Preparation and characterisation of poly (ethylene terephthalate) and poly (vinyl alcohol)/ clay nanocomposites

By

Leena-Marie Döppers

A thesis submitted in part fulfilment of the requirements of Sheffield Hallam University for the degree of Doctor of Philosophy

October 2004

Abstract

The formation of poly (ethylene terephthalate) (PET)/organo-montmorillonite and poly (vinyl alcohol)(PVOH)/ montmorillonite nanocomposites and the diffusion behaviour of water and acetone/ water mixtures into the latter have been investigated. Nanocomposites of PET and various, commercially available, organoclays have been prepared by solution intercalation and the structure of the resulting composite investigated in dependence of surfactant on the organoclay, clay loading, solvent, stirring time, polymer concentration, polymer type and drying temperature. All samples prepared had an intercalated structure with layer spacing depending mainly on the type of surfactant present on the clay. Thermal stability of the samples was similar to that of PET, yet decomposition was found to start at temperatures up to 40 °C lower than for the pristine polymer.

Formation of nanocomposites of PVOH and montmorillonite has been achieved by solution intercalation from aqueous solutions. For these samples the influence of molecular weight of the PVOH, clay loading, clay structure and interlayer cations has been investigated. PVOH/ clay (nano-) composites have been prepared over the full range of compositions, from "true" nanocomposites to PVOH adsorbed on clay. For clay loadings up to 10 wt% XRD silent nanocomposites have been obtained. Clay loadings between 20 and 40 wt% resulted in intercalated nanocomposites with wide ranges of layer spacings, while clay loadings of 45 – 75 wt% resulted in intercalated composites with a narrower distribution of spacings. Above this loading adsorption of PVOH onto clay with two distinct layer spacings could be observed. Results were similar for higher molecular weight PVOH. Thermal stability of these samples was also found to depend on the clay loading. An increase of the degradation onset temperatures by 10-20 °C was measured for nanocomposite samples. Lithium and sodium montmorillonites showed similar dispersion patterns. Charge reduction of the lithium clay had a strong influence on the dispersion of the clay. Lower charged layers resulted in poorer dispersion. Li^+ MCBP fired at 210 °C did not form nanocomposites with PVOH independent of the clay loading.

Diffusion measurements of water into PVOH showed strong influences of swelling, gelling and dissolution of the samples. Generally, diffusion into the nanocomposites showed shorter time delays before it became measurable, yet the diffusion coefficient decreased with increasing clay content. Diffusion was found to be dependent on the dispersion of the clay with microcomposite structures resulting in better barrier properties than their nanocomposite counterparts. Higher temperatures resulted in faster diffusion rates. During the diffusion of water crystalline regions of the PVOH were dissolved and the clay remained dispersed in the swollen PVOH.

Diffusion of acetone/ water mixtures was found to be strongly dependent on the concentration of water in the diffusant. In mixtures with an excess of water or a molar ratio of acetone: water of 1:1 the diffusion of acetone and water proceeded at the same time in PVOH and its nanocomposites. This has been attributed to formation of acetone/ water complexes. At excess levels of acetone in the diffusant acetone diffusion is delayed and occurs at a slower rate. Presence of clay in these samples leads to longer delay times before diffusion can be measured and slower diffusion rates. Microcomposite samples were again found to have better barrier properties than the nanocomposites and it is assumed that partial delamination of the clay layers in these samples increases the aspect ratio of the clay. Swelling is found to decrease with decreasing water content as well as increasing clay content. Crystallinity of the polymer is initially decreased, yet some crystallinity is recovered over the course of the experiment in the neat polymer. Presence of clay reduced the extent to which crystallinity was recovered. Analysis of the hydrogen bonding of the water within the polymer in the equilibrium spectra showed decrease of strongly and weakly hydrogen bonded water with increasing acetone/ contents in the diffusant. In the nanocomposites only decrease of the weakly hydrogen bonded water could be observed. Following the changes in hydrogen bonding over the course of the experiments showed increases in weakly hydrogen bonded water while strongly hydrogen water decreased due to break down of the hydrogen bonding network. Hydrogen bonding of the polymer also decreased due to swelling of the polymer.

Acknowledgements

"Thank you" ...two small words that can mean so much. I would like to use this opportunity and thank some people for whose help and support during the work on this thesis I cannot express enough gratitude.

First of all, I would like to thank Jack Yarwood for his scientific input and many interesting and helpful discussions. Thanks also to Chris Sammon for providing many character building exercises and making time to answer all the questions I could come up with (or at least most of them) and Chris Breen for helping me see results from a completely different angle.

A big thank you is also directed at my parents, Elfriede and Hans-Hermann Döppers, for their support throughout my studies no matter how far away from home I chose to be. You might not fully understand what I have been doing those past three years or why I have been doing it yet tried to help me wherever possible.

Thanks also to everyone in the office and all members of the PCAS group for sharing the fun and disappointments of research and making sure that there was always enough distraction when work got too tedious.

And finally thanks to Michael for providing ample distraction with discussions of "mad science" yet letting me get on with the "puny earth science" first and never failing to help me find motivation again when I got too annoyed by one thing or another.

Table of contents

List of abbreviations

AFM	atomic force microscopy
ATR	attenuated total reflection
BHET	bis (hydroxy ethyl) terephthalate
CEC	cation exchange capacity
DTGS	deuterated triglycine sulfate
FPA	focal plane array
FTIR	Fourier transform infrared spectroscopy
MCT	mercury cadmium telluride
MMT	montmorillonite
NMR	nuclear magnetic resonance
PA	polyamide
PBT	poly (butylene terephthalate)
PE	polyethylene
PEO	poly (ethylene oxide)
PET	poly (ethylene terephthalate)
PI	polyimide
PP	polypropylene
PS	polystyrene
PVOH	poly (vinyl alcohol)
TEM	transmission electron microscopy
TEOS	tetraethoxysilane
TG	thermogravimetry
XRD	x-ray diffraction

Postgraduate courses and accompanying coursework

- Research methods unit:
    - Literature Review
    - Project Planning and Management
    - Project Proposal
    - Scientific Communication
    - Data Analysis and/or Experimental Design
- MRI seminars
- Group seminars of the polymer, surfaces and composites group within M(E)RI
- Workshop on Vibrational spectroscopy
- Workshop on X-ray diffraction

Attended conferences

- Clay Minerals Group, Autumn Meeting, University of Huddersfield, 10th October 2001
- Materials Research Institute Research Day, 25th January 2002
- Hybrid Net 3rd Meeting, Sheffield Hallam University, 26th February 2002
- 6th IRDG Martin & Willis Prize Award Meeting and 168th IRDG Meeting, University of Strathclyde, 10th/11th April 2002
- IRDG Christmas meeting, King's College, London, 18th December 2002
- Materials Research Institute Research Day, 22nd January 2002
- 15th European Symposium on Polymer Spectroscopy, Heraklion, Crete, 8th - 12th June 2003
- 172nd IRDG Meeting, UMIST, Manchester, 15th October 2003
- IRDG Christmas meeting, King's College, London, 18th December 2003
- Materials Research Institute Research Day, 19th January 2004
- International Bunsen Discussion Meeting "Raman and IR Spectroscopy in Biology and Medicine", Friedrich Schiller University Jena, 29th February – 2nd March 2004
- Macro Group UK, Young Reseacher's Meeting, University of Sheffield, 6th – 7th April 2004
- Materials and Engineering Research Institute Science Day, 10th September 2004

1 Introduction

1.1 Aims and Objectives

The aim of this project was to explore the possibility of synthesising polymer/ clay nanocomposites and characterise these materials especially with respect to their diffusion/ barrier properties. Such nanocomposites are expected to exhibit improved barrier properties compared to their unfilled parent polymers.

Two different polymer systems were chosen for this study. First, experiments were performed on the preparation of poly (ethylene terephthalate) (PET)/ organoclay nanocomposites. This polymer was chosen because it finds applications in many areas where good barrier properties are necessary. Further, extensive work has been carried out within our group to characterise the diffusion behaviour of small molecules into the pristine polymer.

The second polymer system chosen for analysis was poly (vinyl alcohol) (PVOH). This polymer was chosen because of its high hydrophilicity and good compatibility with the hydrophilic layered silicates. Because of these characteristics, preparation of nanocomposites is expected to be easier to achieve compared to many other polymers, including PET. This polymer also has high barrier properties towards gases and water vapour, while its performance as a barrier material is severely impeded by the presence of moisture. The work described in this thesis will therefore be centred on the influence of clay on the diffusion of liquids (water and aqueous mixtures) into PVOH nanocomposites.

All nanocomposites were prepared by solution intercalation. Thin films, which can be used in the study of diffusion behaviour by attenuated total reflection – Fourier transform infrared spectroscopy (ATR-FTIR), could be cast from the same solution that was used to prepare samples for structural analysis. These measurements were performed to gain information on the diffusion kinetics, the interactions of the diffusant with the polymer and on changes in the structure of the polymer which are induced by the solvent (such as swelling or changes in crystallinity).

To relate the observed transport properties to the structure of the nanocomposites, the dispersion of the clay layers within the polymer was evaluated from x-ray diffraction analysis (XRD) data. Furthermore, information on the thermal stability of these materials was gained from thermogravimetric measurements.

The challenges expected during this work will be summarised at the end of this chapter, after an introduction of the materials, and an overview of the available literature relevant to this work has been given.

1.2 Poly (ethylene terephthalate) (PET)

1.2.1 Synthesis and structure of poly (ethylene terephthalate)

Poly (ethylene terephthalate) (PET) was first synthesised by Whinfield and Dickson at Calico Printers Associate Ltd in 1941. Permission to commercially produce this polymer was given to ICI and DuPont. PET has been manufactured on a large scale since 1953. It has since become one of the major polymers with a wide range of applications [1.1 - 1.3].

PET can be produced from various monomers and oligomers. The common production process of PET involves four stages. At first the monomer, bis (hydroxy ethyl) terephthalate (BHET), is synthesised by esterification of terephthalic acid and ethylene glycol or transesterification of dimethyl terephthalate with ethylene glycol. BHET then undergoes pre-polymerisation to form oligomers. These oligomers are then reacted in a polycondensation reaction in the melt under near vacuum and temperatures around 280 °C, with the addition of a catalyst to form longer polymer chains. This step is followed by a solid state polycondensation step [1.1, 1.4]. The general equation for this reaction is given in Figure 1-1.

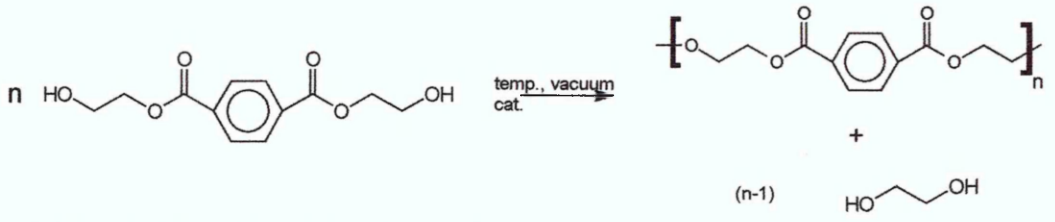

Figure 1-1 Polycondensation of BHET

PET is a colourless, rigid, semi crystalline polymer. It's physical properties are greatly affected by the crystallinity which, at the same time, is strongly influenced by its thermal and processing history [1.2]. X-ray diffraction studies have shown that PET molecules are nearly planar and have a centre of symmetry [1.5]. The unit cell of PET crystals was found to be triclinic with the following cell dimensions: a = 4.56 Å, b = 5.96 Å, c = 10.75 Å, α = 98.5°, β = 118°, γ = 112°. These measurements were obtained from x-ray diffraction studies on PET fibres [1.6]. An illustration of the unit cell is presented in Figure 1-2, and the arrangement of the polymer chains within that cell is shown in Figure 1-3.

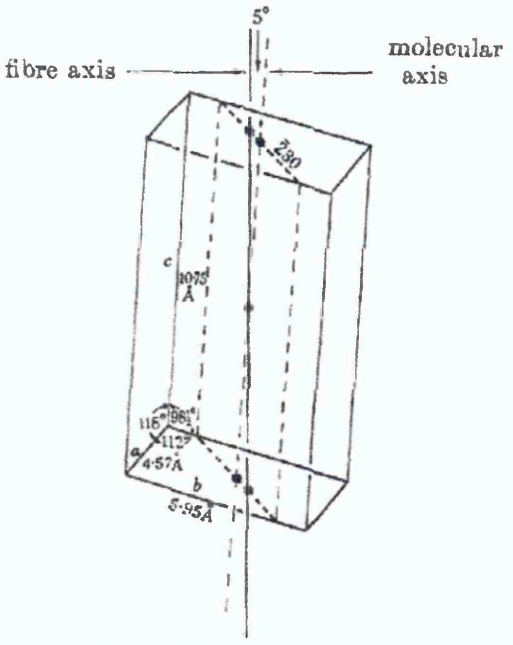

Figure 1-2 Unit cell and direction of tilt in relaxed PET fibres [1.6]

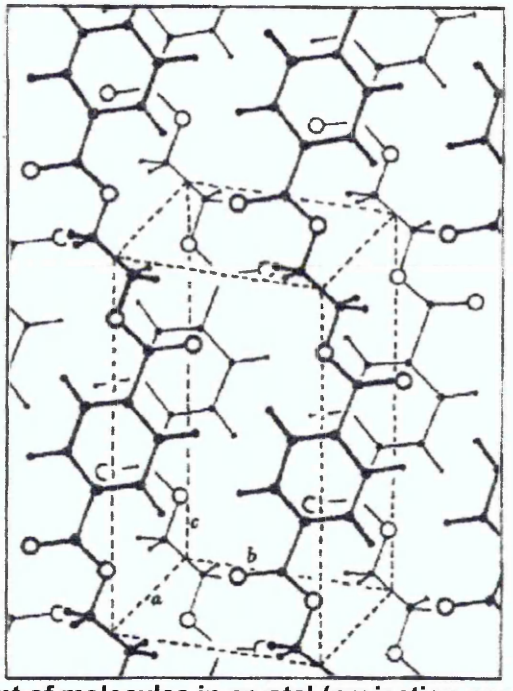

Figure 1-3 Arrangement of molecules in crystal (projection normal to 010 plane) [1.6]

Crystalline regions are comprised of PET molecules in which the ethylene glycol moiety is in a trans configuration. Gauche conformers of the ethylene glycol segment can be found in the amorphous regions of the polymer [1.7, 1.8]. Figure 1-4 shows the molecular structures for PET chains having adopted all trans conformation and a mixed trans and gauche conformation.

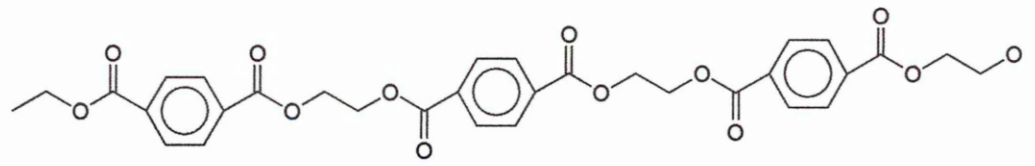

All trans conformation

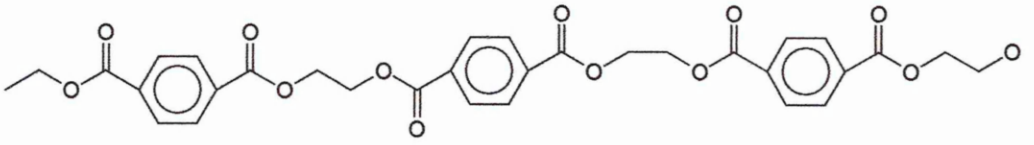

Mixed trans and gauche conformation

Figure 1-4 Structure of PET

Crystallinity can be induced in amorphous PET by thermal annealing or solvent treatment. The structure of samples crystallised by these two methods was found to be similar, though the mobility of polymer chains is much higher during annealing at 140 °C than during solvent induced crystallisation [1.9]. Solvent diffusion in the polymer is mainly thought to occur in the amorphous regions. The effective solubility of a polymer can therefore be given by the ratio of the measured solubility to the amorphous fraction. Solvent induced crystallisation can take place at temperatures well below the glass transition temperature for certain strongly interacting solvents. While thermal crystallisation affects the whole specimen, solvent induced crystallisation is more localised as it only occurs in regions that have been penetrated by the solvent [1.10].

1.2.2 Uses for poly (ethylene terephthalate)

PET possesses excellent chemical resistance, thermal stability, melt mobility and spinability [1.11]. These properties make it suitable for many applications and it is used extensively in the form of fibres, films and moulding materials. Fibres find application in the clothing industry for quick drying fabrics as well as industrial fabrics (e.g. filter cloth, conveyer belts) and marine uses (fishing nets, sailing cloth). Films are produced for the packaging industry, for electrical insulation and as substrates for magnetic tape [1.1, 1.3]. Moulded materials include bottles and jars for food and beverage packaging. Furthermore, PET finds use as reinforcement in tyres and rubber goods [1.12].

1.2.3 Infrared analysis of poly (ethylene terephthalate)

Vibrational spectroscopic methods have been extensively used to characterise the structure of PET. The bulk of the investigations have been carried out by transmission FTIR. The focus of this work was on the weaker bands in the spectrum, since saturation has been observed for some of the stronger bands for films thicker than 2 μm [1.13 - 1.19]. To avoid saturation, other techniques such as ATR and front surface reflection [1.20 - 1.23] have also been applied to the study of PET.

The spectrum of poly (ethylene terephthalate) is rather complex, with respect to the number of bands that can be observed. A typical ATR-FTIR spectrum is presented in Figure 1-5 and band assignments for some of these bands in the mid-IR region are given in Table 1-1. Peak positions in this table refer to the positions observed in spectra recorded in transmission mode. While relative intensities of the peaks can vary between transmission and ATR spectra, due to the wavelength dependence of the absorption in ATR, the peak positions remain similar.

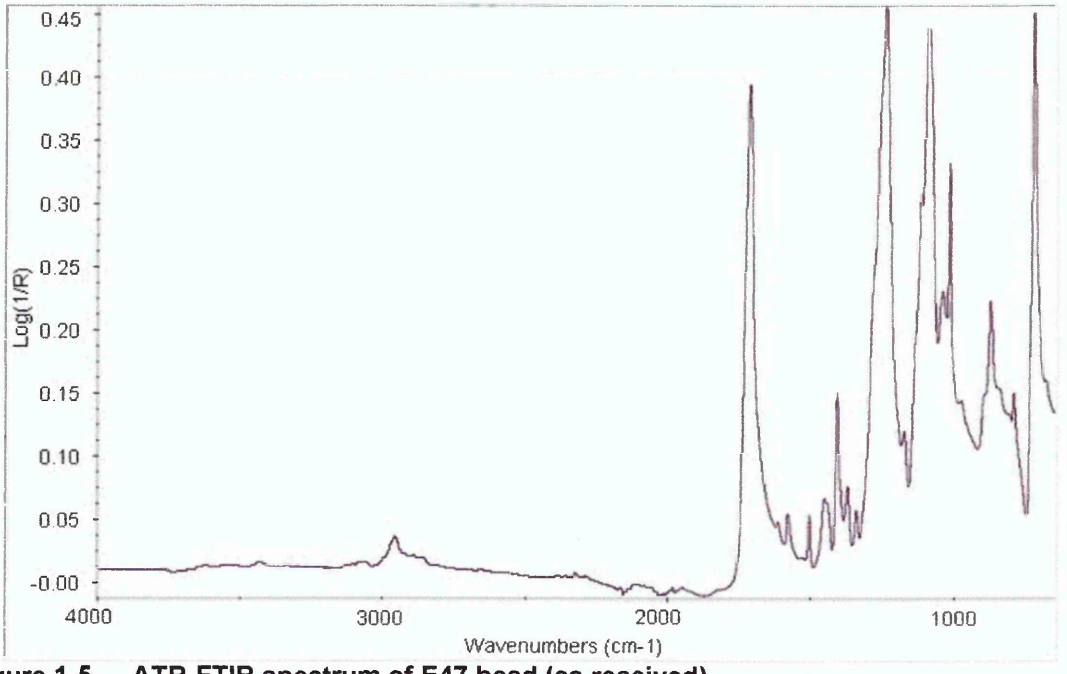

Figure 1-5 ATR-FTIR spectrum of E47 bead (as received)

Band position [cm^{-1}]	Assignment	Morphology
3081	$\nu_{ring}(CH)$	A/C
3067		
2962	$\nu_a(CH_2)$	A/C
2912	$\nu_s(CH_2)$	A/C
1734	$\nu(C=O)$	A
1722		C
1720		A
1714		C
1685	$\nu_{end\ group}(C=O)$	A/C
1615	ν_{ring} (C-C)	C
1580	ν_{ring} (C-C)	A
1507	in plane $\delta(CH)$	A/C
1470	$\delta(CH_2)$	C
1453		A
1410	in plane $\delta(CH)$	A/C
1385		C
1370	$\gamma_w(CH_2)$	A
1339		C
1287	---	A
1265	---	A/C
1248	---	C
1178	in plane $\delta(CH)$	A
1138	---	A
1126	---	C
1110	---	C
1102	$\nu(C-O)$	A/C
1043	$\nu(C-O)$	A
1023	in plane $\delta(CH)$	C
1020		A
1019		A
972	$\nu(O-CH_2)$	C
896	$\gamma_r(CH_2)$	A
875	out of plane $\delta(CH)$	A/C
850	$\gamma_r(CH_2)$	C
793	out of plane $\delta(C=O)$	A/C
734	out of plane $\delta(CH)$ + out of plane $\delta(C=O)$	A
724		C

Table 1-1 Band assignments for PET infrared spectrum [1.5, 1.13, 1.20, 1.24, 1.25] (table adapted from 1.26)

Studying model compounds Štokr et al. [1.27] identified four groups of peaks in vibrational spectra of PET:

1 peaks that do not change upon transition from amorphous to crystalline state or in solution
2 peaks appearing only in spectra of crystalline samples and bands that have much higher intensity than in spectra of amorphous samples or solutions
3 peaks appearing only in spectra of amorphous samples and bands that have much higher intensity than in spectra of crystalline samples or solutions
4 peaks which appear in IR and Raman spectra of amorphous samples but only in IR or Raman for crystalline samples.

Bands at 1470 cm^{-1}, 1337 cm^{-1}, 973 cm^{-1} and 843 cm^{-1} have been found to increase with increasing crystallinity, while bands at 1453 cm^{-1}, 1370 cm^{-1}, 1040 cm^{-1} and 778 cm^{-1} decrease with increasing crystallinity [1.25]. Two explanations have been published for these observations. Ward et al. [1.28] attributed these changes to rotational isomerism of the ethylene glycol segments, while Liang and Krimm [1.29] argued that they are caused by changes in symmetry and resonance characteristics of the substituted benzoid ring framework. Calculation of the PET spectrum, using a valance force field, supports the assignment of these bands to the ethylene glycol segments [1.25].

The degree of crystallinity of polymers can be calculated from their infrared spectra. Such calculations require data on two bands that are attributed to crystalline and amorphous structures. For transmission spectra direct comparison of such bands can be used, since the sampling thickness is equal to the thickness of the specimen. For ATR measurements one has to correct the data for the wavelength dependence of the sampling depth in order to get meaningful results. Such correction can be achieve by two methods; the experimental one, where spectra are recorded at different angles of incidence to achieve the same sampling depth for all bands of interest and the theoretical one, by which data is corrected for differences in sampling depth by means of theoretical mathematical data treatment [1.30].

By means of spectral subtraction, several research groups have obtained spectra of 'pure trans' and 'pure gauche' configurations [1.16, 1.21, 1.23]. Using such subtraction methods three different spectra could be identified; for the trans conformation in the crystalline region and the amorphous region respectively; and for the gauche conformation in the amorphous region.

1.3 Poly (vinyl alcohol) (PVOH)

1.4 Synthesis and structure of poly (vinyl alcohol)

Poly (vinyl alcohol) is a semi-crystalline, water soluble polymer. It is usually synthesised by free radical polymerisation of vinyl acetate and subsequent hydrolysis. Commercially available PVOH is predominantly atactic as monomers polymerise in a head to tail alignment with about 2 % glycol structures [1.31]. The polymer exhibits strong inter- and intra-molecular hydrogen bonding. The presence of water within the polymer structure can plasticise the material, leading to a reduction in the glass transition temperature. If such samples are annealed, higher crystallinities are achieved compared to the crystallinities obtained by annealing fully dried samples [1.32, 1.33].

Fully hydrolysed PVOH is completely water soluble above its 'dry' glass transition temperature of 85 °C [1.33]. Heating the dry polymer above 60 °C can lead to some degradation and discoloration of the sample [1.34].

Gels formed from PVOH and water are classified as physical gels which exhibit thermo-reversible phase transitions. Studying these phase transitions by fluorescence measurements, with the use of flourescein as a probe, shows that not all water molecules in the gels are available for dye hydration and changes in the interactions between the polymer, water and the dye can be observed [1.35].

X-ray diffraction studies of PVOH showed that the polymer crystals can be described by a two molecule monoclinic cell with the following dimensions: a=7.81 Å, b=2.52 Å, c=5.51Å and β=91° 42' [1.36]. These distances agree well with a polymer structure where the hydroxyl groups are randomly placed at either side of the zig-zag shaped polymer backbone (atactic polymer).

1.4.1 Uses for poly (vinyl alcohol)

Poly (vinyl alcohol) finds commercial application in the form of films, coatings and gels. It is used in paper coating, textile sizing and water soluble packaging and mulching films [1.37, 1.38]. As a gel PVOH finds application as a column packaging material for the separation of aqueous solutions [1.39]. PVOH hydrogels are important in the biomedical field due to their compatibility with living tissue [1.35]. PVOH also finds application as an adhesive and as a binder [1.40]. The study of diffusion of water and acetone/ water mixtures into the polymer can therefore give information on the diffusion of these molecules into adhesive layers and how the polymer/ substrate interface is affected by this diffusion.

1.4.2 Infrared analysis of poly (vinyl alcohol)

The infrared spectrum of poly (vinyl alcohol) between 2000 cm^{-1} and 800 cm^{-1} was first published by Barnes et al. in 1943 [1.41]. Two years later Thompson and Torkington [1.42] published an IR spectrum of the polymer recorded between 3400 cm^{-1} and 550 cm^{-1} and provided some band assignments.

Bands at 1710 cm^{-1} and 1265 cm^{-1} have since been attributed to residual acetate groups while a band observed at 1650 cm^{-1} has been assigned to the bending mode of water within the polymer as it can be removed by drying the sample through heating.

Based on group theoretical considerations Krimm [1.31] published band assignments for most bands observed in the PVOH spectrum. A typical spectrum of PVOH recorded by ATR - FTIR is shown in Figure 1-6 and a summary of these assignments based on peak positions in transmission spectra is given in Table 1-2.

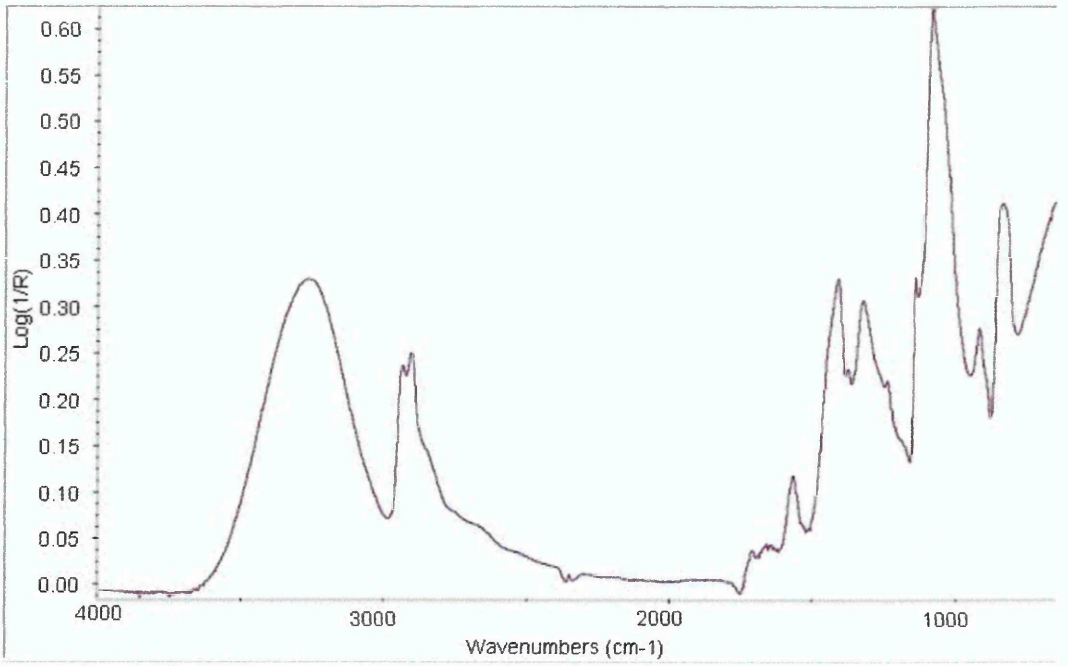

Figure 1-6 ATR-FTIR spectrum of poly (vinyl alcohol)

Wavenumber [cm^{-1}]	Intensity	Polarisation	Assignment
3340	vs (broad)		ν(OH)
2942	s	σ	$\nu_a(CH_2)$
2910	s	σ	$\nu_s(CH_2)$
2840	sb	σ	ν(CH)
1446	s	π	δ(CH+OH)
1430	s	σ	$\delta(CH_2)$
1376	w	π?	$\gamma_w(CH_2)$
1326 1320	m	σ	δ(CH+OH)
1235	w	π	γ_w(CH)
1215	vw	σ	
1144	m	σ	ν(C-O-C)
1096 1087	s	σ	ν(CO)
1040	sh	σ	
917	w	σ	$\gamma_r(CH_2)$
890	vw	σ	$\delta(CO)+\gamma_w(CO)$?
851	m	σ	$\gamma_r(CH_2)$ (amorphous)
825	vw	σ	$\gamma_r(CH_2)$

Table 1-2 Band and their assignments in the infrared spectrum of poly (vinyl alcohol) [1.5, 1.31]

Some question, however, remains about the assignment of the band around 1141 cm^{-1}. This band has been used as an indication for the crystallinity of the polymer, and has been assigned to various different vibrations. Krimm [1.31]

assigned it to C-O-C stretching vibrations arising from temperature induced cross-linking in the crystalline region. Peppas [1.43] later assigned it to the C-C symmetric stretching vibration, while Xu et al. [1.40] attributed it to a combination of symmetric C-C and C-O stretching vibrations in the crystalline regions. Kenney and Willcockson [1.44] did, however, note that the calculation of crystallinity from these bands is less reliable than the determination from density measurements.

The intensity of the band increases with increasing drying temperatures of the polymer samples with a maximum for samples heated around 200 °C. At higher temperatures it is found to decrease, probably due to melting and degradation of the polymer [1.43]. Humidification of the polymer, which is thought to result in an increase in the relative amount of ordered regions, also leads to an increase of this band [1.5].

Furthermore, bands at 916 cm^{-1} and 1096 cm^{-1} have been shown to be sensitive to the intermolecular structure of the polymer. [1.43, 1.45] Suguira et al. [1.45] found that the ratio of the bands as 916 cm^{-1} and 849 cm^{-1} provides a measure of the tacticity of the sample.

Analysing transmission infrared spectra of PVOH with different molecular weights El-Kader and Orabi [1.46] did not observe any changes in the positions for the C=O nor C-C stretches. The spectra presented in this paper did, however, show saturation in the OH and C=O stretching bands which makes the results questionable.

1.4.3 Diffusion of water into poly (vinyl alcohol)

The control of poly (vinyl alcohol) (PVOH) solubility is currently limited because the influence of heat and chemical treatments on the solubility is poorly understood. Therefore, the scientific and technological interest in the interactions of water and PVOH has been considerable in the past few years [1.47]. Understanding the interactions between the polymer and water is also essential to understanding the swelling process of the material. Studies show that samples with higher crystallinity swell less. This effect has been attributed to the observation that water is not penetrating crystallites [1.48].

One application for PVOH membranes is the separation of aqueous organic mixtures. Due to its high hydrophilicity PVOH is highly selective to water permeation. This makes PVOH membranes particularly useful for the separation of mixtures such as ethanol/ water mixtures that cannot be completely separated by distillation, due to formation of an azeotrope. [1.49].

Pervaporation experiments of water through PVOH membranes showed no apparent correlation between the crystallinity of the membrane and its transport properties. The water diffusivity was, however, found to increase exponentially with increasing molar water content in the membrane [1.50].

Diffusion studies of water into PVOH have shown that while water does not inhabit crystalline regions its presence in the sample does result in a reduction of crystallinity. The reduced crystallinity is due to dissolution of crystallites by attack of the amorphous/ crystalline interface resulting in unfolding of the chains that form the crystals [1.33, 1.47, 1.51, 1.52]. Reduction of crystallinity only occurs during the diffusion of liquid water into PVOH while water vapour diffusion does not cause any changes in crystallinity [1.53]. The rate of polymer dissolution was found to be dependent on temperature, as well as molecular weight and degree of hydrolysis of the samples. At higher temperatures PVOH dissolved faster in water while higher molecular weight samples exhibited a more gradual dissolution and reduction in crystallinity [1.52]. Water solubility was found to increase with increasing degrees of hydrolysis (lower vinyl acetate content) [1.54, 1.55].

Ngui and Mallapragada [1.34] showed that elevated temperatures increased the drying rate of PVOH and reduced the residual water content of the samples. During the drying process the polymer changes from a rubbery state to a glassy one. Once PVOH has become glassy, the drying rate undergoes a sharp decrease compared to PVOH in its rubbery state.

Hodge et al. [1.33] observed that water initially enters PVOH in form of single water molecules, which hydrogen bond to the hydroxyl groups of the polymer. Ping et al. [1.54] proposed that one water molecule binds to each hydroxyl group. During the initial phase of diffusion an increase of density of the polymer could be observed. This has been attributed to water filling free volume cavities

in the polymer, without causing any swelling. Water contributes to the plasticisation of PVOH in a two fold manner. Through disruption of the hydrogen bonding network of the polymer the size of free volume cavities is increased; while the lubrication also leads to higher polymer chain mobility [1.33, 1.51].

Ping et al. [1.55] observed that the subtraction a dry poly (vinyl alcohol) spectrum from that of the hydrated polymer gives rise to two peaks with peak centres at 3400 and 3280 cm^{-1}. They assigned these two peaks to water molecules of the first and second hydration layer of the polymer and noticed that these peaks increase in different proportions with an increase in the water level.

Incorporation of tetraethoxysilane (TEOS) into PVOH was found to decrease the swelling of PVOH membranes while increasing the "perm selectivity" for water, and the density of the hybrid material [1.49]. These improvements of the material were attributed to the formation of hydrogen bonds between the silanol groups of the TEOS and the hydroxyl groups of the PVOH.

1.5 Clays and organoclays

1.5.1 Clay structure

Clay minerals (phyllosilicates) are among the most important industrial minerals. Their physical and chemical properties are closely related to their structure and composition [1.56]. Because of their properties clays are often used as filler materials in formulations such as dry wall finishings, joint treatment compounds or wallboard compounds providing thickening properties and thixotropic characteristics [1.57].

Bentonite is a naturally occurring clay comprised of a mixture of various (clay) minerals. The most common type of clay found in bentonite are smectites, a group of 2:1 layered clays. Natural deposits of bentonite have either sodium or calcium as the dominant interlayer cation. Main deposits of sodium bentonite are located in South Dakota, Wyoming and Montana while calcium bentonites can be found in Texas, Mississippi, England, Germany, Greece, Italy, Spain and India [1.56].

The crystal structure of these materials is formed by two layers of tetrahedrally co-ordinated silicon atoms, which are fused to opposite sides of an octahedral sheet of either aluminium or magnesium oxide. The fusion of the different layers occurs by sharing of oxygen atoms in the structure. The thickness of such 2:1 layers is around 1 nm and lateral dimensions may vary from several nanometres to several micrometers. These layers organise themselves to form stacks with a regular van der Waals gap between them. This gap is referred to as the interlayer or gallery. Figure 1-7 shows a schematic representation of these layers [1.58, 1.59]. The position of the silicon atoms at the centre of the tetrahedra, which are formed by the oxygen atoms surrounding them, has been omitted in this diagram for clarity of the schematic.

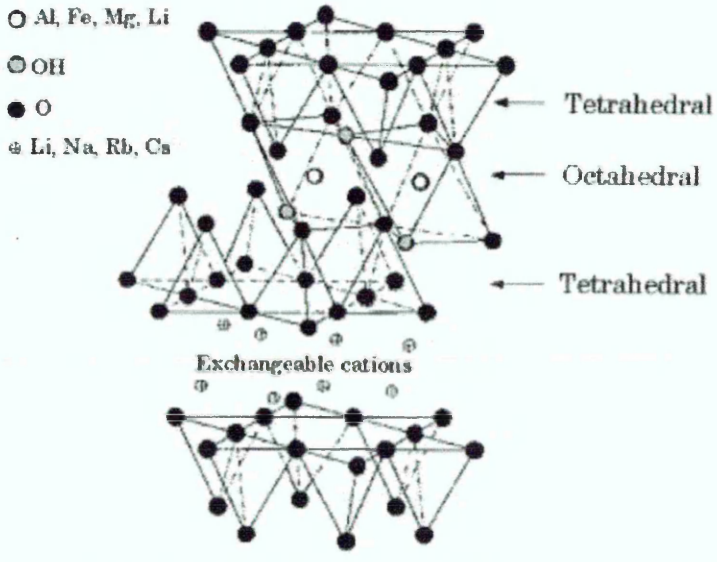

Figure 1-7 Schematic diagram of the structure of a 2:1 phyllosilicate [1.60]

Isomorphous substitution of Al^{3+} for Si^{4+} in the tetrahedral sheet or Fe^{2+}, Mg^{2+} for Al^{3+} in the octahedral sheet creates an excess of negative charge in the clay layers that is counterbalanced by cations (usually alkali or alkaline earth cations) in the clay galleries. The distance between sites of negative charge depends on the extent of the isomorphous substitution. The predominant exchangeable cations are calcium, magnesium, sodium and potassium. Most of these exchangeable cations are situated in the clay gallery. Cations associated with edges of the layers, where structural atoms can exhibit unsatisfied valences, can also be exchanged [1.61, 1.62]. It is generally accepted that 80% of the exchangeable cations occupy sites within the gallery.

The maximal amount of cations that can be exchanged by other cations is given by the cation exchange capacity (CEC). It is measured in milliequivalents (meq) per 100 grams. The CEC varies, depending on the extent of isomorphous substitution, but is similar for clays with similar sum chemical formulae.

Different clays can be summarised in classes according to their sum chemical formula. Some characteristics for commonly used 2:1 layer clays are summarised in Table 1-3.

Class	Chemical formula	Cation exchange capacity [meq/ 100g]	Particle length [nm]
Montmorillonite	$M_x(Al_{4-x}Mg_x)Si_8O_{20}(OH)_4$	110	100 - 150
Hectorite	$M_x(Mg_{6-x}Li_x)Si_8O_{20}(OH)_4$	120	200 – 300
Saponite	$M_xMg_6(Si_{8-x}Al_x)Si_8O_{20}(OH)_4$	86.6	50 - 60

M = monovalent cation, x = degree of isomorphous substitution (between 0.5 and 1.3)

Table 1-3 Summary of characteristics of commonly used 2:1 layer clays [1.59]

Clay is hydrophilic and water can usually be found in the galleries, solvating the cations present [1.61]. Water molecules in the galleries can be present in two different environments. They can either be directly co-ordinated to the exchangeable cations, hydrogen bonded to the water in the first coordination sphere of the cations, or be physio-sorbed onto the clay layers.

Reference intensity ratios for peaks in XRD traces of clays are hard to obtain because of differences in the amorphous content, and the preferred orientation of crystallites in these natural materials. Furthermore, humidity during the analysis and Lorentz polarisation effects are known to alter the ratio of peaks observed in such measurements. In smectite clays for example, a peak at 23.8 Å can be observed which arises from the ordered interstratification of layers containing one layer of water molecules and dehydrated layers. A schematic representation of dehydrated and swollen clay layers is given in Figure 1-8 [1.63].

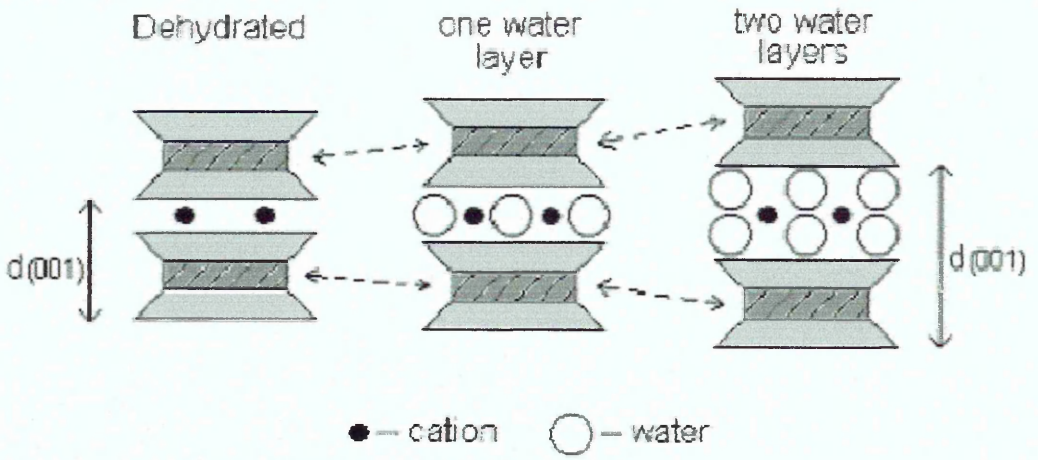

Figure 1-8 Swelling of clay in the presence of water

Measuring water adsorption and desorption kinetics by the weight changes of the clay showed slightly higher values during desorption of water than for the adsorption process. This hysteresis effect has been attributed to higher water contents on the external surfaces during the drying process. Charge reduction in lithium clays heated to 110 °C and 135 °C respectively showed only minor effects on the water adsorption. Lithium clays heated at 160 °C and 300 °C however showed strongly decreased adsorption which can be attributed to the formation of non-swelling layers in these samples [1.64].

Smectites are often compositionally and structurally heterogeneous materials. XRD analysis can be used to estimate the layer charge of these clays, but no information on the charge location can be obtained by this method. To further clarify the distribution of charges in clay layers Christidis and Eberl [1.65] compared XRD traces of various glycol expanded smectites with calculated traces. The calculated XRD patterns had been based on different ratios of layers with low charge (containing double glycol layers), intermediate charge (one glycol layer) and high charge (collapsed layers)

Structural OH and Si-O vibrations in infrared spectra of clays can be used to differentiate various types of clay. The positions and intensities of the metal-OH bending modes, which can be observed in the region of 1000 – 800 cm^{-1}, can give information on the chemical composition of the octahedral layer. In smectite clays only a single band can be observed in the ν(OH) region which arises from water sorbed in the clay layers. FTIR is sensitive to structural

modification. Acid activation of the clay surface, for example, shifts the Si-O stretching vibration in montmorillonite from 1030 cm^{-1} to 1100 cm^{-1} [1.66].

1.5.2 Organically modified clays

Interactions between clays and organic molecules are of major interest for many industrial applications. Due to their sorption properties clays are often used to retain hazardous materials in landfills or waste treatment.

Adsorption of organic cations renders the surface of clay layers organophillic. Such exchange reactions are possible because most cations are preferentially sorbed over most organocations, due to a combination of electrostatic and non-coulombic forces. Organo-modified clays can be used as gelling agents, thickeners, fillers, chromatography column packing materials, and for sorption of hydrophobic pollutants [1.62].

Alkylammonium cations or cationic surfactants are the most common organic modifiers used to improve compatibility between polymers and clay surfaces. These organic cations may also contain functional groups which react with the polymer to form covalent bonds thereby improving the adhesion between the organic and inorganic phase of a nanocomposite [1.67]. Other materials used to create organophilic clay surfaces are amino acids and silanes [1.61]. Organically modified clays are commercially available from a number of suppliers, but they may not always have the optimal surfactant loading required for a particular application [1.68].

The cation exchange process can be described as a two stage process. Initially, the bulk solution will penetrate into the galleries, and exchange of cations close to the edges can be observed. Over time, diffusion of solution further into the interlayer will result in exchange of the cations that are occupying sites further away from the edges of the clay particles [1.61]. To exchange the cations of natural clays for organocations the clay is dispersed in a solution of the organocation. Ion exchange takes place due to preferred sorption of these organic molecules over the inorganic ions [1.59, 1.68, 1.69].

Usuki et al. [1.70] observed that amino acids were adopting different orientations when intercalated into montmorillonite. With increasing chain length of the amino acid larger basal spacings were observed for the clays. When the

chain length was shorter than C = 8 amino acids were aligned parallel to the clay layers while chains with 11 or more carbon atoms adopted an inclined alignment. Addition of ε-caprolactam was found to further swell the clay as the clay layers expand to accommodate the caprolactam which also results in a realignment of the amino acids.

Similar observations have been made for alkylammonium ions. When intercalated into the clay, the ammonium head groups reside preferentially on the clay surface leaving the alkyl chain(s) to radiate away from the surface. Depending on the CEC of the clay and the alkyl chain length, different arrangements are adopted by the alkylammonium ions. At low CEC's these chains are thought to form mono- or bi-layers with the alkyl chains aligned parallel to the clay surface. At higher CEC's paraffin like mono- or bi-layers can be observed (see Figure 1-9). Since each of these arrangements results in a different spacing of the clay layers, XRD analysis can be used to gain information on the orientation of alkylammonium ions within the clay galleries [1.58, 1.71].

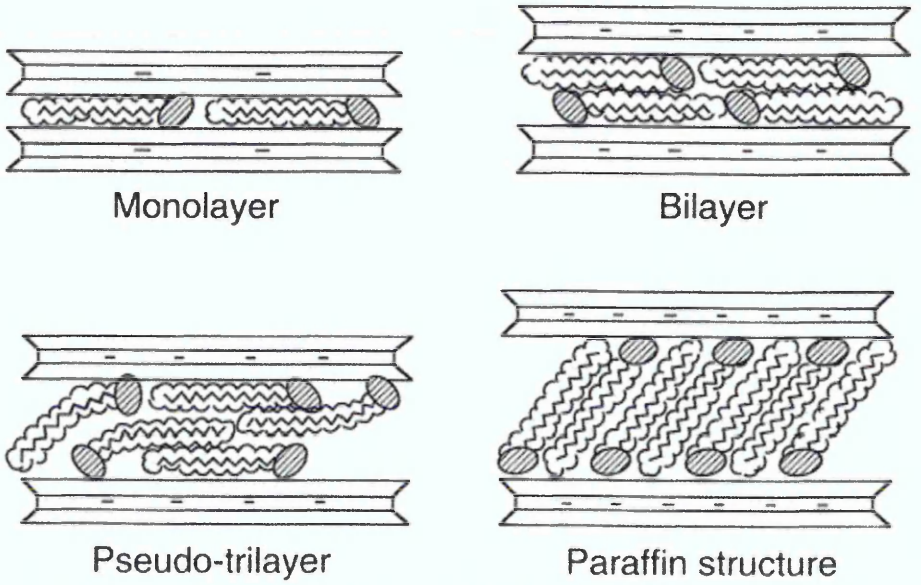

Figure 1-9 Alkyl chain orientation and aggregation in clay galleries [1.72]

1.5.3 Charge reduction in Li^+ montmorillonites

A change in the negative residual charge of clay layers causes a marked change in the properties of smectites, such as hydrophobic character or the

ordering of aliphatic chains of alkylammonium ions sorbed in the interlayer [1.73].

Lithium saturated montmorillonites lose their expandable character and exhibit a loss of exchangeable lithium ions upon heating. Two different mechanisms have been suggested to explain these observations but the final position of lithium ions fixed in the clay sheets remains ambiguous, and is likely to depend on the type of montmorillonite (MMT) used, and its total charge and/or octahedral to tetrahedral charge ratio [1.74]. The first mechanism, which describes a migration into the vacant octahedral sites, is based on the observation that montmorillonite is the only mineral of the smectite group which exhibits this effect, and the fact that the major charge deficit in MMT arises from isomorphous substitution in the octahedral layer. The second mechanism explains this behaviour by diffusion of the lithium ions into the bottom of the hexagonal cavities, or basal surfaces of the octahedral layer. [1.75].

The degree of charge reduction achieved by heating lithium exchanged montmorillonites depends on the time and temperature of the heating process [1.76, 1.77]. Increased temperatures allow the lithium ions to gain enough kinetic energy to overcome the energetic barrier to move into the clay sheets [1.73]. The charge reduction can also be influenced by the fraction of lithium ions in the galleries prior to heat treatment [1.78].

Exchanging charged reduced clays with alkylammonium ions can prevent the collapse of low charge layers upon removal of the solvent. When the lithium content in the galleries prior to heat treatment does not exceed 40% alkylammonium ions can still be intercalated into all clay layers. At higher lithium fractions non-charged layers are created that can only be swollen by ethanol, but no alkylammonium ions can be intercalated into these layers. These observations confirm that charge reduction is a non-homogenous process [1.78].

Hrobarikova et al. [1.74] observed that the charge of the tetrahedral layers remained unchanged by lithium fixation. Furthermore, highest reductions of the cation exchange capacity of heat treated lithium clays were obtained for clays with the lowest tetrahedral and highest octahedral charges [1.79].

Calvet and Prost [1.76] showed that deuteration does not affect the structural OH groups but only interlayer water. This technique could therefore be used to study the structural effects of heat treatment of lithium exchanged clays by FTIR without interferences of the OH vibrations of interlayer water. In the OH stretching region, heating caused a shift to higher wavenumbers and the appearance of a dichroic band which has been attributed to a change in the orientation of OH groups upon migration of small cations into the octahedral layer. The metal-hydroxide bending modes also shifted to higher wavenumbers upon heating and decreased in their intensities [1.74 - 1.76, 1.79].

The main changes in the infrared spectra of heated lithium MMT's can be observed in the ν(Si-O) band which exhibits broadening and shifts to higher frequencies [1.75]. Further analysis of the region between 1200 and 950 cm^{-1}, by Fourier deconvolution of the Si-O-Si and Si-O-metal stretching vibrations, reveals shifts in the relative intensities of these bands, dependent on the metal ion involved [1.80].

The fixation of lithium in the octahedral sheet of montmorillonite is accompanied by a re-orientation of the structural hydroxyl groups. These structural changes can be observed when lithium exchanged clays are heated above 160 °C [1.77]. Furthermore, differences in the perturbation of the OH bending mode give information on the position of the fixed lithium ions [1.79]. To determine the final position of lithium ions fixed in the clay sheets the whole spectrum between 4000 and 400 cm^{-1} needs to be analysed. Near infrared data of these samples was found to provide similar information, showing changes in all combination bands arising from the different OH vibrational modes upon heating of the samples [1.81].

Lithium clays, collapsed at temperatures over 300 °C, have often been reported to be non-expandable. However Alvero et al. [1.75] reported that they were able to re-expand such clays by treating them with water vapour, at high pressures around 8.5 MPa. Under these conditions, they reported the formation of a double water hydration layer around lithium ions in the clay galleries. They used their observations as further proof for the second mechanism. They stated that lithium ions migrate to the bottom of the pseudo-hexagonal holes in the

tetrahedral layer upon heat treatment, causing a complete dehydration of the galleries of these materials.

Madejova et al. [1.79] reported that temperatures of 220 °C are sufficient to achieve maximum charge reduction in lithium exchanged clays. Previously published data stated temperatures of 250-300 °C to achieve this level of reduction in the cation exchange capacity.

Charge reduction in MMT can be achieved with different cations in the interlayer. The effect is strongest for lithium ions with weaker charge reduction for copper or cadmium exchanged clays. The temperatures required to fix previously exchangeable cations in the structure increase with the size and charge of the cation. If lithium is present with copper, preferred fixation of the lithium ions can be observed [1.82].

Studying the behaviour of various cations in the interlayer of clays Karakassides et al. [1.83] concluded that the structural site to which the metal ion is fixed upon heating depends on the valency and size of the cation. Lithium ions were found to be trapped in previously vacant octahedral positions, and within the hexagonal holes of the tetrahedral sheet. Copper ions on the other hand were only fixed deep in the hexagonal holes, while the larger cadmium ions were only fixed loosely in the hexagonal holes [1.77, 1.82, 1.83].

1.6 Polymer/ clay nanocomposites

Although Unichika (Japan) filed a patent for a nylon–6/ montmorillonite nanocomposite in 1976, the first nanocomposite material to be commercialised was a nylon-6/ montmorillonite hybrid developed at the Toyota Research Laboratory in 1988 [1.84]. After failing to disperse alkylammonium exchanged clays in the polymer by melt intercalation, in-situ polymerisation of ε–caprolactam intercalated into C_{12} -ammonium exchanged montmorillonite was found to produce a composite with largely improved properties [1.85 – 1.89]. The publication of these findings sparked a worldwide interest in these materials and research has since been carried out on many different polymer/ clay systems.

Nanocomposites are two phase materials which consist of a phase with dimensions on the nanometre (10^{-9} m) scale dispersed in a second one [1.61]. Types of nanofillers are classed according to the number of dimensions of the material that are on a nanometre scale as summarised in Table 1-4.

Number of dimensions on nanometre scale	Type of nanofiller
one	layered crystals, e.g. clay
two	Nanotubes or whiskers
three	Spherical silica nanoparticles

Table 1-4 Types of nanofiller materials [1.58]

While the term "nanocomposite" has only recently been introduced, and systematic investigations of such materials have been carried out only in the last two decades such materials have been in use in industry for at least a century, and have always been present in nature e.g. vegetables, minerals or bones and cartilage [1.90]. The introduction of small particle powders such as calcium carbonate, silica, silicates or carbon black into polymers as reinforcing fillers has been mentioned in the literature in the 1950's, and particle size has been known to influence the characteristics of the composite material since then [1.91, 1.92].

Clays have been used as filler materials in polymers for a long time. However, dispersing the individual clay layers in a polymeric matrix to form nanocomposites is a relatively new technique. Smectite clays like montmorillonite, hectorite or saponite are among the most commonly used

layered silicates in the industry in general [1.61, 1.93], and in nanocomposite preparations [1.94].

The interactions between polymers and clays have been extensively studied since the 1960's. Yet most of these studies concerned the adsorption of polymers onto the clay layers [1.61]. Adsorption of polymers onto non-porous adsorbents is a fairly rapid process while adsorption of polymers onto clays may require several hours or days to reach equilibrium. When adsorbing a polymer from solution the competitive sorption of polymer and solvent is the predominant factor influencing the sorption process [1.57].

Polymer/ layered silicate nanocomposites present a radical alternative to conventionally filled polymers [1.94]. They often exhibit large improvements of various properties, without the trade-offs observed for many conventional fillers [1.95].

Nanocomposites have been prepared using many different polymer matrices [1.59, 1.61, 1.71, 1.90]. Over the years, nanocomposites have been reported for thermosets like epoxy resins [1.96], unsaturated polyesters [1.97 - 1.100] and polyurethanes as well as thermoplastics e.g. polyamides (PA) [1.85 – 1.89], poly ethylene oxide (PEO) [1.73], polyimides (PI) [1.101, 1.102], polystyrene (PS) [1.103], polypropylene (PP) [1.104], poly (ethylene terephthalate) (PET) [1.105, 1.106], poly (vinyl alcohol) (PVOH) [1.107, 1.108] or polyelectrolytes [1.109].

1.6.1 Structures of polymer/ clay nanocomposites

Among the controllable variables known to influence the properties of the final composite material are type of clay and clay pre-treatment (organic modification), the type and properties of the polymer component and the method used to disperse the clay in the polymer matrix [1.68].

Three different types of clay dispersion in polymers have been identified. When the compability of the polymer and the clay is insufficient, so-called conventional microcomposites are formed. These are usually phase separated structures that do not exhibit the same property enhancement as their nanocomposite counterparts. For the nanocomposites two different types of dispersion can be observed. Often both types can be found in different regions of a

nanocomposite material. The first type of nanocomposite is the intercalated nanocomposite. Here the general order of the layer stacking is maintained and clay layers are merely moved further apart by the presence of polymer chains in the galleries. Such nanocomposites show diffraction peaks in their XRD patterns, as long as the layer spacing is within the range that can be measured by this method (usually up to 5 nm). Nanocomposites, in which the order of the clay is completely abandoned and single sheets of silicate are dispersed in the polymer, are called exfoliated nanocomposites. These do not show any diffraction peaks that could be attributed to the clay when examined by XRD [1.59, 1.61, 1.67, 1.68, 1.71, 1.94, 1.110]. A schematic representation of the different polymer/ clay composite structures is given in Figure 1-10.

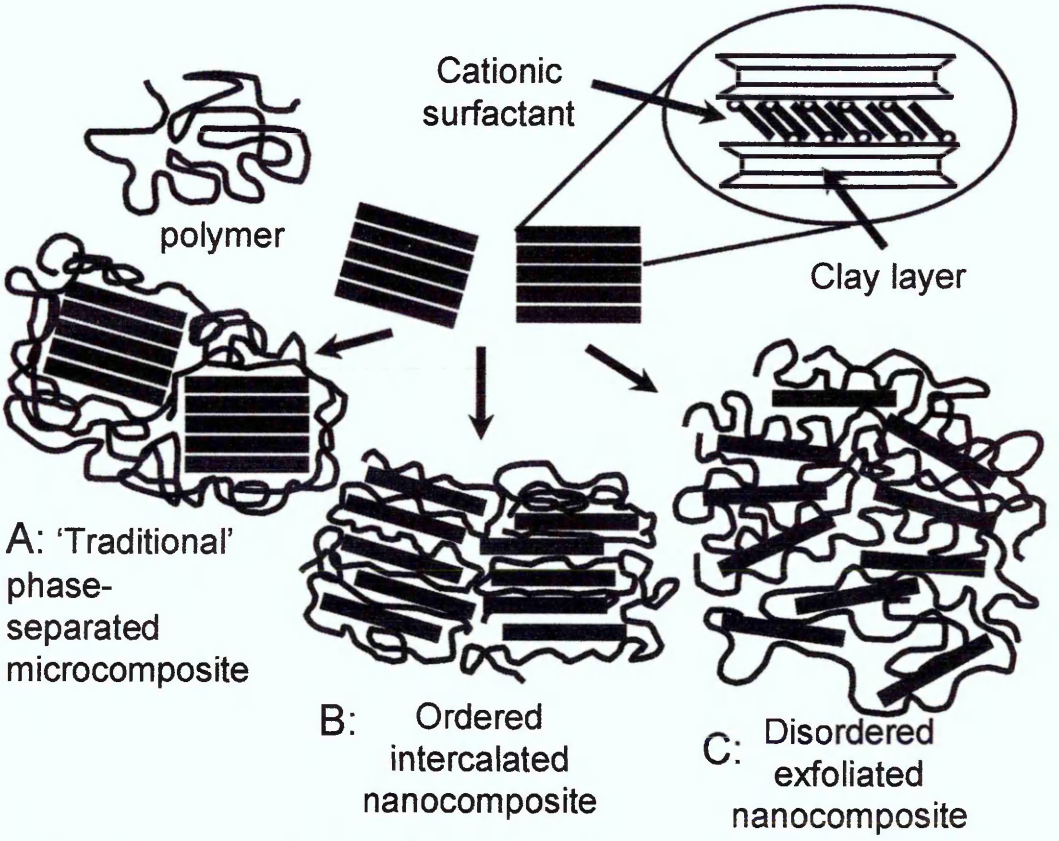

Figure 1-10 Structures of polymer/ clay composites (not to scale)

To elucidate the structure of polymer/ clay nanocomposites several methods are required to give complementary information. The most commonly used techniques are x-ray diffraction analysis (XRD) which gives information on the spacing of the clay layers and crystallinity of the polymer and transmission electron microscopy (TEM) which can help understand XRD traces that do not show any peaks for the clay [1.59, 1.69]. Furthermore, atomic force microscopy

(AFM), nuclear magnetic resonance spectroscopy (NMR) and neutron scattering have been used to investigate the structure of polymer/ clay hybrids. [1.110]

The extent to which nanocomposites improve the properties of the parent polymer is closely related to the structure of the nanocomposite, i.e. the dispersion of the clay in the polymer matrix. Few theories exist which pinpoint or predict the thermodynamic stability of a polymer/ clay mixture accurately. Because of this lack of theoretical descriptions synthetic chemists have to create a whole range of samples with different compositions to isolate the desired materials. Understanding the interactions between the organically modified clay surfaces and the polymer chains can, however, provide a better understanding of how to achieve certain types of polymer/ clay nanocomposite [1.111 – 1.113].

To this end, Balazs et al. [1.111, 1.112] modelled the interactions between surfactant modified clay surfaces and surrounding polymer melt using self-consistent field theory. They found that the phase behaviour and morphology of the nanocomposite can be affected by the kinetic mechanism which controls the polymer penetration into the clay interlayer. During melt intercalation, the polymer diffuses into the interlayer from the edge to the middle maximising the contact with any organophilic surfaces. If there is strong attraction between the organic modification of the clay and the polymer the resulting polymer/ clay nanocomposite will be intercalated, since the clay layers are stuck together by the polymer/ surfactant interactions. Using this model Singh and Balazs [1.114] also found that higher branching of the polymer at constant molecular weights increases the miscibility of these systems.

Exfoliated nanocomposites can be achieved by using polymers that have fragments which are highly attracted to the organically modified surface (to attract the polymer into the gallery) and fragments that are not attracted to this surface (to expand the gallery space). Optimal polymeric candidates for exfoliated nanocomposites are therefore materials that constitute optimal steric stabilisers for colloidal suspensions of clay [1.112, 1.113].

Modelling the behaviour of a polymer melt containing functionalised chains between two infinite planar surfaces using scaling theory, Kuznetsov and Balazs [1.115] reported that no thermodynamically stable intercalated states exist for telechelic chains. At sufficiently high adsorption energies these materials formed an exfoliated system while lower adsorption energies resulted in an immiscible mixture. From these results they deduced that organo-modified clay can be exfoliated in a polymer melt of reactive di-functionalised chains requiring little processing.

Analysing nanocomposites prepared from nylon-6 with amino acid exchanged clay, Usuki et al. [1.89] found that the carboxyl groups of the amino acid helped initiate polymerisation of the ε-caprolactam in the galleries and creating bonds between the clay and polymer. With increasing clay content the ratio of bonded to non-bonded polymer was increased.

Interaction of clay surfaces with polymers has been found to influence the crystal structure of semi-crystalline polymers [1.85]. For nylon-6 nanocomposites, Kojima et al. [1.86] reported a reduced crystallinity in the nanocomposite compared to the pristine polymer.

Studying nanocomposites of polyester resin with Cloisite 30B®, Bharadwaj [1.97] found that these materials showed no d_{001} peaks in their XRD patterns, with a clay content up to 10 wt%. This indicates that either the clay layer spacing was higher than that measurable by the system, or the ordered stacking of the clay layers was sufficiently disturbed not to result in a peak, as would be the case in exfoliated nanocomposites. Transmission electron microscope (TEM) images of these materials confirmed these findings, and showed that these samples contained a mixture of intercalated and exfoliated regions.

Bujdak [1.73] showed that the amount of polymer absorbed onto a clay is controlled by the layer charge density of the clay by intercalating poly (ethylene oxide) (PEO) into lithium exchanged clays with different layer charges. Some intercalation could be observed by mixing the clay and low molecular weight polymer at room temperature. In general, heating to just below the melting temperature of the PEO was, however, necessary to achieve an even

intercalation. High charge silicates were found to produce a mixed layer structure with galleries containing two polymer layers and others having one or no polymer layer. At lower charges the structure was more uniform and the d spacings increased with decreasing layer charges. The method of preparation had only minor effects on the final nanocomposite for these samples as solution and melt intercalation produced similar results.

Epoxy resin/ clay nanocomposites often have exfoliated structures. If, however, only small amounts of epoxy are added to the clay swelling occurs. Pre-swelling organoclays with epoxy was found to improve the dispersion of these clays in other polymers such as PVOH [1.107] or PBT [1.116].

By treating montmorillonite with silanes to activate the surface, Kornmann et al. [1.98] were able to create a nanocomposite of unsaturated polyester resin with montmorillonite, which showed no d_{001} peaks for clay loadings up to 10 wt%. Mechanical testing of these materials showed improved tensile strength and toughness.

Suh et al. [1.99] investigated the influence of "all at once" and 'sequential' mixing of uncured unsaturated polyesters, styrene and organophilic montmorillonite on the structure of the final nanocomposites. They found that sequential mixing, where the clay was pre-intercalated with the polyester before addition of styrene, resulted in higher d spacings, and greater improvement in the polymer properties. Allowing longer mixing times also led to larger d spacings of the clay. This observation was attributed to the higher mobility of the styrene, which results in higher styrene concentrations in the galleries, and therefore lower cross-linking of the resin.

Polymer/ clay nanocomposites offer a unique avenue for the study of the static and dynamic properties of polymers in confined spaces. Following the intercalation process of polystyrene into organoclay in the melt by XRD measurements, Krishnamoorti et al. [1.116] found that the mass transport of the polystyrene chains appears to be unhindered, since the diffusion coefficient measured was similar to the diffusion coefficient of polystyrene chains in the bulk.

The influence of surfactant surface coverage on the dispersion of various organo modified montmorillonites in poly (vinyl carbazole) was investigated by Suh and Park [1.100]. While higher surface coverage of the surfactant led to higher d spacings in the clay nanocomposites, this would indicate only intercalated structures. If the clay surface was only partially covered by surfactant, exfoliation occurred due to formation of coil like polymer structures in contact with untreated clay surfaces.

Delozier et al. [1.117] investigated the dispersion of charged reduced clays in polyimides. The charge reduction had been achieved by heating lithium exchanged montmorillonite to 120 °C, 130 °C, 140°C and 150°C respectively, before exchanging the lithium for organic cations. Clays with lower charges were found to agglomerate more when intercalated into polyimides, with the best dispersion observed for the clay heated at 130 °C.

1.6.2 Preparation techniques

Nanocomposites can be prepared via different routes. The choice of the preparation method usually depends on the properties of the polymer matrix and the type of clay. Some types of nanocomposite can be prepared using several of these strategies and the structure of the resulting material can be influenced by the method of preparation. The four main processes that have been considered in the preparation of polymer/ clay nanocomposites are exfoliation – adsorption, in-situ intercalative polymerisation, melt intercalation and template synthesis [1.58, 1.61, 1.90, 1.92]. In-situ polymerisation and solution intercalation are often limited in their use in technological applications, since compatible clay/ monomer systems or clay/ polymer/ solvent systems are not always available [1.67].

The exfoliation – adsorption or solution intercalation mechanism is widely used with water soluble polymers such as poly (vinyl alcohol), poly (ethylene oxide), poly (vinylpyrrolidone) or poly (acrylic acid). To form nanocomposites the clay is exfoliated by dispersing it in a solvent in which the polymer is soluble. The polymer is then adsorbed onto the clay layers from solution. Nanocomposites prepared by this method often have intercalated structures as the clay layers reassemble to a certain degree during the evaporation of the solvent. In some cases, where nanocomposites of insoluble polymers such as polyimide are

prepared, a pre-polymer is adsorbed onto the clay layers, which is afterwards chemically or thermally converted into the desired polymer. This process also describes emulsion polymerisations, where the layered silicate is dispersed in the aqueous phase.

During in-situ intercalative polymerisation, the clay is swollen within the liquid monomer or a monomer solution. Polymerisation can then be initiated by heat, radiation, the diffusion of a suitable initiator, or by an organic initiator or catalyst fixed to the clay surface by cation exchange prior to swelling of the clay. Nanocomposites prepared via this route have been reported for thermoplastic materials like polyamides, poly (ε-caprolactone), polystyrene and polyolefins as well as thermosets, such as epoxy or unsaturated polyester resins, and elastomeric materials like rubber or elastomeric epoxies and polyurethanes.

Melt intercalation of high polymers into clay is a powerful approach to synthesise polymer/ clay nanocomposites. It is applicable to a wide range of commodity polymers [1.94]. In this process the polymer is mixed with the layered silicate in a molten state. If the clay surface is sufficiently compatible with the polymer intercalation and exfoliation occurs in the melt due to entropic and enthalpic factors, without the need of any solvent. Dispersion of the inorganic phase is often aided by shear forces when samples are prepared by extrusion. Melt intercalation has been applied to a wide range of polymers e.g. polystyrene, nylon-6, polypropylene, rubbers or poly (ethylene oxide) and copolymers of ethylene and vinyl acetate or styrene and butadiene.

The fourth preparation method for nanocomposites, template synthesis, uses the polymer as a template to crystallise layered silicate structures. It is widely used to prepare double-layer hydroxide-based nanocomposites, and also for preparation of polymer/ clay nanocomposites. Synthetic clays produced in this manner can be preferable to natural clays because their purity and composition can be controlled with better reproducibility. Synthetic clays generally have smaller crystallite sizes and lower aspect ratios than their natural counterparts giving them higher surface areas. Since crystallisation of layered silicates requires heat to be initialised, not all types of clay can be produced within polymers due to degradation of the polymer matrix at higher temperatures.

Crystallisation conditions for hectorite are mild enough for polymers to be used as templates. The final product can either be used in nanocomposite applications or the polymer can be extracted to use the clay as a catalyst or in similar applications that require mesoporous materials [1.118].

1.6.3 Property enhancement in polymer/ clay nanocomposites

Polymer clay nanocomposites have been found to enhance many different properties of the parent polymer without showing the penalties often observed when using conventional filler materials. Polymer nanocomposites are lighter in weight than their conventionally filled counterparts. Integrating single dispersed clay layers into a polymeric matrix can improve stiffness and strength, dimensional stability, flame retardancy, solvent and UV resistance and barrier properties of the polymer [1.58, 1.59, 1.71, 1.94, 1.97].

Properties like thermal or mechanical stability that depend on the surface area of the filler can show similar improvements for small amounts of nanometre thin layered inorganic fillers as for 30 - 50 wt% conventional micro-sized fillers [1.108].

An example of the improvement that can be achieved in nylon-6 nanocomposites with different degrees of clay dispersion is given in Table 1-5.

Composite type	wt% clay	Tensile strength [MPa]	Tensile modulus [GPa]	Impact strength [KJ m^{-2}]	Heat distortion temperature [°C]
Exfoliated	4.2	107	2.1	2.8	145
Intercalated	5.0	61	1.0	2.2	89
Pristine polymer	0.0	69	1.1	2.3	65

Table 1-5 Mechanical properties for nylon-6 and nylon-6/ MMT nanocomposites [1.88, 1.89]

Requiring only low volume fractions of fillers makes polymer/ clay nanocomposites attractive materials since, unlike many other filled polymers, they can be processed in the same manner as the unfilled polymer [1.67].

Thermogravimetric analysis (TGA) is often used to asses the thermal stability of polymers. Whether thermal properties of a nanocomposite will be increased often depends on the polymer matrix and its interactions with the clay. For nylon-6 nanocomposites, Kojima et al. [1.86] observed melt and glass transition

temperatures in the composites were similar to those of the pristine polymer. The thermal properties of polymer/ clay nanocomposites can also be influenced by the organic modifiers used to compatibilise the clay and polymer components. Kotsilkova et al. [1.96] found that the thermal breakdown patterns of epoxy/ smectite nanocomposites showed the degradation of both the surfactant and the polymer.

The heat release rate of a material is the single most important variable in a fire. Therefore it is desirable to synthesise materials with low heat release rates. Cone calorimetric measurements have shown that the heat release rate in nanocomposites of polyamide, polystyrene and polypropylene with organically modified clays is significantly reduced at clay loadings of 2 - 5 wt% [1.93]. The improvement in polystyrene nanocomposites containing 3 wt% organically modified clay was found to be similar to that of polystyrene with 30 wt% of decabromodiphenyloxide and antimony trioxide.

The improved thermal stability and fire retardancy of nanocomposite materials has been attributed to the promotion of delayed degradation and char formation by the organoclay.

Mechanical properties of polyester/ organo - MMT nanocomposites were found to be decreasing compared to the pristine polymer. The reduction in storage, loss and tensile modulus was attributed to a reduction in cross-linking in the presence of clay, since the sample with the best clay dispersion (at 2.5 wt% clay loading) was found to have the weakest mechanical properties [1.97]. At the same time, a decrease in oxygen permeability could be observed with the 2.5 wt% sample exhibiting the best barrier properties.

The decrease of permeability observed in many nanocomposite materials has often been attributed to the increase in tortuosity caused by the clay layers. A further factor contributing to the improvement of barrier properties may be the constraint exerted on the polymer chains in the presence of clay layers [1.61].

Messersmith and Giannelis [1.119] reported the formation of poly (ε-caprolactone)/ amino acid - montmorillonite composites by in-situ polymerisation. Measurement of water vapour transmission in solvent cast films of this material according to ASTM Standard E96 showed a linear reduction of

the relative permeability of the nanocomposites, with increasing volume fractions of clay.

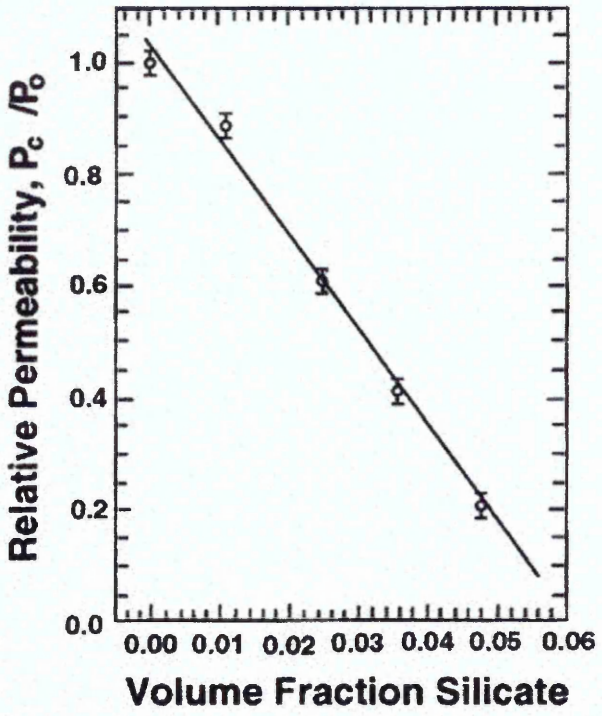

Figure 1-11 Relative permeability versus volume fraction of silicate in nanocomposite films [1.119]

Water vapour permeability was also found to decrease in poly urethane urea/ layered silicate nanocomposites. The reduction in permeability was found to reach up to 5-fold at the highest clay content (20 wt%). The magnitude of this reduction is considerably larger than that observed when modifying this polymer with the usual chemical methods [1.120].

Films of polyimide/ montmorillonite nanocomposites prepared by casting films from a mixture of solution polymerised polyamic acid and organophilic montmorillonite and heating these to form imides showed similar water adsorption to the neat polymer. The permeability to water vapour, oxygen and helium was however greatly reduced [1.101]. Using different smectite clays to form nanocomposites with polyimides Yano et al. [1.102] also found that the barrier properties changed with size of the clay platelets. Synthetic mica provided the best barrier properties followed by montmorillonite, and saponite with hectorite causing the lowest improvement in barrier properties.

Lape et al. [1.121] reported reduced acid permeability for poly (vinyl alcohol)/ mica nanocomposites containing zinc oxide. The improvement of the barrier properties for these samples was attributed to the combination of a highly impenetrable polymer with a flake filler and reactive groups. Preparation of these materials required the dispersion of the constituent materials in separate solutions before mixing them together.

Poly (vinyl alcohol)/ MMT hybrids with clay loadings between 4 and 6 wt% have been found to exhibit a reduction in water vapour permeability by 40 wt%. Furthermore, Strawhecker and Manias [1.108] reported a 300% increase in Young's modulus with only 20% decrease in toughness and no change in the value for stress at break for these nanocomposites.

1.6.4 Uses and commercial applications for polymer/ clay nanocomposites

Polymer/ layered silicate nanocomposites offer unique property profiles which are not shared by their conventional microcomposite counterparts. These properties make nanocomposite materials attractive for use in new technologies and present business opportunities. Even though many different polymer/ clay systems have been investigated on a lab scale, only relatively few polymer/ clay nanocomposites have been commercialised so far [1.67].

In order to commercialise such systems, scale up problems and interactions of other additives with the clay have to be solved [1.85, 1.92]. Furthermore, processing routes such as melt compounding can lead to materials inferior to those first synthesised [1.68]. For nylon-6/ MMT nanocomposites the type of processing most suitable depended on the clay loading of the material. Usuki et al. [1.89] were able to injection mould nanocomposites with clay loadings up to 8 wt%, while materials with clay contents over 15 wt% required press moulding.

Mülhaupt et al. [1.122] summarised the advantages and disadvantages of nanocomposites for commercial applications as given in Table 1-6.

Polyamide -6/ clay nanocomposites are the most readily available nanocomposite to date [1.84]. Some examples for other commercially available polymer/ clay nanocomposite systems and their main applications are given in Table 1-7 [1.68, 1.84].

Advantages	Disadvantages
- only low percentages layered silicate filler needed to modify properties - recyclable - low specific density - smooth surfaces - improved mechanical properties - improved barrier properties against gases and liquids - low stress materials - improved long term properties - improved tensile strength at increased elongation in rubbers - improved resistance to aging - improved thermal stability - reduced flammability without addition of halogens - reducing solubility of water soluble polymers - improved stiffness in flexible polymers - control of biodegradation in poly lactic acid and starch - dispersion and fixation of pigments and fillers	- production costs - reduced extensibility in some thermoplastic blends - discoloration in cation activated bentonites - orientation and properties dependent on direction of shear - no adequate replacement of silica or carbon fibre reinforcement yet - high adhesive content in non-polar polyolefins

Table 1-6 Advantages and disadvantages of polymer/ clay nanocomposites [1.122]

Company	Material	Application
Toyota	Polyamide-6/ MMT	Timing belt covers
Ube Industries	Polyamide/ MMT	Barrier films for food packaging; fuel tank and fuel line components
Bayer	Polyamide-6/ MMT	Barrier films
Honeywell	Polyamide-6/ MMT	Barrier films
RTP	Polyamide-6/ MMT	Barrier films
Eastman	Polyethylene/ organoclay	Food packaging
ICI	PET/ organoclay	Barrier films

Table 1-7 Examples for commercially available nanocomposites and their applications

Research is also being conducted by Triton systems/ US army [1.68] to find a material with improved barrier properties. The aim is to produce a non-refrigerated packaging system capable of maintaining food freshness for three years. Blown films of nanocomposites of biocompatible polymers might also be considered in the research for materials to create artificial intestines.

Standard commercially used flame retardants often have the disadvantage of requiring high loadings, which alter the properties of the polymer and are of environmental concern, as many of these substances are halogenated. Therefore polymer/ clay nanocomposites are a welcome new material that can be used as an environmentally friendly alternative coating material for cables [1.93].

The formation of a ceramic char upon pyrolysis means that polymer/ clay nanocomposites can potentially be used as ablative materials. Nanocomposites have been found to have vastly improved ablative properties compared to the neat polymers but further research and improvements are needed before these materials can be used as heat protection in applications like space and launch systems or protecting aerodynamic surfaces [1.123].

Lithium salts dissolved in flexible polymers such as poly (ethylene oxide) are of particular interest to the battery industry. Lithium exchanged clay nanocomposites of these polymers are therefore investigated as a means of improving conductivity and dispersion of the Li ions [1.68, 1.73].

1.6.5 Some challenges expected to be encountered in this work

Several challenges were expected to be encountered during the preparation of nanocomposites by solution intercalation, and the study of diffusion of small molecules into nanocomposite films by ATR-FTIR. A brief summary of these will be given here while discussion of many of these aspects will follow in the later chapters.

For the preparation of PET nanocomposites by solution intercalation a suitable solvent needs to be found, which fully dissolves the polymer, and is also capable of swelling the clay, as swelling facilitates the dispersion of the clay in the polymer. The study will therefore include various organically modified clays, solvents and types of polymer. As crystallinity is a major factor in the diffusion behaviour of small molecules into PET, the influence of the clay on the crystallinity needs to be investigated in order to compare samples of similar crystallinities.

As final crystallinity depends on the conditions under which the samples are dried, as well as the solvent used to prepare the polymer solutions, some

difficulties in the reproducibility of films with the same crystallinity are expected. Furthermore complications are expected in obtaining uniform thin films, which are required for the ATR-FTIR diffusion experiment.

For the preparation of PVOH nanocomposites the main problem expected is the reproducibility of dispersion and clay content within cast films. The preparation of nanocomposites from aqueous PVOH solutions and dispersions of untreated clays should be relatively straight forward.

The main difficulties are expected during the interpretation of the data obtained on the diffusion of water into PVOH and PVOH nanocomposites. As PVOH is fully water soluble at elevated temperatures and forms swollen gels with small amounts of water at room temperature, the data is likely to be influenced by a combination of swelling and dissolution of the polymer. Such severe changes in the polymer might make it difficult or even impossible to describe the process in terms of a simple diffusion model. Furthermore, reproducibility of these results may be hampered by difficulties in obtaining fully dried films or at least films with comparable moisture content.

To reduce the influence of swelling and dissolution on the diffusion and experiments with mixtures of acetone and water will be carried out. In these experiments the concentration of water in the diffusant will be lowered enough to observe its diffusion, without complete dissolution of the polymer. These experiments are also expected to yield information on the influence of the presence of a solvent (water) on the diffusion of a non-solvent (acetone) into PVOH and how the diffusion characteristics of these two liquids are influenced by the presence of clay within the samples.

1.7 References

1.1 Ravindranath K, Mashelkar RA, *Chem. Eng. Sci.*, **41**, 2197 (1986)
1.2 'Organic Polymer Chemistry', (Ed. Saunders KJ), Chapmann and Hall, London (1973)
1.3 'Fibres, Films, Plastics and Rubbers', (Eds. Roff NJ, Scott JR), Butterworth, London (1973)
1.4 http://www.psrc.usm.edu/macrog/pet.htm Last accessed: 08/2004
1.5 Krimm S, *Fortschritte der Hochpolymeren Forschung*, **2**, 51 (1960)
1.6 Daubeny R de P, Bunn CW, Brown CJ, *Proc. Roy. Soc.*, **A226**, 531 (1954)
1.7 Stokr J, Schneider B, Doskocilová D, Lövy J, Sedlácek P, *Polymer*, **23**, 714 (1982)
1.8 Ruvolo-Filho A, de Carvalho GM, *J. Macromol. Sci.*, **B35**, 255 (1996)
1.9 Ouyang H, Shore SH, *Polymer*, **40**, 5401 (1999)
1.10 Jameel H, Waldman J, Rebenfeld L, *J. Appl. Polym. Sci.*, **26**, 1795 (1981)
1.11 Chang JH, Park DK, *J. Polym. Sci.*, **39**, 2581 (2001)
1.12 Davis CH, Mathias LJ, Gilman JW, Schiraldi DA, Shields JR, Trulove P, Sutto TE, Delong HC, *J. Polym. Phys.*, **40**, 2661 (2002)
1.13 D'Esposito L, Koenig JL, *J. Polym. Sci. Polym. Phys. Ed.*, **14**, 1731, (1976)
1.14 Lin SB, Koenig JL, *J. Polym. Sci. Polym. Phys. Ed.*, **20**, 2277, (1982)
1.15 Lin SB, Koenig JL, J. *Polym. Sci. Polym. Phys. Ed.*, **21**, 2365, (1983)
1.16 Fina LJ, Koenig JL, *Macromol.*, **17**, 2572, (1984)
1.17 Lapersonne P, Bower DI, Ward IM, *Polymer*, **33**, 1277, (1992)
1.18 Ajji A, Cole KC, Dumoulin MM, *Polymer*, **36**, 4023, (1995)
1.19 Qian R, Shen D, Sun F, *Macromol. Chem. Phys.*, **197**, 1485, (1996)
1.20 Cole KC, Guèvremont J, Ajji A, Dumoulin MM, *Appl. Spec.*, **48**, 1513, (1994)
1.21 Guèvremont J, Ajji A, Cole KC, Dumoulin MM, *Polymer*, **36**, 3385, (1995)
1.22 Cole KC, Guèvremont J, Ajji A, Dumoulin MM, *Mikrochim. Acta [suppl.]*, **14**, 403, (1997)
1.23 Cole KC, Ajji A, Pellerin E, *Macromol.*, **35**, 770, (2002)
1.24 Miyake A, *J. Polym. Sci.*, **38**, 479 (1958)
1.25 Bahl SK, Cornell DD, Boerio FJ, McGraw GE, *J. Polym. Sci. Polym. Lett.*, **12**, 13 (1974)
1.26 Sammon C, PhD Thesis, (1997)
1.27 Štokr J, Schneider B, Doskocilová D, Lövy J, Sedlácek P, *Polymer*, **23**, 714 (1982)
1.28 Ward IM, *Chem. and Ind.*, (London) 1102 (1957)
1.29 Liang CY, Krimm S, *J. Mol. Spectrosc.*, **3**, 554 (1959)
1.30 Belali R, Vigourex JM, *Appl. Spec.*, **48**, 465 (1994)
1.31 Krimm S, Liang CY, Sutherland GBBM, *J. Polym. Sci.*, **22**, 227 (1956)
1.32 Assander HE, Windle AH, *Polymer*, **39**, 4295 (1998)
1.33 Hodge RM, Bastow TJ, Edward GH, Simon GP, Hill AJ, *Macromol.*, **29**, 8137 (1996)
1.34 Ngui MO, Mallapragada SK, *J. Polym. Sci. B Polym. Phys.*, **36**, 2771 (1998)
1.35 Dibbern-Brunelli D, Atvars TDZ, *J. Appl. Polym. Sci.*, **75**, 815 (2000)
1.36 Bunn CW, *Nature*, **161**, 929 (1948)

1.37 Chang JH, Jang TG, Ibn KJ, Lee WK, Sur GS, *J. Appl. Polym. Sci.*, **90**, 3208 (2003)
1.38 Chiellini E, Corti A, Politi B, Solaro R, *J. Polym. Environ.*, **8**, 67 (2000)
1.39 Murakami R, Hachisako H, Yamada K, Motozato Y, *J. Mater. Sci. Lett.*, **14**, 937 (1995)
1.40 Xu JY, Hu Y, Song L, Wang QG, Fan WC, Liao GX, Chen ZY, *Polym. Degrad. Stabil.*, **73**, 29 (2001)
1.41 Barnes RB, Liddel U, Williams VZ, *Ind. Eng. Chem.*, **15**, 659 (1943)
1.42 Thompson HW, Torkington P, *Trans. Faraday Soc.*, **41**, 246 (1945)
1.43 Peppas NA, *Makromol. Chem.*, **178**, 595 (1977)
1.44 Kenney JF, Willcockson GW, *J. Polym. Sci.*, **4**, 679 (1966)
1.45 Sugiura K, Hashimoto M, Matsuzawa S, Yamaura K, *J. Appl. Polym. Sci.*, **82**, 1291 (2001)
1.46 El-Kader KMA, Orabi AS, *Polym. Test.*, **21**, 591 (2002)
1.47 Assander HE, Windle AH, *Polymer*, **39**, 2581 (2001)
1.48 Gref R, Nguyen QT, Rault J, Neel J, *Europ. Polym. J.*, **28**, 1007 (1992)
1.49 Uragami T, Okazaki K, Matsugi H, Miyata T, *Macromol.*, **35**, 9156 (2002)
1.50 Gref R, Nguyen QT, Schaetzel P, Néel J, *J. Appl. Polym. Sci.*, **49**, 209 (1993)
1.51 Hodge RM, Edward GH, Simon GP, *Polymer*, **37**, 1371 (1996)
1.52 Mallapragada SK, Peppas NA, *J. Polym. Sci.: Pt. B Polym. Phys.*, **34**, 1339 (1996)
1.53 Krzeminski J, Molisak-Tolwinska H, *J. Macromol.. Sci. Chem.*, **A28**, 413 (1991)
1.54 Ping ZH, Nquyen QT, Chen SM, Zhou JQ, Ding YD, *Polymer*, **42**, 8461 (2001)
1.55 Nguyen QT, Favre E, Ping ZH, Neel J, *J. Membrane Sci.*, **113**, 137 (1996)
1.56 Murray HH, *Clay Miner.*, **34**, 39 (1999)
1.57 Chang SH, Ryan ME, Gupta RK, Swiatkiewicz B, *Colloid Surface*, **59**, 59 (1991)
1.58 Alexandre M, Dubois P, *Mater. Sci. Eng.*, **28**, 1 (2000)
1.59 Ray SS, Okamoto M, *Prog. Polym. Sci.*, **28**, 1539 (2003)
1.60 Giannelis EP, Krishnamoorti R, Manias E, *Adv. Polym. Sci.*, **118**, 108 (1999)
1.61 Kornmann X, http://www.mb.luth.se/a_mpp/mpp_staff/Xavier.Kornmann/Xavier.Kornmann.htm, last accessed 07/2002
1.62 Johnston CT, *CMS Workshop Lectures*, **8**, 1 (1996)
1.63 Chipera SJ, Bish DL, *Clays Clay Miner.*, **49**, 398 (2001)
1.64 Komadel P, Hrobarikova J, Smrcok L, Koppelhuber-Bitschnau B, *Clay Miner.*, **37**, 543 (2002)
1.65 Christidis GE, Eberl DD, *Clays Clay Miner.*, **51**, 644 (2003)
1.66 Madejova J, *Vib. Spec.*, **31**, 1 (2003)
1.67 Giannelis EP, *Adv. Mater.*, **8**, 29 (1996)
1.68 Hay JN, Shaw SJ, www.nano.org.uk/nanocomposites_review.pdf, last accessed 10/2003
1.69 Zanetti M, Lomakin S, Camino G, *Macromol. Mater. Eng.*, **279**, 1 (2000)
1.70 Usuki A, Kawasumi M, Kojima Y, Okada A, Kurauchi T, Kamigaito O, *J. Mater. Res.*, **8**, 1174 (1993)
1.71 LeBaron PC, Wang Z, Pinnavaia TJ, *Appl. Clay Sci.*, **15**, 11 (1999)
1.72 Lagaly G, *Solid State Ionics*, **22**, 43 (1986)

1.73 Bujdak J, Slosiarikova H, Novakova L, Cicel B, *Chem. Papers*, **45**, 499 (1991)
1.74 Hrobarikova J, Madejova J, Komadel P, *J. Mater. Chem.*, **11**, 1452 (2001)
1.75 Alvero R, Alba MD, Castro MA, Trillo JM, *J. Phys. Chem.*, **98**, 7848 (1994)
1.76 Calvet R, Prost R, *Clays Clay Miner.*, **19**, 175 (1971)
1.77 Madejova J, BujdaK J, Gates WP, Komadel P, *Clay Miner.*, 31, 233 (1996)
1.78 Clementz DM, Mortland MM, *Clays Clay Miner.*, **22**, 223 (1974)
1.79 Madejova J, Bujdak J, Petit S, Komadel P, *Clay Miner.*, **35**, 739 (2000)
1.80 Karakassides MA, Gournis D, Petridis D, *Clay Miner.*, **34**, 429 (1999)
1.81 Madejova J, Bujdak J, Petit S, Komadel P, *Clay Miner.*, **35**, 753 (2000)
1.82 Madejova J, Arvaiova B, Komadel P, *Spectrochim. Acta*, **55**, 2467 (1999)
1.83 Karakassides MA, Madejova J, Arvaiova B, Bourlinos A, Petridis D, Komadel P, *J. Mater. Chem.*, **9**, 1553 (1999)
1.84 Lawton G, *Chem. Ind. - London*, **6**, 174 (2001)
1.85 Kawasumi M, *J. Polym. Chem.*, **42**, 819 (2004)
1.86 Kojima Y, Usuki A, Kawasumi M, Okada A, Fukushima Y, Kurauchi T, Kamigaito O, *J. Mater. Res.*, **8**, 1185 (1993)
1.87 Okada A, Usuki A, *Mater. Sci. Eng.*, **39**, 251 (1996)
1.88 Usuki A, Kawasumi M, Kojima Y, Okada A, Kurauchi T, Kamigaito O, *J. Mater. Res.*, **8**, 1174 (1993)
1.89 Usuki A, Kojima Y, Kawasumi M, Okada A, Fukushima Y, Kurauchi T, Kamigaito O, *J. Mater. Res.*, **8**, 1179 (1993)
1.90 Oriakhi CO, *J. Chem. Edu.*, **77**, 1138 (2000)
1.91 Donnet JB, *Comp. Sci. & Tech.*, **63**, 1085 (2003)
1.92 Lagaly G, *Appl. Clay. Sci.*, **15**, 1 (1999)
1.93 Beyer G, *Plastic Additives and Compounding*, 22 (2002)
1.94 Giannelis EP, *Appl. Organomet. Chem.*, **12**, 675 (1998)
1.95 Schmidt D, Shah Deepak, Giannelis EP, *Curr. Opin. Solid St. M.*, **6**, 205 (2002)
1.96 Kotsilkova R, Petkova V, Pelovski Y, *J. Therm. Anal. Calorim.*, **64**, 591 (2001)
1.97 Bharadwaj RK, Mehrabi AR, Hamilton C, Trujillo C, Murga M, Fan R, Chavira A, Thompson AK, *Polymer*, **43**, 3699 (2002)
1.98 Kornmann X, Berglund LA, Sterte J, Giannelis EP, *Polym. Eng. Sci.*, **38**, 1351 (1998)
1.99 Suh DJ, Lim YT, Park OO, *Polymer*, **41**, 8557 (2000)
1.100 Suh DJ, Park OO, *J. Appl. Polym. Sci.*, **83**, 2143 (2002)
1.101 Yano K, Usuki A, Okada A, *J. Polym. Sci A – Polym. Chem.*, **35**, 2289 (1997)
1.102 Yano K, Usuki A, Okada A, Kurauchi T, Kamigaito O, *J. Polym. Chem.*, **31**, 2493 (1993)
1.103 Moet AS, Akelah A, *Mater. Lett.*, **18**, 97 (1993)
1.104 Hasegawa N, Kawasumi M, Kato M, Usuki A, Okada A, *J. Appl. Polym. Sci.*, **67**, 87 (1998)
1.105 Ke YC, Long CF, Qi ZN, *J. Appl. Polym. Sci.*, **71**, 1139 (1999)
1.106 Ke YC, Yang ZB, Zhu CF, *J. Appl. Polym. Sci.*, **85**, 2677 (2002)
1.107 Ishida H, Campbell S, Blackwell J, *Chem. Mater.*, **12**, 1260 (2000)
1.108 Strawhecker KE, Manias E, *Chem. Mater.*, **12**, 2943 (2000)

1.109 Liao B, Song M, Liang HJ, Pang YX, *Polymer*, **42**, 10007 (2001)
1.110 Morgan AB, Gilman GW, *J. Appl. Polym. Sci.*, **87**, 1329 (2003)
1.111 Balazs AC, Singh C, Zhulina E, *Macromol.*, **31**, 8370 (1998)
1.112 Balazs AC, Singh C, Zhulina E, Lyatskaya Y, *Acc. Chem. Res.*, **32**, 651 (1999)
1.113 Lyatskaya Y, Balazs AC, *Macromol.*, **31**, 6679 (1998)
1.114 Singh C, Balazs A, *Polym. Int.*, **49**, 469 (2000)
1.115 Kuznetsov DV, Balazs AC, *J. Chem. Phys.*, **112**, 4365 (2000)
1.116 Krishnamoorti R, Vaia RA, Giannellis EP, *Chem. Mater.*, **8**, 1728 (1996)
1.117 Delozier DM, Orwoll RA, Cahoon JF, Ladislaw JS, Smith Jr JG, Connell JW, *Polymer*, **44**, 2231 (2003)
1.118 Carrado KA, *Appl. Clay Sci.*, **17**, 1 (2000)
1.119 Messersmith PB, Giannelis EP, **6**, 1719 (1994)
1.120 Xu RJ, Manias E, Snyder AJ, Runt J, *Macromol.*, **34**, 337 (2001)
1.121 Lape NK, Yang CF, Cussler EL, *J. Mem. Sci.*, **209**, 271 (2002)
1.122 Mülhaupt R, Engelhardt T, Schall N, *Kunststoffe*, **91**, 178 (2001)
1.123 Vaia RA, Price G, Ruth PN, Nguyen HAT, Lichtenhan J, *Appl. Clay Sci.*, **15**, 67 (1999)

2 Characterisation methods

2.1 Infrared spectroscopy

2.1.1 General theory

2.1.1.1 Frequencies and time scales

Infrared radiation (IR) is electromagnetic radiation with wavelength situated between the visible and microwave regions of the electromagnetic spectrum. The molecular energies obtained from this region carry information on the vibrational and rotational changes within the molecules. The IR region can be divided into three sub-regions, the near IR region which encompasses the range of 14,000 – 4000 cm^{-1}, the mid-IR region (4000 – 400 cm^{-1}) and the far IR between 400 and 20 cm^{-1}. An illustration of the regions of the electromagnetic spectrum is given in Figure 2-1.

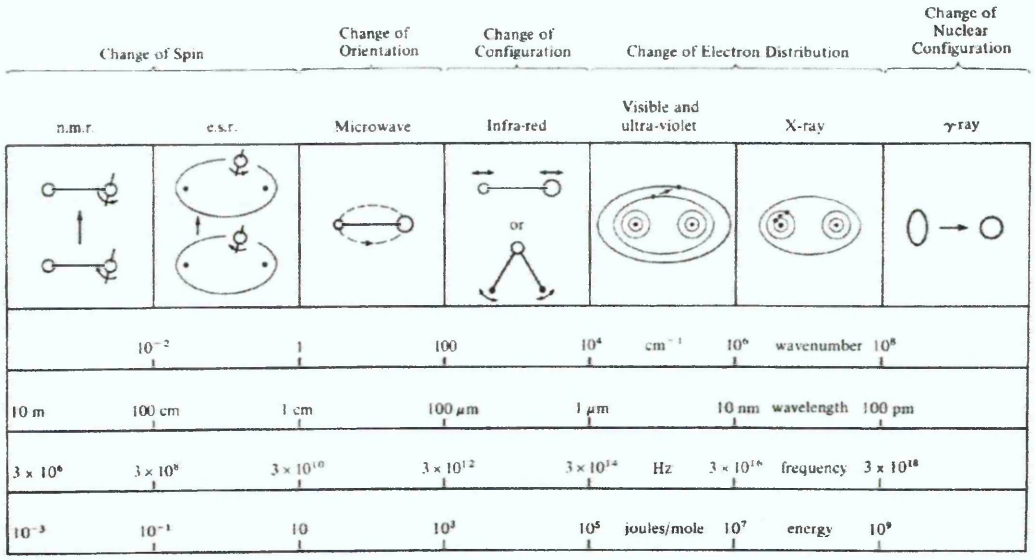

Figure 2-1 Regions of the electromagnetic spectrum [2.1]

The time scale for infrared transitions determines which types of processes can be observed by infrared spectroscopy. The timescale for an infrared transition is on the order of 10^{-13} to 10^{-15} seconds. Spectroscopic methods can investigate phenomena on different timescales depended on the change that is measured (see Figure 2-1). These variations in the timescale have to be taken into account when data obtained by different methods is compared [2.2].

Using infrared spectroscopy as a means of chemical analysis has been indicated in the 1930's. The technique did, however, not experience any real growth until after World War II [2.3].

An infrared spectrum is formed as a consequence of the absorption of electromagnetic radiation at frequencies that correlate to the vibration of specific sets of chemical bonds within a molecule [2.2]. In the following a brief summary of the equations relating to these vibrations and the absorption of the IR radiation will be given.

2.1.1.2 Molecular vibrations

The basic process of molecular vibrations can be described by simplistic models [2.4, 2.5]. Even though classical mechanics is inadequate to fully describe the processes resulting in IR spectra considering a diatomic molecule as a spring and ball assembly can explain some of the observations. The forces in a stable diatomic molecule can in this case be described by Hooke's law.

$$f = -k(r - r_{eq}) \qquad \textbf{Equation 2-1}$$

where f is the restoring force
k is the force constant
r is the internuclear distance

Such a system is known as a simple harmonic oscillator and the potential energy curve for this model has a parabolic shape and is given by equation 2-2.

$$E = -\frac{1}{2}k(r - r_{eq})^2 \qquad \textbf{Equation 2-2}$$

Since vibrational energies are quantised the allowed vibrational energies can be calculated from the Schrödinger equation. The relationship between these allowed vibrational energies, the vibrational quantum number, Planck's constant and the oscillating frequency is given by equation 2-3.

$$E_v = \left(v + \frac{1}{2}\right)h\varpi_{osc} \qquad \textbf{Equation 2-3}$$

where v is the vibrational quantum number (v = 0, 1, 2,)
h is Planck's constant
ω_{osc} is the oscillating frequency

The corresponding vibrational frequencies can be calculated using equation 2-4.

$$\nu = \left(\frac{1}{2}\pi\right)\sqrt{\frac{k}{\mu}} \qquad \textbf{Equation 2-4}$$

where k is the force constant

μ is the reduced mass given by $\mu = \frac{m_1 m_2}{(m_1 + m_2)}$

The electrical and mechanical behaviour of a real diatomic molecule is, however, not accurately harmonic [2.5]. At low amplitudes of vibration Hooke's law represents a good approximation of the mechanical behaviour of a real molecule but with increasing extensions of the bond the molecules are likely to dissociate. As dissociated atoms do not influence each other any further the force constant is 0, while the distance between the atoms can be increased to infinity with no further change of the potential energy. While electrical anharmonicity is usually a minor effect and its influence can mainly be observed for overtones ($\Delta v = 2,3...$) mechanical anharmonicity modifies the intensities of IR vibrations. An empirical approximation of this behaviour is given by equation 2-5 which is known as the Morse function.

$$E = D\left[1 - \exp\{a(r_{eq} - r)\}\right]^2 \qquad \textbf{Equation 2-5}$$

where D is the depth of the potential minimum
a is a constant

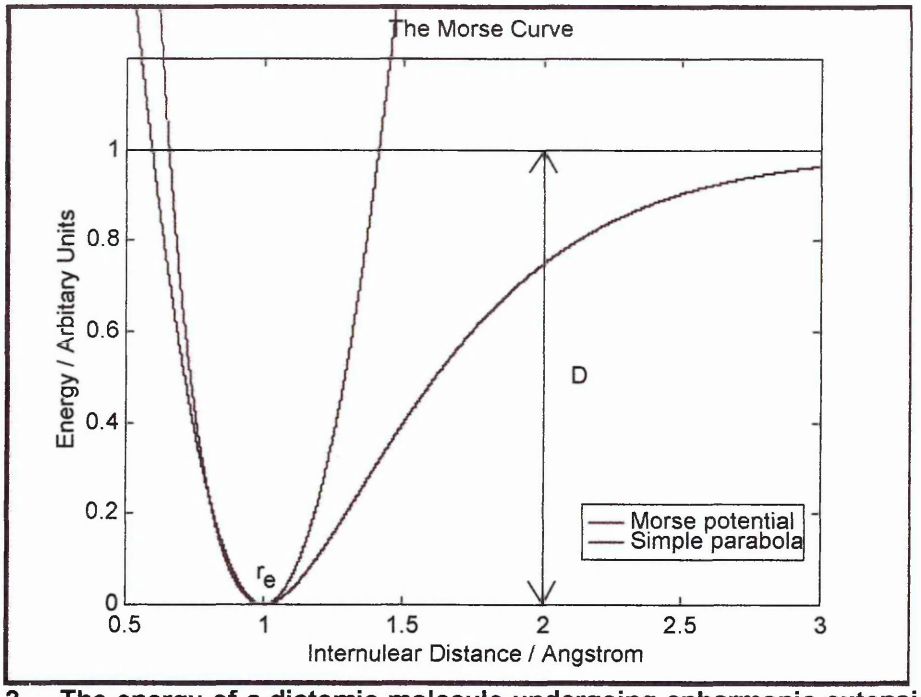

Figure 2-2 The energy of a diatomic molecule undergoing anharmonic extensions and compressions

Using this function to calculate the allowed vibrational energies from the Schrödinger equation yields equation 2-6:

$$\varepsilon_v = \left(v+\frac{1}{2}\right)\varpi_e - \left(v+\frac{1}{2}\right)^2 \omega_e x_e \qquad \textbf{Equation 2-6}$$

where x_e is the anharmonicity constant

Re-arrangement of equation 2-6 yields a general expression for the energy levels, which can be used to find the dissociation energy of a molecule.

$$\varepsilon_v = \varpi_e\left\{1-x_e\left(v+\frac{1}{2}\right)\right\}\left(v+\frac{1}{2}\right) \qquad \textbf{Equation 2-7}$$

A diagrammatic representation of this equation is presented in Figure 2-3.

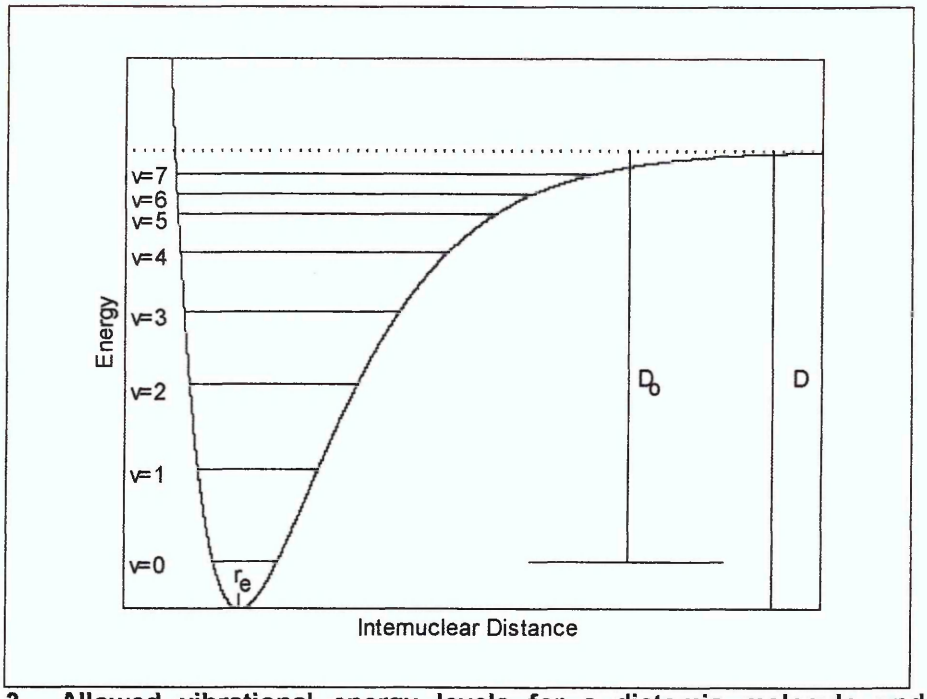

Figure 2-3 Allowed vibrational energy levels for a diatomic molecule undergoing anharmonic oscillations

Generally, only the transitions v=1←0 (fundamental), v=2←0 (1st overtone) and v=3←0 (2nd overtone) are relevant to IR spectroscopy. Note that the energy corresponding to v=0 is not zero but termed the zero-point energy.

Extending the discussion to polyatomic molecules one has to consider far more complex molecular motions. For polyatomic molecules the number of normal modes of motions for N atoms is given by 3N-6. In case of linear molecules this number is given by 3N-5.

The intensities of any bands that can be observed in the infrared spectrum of a sample depend on the symmetry of the molecule (selection rules), the population of the relevant vibrational levels and the amount of sample interacting with the IR beam.

Selection rules are derived from the transition probability. They indicate whether a particular transition is 'allowed' or 'forbidden'. For vibrational transitions the transition probability is given by:

$$\rho^{v'v''} \propto N_i \left[\varphi_{v'} \hbar \varphi_{v''} dQ\right]^2 \qquad \textbf{Equation 2-8}$$

where ∇ is the corresponding operator (for IR the molecular dipole moment μ_k)
$\varphi_{v'}$ is the wave function of the excited state
$\varphi_{v''}$ is the wave function of the ground state
Q is the displacement 'normal coordinate'

This function can be rewritten for IR vibrational transitions

$$\mu_k = \mu_0 + \left(\frac{\partial \mu}{\partial Q}\right)Q + \frac{1}{2}\left(\frac{\partial^2 \mu}{\partial Q^2}\right)Q^2 + \ldots$$ **Equation 2-9**

Normal modes of vibration are only infrared active if they alter the molecular dipole moment μ_k [2.2]. The intensity of infrared active bands is proportional to the square of the transition dipole moment.

$$I \propto \left(\frac{\partial \mu}{\partial Q}\right)^2$$ **Equation 2-10**

Some infrared bands have zero intensity as they are forbidden by symmetry considerations. Vibrations can also be degenerate, which results in a reduction of the observed number of bands. For benzene, for example, only four fundamental bands can be observed in the infrared spectrum even though the molecule should have 30 normal modes of motion.

The population of a particular energy level, which also influences the intensities of bands in the IR spectrum, can be calculated from the Boltzmann distribution.

$$\frac{N_i}{N_0} = \frac{g_i}{g_0}\exp\left(-\frac{\Delta E}{kT}\right)$$ **Equation 2-11**

where N_0 is the ground state
N_i is the energy level of interest
g_0 and g_i are the degeneracies of the particular levels
ΔE is the energy difference between the levels
T is the temperature

For most systems the ground state is the most heavily populated state at room temperature. Therefore, the intensities of transitions from the ground state to higher energy levels will result in the strongest bands. Elevated temperatures can lead to the population of higher energy levels, which can result in the occurrence of so-called "hot" bands.

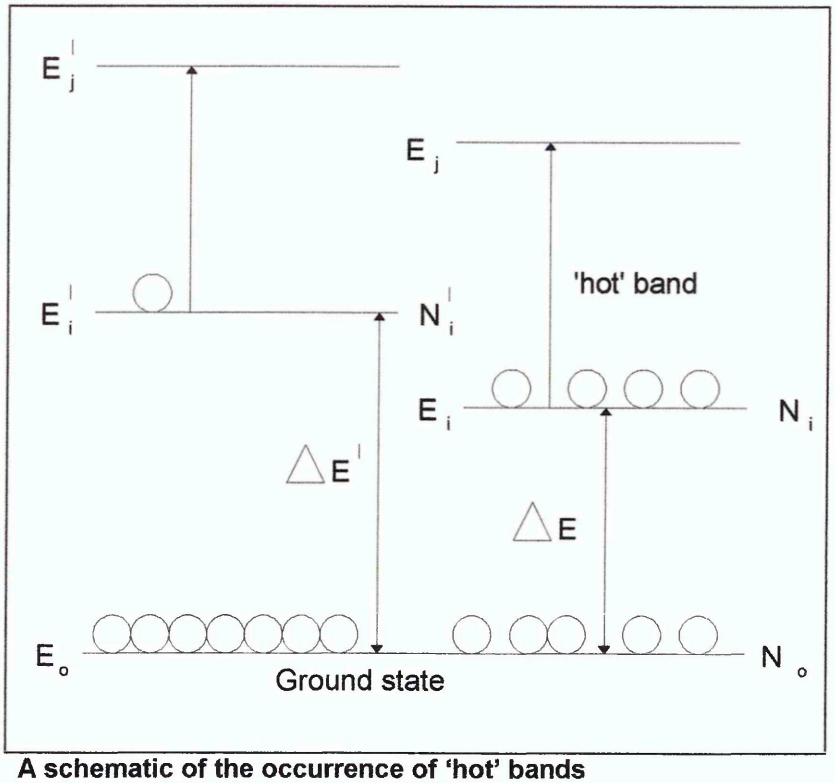

Figure 2-4 A schematic of the occurrence of 'hot' bands

The most important influence on the intensity of the bands observed in the IR spectrum is the number of molecules sampled by the IR beam. The relationship between the initial intensity of the beam (I_0), the transmitted intensity (I) and the sample concentration (c) is given by the Beer-Lambert law:

$$I = I_0 \exp(-\varepsilon\ cL) \qquad \textbf{Equation 2-12}$$

where ε is the molar absorption coefficient
L is the sample (or cell) thickness

2.1.2 Fourier transform infrared spectroscopy (FTIR)

Traditional (dispersive) infrared spectrometers utilised a prism and later a grating to separate the wavelengths before they reached the detector. Taking spectra with these systems was often time consuming and gave poor signal to noise ratios. Both these facts cause problems when one considers kinetic investigations. Poor signal to noise ratios result in large inherent errors in the data and long sampling times make in-situ observations difficult, if not impossible. These problems were solved by the invention of the Fourier transform infrared spectrometer (FT-IR). This instrument is based on a Michelson interferometer and a mathematical procedure developed by Fourier to convert data from the time domain to the frequency domain [2.6 – 2.8].

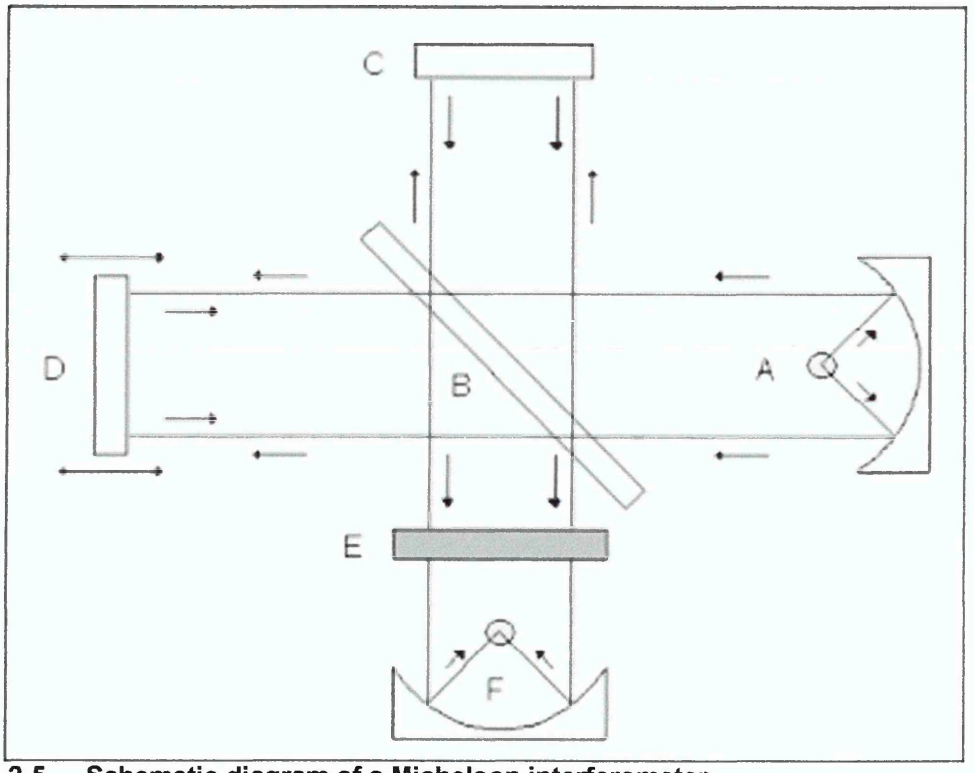

Figure 2-5 Schematic diagram of a Michelson interferometer

Figure 2-5 presents a schematic of the Michelson interferometer. In such a system a parallel, polychromatic beam of radiation is directed from its source (A) onto a beam splitter (B). The radiation source can be a mercury lamp or a silicon carbide rod. The beam splitter is made from an infrared transparent material (e.g. KBr). Beam splitter materials are chosen with respect to the region that is investigated as the window of transparency influences the measurable radiation. The beam splitter reflects approximately half the light

onto a fixed mirror (C) which in turn reflects the light back to the beam splitter. The light that is not reflected of the beam splitter is passed through it onto a continuously moving mirror (D). This mirror moves at a constant, known velocity. The light is reflected off this mirror and recombined with the light reflected off the fixed mirror at the beam splitter. The radiation is then passed through the sample (E) onto a detector. The detector is sufficiently sensitive to cope with the time domain changes from the modulation of the interferometer. Commonly used detectors are the liquid nitrogen cooled mercury cadmium telluride (MCT) detector or the (less sensitive) deuterated triglycine sulfate (DTGS) detector.

The recombination of the two beams results in both destructive and constructive interference dependent on the position of the moving mirror and therefore the phase difference between the two beams. The position of the moving mirror changes constantly, resulting in different wavelength of radiation being in-phase or out-of-phase at a frequency that is dependent on the mirror velocity and the frequency of the radiation. The resulting complex pattern of overlaid sinusoidal waves of light is known as the interferogram. This interferogram, which is in the time domain, can be converted to a spectrum, a frequency distribution, by means of a Fourier transform.

FTIR has several advantages over the traditional dispersive approach to record an infrared spectrum. These systems build up a spectrum by passing only discrete frequencies onto the detector, which results in a time consuming process that is reliant on many moving parts to accurately separate these frequencies.

Three major advantages have been noted for recording of spectra by FTIR which will be described here:

- throughput advantage (Jaquinot advantage)
- multiplex advantage (Fellgett advantage)
- Connes advantage

The throughput or Jaquinot advantage is realised due to the inherent simplicity of the FT system, which does not require any slits that can attenuate radiation. The intensity of the radiation reaching the detector is therefore much greater

than that observed in dispersive systems resulting in improved signal to noise ratios.

In order to compare the optical conductance of a dispersive system to that of an FTIR system one must choose an equal beam area of the interferometer to that of the grating. The optical conductance of a grating system is given by equation 2-13, while the equivalent for an FT system is given by equation 2-14.

$$G_{\bar{\nu}}^{G} = \frac{hH}{f\bar{\nu}} R_0$$ **Equation 2-13**

where $G_{\bar{\nu}}^{G}$ is the optical conductance per wavenumber of grating
h is the length of the entrance slit
H is the height of the grating
F is the focal length of the collimator
R_0 is the theoretical resolving power

$$G_{\bar{\nu}}^{I} = \frac{2\pi H^2}{\bar{\nu}}$$ **Equation 2-14**

The ratio of these two optical conductances is therefore given by equation 2-15, which equates to throughput about 100 times higher in an interferometer than in a dispersive system.

$$\frac{G_{\bar{\nu}}^{I}}{G_{\bar{\nu}}^{G}} \approx \frac{2\pi f}{h}$$ **Equation 2-15**

The multiplex or Fellgett advantage is achieved because all elements of the light reach the detector simultaneously. The time necessary to record a spectrum is shortened considerably. If one considers a spectrum to be made up of M individual measurements as is the case for dispersive systems than the sampling time increases with increasing numbers of spectral elements which in turn influence the spectral detail.

This advantage also impacts the signal to noise ratio. While this ratio is proportional to the ratio of the square root of the time required to run an experiment and the square root number of spectral elements in dispersive systems it is only proportional to the recording time in FT systems resulting in an improvement of the signal to noise ratio on the order of $\sqrt{M}$.

The Connes advantage is derived from the method the wavelength is determined. In an FT system the spectral wavelength is known very accurately as it is obtained by sampling at accurately known time intervals given by the output of a laser (usually at fixed wavelength of 623.8 nm). This accurate time measurement then allows accurate determination of wavelength when the data is converted from the time domain to the frequency domain. This absolute control of the spectrum allows manipulative techniques such as spectral additions to further improve the signal to noise ratio.

Some disadvantages can be noted for FTIR systems, which are, however, outweighed by the advantages mentioned before. When these systems were first commercialised the cost for an FTIR spectrometer was significantly higher than that of a dispersive system. Furthermore, some computational support was necessary to convert the interferogram, which is difficult to interpret for most people into a spectrum. Both these disadvantages have been overcome over the years and the cost of FTIR systems nowadays is similar to that of a dispersive system. Cheap and fast CPU's allow Fourier transforms to be carried out within fractions of a second on a bench top instrument.

Another disadvantage, the Fellget disadvantage, means that if the light source produces a 'noisy' output noise will be detected at all frequencies even if the noise only occurs within a certain frequency range.

Finally, the presence of unwanted bands in the spectrum from CO_2 or water vapour absorption, which could be eliminated in dispersive instruments by use of a reference beam (dual beam system), can only be removed by purging the instrument with a dry, infrared inactive gas e.g. nitrogen or subtraction of a spectrum of the sample compartment in absence of a sample. Similar subtraction of spectra can be used to simplify experimental data and extract information on overlapping bands. Difference spectra can, therefore, be classed in two groups. The first one includes spectra where subtraction is used to eliminate unwanted absorption from solvent residues or water vapour. The second group of difference spectra describes spectra obtained from subtraction of two similar spectra to isolate only those bands that have changed between these two spectra. For spectral subtraction to give meaningful results the relevant spectra have to be recorded at a constant temperature and with the

same parameters (technique, spectral resolution, data treatment during Fourier transformation, number of scans) as all these parameters influence the absorbance of a molecule [2.9].

The most basic sampling technique in infrared spectroscopy is the transmission set-up. Here the light from the source is passed through the sample onto the detector.

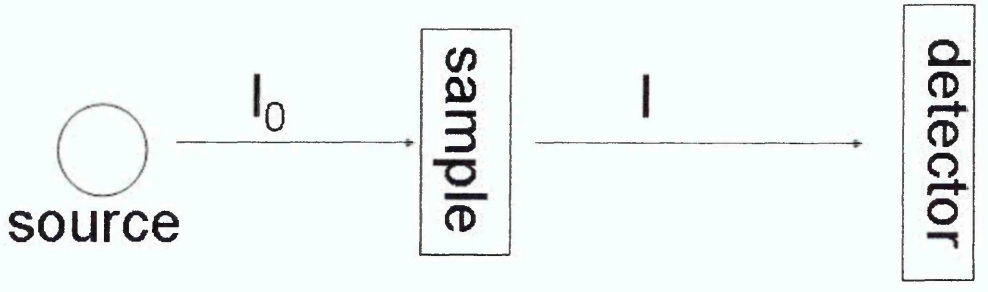

Figure 2-6 Schematic representation of transmission set-up

With this technique information on the bulk of the sample can be obtained. The thickness of samples that can be analysed by this method depends on the absorption properties of these samples. For strongly absorbing samples only thin films can be analysed. Samples can also be presented pressed into KBr discs. This sample preparation can however be time consuming and difficult to reproduce. The transmission in this set-up is given by equation 2-16.

$$T = \frac{I}{I_0} = \exp(-\alpha L) \qquad \textbf{Equation 2-16}$$

where I is the transmitted intensity
I_0 is the incident intensity
α is the absorption coefficient
L is the sample thickness

2.1.2.1 Attenuated total reflection – Fourier transform infrared spectroscopy (ATR – FTIR)

Attenuated total reflectance (ATR) spectroscopy, also known as internal reflection spectroscopy (IRS), is especially suitable for the analysis of samples that are difficult to investigate by transmission measurements such as thick samples, strongly absorbing solids or liquids. Here only a brief discussion of the theory will be given. More detailed explanations can be found in the literature. [2.10 – 2.13]

Even though the existence of an evanescent field in a medium of lower refractive index in contact with a higher refractive index medium in which a propagating wave of radiation undergoes total internal reflection has been first observed by Newton about two centuries ago this phenomenon has not been exploited for the production of absorption spectra until the 1960's. The theoretical principles of this method had actually been discussed in a series of papers by Taylor and co-workers three decades earlier but it was not until pioneering development work was carried out simultaneously by Harrick [2.11, 2.12] (using multiple reflections) and Fahrenfort [2.13] (using a single reflection) on the experimental implementation of these principles that spectra were recorded by this method. The initial publications sparked a multitude of studies even though the general use of this method was initially hampered by doubts about its reproducibility and capability for quantitative measurements. The commercial availability of FTIR systems led to the possibility of investigating a wide variety of theoretical and experimental questions concerning the ATR method which require high quantitative accuracy and large data-handling capability.

ATR spectroscopy is a surface technique and its most important theoretical feature is associated with the properties of the evanescent field created at the surface of the ATR crystal.

Light (in this case infrared radiation) travelling at an angle greater than the critical angle through a medium with a high refractive index (the ATR crystal) undergoes total internal reflection at the interface with a material of lower refractive index. The infrared radiation propagates through the ATR crystal but

an electric field penetrates into the sample. This non-transverse wave is known as the evanescent field and its intensity decays exponentially with increasing distance from the interface. The rate of decay of the evanescent field depends on the wavelength, the angle of incidence of the light and the refractive indices of the denser and rarer medium (ATR crystal and sample).

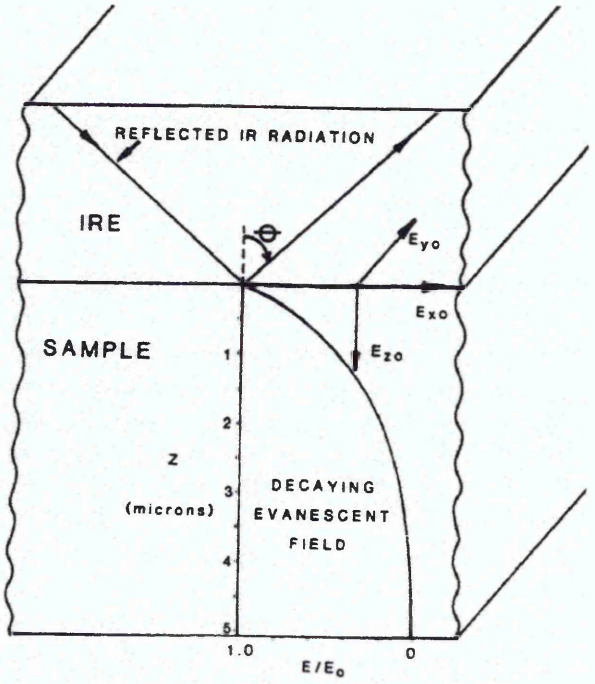

Figure 2-7 representation of the basic ATR experiment [2.10]

If the rarer medium is non-absorbing the intensity of the reflected light will be equal to that of the incident light. In most instances the rarer medium is, however, absorbing and the reflection is said to be attenuated.

Ideally no radiation is lost during reflection unless it is absorbed by the propagating medium. ATR crystals are therefore required to be infrared transparent and made from materials of high refractive index. Some common materials for ATR crystals are listed in Table 2-1.

Material	Refractive index
ZnSe	2.54
Diamond	2.4
Ge	4.0
Si	3.4

Table 2-1 Common ATR crystal materials and their refractive indices

When diamond crystals are used one has to keep in mind that while diamond can transmit electromagnetic radiation from the UV/Vis to the Far IR region its

lattice vibrations result in absorption of radiation around 2000 cm^{-1}. Careful optical design and short path lengths can, however, compensate for this absorption. An advantage of using diamond crystals is the high thermal conductivity of the material which allows measurement of samples at temperatures up to 200 °C [2.14].

The properties of the evanescent field can be summarised as follows:

- The field intensity in the rarer medium is not zero but there is an instantaneous normal component of energy flow into the rarer medium whose time average is zero. The propagating radiation in the denser medium is therefore totally internally reflected.
- The evanescent field is a non-transverse wave with components in all spatial directions.
- The evanescent field is confined to the vicinity of the surface decreasing with in intensity with increasing distance.
- There is a non-zero energy flow parallel to the surface which results in displacement of the incident and reflected waves. This displacement is known as the Goos-Hänchen shift.

The decay of the electric field amplitude of the evanescent field from a value E_0 at the interface to a value E at distance z is given by equation 2-17.

$$E = E_0 \exp - \frac{2\pi}{\lambda_1}\left(\sin^2\theta - n_{21}^{\ 2}\right)^{\frac{1}{2}} z \qquad \textbf{Equation 2-17}$$

where $\lambda_1 = \lambda / n_1$

The exponential constant in equation 2-17 can be replaced by the electric field amplitude decay coefficient γ yielding:

$$E = E_0 \exp\left[-\gamma\, z\right] \qquad \textbf{Equation 2-18}$$

$$\gamma = \frac{2\pi\left(\sin^2\theta - n_{21}^{\ 2}\right)^{\frac{1}{2}}}{\lambda_1} \qquad \textbf{Equation 2-19}$$

The depth at which the E has dropped to E_0 exp [-1] has been defined as the depth of penetration, $d_p = 1/\gamma$. This parameter has been arbitrarily defined by Harrick and the naming has caused some confusion. It is often used as a

measure of the depth that is sampled in the ATR experiment. As the electric field amplitude at this point is however 37% of its value at the surface the actual sampling depth appears to be greater than d_p. Mirabella [2.15] tested the actual maximum sampling depth (d_s) for polypropylene and polystyrene samples measured on a KRS-5 crystal and found that it was about three times d_p.

The effective thickness (d_e) is defined as the thickness of a sample material which would give the same absorbance for a transmission experiment at normal incidence. For weak absorbers the relationship between the reflectivity and the effective thickness is given by equation 2-20. In order to calculate the effective thickness from the basic ATR parameters one first has to derive the expressions for the electric field amplitudes at the surface of the rarer medium.

$$R = e^{-\alpha d_e} \cong 1 - a \qquad \textbf{Equation 2-20}$$

where R is the reflectivity $\left(R = \frac{I}{I_0}\right)$

α is the absorption coefficient (same as for transmission)

a is the absorption parameter ($a = \alpha\ d_e$ for a single reflection)

The light can be polarised in two directions. These polarisations are described as the transverse magnetic polarisation referred to as TM or P wave, which is parallel to the plane of incidence and the transverse electric polarisation (TE or S wave) which is perpendicular to the plane of incidence. In this case the plane of incidence is perpendicular to the plane formed by the surfaces of the rarer and denser medium. The TE wave only has components in the y plane while the TM wave has components in both the x and z planes.

$$TE = E_y \qquad \textbf{Equation 2-21}$$

$$TM = \sqrt{|E_x|^2 + |E_z|^2} \qquad \textbf{Equation 2-22}$$

For the thickness of the rarer medium (sample) two distinct cases can be defined, the semi-infinite case, where the sample thickness is much greater than the depth of penetration, and the thin film, where the sample film is much thinner than the depth of penetration. In the first case the electric field amplitude falls to a very low value entirely within the film while it remains essentially constant within the sample film for the second case. For thin films the properties

constant within the sample film for the second case. For thin films the properties of the film are only having a minor impact on the evanescent field and the controlling refractive index is that of the next medium (n_3).

In the following only the semi-infinite case will be considered, since all experiments presented in this thesis fall into that category. In this case the electric field amplitudes are given by equation 2-23 to 2-25.

$$E_y = \frac{2\cos\theta}{\sqrt{1-n_{21}^{\ 2}}}$$ **Equation 2-23**

where $n_{21} = \frac{n_2}{n_1}$

$$E_x = \frac{2\cos\theta\sqrt{\left(\sin^2\theta - n_{21}^{\ 2}\right)}}{\sqrt{\left(1-n_{21}^{\ 2}\right)}\sqrt{\left(1+n_{21}^{\ 2}\right)\sin^2\theta - n_{21}^{\ 2}}}$$ **Equation 2-24**

$$E_z \frac{2\cos\theta\ \sin\theta}{\sqrt{\left(1-n_{21}^{\ 2}\right)}\sqrt{\left(1+n_{21}^{\ 2}\right)\sin^2\theta - n_{21}^{\ 2}}}$$ **Equation 2-25**

Plotting these electric field amplitudes for different angles of incidence as presented in Figure 2-8 clearly shows that E_y and E_z reach maxima at the critical angle, while E_x is equal to zero at this point. At 90° the electric field amplitude reaches 0 in all directions.

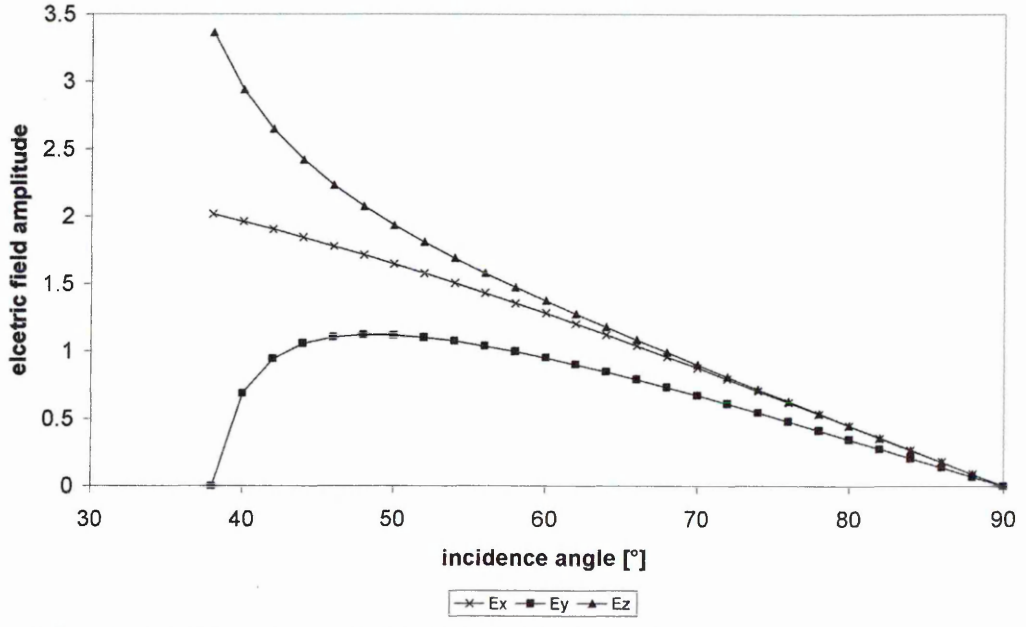

Figure 2-8 Variations of calculated electric field amplitudes for polarised radiation for n_1=1.5 and n_2=2.4

The relation between the electric field, E, and the absorption parameter, a, for weak absorbing samples of semi-infinite thickness is given by equation 2-26 which can be integrated over the film thickness to yield equation 2-27.

$$a = \frac{A}{N} = \frac{n_{21}\alpha\ c}{\cos\theta}\int_0^\infty E^2 dz \qquad \textbf{Equation 2-26}$$

where A is the absorbance
N is the number of reflections
c is the concentration
α is the molar absorption coefficient

$$a = \frac{n_{21}\alpha\ dE_0^{\ 2}}{2\gamma\ \cos\theta} \qquad \textbf{Equation 2-27}$$

As $a = \alpha d_e$, one can re-arrange equation 2-27 to give the effective thickness. If one substitutes equations 2-19, 2-23, 2-24 and 2-25 into equation 2-27 the effective thickness for the TE and TM waves for the bulk (= semi-infinite) case is given by equations 2-28 and 2-29 respectively. Note that for the parallel polarisation $E_0^{\ 2} = E_x^{\ 2} + E_z^{\ 2}$.

$$d_{e\,\text{perpendicular}} = \frac{n_{21}\dfrac{\lambda}{n_1}\cos\theta}{\pi\left(1-n_{21}^{\ 2}\right)\sqrt{\left(\sin^2\theta\ -n_{21}^{\ 2}\right)}} \qquad \textbf{Equation 2-28}$$

$$d_{e\,\text{parallel}} = \frac{n_{21}\dfrac{\lambda}{n_1}\cos\theta\left(2\sin^2\theta\ -n_{21}^{\ 2}\right)}{\pi\left(1-n_{21}^{\ 2}\right)\left[\left(1+n_{21}^{\ 2}\right)\sin^2\theta\ -n_{21}^{\ 2}\right]\sqrt{\left(\sin^2\theta\ -n_{21}^{\ 2}\right)}} \qquad \textbf{Equation 2-29}$$

For unpolarised radiation the effective sampling thickness is given by

$$d_e = \frac{d_{e\,\text{perpendicular}} + d_{e\,\text{parallel}}}{2} \qquad \textbf{Equation 2-30}$$

Equations 2-28 and 2-29 show that the effective sampling thickness is dependent on the electric field decay constant (γ), the wavelength of the radiation (λ), the electric field at the surface (E_0^2), the angle of incidence (θ), the sampling area and the respective refractive indices of the sample and the ATR crystal. To illustrate the changes in the effective thickness in the mid-IR region plots of d_e versus wavenumber for several angles of incidence are presented in

Figure 2-9. The thicknesses have been calculated for a typical polymer sample (n_2 = 1.5) and a diamond crystal (n_1 = 2.4).

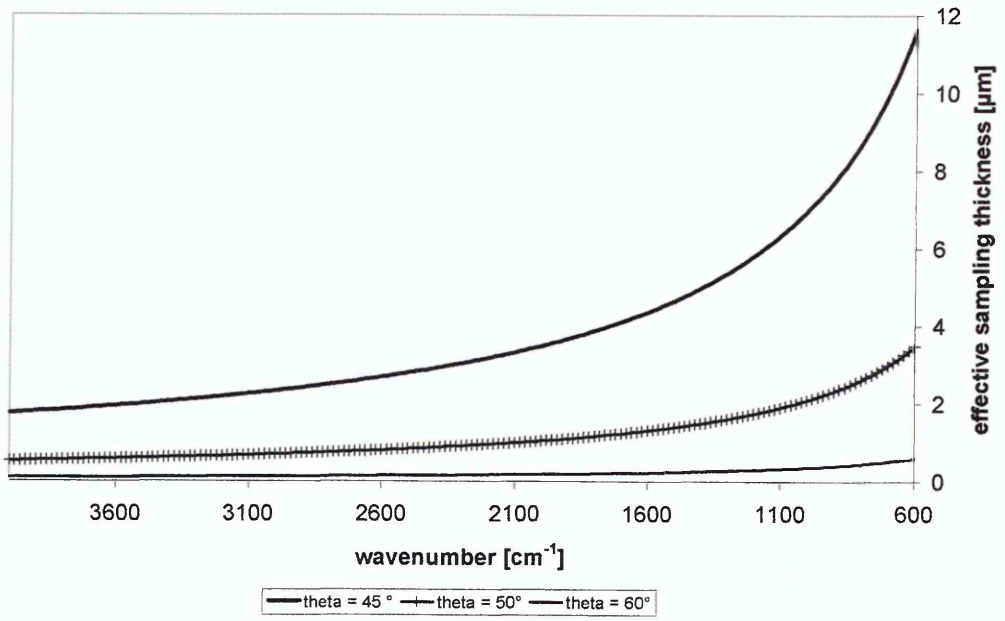

Figure 2-9 Effect of wavelength and angle of incidence on the effective sampling thickness

These relatively short sampling depths make it necessary to have very good contact between the sample and the ATR crystal. Contact is usually ensured by applying a pressure to the sample that is strong enough to press the sample against the crystal, yet does not damage the crystal or the sample. To obtain reproducible results the applied pressure has to remain constant [2.16].

2.1.2.2 Fourier transform infrared imaging

FTIR microspectroscopy is a technique of obtaining IR spectra from small areas by focussing the IR radiation through a microscope onto the sample. Microspectroscopy did only really become viable with the coupling of spectrometers to computers and the use of interferometry, as well as the utilisation of fast, sensitive detectors like MCT detectors [2.3].

FTIR microscopy is nowadays used extensively in industry for point identifications and point mapping of defects and inhomogeneities within sample films or laminates. Point mapping does, however, require large amounts of time which is determined by the size of the area sampled (overall area and number of sampling points) and the quality of the spectra (spectral resolution and number of scans). Using the ATR technique sample contact can also influence the results. FTIR imaging using a focal plane array detector rather than a single detector has been able to reduce the time necessary to obtain information of various points in an area and the improve the spatial resolution between the sampling points [2.3, 2.17].

The use of indium antimonide focal plane array detectors to record FTIR images of sample areas has first been described by Lewis et al. [2.18, 2.19] in 1995. They used a 128 x 128 array coupled to a microscope and a step scan spectrometer to collect transmission FTIR images of an optical resolution target as well as imaging the dispersion of a surfactant in water. The data for the later set was presented as chemical absorbance images created by plotting the area of the relevant absorption band at each recorded point. A method using ATR FTIR as imaging sampling technique was probably first mentioned in a publication by Sommer et al. [2.21] in 2001. They described the use of an ATR microscope coupled to a step scan FTIR spectrometer with a 64 x 64 element focal plane array (FPA) MCT detector.

The FPA detector works like an IR sensitive camera with each pixel corresponding to a unique region on the sample. The spatial resolution of an image acquired with the FPA is essentially wavelength limited while it is limited by the aperture sizes in point mapping [2.22]. A diagram of the concept of the imaging set-up is presented in Figure 2-10.

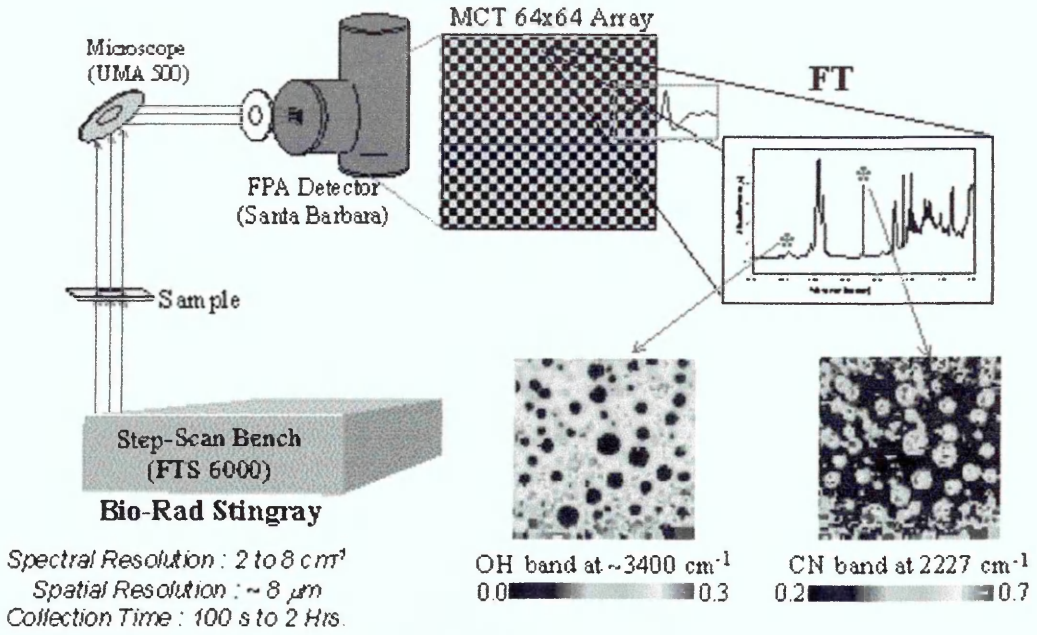

Figure 2-10 Concept of FTIR imaging [2.23]

FPA detectors require greater acquisition times and have poorer signal to noise ratios than single element detectors [2.24]. This results in imaging data having only moderate quality yet data acquisition for an area is still orders of magnitude faster than point mapping with a single element detector. The modification of the data acquisition to improve the spectra has mainly focussed on the design of FPA detectors and the parameters of the step scan method used to collect the spectra. For small arrays (16 x 16 or 32 x 32 elements) it is possible to use a rapid scan system with continuous scans being performed at mirror velocities greater 0.01 cm/s. Another possibility has been discussed by Huffmann et al. [2.25]. They suggest the use of a slower detector and use two scans with different time delays for the sampling of the interferogram and assembly of the full waveform from these two separate scans.

2.2 Thermogravimetric analysis (TGA)

Thermal analysis refers to a group of methods in which the change in a physical property is continually monitored as a function of temperature. Dependent on the physical property that is examined the measurements are described by the following techniques:

- Thermogravimetric analysis (changes in weight)
- Differential scanning calorimetry (changes in energy)
- Thermomechanical analysis (changes in dimension)
- Thermoacoustimetry (changes in acoustical properties)
- Thermoptometry (changes in optical properties)
- Electrothermal analysis (changes in electrical conductivity)
- Thermomagnetometry (changes in magnetic properties)

In case of thermogravimetric measurements the change in sample weight with temperature is recorded. Such changes in weight of a sample occur when volatile materials desorb or the sample decomposes (weight loss) or when chemical processes, such as oxidation, occur (weight gain) [2.26 - 2.29].

Thermogravimetric measurements are performed to assess the thermal stability of the samples. The equipment basically consists of a precision balance, a furnace controlled by a temperature programmer and a recorder e.g. a computer. A schematic of such a system is presented in Figure 2-11.

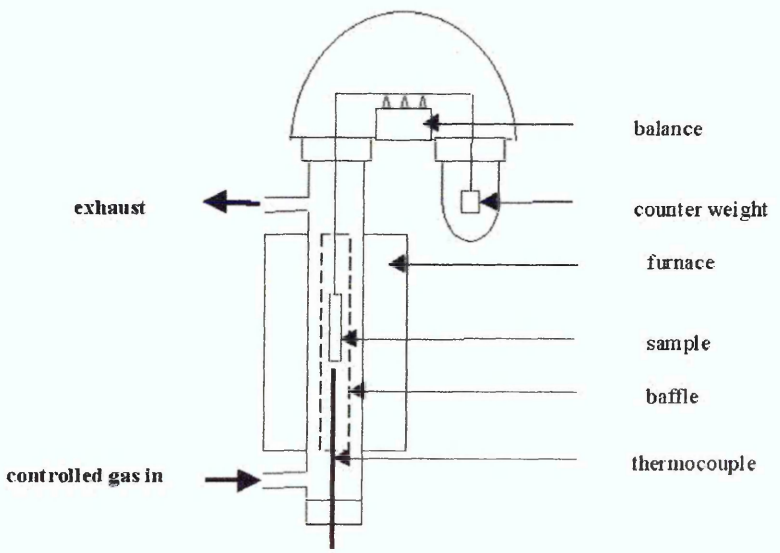

Figure 2-11 Schematic diagram of a TGA instrument

During the measurement a sample weighing a few milligrams is usually subjected to a linear temperature gradient. It is contained in a refractory crucible and weight is recorded by means of a sensitive balance. Depending on the instrumentation and sample set-up measurements can be performed from room temperature up to 1000 °C or higher. To prevent oxidation measurements are often performed under a nitrogen atmosphere. The shape of the weight loss curve can be affected by various factors [2.26]:

- sample size → large samples may result in poorly resolved events due to temperature gradients and/or trapping of volatile materials
- particle size distribution and packing density → variations in these parameters can lead to poor reproducibility of results
- use of inert atmospheres and gas flow rate → oxidation of organic materials is suppressed when experiments are run under nitrogen
- sample holder → To ensure conclusive results the sample holder must not react with the sample. The depth of this crucible can also influence the quality of the data
- heating rate → slow heating rates are beneficial as they ensure that the sample temperature is close to the recorded temperature

The output of such measurements, the thermogram, plots the change in weight as a function of time. Often the negative first derivative of this curve is chosen to present the data since this enables plotting of the maximum rate of weight losses as maxima.

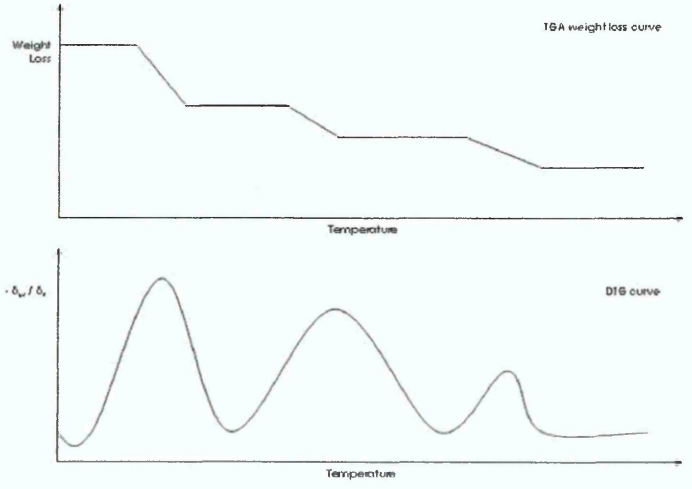

Figure 2-12 Diagrammatic representation of TGA and derivative TG (dTG) data curves

2.3 X-ray diffraction analysis (XRD)

X-rays are a high frequency (around 10^{18} hertz) form of electromagnetic radiation that is produced when atoms of any substance are struck by high speed electrons. This form of radiation was first analysed and reported by Wilhelm Röntgen in 1895. When experimenting with high energy electrons Röntgen discovered that radiation with the following properties was being produced [2.30 – 2.32]:

- travels in straight lines
- is exponentially absorbed by matter with the exponent being proportional to the mass of the absorbing material
- darkens photographic plates
- creates shadows of absorbing material on photosensitive paper

These experiments initiated radiography but at that point the radiation used was not understood. The exact nature of x-rays was not established until 1912 when the phenomenon of x-ray diffraction by crystals was discovered proving the wave nature of x-rays and establishing a new method to investigate fine structures at the same time. While radiography can resolve details on the order of 10^{-3} mm, the diffraction method is capable of revealing structural details of the order of 10^{-7} mm.

The x-ray diffraction phenomenon was discovered by the German physicist von Laue who reasoned that if crystals were composed of regularly spaced atoms, which might act as scattering centres for x-rays, and if the wavelength of x-rays was about equal to the inter-atomic distance in crystals, then it should be possible to diffract x-rays by means of crystals. He tested this hypothesis together with two co-workers, Friedrich and Knipping, by positioning a crystal of copper sulphate between the source of a narrow beam of x-rays and a photographic plate.

The account of these experiments led the English physicists W.H. Bragg and his son W.L. Bragg to derive an expression for the necessary conditions for x-ray diffraction to occur in much simpler mathematical terms than von Laue had used in the same year. Within the following year they were able to solve the structures of NaCl, KCl, KBr and KI.

Bragg's description of diffraction proposed that planes of particles were capable of scattering constructive interference in certain directions. The particles behave like reflecting planes. X-ray reflection can only occur at certain angles, which depend upon the interplanar spacing of the reflecting planes. The relation between the order of diffraction, the wavelength of the radiation, the angle of diffraction and the distance between the reflecting planes is given by equation 2-31. It was first formulated by W.L. Bragg and is referred to as Bragg's law.

$$n\lambda = 2d\sin\theta \qquad \textbf{Equation 2-31}$$

where n is the order of diffraction
λ is the x-ray wavelength
d is the distance between reflecting the planes
θ is the angle of diffraction

In an x-ray diffractometer x-rays are generated inside the vacuum of the x-ray tube by bombarding a metal target with high energy electrons from a tungsten filament, the cathode. The electrons produced by the cathode are accelerated through a potential difference typically between 15 and 60kV before they strike the target which is acting as the anode. The most commonly used material for the target and, therefore, the source of the x-rays is copper. Other target materials include cobalt, molybdenum, chromium and iron. The wavelength for the Kα lines of x-rays produced by these metals are summarised in Table 2-2.

Material	Wavelength Kα line [Å]
Chromium	2.291
Cobalt	1.79026
Copper	1.54186
Iron	1.93735
Molybdenum	0.71073

Table 2-2 Summary of wavelength of x-rays produced by various metals

The x-rays are then targeted onto the sample in form of a collimated beam. X-rays hitting the sample will be scattered and a diffraction pattern can be recorded if the sample has a regular, oriented structure (crystal structure) of which the beams are scattered.

For the measurements presented in this thesis powder diffraction measurements in reflection were performed using a Bragg - Brentano parafocusing geometry, which is employed in most commercially available systems. A schematic of the x-ray diffractometer is presented in Figure 2-13.

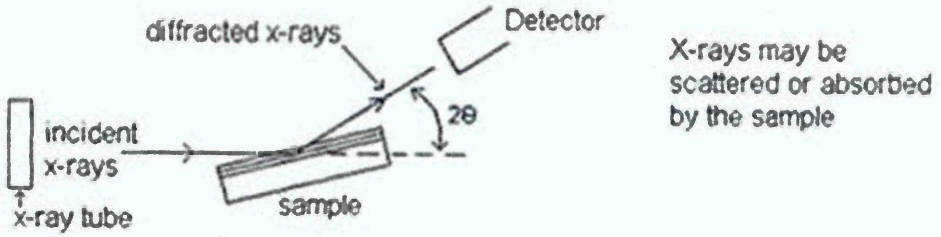

Figure 2-13 Schematic of x-ray diffractometer

The use of powder diffraction in the analysis of polymer/ clay nanocomposites is largely based on the established procedures developed for the identification and characterisation of layered silicate minerals. From the diffraction pattern information on the crystal structure, such as unit cell type and its dimensions, can be gained. For polymer/ clay nanocomposites the 00ℓ basal reflections, which give information about the stacking order of the clay layers, are generally used to characterise the morphology of the material. [2.33] The interlayer spacing of the layered silicates is usually calculated from the position of the 001 peak by employing Bragg's law (equation 2-31) after re-arrangement as given in equation 2-32.

$$d = \frac{n\lambda}{2\sin(\theta)}$$ **Equation 2-32**

2.4 References

2.1 'Fundamentals of Molecular Spectroscopy' 3rd Ed.(Ed. Banwell CN), McGraw-Hill, London (1972)
2.2 Coates J, *Encyclopedia of Analytical Chemistry*, 10815 (2000)
2.3 Katon JE, *Micron*, **27**, 303 (1996)
2.4 'Infrared Spectroscopy of Polymer Blends, Composites and Surfaces', (Ed. Garton A), Hanser Publishers, Munich (1992)
2.5 'Modern Spectroscopy', (Ed. Hollas JM), 2nd Edition, Wiley&Sons, New York (1992)
2.6 'Fourier Transform Infrared Spectrometry', (Ed. Griffiths P, de Haseth JA), Wiley&Sons, New York, (1986)
2.7 http://www.shu.ac.uk/schools/research/mri/pcas/, last accessed 09/04
2.8 Maddams B, *Internet. J. Vibr. Spectrosc.*, **5**, 3 (2001)
2.9 Grdadolnik J, *Vib. Spectrosc.*, **31**, 279 (2003)
2.10 Mirabella FM, *Appl. Spec. Rev.*, **21**, 45 (1985)
2.11 Harrick NJ, *Phys. Rev. Lett.*, **4**, 224 (1960)
2.12 Harrick NJ, *J. Phys. Chem.*, **64**, 1110 (1960)
2.13 Fahrenfort J, *Spectrochim. Acta*, 698 (1962)
2.14 Coombs D, *Internet. J. Vibr. Spectrosc.*,**2**
2.15 Mirabella FM, *J. Polym. Phys., Polym. Phys. Ed.*, **21**, 2403 (1983)
2.16 Buffeteau T, Desbat B, Eyquem D, *Vib. Spectrosc.*, **11**, 29 (1996)
2.17 Chalmers JM, Everall NJ, Schaeberle MD, Levin IW, Lewis EN, Kidder LH, Wilson J, Crocombe R, *Vib. Spectrosc.*, **30**, 43 (2002)
2.18 Treado PJ, Levin IW, Lewis EN, *Appl. Spectrosc.*, **48**, 607 (1994)
2.19 Lewis EN, Treado PJ, Reeder RC, Story GM, Dowrey AE, Marcott C, Levin IW, *Anal. Chem.*, **67**, 3377 (1995)
2.20 Lewis EN, Crocombe RA, *Mikrochim. Acta*, **14**, 589 (1997)
2.21 Sommer AJ, Tisinger LG, Marcott C, Story GM, *Appl. Spectrosc.*, 55, 252 (2001)
2.22 Bhargava R, Wall BG, Koenig JL, *Appl. Spectrosc.*, 54, 470 (2000)
2.23 http://home.cwru.edu/~rxb29/introduction.htm, last accessed 09/04
2.24 Snively CM, Koenig JL, *Appl. Spectrosc.*, 53, 170 (1999)
2.25 Huffmann SW, Bhargava R, Levin IW, *Appl. Spectrosc.*, 56, 965 (2002)
2.26 'Thermal Methods' (Eds. Dodd JW, Tonge KH), Wiley&Sons on behalf of ACOL, London (1987)
2.27 'CMS Workshop lectures: Thermal analysis in clay science', (Eds. Stucki JW, Bish DL, Mumpton FA), The Clay minerals society, USA (1990)
2.28 'An introduction to Thermogravimetry', 2nd edition, (Eds. Keattch CJ, Dollimore D), Heyden&Sons, London (1975)
2.29 'Taschenatlas der Analytik, 2nd edition, (Ed. Schwedt G), Thieme, Stuttgart (1996)
2.30 'Elements of x-ray diffraction', 3rd edition, (Eds. Cullity BD, Stock SR), Prentice Hall, London (2001)
2.31 'Modern Powder Diffraction' (Eds. Bish DL, Post JE), Mineralogical Society of America (1989)
2.32 'X-ray diffraction and the identification and analysis of clay minerals', 2nd edition, (Eds. Moore DM, Reynolds Jr. RC), Oxford University Press, Oxford (1997)
2.33 Vaia RA, Liu WD, *J. Polym. Sci. Pt. B Polym. Phys.*, **40**, 1590 (2002)

3 Preparation and characterisation of polymer/ clay nanocomposites

3.1 Introduction

In this chapter the methods used to prepare nanocomposites of montmorillonite clays with PET and PVOH respectively will be discussed. Furthermore, the results of the characterisation of these samples by XRD, TGA and in some cases FTIR and FTIR imaging will be presented and discussed.

It would have been desirable to perform transmission electron microscopy (TEM) on some of the nanocomposite samples which did not show any d_{001} peaks of the clay. However, difficulties in sample preparation and unavailability of the TEM instrument meant that no such measurements have been performed.

3.2 Instruments and instrument settings used for the characterisation of polymer/ clay nanocomposites

3.2.1 XRD analysis

X- ray diffraction traces were recorded on two different instruments with a chromium and a copper target respectively. Measurements with a chromium target ($\lambda_{K\alpha}$ = 2.291 Å) were performed on a Phillips PW 1830 X-ray diffractometer. Settings for these runs are summarised in Table 3-1.

Parameter	Setting
Generator tension [kV]	30
Generator current [mA]	40
Starting angle [°]	1.8
End angle [°]	45
Step size [°]	0.02
Time per step [sec]	1

Table 3-1 Settings for XRD measurements using a chromium target

Measurements using a copper target ($\lambda_{K\alpha}$ = 1.542 Å) were performed on a Phillips PW3710 X-ray diffractometer. Settings for these runs are summarised in Table 3-2.

Parameter	Setting
Generator tension [kV]	40
Generator current [mA]	40
Starting angle [°]	2
End angle [°]	80
Step size [°]	0.02
Time per step [sec]	1

Table 3-2 Settings for XRD measurements using a copper target

3.2.2 TGA analysis

Thermogravimetric analysis was performed on a Mettler Toledo TG 50 Thermogravimetric Analyser. Data was recorded at a heating rate of 20 °C/min for temperatures between 35 °C and 800 °C after an isothermal stage where the sample was kept at 35 °C for 15 minutes. The analysis was performed in a nitrogen atmosphere at a flow rate of 30 mL/ min in case of the PVOH samples and 10 mL/ min for the PET samples.

3.2.3 ATR – FTIR

Attenuated total reflection – Fourier transform infrared spectra were recorded on a Nicolet Magna 860 and in some cases a Nicolet Nexus FTIR spectrometer equipped with a Graseby - Specac Golden Gate™ accessory and a mercury cadmium telluride (MCT) detector. The Golden Gate™ accessory has a single reflection diamond crystal and a heating stage which allows data collection at temperatures up to 200 °C. Spectra on the Nicolet Magna 860 were recorded with the settings summarised in Table 3-3 and saved as reprocessed spectra in the Log 1/R format or as single beams.

Parameter	Setting
Number of scans	64
Mirror speed [cm/sec]	1.8988
Resolution [cm^{-1}]	4
Apodisation function	Triangular
Spectral region [cm^{-1}]	4000 - 650

Table 3-3 Settings for ATR – FTIR measurements on the Nicolet Magna 860

Spectra on the Nicolet Nexus were recorded with the settings summarised in Table 3-4 and saved as single beams.

Parameter	Setting
Number of scans	10
Mirror speed [cm/sec]	1.8988
Resolution [cm^{-1}]	4
Apodisation function	Triangular
Spectral region [cm^{-1}]	4000 - 650

Table 3-4 Settings for ATR – FTIR measurements on the Nicolet Nexus

3.2.4 ATR imaging

ATR images were recorded on a Digilab Stingray with a 16 by 16 mercury cadmium telluride – Focal plane array detector (MCT-FPA). Settings are summarised in Table 3-5.

Parameter	Setting
ATR crystal	Si
Spectral region [cm^{-1}]	4000 - 900
Resolution [cm^{-1}]	8
Imaging area [µm x µm]	88 x 88
Spacial resolution [µm]	5.5

Table 3-5 Settings for ATR imaging

3.3 Clays and polymers used for the work in this thesis

3.3.1 Data for the clays

For the preparation of the nanocomposites various commercially available sodium and organo montmorillonites were used. All clays were used without further treatment or purification. Poly (ethylene terephthalate) nanocomposites were prepared using three different organo – modified montmorillonites and Poly (vinyl alcohol) nanocomposites were prepared using sodium montmorillonites and lithium exchanged montmorillonites.

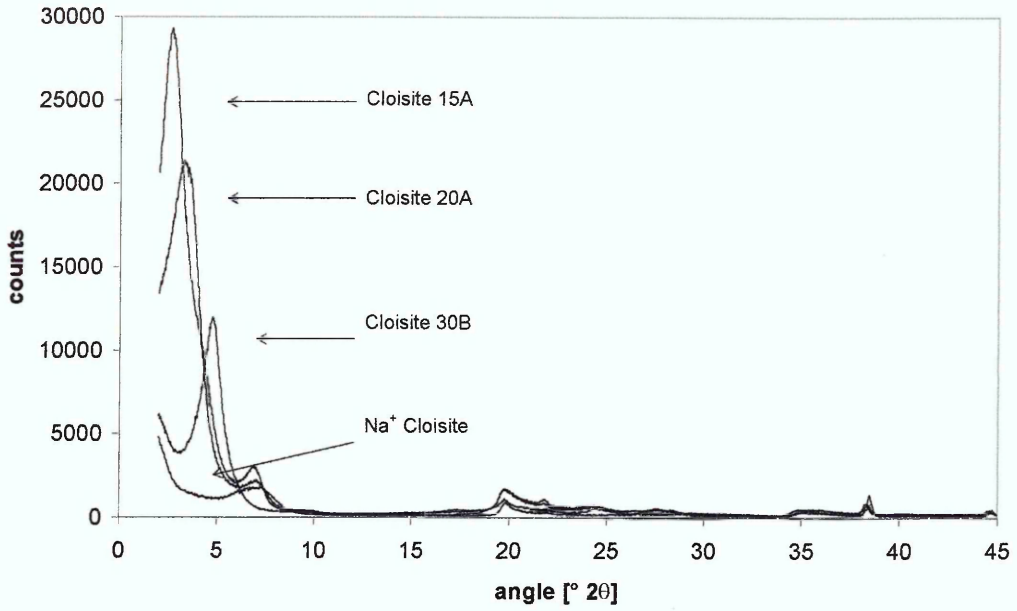

Figure 3-1 Powder x-ray diffraction traces (Cu tube) for the Cloisites used

Clay	Supplier	Cation	CEC (Na^+ clays)/ surfactant concentration) [meq/ 100g clay]	Literature values for d_{001} spacing [Å]
Mineral Colloid British Pharma-copoeia (MCBP)	ECC International Ltd.	Na^+	81	n/a
Na^+ Cloisite®	Southern Clay	Na^+	92.6	11.7
Cloisite® 15A	Southern Clay	dihydrogenatedtallow, quaternary ammonium	125	31.5
Cloisite® 20A	Southern Clay	dimethyl, dihydrogenatedtallow, quaternary ammonium	95	24.2
Cloisite® 30B	Southern Clay	methyl, tallow, bis-2-hydroxyethyl, quaternary ammonium	90	18.5

Table 3-6 Summary of data for clays used to prepared nanocomposites [3.1]

During the analysis of the Na^+ Cloisite® samples a contamination of some of the clay with organic surfactants was found. To ensure that the observed results were not influenced by this contamination, experiments were repeated with the

clay obtained from a new batch of Na^+ Cloisite®. X-ray fluorescence analysis of the sodium clays revealed only minor differences between the clean and contaminated Na^+ Cloisite® clays. The Na^+ MCBP had a lower content in sodium and higher levels of calcium and potassium.

	Contaminated Na^+ Cloisite ®	clean Na^+ Cloisite ®	Na^+ MCBP
Na2O	4.67	4.07	1.98
MgO	3.17	2.10	1.91
Al2O3	22.35	22.63	19.02
SiO2	64.30	65.50	71.28
P2O5	0.00	0.01	0.01
SO3	0.41	0.48	0.44
K2O	0.07	0.07	0.15
CaO	0.21	0.21	0.91
TiO2	0.12	0.12	0.10
Cr2O3	0.00	0.00	0.00
Mn3O4	0.01	0.02	0.01
Fe2O3	4.67	6.21	4.16
ZnO	0.01	0.02	0.01
BaO	0.02	0.03	0.01

Table 3-7 XRF results for Na^+ Cloisite® and Na^+ MCBP

3.3.2 Data for the polymers

3.3.2.1 Poly (ethylene terephthalate)

Two different PET polymers were used to prepare the nanocomposites. The polymer was provided in form of extruded chips by Dupont Teijin films. Some characteristics of these polymers are summarised in Table 3-8.

Type	Isophthalate content [%]	Mean molecular weight (M_w)	Glass transition temperature (T_g) of the polymer chips [°C]
E47	0	70,000	73
E99	18	60,000	67

Table 3-8 Summary of characteristics of PET chips [3.2]

The isophthalate in the E99 causes this polymer to have a lower crystallinity as the isophthalate units introduce kinks in the polymer backbone which hinders the regular stacking observed in PET crystallites. A schematic of the two polymer structures is presented below.

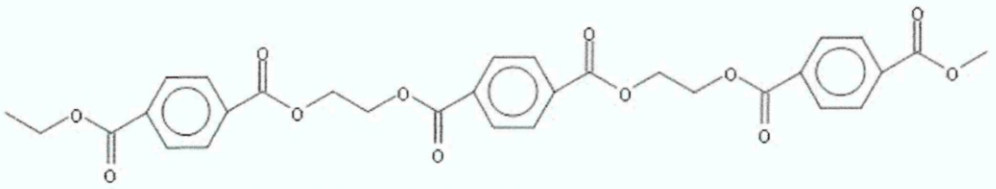

pure terephthalate

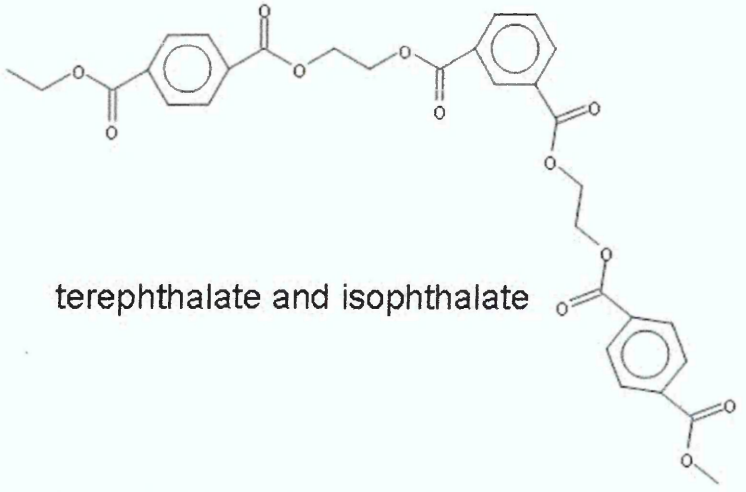

terephthalate and isophthalate

Figure 3-2 Schematic representation of poly (ethylene terephthalate) and poly (ethylene terephthalate-co-isophthalate)

3.3.2.2 Poly (vinyl alcohol)

Two poly (vinyl alcohol) polymers with different molecular weights were used in the preparation of nanocomposites samples. Both polymers were obtained from Aldrich. Samples referred to as low molecular weight PVOH had an average molecular weight of 31000 – 50000 and the high molecular weight PVOH had an average molecular weight of 146000 – 186000. The degree of hydrolysis was 98-99% for both polymers.

3.4 Poly (ethylene terephthalate)/ montmorillonite nanocomposites

3.4.1 Introduction

Preparation of poly (ethylene terephthalate)/ organoclay nanocomposites has been attempted by several researchers but so far results are less promising than those achieved in polyamides. Publications on the preparation of PET/ organoclay nanocomposites can be found describing in-situ intercalation, melt intercalation and solution intercalation procedures.

Ke et al. [3.3] used in-situ polymerisation in the presence of clay slurries to produces nanocomposites that had improved heat distortion temperatures as well as higher decomposition and melting temperatures with increasing clay loadings. They found that the clay particles play a nucleating role during the crystallisation of PET. Using a similar production method to synthesise a PET-derivative [3.4] they were able to show that increasing the clay level increases the molecular weight of the samples.

In-situ polymerisation of bis (hydroxy ethyl terephthalate) (BHET) with 4 wt% expandable fluorine mica and different concentrations of compatibiliser resulted in intercalated nanocomposites [3.5]. The d spacing of the clay and the glass transition was found to decrease with increasing compatibiliser concentrations, while the crystallite size increased yet overall crystallinity remained constant.

Zhang et al. [3.6, 3.7] used in-situ polymerisation to produce PET nanocomposites with clay exchanged with a hydroxyethyl isonicotinamide (HENA) anchor monomer. These samples formed good hybrids but had a brownish coloration due to degradation of the pyridinium substituent of the modifier. The interlayer spacing of these samples was found to increase upon polymerisation. Similarly Zhang et al. [3.8] showed that PET/ clay nanocomposites could be synthesised by the reaction of PET oligomers in the presence of clays. These samples had improved mechanical and thermal properties.

Melt intercalation studies have been performed by Boesel and Pessan [3.9] to investigate the morphology of PET/ organoclay nanocomposites in dependence

of population and packing density of the organic modifier in the interlayer. Using three clays with varying amounts of organic modifier present, they found that two of these clays had the same d spacing even though higher amounts of surfactant were present, which meant that the packing density for the higher surfactant loading with this spacing was greater. Mixing these clays with a PET melt to form 10 wt% composites provided a microcomposite in case of the clay with highest packing density. The intermediate sample showed partial intercalation while a mixture of exfoliated and intercalated clay layers could be found in the sample with the lowest packing density.

Davis et al. [3.10] melt blended PET with 1, 2-dimethyl-3-N-hexadecyl imidazolium modified clay or N, N-dimethyl-N, N-dioctadecylammonium (DMDODA) modified clay in a twin screw extruder at different screw speeds and mixing times. The melt-processing was kept at 285 – 290 °C, which is well above the melting point of the polymer (T_m (PET) = 254 °C). The nano-composites prepared with the DMDODA clay were discoloured because of surfactant decomposition occurring under these mixing conditions. At high and low mixing times (2 and 7 minutes) mixed intercalated and exfoliated nanocomposites with a d_{001} peak in the XRD trace were formed, while an intermediate mixing time produced a nanocomposite that only had a raised background at low angles in the XRD trace. TGA analysis presented no differences between the nanocomposites and the pristine polymers.

Injection moulded samples of poly (butylene terephthalate) (PBT) and various commercially available organoclays were investigated by Li et al. [3.11] Mixing the polymer with Cloisite® 6A resulted in a microcomposite structure. With Cloisite® 30B partial intercalation could be achieved while Cloisite® 10A proved to be the most compatible organoclay yielding a mixed structure of intercalated and exfoliated clay layers. The addition of epoxy as a modifier did not have any effect on the dispersion of Cloisite® 6A while that of Cloisite® 10A was poorer in presence of epoxy. Cloisite® 30B was found to disperse better in PBT if epoxy was added to the polymer/ clay mixture though the structure remained mainly intercalated.

Xu and Li [3.12] compared melt intercalated and in-situ polymerisation intercalated nanocomposites of PET and organically modified montmorillonite.

They found that while MMT acts as a nucleating agent it also inhibits the crystals from growing to larger sizes. The rate of crystallisation was more affected by clay in melt intercalation samples.

Studying the intercalation behaviour of BHET and poly (ethylene glycol) (PEG) into organoclays Yi and Zhang [3.13] observed exfoliation of the clay layers if less than 10 wt% clay was present in BHET. PEG on the other hand formed intercalated structures with 1 - 3 layers of PEG in the clay galleries.

Using solution intercalation in a mixture of 3:1 (w/w) phenol and chloroform Ou et al [3.14] formed nanocomposites of PET with a cetyltrimethylammonium exchanged MMT. The layer spacing decreased with increasing clay loadings. XRD traces showed d_{001} peaks at increased spacings for samples above 10 wt%. Below this clay loading only a raised background at low angles could be observed, while a clay content of 15wt% resulted in a d_{001} peak around 2.46° 2θ indicating layers with a slightly increased spacing compared to that of the organoclay. The presence of clay was found to increase the rate of crystallisation, therefore acting as a nucleating agent. The highest rate of crystallisation was measured for the 10 wt% nanocomposite while higher clay loadings had decreasing rates of crystallisation.

Barber et al. [3.15] compared the morphology and thermal stability of PET/ Cloisite® 30A and sulfonated PET/ Cloisite® 30A nanocomposites with various degrees of sulfonation prepared by solution intercalation in a 1:1 mixture of hexaflouro-2-propanol and chloroform. They reported the formation of intercalated PET nanocomposites and observed that the sulfonated PET acts as a compatibiliser resulting in exfoliated structures for these nanocomposites.

Furthermore, some interest has been shown in nanocomposites of PET blends. Chang and Park [3.16] investigated nanocomposites of poly (ethylene terephthalate –co – naphthalate) with a PET content in the polymer of 92 mol%. Nanocomposites were prepared by solution intercalation in dimethylacetamide using a montmorillonite modified with a surfactant with an alkyl chain length of 16 carbon atoms. At 1 wt% clay loading only an increased background could be observed in the XRD trace. Samples with 2 to 4 wt% clay showed an increased layer spacing while a 6 wt% sample had a similar layer spacing to that of the

organoclay. DSC analysis showed virtually no changes in the glass transition and melting temperatures of these materials. The onset of thermal decomposition was delayed by 4 - 14 °C for the nanocomposites but the maximum decomposition temperature remained the same as that of the pristine polymer.

Using different organic modifiers Chang and Park [3.17] obtained similar results for those mentioned above for a dodecyltrimethyl ammonium (DTA) exchanged clay and Cloisite® 30A. With Cloisite® 25A an exfoliated system was obtained for a clay loading of 4 wt%.

3.4.2 Preparation

Samples were prepared by solution intercalation. This method was chosen because it provided an easy means to cast films once the nanocomposites were formed. A wide range of samples was prepared to investigate the influence of different organically modified montmorillonites, polymer structures, stirring times to expand the clay layers, drying temperatures of the cast films, solvent, clay loading and polymer concentration in solution.

Three different commercially available organo-clays were used for intercalation in PET. A description of these clays can be found in chapter 3.3.1. To investigate the influence of the polymer structure on the clay dispersion two different kinds of PET were used for the formation of nanocomposites as described in chapter 3.3.2.1.

Initially solutions of 10 wt% poly (ethylene terephthalate) were prepared. The clay content was varied between 2.5 wt% and 10 wt% with respect to the amount of polymer. A summary of the parameters used for preparation of various PET nanocomposites is given in Table 3-9.

Two different solvents were used, tetrachloroethane (TCE) and o-chlorophenol (OCP). These solvents were chosen based on previous work performed on PET [3.3] in our group, which identified these two solvents suitable for solvent casting of thin films. In pure PET these two solvents induce different crystallinities in the polymer and the general structure (surface roughness) of the films is influenced by the solvent. (Films cast from TCE dry faster due to the lower boiling point of the solvent but also have a considerably rougher surface.)

In general, the clay was dispersed in a solvent by stirring for a certain amount of time (see Table 3-9) before addition of PET pellets and heating of the sample under continuous stirring using a magnetic stirrer for two days.

Films were then cast by dispensing 2 mL of these mixtures onto microscope slides. The films were allowed to form at room temperature before being dried at elevated temperatures in an oven.

wt% PET (with respect to solvent)	wt% clay (with respect to PET)	clay	PET	solvent	stirring time for clay in solvent
10	5	15A	E47	o-chlorophenol (OCP)	3 days
10	5	20A			
10	5	30B			
10		---			
10	5	15A			2 days
10	5	20A			
10	5	30B			
10	5	15A			1 day
10	5	20A			
10	5	30B			
10	5	15A			12 hours
10	5	20A			
10	5	30B			
10	5	15A			6 hours
10	5	20A			
10	5	30B			
10	5	15A			1 hour
10	5	20A			
10	5	30B			
10	5	15A			directly all
10	5	20A			
10	5	30B			
10	5	15A			1 day, separately dissolve PET
10	5	20A			
10	5	30B			
10	---	---	E99		
10	5	15A			
10	5	20A			
10	5	30B			
10	5	20A			3 days
10	5	30B			
10	5	20A			2 days
10	5	30B			
10	5	20A			1 day
10	5	30B			
10	5	20A			1 hour
10	5	30B			
2.5	5	20A			
5	5				
7.5	5				
10	2.5				
10	7.5				
10	10				
5	5			1,1,2,2-tetrachloroethane (TCE)	
5	10				
10	5				
10	10				

Table 3-9 Summary of nanocomposite preparation parameters

3.4.3 Determination of degree of crystallinity of poly (ethylene terephthalate] from ATR-FTIR spectra

The degree of the crystallinity of PET can be calculated from the ratio of the CH wagging mode bands at 1370 cm^{-1} (gauche conformer) and 1340 cm^{-1} (trans conformer) of the ethylene glycol moiety. The trans conformer is associated with crystalline regions, while the gauche conformer is predominant in amorphous regions. Figure 3-3 shows typical spectra for samples with high and low crystallinities.

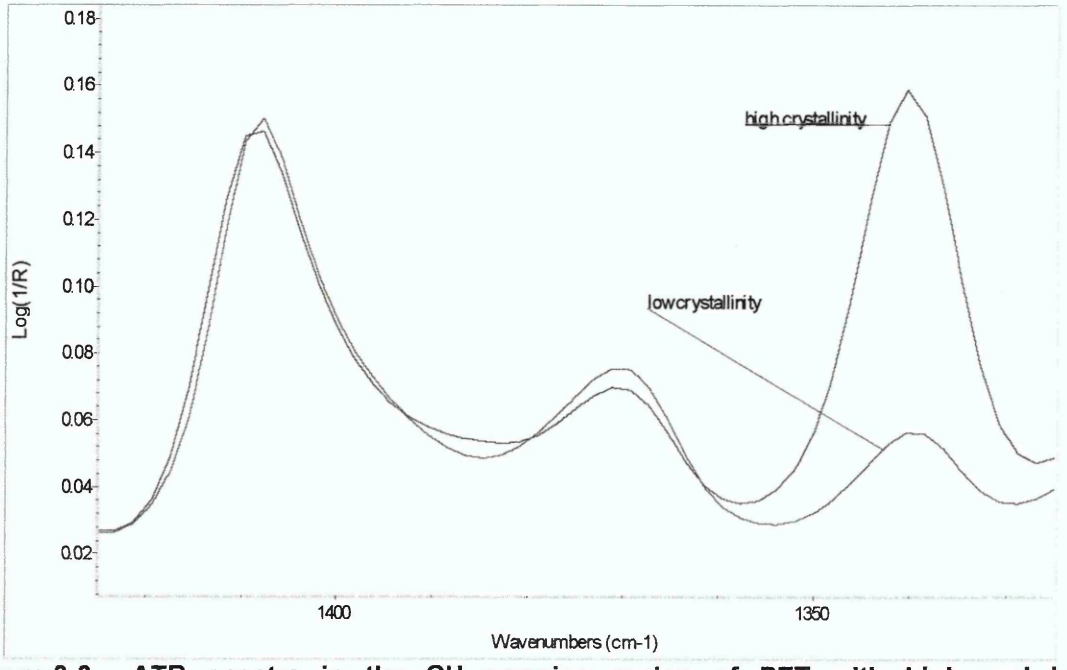

Figure 3-3 ATR spectra in the CH wagging region of PET with high and low crystallinities

Peak areas for these two bands were obtained by fitting mixed Gaussian/Lorentzian bands with at least 80% Lorentzian shape. The values obtained were then corrected for influence of an OCP band at 1338 cm^{-1} on the area for the trans conformer band.

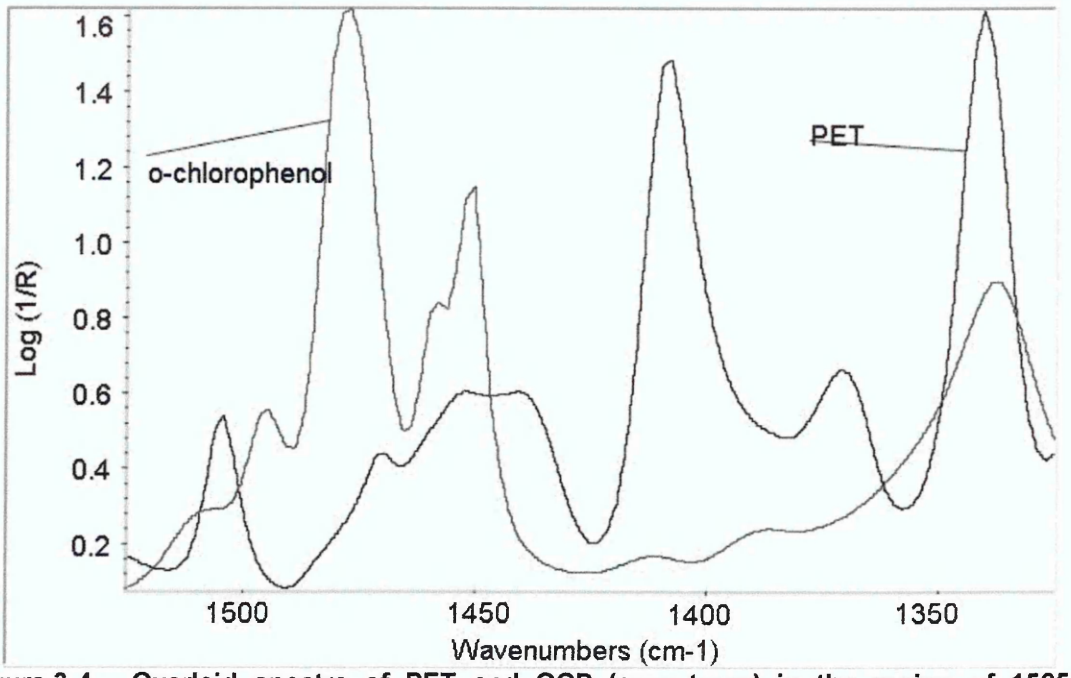

Figure 3-4 Overlaid spectra of PET and OCP (grey trace) in the region of 1525 - 1325 cm^{-1}

Belali and Vigoreux [3.18] discussed the correction of the crystallinity calculations needed to apply the equation used for transmission spectra to ATR spectra. For ATR spectra they published the following calculation for the determination of crystallinity in PET samples.

$$x_c = \frac{a_i - a_j\left(\frac{A_i}{A_j}\right)\left(\frac{\nu_i}{\nu_j}\right)}{(c_j - a_j)\left(\frac{A_i}{A_j}\right)\left(\frac{\nu_i}{\nu_j}\right) - (c_i - a_i)}$$

Equation 3-1

where a_i, c_i: molar absorption coefficients for the 1370 band
a_j, c_j: molar absorption coefficients for the 1340 band
A_i, A_j: area of the 1370 and 1340 band respectively
ν_i, ν_j: wavenumbers of the 1370 and 1340 band respectively

The values for the molar absorption coefficients are given in Table 3-10.

ν [cm^{-1}]	a $\left[\frac{l}{cm*mol}\right]$	c $\left[\frac{l}{cm*mol}\right]$
1370	0.160	0.050
1340	0.080	0.900

Table 3-10 Molar absorption coefficients for bands at 1370 cm^{-1} and 1340 cm^{-1} [3.18]

3.4.4 Determination of peak positions and errors associated with this determination

Peak positions for the d_{001} peaks, which were used to deduce information on the dispersion and the layer spacing of the clay dispersed in the polymer, were determined from the XRD traces by eye. In many cases the peaks were broad with no clear peak centre. Exact determination of the peak position was also hampered by the poor signal to noise ratio of some measurements. Therefore, the angle of 2 θ could often only be determined with an accuracy of ± 0.2°.

This uncertainty can lead to rather large errors for the layer spacings calculated from peaks at low angle. An overview of the angles expected for nanocomposite samples and resulting layer spacings including the errors associated with the layer spacings based on the uncertainty in the determination of the angle 2θ is given in Table 3-11 for the measurements with a copper target and Table 3-12 for the measurements with a chromium target.

Angle 2θ [°]	D spacing [Å]	Error d spacing [Å]	Error d spacing [%]
2	44.2	4.5	10
3	29.5	2.0	6.7
4	22.0	1.0	5
5	17.7	0.7	4
6	14.7	0.5	3.3
7	12.6	0.36	2.8
8	11.0	0.28	2.5
9	9.8	0.22	2.2
10	8.9	0.18	2
11	8.0	0.15	1.8
12	7.4	0.12	1.6
13	6.8	0.11	1.5
14	6.3	0.09	1.4
15	5.9	0.08	1.3
16	5.5	0.07	1.2

Table 3-11 Errors in the calculated d spacings for XRD traces from a copper source

Angle 2θ [°]	D spacing [Å]	Error d spacing [Å]	Error d spacing [%]
2	65.6	6.5	10
3	43.8	3	6.7
4	32.8	1.6	5
5	26.3	1	4
6	21.9	0.7	3.3

Table 3-12 Errors in the calculated d spacings for XRD traces from a chromium source

3.4.5 Results and discussion

Even though a wide range of samples was prepared using E47 XRD analysis of these samples proved difficult because the films were very brittle and delaminated from the glass slides on which they were cast. Diffraction measurements of these films could, therefore, not always be taken and the results and discussion presented here focus mainly on data obtained from E99 nanocomposites, which were easier to handle as the general crystallinity of this polymer is lower than that of the E47.

Using either of the two polymers production of uniform thin nanocomposite films that could be used in ATR diffusion experiments proved very difficult. As film production via solvent casting for these samples was found to suffer from poor reproducibility no diffusion experiments could be performed due to a lack of suitable sample films.

3.4.5.1 Effect of organic modification of the clay

The dispersion of three commercially available organically modified clays in PET (E47) was investigated. Two of the clays (Cloisite® 15A and Cloisite® 20A) were modified with the same surfactant in different concentrations, while the third clay, Cloisite® 30B, was modified with a slightly different surfactant molecule. Details for these clays are given in chapter 3.3.1.

3.4.5.1.1 XRD results

All three clays influenced the crystal structure of the PET as can be seen in Figure 3-5. d_{001} peaks were present in all samples even at clay loadings as low as 2.5 wt%. This indicates that the clay is not dispersing too well in PET under the conditions used to prepare these samples. Since these samples were prepared by dispersing the clay for only 90 minutes in the solvent before adding polymer improvements are likely to be achieved by optimising the process as discussed later. The layer spacings obtained for the clay in these samples are, however, increased compared to those of the pure organoclays due to PET intercalating into the clay galleries.

While the layer spacing obtained for the Cloisite® 30B sample was the lowest overall this clay showed the largest increase upon intercalation of PET (from 18.5 Å to 36.5 Å (+ 97%)). The spacing for the Cloisite® 15A and Cloisite® 20A

were the same within the error of the measurement at 44.4 Å and 42.6 Å respectively. The increase in spacing between these samples and the pure clay layer spacing was, however, only 40% for the Cloisite® 15A and 76% for the Cloisite® 20A. This similarity of the layer spacings is probably due to both clays having been modified with the same surfactant. The excess of surfactant present on the Cloisite® 15A is most likely washed off during the dispersion of the clay in the solvent resulting in two similar clay dispersions for Cloisite® 15A and 20A in a solvent.

Cloisite® 30B, therefore, has the highest affinity to PET, which was to be expected as the surfactant in this material contains a hydroxyl group. The higher surfactant concentration in Cloisite® 15A sample compared to Cloisite® 20A results in less PET being able to penetrate into the clay layers, which means that the layers cannot be dispersed in an exfoliated manner as easily as it might be for the Cloisite® 20A under the right preparation conditions.

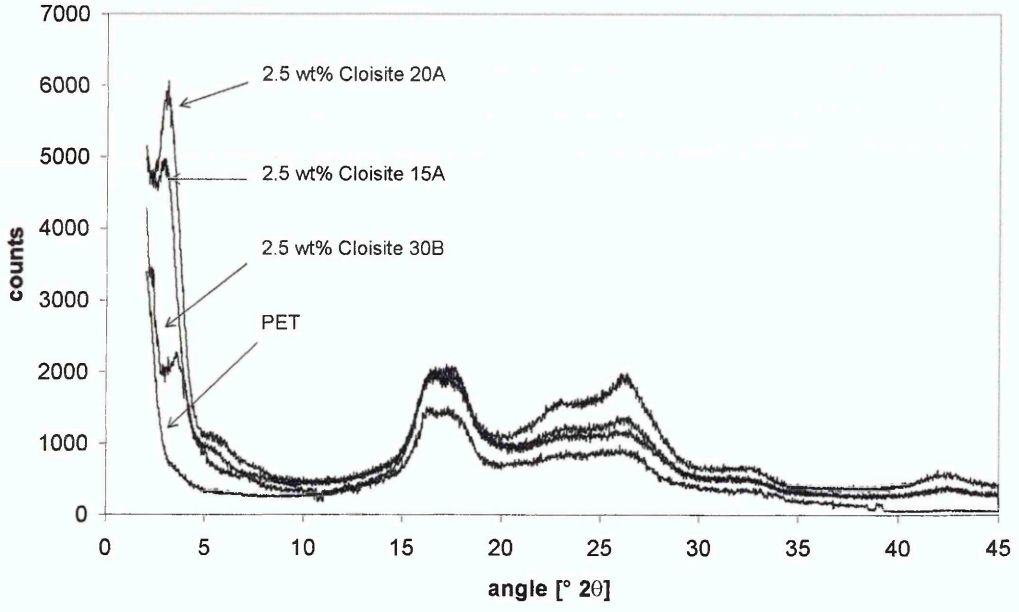

Figure 3-5 XRD traces (Cr tube) for PET (E47) nanocomposites with various organoclays

3.4.5.1.2 TGA results

Thermogravimetric analysis of these materials did not show any major differences for samples with or without clay or with different clays for that matter. Figure 3-6 shows mass loss curves for 2.5 wt% nanocomposites and pristine E47. For all these samples the maximum weight loss temperature remained the same at about 450 °C. The decomposition does, however, start at temperatures 20 - 30 °C lower for the nanocomposites than in the pristine polymer. This is probably due to the clay acting as a catalyst for the decomposition or decomposition of the surfactant prior to the polymer decomposition. Furthermore, it is possible that the solvent residue in these samples varied with higher solvent concentrations in the nanocomposite films, which result in the lowering of the onset temperature for the polymer decomposition.

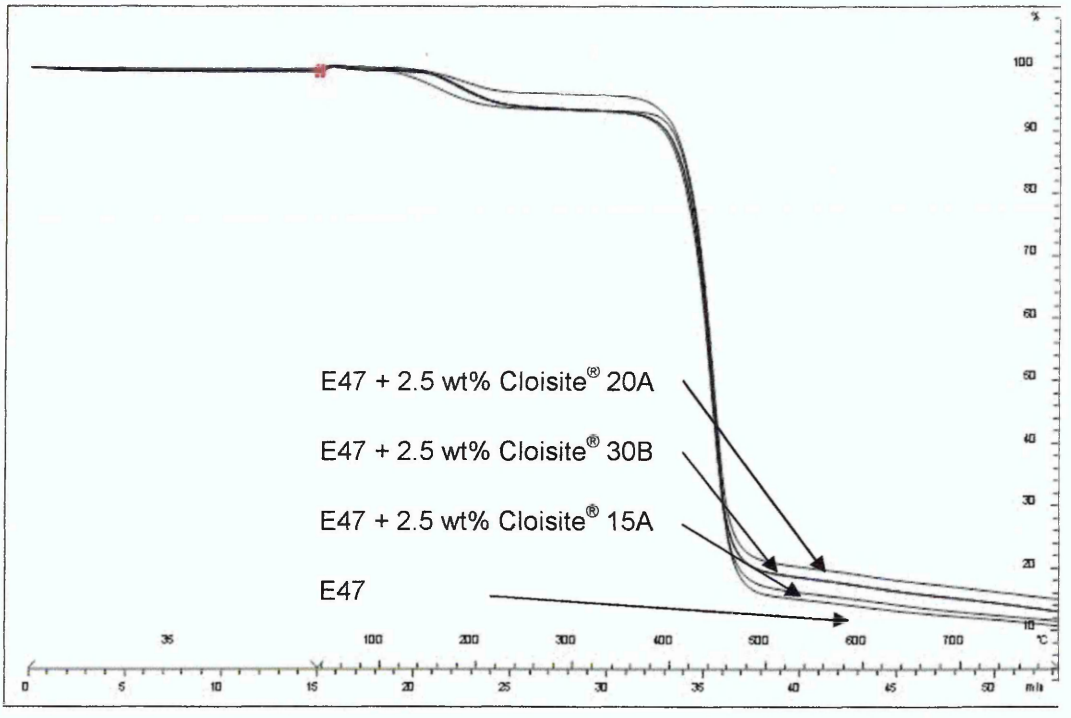

Figure 3-6 Thermograms of E47 and E47/ organoclay nanocomposites

3.4.5.1.3 Summary

Using XRD and TGA analysis it has been shown that the dispersion of clay in PET is dependent on the type and concentration of organic modifier used to render the clay organophilic. All types of clay used in the preparation of nanocomposites led to intercalated structures.

The XRD data showed that the use of Cloisite® 20A resulted in the largest layer spacing of the clay while samples prepared from Cloisite® 30B had the largest percentage increase in layer spacing between that of the clay on its own and clay intercalated with PET.

The thermal stability of the nanocomposites was found to be similar to that of the pristine polymer with a slight reduction in the decomposition onset temperature.

3.4.5.2 Effect of polymer structure

The two PET types used for the preparation had slightly different structures, which influence the packing of the polymer chains and therefore the crystallinity of the material as discussed in chapter 3.3.2.1.

3.4.5.2.1 XRD results

Figure 3-7 presents a comparison for nanocomposites of E99 and E47 with Cloisite® 20A. As could be expected the E99 sample had a poorer clay distribution than the E47 sample which is due to the E99 chains being 'bulkier', i.e. being less ordered and chains having more 'kinks' as shown in Figure 3-2, and, therefore, intercalating less into the clay layers.

While the d_{001} peak in the E99 sample appears at a slightly higher spacing than the main raised background in the E47 the presence of a second peak around 7.4° 2θ, which is the d_{002} reflection, confirms the higher order of the clay layers in the E99 sample. The layer spacing in this E99 sample, which was prepared by stirring the clay in solvent for three days before the addition of polymer is 34.5 Å, which is lower than those observed for the E47 samples of similar clay content and lower stirring times presented in chapter 3.4.4.1.

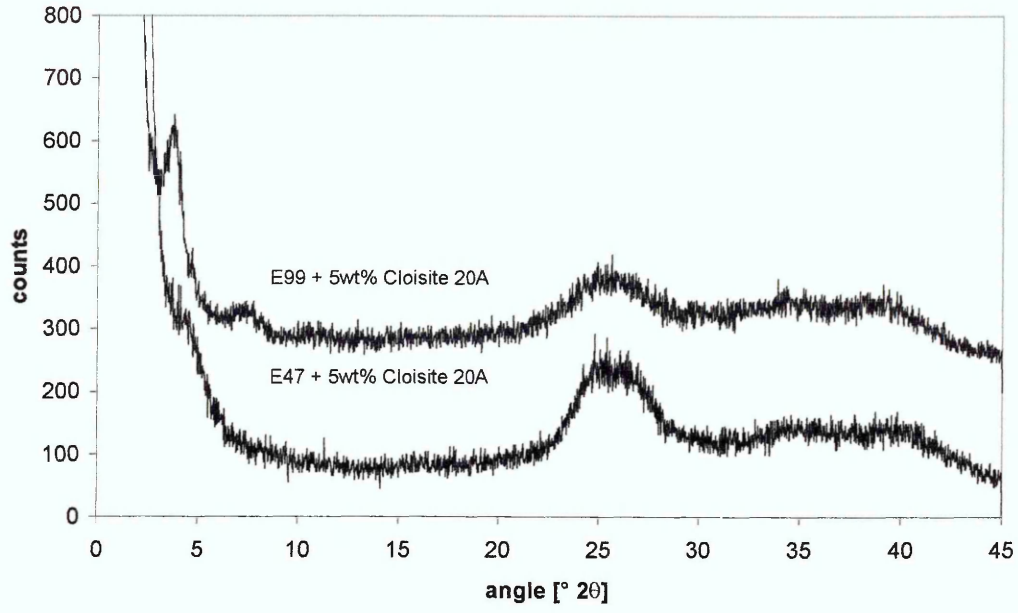

Figure 3-7 XRD traces (Cr tube) for E99 and E47/ Cloisite® 20A nanocomposites (traces offset for clarity)

3.4.5.2.2 TGA results

The thermal stability of E47 and E99 is very similar. For both polymers the onset of decomposition occurred at 360 °C and the maximum decomposition temperature was 440 °C for E99 and 450 °C for E47. The slightly higher decomposition temperature for E47 is due to higher crystallinity of solvent cast films of this polymer.

Nanocomposites of E99 showed similar decomposition behaviour to their E47 counterparts. Decomposition in E99 nanocomposites started around 335 – 340 °C and the weight loss curves are very similar to those for E47 nanocomposites. A direct comparison of weight loss curves for E47 and E99 nanocomposites with 5 wt% Cloisite® 20A is presented in Figure 3-8. The higher weight loss at lower temperatures in the E99 nanocomposite is due to higher solvent residue in the sample which is desorbing around 160 °C.

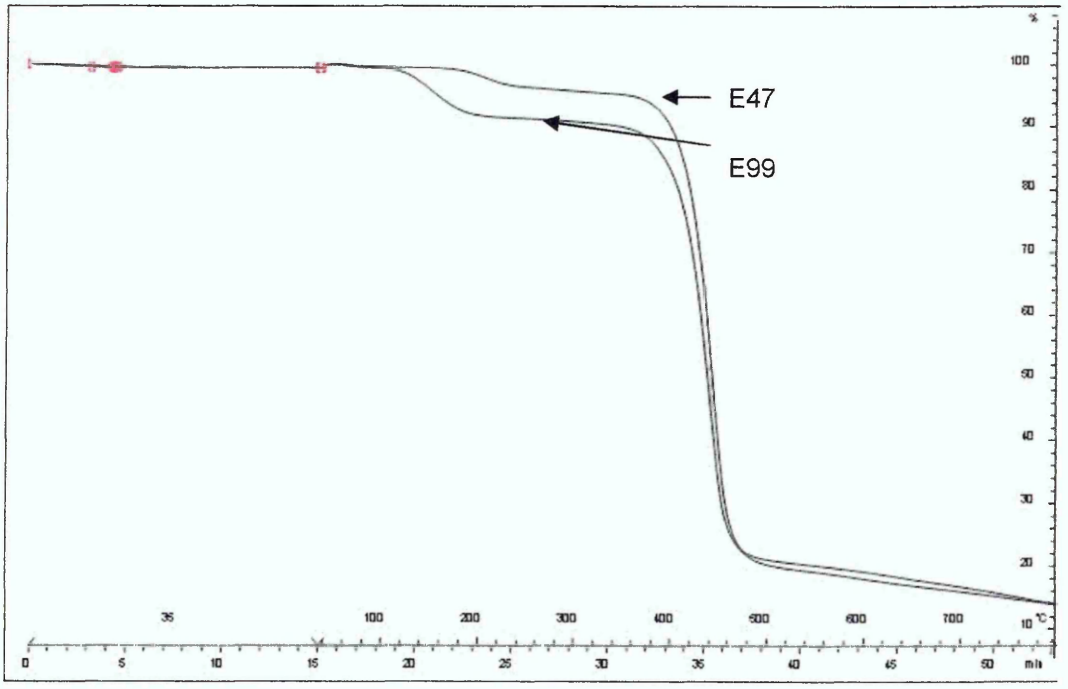

Figure 3-8 Thermograms of E47- and E99/ 5wt% Cloisite® 20A nanocomposites

3.4.5.2.3 Summary

Nanocomposites prepared from these two types of PET polymer by solution intercalation have an intercalated structure. XRD analysis shows that clay layers incorporated in E99 are less disordered as a d_{002} reflection can be seen in the XRD traces of these nanocomposites. Thermal stability of these samples is however very similar.

3.4.5.3 Effect of stirring time

Different stirring times were tested to investigate whether the clay can be better dispersed in the solvent prior to addition of PET by longer stirring times. Clay was dispersed by magnetic stirring for periods of 1 hour to 3 days. E47 samples were also prepared by immediately adding clay and polymer to the solvent.

The samples that were stirred for a day and longer looked similar to pure PET samples. Shorter stirring times appeared to lead to more opaque materials. All samples were relatively brittle and tended to delaminate from the glass slides they were cast on.

3.4.5.3.1 XRD results

The time that was allowed for the clay to disperse in the solvent appears to have no influence on the structure of the final nanocomposite. Figure 3-9 shows representative traces for nanocomposites prepared with various dispersion times for the clay at a clay loading of 5 wt%. The layer spacing for these samples was in the range of 32.2 Å and 32.8 Å. These variations are well within the error of the measurement and similar to those observed between samples cast from the same solution (see Figure 3-10) or indeed between different areas of the same film. For each stirring time, XRD traces were measured on three samples cast from the same solution and two different slices of a film were investigated for each sample. The traces presented below are representative for these repeat measurements. Variations in the peak around 7° 2θ appeared to be random with regard to the stirring times and largely due to variations in the sample thickness or local variations within a sample film.

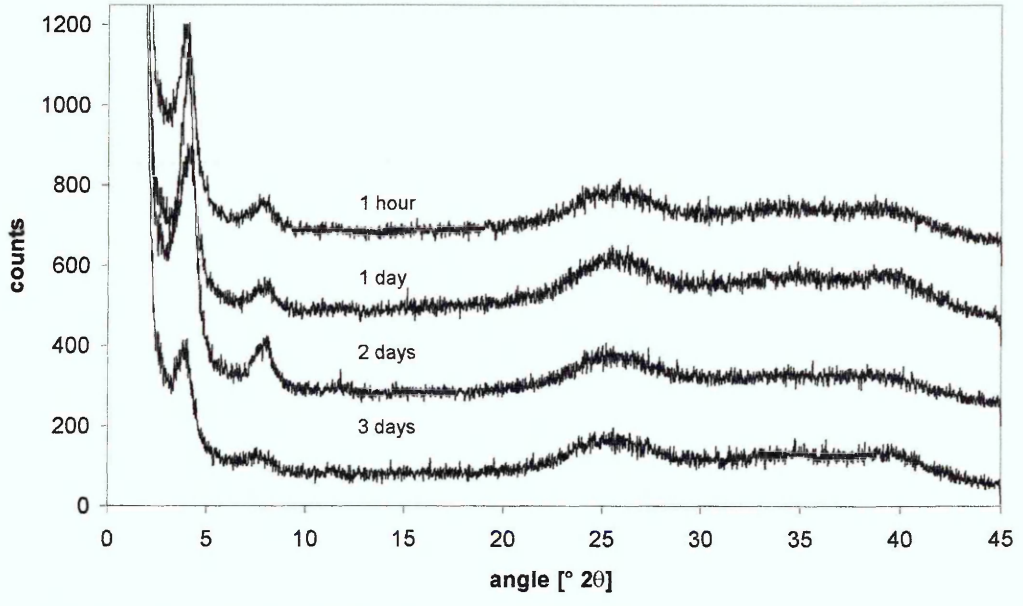

Figure 3-9 XRD traces (Cr tube) for E99/ Cloisite® 20A nanocomposites with different dispersion times for the clay (traces offset for clarity)

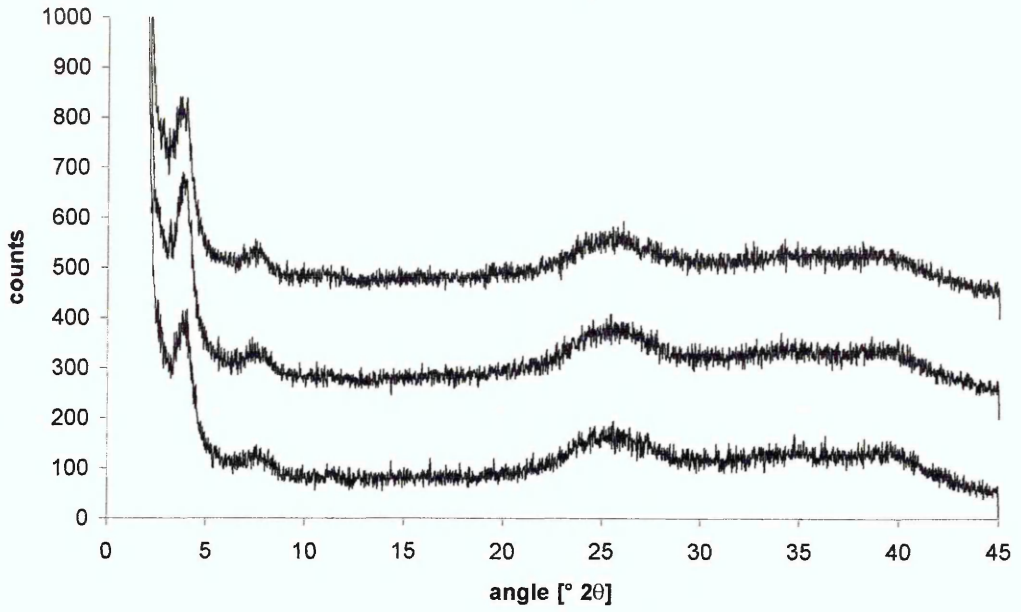

Figure 3-10 XRD traces (Cr tube) for several E99/ Cloisite® 20A nanocomposite samples cast from the same solution (clay stirred for 3 days before adding polymer) (traces offset for clarity)

The layer spacing for E99/ Cloisite® 30B samples remained equally unchanged by the variations in stirring times of the clay/ solvent mixtures. XRD traces for these nanocomposites are presented in Figure 3-11. Apparent variations between the samples in this figure are due to variations of the amount of clay in the sampled area rather than variations due to differences in the overall dispersion.

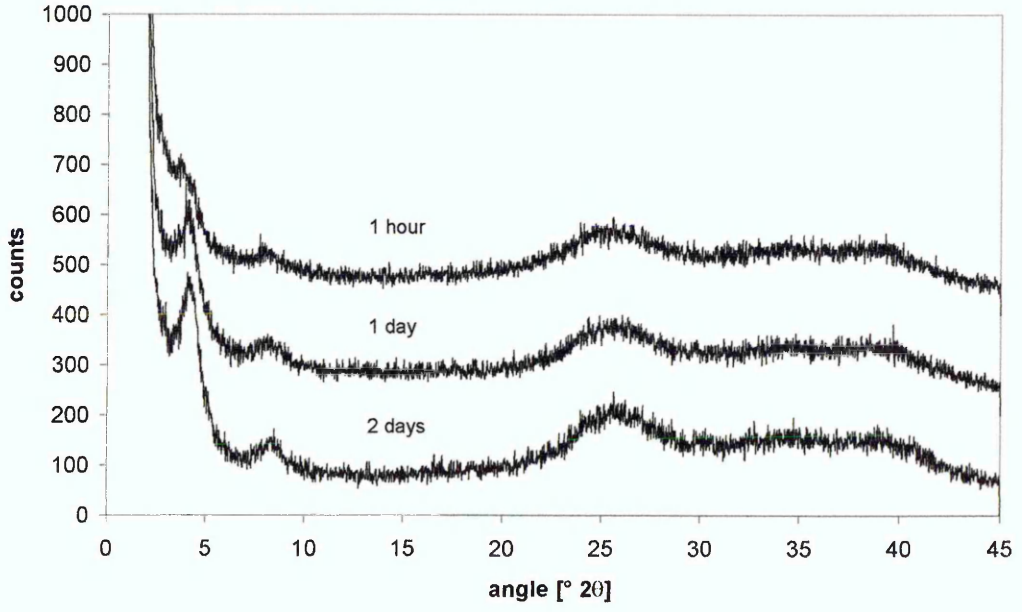

Figure 3-11 XRD traces (Cr tube) for E99/ Cloisite® 30B nanocomposites with different dispersion times for the clay (traces offset for clarity)

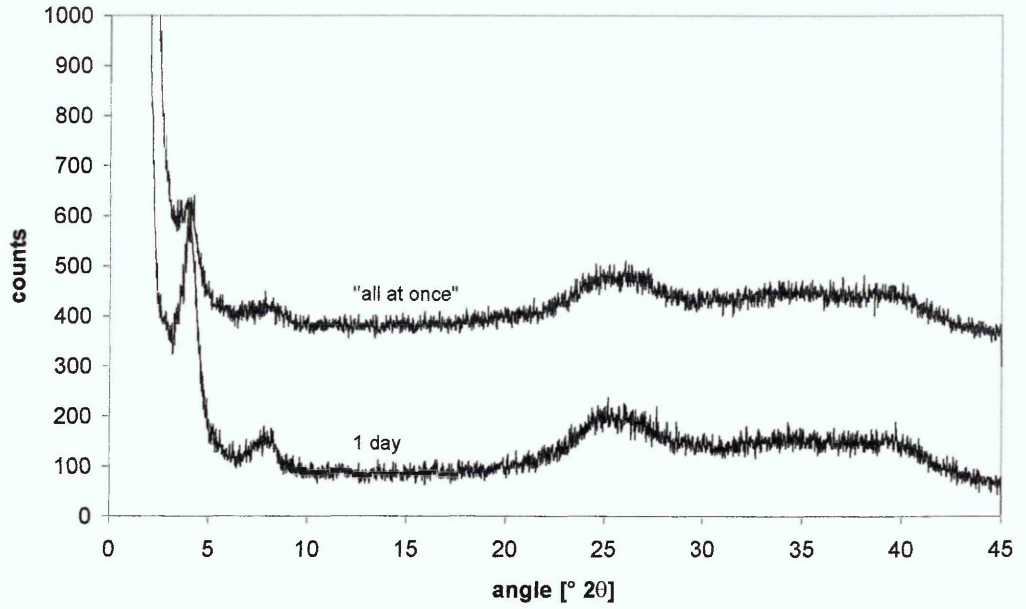

Figure 3-12 XRD traces (Cr tube) for E47/ Cloisite® 20A nanocomposites with different dispersion times for the clay (traces offset for clarity)

When analysing the influence of dispersion time on the structure of E47 nanocomposites samples were also prepared by mixing clay, polymer and solvent without pre-dispersing the clay in the o-chlorophenol. As Figure 3-12 shows this kind of treatment did not have any effect on the layer spacing of the sample. The different intensities for the clay peaks in these samples are more likely to be caused by less clay being present in the part of the sample analysed by XRD than changes in the dispersion as the d_{002} peak around 7° 2θ is still present in the "all at once" sample.

Since the time for which the polymer/ clay dispersions were heated and stirred was kept constant at two days, it appears likely that this relatively long stirring time was enough to allow the polymer to intercalate the clay independent of its dispersion when the polymer was first added to the mixture.

3.4.5.3.2 TGA results

Since variations in the stirring time did not lead to any obvious differences in the structure of the nanocomposites, the thermal stability is expected to remain unchanged. Table 3-13 gives a summary of the data obtained from the dTG curves of these samples. All samples had a weight loss around 160 °C which is due to the residual solvent desorbing from the sample. The weight loss due to solvent desorption was slightly higher for the nanocomposites than the pure

polymer. Casting a thinner film from a solution diluted to a polymer concentration of 2.5 wt% also resulted in a film with less solvent content (due to less solvent being trapped in the film during the drying procedure).

Weight loss of the polymer was lower in the nanocomposites than in the pristine polymer. The decomposition of nanocomposites started at lower temperatures but did not appear to be influenced by the stirring time of the clay in solvent. The maximum decomposition temperature remained constant for all samples.

Clay	stirring	weight loss OCP [%]	weight loss PET [%]	Decomposition onset temperature [°C]	Maximum decomposition temperature [°C]
C20A	3 days	9.9	72.1	340	440
C20A	3 days dilution	6.4	75.8	340	440
C20A	2 days	8.0	70.2	320	440
C20A	1 day	8.9	73.4	325	445
C20A	1 hour	9.1	71.9	335	435
C30B	2 days	8.4	69.2	320	440
C30B	1 day	8.3	70.3	310	440
C30B	1 hour	9.2	72.2	320	440
pure E99		6.2	77.8	360	440

Table 3-13 Summary of TGA data for PET (E99)/ organoclay nanocomposites

3.4.5.3.3 Summary

Dispersion of the clay in the polymers remained unchanged when the time of dispersion of the clay was altered. This is in contrast to data published by Suh et al. [3.19] on the preparation of polyester resin nanocomposites where mixing all components at once resulted in lower layer spacings in the final nanocomposites. The simultaneous mixing sample showed a broad peak in the diffraction trace around 3.5° 2θ (~25Å), while sequential mixing resulting in samples with lower intensity, broad peaks around 2.5° 2θ (~35Å).

Thermal stability also remained unchanged by the stirring time, yet decomposition started at lower temperatures in the nanocomposites compared to the pristine polymer.

3.4.5.4 Effect of drying temperature

The degree of crystallinity in PET can be affected by the temperatures at which the polymer films are dried. Samples in this series of experiments were allowed to dry at room temperature for one day before being dried for six days at 60 °C. This temperature is just below the glass transition temperature of the polymer. Two drying regimes were used for the samples dried at higher temperatures. One set of samples was dried at room temperature for one day then heated to 160 °C for an hour. At this point the samples were cooled to 90 °C and kept at that temperature for an hour. Finally samples were allowed to remain at 60 °C for six days. The second set of samples was only dried at the last two stages of the process described above after they had been dried at room temperature.

3.4.5.4.1 XRD results

Drying the samples at temperatures above their glass transition temperature did not alter the layer spacing significantly. Changes in the intensity of the clay d_{001} peak are likely to be caused by inhomogeneities in the clay dispersion, i.e. low amounts of clay in the analysed sample area rather than improved dispersion. However changes in the peaks between 25° and 40° 2θ, which have been assigned to the d_{010} and d_{100} reflections of the PET crystals, show that the morphology of the polymer matrix is changing [3.21]. Comparison of the changes for E47 samples and E99 samples (see Figure 3-13 and Figure 3-14) shows that the effect is more marked in E99 samples. This is to be expected as these samples have a lower crystallinity when they are initially dried.

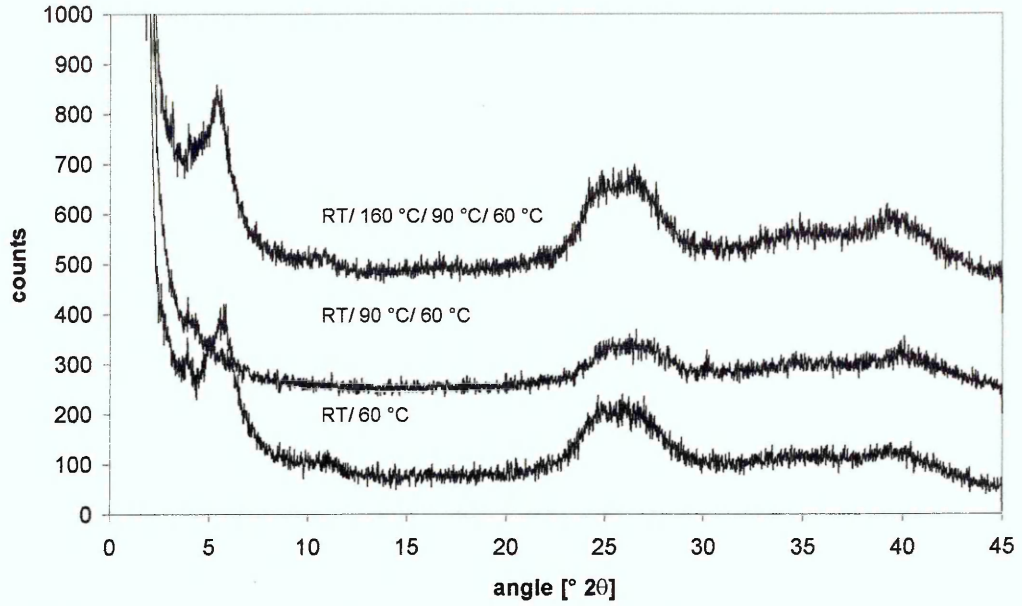

Figure 3-13 XRD traces (Cr tube) for E47/ 5 wt% Cloisite® 30B nanocomposites dried at different temperatures (traces offset for clarity)

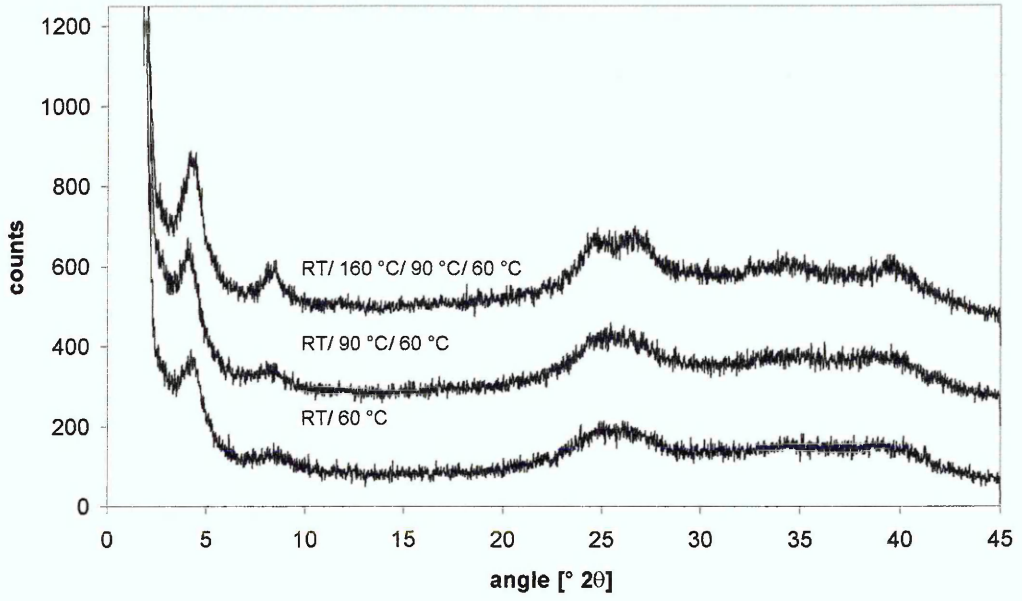

Figure 3-14 XRD traces (Cr tube) for E99/ 5 wt% Cloisite® 30B nanocomposites dried at different temperatures (traces offset for clarity)

3.4.5.4.2 Analysis of ATR – FTIR spectra

ATR-FTIR spectra were taken of various samples dried at different temperatures. For each sample four spectra were collected from different regions of the polymer to account for local changes in the morphology of the PET. Figure 3-15 shows typical changes observed for spectra taken from the same sample. The changes in these spectra are mainly due to variations in the solvent residue (OCP band at 1481 cm^{-1}) and PET crystallinity.

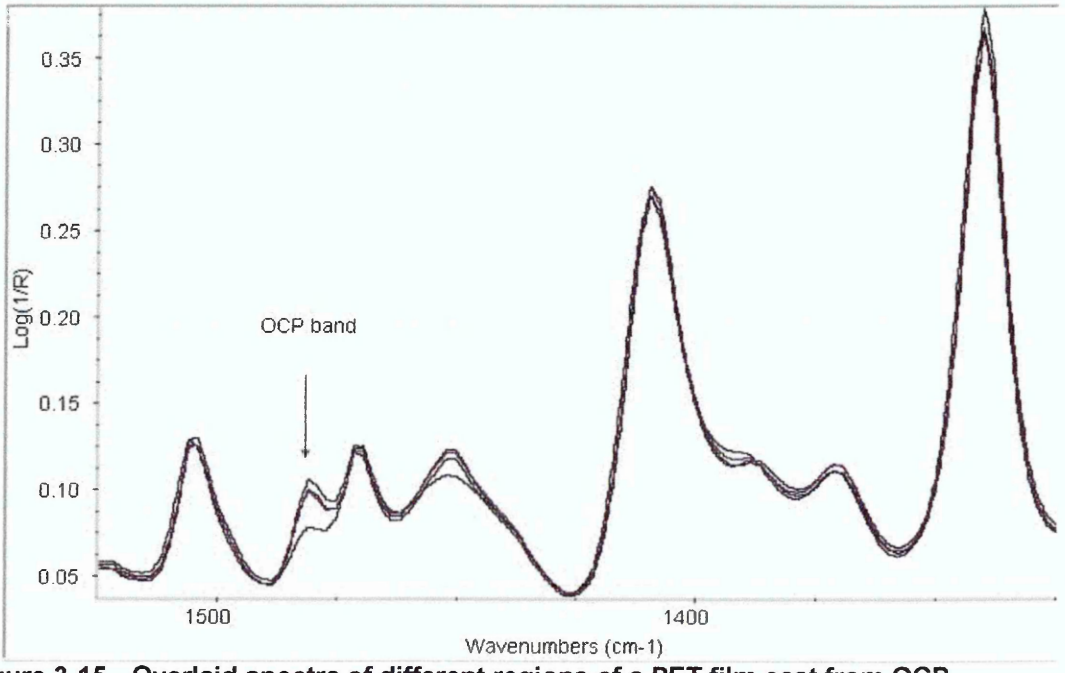

Figure 3-15 Overlaid spectra of different regions of a PET film cast from OCP

As PET has several strong absorbing bands in the fingerprint region any bands arising from the addition of clay to the polymer are hidden under the ester bands of the polymer as can be seen from the spectra presented in Figure 3-16.

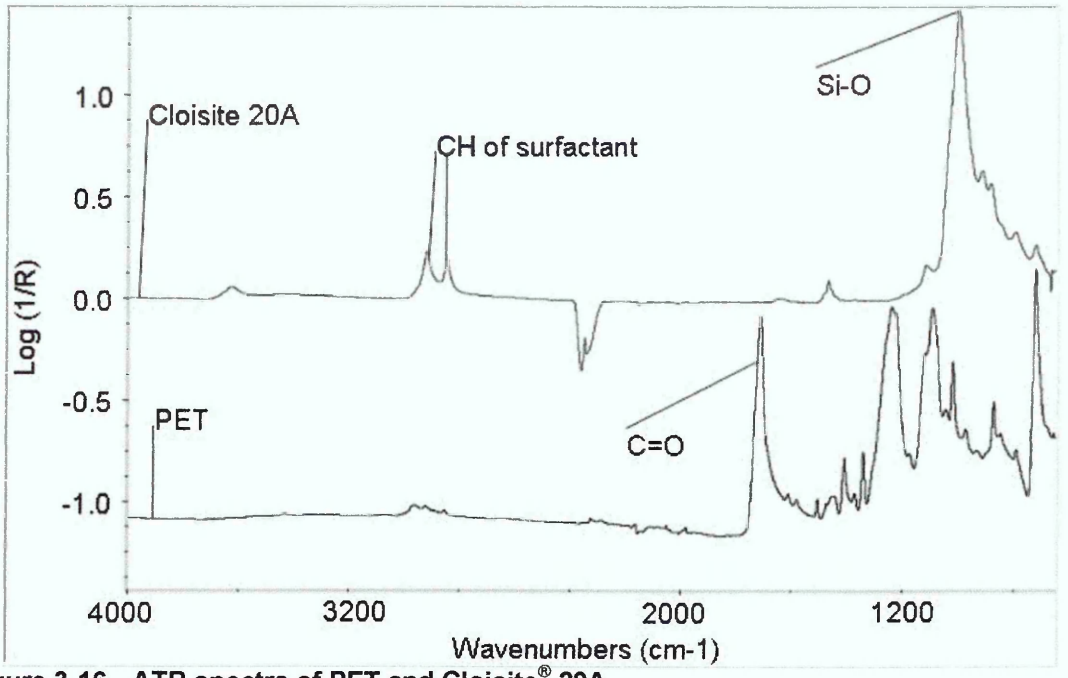

Figure 3-16 ATR spectra of PET and Cloisite® 20A

To investigate any changes occurring in the spectra, the spectra taken on pure PET samples for each drying temperature have been averaged and subsequently been subtracted from the corresponding spectra of the nanocomposites. The aim of averaging the spectra of the pure PET was the production a representative PET spectrum in which the influence of variations in the morphology and solvent residue in the polymer should be minimised. Even though changes in morphology observed in the difference spectra are not necessarily caused by the clay alone it should be possible to identify major changes that are likely to be induced by the presence of the clay.

In the subtraction spectra bands originating from the clay (examples shown in Figure 3-17) could be identified. In the spectra of samples dried at 60 °C the CH_2 stretching modes of the aliphatic chains of the surfactants could be observed at 2922 cm^{-1} and 2850 cm^{-1}. Furthermore, shifts can be observed in the position of the carbonyl stretching band from 1712 cm^{-1} in the PET spectra to 1718 cm^{-1} in the nanocomposite spectra. The ν(Si-O) and δ(metal-OH) bands of the layered silicate can be found in the region between 1089 cm^{-1} and 898 cm^{-1}. These shifts in the carbonyl stretching band of the polymer and the "extra" bands in the region between 1089 cm^{-1} and 898 cm^{-1} were similar for all nanocomposites, irrespective of the organoclay used.

Changes in the stirring time for dispersing the clay during preparation did not lead to any significant changes in the spectra. This is to be expected since XRD analysis showed samples prepared with different clay dispersion times to have similar structures.

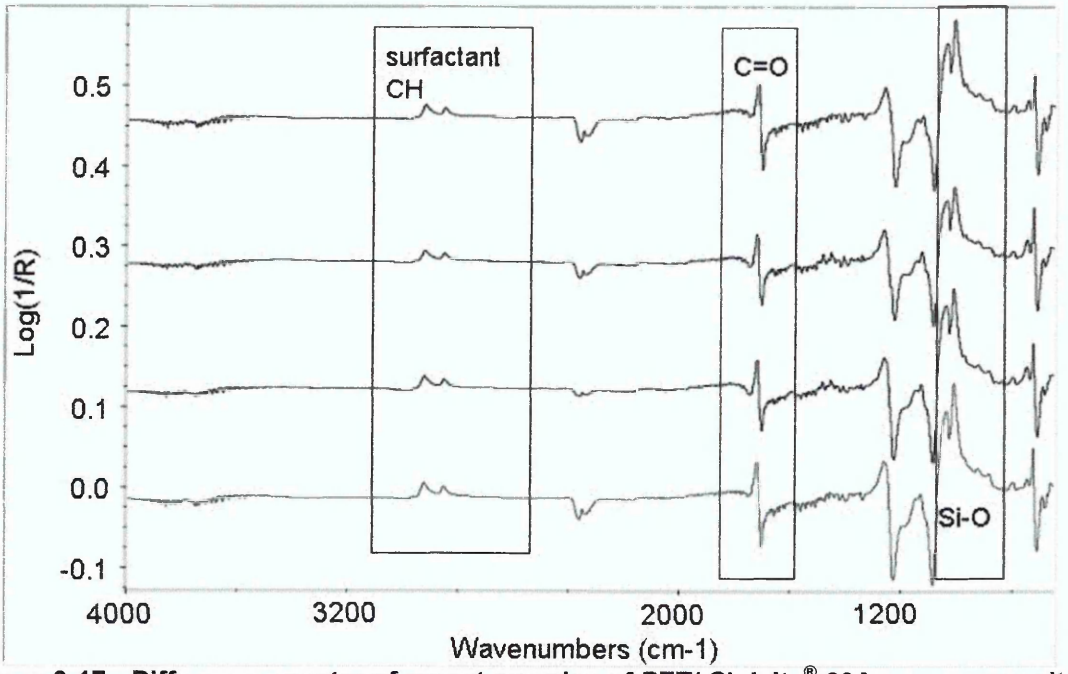

Figure 3-17 Difference spectra of repeat samples of PET/ Cloisite® 20A nanocomposites dried at 60 °C obtained by subtraction of a pure PET spectrum

The samples dried at 90 °C for an hour showed the same types of changes as those described above for samples dried at 60 °C. Figure 3-18 presents typical spectra for samples dried at this temperature. The shift of the carbonyl band is smaller when samples are dried at this temperature.

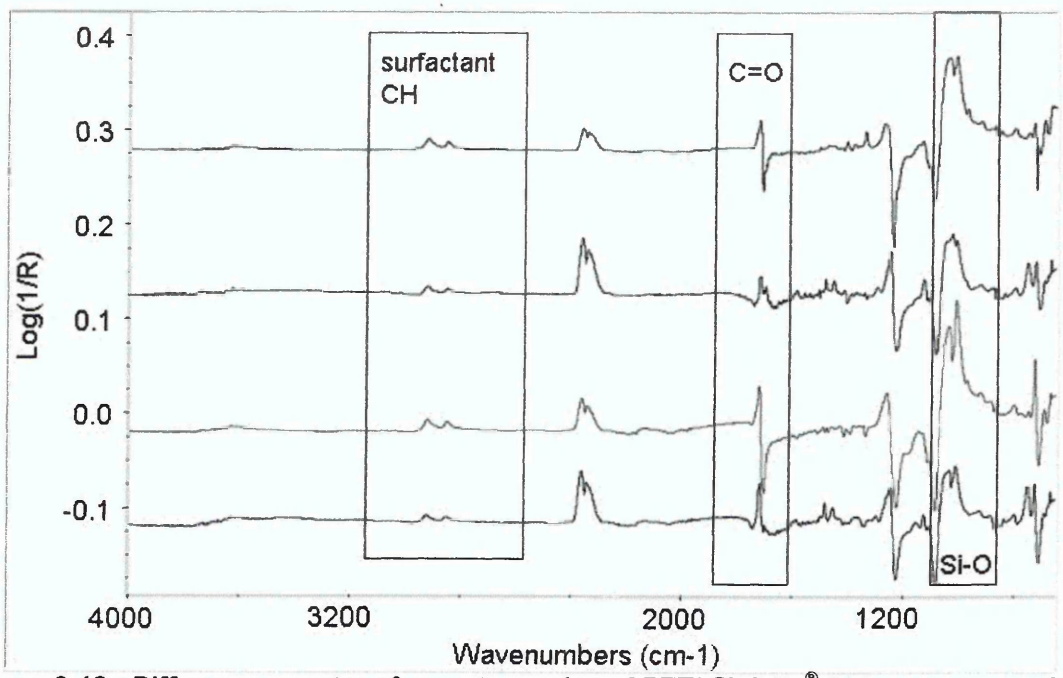

Figure 3-18 Difference spectra of repeat samples of PET/ Cloisite® 20A nanocomposites dried at 90 °C and then 60 °C obtained by subtraction of a pure PET spectrum

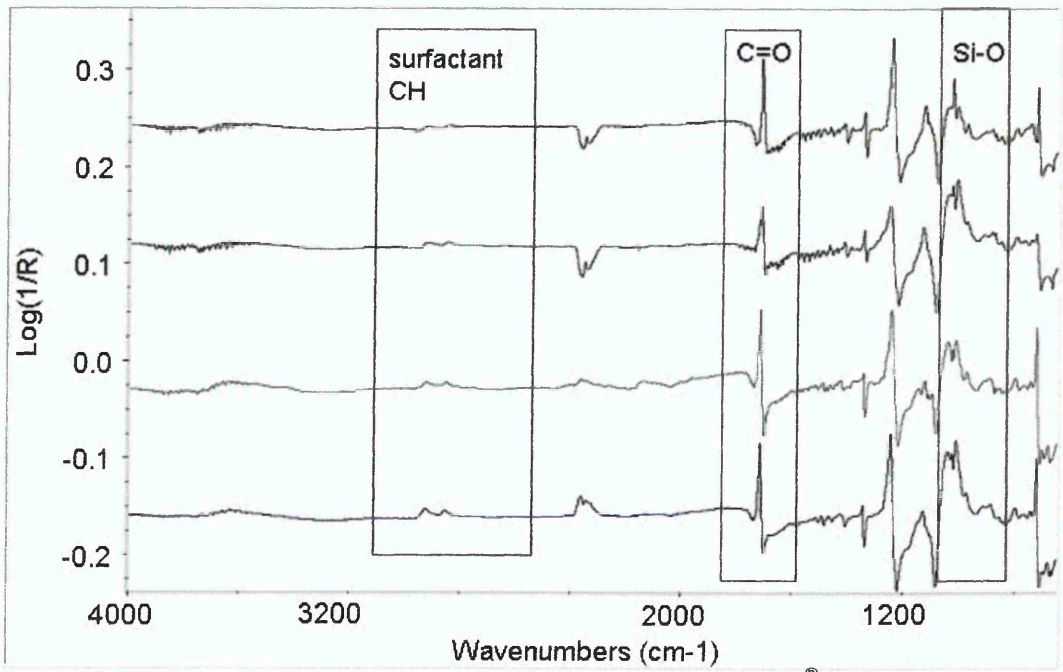

Figure 3-19 Difference spectra of repeat samples of PET/ Cloisite® 20A nanocomposites dried at 160 °C, 90 °C and then 60 °C obtained by subtraction of a pure PET spectrum

When samples are dried at 160°C for an hour the shifts in the carbonyl band is difficult to assess from the subtraction spectra of the nanocomposites. The band does, however, narrow when clay is introduced. As drying at higher temperatures does not only change the morphology of the sample, but also the

solvent residue, the changes observed in the carbonyl band are likely to be due to a combination of the effect of differences in solvent residue at the lower temperatures as well as interaction.of the polymer with the clay.

Changes in the crystallinity of the samples were observed by calculating the crystallinity for each spectrum as described in chapter 3.4.3.

Changes in crystallinity in nanocomposites and pure PET samples dried at three different temperatures are plotted in Figure 3-20. As expected an increase in crystallinity can be observed when samples are dried at higher temperatures similar to the changes noted in the XRD traces of these samples. Values are however similar for the pristine polymer and the nanocomposites. If the clay is inducing crystallinity in PET nanocomposites the effect is too small compared to the variations in crystallinity observed within a PET sample to be identified from these ATR spectra.

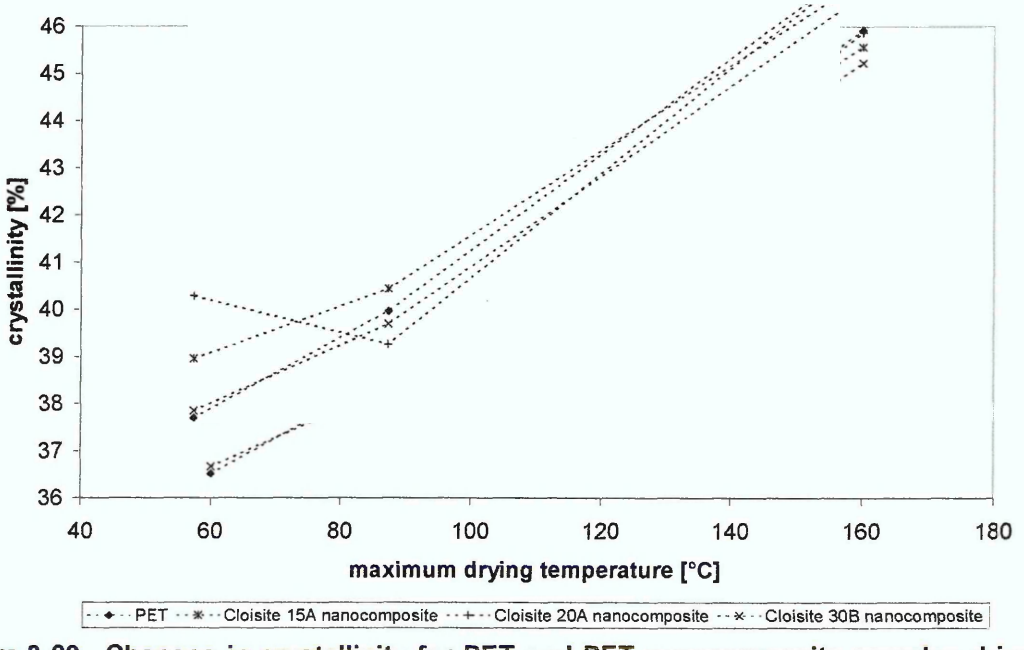

Figure 3-20 Changes in crystallinity for PET and PET nanocomposite samples dried at different temperatures

Longer dispersion times for the clay had also little influence on the surface crystallinity of these films. Changes observed for these samples were similar to those observed for spectra taken from different regions of the same sample.

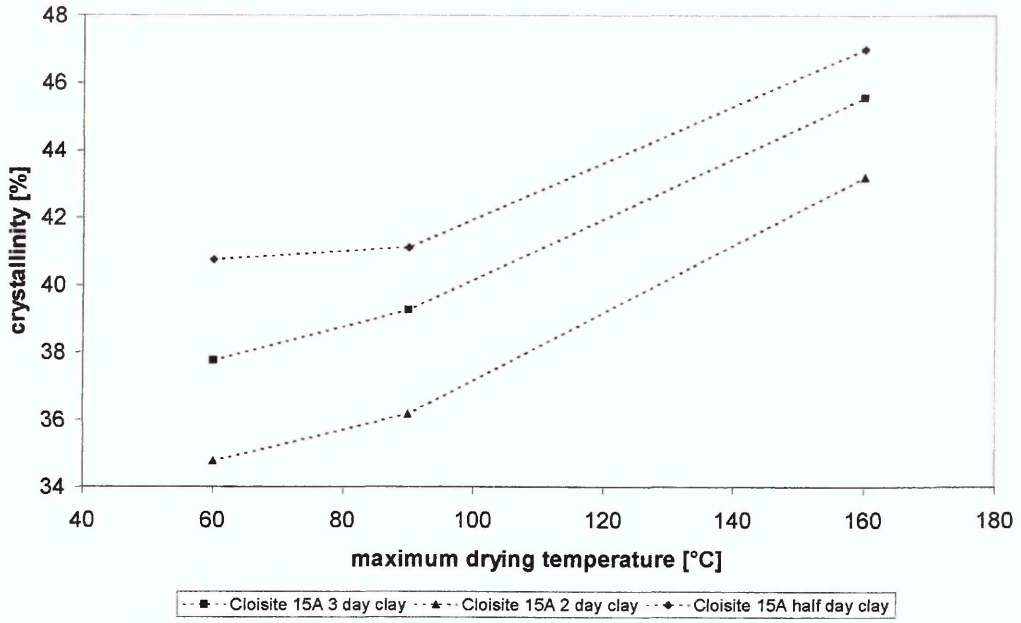

Figure 3-21 Changes in crystallinity for nanocomposites prepared with different clay dispersion times

3.4.5.4.3 Summary

XRD results showed no changes in dispersion for samples dried at temperatures just below and above the glass transition temperature of the pristine polymer. It is, therefore, assumed that heating the sample does not change the mobility of the clay platelets in the polymer matrix enough to cause re-aggregation which has been observed in polypropylene/ clay nanocomposites. Changes can, however, be seen in the peaks arising from the crystalline regions of the PET indicating increased crystallinity in samples heated to higher temperatures. These increases in crystallinity are also confirmed by ATR-FTIR spectroscopic analysis of the samples. Calculations of crystallinity from the ratio of the areas of the $\gamma_w(CH_2)$ bands of PET in trans and gauche conformation showed that crystallinity in E47 samples increased from about 35 % in samples dried at 60 °C to 46 % for samples dried at 160 °C. There were, however, no obvious changes between the crystallinity of the pure polymer and the nanocomposites.

3.4.5.5 Effect of solvent type

The type of solvent used to dissolve the polymer and disperse the clay can affect the structure of the nanocomposites formed by solution intercalation as swelling and dispersion of clay is dependent on the solvent properties. Furthermore, different solvents can induce changes in the morphology of the dried polymer.

3.4.5.5.1 XRD results

Clay films cast from dispersions in o-Chlorophenol (OCP) and 1, 1, 2, 2-tetrachloroethane (TCE) respectively showed a higher apparent d spacing for the samples cast from TCE.

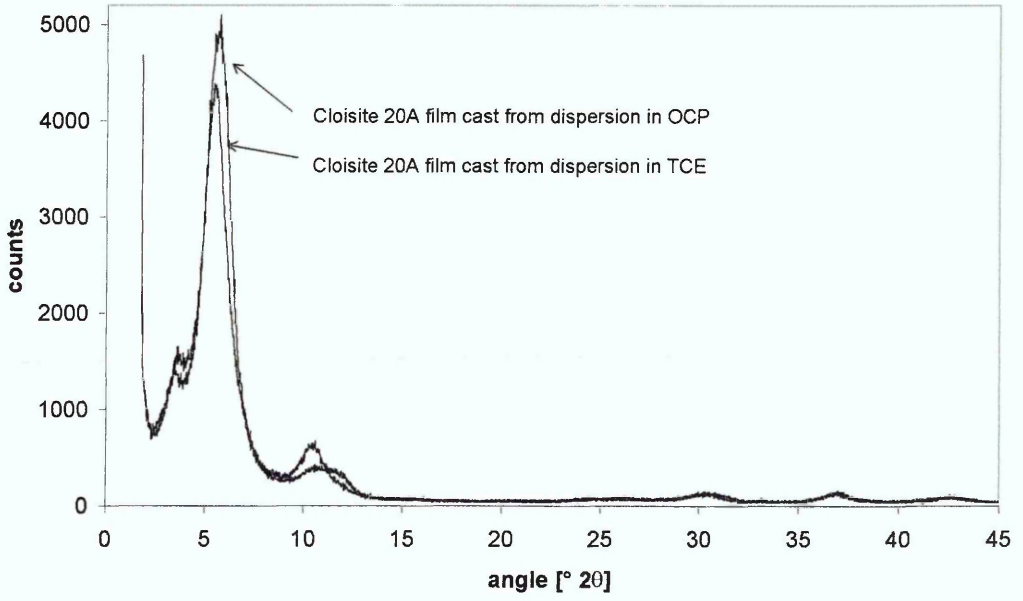

Figure 3-22 XRD traces (Cr tube) for Cloisite® 20A films cast from OCP and TCE

Changes in the d_{001} peaks of films cast from these two solvents were only minor, with TCE samples exhibiting a layer spacing of 23.9 Å and OCP samples having a layer spacing of 23 Å. Based on the errors associated with the analysis these values have to be regarded as being the same, yet repeat measurements for these samples always showed moderately lower angles for the samples cast from TCE. Both these values are slightly below the literature d_{001} spacing for Cloisite® 20A of 24.2 Å when possible errors in the determination of the angle 2θ are disregarded. Measurement of a powder sample of the pristine organoclay under the same conditions resulted in a spacing of 23.2 Å, which is comparable to the values of obtained for the solvent cast films. It is, therefore,

assumed that these solvents are not retained in the galleries when the clay is dried again as no swelling can be observed. The shape of the peak around 11° 2θ which corresponds to the d_{002} reflection indicates a higher order in the film cast from TCE since the peak is much broader in the film cast from OCP. (see Figure 3-22)

Diffraction traces for nanocomposite films prepared by solution intercalation with these two solvents are shown in Figure 3-23 andFigure 3-24. The differences in layer spacing observed in films of the dried clays are also visible in these nanocomposite samples. For samples cast from a solution with higher (10 wt%) polymer concentration the layer spacings are 34.9 Å for the sample cast from TCE and 32.7 Å for the sample cast from OCP. While the difference between these samples appears larger than those observed in the pure clay film traces, these variations are still within the error of the experiment. The nanocomposite samples cast from OCP have a higher crystallinity of the PET as the peaks due to crystalline parts of the polymer have higher intensities and are sharper in the traces for these samples.

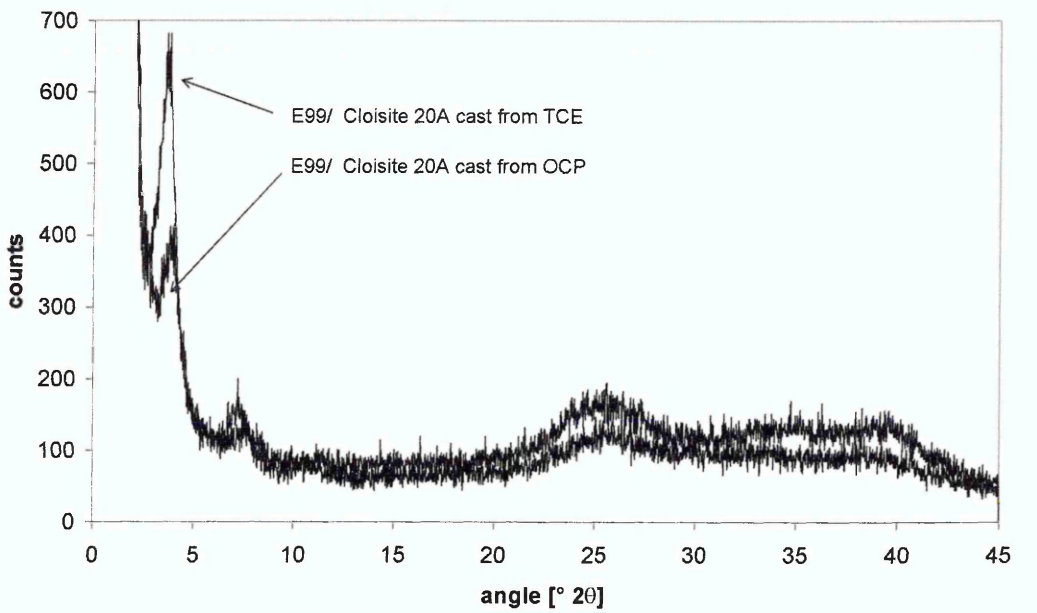

Figure 3-23 XRD traces for 10wt% E99/ 5 wt% Cloisite® 20A nanocomposites cast from different solvents

A reduction in polymer concentration in the solution to 5 wt% (Figure 3-24) reduces the effect of the solvent and the overall spacings observed in these samples are similar. Samples cast from a 5 wt% PET solution in TCE have a layer spacing of 32.5 Å while those cast from OCP have a layer spacing of

31.7 Å. Furthermore, no changes in polymer morphology can be identified from the XRD traces of samples cast from a less concentrated solution.

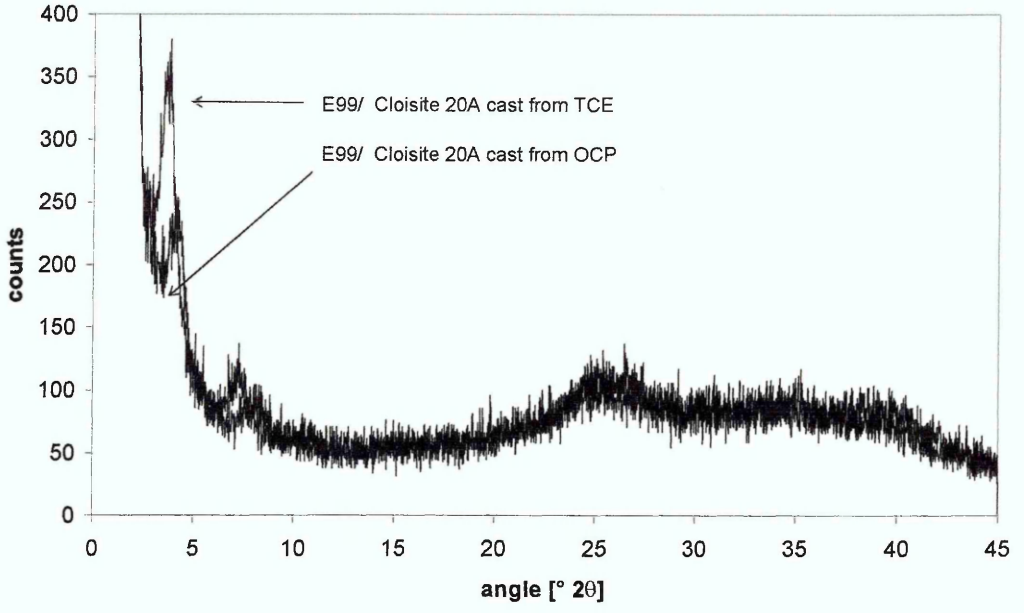

Figure 3-24 XRD traces for 5 wt% E99/ 5 wt% Cloisite® 20A nanocomposites cast from different solvents

3.4.5.5.2 TGA results

Thermal stability of films cast from 1, 1, 2, 2-tetrachloroethane (TCE) and o-chlorophenol (OCP) was relatively similar. TCE desorbed at lower temperatures as its boiling point was lower. Weight loss for the solvent desorption was lower for films cast from TCE, while the weight loss from polymer decomposition as well as the decomposition onset and maximum temperatures remained stable for these nanocomposites.

Clay loading [wt%]	Solvent	weight loss solvent [%]	weight loss PET [%]	Decomposition onset temperature [°C]	Maximum decomposition temperature [°C]
10	OCP	8.4	70.1	350	440
10	TCE	6.6	71.2	350	435
5	TCE	6.5	71.7	340	425

Table 3-14 Summary of TGA data for PET (E99)/ Cloisite® 20A nanocomposites

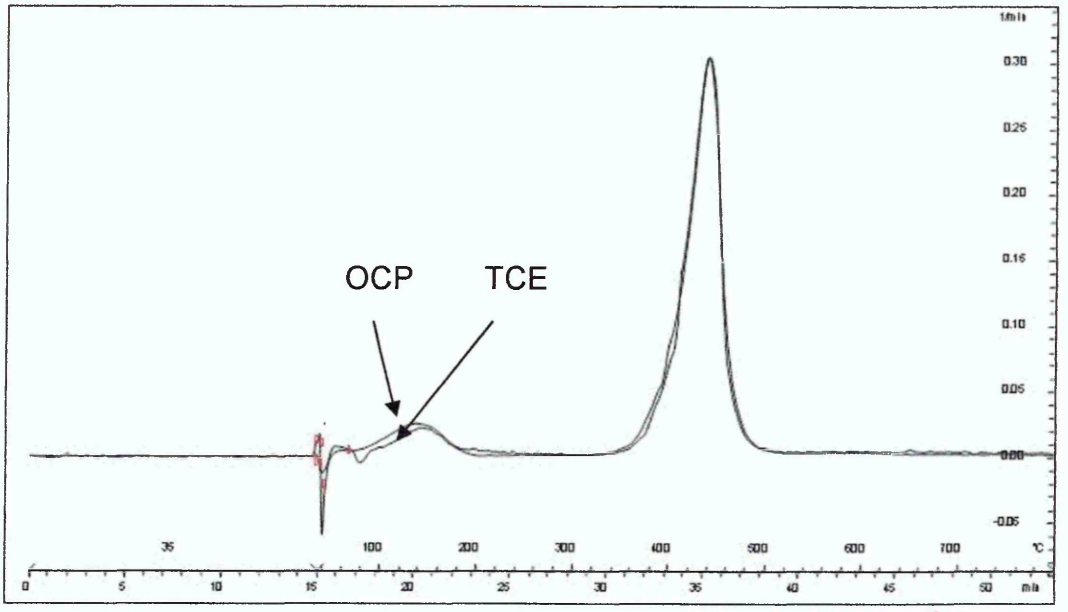

Figure 3-25 Derivative thermograms for E99/ 10 wt% Cloisite® 20A nanocomposite cast from TCE and OCP respectively

3.4.5.5.3 Summary

The two solvents used were found to result in relatively similar swelling of the clay. Films cast from TCE exhibited higher apparent layer spacings for the pure clay as well as for the nanocomposites. The increased swelling in the samples prepared from TCE is likely to be due to the smaller size of the solvent and, therefore, its better ability to diffuse into the clay galleries. The difference between the layer spacings, obtained for nanocomposites cast from these two solvents, was, however, only minor (1-2 Å) and well within the error of the experiment. The different solvents did not lead to any changes in the thermal stability of the samples.

3.4.5.6 Effect of clay loading

Higher clay loadings usually affect the dispersion of the clay in a polymer matrix causing larger areas of intercalated or even agglomerated clay layers.

3.4.5.6.1 XRD results

XRD traces for E99 nanocomposites with 2.5 wt% - 10 wt% of Cloisite® 20A are presented in Figure 3-26. Even at the lowest clay loading the d_{001} peak of the clay can be observed in the diffraction trace. The position of this peak does not shift a great deal with increased clay loading (33.7 Å for the 2.5 wt% sample to 32.3 Å in the 10 wt% sample).This shift is of the same order as the differences within samples cast from the same solution and variations in the determined peak maxima are within the error associated with the determination of these angles. Increased intensity of the d_{001} peak however shows the increase of clay in the sample. It is, therefore, assumed that only a certain amount of PET can intercalate into the galleries without causing exfoliation of the system. At clay loadings up to 10 wt% enough polymer is present to equally intercalate all clay galleries resulting in peaks of similar width and positions for nanocomposites with varying clay loadings.

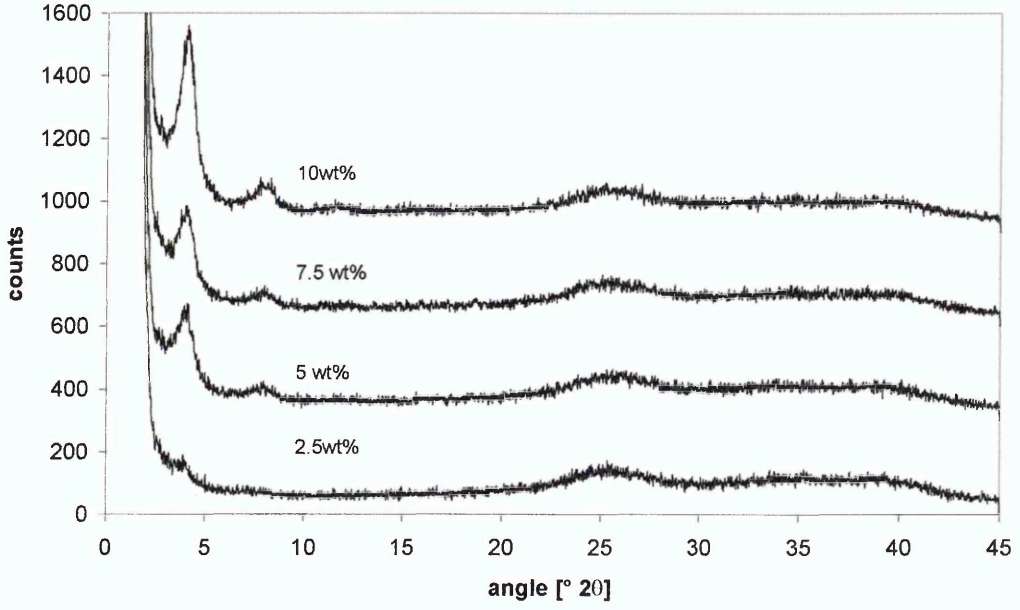

Figure 3-26 XRD traces for E99/ Cloisite® 20A nanocomposites with different clay loadings (traces offset for clarity)

3.4.5.6.2 TGA results

Different clay loadings affected the thermal stability of PET/ organoclay nanocomposites. Generally the weight loss of polymer during the decomposition is decreasing with increasing clay loadings. The onset temperature for the decomposition was reduced by about 20 °C for low clay loadings (2.5 wt% and 5 wt%) and up to 40 °C at higher clay loadings. A summary of the data obtained from TGA for E99/ organoclay nanocomposites is given below.

Clay type	Clay loading [wt%]	weight loss OCP [%]	weight loss PET [%]	Decomposition onset temperature [°C]	Maximum decomposition temperature [°C]
Cloisite® 15A	2.5	6.2	76.8	340	450
	5	5.8	74.8	340	450
	7.5	9.6	70.0	320	440
	10	5.4	73.7	325	450
Cloisite® 20A	2.5	4.1	75.4	340	450
	5	6.7	74.6	340	440
	10	3.1	76.2	335	440
Cloisite® 30B	2.5	5.4	75.4	345	440
	5	4.9	73.0	340	440
	10	6.3	72.6	335	440
Pure E99		6.2	77.8	360	440

Table 3-15 Summary of TGA data for PET (E99)/ organoclay nanocomposites

3.4.5.6.3 Summary

Nanocomposites of PET and organoclays formed by solution intercalation yielded intercalated structures for all clay loadings investigated. Minor increases in layer spacing were observed for samples with 2.5 wt% clay compared to those with higher clay loadings. Higher clay loadings also lead to a decrease in the decomposition onset temperature while the overall weight loss was reduced.

3.4.5.7 Effect of polymer concentration in the solution

Nanocomposites have been prepared from solutions with polymer concentrations of 2.5 wt% to 10 wt% to investigate whether the dispersion of clay is influenced by the concentration of the polymer in the solution which in turn affects the density and viscosity of the solution.

3.4.5.7.1 XRD results

XRD traces for nanocomposites films cast from solutions of different polymer concentrations are shown in Figure 3-27. The layer spacing for these samples remained unchanged. For the lowest polymer concentration stronger clay peaks are observed in the XRD trace. The exact cause of this increased intensity could not be identified. It is most likely due to a combination of the thinner film produced from this solution (all films were cast from the same volume of solution) and sampling of an area with high clay content. Thinner films can result in stronger clay peaks because the relative amount of clay interacting with the clay is higher in a thinner film with the same loading as a thicker film.

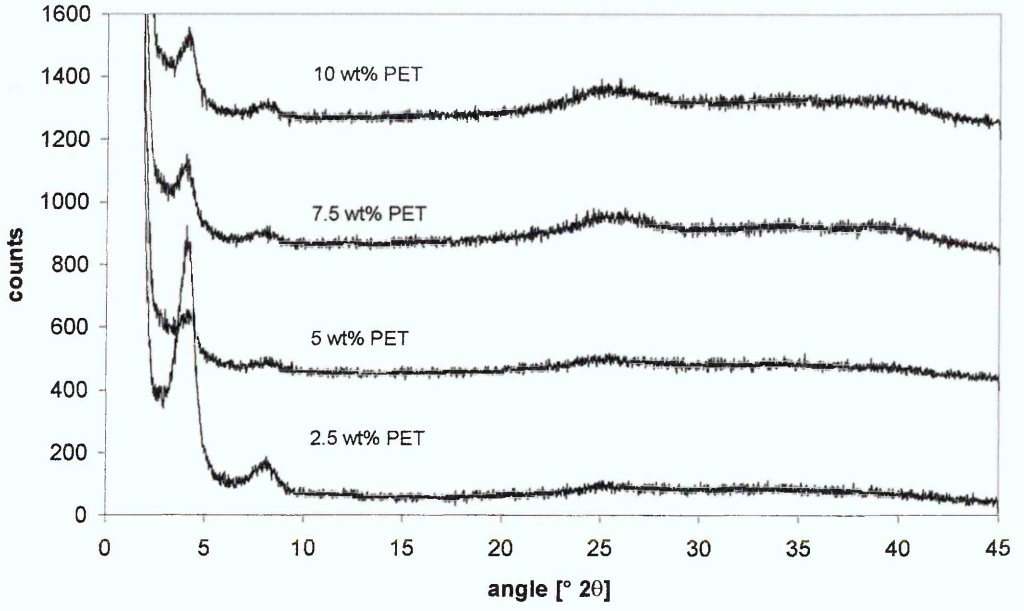

Figure 3-27 XRD traces for E99/ 5 wt% Cloisite® 20A nanocomposites cast from solutions with different polymer concentrations (traces offset for clarity)

3.4.5.7.2 ATR imaging data

Some samples prepared from solutions with different polymer concentration have been analysed by ATR-FTIR imaging. The data has been analysed by creating images of the ratio of the band at 1410 cm^{-1} to the bands at 1370 cm^{-1} and 1340 cm^{-1} respectively. These ratios indicate areas with high amounts of gauche conformers of the ethylene glycol unit when the area of the band at is 1370 cm^{-1} used and areas with high amounts of trans conformers in case of the 1340 cm^{-1} band.

In the pure PET sample, which was cast from a 10wt% polymer solution regions with high concentration of either gauche or trans conformers can be identified (light regions in Figure 3-28 A and B represent high concentrations) The film cast from a 2.5 wt% solution of the nanocomposite is much thinner and appears to have a higher crystallinity as the imaged area is showing predominantly trans conformer. The images of a film cast from a 5 wt% polymer nanocomposite solution show a region of mainly gauche conformer. As only a small area (88 µm x 88 µm) of each sample was imaged it is not entirely clear whether the marked changes in these images are due to overall differences in these films or just local effects of the imaged areas.

Showing variations of the ratio of the band at 1410 cm^{-1} to the trans and gauche band respectively has been chosen for these images rather than the ratio between the trans and gauche band (which gives a measure of the crystallinity as shown in chapter 3.4.3) because variations in sample contact meant that the resulting maps would be a combination of changes in the ratio due to crystallinity changes as well as sample contact changes.

gauche trans

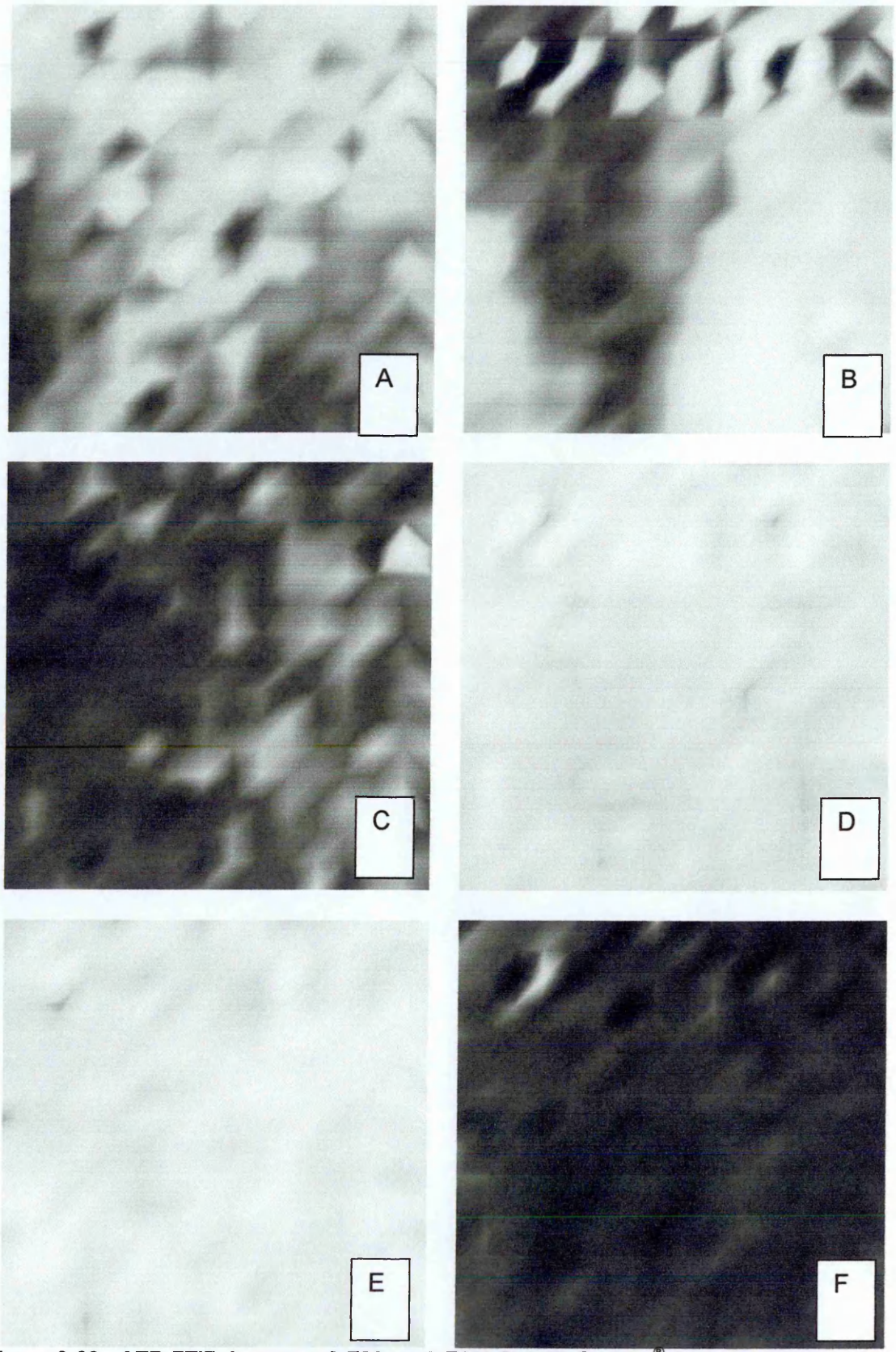

Figure 3-28 ATR-FTIR images of E99 and E99/ 5 wt% Cloisite® 20A nanocomposites (A/B = pure PET, C/D = 2.5 wt% PET solution E/F 5 wt% PET solution)

3.4.5.7.3 Summary

The concentration of the polymer solution did not influence the degree of dispersion of the clay in the polymer. Samples cast from more diluted solutions did however present a higher crystallinity when imaged using ATR-FTIR spectroscopy.

3.4.5.8 Summary of results for the preparation of PET/ organoclay nanocomposites

Nanocomposites of PET and organically modified montmorillonite have been prepared by solution intercalation. The structure of such nanocomposites has been analysed in dependence of several preparation parameters, as well as different PET materials, organic modifiers on the clay and solvents.

Structural analysis by x-ray diffraction revealed that all samples described in this thesis had an intercalated dispersion of the clay layers within the polymer matrix. Higher backgrounds at low angles in the XRD traces of nanocomposites suggest that the samples are very likely to have regions of exfoliated clay layers co-existing with intercalated regions. Further analysis by transmission electron microscopy (TEM) is, however, needed to investigate whether such regions of exfoliated clay layers are present. These results are similar to those published by other groups [3.3, 3.4, 3.6 - 3.8, 3.12] for the preparation of PET/ clay nanocomposites.

The dispersion of the clay in PET did not change with longer stirring times to disperse the clay in the solvent, the temperatures samples were heated to during the drying process or the concentration of the polymer solution during the preparation.

Different degrees of organic modification and changes in the surfactant resulted in changes in the interlayer spacing of the clay when dispersed in PET. Cloisite® 30B exhibited the largest percentage increase in its 001 spacing upon intercalation. The layer spacing of Cloisite® 15A increased least when comparing the organoclay to the nanocomposite but the layer spacing was the largest observed for any of the PET nanocomposites at ~ 44 Å.

The use of a 'bulkier' polymer (E99) resulted in a higher ordering of the clay layers within the nanocomposite. Clay peaks were more intense in these nanocomposites compared to those prepared from E47 indicating that less polymer was moving into the galleries, thereby possibly creating a mainly intercalated nanocomposite.

Layer spacing also appeared to be influenced by the solvent used during the preparation and the weight percentage of clay with respect to the polymer. Nanocomposites prepared from a solution of PET in TCE presented layer spacings that were apparently 1-2 Å larger than those observed for their counterparts prepared from a solution in OCP. Changes of a similar extent were observed for nanocomposites prepared with 2.5 wt% to 10 wt% of clay. Higher spacings were observed for samples with lower clay loadings.

A general overview of the layer spacings obtained for the different PET samples is given in Table 3-16 and Table 3-17. All layer spacings given here are given with the accuracy discussed in chapter 3.4.4.

wt% PET (with respect	wt% clay (with respect to PET)	clay	solvent	stirring time for clay in solvent	D spacing [Å]
10	5	20A	OCP	3 days	34.5
10	5	20A		2 days	32.7
10	5	30B			32.0
10	5	20A		1 day	32.5
10	5	30B			31.7
10	5	20A		1 hour	32.7
10	5	30B			34.4
2.5	5	20A			32.3
5	5				31.7
7.5	5				32.8
10	2.5				33.7
10	5				33.3
10	7.5				32.3
10	10				32.3
5	5		TCE		32.5
10	5				34.9

Table 3-16 Summary of layer spacings for E99/organoclay nanocomposites

wt% clay (with respect to PET)	clay	solvent	stirring time for clay in solvent	D spacing [Å]
2.5	15A	o-chlorophenol	3 days	44.4
2.5	20A			42.6
5				40.2
2.5	30B			36.5
5	20A		1 day	31.2
5			directly all	31.3

Table 3-17 Summary of layer spacings for E47/organoclay nanocomposites

Incorporating clay into PET on a nanoscale dispersion did not improve the thermal stability of these samples when measurements were performed in an inert atmosphere. The thermogravimetric analysis of the nanocomposites under nitrogen showed that polymer degradation set in at temperatures 20 – 40 °C lower than in the neat polymer while the maximum decomposition temperature remained stable at 440 ± 5 °C for E99 samples and 450 ± 5 °C for E47. It is possible that the presence of the clay alters the degradation mechanism when oxygen is present, however no data was collected for these nanocomposites in normal atmosphere.

Crystallinity in the polymer and the nanocomposites was shown to increase with increasing temperatures. These changes could be monitored in the XRD traces and in ATR-FTIR spectra. No obvious differences were observed between polymer and nanocomposite samples where the levels of crystallinity are concerned but the methods used have too low spatial resolution to investigate whether clay is locally inducing crystallinity.

3.5 Poly (vinyl alcohol)/ montmorillonite nanocomposites

3.5.1 Introduction

Poly (vinyl alcohol) easily adsorbs onto clays [3.22]. When clay is dispersed in a solution of poly (vinyl alcohol) it is kept in colloidal dispersion by the steric interactions of the polymer chains and the clay layers. Gentle removal of solvent from such solutions creates a gel with clay layers embedded in it. [3.23, 3.24] When the gels are dried further to form polymer films some re-aggregation of the clay layers can be observed. The extent of this re-ordering was found to depend on the drying conditions. Interaction between PVOH and clay is likely to occur by hydrogen bonding of the hydroxyl groups of the polymer to the oxygen atoms of the clay layers [3.24].

When PVOH is absorbed onto sodium montmorillonite a basal spacing of 30 Å can be observed for the maximal amount that can be absorbed. Calcium montmorillonites swell less but unlike the sodium montmorillonites these clays show increased swelling at raised temperatures [3.25]. The equilibrium sorption level depends almost linearly on the starting concentration of polymer in the solution. Low molecular weight PVOH is preferentially sorbed onto clay layers and higher sorption levels can be observed with an increase in the degree of hydrolysation of the polymer. [3.25, 3.26]

PVOH gels are often formed by co-polymerising PVOH with metal alkoxides. Murakani [3.27] examined the performance of PVOH/ TEOS hybrids as column packaging materials for the separation of aqueous solutions. Measurements showed similar excluded molecular weight for the hybrid and the neat polymer but higher elution volumes, improved separation and better stability under pressure for the hybrid materials.

PVOH and silica components show excellent compatibility on the nanoscale. While the addition of silica reduces the solubility and swelling in water composites with high silica contents are often stiff and brittle [3.28, 3.29]. XRD patterns showed a broadening of the d_{101} peak of PVOH with increasing silica content indicating that crystal growth is inhibited in the presence of silica [3.30].

Chang et al. [3.30] investigated the dispersion of various sodium and organo-clays in poly (vinyl alcohol) by solution intercalation. They found that sodium

clays disperse more readily in poly (vinyl alcohol) than organophilic clays. XRD analysis of such samples showed no peaks for either sodium montmorillonite and sodium saponite hybrids and TEM confirmed the formation of a nanocomposite material. Using organoclays an intercalated structure was formed, which had a higher basal spacing than the pure organoclay. Thermogravimetric analysis of these materials gave slightly higher onset temperatures for the degradation of the nanocomposites than the neat polymer.

Incorporation of graphite oxide into PVOH at low weight percentages led to an intercalated composite. At graphite loadings above 20 wt% intercalated and non-intercalated graphite oxide peaks could be observed in the XRD traces. Glass transition in such composites was increased while mass loss decreased with increasing graphite oxide contents [3.31].

Using solution intercalation of aqueous PVOH solution and Na^+ MMT Strawhecker and Manias [3.32, 3.33] prepared composites over a wide range of compositions. At lower clay contents no clay peaks could be observed in the XRD traces but higher background levels indicate the presence of exfoliated and possibly intercalated layers with layer spacings above 5 nm. TEM of these samples confirmed the presence of a mixture of intercalated and exfoliated regions. Basal spacings and their distribution were found to decrease systematically with increasing clay loadings in samples with high clay content (from 40 to 90 wt%).

Polyvinyl alcohol/ clay nanocomposite formation from solution is a kinetically dictated process with some aggregation of the colloidal clay layers occurring during the drying process while other layers are trapped in a dispersed form in the drying sample.

DSC and XRD measurements confirmed the formation of a new crystalline phase with a higher melting point in nanocomposites. This new phase was found to increase with increasing clay levels showing that its formation is induced by the presence of clay [3.32].

To further investigate the crystallisation behaviour of PVOH/ clay hybrids Strawhecker and Manias [3.33] used atomic force microscopy (AFM). Such measurements showed that crystallisation is predominantly initiated in the final

drying stages. Humidity was having a major effect on the crystallisation with the polymer becoming glassy at low ambient humidities, while water plasticisation allowed for slow cold crystallisation at high humidity. The AFM measurements revealed that crystallisation is initiated in the immediate vicinity of the clay layers and crystals remaining smaller than those in the bulk polymer.

Wang et al. [3.34] investigated PVOH/ MMT spun fibres. They found that the spinning process was hampered by larger clay loadings and only fibres with clay contents up to 2 wt% could be obtained. These fibres showed similar thermal decomposition behaviour to the unfilled polymer. The elongation at break was reduced in nanocomposite samples but strength and initial modulus showed improvements.

Poly (vinyl alcohol)/ clay nanocomposites can also be prepared by in-situ polymerisation of vinyl acetate in alkyl ammonium clays followed by hydrolysation of the acetate groups [3.35]. Nanocomposites prepared in this manner showed no d_{001} peaks for the clay at loadings between 2 and 10 wt% and had slightly improved thermal stability. Measurement of the molecular weight of the polymer after extraction from the clay revealed significantly lower molecular weights than the bulk material.

Carrado et al. [3.26] used poly (vinyl alcohol) with various molecular weights between 9,000 and 146,000 for the hydrothermal crystallisation of synthetic hectorite. The molecular weight had only little effect on the basal spacing of the clay or the amount of polymer that was incorporated between the clay layers.

3.5.2 Preparation

3.5.2.1 Preparation of charged reduced Li+ MCBP

Li^+ MCBP was prepared by exchanging Na^+ MCBP. 75 g of Na^+ MCBP were dispersed in 2 L of de-ionised water by magnetic stirring for 24 hours. 500 mL of a 0.33 M LiCl solution were then added and the dispersion stirred for a further three days. The dispersion was then centrifuged and the clay re-dispersed in de-ionised water before adding further LiCl solution. This process was repeated once more. After the third mixing with LiCl solution the clay was washed by repeatedly dispersing it in de-ionised water and centrifugation to remove any lithium sorbed onto the outer surfaces. Samples were then allowed to dry at room temperature for two weeks.

The temperatures used for the heat treatment to produce charge reduced clays were chosen with reference to those published by Madejova et al. [3.36]. Before heat treatment samples were ground to a powder. 3 g of clay was spread out on a tray and kept at the desired temperature for 24 h. The temperatures used to produce charge reduced clays were 110 °C, 135 °C, 160 °C and 210 °C respectively. Using these temperatures Madejova et al. [3.36] observed an increase in structural Li by a factor of 6.7 between the samples heated to 110 °C and 210 °C, which resulted in a reduction of the exchangeable calcium by a similar factor in their clays.

3.5.2.2 Preparation of nanocomposites

PVOH nanocomposites were prepared by solution intercalation. For the samples prepared from sodium clays the desired amount of clay was dispersed in 20 mL deionised water by stirring with a magnetic stirrer. After two hours PVOH was added to the dispersion and the flasks transferred to an oven heated to 90 °C. The total amount of solids for each sample was 1 g. Samples were heated at 90 °C for four hours to allow for complete dissolution of the PVOH. To ensure good mixing of the clay and polymer the solutions were stirred for 30 – 45 minutes at room temperature before films of 2 mL solution were cast onto microscope slides. These were dried in an oven for two days at 40 °C before being analysed by XRD and TGA.

Nanocomposites were prepared using poly (vinyl alcohol) granules provided by Sigma-Aldrich with two different average molecular weight ranges as described in chapter 3.3.2.2. Nanocomposites of the lithium clays were prepared in a similar manner. As the charged reduced clays dispersed less readily in water these clays were allowed to stir over night before the addition of polymer.

3.5.3 Results and discussion

3.5.3.1 Poly (vinyl alcohol)/ Na+ Cloisite® nanocomposites

3.5.3.1.1 Effect of clay levels

Poly (vinyl alcohol)/ Na^+ Cloisite® composites were prepared with a variety of compositions ranging from 0.5 wt% clay to 97.5 wt% clay. Films of these materials were transparent up to clay loadings of 45 wt%. At higher clay loadings films became brittle and delaminated from the microscope slides they were cast onto.

3.5.3.1.1.1 XRD results

Judging from their x-ray diffraction traces composites of poly (vinyl alcohol) and Na^+ Cloisite® can be divided into four groups. At clay loadings up to 10 wt% no clay peaks can be observed in the diffraction traces of these materials. Increased backgrounds at low angles, however, indicate the presence of some crystal structures. The clay layers in these composites are either intercalated with a d_{001} spacing larger than 70 Å or are fully exfoliated. It is likely that a mixture of both structures is present but XRD on its own gives insufficient information to elucidate the structure of the nanocomposites in this instance. The traces for these nanocomposites are presented in Figure 3-29. The peak in at 29.8° 2θ is the d_{101} reflection of PVOH. This peak remains unchanged by the presence of clay in the samples.

A further increase of the clay loading results in the formation of a predominantly intercalated structure. Composites with clay loadings between 20 and 40 wt% have a wide distribution of d spacings. The XRD traces of these samples show very broad peaks indicating layer spacings between 10 Å and 47 Å. The intensity of this broad peak, caused by a wide range of layer spacings present in the samples, is increasing with increasing clay content in the sample. The

secondary peak, which can be observed around 14.6 ° 2θ, is due to the d_{002} reflection caused by reflections from sodium ions and polymer molecules in the galleries.

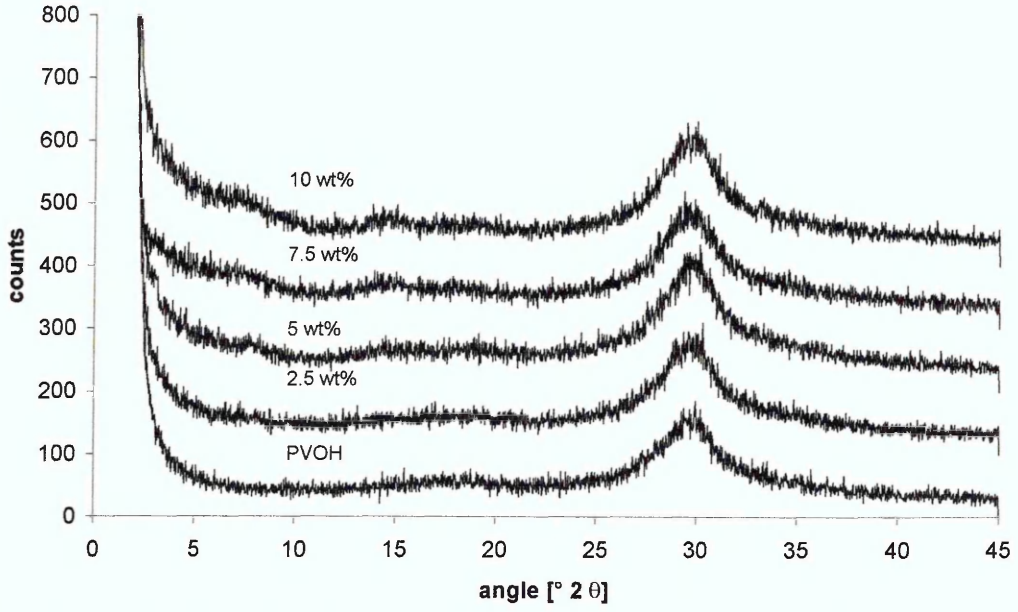

Figure 3-29 XRD traces (Cr tube) for low molecular weight PVOH/ Na^+ Cloisite® nanocomposites at low clay contents (traces offset for clarity)

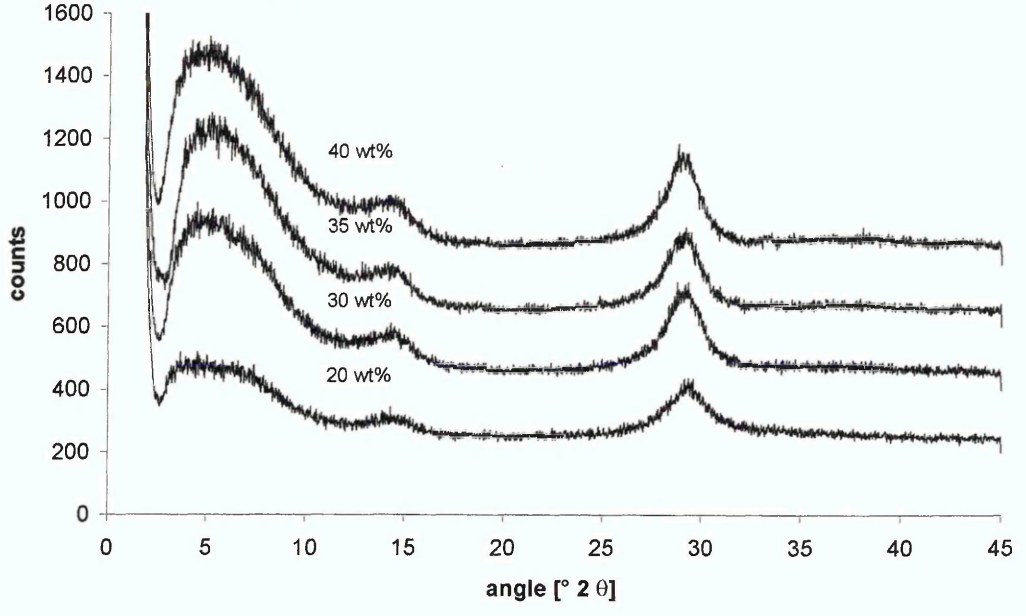

Figure 3-30 XRD traces (Cr tube) for low molecular weight PVOH/ Na^+ Cloisite® nanocomposites at intermediate clay contents (traces offset for clarity)

Further increase of the clay loading in the polymer results in formation of a more uniform dispersion of the clay platelets. PVOH/ Na^+ Cloisite® composites with layered silicate contents of 45 wt% to 75 wt% have an intercalated structure.

The spacing between the clay layers reduces linearly with increasing clay content as less and less polymer is available for intercalation into the clay layers and layers can re-aggregate more easily during the drying of the films. In Figure 3-31 the layer spacing for these nanocomposites is plotted against the clay content in the sample.

At clay loadings above 75 wt% the amount of polymer present was not enough to expand all layers of the clay. The XRD traces (see Figure 3-32) of showed a doublet peak for these samples indicating two layers intercalated with two different polymer amounts or indeed a combination of layers with and without polymer chains present. With increasing clay loading the peak for the higher d spacing was found to decrease, while the secondary peak, which had a spacing similar to that observed in films of Na^+ Cloisite® cast from aqueous solution, increased. The position of the peak resulting from higher spacing of the layers (around 17 Å) did not vary with higher clay loadings, while the spacing of the layers with less or no polymer present decreased with increasing clay content.

Data published for such nanocomposites by Strawhecker and Manias [3.32] showed similar results to those presented in this thesis for the higher clay loading samples. At intermediate clay loadings they reported higher spacings and better dispersions of the clay layers within the PVOH matrix. This is likely to be due to the fact that their samples were sonicated to improve dispersion while samples presented here were mixed by magnetic stirring.

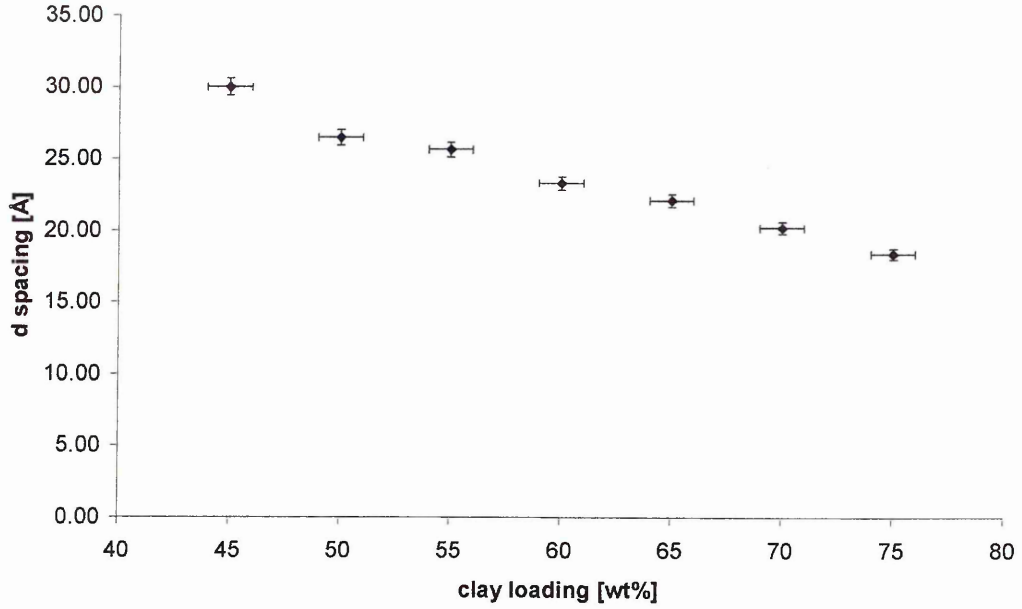

Figure 3-31 Layer spacing for low molecular weight PVOH/ Na^+ Cloisite® composites at higher clay loadings

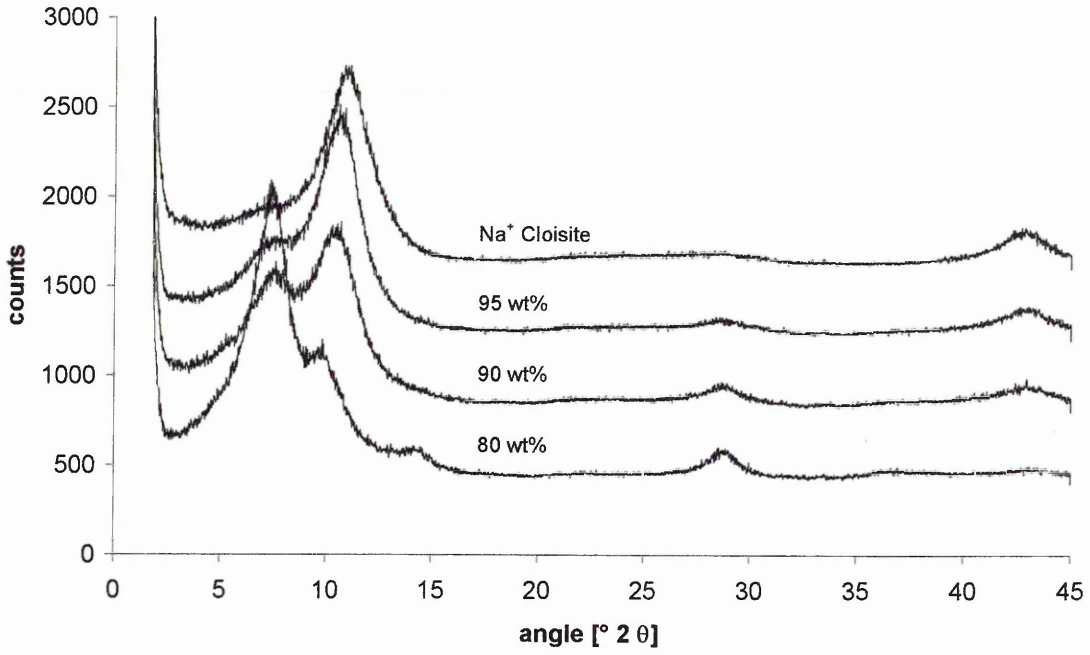

Figure 3-32 XRD traces (Cr tube) for low molecular weight PVOH/ Na^+ Cloisite® composites at high clay contents (traces offset for clarity)

3.5.3.1.1.2 TGA results

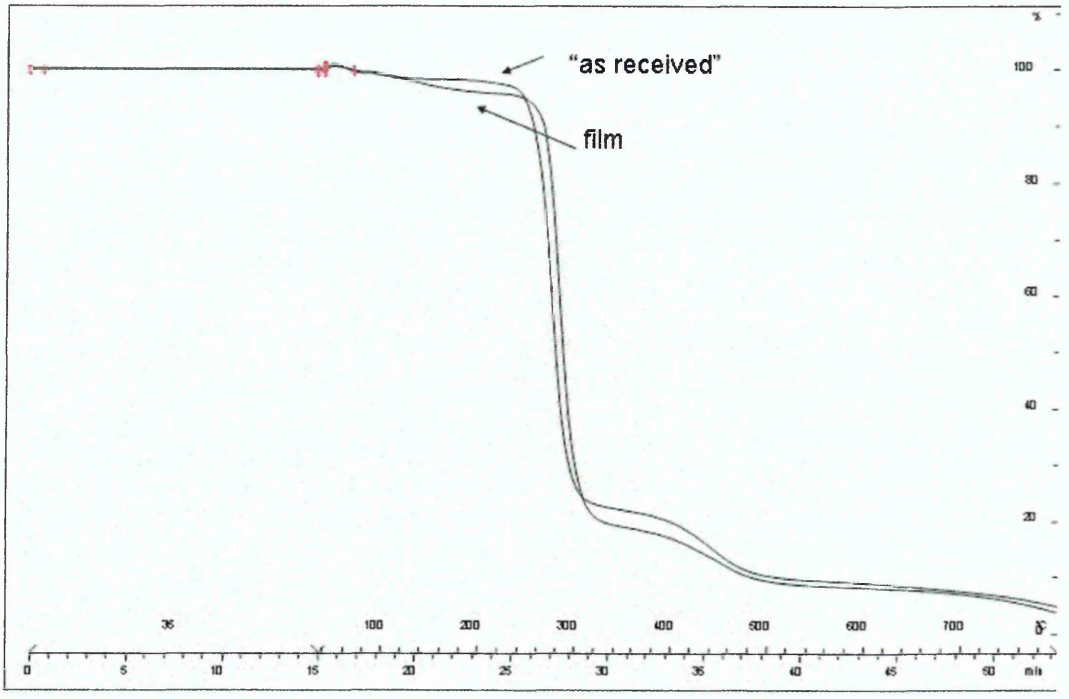

Figure 3-33 Thermograms for PVOH 'as received' and a PVOH film cast from aqueous solution

Films cast from aqueous solution started decomposing at a lower temperature than the neat polymer out of the tub. This decrease in thermal stability is caused by higher amounts of water present in the film as samples could not be fully dried in lab conditions. The PVOH/ clay (nano-) composite samples will therefore be compared to the data obtained from polymer films produced under the same conditions as the PVOH/ clay films.

Introduction of clay raises the temperature at which the decomposition of PVOH starts by 10 - 20 °C to 200 °C in samples with clay contents up to 50 wt%. At higher clay loadings the onset of PVOH decomposition occurs at even higher temperatures of 220 - 240 °C. Such increased temperatures of polymer decomposition in nanocomposites were also found by Chang et al. [3.30] who observed that onset temperatures increased by 10 - 15 °C in their nano-composites compared to the neat polymer.

PVOH decomposition occurs as a two step process with decomposition maxima around 275 °C and 450 °C. Carrado et al [3.24] reported temperatures of 276 °C and 380°C for the decomposition of Ca+ - MMT – PVOH samples, while

Nakane et al. [3.28] observed decomposition maxima at 375 °C and 450°C in PVOH/ silica nanocomposites.

For the samples investigated in this thesis a two stage process has been observed for nanocomposites with clay loadings up to 40 wt%. For samples with clay loadings of 40 – 65 wt% the decomposition at lower temperatures was split into two events with decomposition maxima around 275 °C and 315 °C. Composites with more than 70 wt% clay content again had a two stage decomposition process though the lower temperature decomposition now occurred at around 290 °C. It is therefore assumed that the increase in the maximum decomposition temperature of the first stage of the decomposition process is due to polymer being absorbed onto the clay sheets where they are stabilised by their interactions with the silicate surface. Derivative thermograms for these samples are presented in Figure 3-34 - Figure 3-36.

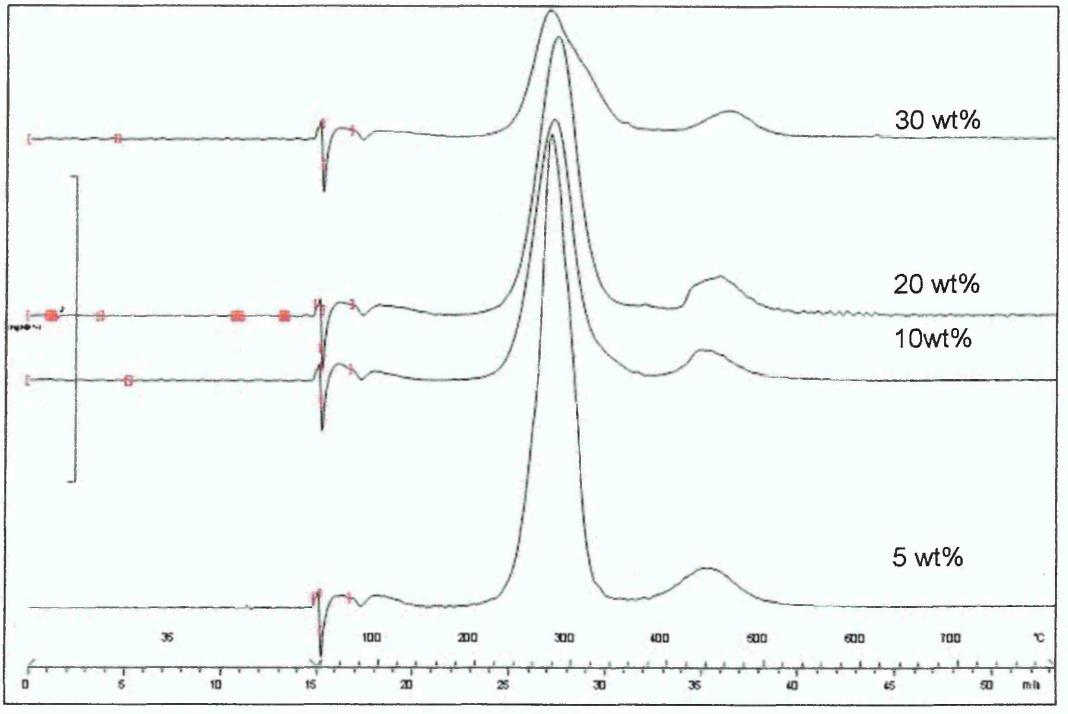

Figure 3-34 Derivative thermograms for PVOH/ Na^+ Cloisite® nanocomposites with low clay loadings

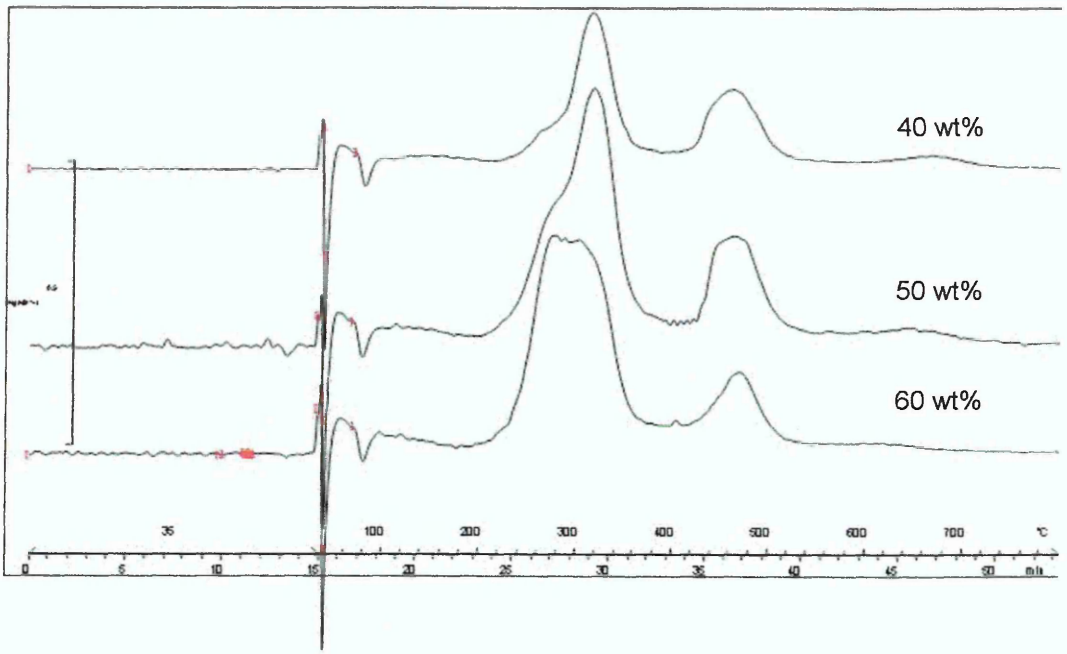

Figure 3-35 Derivative thermograms for PVOH/ Na^+ Cloisite® nanocomposites with intermediate clay loadings

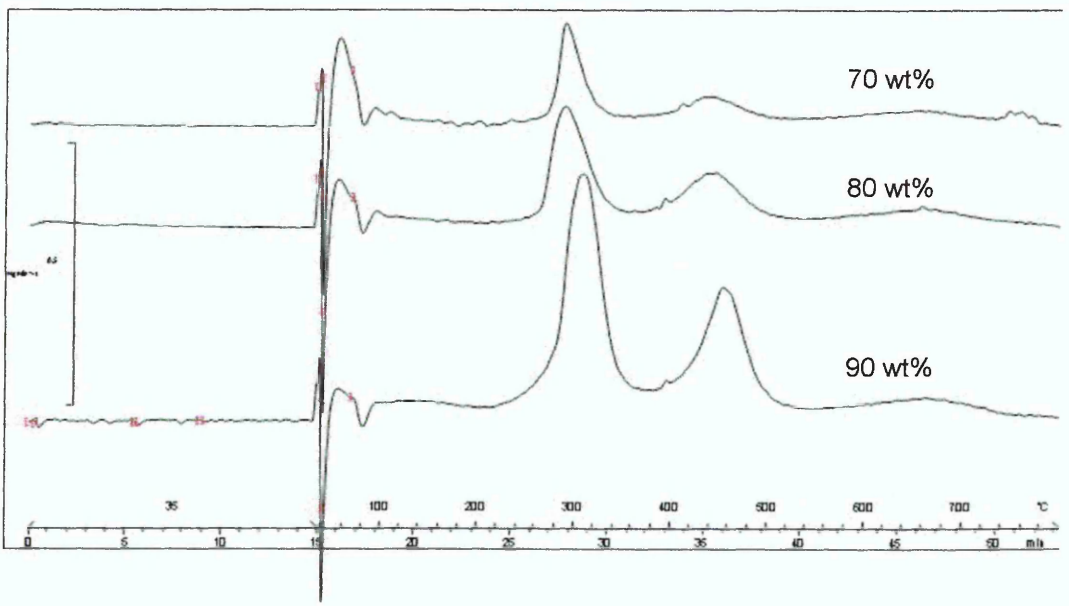

Figure 3-36 Derivative thermograms for PVOH/ Na^+ Cloisite® nanocomposites with high clay loadings

The maximum decomposition temperatures for the first weight loss stage did not change significantly with increasing clay loadings within each of the groups mentioned above. The second stage process did however occur at higher temperatures of 450 – 470 °C for clay loadings between 20 wt% and 70 wt%, while maximum decomposition for this stage occurred around 440 °C for samples with clay loadings lower than 20 wt% or higher than 70 wt%.

The onset temperature of the second decomposition stage increased steadily with increasing clay contents from 365 °C in a film of the neat polymer to 415 °C in samples with 65 wt%. At clay loadings between 75 wt% and 92.5 wt% this temperature decreased again and no weight loss peak was visible in samples of 95 wt% clay and above.

Weight loss during the first decomposition stage decreased with increasing clay loadings. The weight loss during the second decomposition stage on the other hand remained constant at ~11% for clay loadings up to 75 wt%, after which it decreased steadily with further increases in the clay content of the sample. As a result the overall weight loss also decreased with increasing clay loadings.

A weight loss of 5 – 10 wt% around 100 °C in all samples indicated the presence of sorbed water. The amount of water present in each film varied without any obvious trends with regard to clay loading. Samples prepared on the same day did, however, have similar levels of water leading to the assumption that the ambient conditions during the drying of the sample influence the water level in the final films.

3.5.3.1.1.3 Analysis of ATR – FTIR spectra

3.5.3.1.1.3.1 ATR – FTIR spectra

These spectra were taken from pieces of sample that had been delaminated from the microscope slides the films were cast on. Measurements were performed using the Golden gate™ single reflection ATR-FTIR accessory.

Casting films from aqueous solution resulted in materials with lower crystallinity than the original pellets. Furthermore, films retained a higher amount of water after drying than that present in the "as received" sample. The spectra presented in Figure 3-37 show spectra for a PVOH film and the material "as

received" and Figure 3-38 shows typical variations observed between a film of PVOH and a film of PVOH nanocomposite.

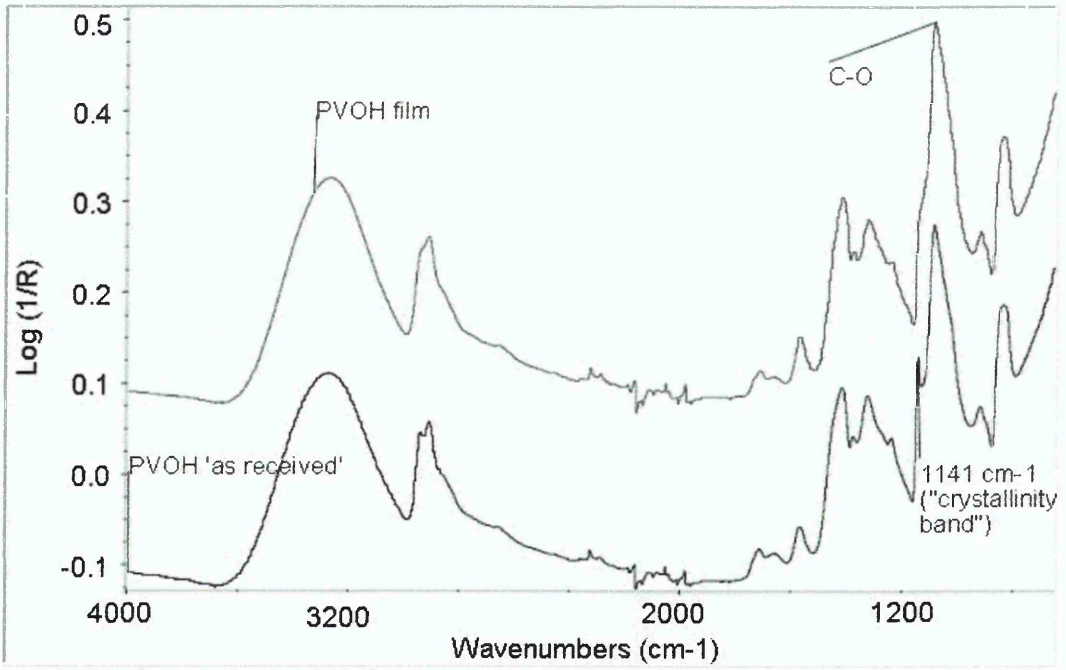

Figure 3-37 Comparison of PVOH "as received" and a film cast from aqueous solution

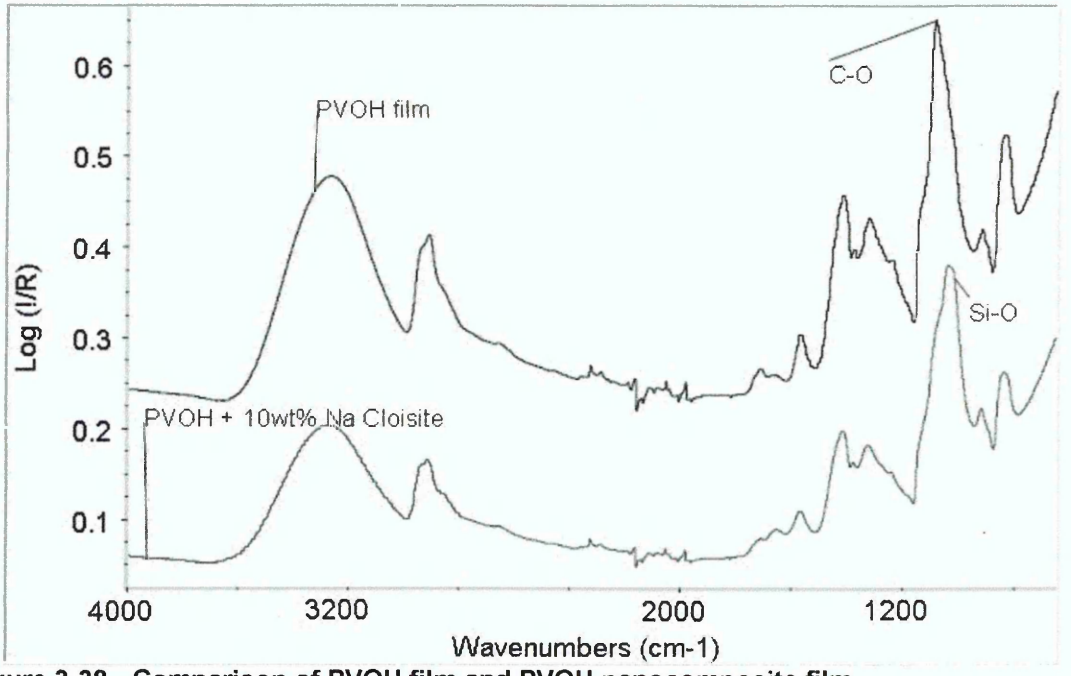

Figure 3-38 Comparison of PVOH film and PVOH nanocomposite film

Direct comparison of the intensities in each spectrum proved difficult, as differences in sample contact with the ATR crystal were quite significant. For samples with up to 40 wt% clay content crystallinity and clay content can, however, be compared by ratioing the area of the band at 1141 cm^{-1} against the

area of the ν(C-O) band for qualitative assessment of the crystallinity and ratioing the area of the ν(Si-O) band against the ν(C-O) for a qualitative measure of the amount of clay in the sample. For these samples crystallinity remains similar in films cast from aqueous solution. The amount of clay detectable from the Si-O stretching vibration is increasing steadily with increasing clay content in the samples. A plot of this data is shown in Figure 3-39.

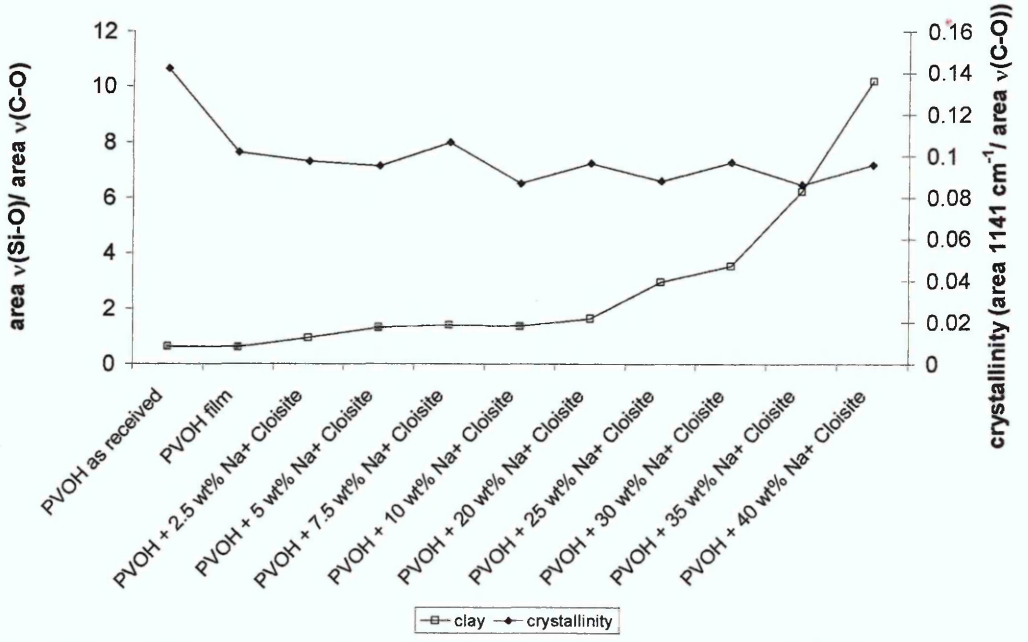

Figure 3-39 Changes in crystallinity and clay level detectable by ATR-FTIR

At higher clay levels this integration is no longer suitable as the spectrum becomes dominated by the ν(Si-O) and δ(metal-OH) vibrations of the clay. With increasing clay levels a shift of the ν(Si-O) to lower frequencies, as shown in Figure 3-40, can be observed which is due to the reduction in polymer/ clay interactions as the amount of polymer sorbed onto the clay is reduced.

This analysis, however, also showed that samples were not very homogeneous and studying only the outer surface of a film can produce contradictory results. Since clay aggregation is a kinetically controlled process, the dispersion of clay in the polymer matrix depends strongly on the drying conditions. Furthermore, aggregation and settling of clay platelets at the interface between the microscope slide and film is more likely to occur with decreasing polymer/ clay ratios. Examples for such spectra are shown in Figure 3-41 presenting a small shift of the ν(Si-O) band to lower wavenumbers with higher clay content.

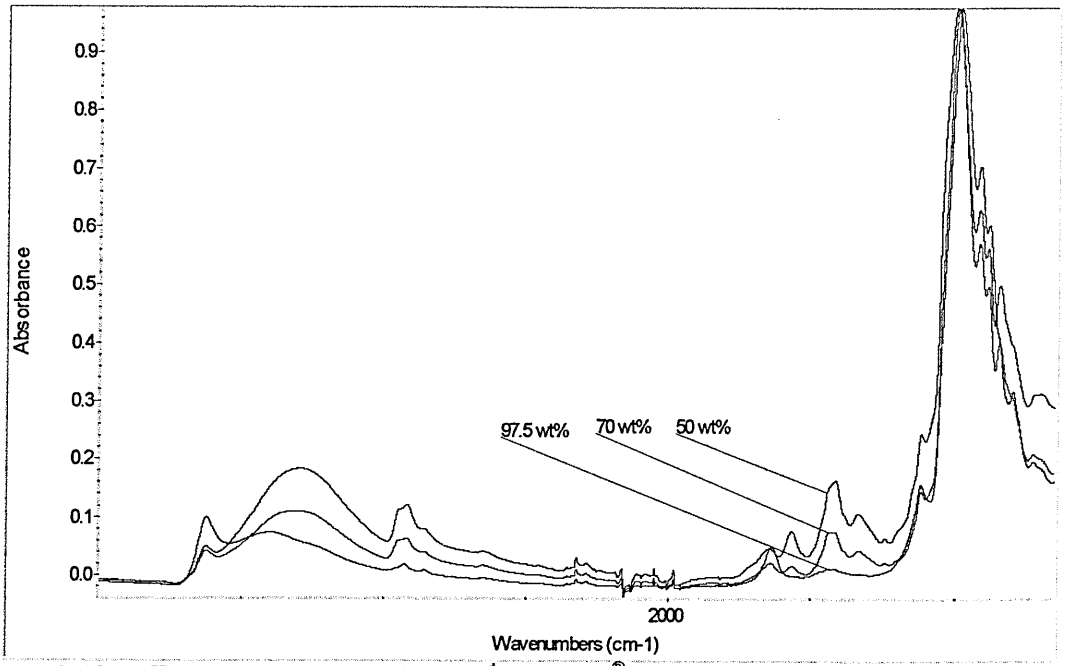

Figure 3-40 ATR spectra of PVOH/ Na^+ Cloisite® composites with clay loadings of 50 wt%, 70 wt% and 97.5 wt%

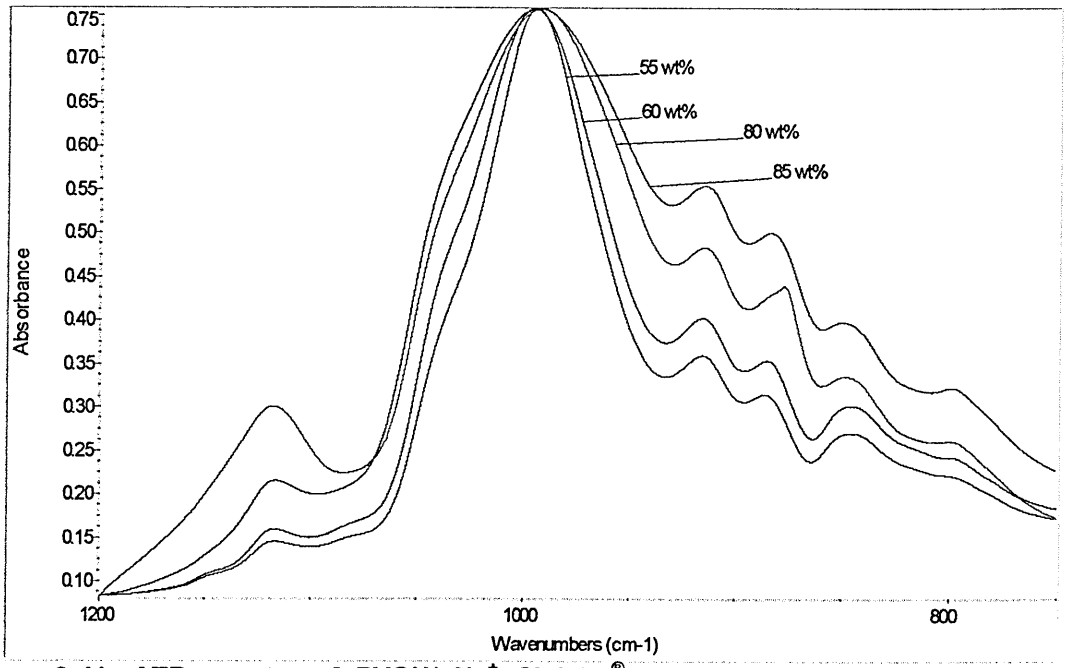

Figure 3-41 ATR spectra of PVOH/ Na^+ Cloisite® composites with clay loadings of 55 wt%, 60 wt%, 80 wt% and 85 wt%

3.5.3.1.1.3.2 ATR – FTIR imaging

ATR images have been recorded of nanocomposite samples with various amounts of clay. Sample contact was judged by the intensity of the ν(C-O) band in the spectra and was found to vary over the imaged area for both the pure polymer and nanocomposite samples. Examples of images indicating the differences in sample contact are shown in Figure 3-42. The dark areas indicate low intensities while light areas have high intensities. These differences in sample contact are most likely due to surface roughness of the sample.

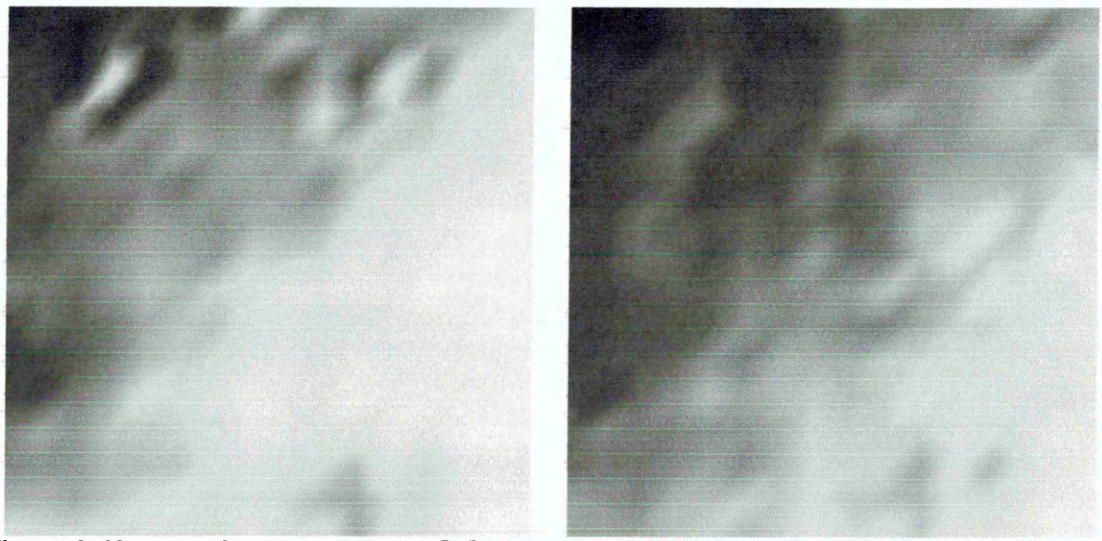

Figure 3-42 sample contact (area C-O) for pure PVOH sample on the left and a 5 wt% PVOH nanocomposite on the right

To adjust for differences in sample contact the bands of interest in the following spectral area were ratioed against the intensity of the ν(C-O). The relative crystallinities of the samples were found to be very similar. The images shown in Figure 3-43 represent the ratio of the crystallinity sensitive band at 1141 cm^{-1} to the ν(C-O) band. The scale for these images is 0.1 - 0.15 with lighter areas indicating higher crystallinity. Crystallinity was relatively constant in the imaged areas of each of these samples.

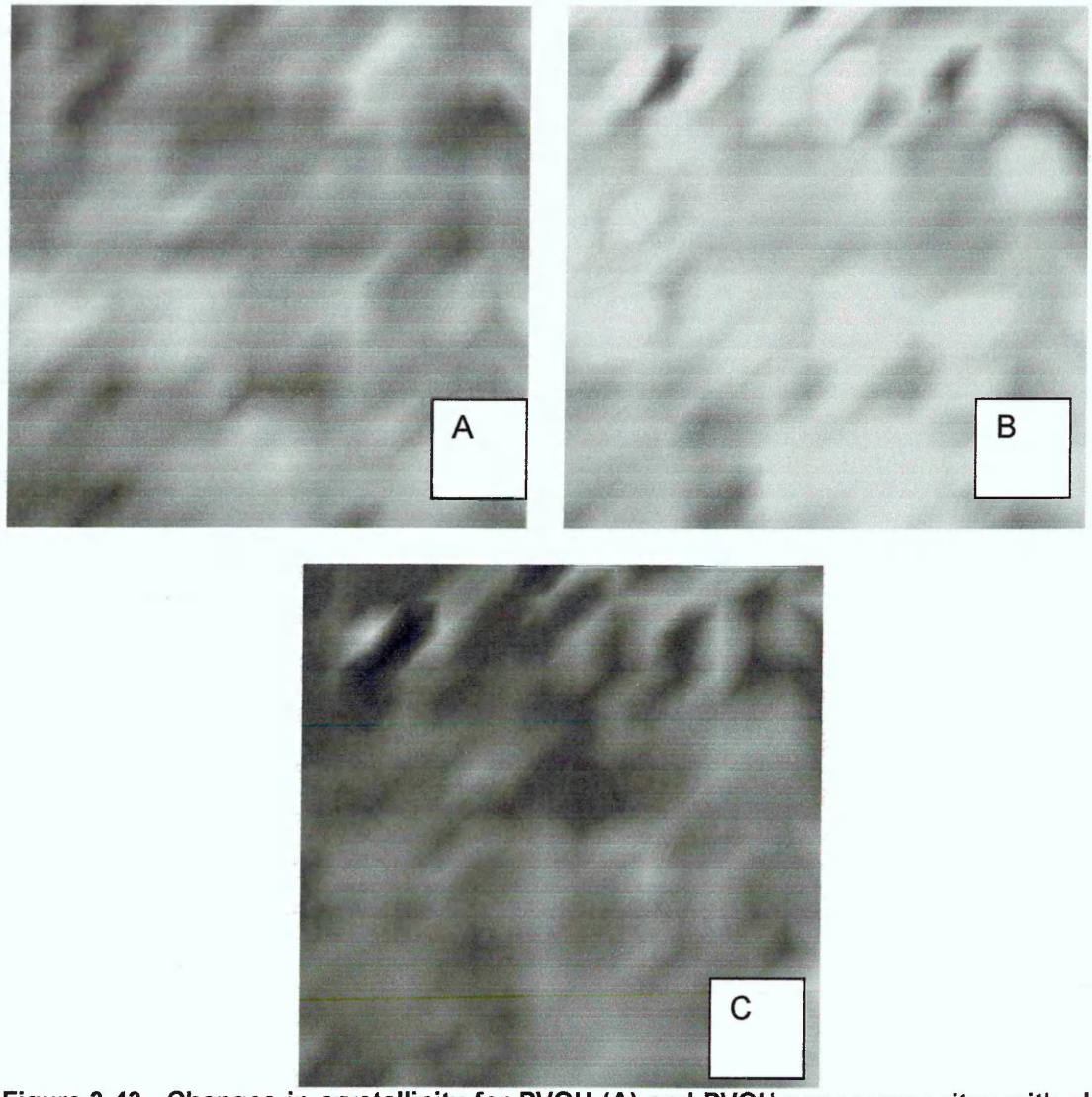

Figure 3-43 Changes in crystallinity for PVOH (A) and PVOH nanocomposites with clay loadings of 1 wt% (B) and 5 wt% (C)

To investigate whether residual water in the films is associated with the clay, the ν(OH)/ν(C-O) ratio and ν(Si-O)/ν(C-O) ratio were compared. The first ratio was, however, found to be influenced strongly by the contribution of the polymer to the intensity of the ν(OH) vibration, making it impossible to monitor residual water in the film from a simple ratio of bands. Regions of low intensity for the first ratio show high intensities for the "clay ratio" and vice versa. The intensity of the clay level ratio is increasing with increasing clay content (see Figure 3-44 B, D and E)

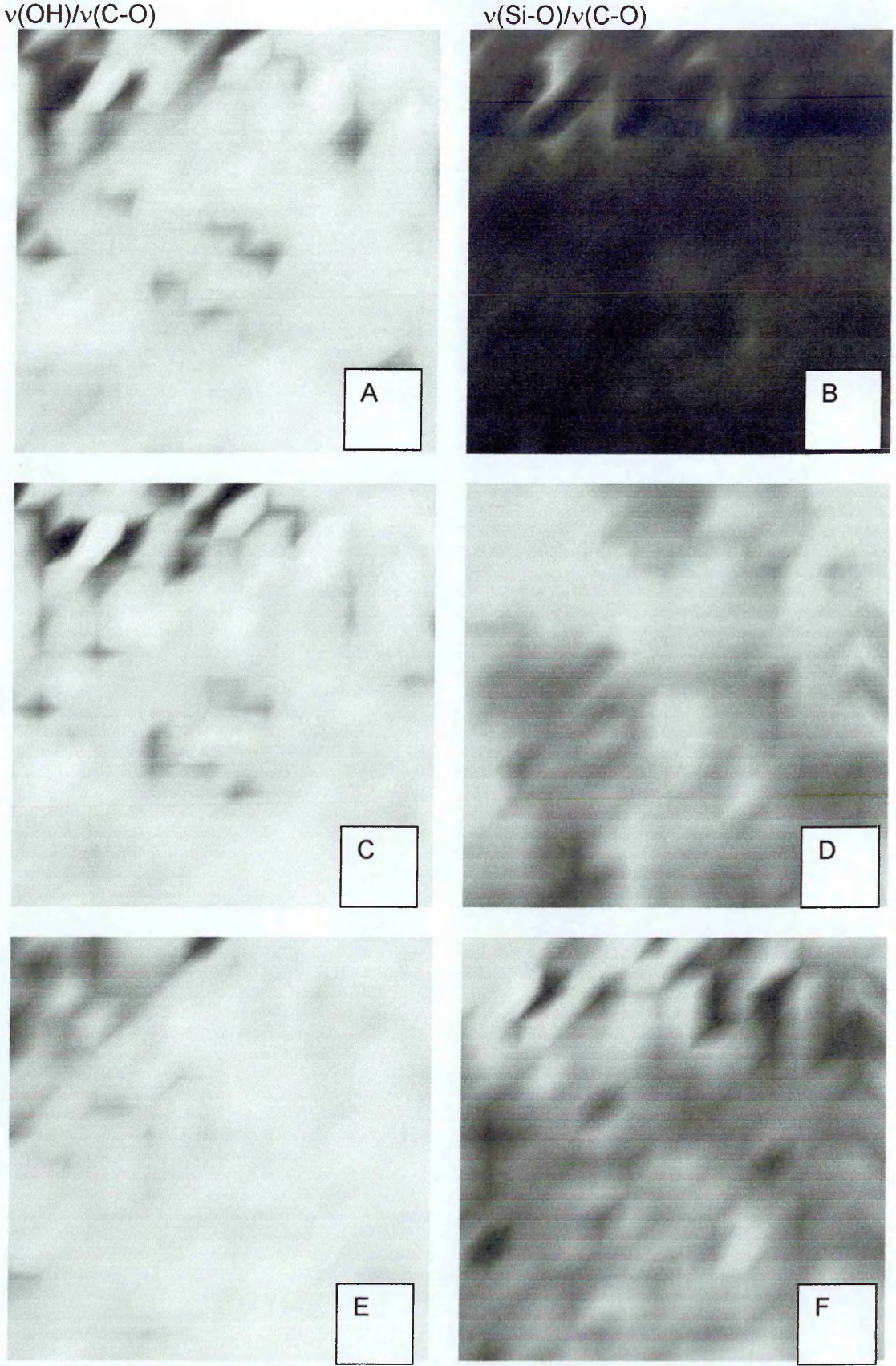

Figure 3-44 **Images of relative intensity of the ν(OH) and ν(Si-O) bands in PVOH nanocomposites with different clay loadings (A/B = 0.5 wt% clay, C/D = 2.5 wt% clay, E/F = 5 wt% clay)**

3.5.3.1.1.4 Summary

PVOH/ MMT Nanocomposites and PVOH/ composites prepared by solution intercalation of Na^+ Cloisite® were investigated. The composites could be divided into four groups with different structural characteristics. At low clay loadings, up to 10 wt%, no clay peaks could be identified in the XRD traces, though the background was raised at low angles 2θ. These samples are assumed to be exfoliated nanocomposites. Increasing the clay loading to values of 20 wt% - 40 wt% decreased the dispersion of the clay in the polymer. These samples have a broad peak in the XRD diffraction trace which corresponds to d spacings of 10 – 47 Å. A further increase in clay loading was found to result in a more ordered intercalated structure in which the spacing between the layers was reduced with increasing loadings up to 75 wt%. For samples containing more than 80 wt% clay a doublet peak was present in the XRD trace arising from clay layers intercalated by PVOH chains and those without PVOH chains present.

Thermal degradation of PVOH under a nitrogen atmosphere occurs as a two stage process. Based on their decomposition behaviour the PVOH composites can be divided into three groups. At lower clay contents (below 40 wt%) the decomposition is comparable to that of the neat polymer though degradation started at temperatures 10 – 20 °C higher than the neat polymer. At intermediate clay levels (40 – 60 wt%) the first decomposition stage occurred as a two step process with decomposition maxima at 275 °C and 315 °C respectively. At higher clay loadings this decomposition maximum is found at 290 °C. The onset temperature for this stage was raised by 10 – 20 °C for clay loadings up to 50 wt% and 40 – 60°C at higher clay loadings.

The onset of the second decomposition stage was delayed by the introduction of clay. The onset temperature rose steadily with increasing clay loadings up to 65 wt% after which it dropped down again.

The weight loss during the first stage decreased with increasing clay content, while the weight loss of the second stage remained virtually unaffected up to 75 wt% clay after which it also decreased.

ATR spectra of the films revealed no significant changes in crystallinity for samples up to 40 wt%. At higher clay loadings this analysis could not be applied any more because the clay bands become dominant compared to the PVOH bands. The intensity of the ν(Si-O) band was found to increase in these samples with increasing clay loadings.

ATR imaging of some of these samples showed a minor increase in crystallinity in samples with 5 wt% clay compared to 1 wt% clay and the neat polymer. As no such variations were observed from the general ATR spectra this increase is likely to be a local feature that could not be observed by "normal" ATR measurements. Furthermore, increased intensities of the ν(Si-O) band could be observed with increasing clay loadings.

3.5.3.1.2 Effect of organic contamination

Further analysis of the clay used to prepare these nanocomposites showed that some of the batch of clay used was contaminated with organic surfactant. As organically modified clay is known to show poorer dispersion in poly (vinyl alcohol) [3.28], experiments were repeated using a new batch of Na^+ Cloisite® to check whether dispersion of the clay and the thermal stability of the resulting nanocomposites had been influenced by this contamination.

3.5.3.1.2.1 XRD results

At clay loadings up to 10 wt% no differences could be observed in the XRD traces of these new samples compared to the observations made previously.

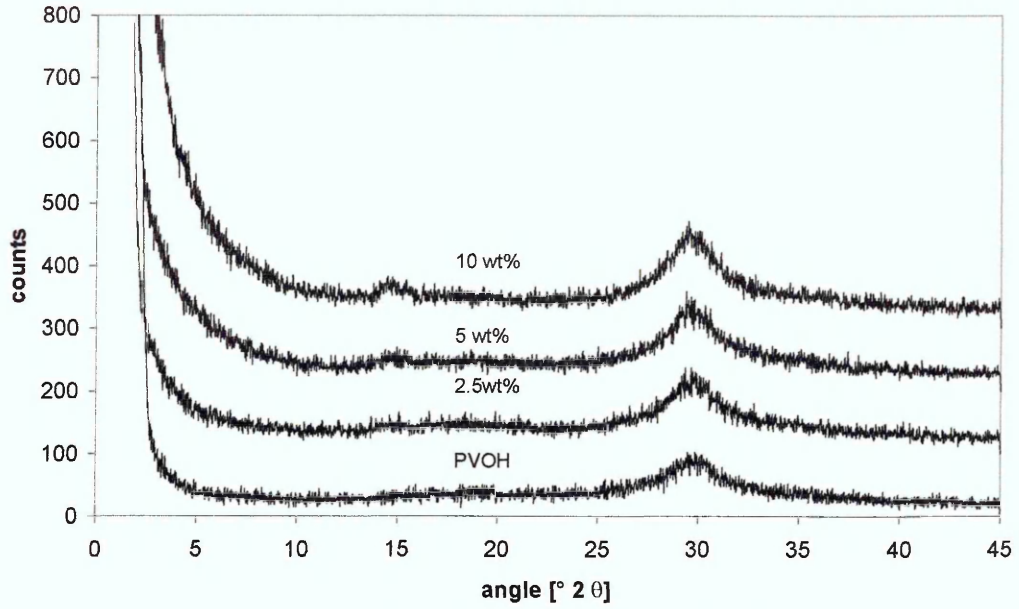

Figure 3-45 XRD traces (Cr tube) for PVOH/ clean Na^+ Cloisite® nanocomposites at low clay contents (traces are offset for clarity)

Even though some differences could be observed in the traces for higher clay loadings (see Figure 3-46) these differences were within the variation observed for samples cast from the same solution. It is, therefore, unlikely that the contamination found in the batch of clay from which the first samples were prepared has had any significant influence on the intercalation of PVOH into Na^+ Cloisite®.

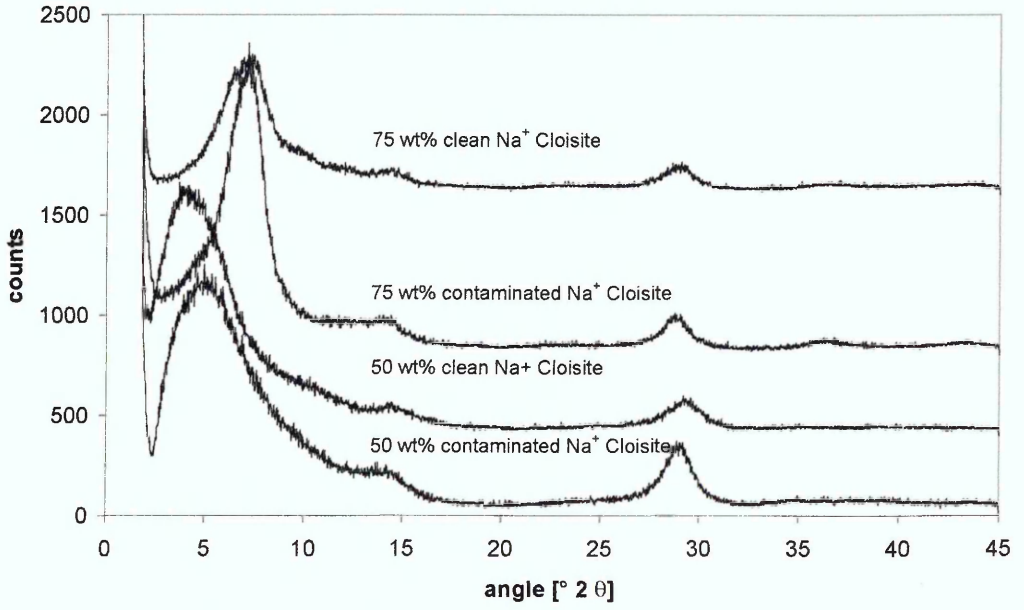

Figure 3-46 Comparison between low molecular weight PVOH/ Na^+ Cloisite® composites prepared from clean and contaminated clay (traces are offset for clarity)

3.5.3.1.2.2 TGA results

The results of the thermogravimetric analysis for nanocomposites prepared with the new, clean, batch of Na^+ Cloisite® were comparable to those obtained for the contaminated clay. As fewer samples were prepared from this material it is however impossible to state whether the ranges observed of similar decomposition behaviour observed in the contaminated clay samples are identical for these clays.

The ratio between the first and second decomposition stage is decreased in these nanocomposites compared to the material prepared from contaminated clay as the second decomposition stage has a weight loss of 14 - 17 % compared to the 11 % weight loss in the contaminated clay samples. Yet the overall weight loss is the same in the clean and contaminated samples.

3.5.3.1.2.3 Summary

Even though organically modified clays have been reported to exhibit worse dispersion behaviour when intercalated into PVOH no such observations could be made when comparing samples prepared from a sodium clay with some organic contamination and a new batch of the same clay that did not have this contamination. Data obtained by XRD and TGA did not show any significant differences for these two clays. It is therefore assumed that the contamination was too small to influence the formation of PVOH/ MMT nanocomposites.

3.5.3.1.3 Effect of molecular weight of the poly (vinyl alcohol)

High molecular weight poly (vinyl alcohol) is expected to show different intercalation patterns when interacting with clay than the polymer of lower molecular weight as its solubility in water is reduced. Furthermore, larger chains are less mobile and intercalation is likely to proceed at a slower rate.

The solutions prepared from this material showed much higher viscosity than the low molecular weight samples. Especially at medium to high clay loadings samples were more gel-like than solutions.

3.5.3.1.3.1 XRD results

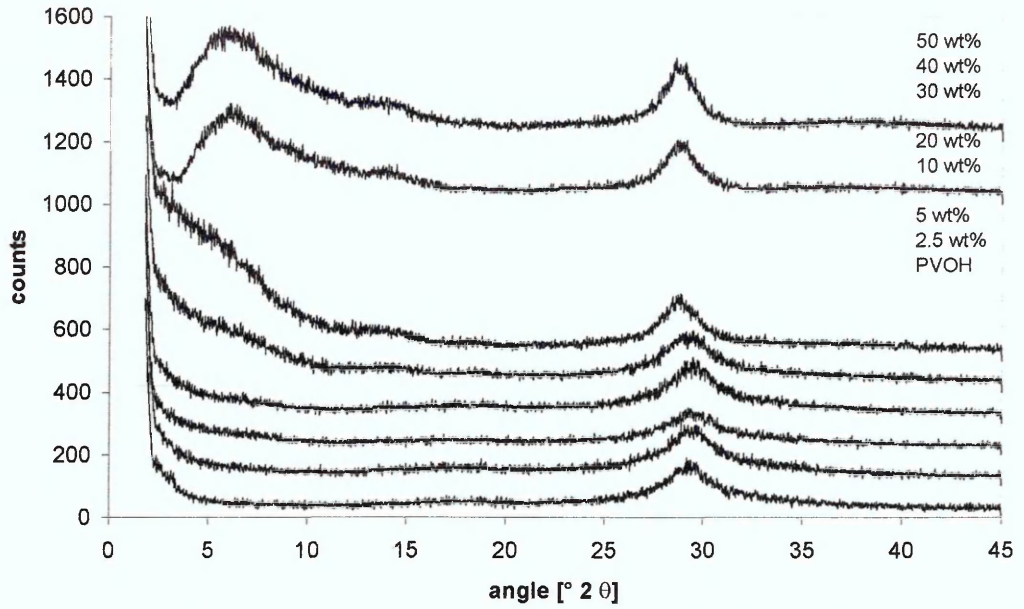

Figure 3-47 XRD patterns (Cr tube) for high molecular weight PVOH/ contaminated Na^+ Cloisite® nanocomposites (traces are offset for clarity)

The traces for the nanocomposites prepared with contaminated Na^+ Cloisite® show no clay peaks for samples below 20 wt% clay loading. For the 2.5 wt% and 5 wt% only a small increase in the background gives indication of the presence of clay in the samples. At 20 and 30 wt% the traces have a significant slope at low angles indicating a wide range of larger clay spacings. Further increase of the clay loading results in a broad distribution of layer spacings ranging between 12 Å and 36 Å.

Similar to the low molecular weight samples no significant differences could be observed in the dispersion from the XRD traces for samples prepared with clean or contaminated clay at low clay loadings. Figure 3-48 shows a comparison of x-ray traces for higher clay contents of samples prepared from clean and contaminated Na^+ Cloisite®. Here some differences could be observed between samples prepared from the different clays. It is, however, not entirely clear how representative the traces shown below are, as differences can be observed within samples cast from the same solution.

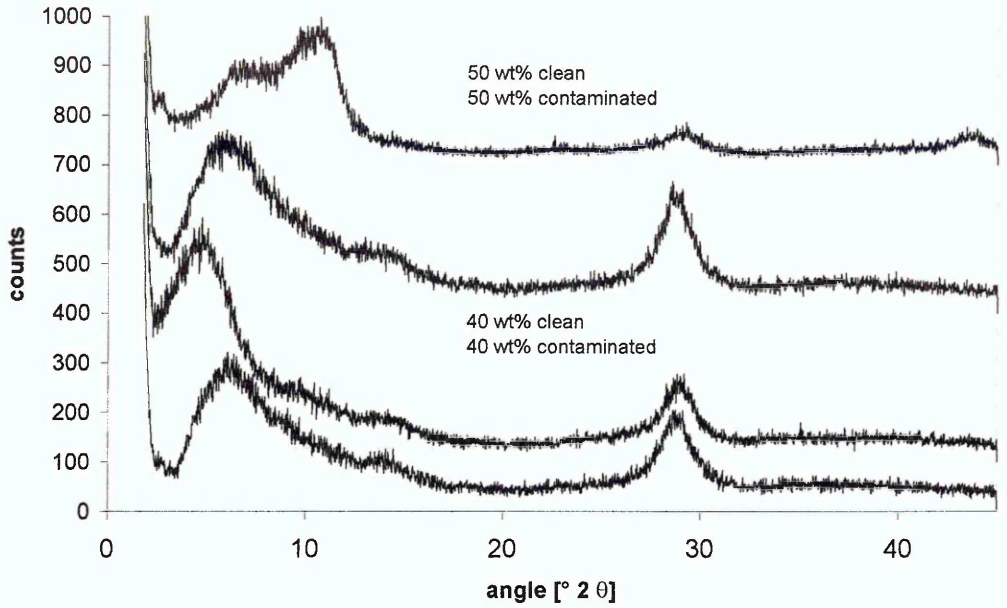

Figure 3-48 Comparison between high molecular weight PVOH/ Na^+ Cloisite® composites prepared from clean and contaminated clay (traces are offset for clarity)

3.5.3.1.3.2 TGA results

The difference in molecular weight between the low and high molecular weight samples did not lead to any apparent differences in the thermal stability of these samples. The two stage decomposition process observed for the low molecular weight samples was also present in the high molecular weight samples.

In the pristine polymer the maxima of the two decomposition stages occurred at 280 °C and 440 °C respectively. Maximum decomposition temperatures for the first stage process were constant at 280 °C for samples prepared from contaminated Na^+ Cloisite®, while they ranged from 260 – 270 °C in samples prepared with clean clay. No explanation has so far been found why clean Na^+ Cloisite® appears to lower the thermal stability of the polymer since the contaminated clay does not have such an effect.

The second weight loss maximum occurred at about 440 °C in all high molecular weight samples. The overall weight loss was decreasing with increasing clay loadings for both, the clean and contaminated clay, nanocomposites and the main changes in the weight loss were due to reduction of weight loss during the first stage process of decomposition.

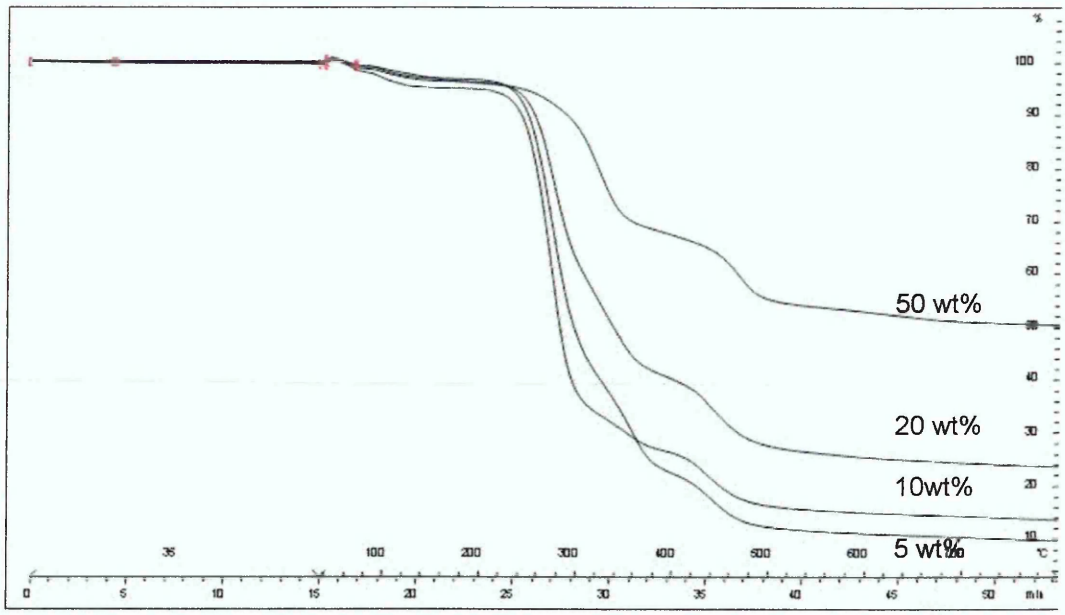

Figure 3-49 Thermograms for high molecular weight PVOH/ Na^+ Cloisite® composites with various clay loadings

3.5.3.1.3.3 Summary

PVOH nanocomposites and PVOH/ clay composites prepared from a higher molecular weight polymer had well dispersed structures at low clay contents, while higher clay contents lead to more and more intercalated structures. At low clay contents no differences were found in the dispersion of clean and contaminated clay in the polymer however traces of higher clay content composites showed some changes in the layer spacing and dispersion of these clays in the polymer. Whether the observed changes are due to the contamination of the clay or just a local feature of the area analysed by XRD is unclear for now and further analysis is needed.

Thermal stability of the high molecular weight samples did present differences between samples prepared from clean and contaminated clay. In the contaminated clay samples no differences between the pristine polymer and the polymer/ clay (nano-)composites could be observed, while the clean clay led to a reduction of the onset and maximum decomposition temperatures of the first decomposition stage similar to that observed for the low molecular weight samples.

3.5.3.1.4 Summary of results for PVOH/Na+ Cloisite® nanocomposites

Samples have been prepared using low and high molecular weight poly (vinyl alcohol). During the preparation of samples it was discovered that the batch of Na^+ Cloisite® used had been contaminated by small amounts of organic material. Therefore, experiments were repeated using a new batch of Na^+ Cloisite® to check whether this contamination had any influence on the dispersion of the layered silicate in the polymer matrix.

Comparisons between samples prepared from the clean and contaminated clays showed no differences in the traces for samples containing up to 10 wt% of clay. As these samples did, however, not have any distinct peaks from the clay, it cannot be ruled out that some differences in dispersion exist which cannot be detected using wide angle XRD. At higher clay loadings minor differences could be observed for some samples, while others showed similar traces for samples prepared with the same weight percentage of clay. As some differences could also observed for samples cast from the same solution no conclusions about the influence of the clay contamination can be drawn just from the XRD data.

Comparison for samples prepared from poly (vinyl alcohol) with different molecular weights did not show any obvious differences. It is, therefore, assumed that the dispersion of Na^+ Cloisite® is not affected to any greater extend by the molecular weight of the sample for the two molecular weights investigated.

Thermal stability of all these samples was also comparable for samples prepared from clean and contaminated Na^+ Cloisite® for the low molecular weight PVOH samples. In the high molecular weight samples the incorporation of clean sodium clay was found to decrease the onset and maximum decomposition temperatures of the first decomposition stage. The thermal stability of the two PVOH polymers was relatively similar though the first decomposition maximum was about 10 °C higher for the high molecular weight sample.

3.5.3.2 Poly (vinyl alcohol)/ MCBP nanocomposites

3.5.3.2.1 Poly (vinyl alcohol)/ Na+ MCBP nanocomposites

Composites of poly (vinyl alcohol) and Na^+ MCBP were prepared with clay contents ranging from 2.5 wt% to 75 wt%. Compared to the Na^+ Cloisite® clays the MCBP had a slightly lower layer spacing than the Cloisite when films were cast from aqueous solution. (see Figure 3-50) These differences are caused by the differences observed in the structure of the clay layers (relative amounts of Mg, Al, Si in the structure) and the variations in the interlayer cations that were found in x-ray fluorescence (XRF) measurements of the sample (see chapter 3.3.1)

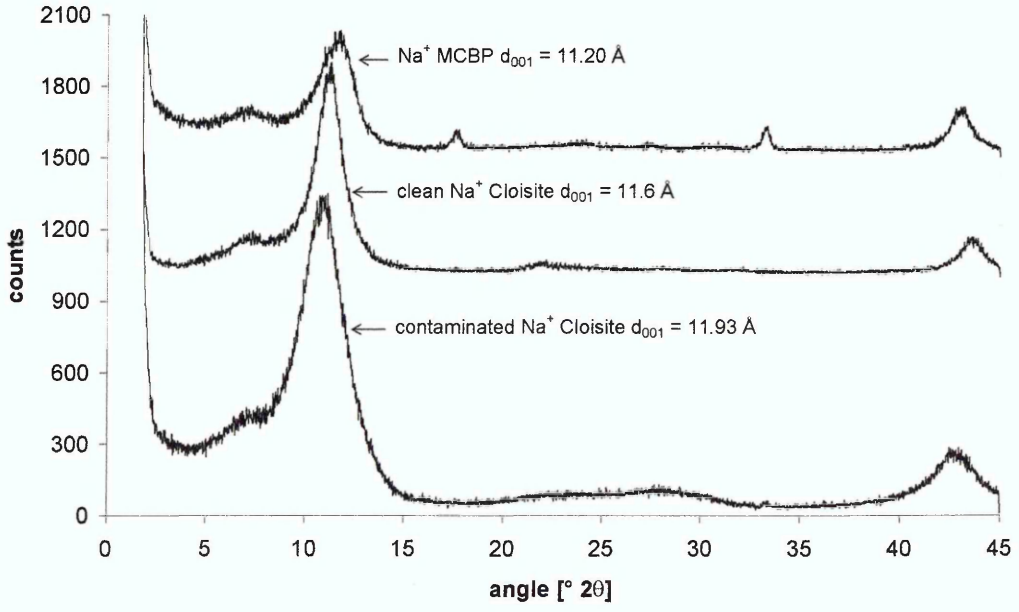

Figure 3-50 XRD traces (Cr tube) for sodium clay films cast from aqueous solution (traces are offset for clarity)

3.5.3.2.1.1 XRD results

The composites of Na^+ MCBP and PVOH showed similar dispersion patterns to those observed for PVOH/ Na^+ Cloisite® composites. At low clay loadings no peaks were present in the trace though elevated backgrounds compared to the pure polymer indicated the presence of clay layers in the sample. At higher angles the diffraction traces showed broad peaks like those observed for the Cloisite samples.

Figure 3-51 shows diffraction traces for composites over the whole range of compositions prepared. The distribution of layer spacings for these samples is similar to the ones for the Cloisite clays but like in the pure clay the spacings are slightly lower.

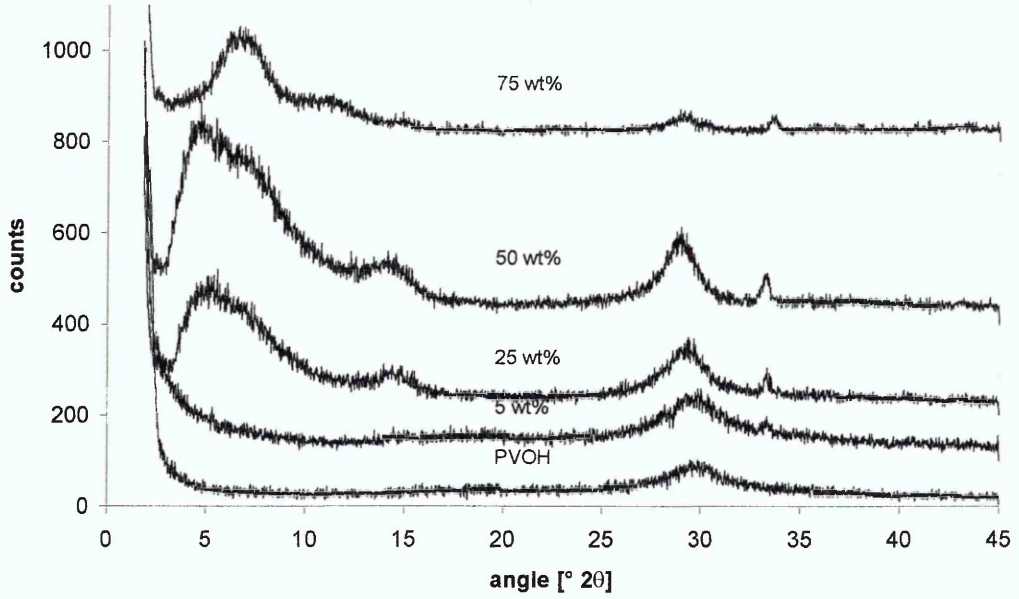

Figure 3-51 XRD patterns (Cr tube) for low molecular weight PVOH/ Na^+ MCBP nanocomposites (traces are offset for clarity)

3.5.3.2.1.2 TGA results

The decomposition behaviour of nanocomposites prepared with Na^+ MCBP was similar to that observed for Na^+ Cloisite® nanocomposites. Fewer samples however meant that no information can be given on the ranges of different behaviour. Because of this lack of information, a direct comparison of the ranges of different behaviour could not be performed. Generally, increasing the clay levels led to decomposition starting at higher temperatures even though the maximum decomposition temperatures remained the same. Weight loss of the samples decreased with increasing clay loadings mainly due to a reduction in weight loss during the first stage. The weight loss during the second stage was slightly higher than that observed for the Na^+ Cloisite® samples remaining steady at 15 %. Thermograms for these samples are shown in Figure 3-52.

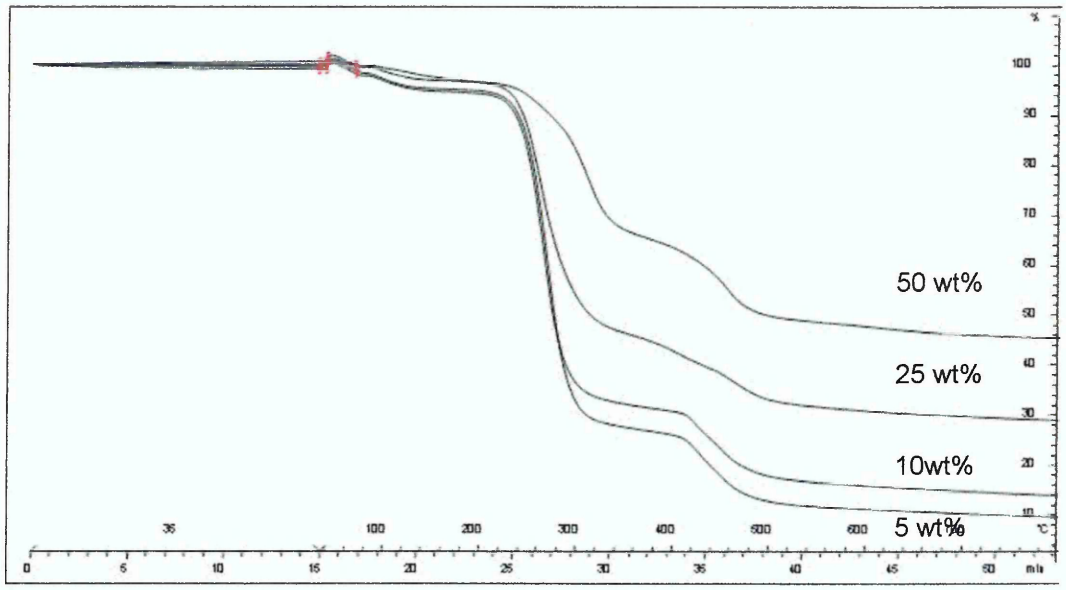

Figure 3-52 Thermograms for PVOH/ Na^+ MCBP composites with various clay loadings

3.5.3.2.1.3 Summary

PVOH/ Na^+ MCBP nanocomposites were found to be very similar to their Na^+ Cloisite® equivalents. At low clay loadings exfoliated nanocomposites were achieved, while higher clay loadings led to intercalated structures.

TGA of these samples showed decomposition was starting at higher temperatures in samples with increased clay loadings. At the same time the overall weight loss decreased with increasing clay loadings.

3.5.3.2.2 Poly (vinyl alcohol)/ Li+ MCBP nanocomposites

For the preparation of low molecular weight PVOH/ Li^+ MCBP composites clays with three different layer charges were used. To compare the influence of the cation in the gallery the unheated Li^+ MCBP was chosen. Furthermore, Li^+ MCBP samples heated at 135 °C and 210 °C respectively for 24 hours were dispersed in PVOH.

3.5.3.2.2.1 Analysis of Li+ MCBP

The lithium clays were prepared by cation exchange as described in chapter 3.5.2.1. X-ray fluorescence analysis of the sodium starting material and the lithium exchanged clay showed that most of the sodium had been exchanged. Furthermore, the calcium content of the lithium sample has been reduced by 70%. A summary of the elemental composition of the two clays is given in Table 3-18.

Compound	Content in wt%	
	Na^+ MCBP	Li^+ MCBP
Na_2O	1.98	0.14
MgO	1.91	1.91
Al_2O_3	19.02	20.30
SiO_2	71.28	72.05
SO_3	0.44	0.03
K_2O	0.15	0.08
CaO	0.91	0.29
TiO_2	0.10	0.10
Mn_3O_4	0.01	0.01
Fe_2O_3	4.16	5.09
ZnO	0.01	0.01
BaO	0.01	0.01

Table 3-18 XRF data for sodium and lithium MCBP

The exchange of calcium ions for lithium ions in the galleries should lead to an increased swelling of the lithium exchanged clay compared to that of the Na^+ MCBP as clay layers intercalated with calcium ions swell less than layers with sodium or lithium ions.

Figure 3-53 presents diffraction traces for powdered samples of Na^+ MCBP and unheated Li^+ MCBP. The Li^+ MCBP has a higher apparent layer spacing (12.4 Å) compared to the Na^+ MCBP (11.9 Å). The broader peak around 6° 2θ

arises from a regular interstratification of layers with and without water present in the galleries [3.35].

Heat treatment collapsed some of the layers in the lithium clay. The XRD traces for such heat treated clays are shown in Figure 3-54.The layer spacing was reduced from 12.4 Å in the unheated powder sample to 10.8 Å and 9.8 Å for the samples treated at 135°C and 210°C. Comparing diffraction traces for powdered samples and films cast from a dispersion of the clay in water show wider d_{001} peaks at higher angles for the films cast from aqueous solutions. These changes were caused by water remaining in the films after drying at 40 °C which caused swelling of various degrees in the clay. Again a decrease in layer spacings could be observed for the heated samples. The d_{001} spacings measured for these films with increasing temperature treatments were 14.3 Å, 12.0 Å and 10.4 Å respectively.

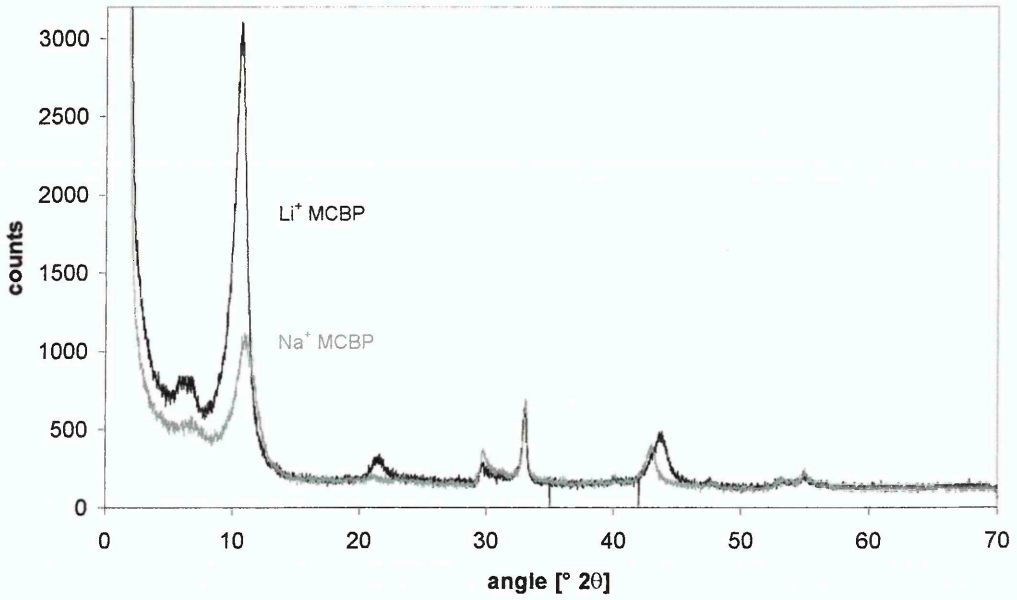

Figure 3-53 XRD Powder diffraction traces (Cr tube) for Na^+ and Li^+ MCBP

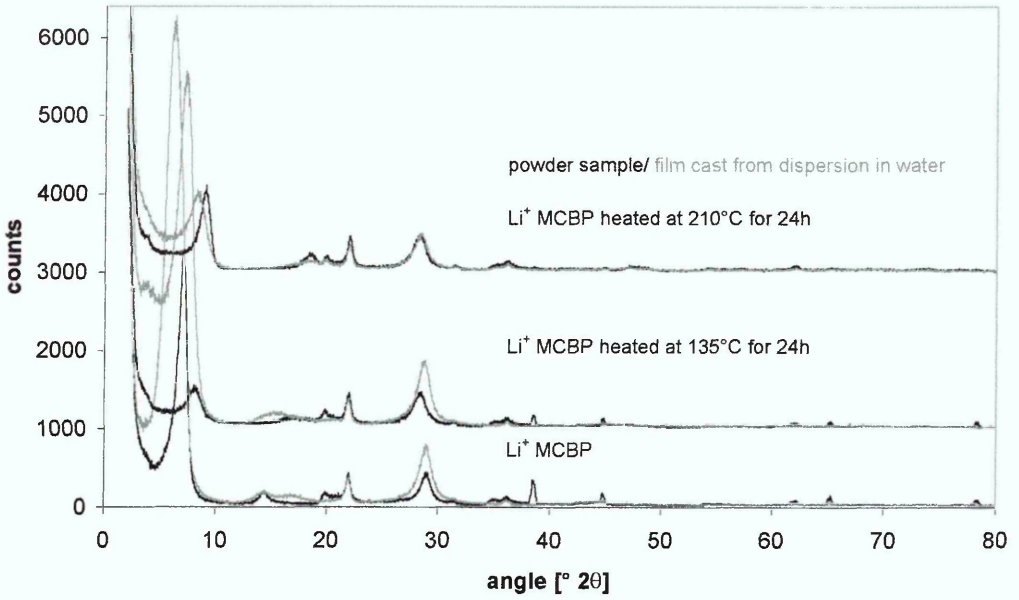

Figure 3-54 Comparison of XRD traces (Cu tube) of powdered and film samples (traces are offset for clarity)

3.5.3.2.2.2 Poly (vinyl alcohol)/ Li+ MCBP (non heat treated) nanocomposites

Poly (vinyl alcohol)/ non heat treated Li^+ MCBP nanocomposites were prepared with clay loadings of 2.5 wt%, 5 wt%, 10 wt% and 25 wt% respectively.

3.5.3.2.2.2.1 XRD results

The Li^+ MCBP disperses in PVOH better than Na^+ MCBP forming intercalated structures with high layer spacings. At the clay loadings investigated for this system no d_{001} peaks were visible in the diffraction traces. With increasing clay content in the samples a higher background could be observed at low angles. All traces furthermore featured a peak around 9.5 ° 2θ. The exact cause of this peak needs to be further investigated. It is, however, possible that it arises from unexpanded clay layers. XRD traces for these samples are presented in Figure 3-55. The better dispersion of the Li^+ MCBP at higher clay loadings is likely to be due to the lower calcium content in these samples making these clays more swellable than the Na^+ MCBP.

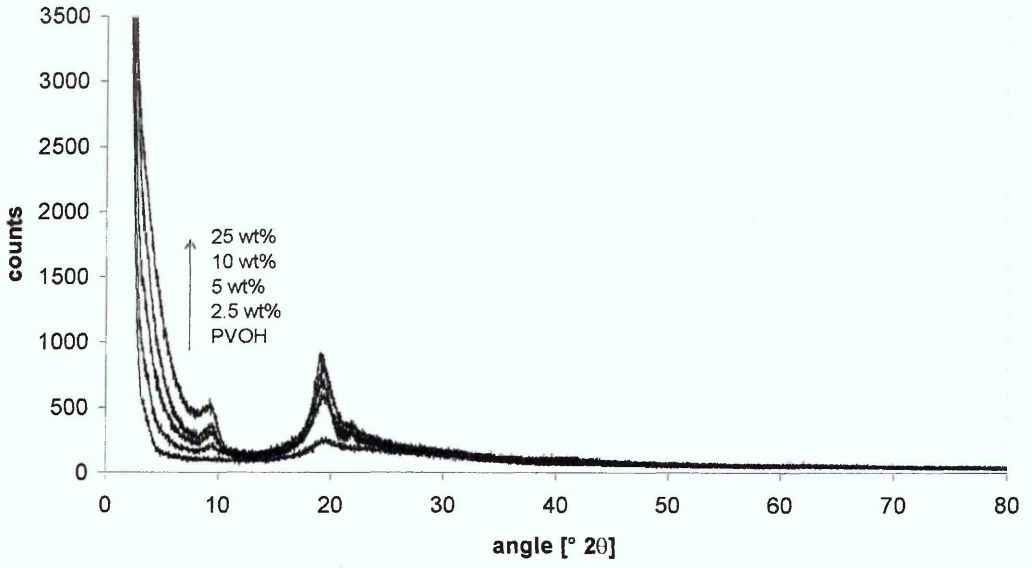

Figure 3-55 XRD traces (Cu tube) for low molecular weight PVOH/ Li^+ MCBP nanocomposites

3.5.3.2.2.2.2 TGA results

The thermal stability of these nanocomposites differed from that of the other nanocomposites discussed so far. The onset temperature for the first decomposition stage was stable at 190 °C for clay loadings up to 25 wt%. The decomposition maximum temperature of this first peak was about 10 °C below that of the pristine polymer. The weight loss was reduced with increasing clay loadings mainly due to a decrease in the weight loss of the first decomposition stage. The weight loss for the second stage was stable around 15 % which is higher than that observed for the neat polymer or the Na^+ Cloisite® nanocomposites but similar to that observed for the Na^+ MCBP.

3.5.3.2.2.2.3 Summary

Lithium exchanged MCBP was found to disperse better in PVOH than its sodium parent compound. Whether this is purely due to the exchange of sodium for lithium or the reduction in calcium in the galleries (which was also replaced by lithium) cannot be stated from the data available.

These slight structural differences led to altered behaviour of decomposition during the first stage in the nanocomposites as onset temperatures remained stable for clay loadings between 2.5 and 25 wt% while the maximum

decomposition temperature of that stage was slightly lower than that of the pristine polymer.

3.5.3.2.2.3 Poly (vinyl alcohol)/ Li+ MCBP (fired at 135 °C) nanocomposites

Poly (vinyl alcohol)/ Li^+ MCBP (fired at 135 °C) composites were prepared with clay loadings between 2.5 wt and 75 wt%.

3.5.3.2.2.3.1 XRD results

Mild charge reduction by heating the clay at 135 °C for 24 hours only had minor effects on the dispersion of the clay in PVOH. Traces for PVOH/ clay composites with clay loadings up to 75 wt% had no d_{001} peak in their XRD trace or, in case of the samples with at least 25 wt% clay, a peak at very low angles (see Figure 3-56). Therefore, general charge appears to have less impact on the structure of PVOH/ MMT nanocomposites than the presence of less expanding layers due to intercalation with calcium.

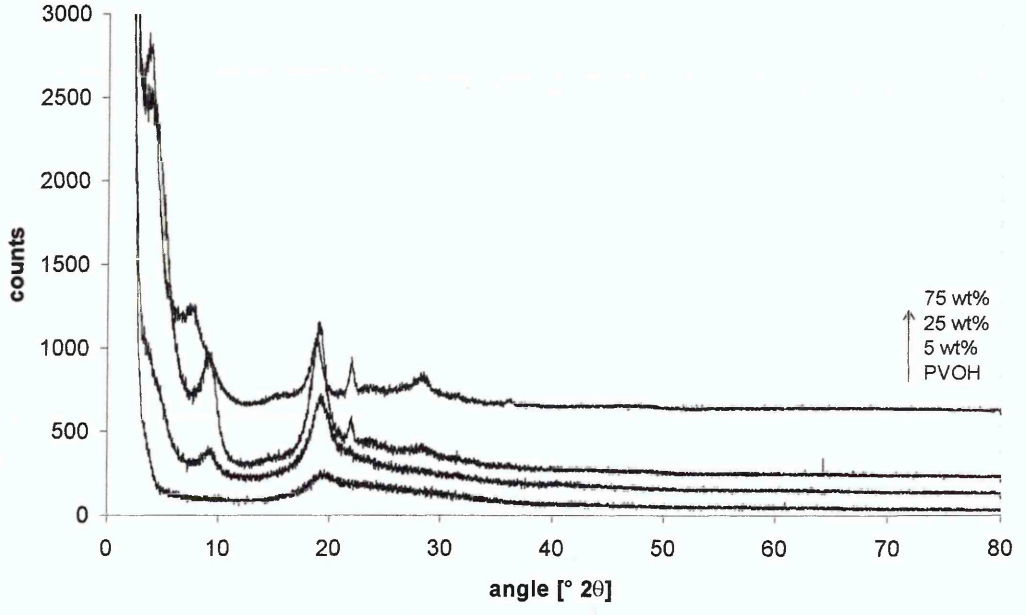

Figure 3-56 XRD traces (Cu tube) for low molecular weight PVOH/ Li^+ MCBP fired at 135 °C nanocomposites (traces are offset for clarity)

3.5.3.2.2.3.2 TGA results

The nanocomposites of Li^+ MCBP with mild charge reduction generally exhibited similar behaviour to those prepared from non heat treated lithium clay. In these nanocomposites the onset temperature of decomposition was raised by 20 °C compared to the neat polymer and did not change with clay loading. The maximum decomposition temperatures of the both decomposition stages were similar to those observed for the pristine polymer for all clay loadings.

Weight loss in these samples reduced with increasing clay loadings, with the main contribution of this change being due to decreased weight loss during the first stage of decomposition. The weight loss of the second stage remained at 13 % for all clay loadings, which is lower than the weight loss observed for the non heat treated Li^+ MCBP nanocomposites, yet higher than that of the neat polymer.

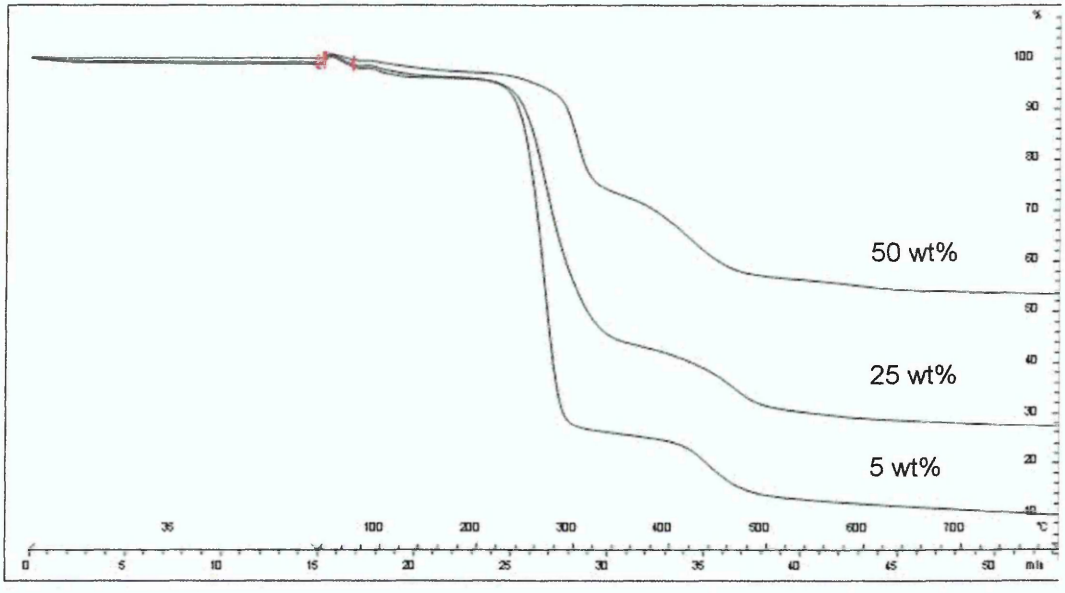

Figure 3-57 Thermograms for PVOH/ Li^+ MCBP (heated at 135 °C) nanocomposites with various clay loadings

3.5.3.2.2.3.3 Summary

Mild reduction in CEC of the clay lead only to minor differences in the dispersion of the clay in the polymer matrix and the thermal stability of the resulting materials. Samples were exhibiting more intercalated character than the nanocomposites of the parent lithium MCBP.

While weight loss of the samples during thermal decomposition decreased with increasing clay loadings, the lower weight loss during the second decomposition stage indicates that dispersion has an influence on the degradation of the polymer, since these samples appear to have poorer dispersion than the non heat treated material, yet slightly better dispersion than the Na^+ Cloisite®.

3.5.3.2.2.4 Poly (vinyl alcohol)/ Li+ MCBP (fired at 210 °C) nanocomposites

Poly (vinyl alcohol)/ Li^+ MCBP (fired at 210 °C) composites were prepared with clay loadings between 2.5 wt and 75 wt%.

3.5.3.2.2.4.1 XRD results

Collapsing most of the clay layers by heating the lithium clay to 210 °C for 24 hours had a profound impact on the structure of polymer/ clay composites prepared using this clay. At all clay loadings non-intercalated layers are present and the layer spacing remains unaffected by the polymer/ clay ratio.

Charge reduction has, in this case, produced uncharged layers that do not swell and, therefore, can not be intercalated by the polymer. Composites formed from this clay are expected to have properties similar to those of the unfilled polymer, as they will have a micro- rather than nano-composite structure.

Figure 3-58 shows examples for XRD traces of composites formed from poly (vinyl alcohol) and Li^+ MCBP fired at 210 °C. With increasing clay content the clay peaks are increasing in intensity. At the same time the PVOH peak at 20° 2θ is narrowing slightly indicating an increase in crystallinity of the polymer in the presence of clay.

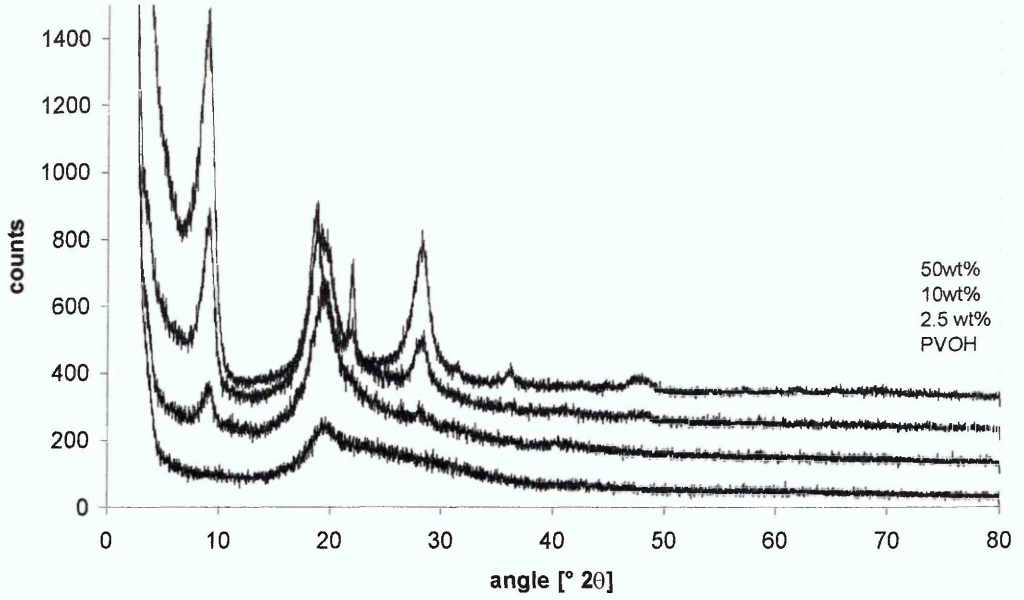

Figure 3-58 XRD traces (Cu tube) for low molecular weight PVOH/ Li^+ MCBP fired at 210 °C composites (traces are offset for clarity)

3.5.3.2.2.4.2 TGA results

The fully charge reduced Li MCBP/ PVOH composites showed very mixed behaviour in their thermal decomposition. At clay loadings up to 10 wt% the onset of decomposition remained stable around 200 °C while the maximum decomposition temperature for the first decomposition stage decreased to 265 °C. This first decomposition stage was then split into two events for samples with 25 and 50 wt%. At the same time the weight loss of the second decomposition stage decreased. For all other composites this decrease could only be observed for samples with more than 75 wt% clay loadings. Examples of thermogravimetric weight loss curves are presented in Figure 3-59.

As these changes in the break down temperatures vary from those observed in nanocomposites formed with all the other clays used in this work, it is assumed that the microcomposite dispersion in these samples is the cause for the differences in decomposition observed for these samples.

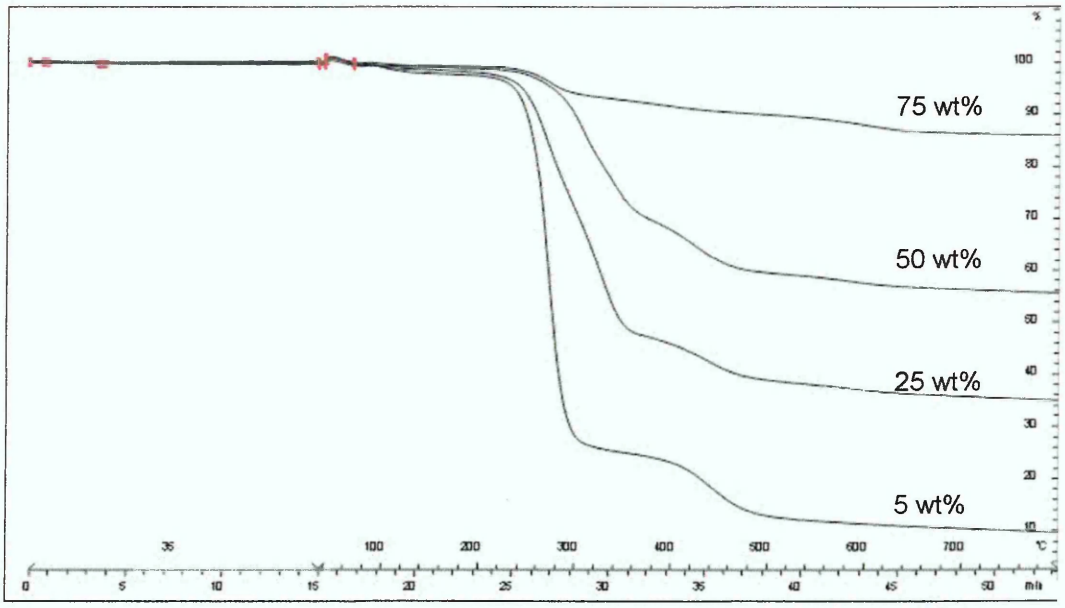

Figure 3-59 Thermograms for PVOH/ Li^+ MCBP (heated at 210 °C) nanocomposites with various clay loadings

3.5.3.2.2.4.3 Summary

PVOH and Li^+ MCBP (fired at 210 °C) could not be mixed as well as the clays with higher charge. The clay was harder to disperse in water as it contained uncharged layers which could not be swollen by liquid water. Due to this the dispersion of the clay particles occurs on a microcomposite level rather than nanocomposite dispersion which results in differences in the thermal decomposition of such samples. While the onset of decomposition appears to be still delayed the maximum decomposition temperatures of the two stage process remained the same as in the neat polymer or decreased in some cases by about 10 °C.

3.5.3.2.3 Summary for PVOH/ MCBP nanocomposites

Charge reduction influenced the dispersion behaviour of the clay in PVOH. Clay layers with lower charge were found to disperse less well in the polymer matrix, which is to be expected as they have less swelling capability. The clay with the lowest CEC could only be dispersed on a microcomposite level.

Comparison of Na^+ and Li^+ MMT nanocomposites with the same CEC showed better dispersion for the lithium clay. At this point it is however impossible to say

whether this improved dispersion is due to the presence of lithium ions or the fact that the cation exchange procedure not only reduced the amount of sodium but also calcium ions found in the clay galleries.

The use of MCBP seemed to influence the second decomposition stage during thermal decomposition of samples more than the Cloisite® as the weight loss was higher in the MCBP samples. Charge reduction of the MCBP did however reduce these levels to those observed in the Cloisite®.

3.5.3.3 Summary for PVOH/ montmorillonite nanocomposites

Nanocomposites and composites of poly (vinyl alcohol) and various montmorillonites have been prepared over the full range of compositions. Samples were investigated with respect to different molecular weight of the polymer matrix, variations in the clay and charge reduced clays.

For clay loadings below 10 wt% at least partially exfoliated structures could be achieved for all clays except the Li^+ MCBP fired at 210 °C. Increasing the clay loading led to a gradual decrease in layer spacing with initially broad distributions of spacings that narrowed down when clay loading was further increased. Above 90 wt% clay non intercalated layers could be observed in the samples.

Using higher molecular weight PVOH to prepare the nanocomposites did not lead to any major changes that could be detected by XRD. Some changes in the dispersion of Na^+ Cloisite® in higher molecular weight PVOH were observed between samples prepared from a contaminated batch of clay and the repeat samples prepared from a clean batch even though the low molecular weight nanocomposites prepared from these two materials did not show any differences.

It was often found difficult to produce samples under the same conditions as humidity of the air during the drying process appeared to influence the levels of water retained in the samples.

A general overview of the d spacings obtained for the different PVOH samples is given in Table 3-19 - Table 3-26. All layer spacings given here are given with the accuracy discussed in chapter 3.4.4.

Clay loading [wt%]	Layer spacing [Å]
2.5	no clay peaks visible
5	no clay peaks visible
7.5	no clay peaks visible
10	slightly sloped at low angle
20	broad peak at ~4° 2 theta (Cr)
30	broad peak at ~5° 2 theta (Cr)
35	broad peak at ~5° 2 theta (Cr)
40	broad peak at ~5° 2 theta (Cr)
45	4.4
50	5.0
55	5.1
60	5.6
65	5.9
70	6.5
75	7.1
80	7.4
90	17.4/12.5
95	17.3/12.5

Table 3-19 Summary of layer spacings for low molecular weight PVOH/ contaminated Na^+ Cloisite® nanocomposites

Clay loading [wt%]	Layer spacing [Å]
2.5	no clay peaks visible
5	no clay peaks visible
10	no clay peaks visible
50	broad peak at ~4° 2 theta (Cr)
75	7.1

Table 3-20 Summary of layer spacings for low molecular weight PVOH/ clean Na^+ Cloisite® nanocomposites

Clay loading [wt%]	Layer spacing [Å]
2.5	no clay peaks visible
5	no clay peaks visible
10	no clay peaks visible
20	slightly sloped at low angle
30	slightly sloped at low angle
40	broad peak at ~6.5° 2 theta (Cr)
50	broad peak at ~6° 2 theta (Cr)

Table 3-21 Summary of layer spacings for high molecular weight PVOH/ contaminated Na^+ Cloisite® nanocomposites

Clay loading [wt%]	Layer spacing [Å]
2.5	no clay peaks visible
10	slightly sloped at low angle
40	broad peak at ~5° 2 theta (Cr)
50	18.8/12.3

Table 3-22 Summary of layer spacings for high molecular weight PVOH/ clean Na^+ Cloisite® nanocomposites

Clay loading [wt%]	Layer spacing [Å]
5	no clay peaks visible
25	broad peak at ~5° 2 theta (Cr)
50	broad peak at ~5° 2 theta (Cr)
75	19.2

Table 3-23 Summary of layer spacings for low molecular weight PVOH/ Na^+ MCBP nanocomposites

Clay loading [wt%]	Layer spacing [Å]
2.5	slightly sloped at low angle
5	slightly sloped at low angle
10	slightly sloped at low angle
25	slightly sloped at low angle

Table 3-24 Summary of layer spacings for low molecular weight PVOH/ Li^+ MCBP nanocomposites

Clay loading [wt%]	Layer spacing [Å]
5	slightly sloped at low angle
25	broad peak at ~4° 2 theta (Cu)
75	22.7

Table 3-25 Summary of layer spacings for low molecular weight PVOH/ Li^+ MCBP (fired at 135 °C) nanocomposites

Clay loading [wt%]	Layer spacing [Å]
2.5	9.6
10	9.9
50	9.7

Table 3-26 Summary of layer spacings for low molecular weight PVOH/ Li^+ MCBP (fired at 210 °C) composites

Thermogravimetric analysis showed complex changes in the decomposition behaviour with increasing clay loadings. The decomposition of PVOH occurred in two stages with maxima in the decomposition occurring at temperatures around 270 °C and 440 °C respectively. All samples exhibited decreased weight loss with increasing clay loadings. In general the onset of decomposition was delayed by the presence of clay. The extent of that delay varied between samples though it is not entirely obvious how much changes in the decomposition temperatures are influenced by the initial water content in the films.

Most of the changes in thermal decomposition occurred in the first decomposition stage. At intermediate clay loadings this peak had a shoulder or was forming a doublet with main weight loss gradually shifting to the higher temperature peak. The weight loss of the second stage usually remained constant at levels similar to the pristine polymer though higher levels have been found in the MCBP nanocomposites.

No trends in changes of crystallinity could be detected by XRD or ATR upon the introduction of clay. If the clay is acting as a nucleating agent the effect is too localised to be noticed by these methods.

3.6 References

3.1 www.nanoclay.com, last accessed : October 2004
3.2 Sammon C, PhD Thesis (1997)
3.3 Ke YC, Long CF, Qi ZN, *J. Appl. Polym. Sci.*, **71**, 1139 (1999)
3.4 Ke YC, Yang ZB, Zhu CF, *J. Appl. Polym. Sci.*, **85**, 2677 (2002)
3.5 Saujanya C, Imai Y, Tateyama H, *Polym. Bull.*, **49**, 69 (2002)
3.6 Zhang GZ, Shichi T, Takagi K, *Mater. Lett.*, **57**, 1858 (2003)
3.7 Zhang GZ, Shichi T, Tong ZW, Takagi K, *Chem. Lett.*, 410 (2002)
3.8 Zhang GY, Yi GZ, Wu LH, Xu X, Song Q, Yang Y, Jin J, Zhong SF, Qi ZN, *Acta Polym. Sin.*, 309 (1999)
3.9 Boesel LF, Pessan LA, J. Metastable and Nanocrystalline Materials, **403**, 89 (2003)
3.10 Davis CH, Mathias LJ, Gilman JW, Schiraldi DA, Shields JR, Trulove P, Sutto TE, Delong HC, *J. Polym. Phys.*, **40**, 2661 (2002)
3.11 Li XC, Kang TY, Cho WJ, Lee JK, Ha CS, *Macromol. Rapid Comm.*, **22**, 1306 (2001)
3.12 Xu JL, Li BG, *Polym. Mater. Sci .& Eng.*, **18**, 149 (2002)
3.13 Yi GZ, Zhang GY, *Acta Polym. Sin.*, 124 (2001)
3.14 Ou CF, Ho MT, Lin JR, *J. Polym. Res. Taiwan*, **10**, 127 (2003)
3.15 Barber GD, Carter CM, Moore RB, *ANTEC 2000*, **1-111**, 3763 (2000)
3.16 Chang JH, Park DK, *J. Polym. Sci.*, **39**, 2581 (2001)
3.17 Chang JH, Park DK, *Polym. Bull.*, **47**, 191 (2001)
3.18 Belali R, Vigourex JM, *Appl. Spec.*, **48**, 465 (1994)
3.19 Suh DJ, Lim YT, Park OO, *Polymer*, **41**, 8557 (2000)
3.20 Suh DJ, Park OO, *J. Appl. Polym. Sci.*, **83**, 2143 (2002)
3.21 Jameel H, Noether HD, REbenfeld L, *J. Appl. Polym. Sci.*, **27**, 773 (1982)
3.22 Chang SH, Ryan ME, Gupta RK, Swiatkiewicz B, *Colloid Surface*, **59**, 59 (1991)
3.23 Lagaly G, *Appl. Clay. Sci.*, **15**, 1 (1999)
3.24 Greenland DJ, *J. Coll. Sci.*, **18**, 647 (1963)
3.25 Chiellini E, Corti A, Politi B, Solaro R, *J. Polym. Environ.*, **8**, 67 (2000)
3.26 Carrado KA, Thiyagarajan P, Elder DL, *Clays Clay Miner.*, **44**, 506 (1996)
3.27 Murakami R, Hachisako H, Yamada K, Motozato Y, *J. Mater. Sci. Lett.*, **14**, 937 (1995)
3.28 Nakane K, Yamashita T, Iwakura K, Suzuki F, *J. Appl. Polym. Sci.*, **74**, 133 (1999)
3.29 Suzuki F, Nakane K, Piao JS, *J. Mater. Sci.*, 1335 (1996)
3.30 Chang JH, Jang TG, Ibn KJ, Lee WK, Sur GS, *J. Appl. Polym. Sci.*, **90**, 3208 (2003)
3.31 Xu JY, Hu Y, Song L, Wang QG, Fan WC, Liao GX, Chen ZY, *Polym. Degrad. Stabil.*, **73**, 29 (2001)
3.32 Strawhecker KE, Manias E, *Chem. Mater.*, **12**, 2943 (2000)
3.33 Strawhecker KE, Manias E, *Macromol.*, **34**, 8473 (2001)
3.34 Wang Y, Wang Y, Wan D, *Polym. Preprints*, **44**, 1102 (2003)
3.35 Yu YH, Lin CY, Yeh JM, Lin WH, *Polymer*, **44**, 3553 (2003)
3.36 Madejova J, BujdaK J, Gates WP, Komadel P, *Clay Miner.*, 31, 233 (1996)
3.37 Chipera SJ, Bish DL, *Clays Clay Miner.*, **49**, 398 (2001)

4 Diffusion of small molecules into polymeric materials

4.1 Introduction

4.1.1 Diffusion background

Diffusion, sorption and permeation are important areas of interest to engineers and scientist in industry and research alike [4.1, 4.2]. In polymers diffusion plays a much greater role than in other solids because mass transport in polymers can be observed at ambient temperatures. Because of this polymers can be used for a variety of applications where diffusion of small molecules is either desired, i.e. controlled drug release, or needs to be reduced to a minimum (protective coatings or (food) packaging can be hampered by diffusion) [4.3, 4.4].

Control of diffusion processes has important implications for many of these technological applications which necessitates the accurate modelling and prediction of properties (and their changes) of polymeric systems during the ingress of small molecules. For systems where the solvent uptake is small macroscopic descriptions, as conveyed by the laws of Fick, have proven useful. Even though deviations from such models can often be observed, most diffusion processes in their isolated form fit these models, once all physical changes in the sample have been taken into account and correctly interpreted [4.5].

Transport of small molecules through membranes occurs due to random molecular motion of individual molecules driven by the concentration difference between the two phases. The nature of the diffusion process is determined by the relative rates of diffusion of penetrant molecules and the relaxation of polymer molecules which leads to a variety of mass transport phenomena. Factors that contribute to the transport process are the nature of the polymer (polymer chemistry and structure), the nature of the penetrant and the nature of cross-links, plasticisers and fillers if they are present in the polymer matrix [4.1 - 4.3, 4.5 - 4.7].

Diffusion through rubbery polymers, a state which is reached at temperatures above the glass transition temperature of the polymer, is usually smooth and modelling the diffusion process does not present many difficulties. Diffusion in glassy polymers is often more complex due to the restricted chain mobility of these polymers [4.1].

For rubbery polymers diffusion is generally expected to follow Fickian diffusion kinetics, whereas diffusion in glassy polymers has often been found to fit case II (plug-flow considerable swelling) models. Changes in the glass transition temperature and, therefore, the state of the polymer induced by the presence of solvent during the diffusion experiment can also lead to a change in the relevant diffusion model [4.6].

The temperature dependence of diffusion can be described by the Arrhenius law in limited temperature regions. Over larger temperature regions data does not follow this law because plasticisation of the polymer changes the activation energy for diffusion into the polymer. The apparent activation energy for diffusion was found to decrease in case of sizeable inclusions of penetrant whereas increases in cohesive energy density or the size of the penetrant result in higher apparent activation energies for diffusion [4.8].

The most common type of measurement performed to obtain diffusion coefficients is the gravimetric, so called "pat and weigh", method [4.9 - 4.12]. Here, the sample size and symmetry is adjusted to the expected rate of diffusion. Samples are immersed in the solvent of interest and weight uptake is measured at specific time intervals by removing the sample from the solvent and blotting of any excess liquid before weighing of the sample. This method can be used to measure diffusion coefficients as low as 10^{-18} cm^2/ sec but errors are easily introduced due to the extensive sample handling [4.13].

Computer modelling has been applied to diffusion with models of diffusion processes being based on two different approaches either investigating the molecular dynamics or by atomistic lattice simulations [4.2].

Typical sorption and permeation kinetics can be described by four different groups named after the shapes of the kinetic data; Fickian diffusion, two stage sorption (which describes a frequently encountered anomalous type of sorption

where fast Fickian diffusion is followed by a slow non-Fickian diffusion process), sigmoidal sorption and case II sorption [4.14].

Using data regression to obtain diffusion coefficients from experimental data provides diffusion rates that are averaged over the whole range of the experimental concentrations [4.15].

Experimental diffusion data can be described by these categories [4.16]:

Case I or Fickian diffusion:	The rate of diffusion is less than the relaxation time of the polymer. The diffusion is slow and constant. This type of diffusion is based on a "random walk" theory without interaction between the diffusant and the polymer.
Case II:	The rate of diffusion is higher than the relaxation time of the polymer. This diffusion is often associated with a sharp penetrant front, which propagates into the polymer at a constant velocity. It is based on strong interactions and a moving interface.
Case III or Non-Fickian diffusion:	The rate of diffusion is similar to the relaxation time of the polymer. This type of diffusion is used to describe all processes that do not fit Case I or II.

Various models have been reported to describe diffusion processes under these conditions. At the same time continuous development of new measurement techniques to try and discern the exact physical processes involved in diffusion leads to a more accurate understanding of the processes [4.17]. Such data is necessary as correct calculation of diffusion kinetics requires knowledge of the viscous response of glassy polymers (obtainable from creep data) and assumptions on how this response changes due to plasticisation of the polymer by the penetrant [4.18].

Barbari [4.19] described an alternative interpretation of the dual mode sorption in terms of maintenance of an "iso-free volume" state in the glassy polymer upon penetrant sorption. This model achieves a constant fractional free volume

by assuming that only a fraction of the total concentration is mobile, which is conceptually identical to a model with partially immobilisation of the solvent. The model could, however, only be used to describe and predict steady-state flux data.

Billovits and Durning [4.20] formulated a model of polymer/ penetrant diffusion accompanied by arbitrarily large polymer displacements. This model gives a general description of unsteady binary diffusion problems in a coordinate system fixed with respect to the reference configuration of one component. The model was found to accommodate two alternate macroscopic formalisms for interdiffusion; the usual engineering formulation which employs species continuity equations, equations of motion for the mixture and constitutive relations for the diffusion mass flux and total stress tensor and a method employing continuity equations, species equations of motion and constitutive relations for the species interaction forces and species partial stress tensors.

4.1.2 General diffusion experiments of water into polymeric materials

Diffusion of small molecules into polymeric materials can alter the physical properties of such systems [4.21]. The extent of these changes usually depends on the amount and properties of penetrant sorbed. Changes induced by polymer/ solvent interactions can occur on the chemical level (e.g. H/D exchange reactions), on the crystal level (changes in crystallinity of semicrystalline polymers) or on the supermolecular level [4.22].

Since polymers are often exposed to atmospheres containing water vapour and/ or organic solvents, the study of diffusion of small molecules into such materials and the changes the presence of these molecules causes are of interest for many applications such as advanced coatings, food packaging and beverage bottling [4.7, 4.23, 4.24].

Water has been found to show anomalous behaviour when incorporated into membranes and to cause disruptions to the structure of the host matrix [4.25, 4.26]. Similarly unusual features in the properties of water can be observed in aqueous polymer solutions due to the disruption of the hydrogen bonding network by the polymer [4.27 - 4.29]. Coyle et al. [4.25] attributed these

changes in water to a reduction in the degrees of freedom when comparing water in a polymer matrix to pure water.

Changes occurring in the polymer during the ingress of water can also affect the mobility of the water molecules. Immobilisation of the penetrant molecules and plasticisation of the polymer can have opposite effects on the mobility of water [4.37]. Water can act as a plasticiser or anti-plasticiser dependent on the temperature and concentration. Since the behaviour of water depends heavily on the experimental conditions, comparison of data produced by different methods can prove problematic [4.25].

The measurement of diffusion coefficients of solvent into polymers can be complicated if the polymer of interest is soluble in the solvent. During the ingress of water, for example, water-soluble polymers can be solvated. Elabd and Barbari [4.30] developed a mathematical model to remove the influence of solvation during the diffusion of methyl ethyl ketone (MEK) vapour at low activities into two vinyl alcohol/ vinyl butyral copolymers. They were able to show that, after the mathematical removal of the effects of solvation of the polymer from the diffusion data obtained by ATR-FTIR, the true diffusion coefficient of the MEK was similar to that of a non-interacting solvent molecule of the same size.

4.1.3 Diffusion of small molecules into organic-inorganic hybrid materials

The barrier properties of a polymer depend on various structural factors such as chemical composition of the polymer, polymer morphology, polymer molecular architecture and plasticisation. Polymers with high barrier properties towards gases generally exhibit poor resistance to polar solvents [4.26]. Improvement of the barrier properties towards such liquids without reducing the gas barrier properties has been of interest for several applications. Barrier properties of polymer membranes and films can be improved by adding layers of barrier materials (usually sandwich structures of polymers with high gas and high water barrier properties) or incorporating materials with higher barrier properties into the polymer matrix as in the case of inorganic filler materials or copolymers [4.31].

Hybrid organic - inorganic materials can be divided into three different groups which are characterised by the different types of interactions between the two components. These groups are materials that exhibit van der Waals forces or hydrogen bonding e.g. microporous beads or clays, materials with covalent bonds between the organic and inorganic phases, and organically modified ceramic membranes [4.32]. In the following only materials of the first group which includes polymer/ clay nanocomposites will be discussed.

Polymer/ clay nanocomposites are a relatively new group of materials. Only few materials have been commercialised so far but several more are being developed for specific purposes [4.31]. The extent of the changes occurring in the diffusion behaviour of polymer/ clay composites depends, among other things, on the distribution of the clay, the aspect ratio of the clay platelets and the volume fraction of the clay [4.33, 4.34, 4.38].

To understand the permeability levels achievable in nanocomposites one should consider the geometry of the clay particles and the molecular level transformations caused by the interactions of polymers with inorganic fillers. While experiments can only measure the combined effect of these factors modelling allows investigation of both separately. Using a model with perfectly aligned randomly distributed platelets Gusev and Lusti [4.23] found that an aspect ratio of 10^3 and arrangement of the platelets at a right angle to the direction of diffusion resulted in the largest improvement in the barrier properties.

Modelling the improvement of gas barrier properties using a purely tortuosity based argument Bharadwaj [4.35] found that longer sheets result in higher barrier properties while wider aggregates (microcomposite like) lower the barrier properties. Permeability was found to be unchanged at volume fractions below 0.05.

Gorrasi et al. [4.33, 4.34] investigated the diffusion behaviour of water vapour into poly (ε-caprolactone) composites with respect to the clay distribution. They found that the introduction of an inorganic compound into the polymer creates a multiphase system in which the coexistence of phases with different permeation

characteristics causes complex transport behaviour that differs significantly from that of the pristine polymer.

Studying the diffusion of water vapour into these systems it was also found that composite materials can absorb higher amounts of water. The amount sorbed depended on the distribution of the clay. Exfoliated nanocomposites were found to absorb the highest amounts of water vapour, which leads to the assumption that water molecules are binding to hydrophilic sites of the clay. Once all these sites are occupied the relationship between the activity of the penetrant and the equilibrium constant was shown to be linear. Such a linear relationship between penetrant activity and equilibrium constant was also observed for the pristine polymer [4.33, 4.34, 4.36].

In polylactide/ montmorillonite nanocomposites water vapour diffusion was found to follow dual sorption behaviour. The amount of water vapour sorbed in intercalated systems appeared to be slightly lower than in exfoliated systems. Intercalated samples only showed minor improvements of the barrier properties compared to the unfilled samples while the D_0 values for exfoliated samples were two orders of magnitude lower than those of either the unfilled polymer or the intercalated nanocomposite [4.37].

Gravimetric measurements of water uptake in various epoxy resin/ organo smectite hybrids showed a reduced equilibrium water uptake in the nanocomposites compared to the neat polymer. The diffusion rate did however remain unaffected by the presence of clay in the samples [4.38].

4.2 Diffusion measurements by attenuated total reflection – Fourier transform infrared spectroscopy

ATR-FTIR measurements of diffusion parameters are especially useful because this technique allows in-situ data collection. At the same time information on the interaction of the polymer and the solvent, as well as changes induced by the ingress of solvent can be monitored through analysis of the spectra [4.13, 4.15, 4.39].

Unlike in gravimetric analysis ATR-FTIR also enables the measurement of diffusion kinetics for the individual components of diffusion mixtures [4.15]. Such diffusion measurements are applicable to any combination of solvents where the various components have clearly distinguishable bands that can be used to monitor the diffusion process [4.4].

Diffusion measurements by ATR-FTIR are a relatively new method. A first investigation of the diffusion of acetone into poly (isobutylene) was described by Lavrentjev et al. in 1975 [4.40]. In the early 1980's studies of the diffusion of small molecules into polyethylene (PE) and the interdiffusion of poly (methyl methacrylate) and styrene-acrylonitrile were published. The first in-situ measurements were reported by Brandt et al. [4.41, 4.42] in 1984/85 for the diffusion of small molecules into PE. After those initial articles no further studies where published until 1992. Since then a steady stream of investigations have been reported [4.4].

The main difficulty of this technique is that good contact between the sample and the ATR-crystal needs to be maintained throughout the experiments to obtain useful information. This often requires samples to be solvent cast or hot pressed onto the ATR crystal, which can alter the morphology of the polymer compared to the "as manufactured" polymer [4.13].

Data obtained from these measurements is comparable to gravimetric measurements though variations can often be observed due to different sample geometries.

The ATR-reflection can change over the course of diffusion measurements because of changes of diffusant concentration and effective thickness of the

sample which results in changes in the absorption over time not only due to the expected changes in the sample but also from changes in the refractive index of the sample film. The changes can, however, be ignored in the interpretation of the data if the diffusant concentration remains always very small compared to the polymer concentration, only minor differences exist between refractive index of the polymer and the solvent and the angle of incidence being sufficiently removed from the critical angle for total reflection [4.15, 4.42].

4.3 Fickian diffusion profiles

Fick's laws provide an empirical relationship stating the rate of transfer of a diffusing substance through a unit area is proportional to the concentration gradient measured normal to the unit area. The first law, which can only be directly applied to diffusion in the steady state, describes the relation between the flux in the x-direction and the concentration gradient as given in equation 4-1.

$$F = -D\frac{\partial c}{\partial x} \qquad \textbf{Equation 4-1}$$

where D is the diffusion coefficient

For non-steady state conditions the rate of change in the penetrant concentration can be expressed in form of the following equation, which is known as Fick's second law of diffusion:

$$\frac{\partial c}{\partial t} = D\left(\frac{\partial^2 c}{\partial x^2}\right) \qquad \textbf{Equation 4-2}$$

where D is the diffusion coefficient
c is the concentration of the penetrant
t is the time

Crank [4.43] summarised solutions to Fick's second law for various geometries and boundary conditions. For the most common type of sorption measurement a film of polymer film of thickness 2L is placed in an infinite bath of penetrant. If the initial penetrant concentration in the film is zero the concentration at any position z in the film at any time t is given by equation 4-3 [4.43 – 4.46]:

$$\frac{c}{c_\infty} = 1 - \frac{4}{\pi}\sum_{n=0}^{\infty}\frac{(-1)^n}{2n+1}\exp\left[\frac{-D(2n+1)^2\pi^2 t}{4L^2}\right]\times\cos\left[\frac{(2n+1)\pi z}{2L}\right] \qquad \textbf{Equation 4-3}$$

where c is the concentration at any point
c_∞ is the concentration at the start
D is the diffusion coefficient
t is the time
L is the sample thickness

Integration of this equation of over the thickness of the film to obtain the sorbed mass yields:

$$\frac{M_t}{M_\infty} = 1 - \sum_{n=0}^{\infty}\frac{8}{(2n+1)^2\pi^2}\exp\left[\frac{-D(2n+1)^2\pi^2 t}{4L^2}\right] \qquad \textbf{Equation 4-4}$$

where M_t is mass sorbed at time t
M_∞ is the mass sorbed at equilibrium
D is the diffusion coefficient
t is the time
L is the sample thickness

For films of thickness 2L and short times equation 4-5 gives a good approximation of equation 4-4:

$$\frac{M_t}{M_\infty} = \frac{2}{L}\sqrt{\left(\frac{D}{\pi}\right)}\sqrt{t} \qquad \textbf{Equation 4-5}$$

For the linear portion of the diffusion curve at $\frac{M_t}{M_\infty} \leq 0.5$ this equation can be used to determine the diffusion coefficient. The error incurred by the use of this approximation is on the order of 0.1% under these conditions [4.46].

The general solution to Fick's second law given in equation 4-4 describes the change in the mass of a penetrant sorbed as a function of time. While it can be used to describe data of the diffusion of solvents into films obtained by various techniques (substituting mass by the appropriate quantity if necessary), it does not apply to ATR-FTIR diffusion measurements in this form as boundary conditions are different.

In the ATR setup the absorbance of a functional group observed in the FTIR spectrum is dependent on the concentration of that group within the sampled depth, which itself is a function of the wavelength and the respective refractive indices of the sample and ATR crystal as discussed in chapter 2.1.2.1. For weak absorbers the absorbance is given by the Beer – Lambert law:

$$dI = \alpha\ Idz = -\varepsilon\ cIdz$$ **Equation 4-6**

where I is the light intensity at position z
α is the absorption coefficient
ε is the molar absorption coefficient

which can be integrated to yield:

$$A = -\ln\left\{\frac{I}{I_0}\right\} = \int_{-L}^{L} \varepsilon\ cdz$$ **Equation 4-7**

where A is the measured absorption
I_0 is the intensity of the incident light
I is the intensity of the transmitted light
2L is the thickness over which the absorbing group is present

Combining the equation for the evanescent field strength with the Beer – Lambert law is possible if one assumes that only weak absorption occur. With this assumption the evanescent field strength can be described by:

$$\frac{I}{I_0} = e^{-A} \approx (1 - A)$$ **Equation 4-8**

or

$$dI = -I_0 dA$$ **Equation 4-9**

Substituting equation 4-9 into the differential form of the Beer – Lambert law as given in equation 4-6 and integrating yields:

$$A = \int_0^L \frac{\varepsilon\ cI}{I_0} dz$$ **Equation 4-10**

or in case of multiple reflections, N:

$$A = \int_0^L N\varepsilon^* cE_0^2 \exp(-2\gamma\ z) dz$$ **Equation 4-11**

where $\varepsilon^* = \frac{\varepsilon}{I_0}$

Substituting the Fickian concentration profile (equation 4-3) into equation 4-11 and integrating gives equation 4-12, which is the equivalent of equation 4-4 for ATR-FTIR measurements.

$$\frac{A_t}{A_\infty} = 1 - \frac{8\gamma}{\pi\left[1-\exp(-2\gamma L)\right]} \times \sum_{n=0}^{\infty}\left[\frac{\exp\left(\frac{-D(2n+1)^2\pi^2 t}{4L^2}\right)\left[\frac{(2n+1)\pi}{2L}\exp(-2\gamma L)+(-1)^n(2\gamma)\right]}{(2n+1)\left(4\gamma^2+\left(\frac{(2n+1)\pi}{2L}\right)^2\right)}\right]$$

Equation 4-12

where A_t is the absorbance at time t
A_∞ is the absorbance at equilibrium

4.4 Choice of diffusion model

Finding a model to describe the diffusion of water into PVOH proved to be complicated by the fact that the ingress of water into this polymer is accompanied by strong interactions between the diffusant and the polymer, as well as significant swelling and partial dissolution of the sample film. Furthermore, PVOH is plasticised by water and its glass transition temperature can be lowered to ambient temperatures when the water content in the sample reaches 10 – 15 wt% [4.47].

The data often shows a time delay before diffusion can be observed followed by in some cases sharp increase in the intensity of the OH bending mode which could suggest that water diffusion is occurring in form of a diffusion front rather than random diffusion. Therefore, attempts have been made to fit the data to a case II model. This case II model [4.46] is given by the following equation.

$$\frac{A_t}{A_\infty} = \frac{1-e^{2\gamma\nu t}}{1-e^{2L\gamma}}$$

Equation 4-13

where ν is the diffusion front velocity
$\gamma = 1/d_p$
L is the film thickness

While this model gives a good representation of the delay time, the overall shape of the diffusion curve is not well represented as is obvious from the example shown in Figure 4-1. Data collected for the diffusion of water into nanocomposites showed even higher deviations from this model possibly indicating a change in the diffusion mechanism with the incorporation of clay.

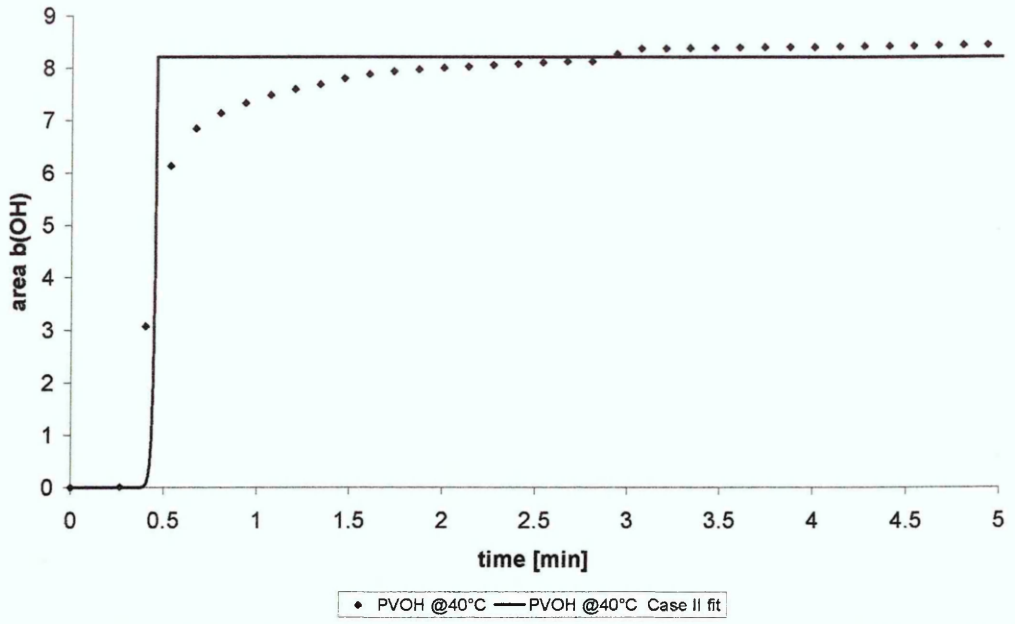

Figure 4-1 Experimental data and Case II fit for diffusion of water into PVOH at 40°C

The shape of the diffusion curves of experimental data were often similar to those expected for a Fickian diffusion process if the initial time delay was neglected. The significant swelling and large water uptake of PVOH films (>10%) are likely to change the state of the polymer from its initial (dry) glassy state to a rubbery state.

The time delay before diffusion can be observed is likely to be a combination of several effects. Initial diffusion could be hindered by formation of a skin with higher crystallinity. Furthermore, swelling and gel formation has been shown to reduce diffusion rates in studies of liquid into tablets and drugs out of tablets in studies of controlled release matrices [4.48 - 4.50]. In these studies the formation of a gel layer through transition of the polymer from a glassy to a rubbery state was found to decrease the diffusion rate. This reduction in the diffusion rate was attributed to reduction of the "free volume" within the polymer. The gel layer was found to slowly increase towards the centre of the sample while diffusion of any molecules active agents is occurring in the opposite direction.

No model was found that would take all changes that are likely to occur within these samples into account. Therefore, diffusion coefficients were approximated by using the short term approximation of the Fickian diffusion model. The short term approximation as described in equation 4-5 could be applied to the data

without any corrections for the ATR effects because only the slope of the diffusion curve was considered in the calculation of diffusion coefficients. Furthermore, these diffusion coefficients were used only as a semi-quantitative measure for comparison of results, so that errors incurred from neglecting the ATR effect on the data should not affect the general trends. Fieldson and Barbari [4.46] discussed that diffusion curves of concentration dependent diffusion could also result in curves that could be fitted by this approximation. In such a case the obtained D values are an average over the applicable concentrations. The use of this approximation for the calculation of diffusion coefficients and consideration of the delay time before diffusion set in as a separate parameter should therefore be valid for determination of diffusion coefficients for the diffusion of liquids into PVOH, which are likely to be concentration dependent in the case of water and aqueous solutions. Initial tests found that the model was adequate to allow a semi-quantitative description and comparison of the data.

Similar problems arose for fitting the data obtained from the diffusion of acetone/ water mixtures into these samples. In mixtures with excess water the diffusion behaviour of both acetone and water was similar to that observed in the diffusion experiments of pure water into PVOH.

With a reduction of the water fraction in the diffusant mixtures the diffusion mechanism appeared to be altered as the shape of the diffusion curves changed. Data for the diffusion acetone fraction in mixtures with an excess of acetone was fitted a dual mode model. This model describes two Fickian diffusion processes occurring at the same time and was found to give a good representation of the shape of the diffusion curve if the time delay at the beginning was treated as a separate parameter. The fitting procedure was, however, a purely mathematical one and values for the single diffusion coefficients obtained from this process as well as the ratio between them varied significantly making a meaningful interpretation of the data difficult.

Application of a more detailed model might, however, be able to give a better representation of the data than this approximation. As it is unlikely that all data could be fitted to one general model and no such model could be found in the literature the short term approximation of Fickian diffusion was deemed

sufficient to enable discussion of the processes observed during the diffusion of water and acetone/ water mixtures into PVOH and its nanocomposites.

4.5 Data fitting process

To calculate diffusion coefficients using the short term approximation given in equation 4-5 data was plotted against √time and the slope of the linear section of this part was determined. In order to do so only the data between the onset of the diffusion process and $\frac{M_t}{M_\infty} = 0.5$ was plotted using an Excel spreadsheet. A linear trendline was then fitted to that data, utilising the functions of the Excel software, to obtain the value for the slope of this line. For some of the faster water diffusion processes only two data points were available within the limits described above. In such cases the next collected data point was included in the fitting to obtain a more representable fit. Some of the data collected showed a very slow increase at short times rather than time delay where the intensity of the bands of interest remained zero. In these cases the diffusion coefficient was determined from the "secondary slope" which could be observed after diffusion had set in.

The relationship between the slope of this linear fit and the diffusion coefficient and sample thickness according to the short term approximation (equation 4-5) is given by

$$m = \frac{2}{L}\sqrt{\frac{D}{\pi}}$$ **Equation 4-14**

which can be re-arranged to calculate the diffusion coefficient

$$D = \pi \left(\frac{mL}{2}\right)^2$$ **Equation 4-15**

The time delay before diffusion could be observed was obtained by calculating the x=0 intercept of the linear fit of the data. In order to use this value for comparisons of data the ratio of this time delay to the sample thickness was calculated. Data for the different diffusion experiments was compared with respect to the time delay/ sample thickness ratio and the diffusion coefficients obtained from equation 4-15.

4.6 References

4.1 George SC, Thomas S, *Prog. Polym. Sci.*, **26**, 985 (2001)
4.2 Paul DR, *ACS Sym. Ser.*, **285**, 253 (1985)
4.3 Bénière F, *Defect and Diffusion Forums*, **194-199**, 897 (2001)
4.4 van Alsten JG, *Trends Polym. Sci.*, **3**, 272 (1995)
4.5 Rossi G, *Trends Polym. Sci.*, **4**, 337 (1996)
4.6 Sammon C, Yarwood J, Everall N, *Polymer*, **41**, 2521 (2000)
4.7 Lagaron JM, Catala R, Gavara R, *Mater. Sci. Tech.-Lond.*, **20**, 1, (2004)
4.8 Hedenqvist M, Gedde UW, *Prog. Polym. Sci.*, **21**, 299 (1996)
4.9 Sfirakis A, Rogers CE, *Polym.Eng. Sci.*, **21**, 542 (1981)
4.10 Billovits GF, Durning CJ, *Polymer*, **29**, 1468 (1988)
4.11 Lim LT, Britt IJ, Tung MA, *J. Appl. Polym. Sci.*, **71**, 197 (1999)
4.12 Shafee EE, Naguib HF, *Polymer*, **44**, 1647 (2003)
4.13 Balik CM, Simendinger III WH, *Polymer*, **39**, 4723 (1998)
4.14 van der Wel GK, Adan OCG, *Prog. Org. Coat.*, **37**, 1 (1999)
4.15 Fieldson GT, Barbari TA, *AIChE J.*, **41**, 795 (1995)
4.16 Linossier I, Gaillard F, Romand M, Feller JF, *J. Appl. Polym. Sci.*, **66**, 2465 (1997)
4.17 Edwards DA, *J. Polym. Sci.: Pt. B Polym. Phys.*, **34**, 981 (1996)
4.18 Thomas NL, Windle AH, *Polymer*, **23**, 529 (1982)
4.19 Barbari TA, *J. Polym. Sci.: Pt. B Polym. Phys.*, **35**, 1737 (1997)
4.20 Billovits GF, Durning CJ, *Chem. Eng. Commun.*, **82**, 21 (1989)
4.21 Marechal Y, *J. Mol. Struct.*, **648**, 27 (2003)
4.22 Iordanskii AL, Razumovskii LP, Krivandin AV, Lebedeva TL, *Desalination*, **104**, 27 (1996)
4.23 Gusev AA, Lusti HR, *Adv. Mater.*, **13**, 1641 (2001)
4.24 Perrin L, Nguyen QT, Clement R, Neel J, *Polym. Int.*, **39**, 251 (1996)
4.25 Coyle FM, Martin SJ, McBrierty VJ, *J. Mol. Liq.*, **69**, 95 (1996)
4.26 Iwamoto R, Murase H, *J. Polym. Sci.: Pt. B Polym. Phys.*, **41**, 1722 (2003)
4.27 Maeda Y, Ide M, Kitano H, *J. Mol. Liq.*, **80**, 149 (1999)
4.28 Maeda Y, Kitano H, *Spectrochim. Acta A*, **51**, 2433 (1995)
4.29 Maeda Y, Tsukida N, Kitano H, Terada T, Yamanaka J, *J. Phys. Chem.*, **97**, 13903 (1993)
4.30 Elabd YA, Barbari TA, *AIChE J.*, **47**, 1255 (2001)
4.31 Lange J, Wyser Y, *Packag. Technol. Sci.*, **16**, 149 (2003)
4.32 Guizard C, Bac A, Barboiu M, Hovnanian N, *Sep. Purif Technol.*, **25**, 167 (2001)
4.33 Gorrasi G, Tortora M, Vittoria V, Galli G, Chiellini E, *J. Polym. Sci.: Pt. B Polym. Phys.*, **40**, 1118 (2002)
4.34 Gorrasi G, Tortora M, Vittoria V, Poller E, Lepoittevin B, Alexandre M, Dubois P, *Polymer*, **44**, 2271 (2003)
4.35 Bharadwaj RK, Mehrabi AR, Hamilton C, Trujillo C, Murga M, Fan R, Chavira A, Thompson AK, *Polymer*, **43**, 3699 (2002)
4.36 Tortora M, Vittoria V, Galli G, Ritrovati S, Chiellini E, *Macromol. Mater. Eng.*, **287**, 243 (2002)
4.37 Gorrasi G, Tammaro L, Vittoria V, Paul MA, Alexandre M, Dubois P, *J. Macromol. Sci. Phys.*, **B43**, 565 (2004)
4.38 Becker O, Varley RJ, Simon GP, *Europ. Polym. J.*, **40**, 187 (2004)

4.39 Farinas KC, Doh L, Venkatraman S, Potts RO, *Macromol.*, **27**, 5220 (1994)
4.40 Lavrentjev VV, Popov VY, Vasenin RM, *J. Polym. Sci. USSR*, **17**, 1869 (1975)
4.41 Brandt VH, Rieger P, *Exp. Techn Phys.*, **32**, 413 (1984)
4.42 Brandt VH, *Exp. Techn Phys.*, **33**, 417 (1985)
4.43 'The Mathematics of Diffusion', 2nd Ed., (Ed. Crank J), Clarenden Press, Oxford (1994)
4.44 'Diffusion in and through Polymers', (Ed. Vieth WK), Hanser Publishers, Munich (1991)
4.45 'Polymer Permeability', 2nd Ed., (Ed. Comyn J), Chapmann & Hall, London (1994)
4.46 Fieldson GT, Barbari TA, *Polymer*, **34**, 1146 (1993)
4.47 Hodge RM, Bastow TJ, Edward GH, Simon GP, Hill AJ, *Macrom.*, **29**, 8137 (1996)
4.48 Colombo P, *Adv. Drug Deliver. Rev.*, **11**, 37 (1993)
4.49 Colombo P, Bettini R, Santi P, Peppas NA, *Pharm. Sci. Technol. To.*, **3**, 198 (2000)
4.50 Siepmann J, Peppas NA, *Adv. Drug Deliver. Rev.*, **48**, 139 (2001)

5 Diffusion of liquid water into poly (vinyl alcohol) and poly (vinyl alcohol)/ clay nanocomposites

5.1 Introduction

Diffusion measurements of liquid water into PVOH and PVOH nanocomposite films prepared from polymers of different molecular weight, and with a variety of sodium and lithium clays have been performed by ATR-FTIR. Most of these experiments where recorded at 40 °C, since films were dried over night at this temperature. Furthermore, running experiments at 40 °C ensured stable temperatures throughout the experiment independent of the temperature in the lab. Additionally, some measurements have been recorded at 30 °C and 50 °C respectively to investigate the temperature dependence of the diffusion process. Information on the kinetic parameters of diffusion was obtained by fitting a straight line to the slope of the data when plotted as integrated area versus the square root of time and calculating diffusion coefficients from the short term approximation of Fickian diffusion as described in the previous chapter.

5.1.1 Vibrational spectra of liquid water

The spectra arising from liquid water have been of interest to spectroscopists for a long time [5.1]. While water is very common comparatively little is known about the structure of this liquid [5.2].

Although infrared spectroscopy is very sensitive to changes in hydrogen bonding, it was rarely used to investigate pure water in early investigations of the water structure. This is mainly due to the fact that water absorption is very strong and therefore saturation of the bands easily occurs. The use of attenuated total reflection Fourier transform infrared spectroscopy (ATR-FTIR) has enabled the collection of water spectra without saturated bands. This has simplified the analysis of water by infrared spectroscopy, because this method only probes a few micrometers of a sample. As a result of this, the number of studies has increased rapidly since the 1980's [5.2].

Overlapping of different vibrational bands and inter- and intra-molecular coupling makes the analysis of pure water or pure heavy water difficult. To

achieve a decoupling of these vibrational modes mixtures of HOD with various concentrations of H_2O or D_2O respectively have been studied [5.3, 5.4].

Throughout the years two different models have been used to explain the spectra observed for water. The continuum model [5.5 - 5.8] interprets the intensity distribution across the ν(OH) band as a distribution of hydrogen bonding energies and geometries. The mixture approach [5.9 – 5.11], on the other hand, interprets water as a mixture of hydrogen bonded and non-hydrogen bonded molecules. The existence of isosbestic points has often been used as apparent proof for the mixture model. However, more detailed analysis showed that these points can only be observed within small temperature intervals and gradually shift to higher frequency with increasing temperatures [5.3, 5.9]. Examples of ATR-FTIR spectra of water recorded at different temperatures are presented in Figure 5-1.

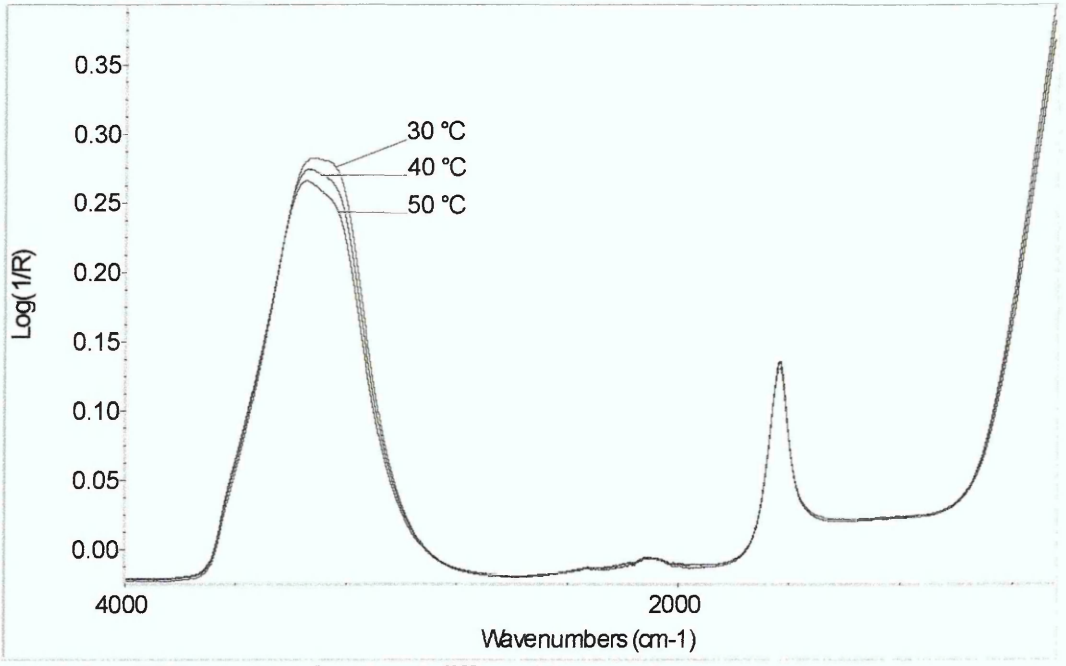

Figure 5-1 ATR spectra of water at different temperatures

Libnau et al. [5.12] used partial least squares analysis (PLS) and evolutionary curve resolution to interpret the spectrum of water in terms of the mixture model. Employing these methods, they were able to show that water can be considered as a two component mixture, in which the two components differ by approximately 0.5 hydrogen bonds per water molecule. They concluded that the water structures proposed by Benson and Siebert [5.11] who suggested that water formed either cubic octamers which break up into tetramers or a

combination of polycyclic decamers and monocyclic pentamers can both be supported by these findings.

5.1.2 States of water in polymers

The state of water in polymers has been investigated by various methods; e.g. dielectric spectroscopy, neutron scattering, nuclear magnetic resonance spectroscopy (NMR), differential scanning calorimetry (DSC) and Fourier transform infrared spectroscopy (FTIR) [5.13].

The number of 'states' of water present in polymers depends on the hydrophilicity of the polymer, and the overall concentration of water. For some hydrated polymer systems, up to four types of water have been reported [5.14]. The intensity of polymer/ water interactions depends on the polarity of the macromolecule fragments, and has a great influence on the sorption and diffusion behaviour observed when water enters polymeric materials [5.15].

DSC studies of water swollen PVOH revealed that no water phase transition can be observed in the samples up to a water content of 24 - 30 weight percent. This form of water has therefore been labelled "non freezable water". At higher water contents, crystallisation of water can be observed at sub zero temperatures. A further increase in water content results in an additional peak in the DSC trace near 0 °C. These two peaks were assigned to "freezable bound water" and "free water" respectively [5.16 – 5.21]. All studies showed that the temperature at which water crystallises, upon cooling of the sample, is about 10 - 20 K lower than the temperature at which melting peaks can be observed, during heating of the sample. These differences have been explained by supercooling of water during cooling runs [5.21].

Rault et al. [5.20] showed that the amount of crystallisable water in PVOH is governed by regulation of the glass transition temperature. As crystallisation of the solvent in the binary systems involves a segregation of the system the concentration of the remaining liquid is decreased thereby changing the properties of the polymer while solvent crystallisation occurs. According to this mechanism non-freezable water in PVOH is not due to strong binding of water to PVOH, but a result of the polymer/ water system reaching a glassy state before the water can crystallise [5.22, 5.23].

Krzeminski [5.24] observed two types of water in PVOH in spectra obtained by IR, Raman, and broad-band NMR spectroscopy; water that is bonded to hydroxyl groups (hydration water) and free (condensation) water. The latter could only be observed above 23 wt% water content in the sample. This limit is similar to the water concentration necessary in PVOH to observe "freezable bound water" in DSC traces.

Spectroscopic methods have so far been unable to corroborate these states of water found in DSC measurements. It appears therefore likely that the identification of different dynamical states of water in hydrogels depends on the process used to probe the system. Using molecular modelling Müller-Plathe [5.25] showed that evidence of two different states of water can only be observed below the freezing point of water.

Investigating the changes occurring in Raman spectra, Maeda and Kitano [5.27] observed three different types of water in aqueous polymer gels; hydration water which is strongly bonded to the polymer, water surrounded by polymer chains and bulk water. The OH stretching band observed for such systems is narrower than that of pure water as water molecules are restricted in their position and orientation in hydration shells by the presence of polymer chains [5.26 - 5.28].

FTIR has been shown to be a powerful tool for the investigation of changes in hydrogen bonding during the hydration of polymers. The time scale of vibration is much smaller than that for the formation and destruction of hydrogen bonds (10^{-14} seconds and 10^{-10} to 10^{-12} seconds respectively) which results in the observation of several bands in the OH stretching region arising from different types of hydrogen bonding [5.13, 5.29]. Hydrogen bonding causes a broadening of bands arising from the structures engaging in hydrogen bonds and enhances their infrared intensities [5.13, 5.29]. At the same time, shifts of the peak centres can be observed with the OH stretching mode generally shifting to lower frequency, and the OH bending mode shifting to higher frequency, with increasing hydrogen bonding [5.5, 5.30, 5.31].

A precise measurement of water molecules in membranes requires accurate knowledge of the relationship between the band intensity and the strength of

hydrogen bonds [5.32]. If this relationship is known, concentrations of different forms of hydrates can be calculated. Studying the changes in hydrogen bonding occurring during the hydration of polymers can give an insight into the mechanism by which hydration occurs [5.2].

For the diffusion of water into PMMA, Sutandar et al. [5.29] observed four bands in the OH stretching region, which they assigned to monomeric non hydrogen bonded water, hydrogen bonded dimers, small hydrogen bonded water clusters and water chains respectively. At short times diffusion of water vapour was observed followed by bulk water leading to an increase of water clusters in the film over time.

Measuring the dehydration of nylon-6 films by FTIR Iwamoto and Murase [5.33] observed significant changes in the OH stretching region when subtracting the spectra of hydrated samples from the dry spectrum. This led to the assumption that water in nylon-6 membranes hydrogen bonds to the carbonyl moieties of the polymer.

Ide et al. [5.34] fitted five Gaussian bands to the OH stretching band observed for water in poly (ethylene glycol dimethyl ether) (PEG-DME). According to their interpretation, these bands were due to monomeric, di- or tri-meric water and three bands arising from water clusters and polymer/ water interactions.

Ping et al. [5.19] observed two distinct water populations in their spectra of hydrated PVOH. Peak centres for these ν(OH) bands were located at 3400 cm^{-1} and 3280 cm^{-1} respectively. The bands were interpreted as water molecules directly attached to active sites, and water molecules in a second hydration layer.

For water in polynaphthoylimide, Chenskaya et al. [5.35] fitted three bands to the ν(OH) region. They assigned a band at 3580 cm^{-1} to non freezing water that is bonded to the carbonyl and amide groups of the polymer. A second band was assigned to bulk water in pores, while the last band was interpreted as clustered water with the polymer.

Studying the diffusion of water into poly (vinyl acetate) Nguyen et al. [5.36] observed initial diffusion of monomeric water, identified by a band at 3620 cm^{-1}

in the infrared spectrum while later in the experiment clusters of water large enough to behave like bulk water can be observed by DSC measurements.

Comparing diffusion data for water diffusion into PET, PVC and SPEES/ PES respectively, Sammon et al. [5.13, 5.31, 5.37, 5.38] found that the water network is broken down into smaller clusters when entering polymeric materials. In all of these polymeric systems, four different types of water have been identified in the spectra of the hydrated samples. Furthermore, a deviation from Beer's law was noted, which is due to perturbation of the electronic field originating from the changing dipole moment of the bonds. For water diffusion into PET, this perturbation was found to be stronger for weaker hydrogen bonded species. Increasing the crystallinity of the sample resulted in a decrease of the overall perturbation of the ν(OH) band [5.12].

Information on polymer/ water interactions is not obvious from interpretation of the OH stretching mode alone. This band is primarily sensitive to changes in water - water hydrogen bonds. Structural information on the polymer can, however, be gained from bands arising from functional groups of the polymer, such as carbonyl or amide groups. Such bands exhibit shifts and changes in intensity, dependent on the strength of hydrogen bonds [5.31].

5.2 Measurement set-up and sample preparation

5.2.1 Schematic of the ATR-FTIR set-up

All measurements were performed using the Golden Gate™ ATR-FTIR attachment manufactured by Graseby Specac. This set-up uses a single reflection diamond crystal and also provides a heating element to perform measurements at various temperatures. Experiments were recorded on a Thermo Nicolet Magna 860 FTIR spectrometer and a Thermo Nicolet Nexus FTIR spectrometer equipped with a mercury cadmium telluride (MCT) detector.

To create the solvent reservoir on top of the film, a standard gas cell from Graseby-Specac was modified to only have a free volume above the crystal. This reduction of the liquid reservoir was found to be necessary to ensure that good contact between the sample, and the crystal could be maintained at all times. Compared to the thickness of the film, the liquid reservoir still remained infinite.

Solvent was introduced via syringes to create an infinite solvent supply in relation to the sampling area. A schematic of the set-up is shown in Figure 5-2.

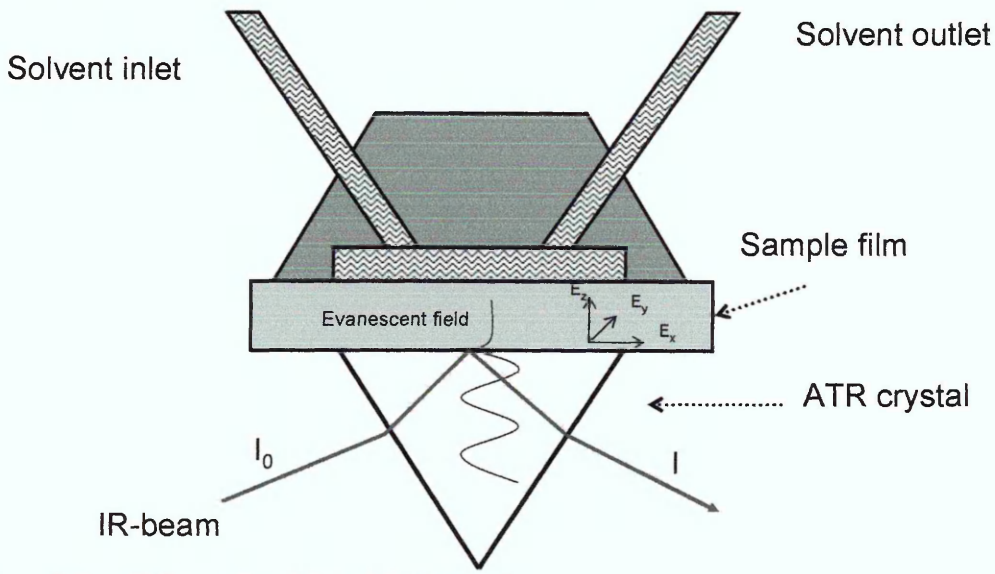

Figure 5-2 Schematic of the diffusion cell

5.2.2 Sample preparation

Polymer and polymer/ clay samples were prepared as described in chapter 3.5.2.2. The nanocomposite mixtures were continuously stirred until the film was cast to prevent the clay from settling out of solution.

Samples were prepared by casting 0.25 mL of an aqueous solution with a combined polymer and clay content of 5 wt% directly onto the Golden Gate accessory. The solution was spread out to completely cover the heatable area of the accessory. Such films had thicknesses of 20 – 30 µm depending on the amount and type of polymer. Samples were dried over night at 40 °C and experiments performed at the same temperature.

For the experiments at 30 °C and 50 °C respectively the temperature was adjusted before running the experiment. Samples were allowed to equilibrate at the new temperature for 45 minutes before the diffusion experiment was started.

5.2.3 Parameters for data collection

Spectra were recorded at various time intervals using a macro to specify the delay times between the collection of individual spectra. The liquid was injected into the cell immediately after the first spectrum was taken.

All work on temperature induced changes was carried out on the Thermo Nicolet Magna 860. Spectra were recorded as averages of 10 scans at 4 cm^{-1} resolution and saved as single beams. Spectra were recorded for 40 minutes. The intervals between the collection of spectra for this set-up are given below.

- 40 spectra without delays (time to collect 1 spectrum: 8 seconds)
- 45 spectra with 12 seconds delay
- 20 spectra with 52 seconds delay

Later in the project, experiments were performed on a newly acquired Thermo Nicolet Nexus FTIR system. This system was capable of collecting spectra of 1 scan without any delays between the spectra. Consequently data collection for the first few minutes could be performed more accurately. Resolution was kept at 4 cm^{-1} and spectra saved as single beams. Sampling intervals for this method are presented below. The collection time for each series was 90 minutes.

- 90 spectra without delays (time to collect 1 spectrum: 1.5 seconds)
- 52 spectra with 3 seconds delay
- 70 spectra with 26 seconds delay
- 60 spectra with 58 seconds delay

Data collection was continued well beyond the diffusion process reaching equilibrium in order to investigate whether changes in the sample due to swelling and plasticisation could be observed at longer times.

For both collection methods, a background spectrum was taken after the removal of the sample at the end of the experiment. The single beam spectra were later reprocessed in two ways. For the first set the single beam spectra were ratioed against a single beam spectrum of the clean crystal (background spectrum), while the second set of spectra was obtained from ratioing against the dry film.

5.3 Obtaining diffusion data

5.3.1 Obtaining kinetic information on the diffusion of water from ATR-FTIR spectra

Changes occurring in the OH stretching region were found to be very complex, since the band is due to overlapping bands arising from stretching vibrations of the PVOH hydroxyl groups, water diffusing into the sample film and polymer/ water interactions.

In the difference spectra the reduction of the contribution of the PVOH hydroxyl stretching vibrations can be observed in the reduced intensity splitting the band into two components around 3280 cm^{-1} (see Figure 5-3). While kinetic data can be obtained by integration of this band (between 3700 and 3000 cm^{-1}), the changes caused by the swelling of the polymer are likely to cause an error in the calculation of diffusion coefficients.

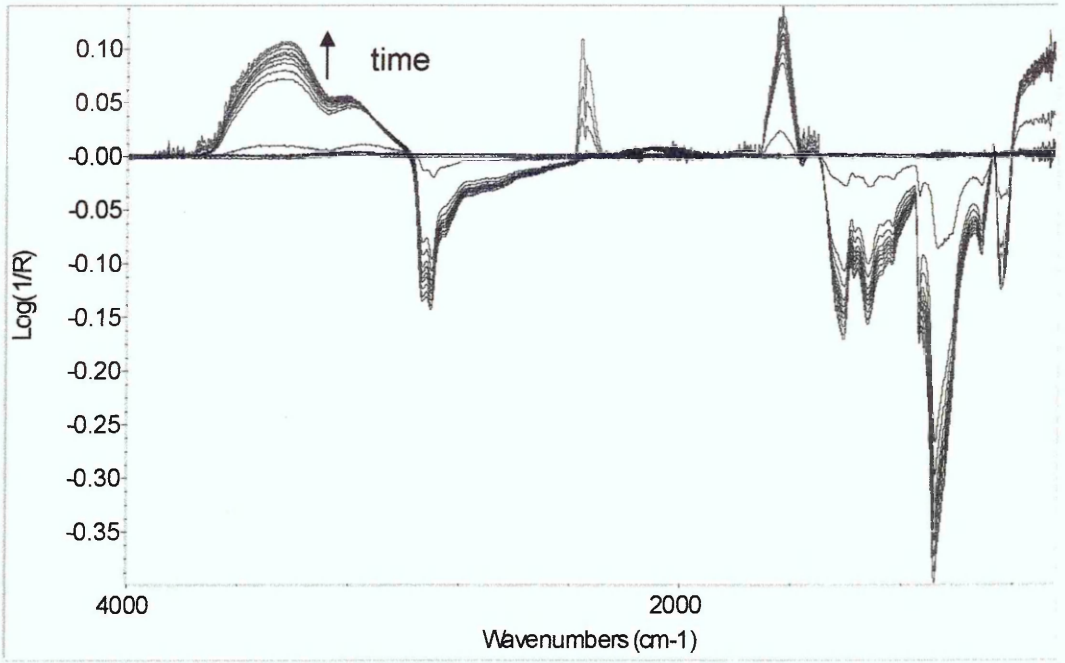

Figure 5-3 Difference spectra (against dry film) of diffusion of water into high molecular weight PVOH

The changes in the δ(OH) region similarly arise from a combination of increasing water levels in the sample, changes in hydrogen bonding and swelling of the polymer. Since the bending mode is less sensitive to different environments, this band is less complex than the ν(OH) mode. Furthermore, the bands arising from the OH bending vibrations of water in the polymer and the OH bending vibrations of the polymer are separated bands with peak centres at 1650 cm^{-1} and 1567 cm^{-1} respectively (see Figure 5-4). The peak position of the δ(OH) band of PVOH is unusually low. However, behaviour of this band appears to indicate that it is indeed arising due to OH vibrations of the polymer, since it reduces and shifts towards higher wavenumbers, with increasing water content in the sample.

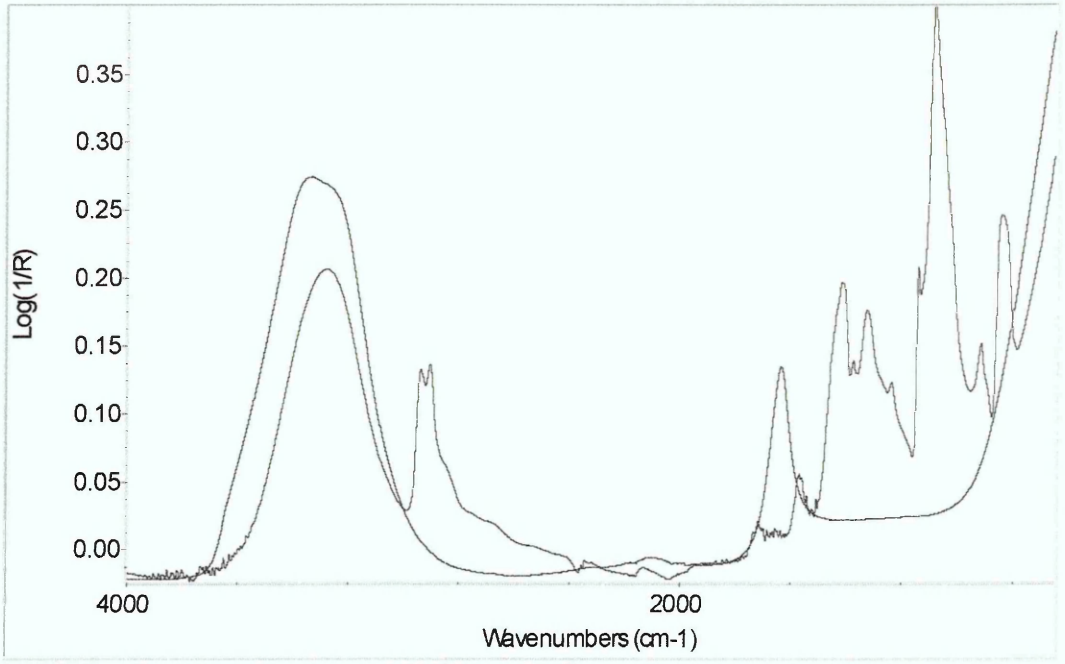

Figure 5-4 Spectra of water and PVOH at 40 °C

Therefore the δ(OH) band was chosen for integration to obtain kinetic data on the diffusion of water into PVOH. The data was obtained by integration of the difference spectra (ratioed against the dry film) between 1740 cm^{-1} and 1565 cm^{-1} with the baseline set to the same limits (see Figure 5-5).

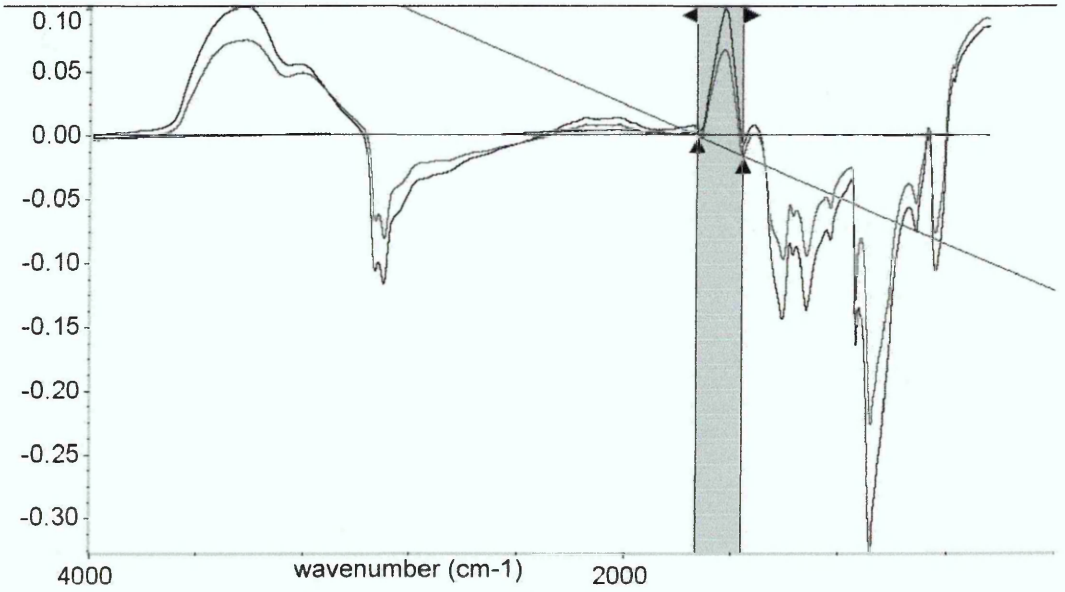

Figure 5-5 Examples for integration of the δ(OH) band

5.3.2 Obtaining information on swelling, changes in crystallinity and clay levels

To assess the changes occurring within the polymer during the diffusion of water into the sample, changes in bands sensitive to changes in crystallinity, clay content and swelling have been followed over time.

The swelling behaviour of the sample film was studied by recording the decrease of the area of the ν(C-O) band over time. This vibration has a very strong peak in the spectrum of dry PVOH and is not overlaid by any water bands. The peak area for this band was obtained from integration between 1133 cm^{-1} and 1057 cm^{-1} with the baseline set between 1160 cm^{-1} and 954 cm^{-1}. The baseline was applied to the spectra between these points to ensure reproducible integration and limit the variation in the baseline applied by the program. Setting the baseline to exactly the same limits as the integration limits, was found to result in peak areas that were influenced strongly by changes in the baseline setting. This was due to shifts and broadening of the peaks of interest, rather than changes in the true baseline.

Changes in the crystallinity were assessed from the ratio of the area of the shoulder at 1140 cm^{-1} to the area of the ν(C-O) peak. The integration limits for the 1140 cm^{-1} band were 1160 cm^{-1} to 1133 cm^{-1}. Baseline was set to the same limits as for the ν(C-O) integration.

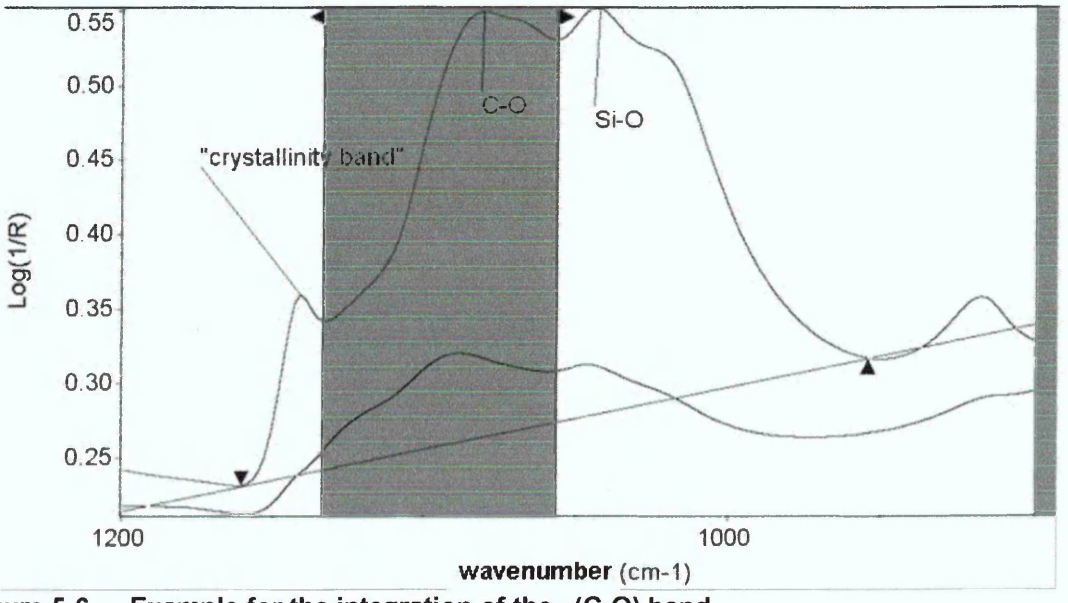

Figure 5-6 Example for the integration of the ν(C-O) band

For the nanocomposites, any changes in the amount of clay in the evanescent field were assessed by following the change in the ratio of the area of the ν(Si-O) band to the area of the ν(C-O) band. The ν(Si-O) band of the clay was seen as a shoulder around 1045 cm^{-1} even at clay levels as low as 2.5 wt%. Integration limits for this band were set to 1057 – 954 cm^{-1} with the baseline set to 1160 – 954 cm^{-1}. An increase in this ratio could point to the clay settling out of the gel, and therefore indicate a phase separation of the composite, which has been observed in nanocomposites formed by kinetic processes.

5.3.3 Obtaining information on changes in the hydrogen bonding of water molecules

The OH stretching vibration is very sensitive to changes in hydrogen bonding, especially changes in the hydrogen bonding of water. Water diffusing into PVOH undergoes changes in its hydrogen bonding network due to interactions with the polymer and restricted movement of water molecules in the polymer matrix. As the concentration of water in the polymer films increases the inter- and intra-molecular hydrogen bonds of PVOH are weakened due to swelling of the sample. This change in hydrogen bonding and the increasing water concentration in the PVOH films led to a shift towards higher frequencies and broadening of the ν(OH) band.

To further assess these changes and compare them to pure water and the dry polymer four peaks were fitted to the ν(OH) band. While DSC studies only found three different states of water in PVOH [5.16 - 5.21], four different strengths of hydrogen bonding have been reported for the diffusion of water into several polymers [5.12, 5.31, 5.37, 5.38]. The result of the peak fitting for pure water is shown in Figure 5-7. These four bands have been labelled strong, moderately strong, moderately weak and weak hydrogen bonded water.

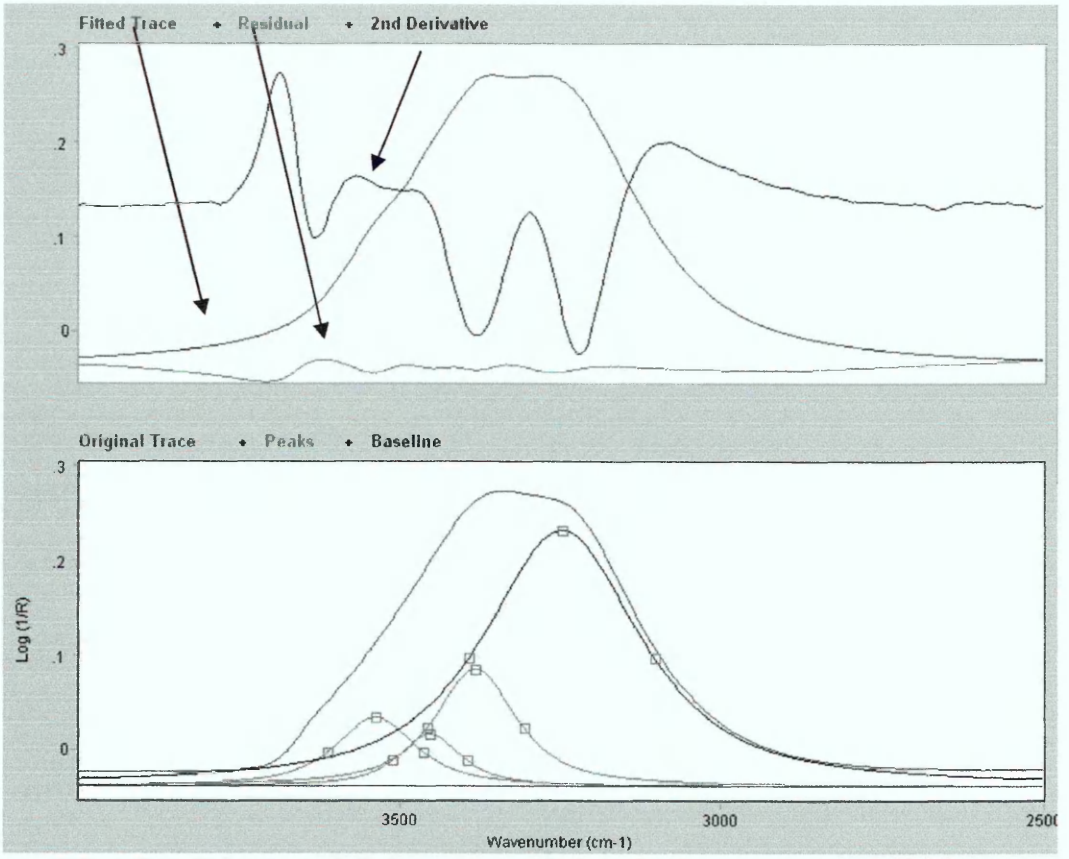

Figure 5-7 Result from peak fitting of the ν(OH) region in pure water at 40 °C

For the PVOH samples, two further peaks were added to the OH stretching region to account for weakly and strongly hydrogen bonded PVOH. The position of these peaks had previously been determined by fitting two bands to the ν(OH) region of spectra of dried PVOH films. Furthermore, three peaks were fitted to the ν(CH) region. All peaks were fitted using a mixed Gaussian and Lorentzian band shape with a minimum Lorentzian contribution of 50%. An example for this fit is shown in Figure 5-8 and parameters for the fitting process are given in Table 5-1.

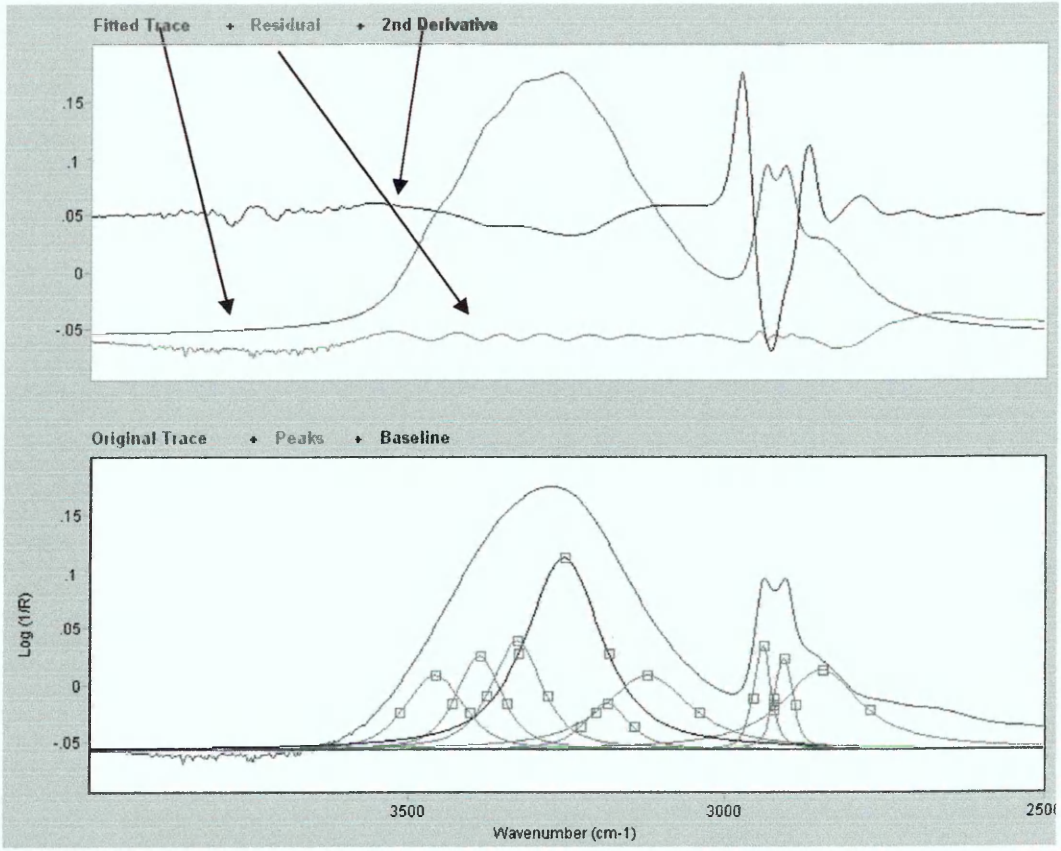

Figure 5-8 Result from peak fitting of the ν(OH) region in low molecular weight PVOH at 40 °C

Peak	restrictions
weakly hydrogen bonded water	position: 3400 – 3500 cm^{-1}, max. width 200 cm^{-1}
weakly hydrogen bonded PVOH	position: 3386 - 3387 cm^{-1}, max. width 200 cm^{-1}
moderately weak hydrogen bonded water	position: 3300 – 3400 cm^{-1}, max. width 200 cm^{-1}
strongly hydrogen bonded PVOH	position: 3253 - 3254 cm^{-1}, max. width 400 cm^{-1}
moderately weak hydrogen bonded water	position: 3100 – 3200 cm^{-1}, max. width 200 cm^{-1}
strongly hydrogen bonded water	position: 3100 – 3200 cm^{-1}, max. width 200 cm^{-1}
$\nu_{as}(CH_2)$	position: 2940 - 2943 cm^{-1}, width 25 - 50 cm^{-1}
$\nu_{s}(CH_2)$	position: 2906 - 2909 cm^{-1}, width 25 - 100 cm^{-1}
ν(CH)	position: 2848 - 2851 cm^{-1}, max. width 150 cm^{-1}

Table 5-1: Fitting parameters for region between 4000 cm^{-1} and 2500 cm^{-1} in PVOH samples

Restricting the bands attributed to OH vibrations of the polymer in their position within one wavenumber, even though spectra were recorded at a resolution of 4 cm^{-1}, was found necessary to obtain meaningful data for the integration of the bands assigned to the different types of hydrogen bonded water within the polymer. While such treatment is disregarding any peak shifts due to changes in the hydrogen bonding strength of the polymer, it allowed collection of data for the changes in hydrogen bonding strength of the water molecules within the polymer.

5.4 Results and discussion

5.4.1 Diffusion of water into low molecular weight poly (vinyl alcohol) and its nanocomposites

Diffusion measurements of water into PVOH and PVOH nanocomposites have been performed on various samples. We have investigated the influence of clay loading, clay structure, molecular weight of the polymer and temperature on the diffusion and the changes occurring during swelling of the PVOH films.

The clays used were Na^+ Cloisite®, Na^+ MCBP and Li^+ MCBP. The sodium clays were used as received. Li^+ MCBP was prepared as described in chapter 3.3.1. The samples referred to as low molecular weight PVOH had an average molecular weight of 31,000 – 50,000, and the high molecular weight PVOH had an average molecular weight of 146,000 – 186,000.

5.4.1.1 Effect of clay loading on the diffusion of water into low molecular weight poly (vinyl alcohol)/ Na+ Cloisite® nanocomposites

Diffusion experiments were performed on samples which were prepared from solutions with clay contents of 0 wt%, 2.5 wt% and 5 wt%. Data on the diffusion of water into these samples was collected on the Nicolet Magna 860 FTIR spectrometer as described in chapter 5.2.3. Due to swelling and gelling of the samples, these could not be peeled of the crystal after the experiment to obtain the exact sample thickness. The thickness was therefore estimated based on the volume of solution used to cast the film and its density, which was calculated from the concentration of the polymer within the solution.

Figure 5-9 presents typical diffusion curves for the diffusion of water into PVOH and PVOH nanocomposites with various amounts of Na^+ Cloisite®. The clay does not appear to have a significant effect on the diffusion rate.

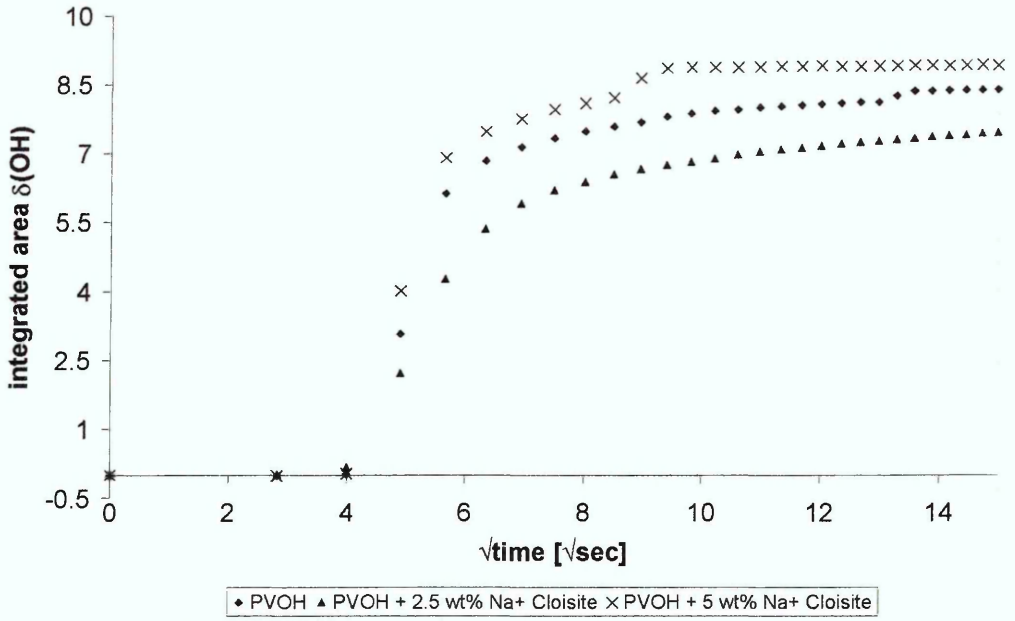

Figure 5-9 Experimental data for diffusion of water into low molecular weight PVOH and its nanocomposites

Samples swelled considerably when water is introduced into the films and formed a gel. As no unique model could be found that would account for the changes occurring during the ingress of water into PVOH films estimates of Fickian diffusion coefficients were obtained by using the short time approximation of Fickian diffusion. The limitations and reasons for choosing this model were discussed in chapter 4.4. Figure 5-10 presents the results of such fitting for the data sets obtained from the diffusion of water into PVOH and a PVOH/ Na^+ Cloisite® nanocomposite with a clay loading of 2.5 wt%.

It is obvious from the data presented in Figure 5-10 that the slope of these diffusion curves is represented by the linear fit reasonably well. The use of this approximation does not, however, take any changes in the general shape of the diffusion curve into account. Furthermore, fits were sometimes found to be poor, as the number of data points within the limits in which this approximation was valid is very limited in these data sets.

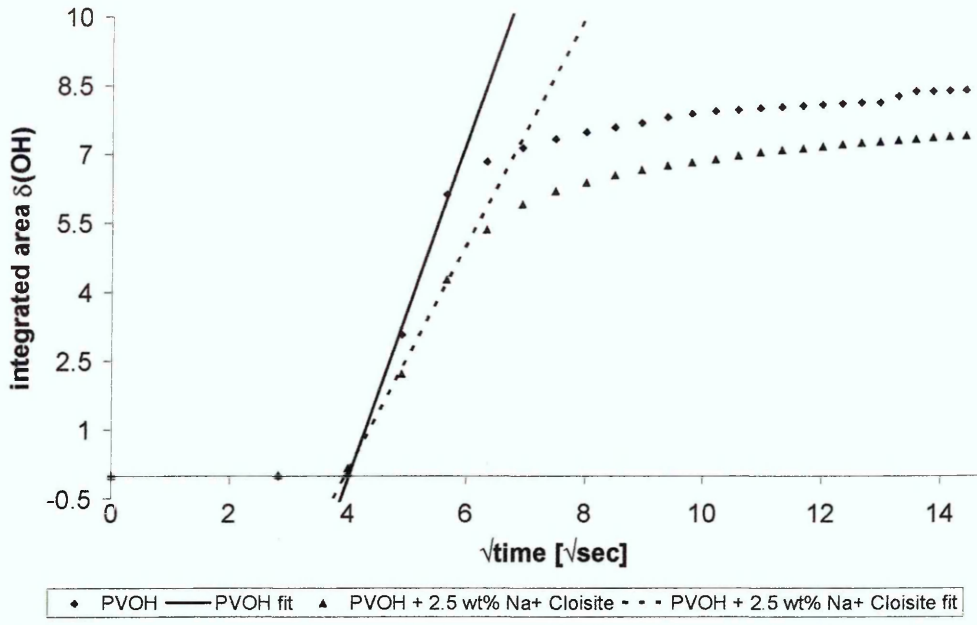

Figure 5-10 Experimental diffusion curves and short term approximation of Fickian diffusion fits for diffusion of water into low molecular weight PVOH and its nanocomposites

The R^2 values for these linear fits were usually above 0.9. The variation of the fitting of the slope caused by the scatter of the data in case of few data points did, however, have limited influence, compared to the uncertainty of the calculated diffusion coefficients introduced by the estimated variations in the thickness of the sample films. For the calculation of diffusion coefficients the thickness of the samples was assumed to be 25 µm ± 5 µm. These thickness estimates were also used to calculate the thickness independent delay time (intercept x=0/ L) before diffusion set in.

Further complications arise from the fact that the polymer changes from a glassy polymer to its rubbery state during the diffusion of water into the sample, since the glass transition temperature is significantly lowered by the presence of water in the sample films [5.39, 5.17]. Hodge et al. [5.17] showed that the glass transition temperature is reduced to ambient temperatures at water contents of 10 - 15 wt%. Though no attempts to quantify the equilibrium water content from the ATR spectra have been made during these experiments, due to lack of a suitable external calibration, it is likely that equilibrium water concentrations reached these levels. The use of the short term approximation of Fickian diffusion to obtain diffusion coefficients also neglects any influence which partial dissolution and gel formation may have on the diffusion mechanism of water through PVOH films. Further study is needed to quantify these influences.

Despite all these factors, limiting the applicability of a simple diffusion model to explain the data, the model used is still likely to enable at least a qualitative investigation of the changes that can be observed between different samples. The influence of the above mentioned uncertainties is expected to be only minor at the short times that are used for the calculation of diffusion coefficients in this case.

A summary of the diffusion coefficients and delay times for the diffusion of water into PVOH and its nanocomposites at 40 °C is given in Table 5-2.

Sample	intercept/L [min/µm]	D [cm²/sec]
PVOH	$1.08 * 10^{-2} \pm 2.24 * 10^{-3}$	$6.66* 10^{-5} \pm 2.66 * 10^{-5}$
PVOH + 2.5 wt% Na^+ Cloisite®	$1.04* 10^{-2} \pm 2.18 * 10^{-3}$	$3.00* 10^{-5} \pm 1.20 * 10^{-5}$
PVOH + 5 wt% Na^+ Cloisite®	$1.05* 10^{-2} \pm 2.20 * 10^{-3}$	$8.48* 10^{-5} \pm 3.39 * 10^{-5}$

Table 5-2 Summary of diffusion parameters for diffusion of water into PVOH and its nanocomposites at 40 °C

These results suggest that the incorporation of clay has little or no influence on the diffusion of water into PVOH films. Figure 5-11 and Figure 5-12 show a comparison of diffusion parameters for the diffusion of water into nanocomposites with different clay loadings at 40 °C. Because films cast from the same solution were found to have different clay levels (due to inhomogeneity of the solutions), clay levels were determined by ratioing the area of the ν(Si-O) band of the clay against the ν(C-O) band of the PVOH in the spectra of the dry films. Peak areas for these bands were obtained as described in chapter 5.3.2. The circled symbols correspond to the diffusion curves presented in Figure 5-10, while the other symbols are repeat runs of films cast from the same solutions. Triangles represent films cast from a solution with a nominal clay content of 2.5 wt%, while squares indicate films cast from 5 wt% solutions.

From these plots one can see that the results summarised in Table 5-2 are further supported by repeat experiments. From data obtained on the diffusion of small molecules into other polymers, one would assume that clay incorporation in the matrix slows down the diffusion process. As this is clearly not the case in the samples investigated here, it is likely that the interactions of water with the

polymer, and the changes these interactions induce, outweigh the influence of low clay levels on the diffusion process.

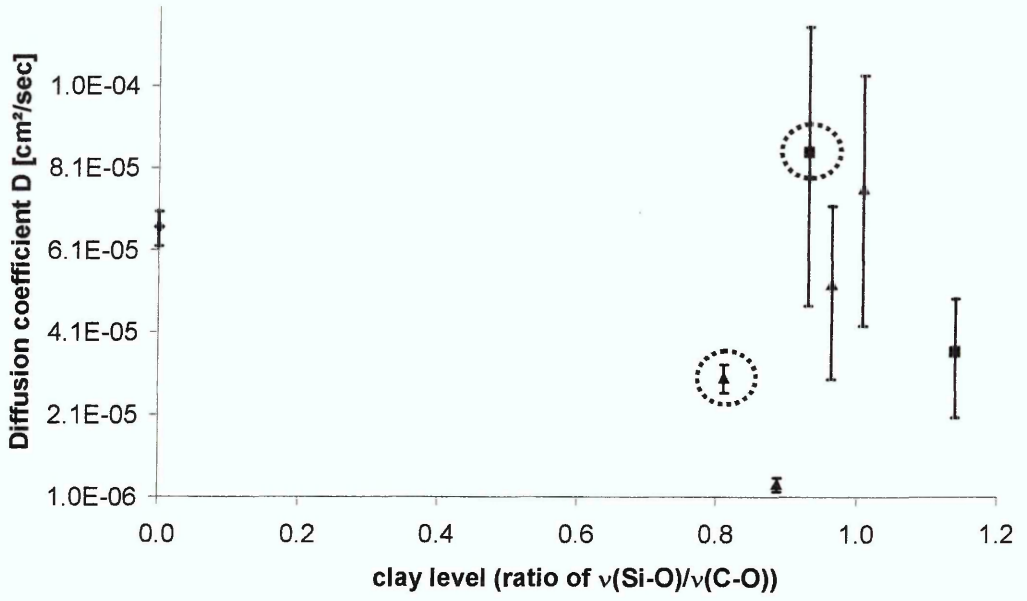

Figure 5-11 Comparison of diffusion coefficients for water diffusion into low molecular weight PVOH/ Na^+ Cloisite® nanocomposites

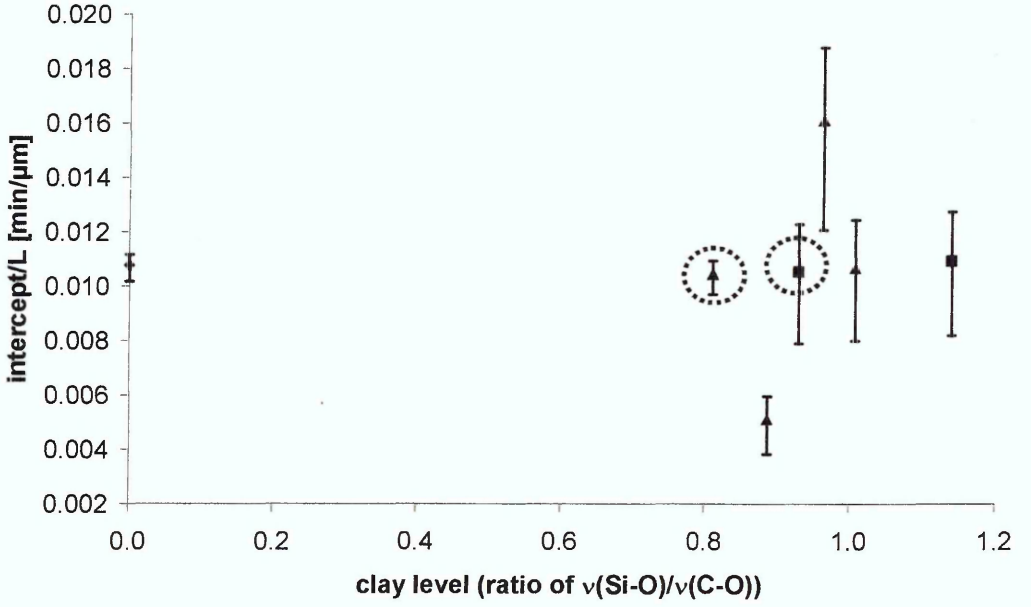

Figure 5-12 Comparison of "onset times" for water diffusion into low molecular weight PVOH/ Na^+ Cloisite® nanocomposites

This determination of the clay content of each film is likely to contain some errors, since only the thin section of the sample directly in contact with the crystal was sampled. This 'section' would only be representative of the whole sample if the clay did not settle out or aggregate during the drying process.

Collecting spectra at short intervals during the drying of some samples did not indicate any changes in the clay levels, once the polymer bands had reached higher intensities than the water bands. No attempts have been made to investigate whether evidence of clay settling out of solution could be extracted data from the spectra early in the drying process which are dominated by the water bands. As all films were about the same thickness and diffusion data was measured using the same method it is reasonable to assume that the data obtained from the ATR spectra gave a good representation in the differences in clay loading in the samples.

5.4.1.1.1 Effect of clay contamination on the diffusion of water into low molecular weight poly (vinyl alcohol)/ Na+ Cloisite® nanocomposites

During the characterisation of the Na^+ Cloisite® nanocomposites it was found that the batch of Na^+ Cloisite® used to prepare these samples had been contaminated by minor amounts of clay modified with an organic surfactant. As discussed in chapter 3.5.3.1.2, the influence of this contamination on the dispersion of the clay in the PVOH matrix appeared to be negligible. Nevertheless, diffusion experiments have been performed on nanocomposites prepared from this batch of clay and a new, clean batch to see if any differences in the diffusion behaviour could be observed in these samples. A comparison of diffusion curves obtained from the pristine polymer and nanocomposites prepared from the two batches of clay are presented in Figure 5-13.

XRD traces of samples with such low clay contents provided no evidence of differences in clay dispersion. This could, however, be due to the samples being either exfoliated or intercalated with a d_{001} spacing higher than 60Å, or a mixture of both, as no clay peaks were present in these XRD traces.

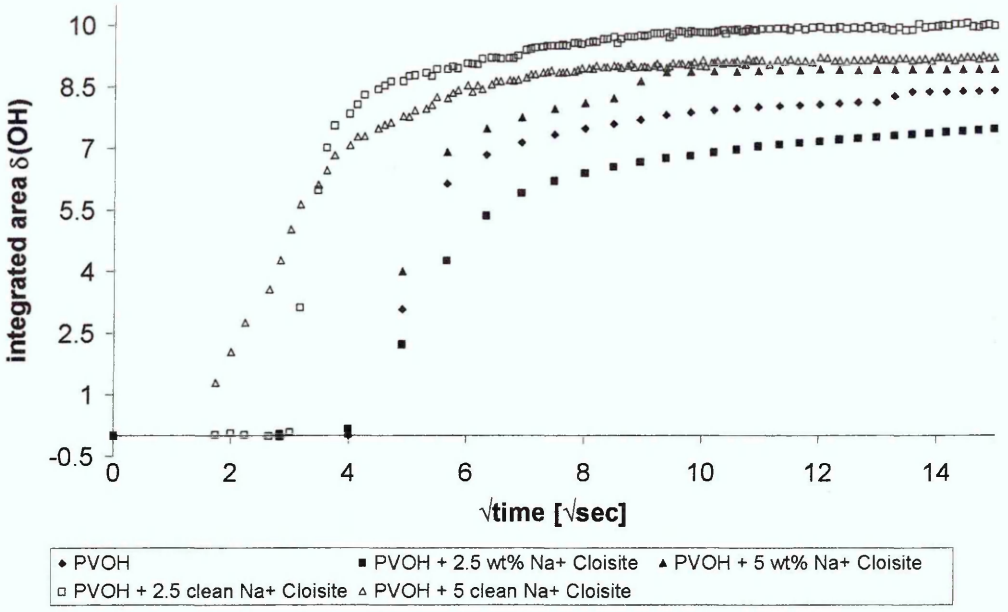

Figure 5-13 Experimental diffusion data for low molecular weight PVOH and its nanocomposites prepared from clean and organically contaminated Na^+ Cloisite®

Direct comparison of the diffusion behaviour shows that the samples prepared from clean Na^+ Cloisite® absorb more water at equilibrium than either the pristine polymer, or the nanocomposites prepared from the clay which had been organically contaminated. Such higher equilibrium sorption in nanocomposites has also been reported by Gorassi et al. [5.40, 5.41] for the diffusion of water vapour into polycaprolactone/ montmorillonite nanocomposites. As the surface of clean clay is more hydrophilic than the contaminated clay, it can be assumed that the higher equilibrium water sorption levels are due to water binding to the hydrophilic surfaces of the clay, and forming hydration layers around the sodium ions in the interlayer of the clay. While such water/ clay interactions are likely to occur in both the clean and the organically modified clay, the extent of water/ clay interaction of clay layers with organic cations is expected to be lower due to the hydrophobic nature of the organic cations.

The higher equilibrium sorption observed for the 2.5 wt% clean clay nanocomposite compared to the 5 wt% clean clay nanocomposite cannot be explained by this assumption. However, adsorption of water vapour in polymer nanocomposites has been shown to increase, with increasing water activity, in measurements of water vapour diffusion [5.40, 5.41]. As no measurements of the humidity and temperature in the lab during the drying process (or the

subsequent diffusion measurement) have been recorded, it cannot be ruled out that changes in the ambient conditions influenced the data enough to create these different levels of equilibrium sorption.

Sample	intercept/L [min/µm]	D [cm²/sec]
PVOH	$1.08 * 10^{-2} \pm 2.24 * 10^{-3}$	$6.66* 10^{-5} \pm 2.66 * 10^{-5}$
PVOH + 2.5 wt% contaminated Na^+ Cloisite®	$1.04* 10^{-2} \pm 2.18 * 10^{-3}$	$3.00* 10^{-5} \pm 1.20 * 10^{-5}$
PVOH + 2.5 wt% clean Na^+ Cloisite®	$5.85* 10^{-3} \pm 1.38 * 10^{-3}$	$7.46* 10^{-4} \pm 2.94 * 10^{-4}$
PVOH + 5 wt% contaminated Na^+ Cloisite®	$1.05* 10^{-2} \pm 2.20 * 10^{-3}$	$8.48* 10^{-5} \pm 3.39 * 10^{-5}$
PVOH + 5 wt% clean Na^+ Cloisite®	$1.01* 10^{-3} \pm 7.76 * 10^{-4}$	$3.37* 10^{-5} \pm 1.66 * 10^{-5}$

Table 5-3 Summary of diffusion parameters for diffusion of water into low molecular weight PVOH and its nanocomposites at 40 °C

The D values in Table 5-3 suggest that diffusion was occurring faster in nanocomposites prepared from the clean batch. While the diffusion coefficients obtained for these samples do not show any clear differences, the ratio of time delay until diffusion occurs to the thickness of the film is reduced by 50 - 100% for the nanocomposites prepared from the clean batch of Na^+ Cloisite®. The shape of the diffusion data also changed (see Figure 5-13).

The change is especially obvious in the nanocomposite sample prepared from 5 wt% clean Na^+ Cloisite®. Despite the fact that no exact diffusion coefficients have been obtained for PVOH and its nanocomposites, the diffusion parameters obtained from the short term approximation of Fickian diffusion behaviour vary enough for the nanocomposites prepared from the clean batch of Na^+ Cloisite® to be considered as evidence for a detrimental effect of clay on the barrier properties of PVOH towards liquid water.

Without further analysis of the dispersion and alignment of the clay layers within the samples it is not entirely obvious how the clay is reducing the barrier properties of the polymer film but it is likely that clay attracts water into the sample and forms channels along which water diffusion can occur.

5.4.1.2 Effect of the type of clay on the diffusion of water into low molecular weight poly (vinyl alcohol)/ clay nanocomposites

5.4.1.2.1 Effect of different montmorillonite clays

Two different commercially available sodium exchanged montmorillonite clays have been used to prepare nanocomposites with PVOH. The main differences between these two montmorillonites are the variations in the relative concentrations of the interlayer cations. A more detailed analysis of the differences between these two clays can be found in chapter 3.3.1.

Diffusion measurements of water into nanocomposites with a clay loading of 5 wt% showed no significant differences between samples. This is to be expected as the general structure of these clays is the same and dispersion should therefore be similar. Figure 5-14 shows typical diffusion curves for these materials and Figure 5-15 presents representative fits of the data to the short term approximation of Fickian diffusion. The differences in time before water can be detected in the evanescent field are likely to be due to a combination of differences in sample thickness and overall clay loading in the film. The actual clay levels observed in the spectra (see Figure 5-16) showed some variation with the contaminated Na^+ Cloisite® sample showing the highest, and the clean Na^+ Cloisite® sample showing the lowest apparent clay level.

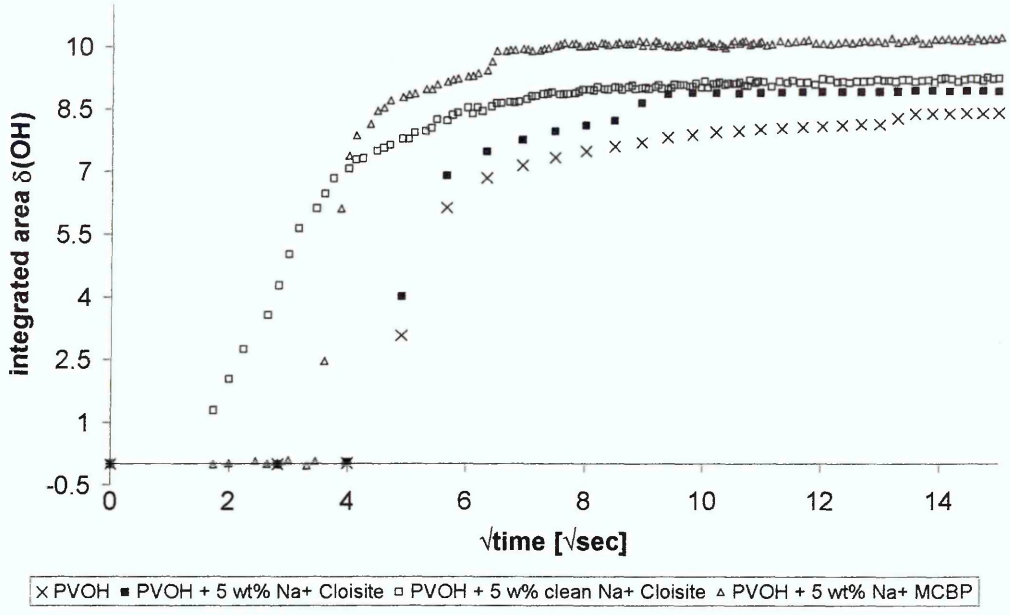

Figure 5-14 Experimental diffusion data for water diffusion into low molecular weight PVOH and its nanocomposites prepared from clean and organically contaminated Na^+ Cloisite® and Na^+ MCBP

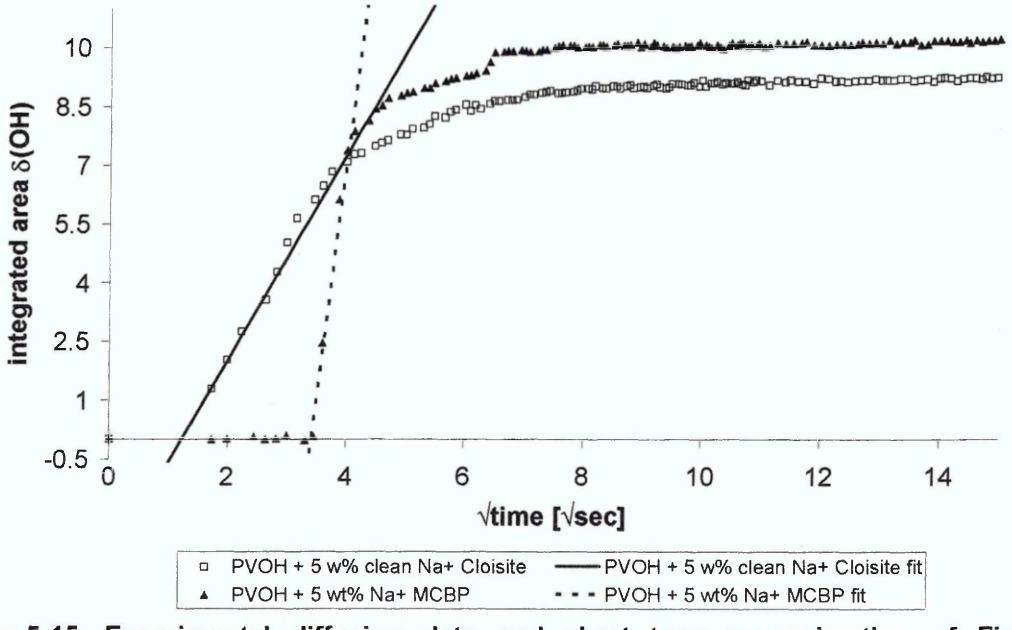

Figure 5-15 Experimental diffusion data and short term approximation of Fickian diffusion fits for water diffusion into low molecular weight PVOH nanocomposites prepared from clean Na^+ Cloisite® and Na^+ MCBP

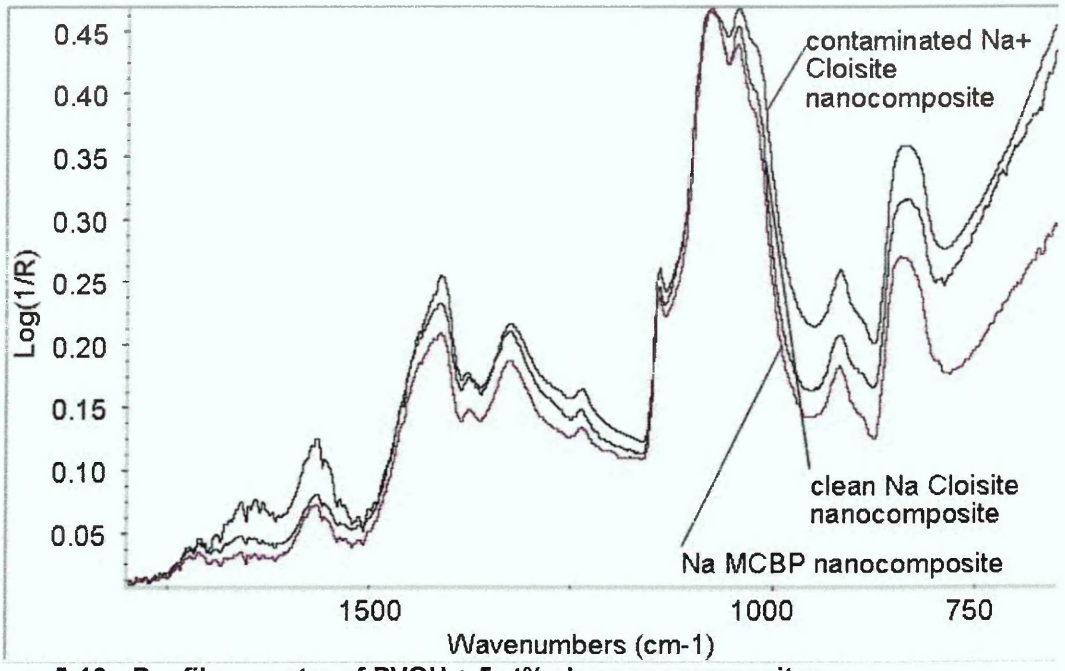

Figure 5-16 Dry film spectra of PVOH + 5wt% clay nanocomposites

Diffusion parameters for these samples are summarised in Table 5-4. The uncertainties in these values are mainly based on differences in the assumed sample thickness, since film thicknesses could not be measured after the experiment, due to the extensive gelling and swelling of the samples.

Sample	intercept/L [min/µm]	D [cm²/sec]
PVOH	$1.08 * 10^{-2} \pm 2.24 * 10^{-3}$	$6.66* 10^{-5} \pm 2.66 * 10^{-5}$
PVOH + 5 wt% contaminated Na^+ Cloisite®	$1.05* 10^{-2} \pm 2.20 * 10^{-3}$	$8.48* 10^{-5} \pm 3.39 * 10^{-5}$
PVOH + 5 wt% clean Na^+ Cloisite®	$1.01* 10^{-3} \pm 7.76 * 10^{-4}$	$3.37* 10^{-5} \pm 1.66 * 10^{-5}$
PVOH + 5 wt% Na^+ MCBP	$7.08* 10^{-3} \pm 9.75 * 10^{-4}$	$7.27* 10^{-4} \pm 1.31 * 10^{-4}$

Table 5-4 Diffusion parameters for diffusion of water into PVOH/ Na^+ Cloisite® and PVOH/ Na^+ MCBP nanocomposites

The intercept time obtained for the MCBP sample is longer than those obtained for the other nanocomposites while the diffusion coefficient is much faster. As both these values were obtained from the fit of a straight line to the diffusion curve at short times (= short term approximation fit), this data does not represent the difference in the overall shape of the diffusion curves. The two clays (Cloisite® and MCBP) have only minor differences in their structure, which do not explain the large differences in the diffusion parameters listed in Table 5-4. It is possible that the changes are related to differences in the dispersion and swelling of the clay. The calcium content in the interlayers of the MCBP is about four times higher than that of the Cloisite®. Calcium clays generally swell

less, and layers do not exfoliate as readily as in their sodium counterparts which could lead to different dispersion pattern of the MCBP. Because XRD analysis did not indicate any obvious changes in dispersion, further analysis of the samples by TEM is necessary to confirm this possibility.

5.4.1.2.2 Effect of different cations in the interlayer

Cation exchanging the Na^+ MCBP with Li^+ ions did not only exchange the sodium present in the galleries but also a considerable amount of the calcium present in the original Na^+ MCBP. The XRF and XRD data for these two MCBP forms is presented in chapter 3.5.3.2.2.1.

The diffusion curves for 5 wt% nanocomposites of these clays were quite different. In the lithium clay nanocomposite ingress of water is immediately visible, while the Na^+ MCBP nanocomposite had a delay before diffusion set in (even though film thickness and clay levels in the evanescent field were comparable). Typical diffusion curves for these two nanocomposites are presented in Figure 5-17 and diffusion parameters are given in Table 5-5.

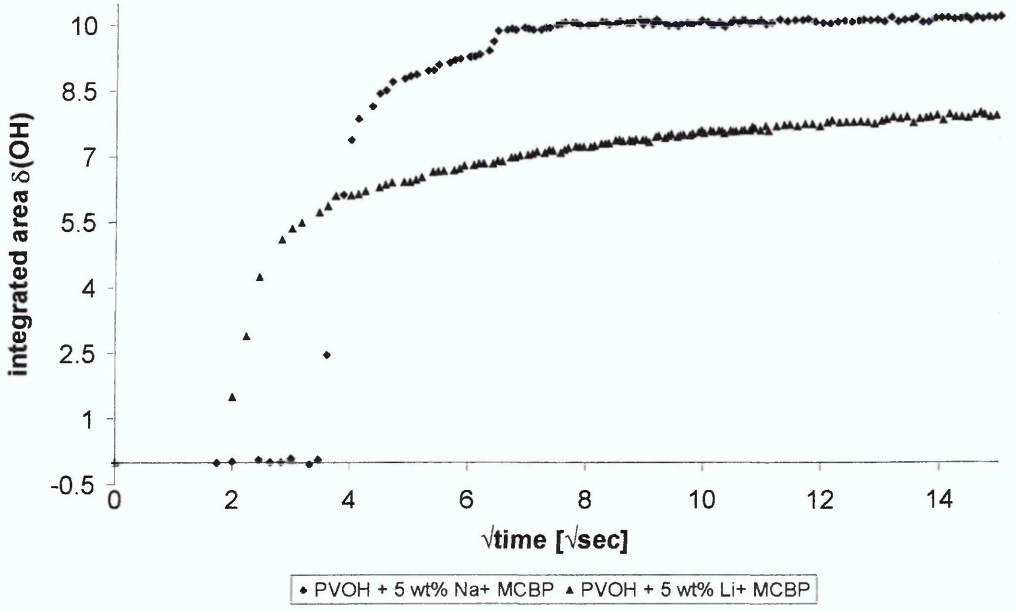

Figure 5-17 Experimental diffusion data for low molecular weight PVOH nanocomposites with Na^+ MCBP and Li^+ MCBP

Sample	intercept/L [min/µm]	D [cm²/sec]
PVOH+ 5 wt% Na^+ MCBP	$7.08 * 10^{-3} \pm 9.75 * 10^{-4}$	$7.27 * 10^{-4} \pm 1.31 * 10^{-4}$
PVOH + 5 wt% Li^+ MCBP	$2.06 * 10^{-3} \pm 1.82 * 10^{-4}$	$4.29 * 10^{-4} \pm 7.30 * 10^{-5}$

Table 5-5 Diffusion parameters for diffusion of water into PVOH/ Na^+ MCBP and PVOH/ Li^+ MCBP nanocomposites

Diffusion in the lithium clay nanocomposite occurs at a faster rate, and the initial delay time is lower than that of the pristine polymer, as well as the Na^+ MCBP nanocomposite. This clay had lower calcium content, which is known to reduce the swelling in clays. It is therefore assumed that the Li^+ MCBP is better dispersed in the polymer matrix, even though no evidence for this could be found in the XRD traces. Such better dispersion results in a greater disruption of the inter- and intra-molecular hydrogen bonding of the polymer which reduces the barrier properties of the material. The better barrier properties of the Na^+ MCBP nanocomposite compared to the Li^+ MCBP nanocomposite could therefore be explained by larger stacks of the Na^+ clay. This would create less disruption of the PVOH hydrogen bonding network than the better dispersed single layers. In the sodium clay case, the disruption of the PVOH structure would be due to interactions between the clay surfaces and the polymer chains. A better dispersion of the clay layers results in more structural disruption because single dispersed layers have a higher surface area which can interact with the polymer than stacks of clay sheets of comparable width.

5.4.1.2.3 Effect of charge reduction in Li+ MCBP

Charge reduction in Li^+ MCBP has been achieved by heating the clay at different temperatures, in order to partially collapse the galleries between the clay layers. Such treatment results in poorer dispersion of the clay in the polymer as the collapsed layers cannot be intercalated by the polymer.

The XRD data of these nanocomposites showed no d_{001} peak in the trace for the PVOH/ Li^+ MCBP. At the same clay loading, a shoulder at the highest measurable d spacings could be seen in the trace for the nanocomposite of PVOH with Li^+ MCBP fired at 135 °C. The clay layer spacing of the nanocomposite formed from PVOH and Li^+ MCBP fired at 210 °C was similar to that of the pristine clay. This sample is therefore likely to be a microcomposite

with clusters of clay dispersed in the polymer matrix. (XRD results are discussed in detail in chapter 3.5.3.2.2.4)

To investigate the influence of clay dispersion and charge reduction on the diffusion of water into PVOH nanocomposites experiments have been performed on nanocomposites with 5 wt% clay loading.

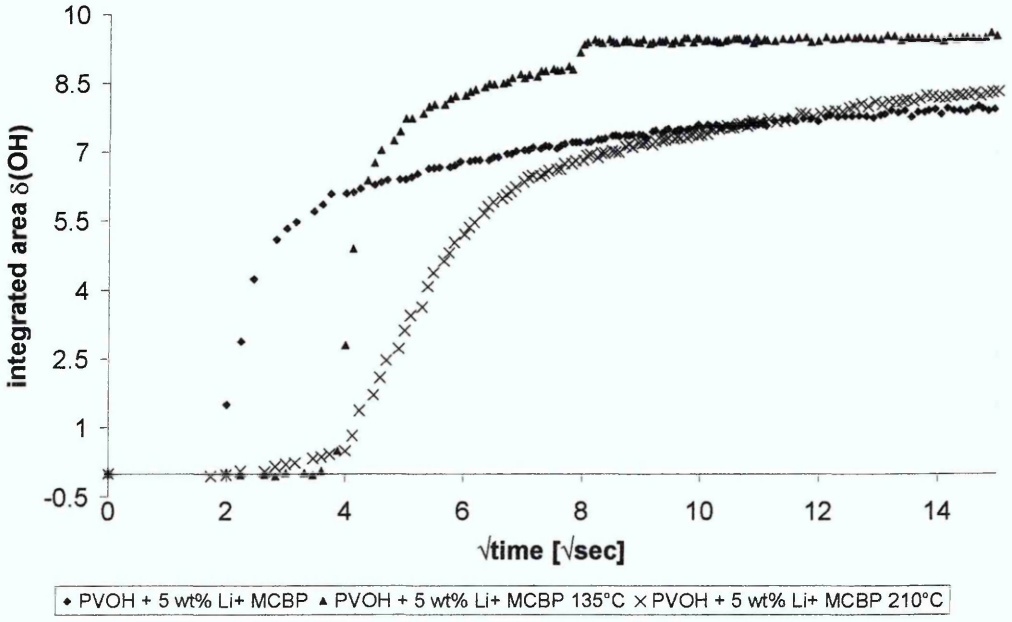

Figure 5-18 Experimental diffusion data for low molecular weight PVOH/ Li^+ MCBP nanocomposites with different clay layer charges

Figure 5-18 shows representative experimental data for water diffusing into PVOH/ Li^+ MCBP (nano) - composites. Diffusion occurs faster when the clay is better dispersed in the polymer matrix. The shape of the diffusion curves for these nanocomposites varied significantly, which means that the diffusion parameters obtained from the short term approximation of Fickian diffusion are not necessarily a good representation of the overall data. From examples for the linear fits of this data which are presented in Figure 5-19, one can however see that the model is a reasonable representation of the experimental data at short times.

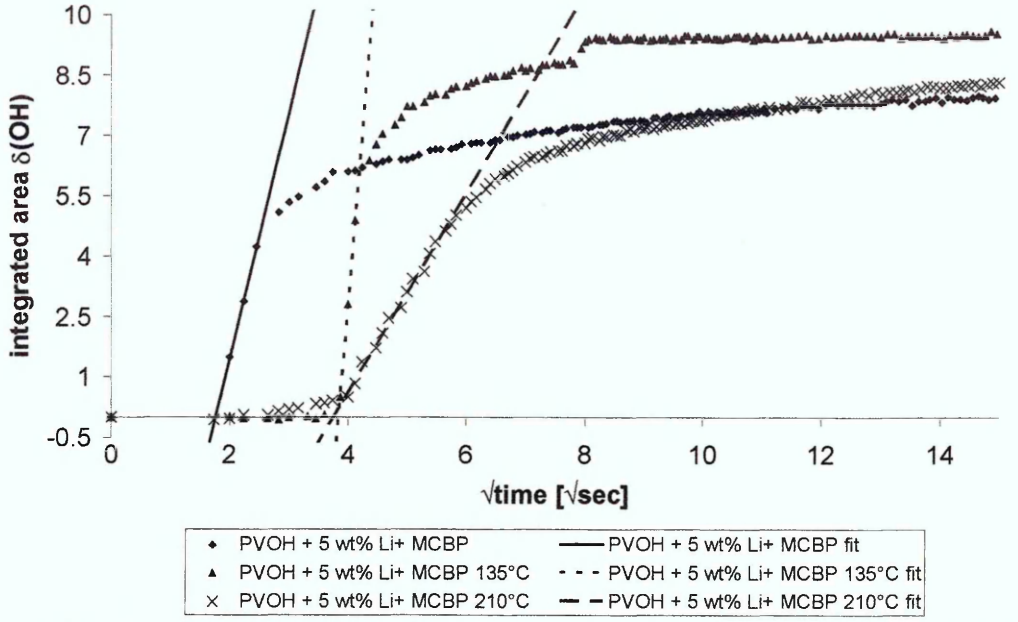

Figure 5-19 Experimental diffusion data and short term approximation of Fickian diffusion fits for low molecular weight PVOH/ Li^+ MCBP nanocomposites with different clay layer charges

A summary of the diffusion parameters obtained from these fits is given in Table 5-6. This data shows that the time before diffusion is observed decreases with the incorporation of clay and diffusion occurs at a faster rate.

Sample	intercept/L [min/µm]	D [cm²/sec]
PVOH + 5 wt% Li^+ MCBP	$2.92 * 10^{-3} \pm 6.10 * 10^{-4}$	$1.21 * 10^{-5} \pm 4.87 * 10^{-6}$
PVOH + 5wt% Li^+ MCBP fired at 135 °C	$9.85 * 10^{-3} \pm 2.05 * 10^{-3}$	$1.52 * 10^{-3} \pm 6.09 * 10^{-4}$
PVOH + 5wt% Li^+ MCBP fired at 210 °C	$9.41 * 10^{-3} \pm 1.98 * 10^{-3}$	$3.02 * 10^{-5} \pm 1.21 * 10^{-5}$
PVOH	$1.08 * 10^{-2} \pm 2.24 * 10^{-3}$	$6.66 * 10^{-5} \pm 2.66 * 10^{-5}$

Table 5-6 Diffusion front velocities for diffusion of water PVOH/ Li^+ MCBP nanocomposites with different clay layer charges

Better dispersion of the clay also results in higher equilibrium sorption of water in these samples. This is to be expected if the extra sorption capacity of the sample is due to water being adsorbed onto the clay surfaces, since more clay surfaces are accessible when the clay layers are better dispersed.

These observations give further proof that incorporation of clay into PVOH opens up the structure of the polymer and thereby causes a decrease in the barrier properties of the nanocomposite materials against the diffusion of liquid water. Clay has, however, been found to generally improve barrier properties of other polymers against water vapour [5.40, 5.41], and also of PVOH against liquid water in mixed solvents (see chapter 6).

In the films prepared from PVOH and Li^+ MCBP fired at 210 °C, clay particles were clearly visible to the unassisted eye. This observation indicates that the agglomerates of clay particles are fairly large. It is possible that the charge reduced clays are partially delaminating when they are dispersed in PVOH, with layers remaining overlapping. Such dispersion creates clay particle agglomerates of greater length compared to the individual layers which increase the time until evidence of water entering the evanescent field can be observed in the ATR spectra and generally appear to improve the barrier properties of the material.

5.4.1.3 Effect of temperature on the diffusion of water into low molecular weight poly (vinyl alcohol)/ Na+ Cloisite® nanocomposites

Diffusion processes are temperature dependent. Higher temperatures usually result in faster diffusion, as the mobility of both the solvent and polymer molecules is increased.

To investigate whether these changes can be observed in PVOH and PVOH nanocomposites, diffusion measurements were performed at 30°C, 40°C and 50°C. The samples for all these experiments were allowed to dry overnight at 40°C. For the diffusion measurements at 30°C and 50°C the sample was allowed to equilibrate at the desired temperature for 45 minutes, before water was introduced into the system. Variations in sample crystallinity for samples measured at different temperatures were found to be similar to the variations observed between repeat samples measured at the same temperature.

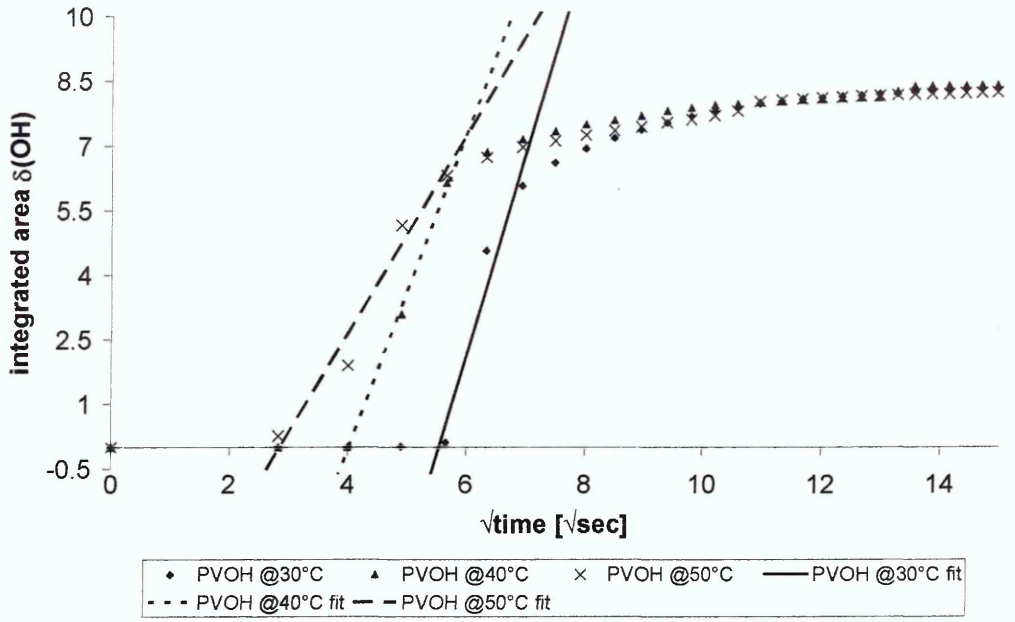

Figure 5-20 Experimental data and short term approximation of Fickian diffusion fits for diffusion of water into low molecular PVOH at various temperatures

Equilibrium sorption levels are similar for the temperatures investigated. For the pristine polymer the delay time before diffusion can be observed decreases with raised temperatures as would be expected. The slopes of these curves, and therefore the approximated diffusion coefficient, decreased with increasing temperatures. The films subjected to diffusion measurements at the higher temperatures are quite likely to contain lower residual water than the samples run at 30 °C. It is therefore possible that this unexpected decrease in the rate of diffusion with increased temperatures is due to differences in structure of the "dry films" at the beginning of each experiment which could be observed in the FTIR spectra of these films taken at the beginning of the experiment. These spectra show a decrease in the intensity of the ν(OH) and δ(OH) bands with increasing temperatures, indicating the variations in residual water in the films. (see Figure 5-21)

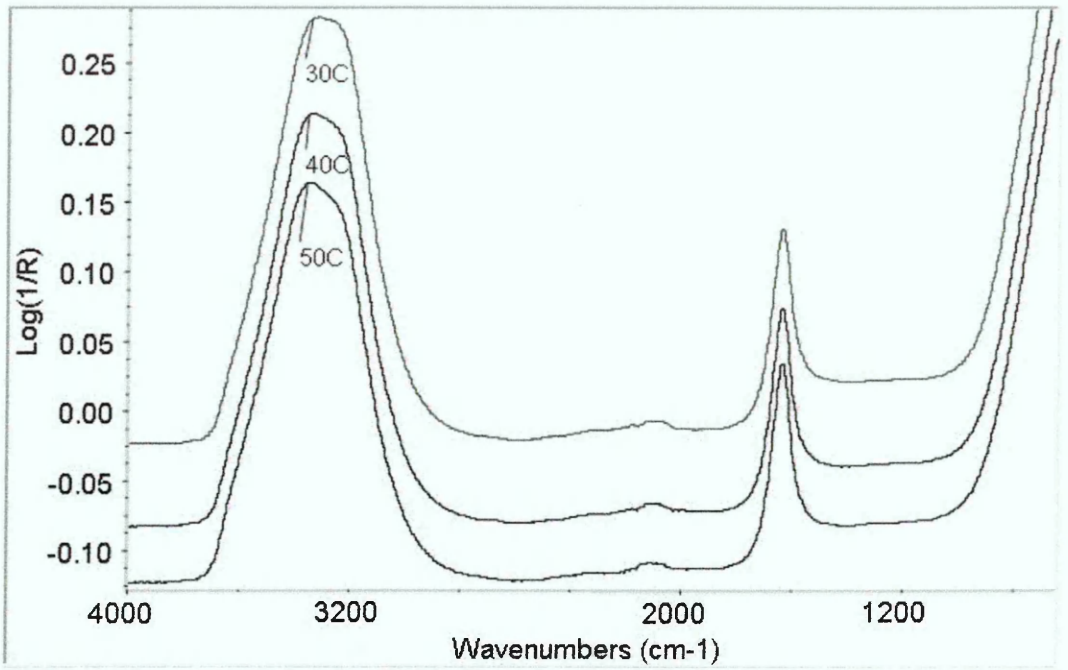

Figure 5-21 Spectra of the dry PVOH films for the diffusion measurements recorded at 30 °C, 40 °C and 50 °C

The data for the nanocomposites presents a more complicated picture. Direct comparison of diffusion curves was, in this case, complicated by variations in clay levels in the evanescent field and film thicknesses. To enable comparison of the data, runs were chosen that appeared to have similar clay contents (according to their dry film FTIR spectra). Experimental data for such films cast from PVOH solutions with 2.5 wt% and 5 wt% Na^+ Cloisite® respectively are shown in Figure 5-22 and Figure 5-23.

Comparison of the data in dependence of the clay levels detected in the dry spectra, as presented in Figure 5-24 and Figure 5-25, shows that diffusion proceeded faster at higher temperatures, when diffusion runs at 30 °C and 40°C were compared. The data collected at 50°C does, however, not follow this general trend. It is not clear at this point whether this is due to the inaccurate determination of actual clay levels in the sample, or changes in the structure of the samples, as indicated for the pristine polymer films. A further possibility is that residual water in some of these films is sufficient to lower the glass transition temperature of the PVOH enough to fall into the range of temperatures chosen for these experiments. If this is the case, samples measured at 40 °C might be just below the glass transition temperature, while samples measured at higher temperatures could have rubbery characteristics.

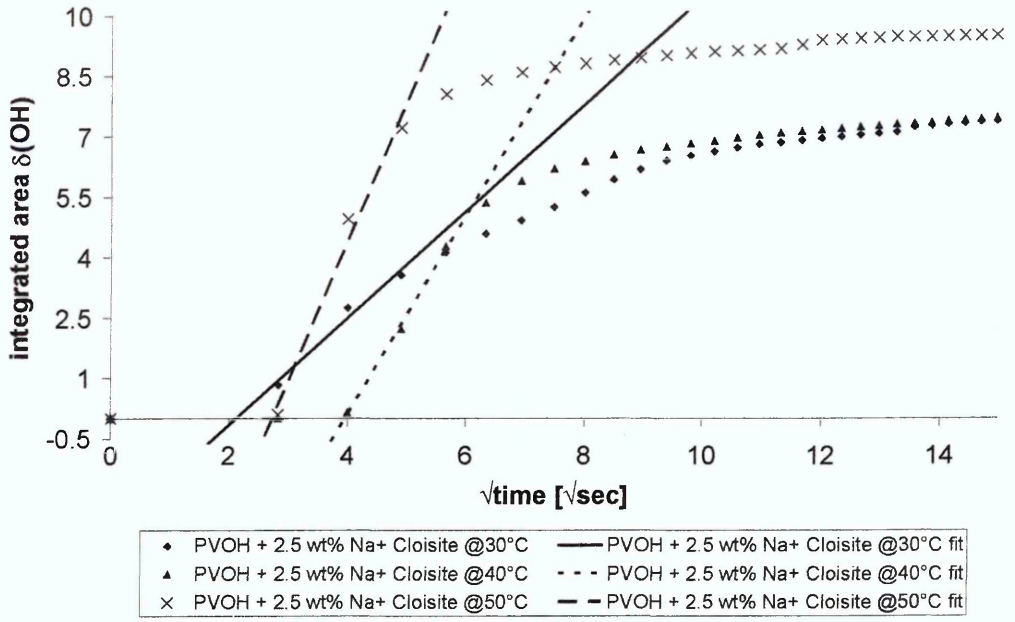

Figure 5-22 Experimental data and short term approximation of Fickian diffusion fits for diffusion of water into low molecular PVOH + 2.5 wt% Na^+ Cloisite® at various temperatures

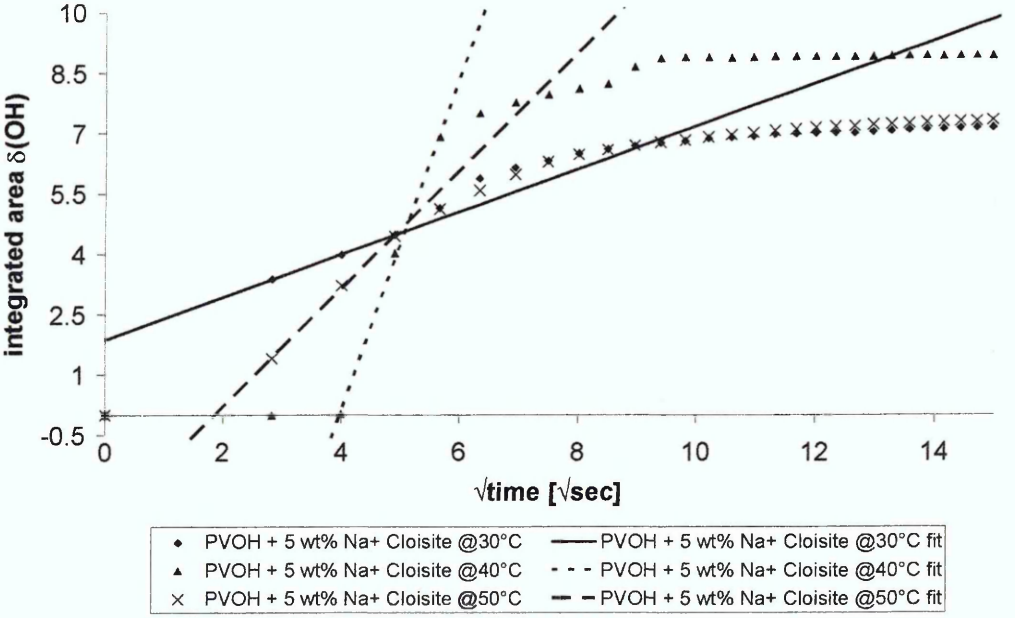

Figure 5-23 Experimental data and short term approximation of Fickian diffusion fits for diffusion of water into low molecular PVOH + 5 wt% Na^+ Cloisite® at various temperatures

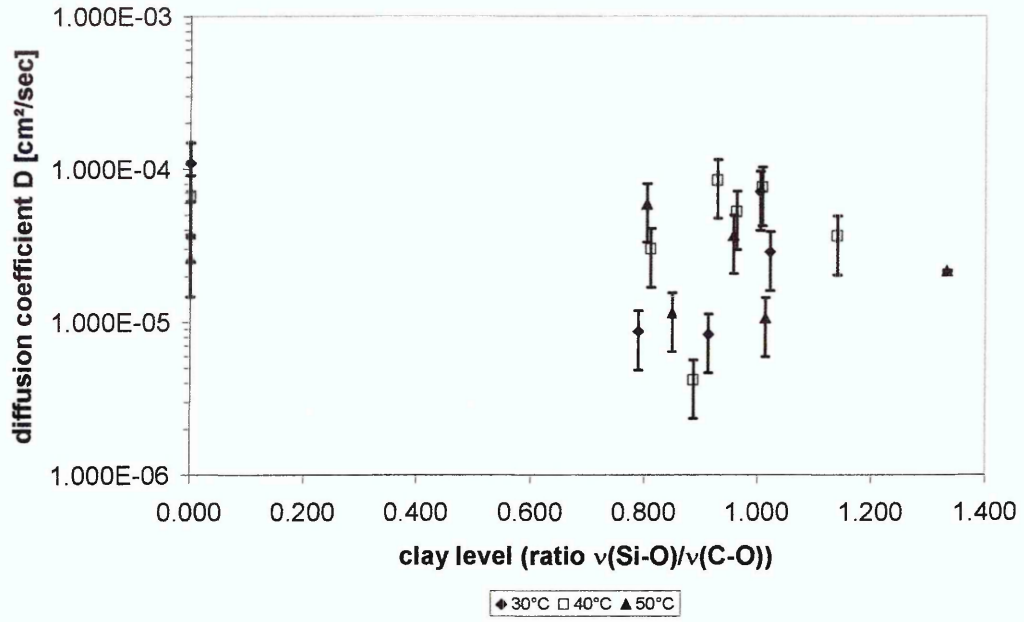

Figure 5-24 Comparison of diffusion rates for water diffusion into low molecular weight PVOH/ Na^+ Cloisite® nanocomposites at various temperatures

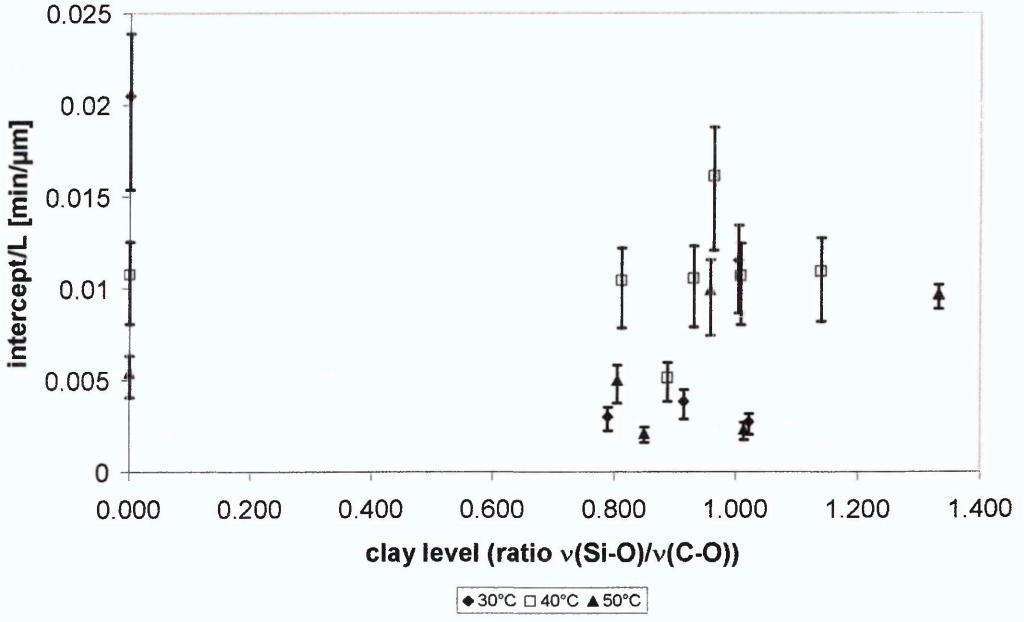

Figure 5-25 Comparison of "onset times" for water diffusion into low molecular weight PVOH/ Na^+ Cloisite® nanocomposites at various temperatures

Plotting the natural logarithm of the diffusion coefficients obtained for PVOH and the nanocomposites at each of these temperatures against the reciprocal temperature as presented in Figure 5-26 results in a wide spread of data.

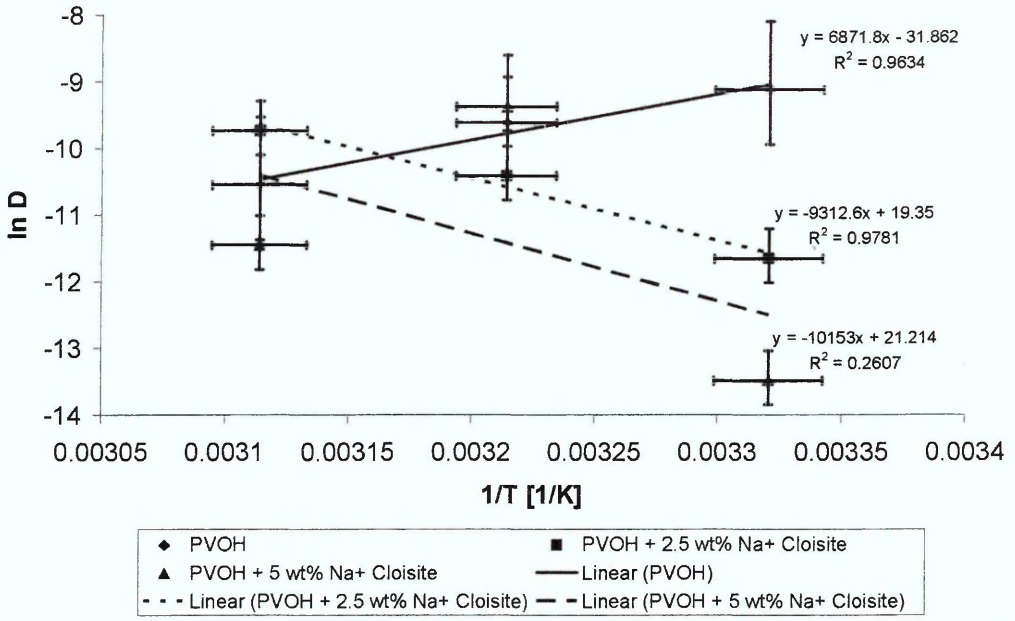

Figure 5-26 Arrhenius plot for diffusion coefficients of PVOH and PVOH nanocomposites

The data generally follows a linear relationship allowing calculation of the activation energy, for the diffusion of water into these samples, by means of the Arrhenius equation. The data for the pristine polymer, however, showed the exact opposite of the expected behaviour. When only the diffusion coefficients are considered, diffusion is found to occur at a faster rate at lower temperatures. This surprising result is likely to be caused by the variations in the water content of the dry films between these experiments and the huge uncertainties in the values obtained for the diffusion coefficients. This is due to the error in estimation of the sample thickness, and few available data points at short times. Data for the nanocomposites portrays the expected behaviour with diffusion rates increasing with increasing temperatures. For the 5 wt% nanocomposites the value at 40°C appears to be too high resulting in a poor fit. Nevertheless activation energies have been calculated based on this data using the Arrhenius relationship given in equation 5-1.

$$k = Ae^{-\frac{E_a}{RT}}$$ **Equation 5-1**

where E_a is the activation energy
R = 8.314 J/mol·K
T is the temperature in Kelvin
A is a factor

The values for the activation energies of the diffusion of water presented in Table 5-7 were calculated without taking the errors in the individual data points into account. They are therefore only a rough indication of the changes in the activation energy for the diffusion of water that can be observed when clay is introduced into the samples. As this model has been developed for a single phases, it is not surprising that a two phase system like nanocomposites cannot always be fully described using this relationship. Some of the deviations observed in Figure 5-26 are also due to different actual clay loadings, in samples cast from solutions of same nominal clay content. The influence of these variations was, however, very small compared to the uncertainties introduced by variations in the "dryness" of the starting films and the film thickness and has not been quantified.

Sample	Activation energy E_a [kJ/ mol]
PVOH	-57.14
PVOH + 2.5 wt% contaminated Na^+ Cloisite®	77.43
PVOH + 5 wt% contaminated Na^+ Cloisite®	84.42

Table 5-7 Activation energies for the diffusion of water into PVOH and its nanocomposites

Generally, an increase in activation energy for diffusion is expected with increasing cohesive energy density of the polymer and size of the penetrant [5.42]. As clay is expected to decrease the cohesive energy of the polymer by disrupting the intermolecular polymer network the activation energy for diffusion in polymer/ clay nanocomposites is expected to be lowered. The clay platelets do however increase tortuosity resulting in a decrease of diffusion rates. It is possible that this effect and the fact that nanocomposites are two phase systems, makes calculation of the activation energy by means of the Arrhenius relationship not applicable.

5.4.2 Diffusion of water into high molecular weight poly (vinyl alcohol) and its nanocomposites

Similar data collected for the diffusion of water into lower molecular weight PVOH experiments have been carried out using higher molecular weight PVOH and clay loadings of 2.5 wt% and 5 wt% respectively.

5.4.2.1 Effect of clay loading on the diffusion of water into high molecular weight poly (vinyl alcohol)/ Na+ Cloisite® nanocomposites

Figure 5-27 shows typical data obtained for the diffusion of water into high molecular weight PVOH and its nanocomposites. While data collected for the samples prepared from low molecular weight PVOH showed only minor differences in the diffusion coefficients and delay times changes are more obvious for these samples.

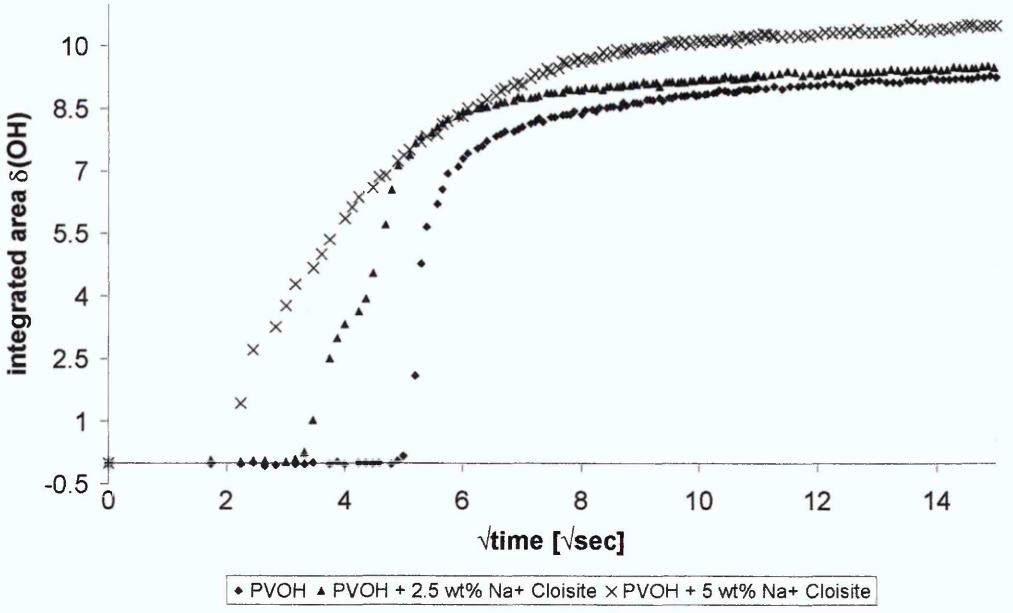

Figure 5-27 Experimental data for diffusion of water into high molecular weight PVOH and its nanocomposites

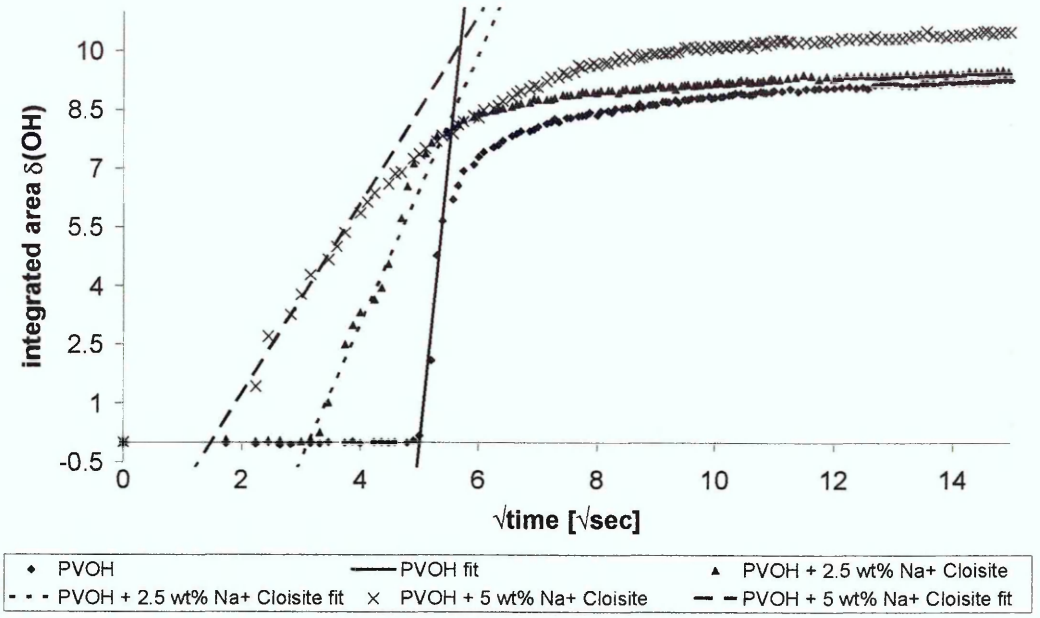

Figure 5-28 Experimental diffusion curves and short term approximation of Fickian diffusion fits for diffusion of water into high molecular weight PVOH and its nanocomposites

With increasing clay loading, the delay time before diffusion can be observed is reduced. The slope of the diffusion curve become shallower with increasing clay loadings, and diffusion coefficients obtained from this data decrease with increasing clay content. A summary of the diffusion parameters calculated for these curves is given in Table 5-8. The film thickness of these samples could be determined more accurately as films remained intact, and could be recovered from the crystal, after a drying period at the end of the experiment.

Sample	Film thickness [µm]	intercept/L [min/µm]	D [cm²/sec]
PVOH	54	$7.73 * 10^{-3}$	$5.08 * 10^{-3}$
PVOH + 2.5 wt% Na^+ Cloisite®	22	$7.42 * 10^{-3}$	$4.54 * 10^{-5}$
PVOH + 5 wt% Na^+ Cloisite®	22	$1.66 * 10^{-3}$	$2.22 * 10^{-5}$

Table 5-8 Summary of diffusion parameters for diffusion of water into high molecular weight PVOH and its nanocomposites at 40 °C

Overlaying the diffusion data collected for each series can be misleading as films differ in thickness. Taking the differences in thickness into account the delay before diffusion sets in is decreased. However, the decrease is of less extent than the comparison of the curves presented in Figure 5-27 suggest. The

diffusion coefficient for the diffusion of liquid water into the nanocomposites is significantly lower than that for the pristine polymer.

Plotting diffusion parameters versus the clay content in the sample, as presented in Figure 5-29 and Figure 5-30, illustrates that the samples investigated showed only little variation in the actual clay content detectable in the dry film. Therefore only small differences should be observed in the diffusion coefficient. The extent of the variations observed between samples with different clay contents is similar to the variations found between repeat runs of diffusion experiments on the neat polymer. It is, therefore, likely that doubling the clay loading of the nanocomposites from 2.5 to 5 wt% has less influence on the diffusion parameters than the initial addition of clay to the neat polymer and variations observed within samples of the same type. It appears likely that the introduction of clay into the polymer increases the number and size of voids or defects in the structure of the polymer. This "free volume" within the sample film is initially filled, resulting in the reduction in the delay time before diffusion can be observed. After this "true" diffusion, which is slowed down by the presence of the clay platelets due to an increase in the tortuosity may begin.

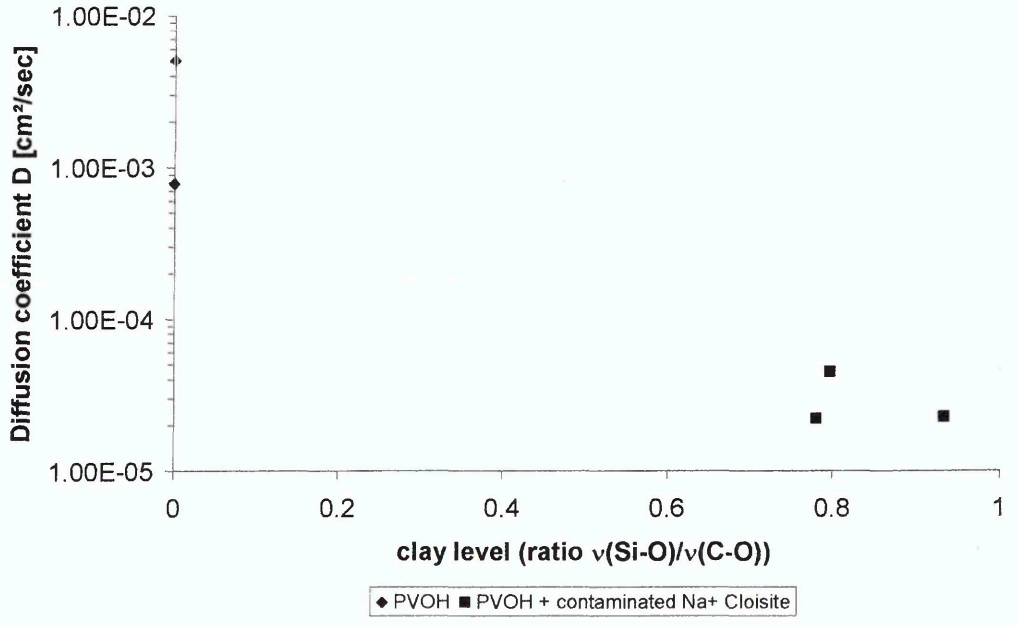

Figure 5-29 Comparison of diffusion coefficients for water diffusion into high molecular weight PVOH/ Na+ Cloisite® nanocomposites

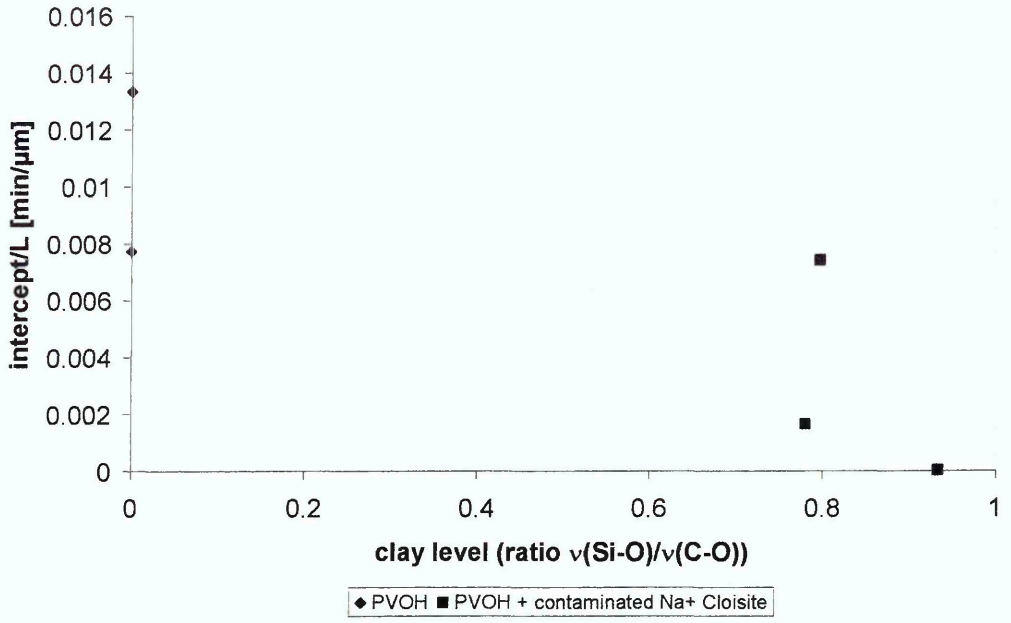

Figure 5-30 Comparison of "onset times" for water diffusion into high molecular weight PVOH/ Na+ Cloisite® nanocomposites

5.4.2.2 Effect of clay contamination on the diffusion of water into high molecular weight poly (vinyl alcohol)/ Na+ Cloisite® nanocomposites

Contamination of the clay by a small amount of organic surfactant resulted in changes in the diffusion behaviour of water into low molecular weight PVOH. Therefore the experiments were repeated with high molecular weight PVOH to investigate whether the influence of the clay contamination can also be observed in these samples.

Figure 5-31 shows that equilibrium sorption levels of water are increased in the presence of clean Na^+ Cloisite® in the high molecular weight PVOH samples like they were for the low molecular weight PVOH nanocomposites. Higher clay levels resulted in higher water sorption. Clay therefore increases the amount of water sorbed in polymer films, independent of molecular weight of the polymer matrix.

The general diffusion behaviour of the nanocomposites prepared from clean Na^+ Cloisite® is comparable to that of the nanocomposites created from organically contaminated Na^+ Cloisite®. The delay time for diffusion to occur is

decreased with increasing clay loadings while diffusion rates are slower in for the nanocomposites than for the neat polymer.

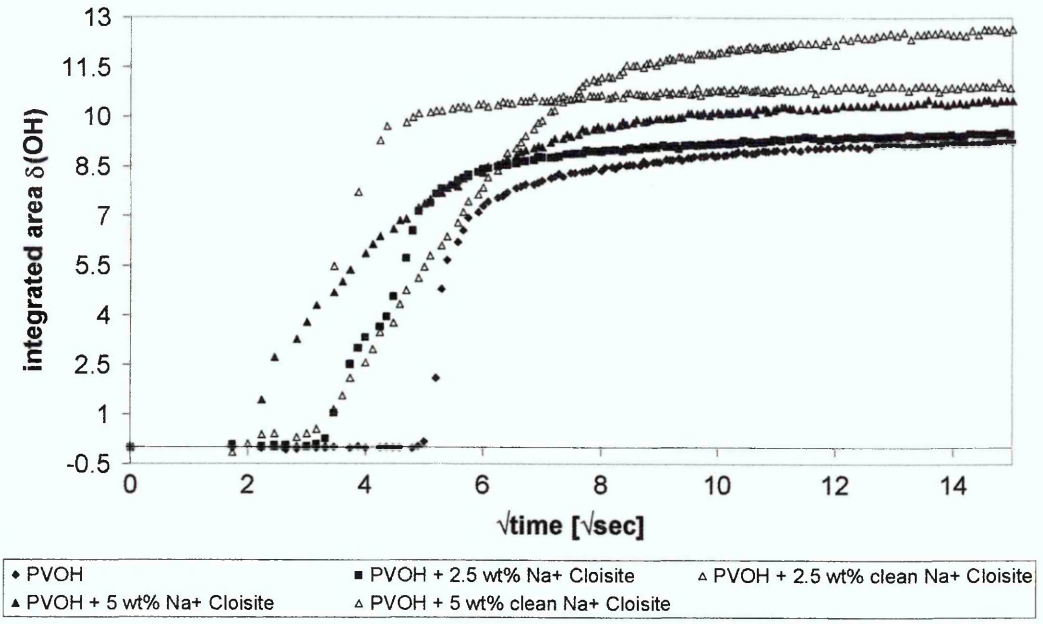

Figure 5-31 Experimental diffusion data for high molecular weight PVOH and its nanocomposites prepared from clean and organically contaminated Na^+ Cloisite®

Sample	Film thickness [μm]	intercept/L [min/μm]	D [cm²/sec]
PVOH	54	$7.73 * 10^{-3}$	$5.08 * 10^{-3}$
PVOH + 2.5 wt% clean Na^+ Cloisite®	29	$5.82 * 10^{-3}$	$9.44 * 10^{-4}$
PVOH + 5 wt% clean Na^+ Cloisite®	45	$3.35 * 10^{-3}$	$1.17 * 10^{-4}$

Table 5-9 Summary of diffusion parameters for diffusion of water into high molecular weight PVOH and its nanocomposites prepared from clean Na^+ Cloisite® at 40 °C

Estimating the apparent clay level by ratioing the area of ν(Si-O) band to that of the ν(C-O) band in these samples gives lower values for the same nominal clay levels than those of obtained from low molecular weight samples. The reason for these differences in apparent clay levels in the evanescent field between high and low molecular weight samples, could either be a different dispersion of the clay within the film (less clay in the evanescent field) or a different relative intensity of the ν(C-O) band in high molecular weight PVOH compared to the lower molecular weight samples. Such a change in relative band intensity of the ν(C-O) compared to the ν(Si-O) could be due variations in the number of C-O

investigated, or shifts in the ν(C-O) band due to a different ratio of C-OH and COOH groups within the polymer.

The samples prepared from the clean clay generally had a lower apparent clay level in the evanescent field making direct comparison of the diffusion parameters difficult. Plotting the diffusion parameters against the apparent clay loading as presented in Figure 5-32 and Figure 5-33, however, implies that diffusion is occurring at a faster rate in nanocomposites of high molecular weight PVOH with the clean Na^+ Cloisite®.

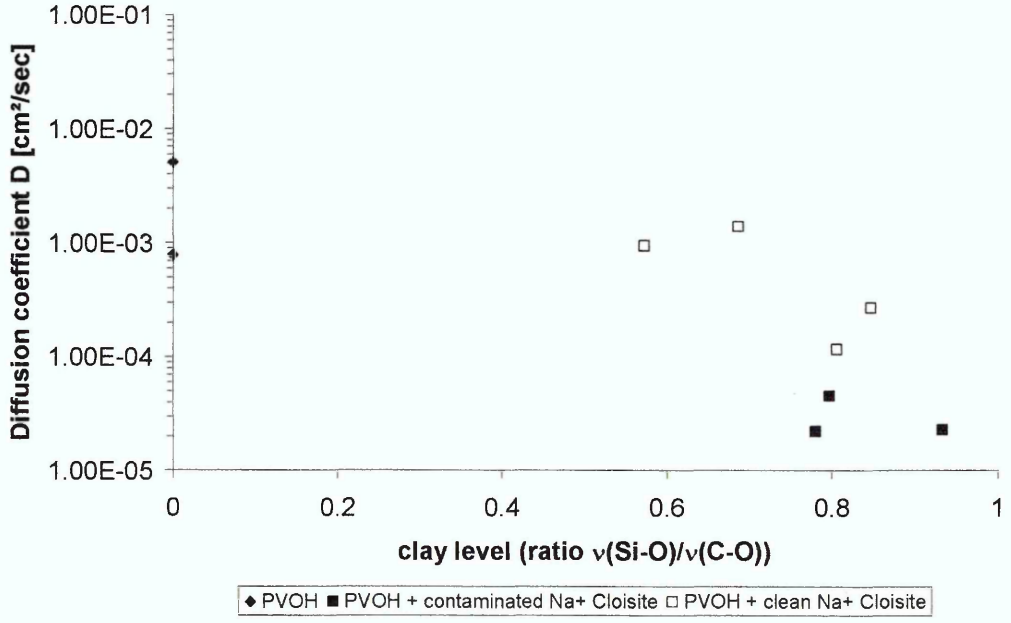

Figure 5-32 Comparison of diffusion coefficients for water diffusion into high molecular weight PVOH/ Na^+ Cloisite® nanocomposites with clean and contaminated clay

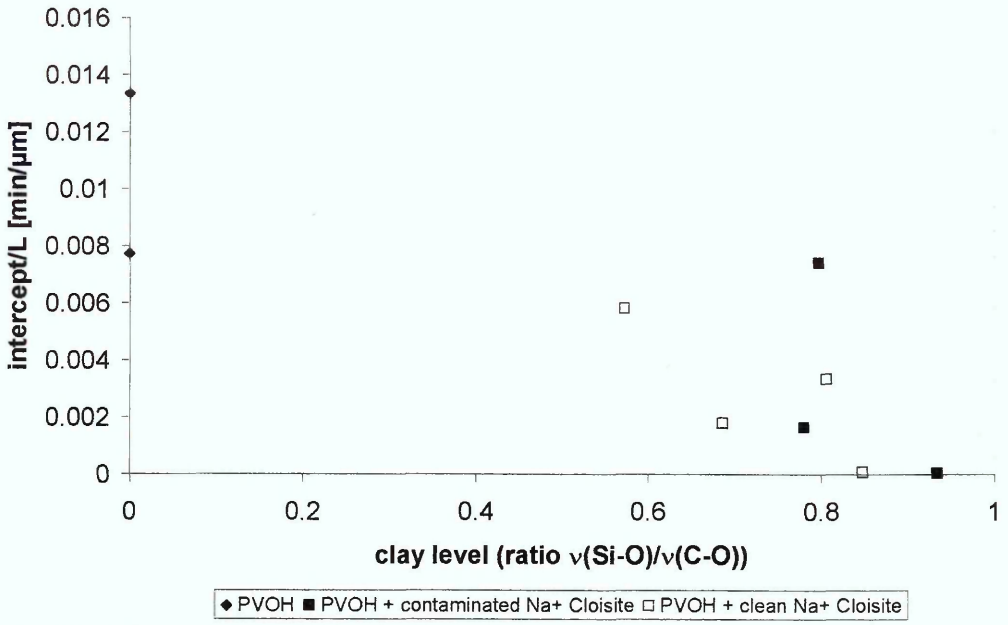

Figure 5-33 Comparison of "onset times" for water diffusion into high molecular weight PVOH/ Na^+ Cloisite® nanocomposites with clean and contaminated clay

While the delay times before diffusion can be observed show no real trend when comparing the two types of nanocomposites, diffusion coefficients for the clean clay nanocomposites are much faster than those for the nanocomposites prepared from the organically contaminated batch of clay. This effect is probably caused by variations in the dispersion of these two clays within the PVOH matrix. While no such differences were visible in the XRD traces of the nanocomposites the clean clay is expected to be better dispersed as it is more hydrophilic and should therefore swell better in water. It should therefore disperse better in the hydrophilic PVOH. This better dispersion would result in more disruption to the polymer structure, which would make it more susceptible to the ingress of water. It is also possible that the higher hydrophilicity of the clean clay compared to the organically contaminated clay attracts water into the film, thereby increasing the diffusion rates.

5.4.2.3 Influence of molecular weight on the diffusion of water into poly (vinyl alcohol)

Comparing the data presented above, with regard to differences in molecular weight of the samples, showed much faster diffusion rates for the high and low molecular weight PVOH samples compared to the nanocomposites. High molecular weight samples generally appear to have poorer barrier properties than the lower molecular weight samples. As the high molecular weight samples

had about twice the thickness of the low molecular weight samples overlaying the data obtained from the integration of the δ(OH) band over time as presented in Figure 5-34 does not show these differences. A summary of diffusion parameters for high and low molecular weight PVOH nanocomposites is given in Table 5-10.

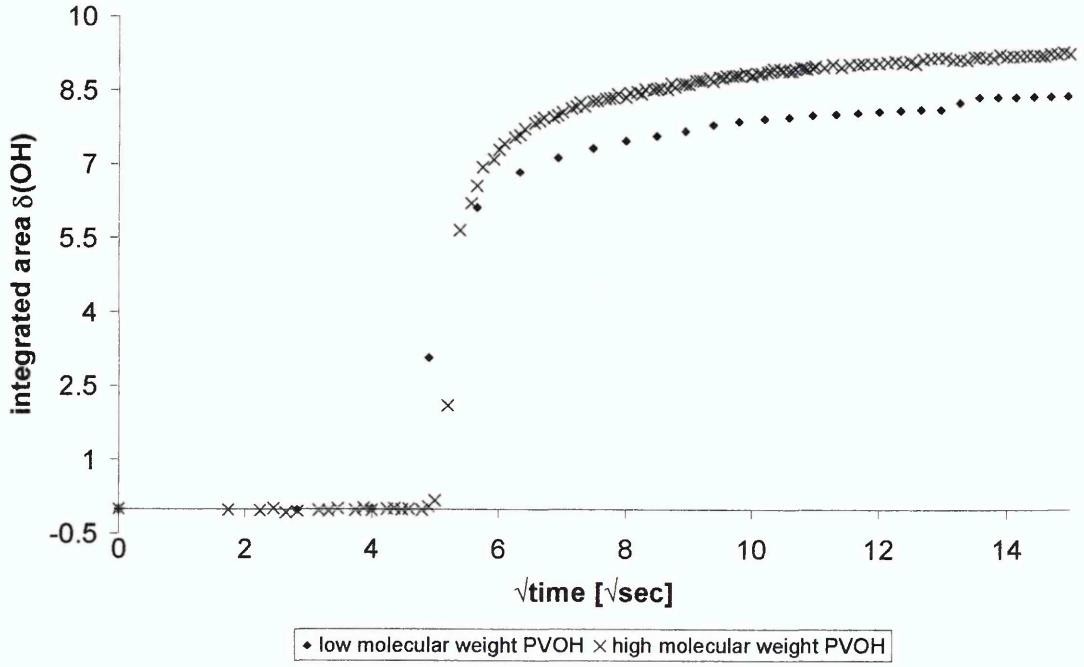

Figure 5-34 Experimental data for diffusion of water into PVOH with different molecular weights

	low molecular weight		high molecular weight	
	intercept/L [min/µm]	D [cm²/sec]	intercept/L [min/µm]	D [cm²/sec]
PVOH	$1.08 * 10^{-2} \pm 2.24 * 10^{-3}$	$6.66* 10^{-5} \pm 2.66 * 10^{-5}$	$7.73 * 10^{-3}$	$5.08 * 10^{-3}$
PVOH + 2.5 wt% Na^+ Cloisite®	$1.04* 10^{-2} \pm 2.18 * 10^{-3}$	$3.00* 10^{-5} \pm 1.20 * 10^{-5}$	$7.42 * 10^{-3}$	$4.54 * 10^{-5}$
PVOH + 2.5 wt% clean Na^+ Cloisite®	$5.85* 10^{-3} \pm 1.38 * 10^{-3}$	$7.46* 10^{-4} \pm 2.94 * 10^{-4}$	$5.82 * 10^{-3}$	$9.44 * 10^{-4}$
PVOH + 5 wt% Na^+ Cloisite®	$1.05* 10^{-2} \pm 2.20 * 10^{-3}$	$8.48* 10^{-5} \pm 3.39 * 10^{-5}$	$1.66 * 10^{-3}$	$2.22 * 10^{-5}$
PVOH + 5 wt% clean Na^+ Cloisite®	$1.01* 10^{-3} \pm 7.76 * 10^{-4}$	$3.37* 10^{-5} \pm 1.66 * 10^{-4}$	$3.35 * 10^{-3}$	$1.17 * 10^{-4}$

Table 5-10 Comparison of diffusion parameters for nanocomposites prepared from high and low molecular weight PVOH

Diffusion generally occurs at a faster rate in the high molecular weight samples and delay times (before diffusion can be observed) are longer in the low molecular weight nanocomposites. The high molecular weight PVOH therefore appears to have a structure that results in a reduction of the barrier properties compared to the lower molecular weight polymer. It is quite likely that the longer chain length of the high molecular weight PVOH results in a less dense packing and a more open structure which enables faster diffusion.

Direct comparison of the diffusion parameters as a function of observed clay levels in the sample has not been carried out. There is some doubt whether the use of the ratio between the ν(C-O) band of PVOH and the ν(Si-O) band of the clay is an accurate means of comparing clay levels in samples with different molecular weights. Higher molecular weight nanocomposites appeared to have lower clay contents at the same clay loading (in the solution) than their high molecular weight counterparts. It remains uncertain whether the observed changes are due to changes in the samples or artefacts of the data extraction.

5.4.3 Changes in the polymer during ingress of water

During the diffusion of water into PVOH and PVOH nanocomposites several changes to the structure of the polymer were observed. PVOH swells considerably when in contact with water, changing from a polymer film to a gel. The extent of swelling can be followed by ATR-FTIR only to a certain extent as spectra of PVOH gels with high water contents are dominated by the spectrum of water. Furthermore, changes in crystallinity and clay levels detectable in the evanescent field can be observed during these experiments. Again only changes in the early part of the experiment can be followed without extensive data treatment. Once equilibrium has been reached no further changes could be observed in the spectra. As no subtraction methods have been used in this analysis it is possible that changes in the gel went unnoticed due to the spectra being dominated by the water bands.

5.4.3.1 Swelling of the polymer and polymer nanocomposite films

The swelling of PVOH and PVOH nanocomposite materials during the ingress of water has been qualitatively investigated by monitoring the decrease of the ν(C-O) band over time. Swelling is dependent on the amount of water sorbed in the film. PVOH can absorb high amounts of water, forming a gel in the process.

Figure 5-35 and Figure 5-36 present the process of swelling during the diffusion of water into low and high molecular weight samples respectively. For both types of samples swelling could be observed in the ATR spectra by changes in the intensities of the polymer bands once water can be detected in the evanescent field. Swelling occurs at a similar rate to the diffusion of water into the films. Plotting the changes in the area of the ν(C-O) band over time results in a curve which mirrors the shape of the water uptake curve obtained from the changes in area of the δ(OH) band.

The addition of clay does not have any apparent effect on the extent of swelling in low molecular weight PVOH, while a minor reduction of the swelling can be observed in the high molecular weight PVOH nanocomposites.

Since the spectra are dominated by water after about 2 minutes into the experiment, it is unclear how accurate this data is. Changes observed could partially be due to changes in the baseline, created by different water levels in the samples.

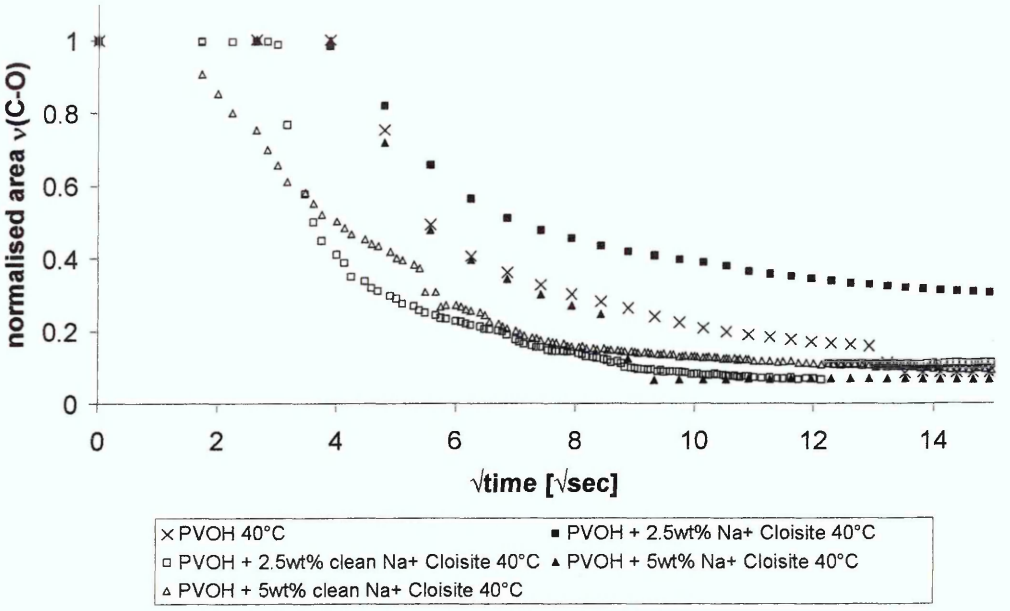

Figure 5-35 Swelling of PVOH and PVOH nanocomposites films of low molecular weight during diffusion of water

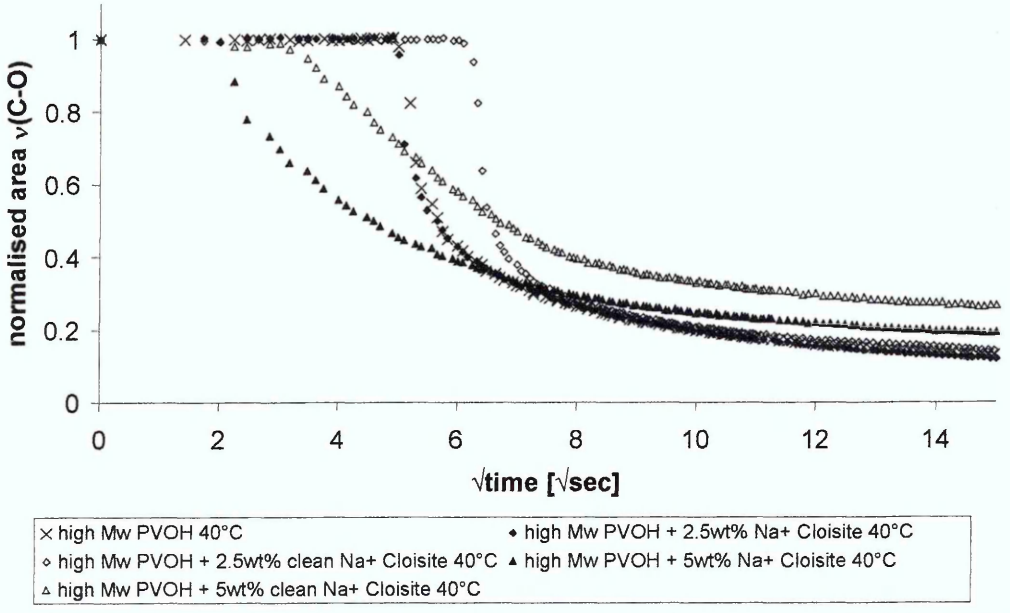

Figure 5-36 Swelling of PVOH and PVOH nanocomposites films of high molecular weight during diffusion of water

As the introduction of clay had little influence on the swelling of the sample, and diffusion rates appeared to remain unaffected by different clay structures, swelling of these samples is expected to remain similar as well. The results for the charged reduced Li^+ MCBP nanocomposites area, however, varied as can be seen in Figure 5-37.

The film with the highest clay content in the evanescent field, the composites prepared from Li^+ MCBP fired at 210 °C, did show the lowest swelling of the polymer which could be expected as less polymer is present in the evanescent field at the beginning. The swelling for the other MCBP were less predictable with the nanocomposite of the clay fired at 135 °C exhibiting higher swelling than the non heat treated Li clay.

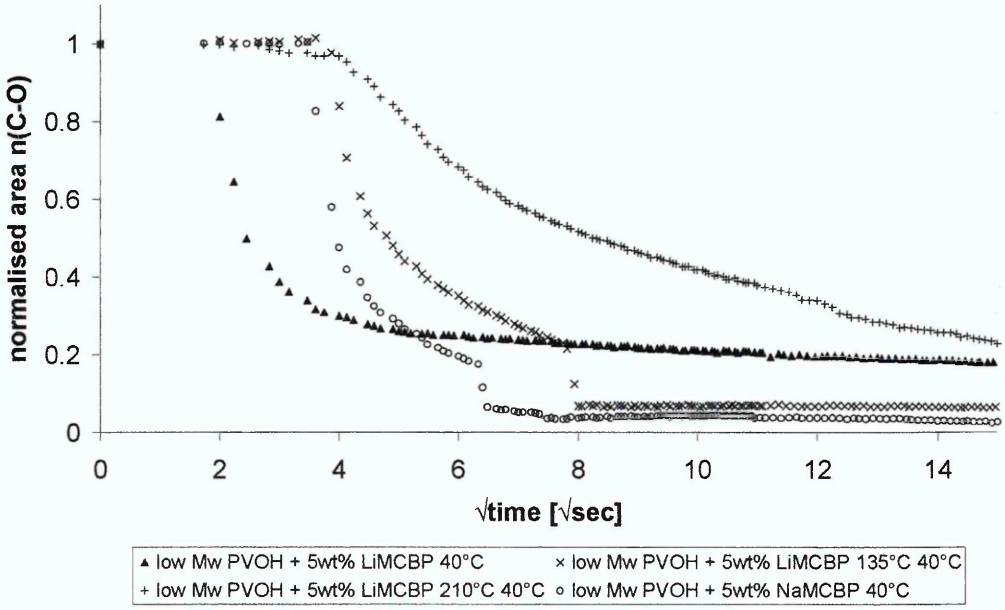

Figure 5-37 Swelling of PVOH and PVOH/ MCBP nanocomposites films of low molecular weight during diffusion of water

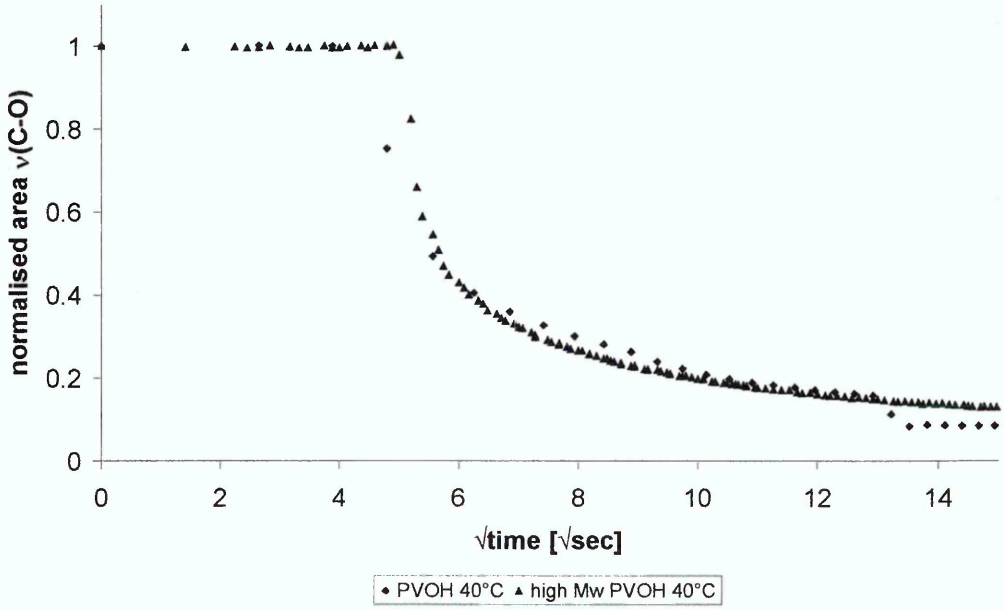

Figure 5-38 Swelling of PVOH films of different molecular weights during diffusion of water

Comparing the swelling measured in this manner for high and low molecular weight samples did not show any differences in the extent of swelling.

Introduction of clay into these samples, however, resulted in a reduction of swelling in the high molecular weight samples compared with low molecular weight samples of the same nominal clay content. The clay content in the evanescent field of these samples was found to be higher in the low molecular weight samples.

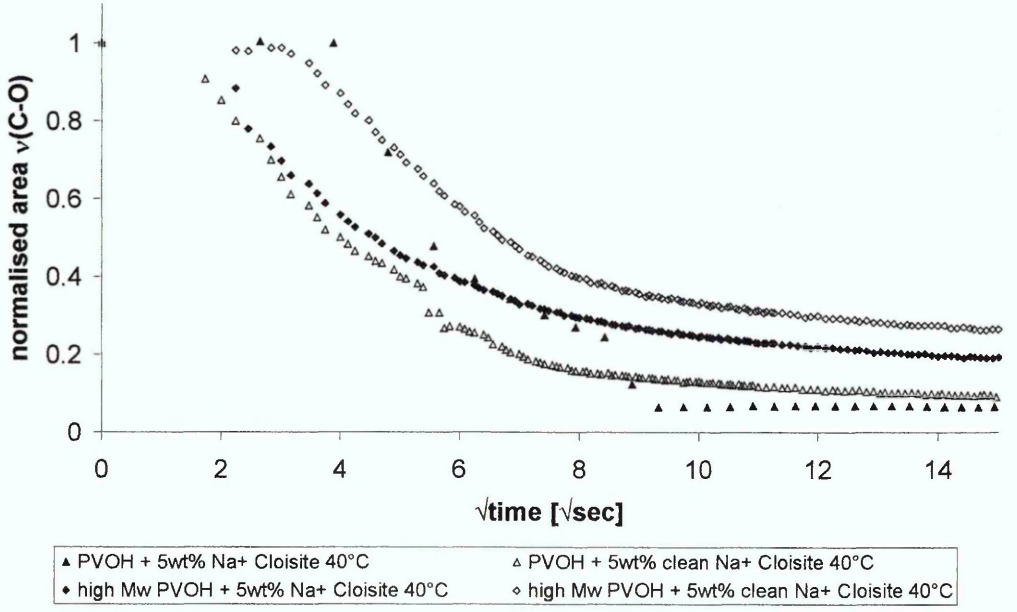

Figure 5-39 Swelling of PVOH and PVOH nanocomposites films of different molecular weights during diffusion of water

Like clay content changes in temperature did not result in any significant differences in the swelling observed for low molecular weight PVOH and PVOH nanocomposite samples.

5.4.3.2 Crystallinity changes of the polymer and polymer nanocomposites

It is generally accepted that diffusion in polymers takes place mainly in the amorphous regions of the sample. The ingress of a solvent can however dissolve crystallites and lead to changes in the overall crystallinity of the film. Crystallinity has been found to decrease during swelling of PVOH samples with water when the overall crystallinity was low, while in higher crystallinity samples, no significant changes were observed. [5.43]

FTIR allows a semi-quantitative determination of crystallinity by ratioing the band at 1141 cm^{-1} which has been found to be sensitive to changes in crystallinity against the ν(C-O) band which is insensitive to the degree of crystallinity. [5.39, 5.44 - 5.46]

As the intensities of the PVOH bands exhibit strong reductions during the diffusion of water into the sample (due to swelling), the values obtained from ratioing the relevant bands give misleading results as the crystallinity band is disappearing while the ν(C-O) band is broadening with increasing water content. Therefore, only spectra showing the reduction of crystallinity in comparison with the dry film spectra will be discussed in the following.

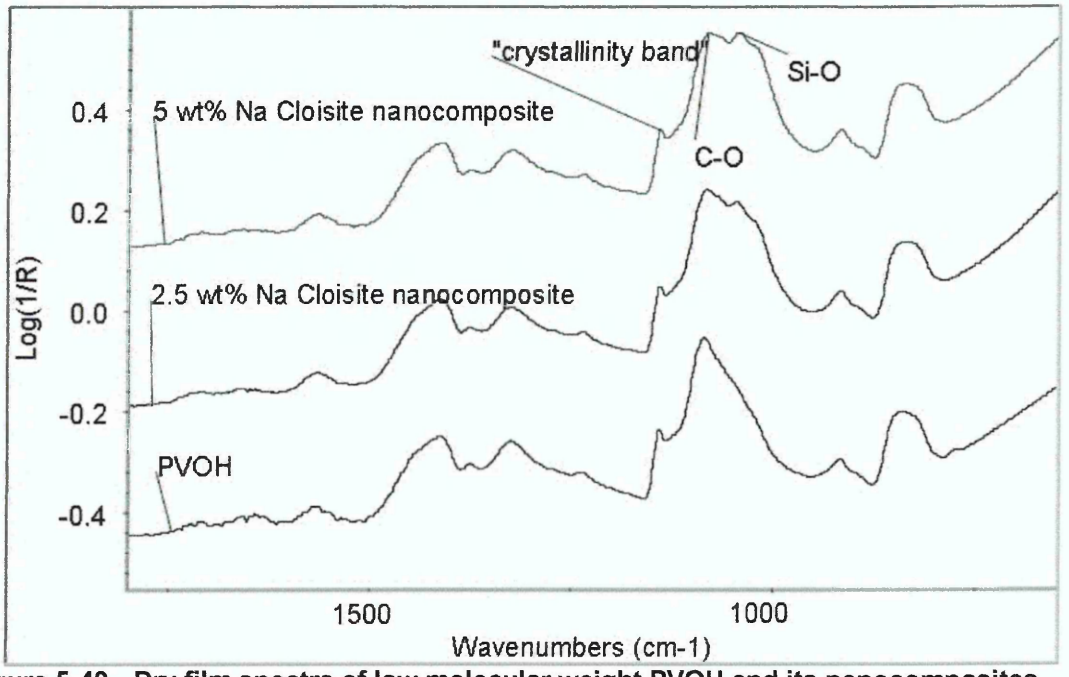

Figure 5-40 Dry film spectra of low molecular weight PVOH and its nanocomposites

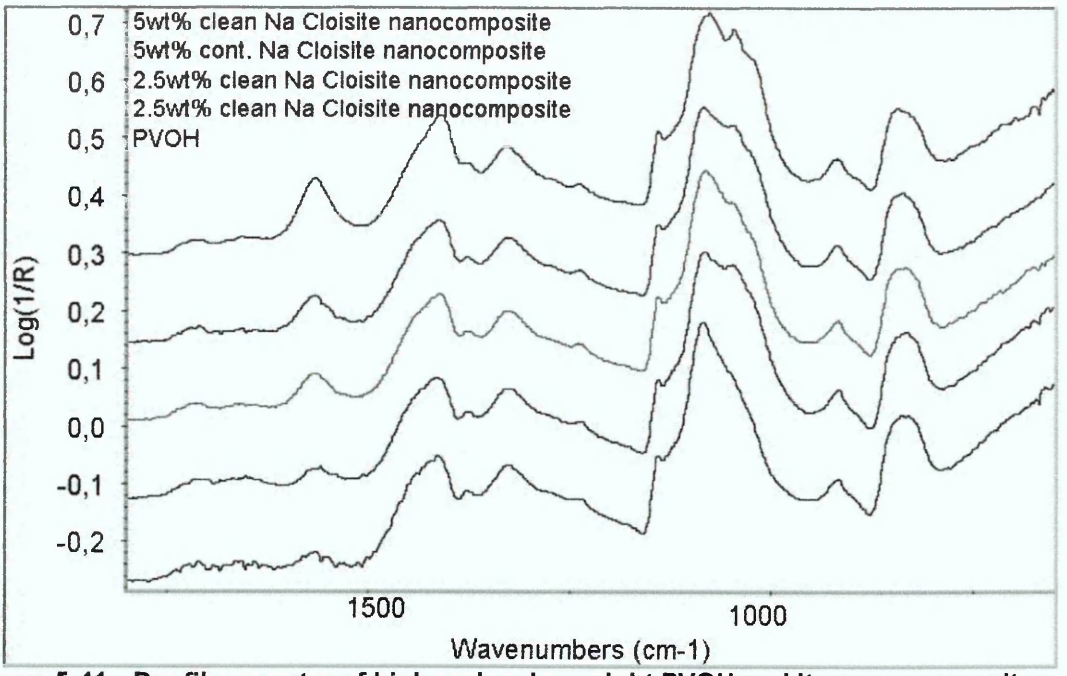

Figure 5-41 Dry film spectra of high molecular weight PVOH and its nanocomposites

Figure 5-40 and Figure 5-41 show that crystallinity levels in the dry films remain similar in the nanocomposites to those of the pristine polymer. As a result of this, the level of crystallinity that can be determined from the ATR-FTIR spectra is considered to be independent of clay level and the overall crystallinity of the polymer in the evanescent field remains unaffected by the addition of clay. It is, however, possible that clay platelets induce localised higher crystallinity that cannot be measured by this method.

Figure 5-42 - Figure 5-44 present examples of the changes occurring during the diffusion of water into PVOH and PVOH nanocomposites with different clay contents. In all cases the band at 1141 cm^{-1} is found to decrease over time and disappear from the spectrum well before diffusion has reached equilibrium, indicating a reduction in crystallinity. This reduction occurs once water has entered the sample causing swelling and increased chain mobility which ultimately results in the dissolution of the polymer crystallites.

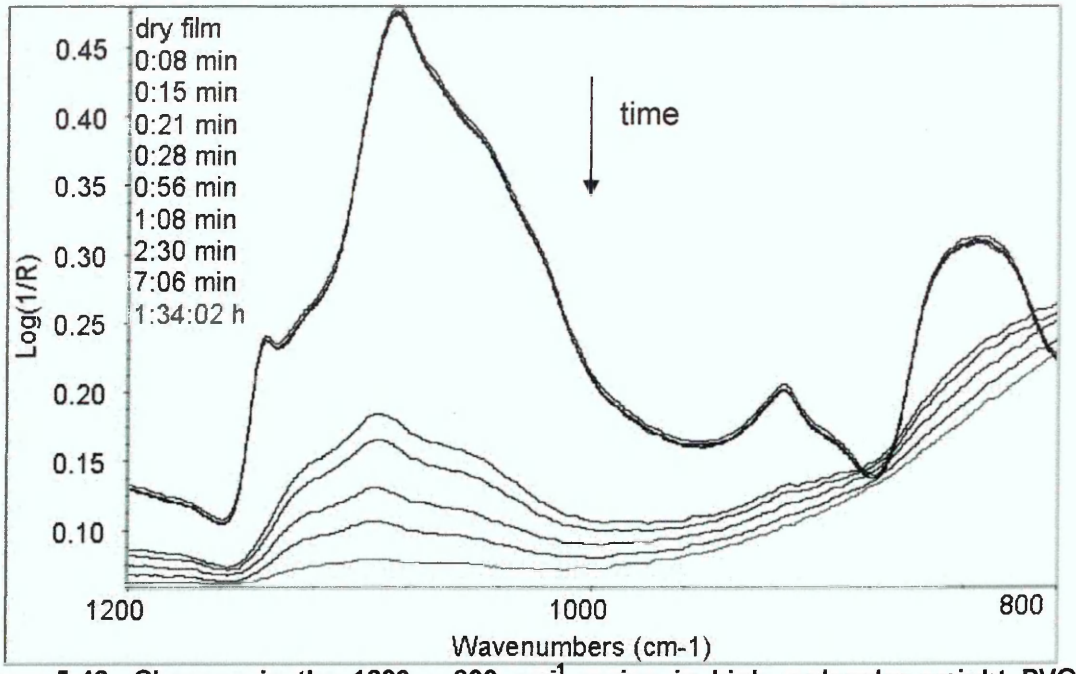

Figure 5-42 Changes in the 1200 – 800 cm^{-1} region in high molecular weight PVOH during the diffusion of water into the sample

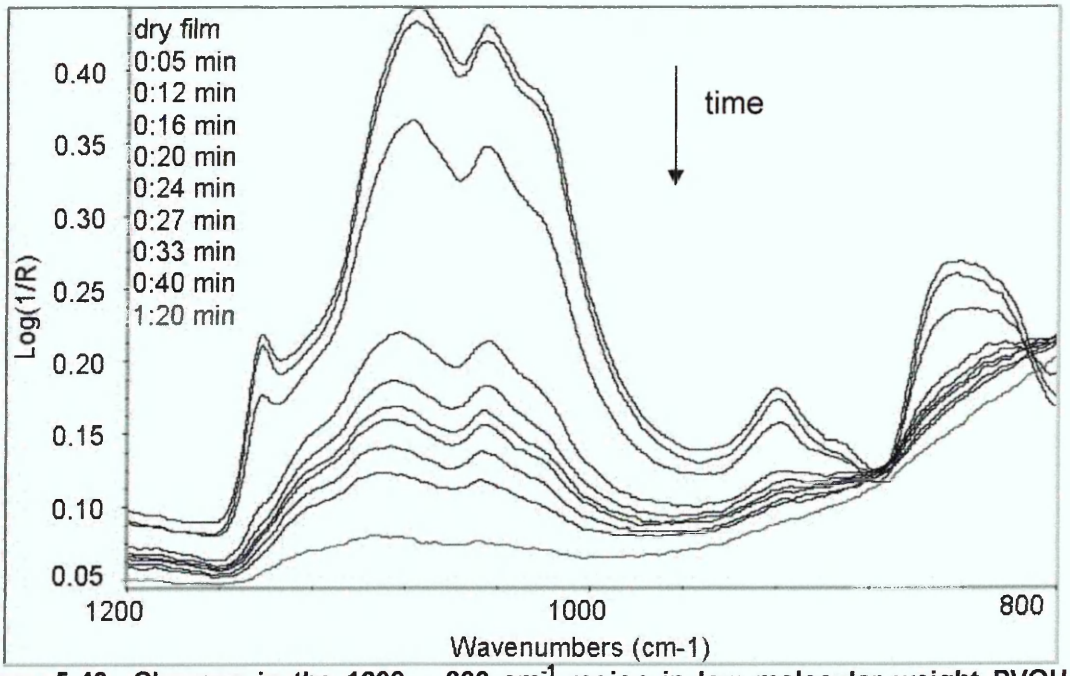

Figure 5-43 Changes in the 1200 – 800 cm^{-1} region in low molecular weight PVOH + 5 wt% clean Na^+ Cloisite® during the diffusion of water into the sample

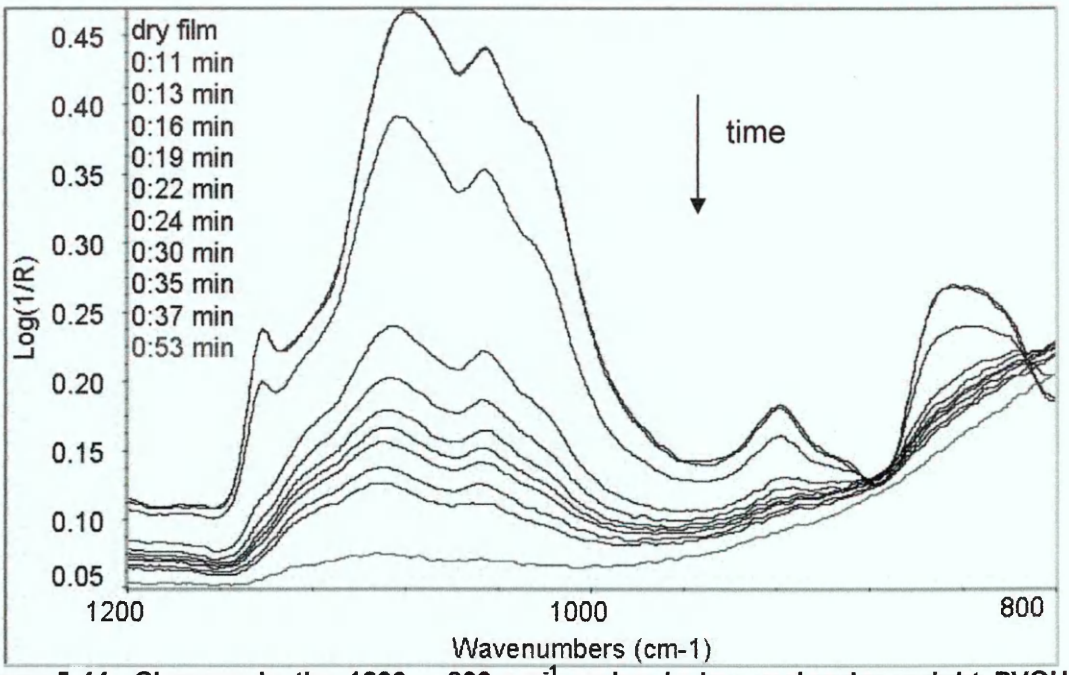

Figure 5-44 Changes in the 1200 – 800 cm^{-1} region in low molecular weight PVOH + 5 wt% Na^+ MCBP during the diffusion of water into the sample

5.4.3.3 Clay level changes in the nanocomposites

Changes in the clay level observed in the evanescent field are of interest in these samples and have been investigated to determine whether the clay is moving within the film, once the sample is swollen and plasticised by water. In the dispersions from which the nanocomposite films were cast, clay was found to settle out when the liquid was no longer agitated.

If clay is showing similar behaviour in the swollen nanocomposite films an increase of the intensity of the ν(Si-O) band around 1040 cm^{-1} compared to that of the ν(C-O) band (ca. 1085 cm^{-1}) should be observed.

As in the case of crystallinity changes, in the clay level can only be qualitatively measured. The strong swelling of the sample makes sensible integration results difficult to obtain. Therefore changes will be discussed from the spectra shown.

In the dry film spectra different clay levels can easily be observed from the shape of the broad band between 1160 cm^{-1} and 950 cm^{-1}. In the nanocomposites, this band arises due to a combination of the ν(C-O) and ν(Si-O) vibrations.

Following the changes in this area during the diffusion of water into nanocomposite films shows that the band is decreasing at a similar rate as the

ν(C-O) band. (see Figure 5-45 - Figure 5-47) At later times, the clay band is even weaker in comparison to the ν(C-O). Therefore one can assume that the clay does not settle out of the polymer matrix but its intensity is reduced due to reduction of clay layers in the evanescent field due to swelling of the polymer, and possibly swelling intercalated clay layers.

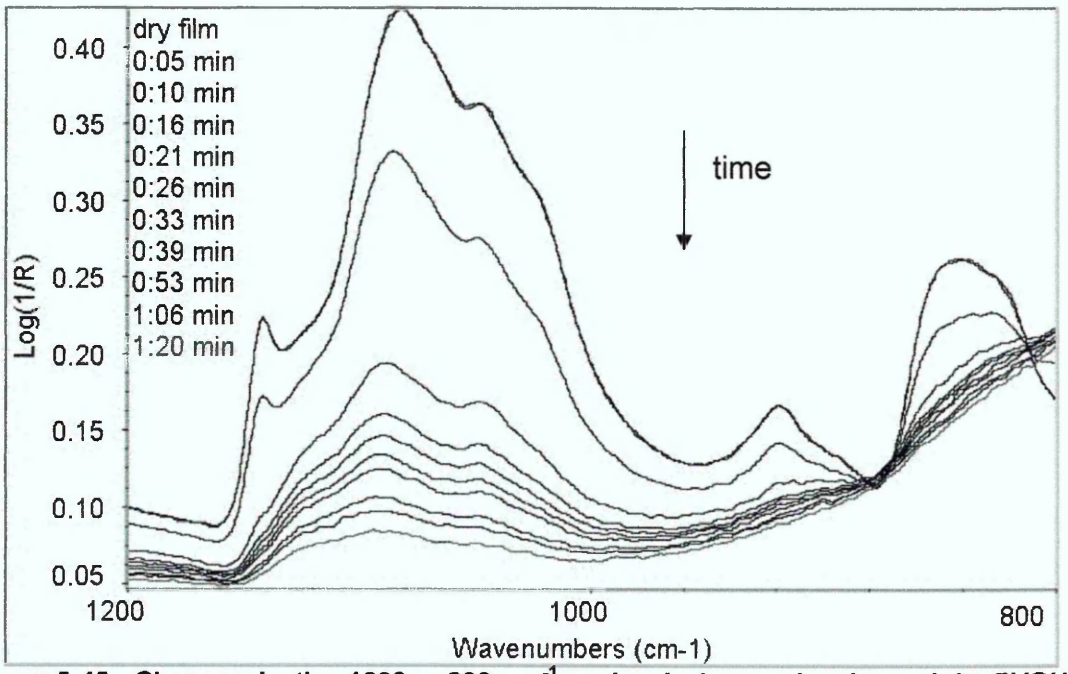

Figure 5-45 Changes in the 1200 – 800 cm^{-1} region in low molecular weight PVOH + 2.5 wt% clean Na^+ Cloisite® during the diffusion of water into the sample

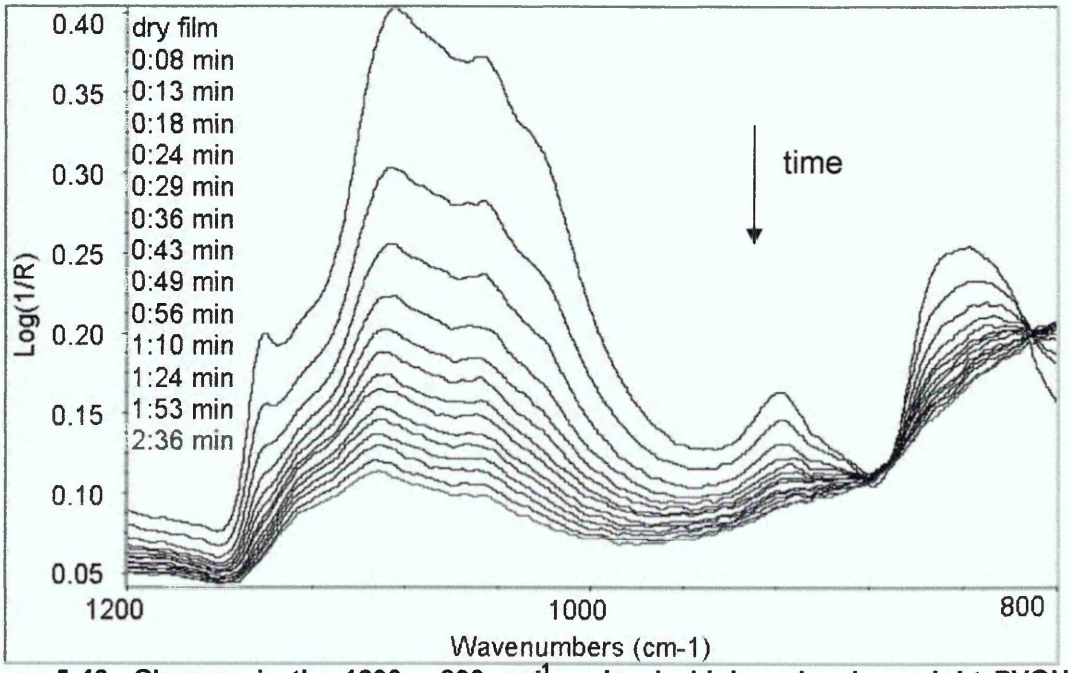

Figure 5-46 Changes in the 1200 – 800 cm^{-1} region in high molecular weight PVOH + 5 wt% clean Na^+ Cloisite® during the diffusion of water into the sample

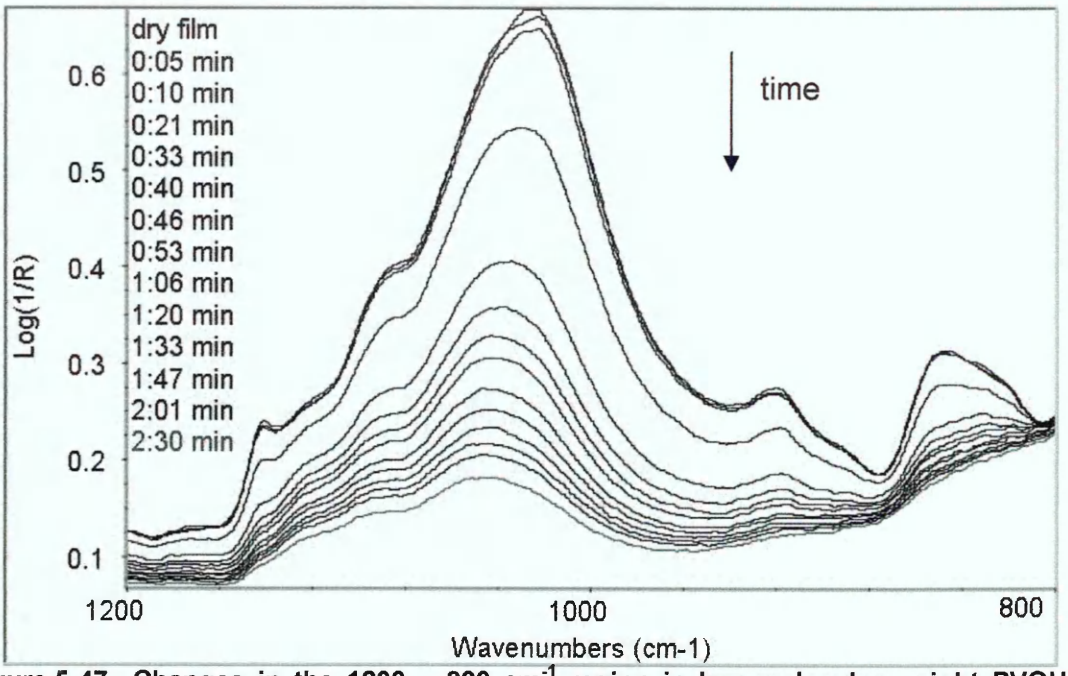

Figure 5-47 Changes in the 1200 – 800 cm^{-1} region in low molecular weight PVOH + 5 wt% Li^+ MCBP fired at 210 °C during the diffusion of water into the sample

5.4.4 Changes in the hydrogen bonding of water and poly (vinyl alcohol)

5.4.4.1 Hydrogen bonding in pure water

The OH stretching mode of water shows a rather complex band, consisting of contributions from molecules exhibiting different degrees of hydrogen bonding in the network. Analogues with the hydrogen bonding strengths identified in pure water, and in other polymers [5.12, 5.31, 5.37, 5.38], four bands have been fitted in the ν(OH) region. These bands correspond to weakly (highest wavenumber), moderately weak, moderately strong and strongly (lowest wavenumber) hydrogen bonded water.

Hydrogen bonding is dependent on temperature. At increased temperatures the hydrogen bonding network weakens which results in a shift of the OH stretching band to higher wavenumbers [5.9]. (see Figure 5-1)

Plotting the relative intensity of the different bands fitted to the ν(OH) region in pure water at 30, 40 and 50°C respectively as presented in Figure 5-48 shows changes in the relative peak areas as expected; the fractions of weakly hydrogen bonded and moderately weak hydrogen bonded water increase while those of moderately strong and strongly bonded water decrease with increasing temperatures.

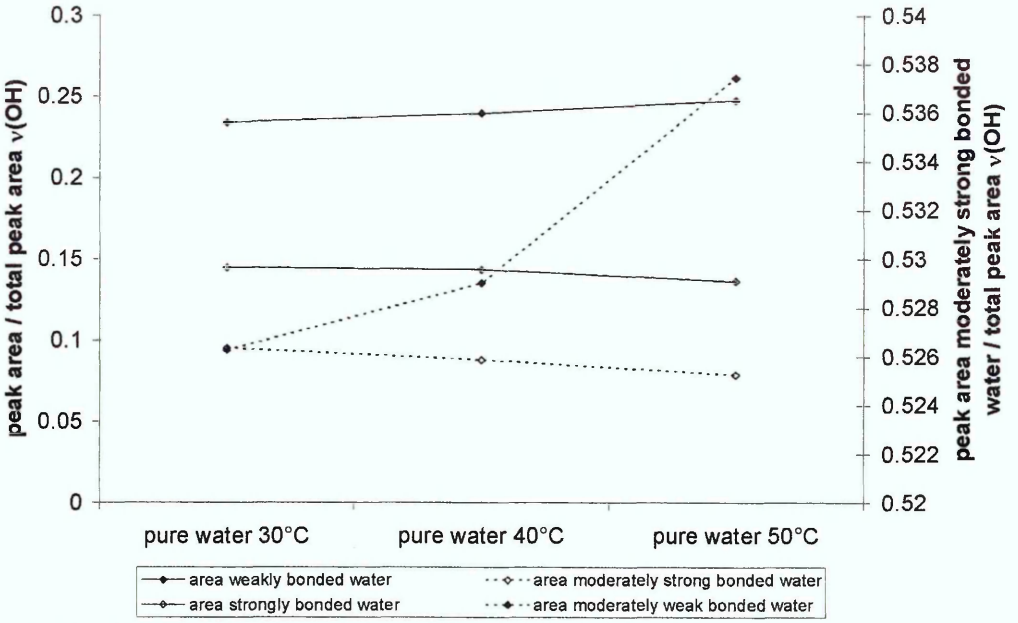

Figure 5-48 Changes in hydrogen bonding in pure water at different temperatures

5.4.4.2 Changes in the equilibrium spectra of the diffusion experiments

Comparison of the equilibrium spectra from the measurements of liquid water diffusing into PVOH and PVOH nanocomposites shows that the hydrogen bonding in these samples is influenced by the temperature at which the diffusion experiment was conducted, the clay loading of the nanocomposites and the clay layer charge/ clay dispersion in the nanocomposites.

In the equilibrium spectra of diffusion experiments of water into low molecular weight at different temperatures a similar trend as that for pure water can be observed (see Figure 5-49). In general the fractions of stronger hydrogen bonded molecules are decreasing with increasing temperatures while the bands assigned to weaker hydrogen bonding increases. The bands assigned to hydrogen bonded PVOH are changing in similar fashion to the water bands. These changes are to be expected as increased temperatures result in a weakening of hydrogen bonding due to higher molecular motion.

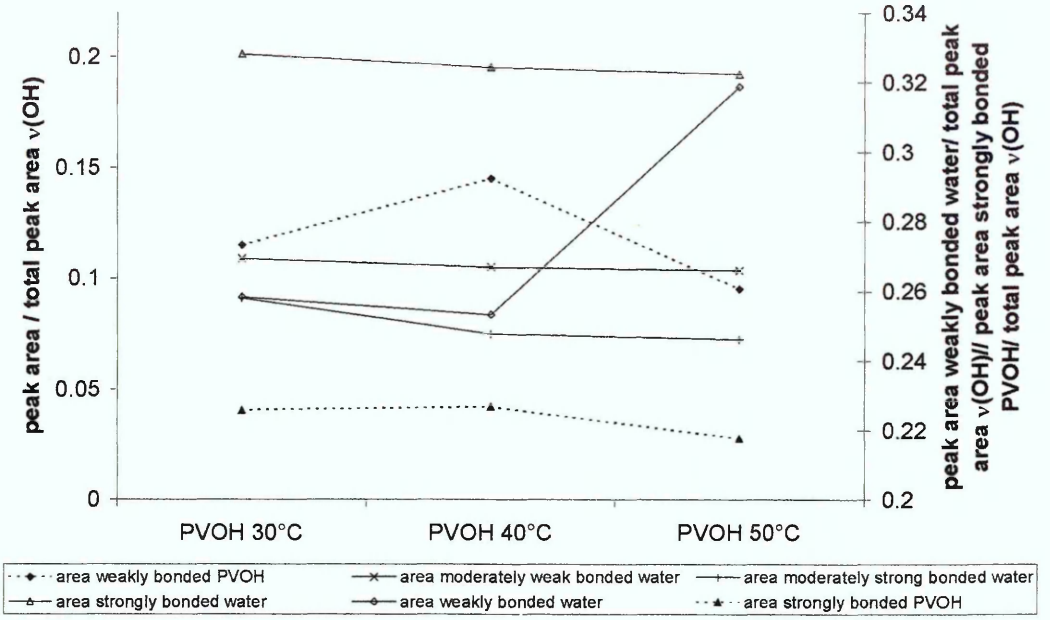

Figure 5-49 Changes in the hydrogen bonding at equilibrium of water diffusion into low molecular weight PVOH at different temperatures

Introduction of clay into PVOH enhances the changes in hydrogen bonding observed for equilibrium spectra of water diffusion. Figure 5-50 presents the changes in relative peak areas for the different hydrogen bonding types in low molecular weight PVOH + 5 wt% Na^+ Cloisite® nanocomposites. Unlike what is found in the pristine polymer, the band for moderately hydrogen bonded water decreases with increasing temperature, while the band for moderately strong hydrogen bonded water increases. The bands for the hydrogen bonded polymer both decrease with increasing temperatures. As actual clay loadings in these samples can vary, the changes observed cannot be attributed entirely to changes related to increased temperature. The observations made for these samples most likely arise from a combination of temperature effects and differences in clay loading, since one would expect the weakly hydrogen bonded PVOH fraction to increase with rising temperatures (due to a weakening of bonds by the higher mobility of the polymer chains at increased temperatures).

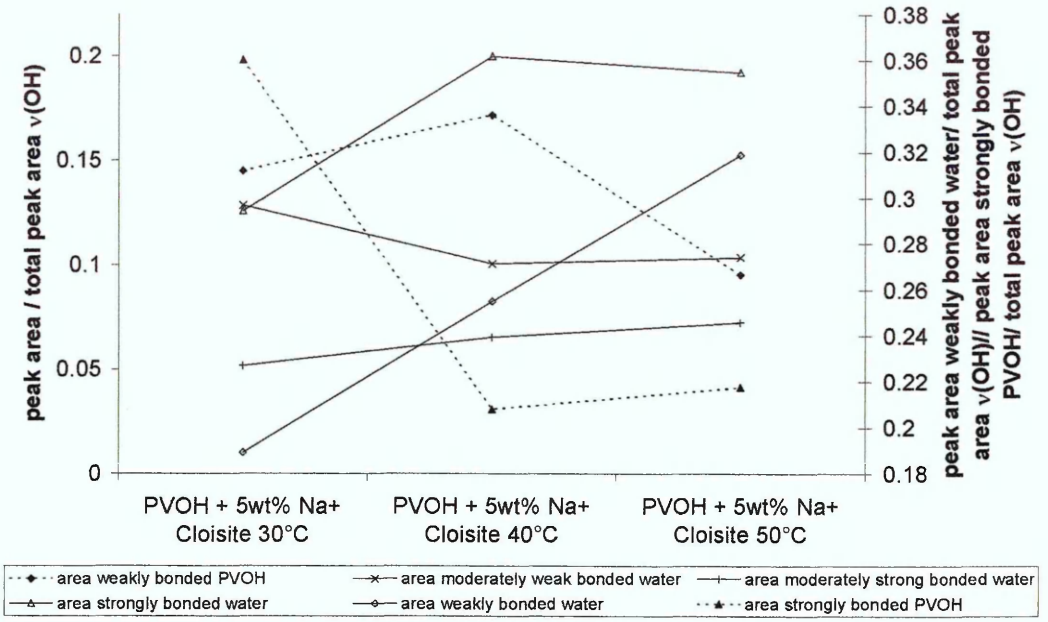

Figure 5-50 Changes in the hydrogen bonding at equilibrium of water diffusion into low molecular weight PVOH/ Na^+ Cloisite® nanocomposites at different temperatures

Figure 5-51 and Figure 5-52 summarise the data obtained for the equilibrium spectra of water diffusing into PVOH and PVOH/ Na^+ Cloisite® nanocomposites. Some differences can be observed between samples prepared from PVOH with different molecular weight, while clay contamination did not appear to have any significant influence on the hydrogen bonding observed in these types of samples. No peaks can be observed for water hydrogen bonding to clay surfaces in these samples due to low clay contents and strong overlapping of the various bands in the OH stretching region. Therefore, one cannot determine whether there really are no changes due to organic contamination of the clay.

In nanocomposites of low molecular weight PVOH bands assigned to weakly bonded PVOH, weakly hydrogen bonded water and moderately weak hydrogen bonded water remain relatively unchanged with increasing clay levels. Bands for moderately strong hydrogen bonded water and strongly hydrogen bonded water are found to decrease with increasing clay levels while the strongly hydrogen bonded PVOH is lowest in the 2.5 wt% clay sample. As this band has a similar relative intensity in the higher clay sample to that in the pristine polymer, this difference is likely to be an artefact of the fitting process.

The high molecular weight nanocomposites exhibit only minor changes in relative areas of the bands assigned to weakly hydrogen bonded PVOH and

moderately strong and moderately weak hydrogen bonded water as well as strongly hydrogen bonded water. Increasing the amount of clay in the sample results in a strong increase in weakly hydrogen bonded water and a decrease of strongly hydrogen bonded PVOH. These changes are probably due to clay disrupting the hydrogen bonding network of the water molecules in the polymer and the inter- and intramolecular hydrogen bonding of the polymer itself.

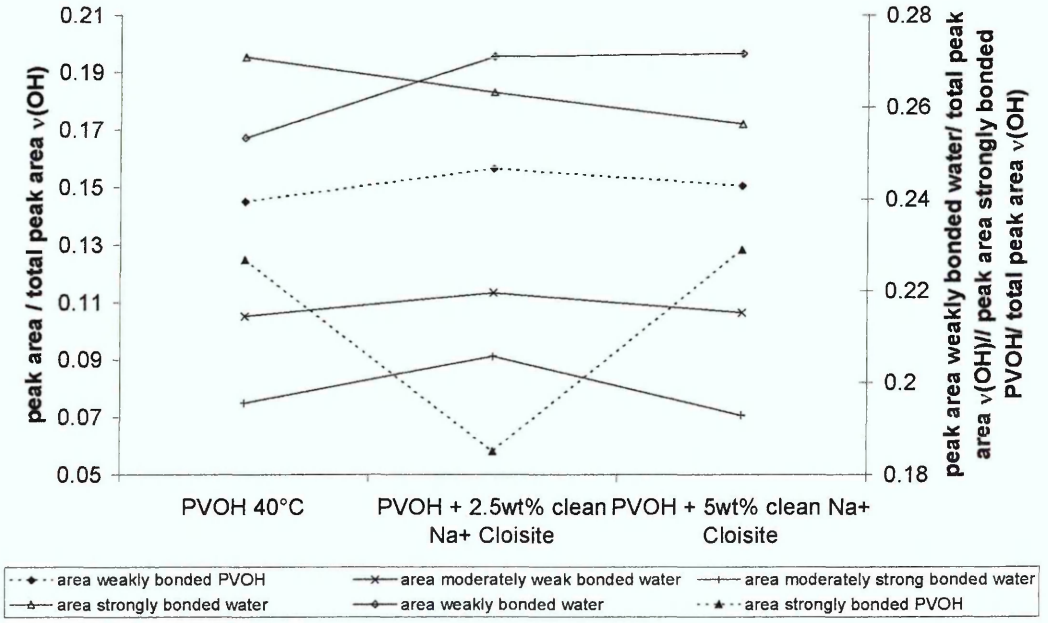

Figure 5-51 Changes in the hydrogen bonding at equilibrium of water diffusion into low molecular weight PVOH/ clean Na^+ Cloisite® nanocomposites at different clay loadings

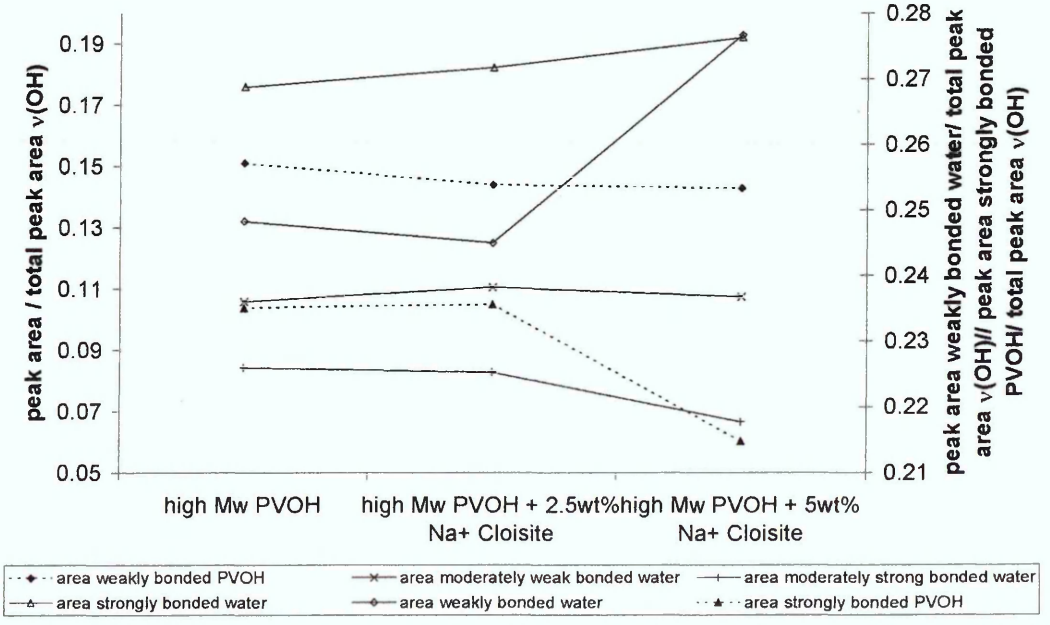

Figure 5-52 Changes in the hydrogen bonding at equilibrium of water diffusion into high molecular weight PVOH/ Na^+ Cloisite® nanocomposites at different clay loadings

Changes due to different clay layer charges and therefore different degrees of dispersion in the polymer matrix proved more difficult to assess. Some bands exhibit stronger changes in the sample prepared with Li^+ MCBP fired at 135°C than in that prepared with Li^+ MCBP fired at 210°C. In general, better dispersion of the clay favours strong hydrogen bonding of the polymer and strong and weak hydrogen bonding of the water within the polymer film.

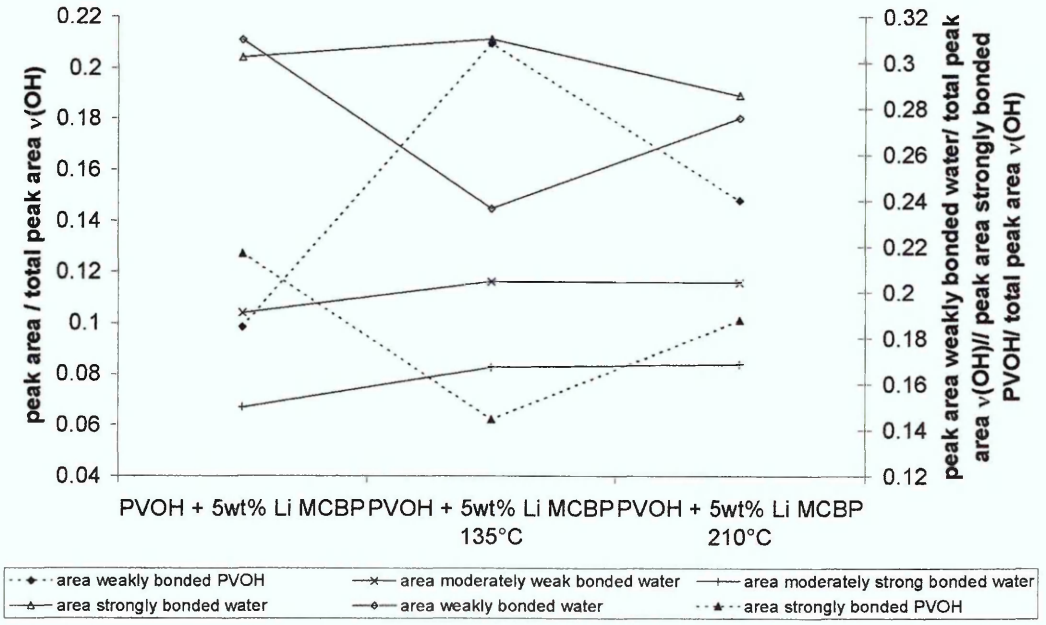

Figure 5-53 Changes in the hydrogen bonding at equilibrium of water diffusion into low molecular weight PVOH/ Li^+ MCBP nanocomposites with different clay layer charges

5.4.4.3 Changes during diffusion of water

Following the changes occurring in hydrogen bonding during the diffusion of water into the sample shows that all bands increase in intensity with increasing water content. The extent of this increase, however, varies for each of the bands. Increases of all bands assigned to water in the polymer are to be expected as the level of water within the sample increases. Such increases have been observed for various types of hydrogen bonded water during the diffusion of water into PET and PVC [5.37].

The increase of the bands assigned to hydrogen bonded polymer is, however, unusual; as one would expect these bands to decrease with increasing water content due to swelling and therefore reduction of the relative amount of polymer in the evanescent field. As PVOH is a hygroscopic polymer, and films have been produced at ambient atmosphere, it is likely that even the films dried

at raised temperatures contained some bound water. The bands assigned to hydrogen bonded polymer will therefore contain some contribution from water bound in the dry films used to obtain the peak positions for the PVOH peaks. Furthermore, the peaks could exhibit increases due to overlapping of different water and polymer vibrations that are not accounted for by the bands fitted in this analysis.

Changes occurring during the diffusion of water into low molecular weight PVOH at 30°C and 40°C respectively are presented in Figure 5-54 and Figure 5-55. Temperature does not affect the general trends observed with increasing water levels. In both cases changes in the hydrogen bonding of the polymer are relatively minor. The water bands most affected by increasing water levels are those of strongly and weakly hydrogen bonded water. The two bands for moderately hydrogen bonded water only exhibit minor changes. Most of the water in PVOH at equilibrium is weakly hydrogen bonded. The relative intensities of the bands for hydrogen bonded PVOH are reducing as one would expect due to the swelling of the sample.

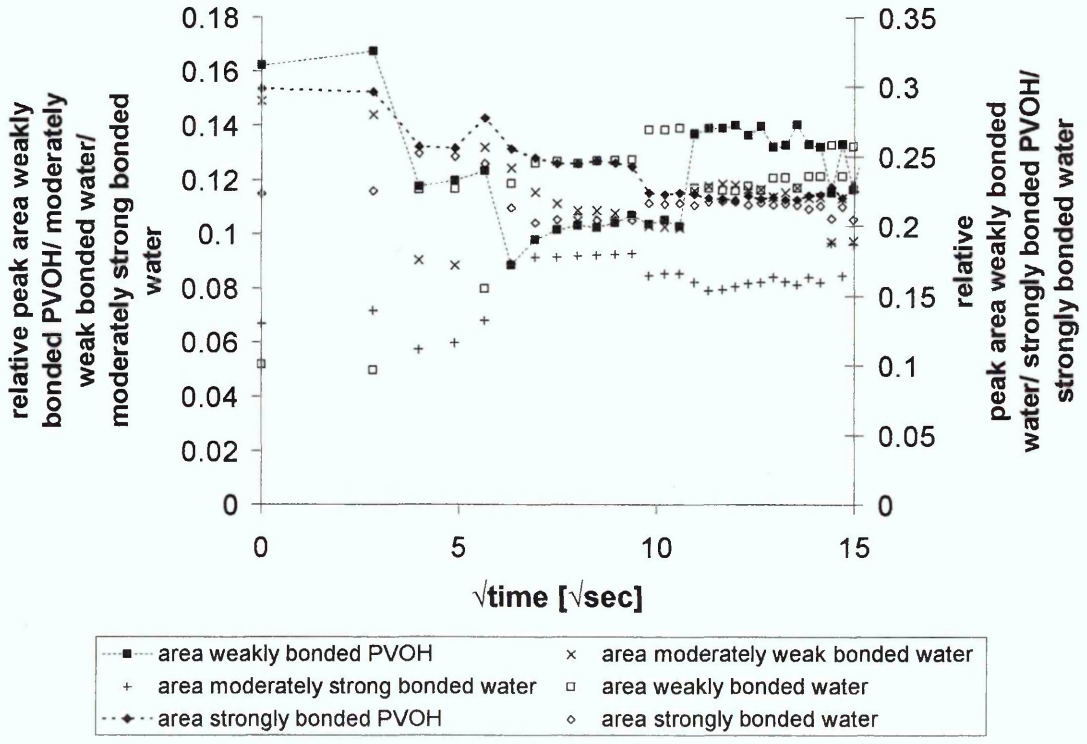

Figure 5-54 Changes in the relative peak areas for the bands assigned to different types of hydrogen bonding during diffusion of water into low molecular weight PVOH at 30 °C

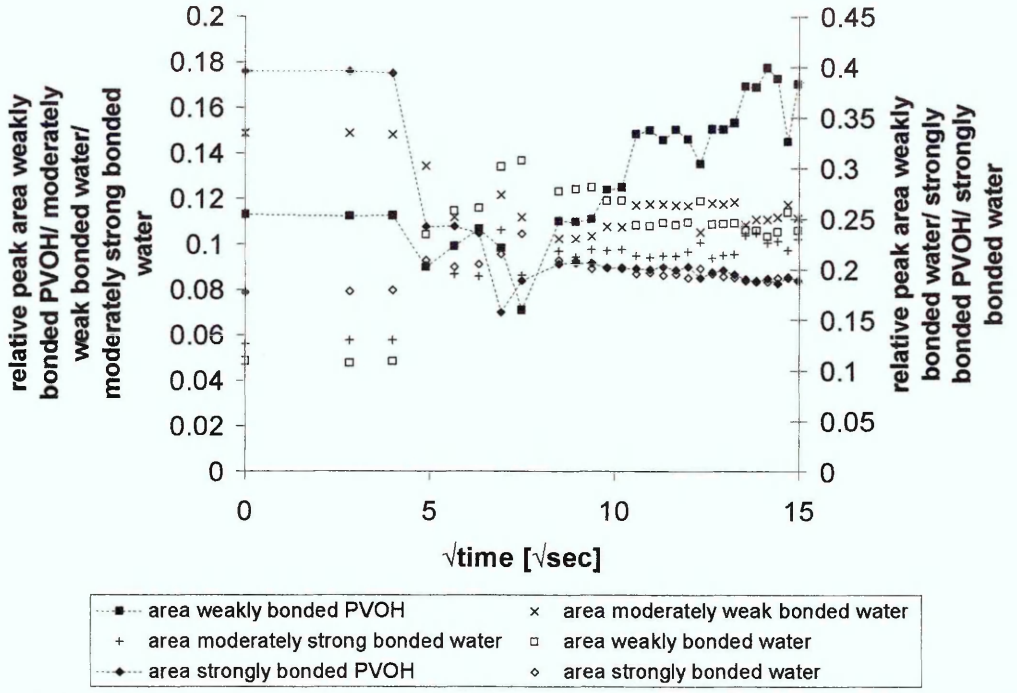

Figure 5-55 Changes in the relative peak areas for the bands assigned to different types of hydrogen bonding during diffusion of water into low molecular weight PVOH at 40 °C

Collecting data from only one scan per spectrum allows shorter sampling intervals. This enables a more detailed investigation of the changes in hydrogen bonding occurring during the diffusion of water into PVOH. In the high molecular weight sample, a reduction in intensity of bands assigned to hydrogen bonded PVOH is observed at the same time as the water front reaches the polymer. After this initial drop in intensity of these bands the band for weakly bonded PVOH is found to increase. As the limited data for the low molecular weight polymer also shows an increase in the weakly hydrogen bonded PVOH it is likely that this is due to reformation of the inter molecular hydrogen bonds in the PVOH after initial disruption of these bonds through the presence of water.

The data for diffusion of water into high molecular weight PVOH is presented in Figure 5-56. As for the low molecular weight sample the increases in the relative intensity of weakly hydrogen bonded water is the dominant change with this fraction becoming the largest at equilibrium.

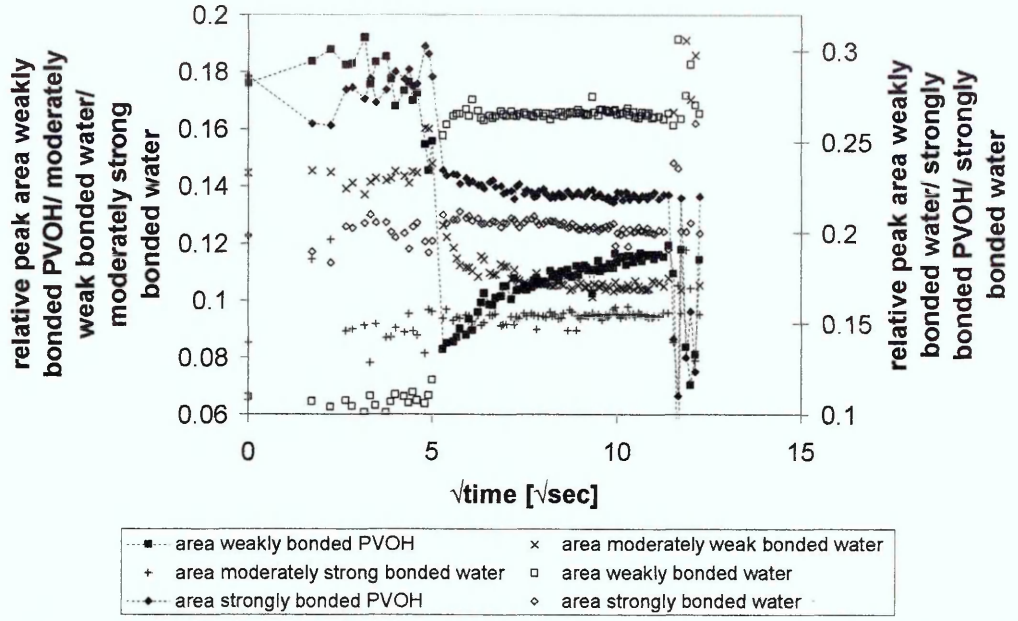

Figure 5-56 Changes in the relative peak areas for the bands assigned to different types of hydrogen bonding during the diffusion of water into high molecular weight PVOH at 40 °C

Addition of clay to the samples does not change these trends in the changes of the relative peak areas. Figure 5-57 -Figure 5-59 present the data for nanocomposites with 5 wt% Na^+ Cloisite®, Li^+ MCBP and Li^+ MCBP fired at 210 °C respectively. The data appears to be more variable which is probably due increased water vapour in these spectra influencing the peak fitting procedure.

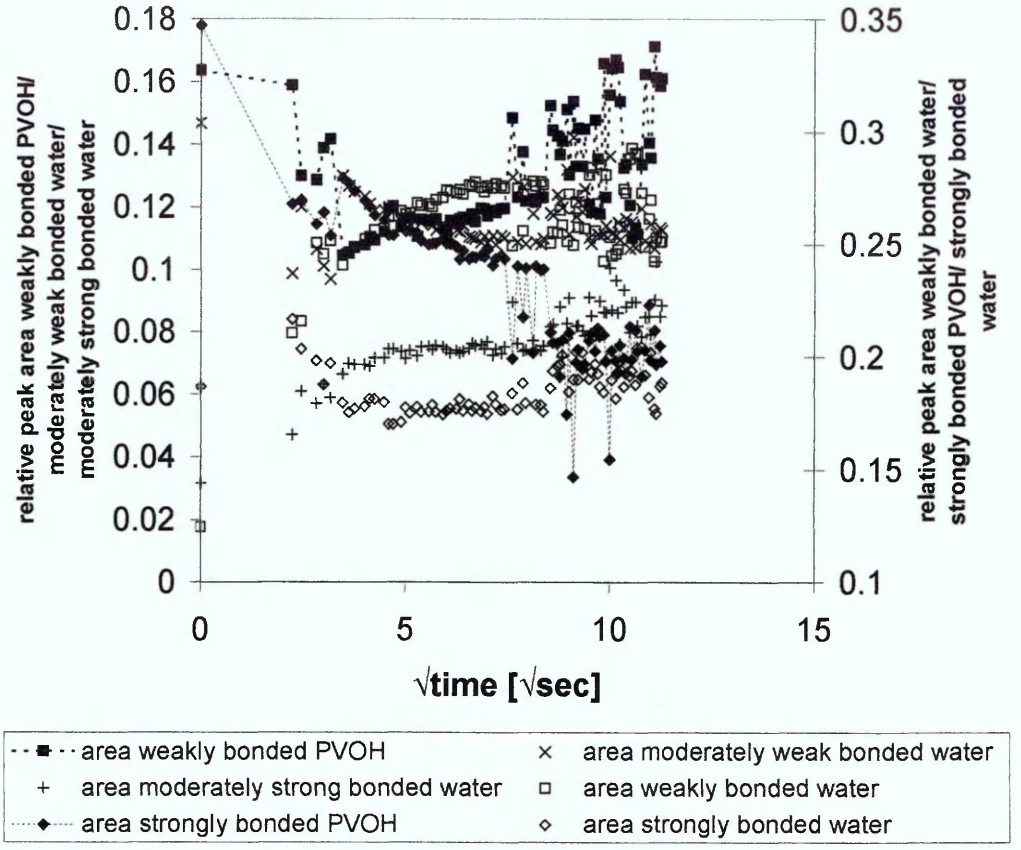

Figure 5-57 Changes in the relative peak areas for the bands assigned to different types of hydrogen bonding during diffusion of water into high molecular weight PVOH + 5 wt% Na^+ Cloisite® at 40 °C

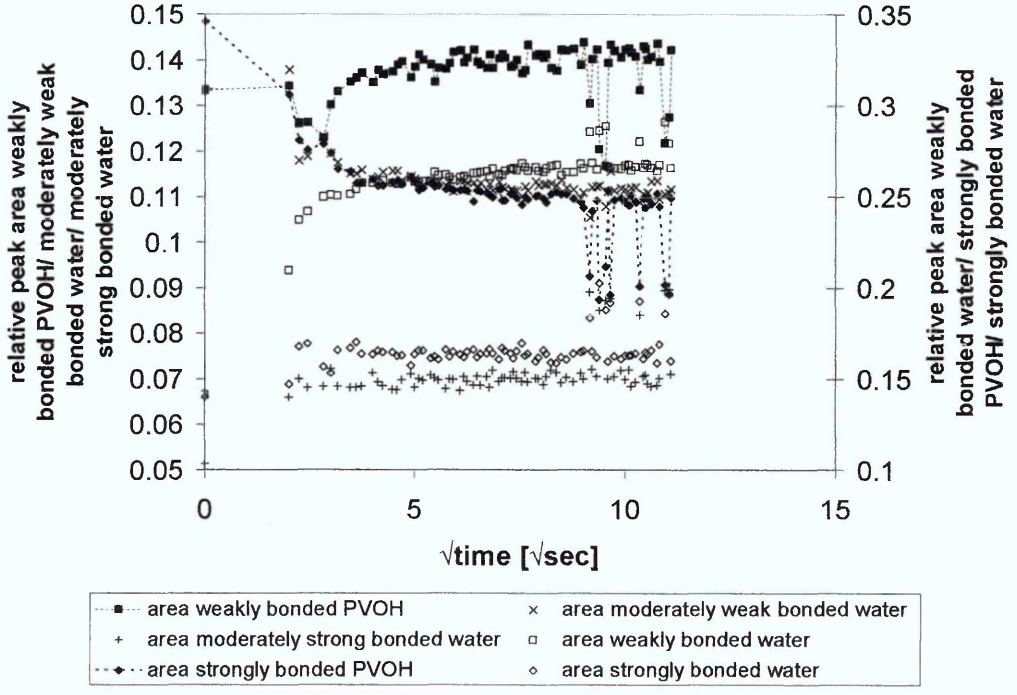

Figure 5-58 Changes in the relative peak areas for the bands assigned to different types of hydrogen bonding during diffusion of water into low molecular weight PVOH + 5 wt% Li^+ MCBP at 40 °C

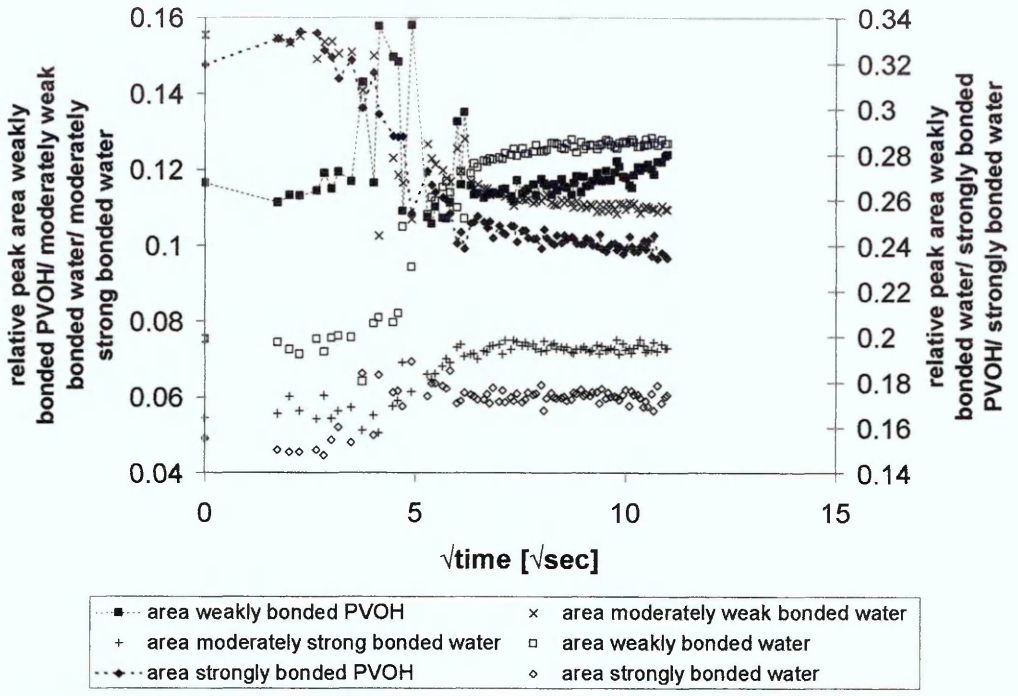

Figure 5-59 Changes in the relative peak areas for the bands assigned to different types of hydrogen bonding during diffusion of water into low molecular weight PVOH + 5 wt% Li^+ MCBP fired at 210 °C at 40 °C

5.4.5 Summary

The diffusion of water into PVOH and PVOH nanocomposites can be followed by ATR – FTIR. Interaction with water causes widespread changes in the polymer film, since PVOH is very hydrophilic and dissolves in water.

Data could be fitted to the short term approximation of Fickian diffusion. Using this model is, however, a simplification since the changes observed in the infrared spectra are not only due to diffusion of water into the sample. There are also contributions from swelling and dissolution of the polymer film.

The formation of nanocomposites resulted in a reduction of the delay time before diffusion could be observed, while the diffusion rate generally decreased with increasing clay content. For the low molecular weight samples, this behaviour was not as obvious as for the high molecular weight samples.

The data collected on charge reduced clay suggests that clays with lower layer charges and therefore poorer dispersion when incorporated into PVOH have less impact on the barrier properties of PVOH.

Measurements at different temperatures showed that the induction time was reduced with increasing temperatures. This trend could not be observed as

obviously in the nanocomposites. This was most likely due to the inhomogeneity of the nanocomposite samples and therefore different actual clay loadings measured at different temperatures. Diffusion coefficients measured for low molecular weight PVOH appeared to decrease with increasing temperature. However, it cannot be ruled out that uncertainties and errors in the measurement are responsible for this counter-intuitive result. It is possible that most likely changes in the residual water at the start of the experiment influence the diffusion behaviour enough to give these results. The nanocomposites generally showed increased diffusion rates at higher temperature, further supporting the hypothesis that the results obtained for the neat polymer are influenced by changes between the samples, rather than being caused by the raised temperatures.

Higher molecular weight samples were found to have poorer barriers towards water diffusion, both for the pristine polymer and the nanocomposites; exhibiting faster water diffusion than the low molecular weight samples. Here the effects of addition of clay on the diffusion were more obvious than in the low molecular weight samples. The decrease in the diffusion coefficient was found to be larger between the neat polymer and the 2.5 wt% nanocomposite than between the nanocomposites with 2.5 wt% and 5 wt% clay loading.

Organic contamination of the clay used for the preparation of the nanocomposites resulted in materials that showed better barrier properties than nanocomposites prepared from a clean batch of the clay. These results are in line with the observations made for charged reduced clay nanocomposites, where lower layer charges (and therefore poorer dispersion) resulted in better barrier properties because the organically contaminated clay is expected to disperse less well in the polymer, due to lower hydrophilicity of the clay surfaces.

The swelling during the diffusion remains largely unaffected by the presence of clay in the sample. This is surprising, as one would expect the polymer to swell less in the presence of clay due to steric hindrance of polymer chain movement by the clay platelets.

The ingress of water causes a reduction of crystallinity in the polymer film. This reduction can be observed in the pristine polymer and nanocomposite samples independent of the type of clay or the clay loading in the sample.

Investigation of the hydrogen bonding of water in the polymer, and of the polymer itself, shows an increase in weakly hydrogen bonded water with increasing temperatures, in the pristine polymer as well as in the nanocomposites.

With increasing clay levels, one can also observe an increase of the weaker hydrogen bonded molecules in low molecular weight PVOH samples. Changes in hydrogen bonding due to presence of clay in the high molecular weight polymer were less extensive and trends observed were similar to the low molecular weight PVOH.

Observed changes in hydrogen bonding during the diffusion of water into these samples show that the inter- and intra molecular hydrogen bonding in the polymer decreases due to swelling of the samples. Most of the water present in the sample is only 'weakly' hydrogen bonded.

5.5 References

5.1 'An introduction to hydrogen bonding', (Ed Jeffrey GA), Oxford University Press (1997)
5.2 Marechal Y, *J. Mol. Struct.*, **648**, 27 (2003)
5.3 Hare DE, Sorensen CM, *J. Chem. Phys.*, **96**, 13 (1992)
5.4 Libnau FO, Christy AA, Kvalheim OM, *Appl. Spectrosc.*, **49**, 1431 (1995)
5.5 Falk M, *Chemistry and Physics of aqueous gas solutions*, 19 (1975)
5.6 Pople JA, *Proc. R. Soc. London Ser. A*, **205**, 163 (1951)
5.7 Stillinger FH, *Science*, **209**, 451 (1980)
5.8 Sceats MG, Rice SA, *J. Phys. Chem.*, **85**, 1108 (1981)
5.9 Libnau FO, Kvalheim OM, Christy AA, Toft J, *Vib. Spec.*, **7**, 243 (1994)
5.10 Nemethy G, Scheraga HA, *J. Phys. Chem.*, **36**, 3382 (1962)
5.11 Benson SW, Siebert ED, *J. Am. Chem. Soc.*, **114**, 4269 (1992)
5.12 Libnau FO, Toft J, Christy AA, Kvalheim OM, *J. A. Chem. Soc.*, **116**, 8311 (1994)
5.13 Sammon C, Deng CS, Mura C, Yarwood J, *J. Mol. Liq.*, **101**, 35 (2002)
5.14 Coyle FM, Martin SJ, McBrierty VJ, *J. Mol. Liq.*, **69**, 95 (1996)
5.15 Iordanskii AL, Razumovskii LP, Krivandin AV, Lebedeva TL, *Desalination*, **104**, 27 (1996)
5.16 Gref R, Nguyen QT, Schaetzel P,Néel J, *J. Appl. Polym. Sci.*, 9lm209 (1993)
5.17 Hodge RM, Bastow TJ, Edward GH, Simon GP, Hill AJ, *Macrom.*, **29**, 8137 (1996)
5.18 Hodge RM, Edward GH, Simon GP, *Polymer*, **37**, 1371 (1996)
5.19 Ping ZH, Nquyen QT, Chen SM, Zhou JQ, Ding YD, *Polymer*, **42**, 8461 (2001)
5.20 Rault J, Gref R, Ping ZH, Nguyen QT, Neel J, *Polymer*, **36**, 1655 (1995)
5.21 Zhang WZ, Satoh M, Komiyama J, *J. Membrane Sci.*, **42**, 303 (1989)
5.22 Rault J, *Macromol. Symp.*, **100**, 31 (1995)
5.23 Rault J, Ping ZH, Nguyen T, *J. Non-Cryst. Solids*, **172**, 733 (1994)
5.24 Krzeminski J, Molisak-Tolwinska H, *J. Macromol. Sci. Chem.*, **A28**, 413 (1991)
5.25 Müller-Plathe F, *Macrom.*, **31**, 6721 (1998)
5.26 Maeda Y, Ide M, Kitano H, *J. Mol. Liq.*, **80**, 149 (1999)
5.27 Maeda Y, Kitano H, *Spectrochim. Acta A*, **51**, 2433 (1995)
5.28 Maeda Y, Tsukida N, Kitano H, Terada T, Yamanaka J, *J. Phys. Chem.*, **97**, 13903 (1993)
5.29 Sutandar P, Ahn DJ, Franses EI, *Macrom.*, **27**, 7316 (1994)
5.30 Kusanagi H, Yukawa S, *Polymer*, **35**, 5637 (1994)
5.31 Sammon C, Deng CS, Yarwood J, *Polymer*, 44, 2669 (2003)
5.32 Marechal Y, *Farad. Dis.*, **103**, 349 (1996)
5.33 Iwamoto R, Murase H, *J. Polym. Sci.: Pt. B Polym. Phys.*, **41**, 1722 (2003)
5.34 Ide M, Yoshikawa D, Maeda Y, Kitano H, *Langmuir*, **15**, 926 (1999)
5.35 Chenskaya TB, Perov NS, Ponomarev II, *J. Mol. Struct.*, **381**, 149 (1996)
5.36 Nguyen QT, Favre E, Ping ZH, Neel J, *J. Membrane Sci.*, **113**, 137 (1996)
5.37 Sammon C, Mura C, Yarwood J, Everall N, Swart R, Hodge D, *J. Phys. Chem.*, **102**, 3402 (1998)

5.38 Sammon C, Mura C, Hajatdoost S, Yarwood J, *J. Mol. Liq.*, **96-97**, 305 (2002)
5.39 Assander HE, Windle AH, *Polymer*, **39**, 2581 (2001)
5.40 Gorrasi G, Tortora M, Vittoria V, Galli G, Chiellini E, *J. Polym. Sci.: Pt. B Polym. Phys.*, **40**, 1118 (2002)
5.41 Gorrasi G, Tortora M, Vittoria V, Poller E, Lepoittevin B, Alexandre M, Dubois P, *Polymer*, **44**, 2271 (2003)
5.42 Hedenqvist M, Gedde UW, *Prog. Polym. Sci.*, **21**, 299 (1996)
5.43 Perrin L, Nguyen QT, Clement R, Neel J, *Polym. Int.*, **39**, 251 (1996)
5.44 Ngui MO, Mallapragada SK, *J. Polym. Sci.: Pt. B Polym. Phys.*, **36**, 2771 (1998)
5.45 Krimm S, Liang CY, Sutherland GBBM, *J. Polym. Sci.*, **22**, 227 (1956)
5.46 Peppas NA, *Makromol. Chem.*, **178**, 595 (1977)

6 Diffusion of acetone/ water mixtures into poly (vinyl alcohol) and its Na+ Cloisite® nanocomposites

6.1 Introduction

6.1.1 Diffusion measurements of solvent mixtures

Studying the diffusion behaviour of solvent mixtures is important for many membrane-based separations and selective barrier materials. The diffusion behaviour observed for such components is often complicated, as it depends on the interactions of each solvent with the polymer sample as well as the interactions between the solvents in the mixture.

Following the diffusion of a mixture of two solvents is not trivial with conventional (mass uptake) measurements [6.1, 6.2]. Due to this, little attention has been paid to the measurement of diffusion coefficients of solvent mixtures in the past. This has, however, changed recently, as magnetic resonance imaging (MRI) [6.3, 6.4], nuclear magnetic resonance spectroscopy (NMR) [6.5], Fourier-transform infrared spectroscopy (FTIR) [6.3, 6.6 - 6.9], and fluorescence microscopy have been found to be powerful tools for the observation of the diffusion of mixed solvents into polymers. In ATR-FTIR measurements the diffusion of various solvents into a sample film can easily be followed if the solvents of interest have strong absorbing IR-bands that do not overlap with each other or any bands from the sample films.

Several models have been suggested for interpretation of the kinetic data obtained from measurements of solvent mixture ingress into polymers. While it is possible to treat the data for each solvent on its own and obtain diffusion coefficients by fitting this data to binary diffusion models, more complex, tertiary, models also take the diffusion of complexes created from interactions between the solvents in solution into account.

Hong and Barbari [6.7] used a combination of two Fickian diffusion profiles to model the diffusion of toluene/ methyl ethyl ketone (MEK) vapours into poly (isobutylene). Huang et al. [6.2] and Dutheillet et al. [6.3] observed a combination of adsorption and Fickian diffusion in their studies of diffusion of

ethanol/ dichloromethane and ethanol/ ethyl acetate mixtures into polyurethane, and aqueous acetic acid into epoxy resins respectively.

Elabd and Barbari [6.6] describe a model for multi-component diffusion in polymers based on the Onsager framework [6.11], which uses an array of diffusion coefficients through a multi-component, transient form of the continuity equation to describe transport. With this approach they have been able to determine diffusion coefficients for MEK and 1-butanol as well as a complex formed by these two solvents into poly (isobutylene).

Using FTIR imaging Ribar and Koenig [6.9] showed that in a mixture of solvent and non-solvent the solvent will diffuse into the sample first, followed by the non-solvent.

So far very little data has been published on the diffusion of solvent mixtures through polymer/ clay nanocomposites. A study of the dehydration of water/ alcohol mixtures by vapour permeation through PVOH/ clay nanocomposites [6.12] showed that the oxygen permeability and water permeation rate decreased at low clay contents of 1 - 3 wt%, due to the increased tortuosity of the diffusion pathway, while an increase was observed at clay levels of more than 5 wt%. This was attributed to phase separation of the organic and inorganic material.

6.1.2 Acetone/ water mixtures

Understanding the interactions between acetone and water in binary mixtures of the two solvents has been the focus of many studies. FTIR has proven to be a useful tool for probing the changes in the water network upon introduction of acetone.

Investigating acetone/ water complexes in argon matrixes Engdahl [6.14] and Zhang et al. [6.15] found a linear dependence of the bands associated with a 1:1 acetone/ water complex on the water concentration when the acetone concentration was kept below the limit for the formation of acetone dimers. At these concentrations a shift of the ν(OH) band to lower wavenumbers has been observed, while no indication of water interacting with the methyl groups of the acetone molecules could be found from the position of the ν(CH) bands.

In contrast to these findings, Mizuno et al. [6.13] showed evidence of "hydrophobic hydration" of acetone at high water concentrations ($x_{water} > 0.96$). The transition from a hydration state of the CH bonds of acetone to "hydrophobic hydration" was found to be dependent on the acetone: water ratio. Similar findings were published by Symons and Eaton [6.16] who observed that systems that favour clathrate formation will avoid hydrophobic hydration when the water/ solute ratio is greater than that necessary for the formation of clathrates. The shifted position of the ν(C=O) in acetone/ water systems (1696 cm^{-1}) compared to its position in pure acetone is indicative of hydrogen bonding of the carbonyl oxygen to two water molecules.

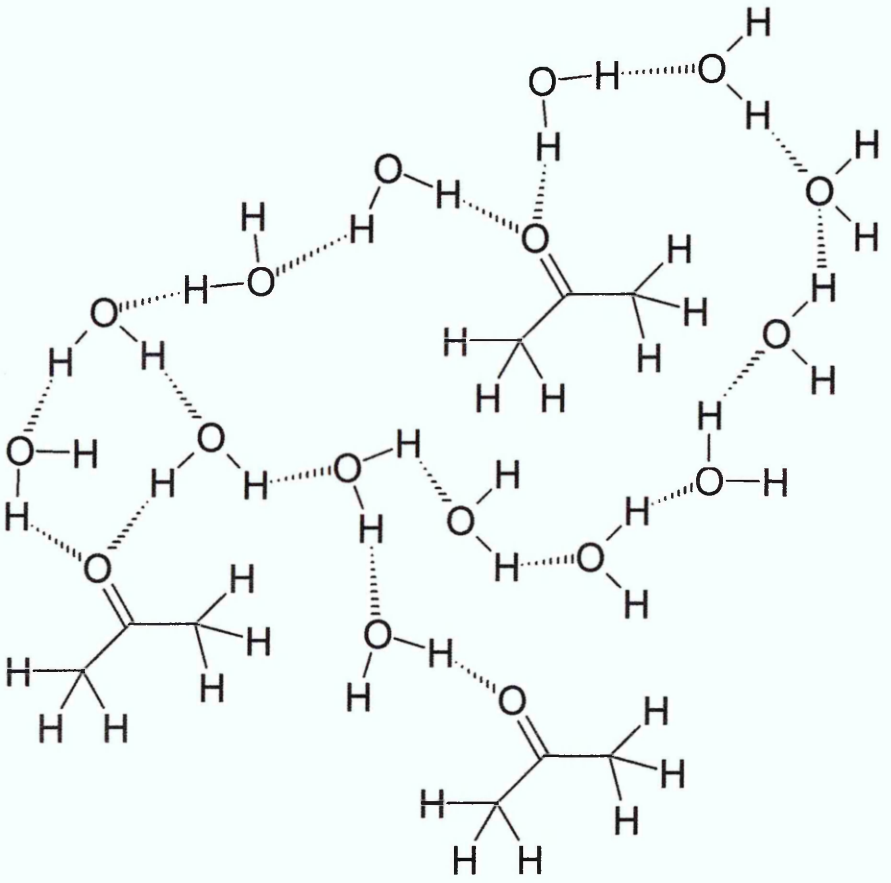

Figure 6-1 Structure of acetone/ water mixture at high water content [6.15, 6.16]

Max and Chapados [6.17] deduced from the spectra of water isolated in acetone that one water molecule is hydrogen bonded to two acetone molecules at these low concentrations.

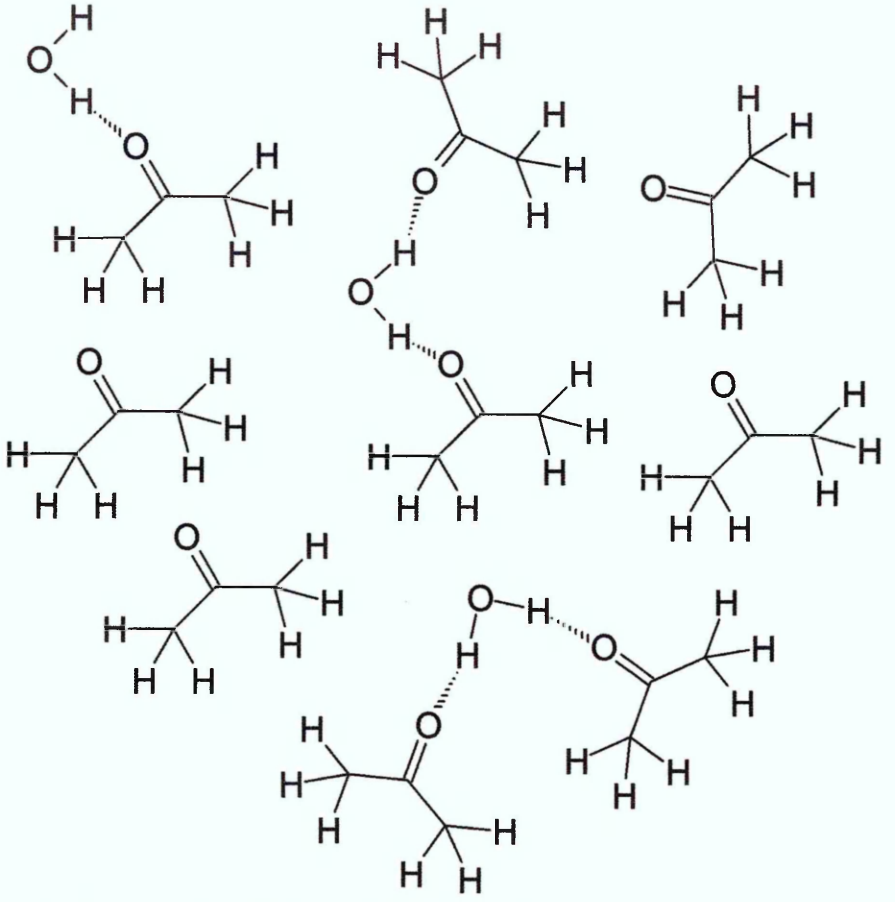

Figure 6-2 Structure of acetone water mixtures at low water content [6.17]

The number of water molecules hydrogen bonded to other water molecules was also found to be highly dependent on the molar fraction of water in the mixture. At $x_{acetone}$ = 0.7 Venables and Schmuttenmaer [6.18] observed dramatic changes in the number of water molecules that are hydrogen bonded to two or more other water molecules. At higher acetone concentrations, only few water molecules with several hydrogen bonds to other water molecules remain, whereas at lower acetone concentrations water remains part of the conventional network.

ATR spectra of the mixtures, used for the experiments presented in this thesis, are shown in Figure 6-3. The overall intensities of these spectra are decreasing with decreasing water concentrations. A closer look at the ν(OH) band shape reveals significant changes of this band in dependence of the water concentration as shown in Figure 6-4.

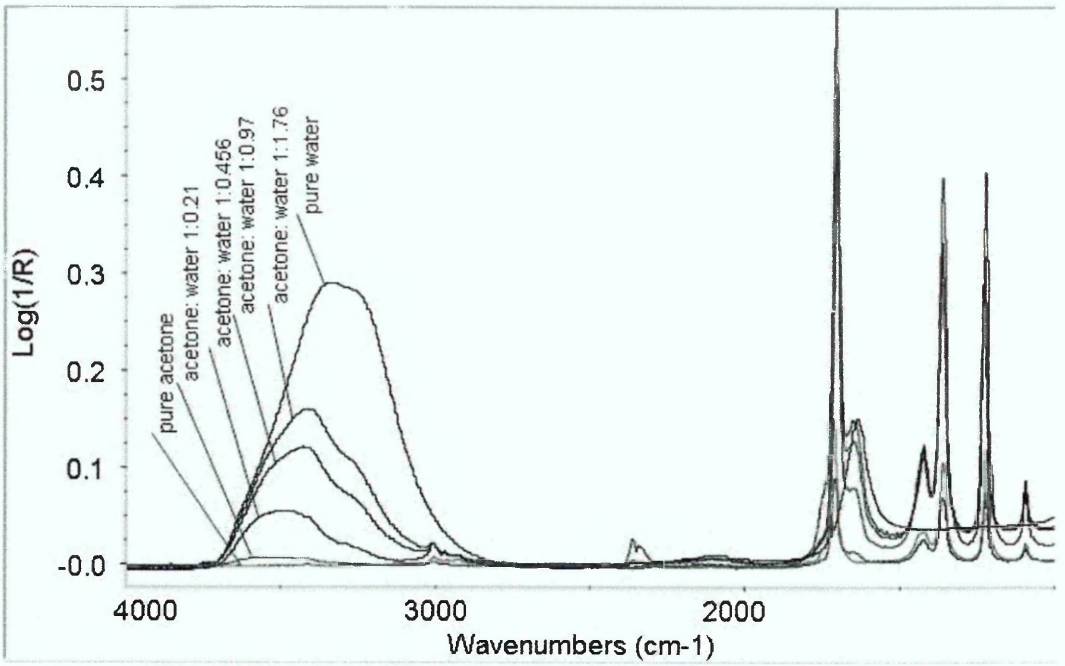

Figure 6-3 ATR spectra of pure water, pure acetone and acetone/ water mixtures

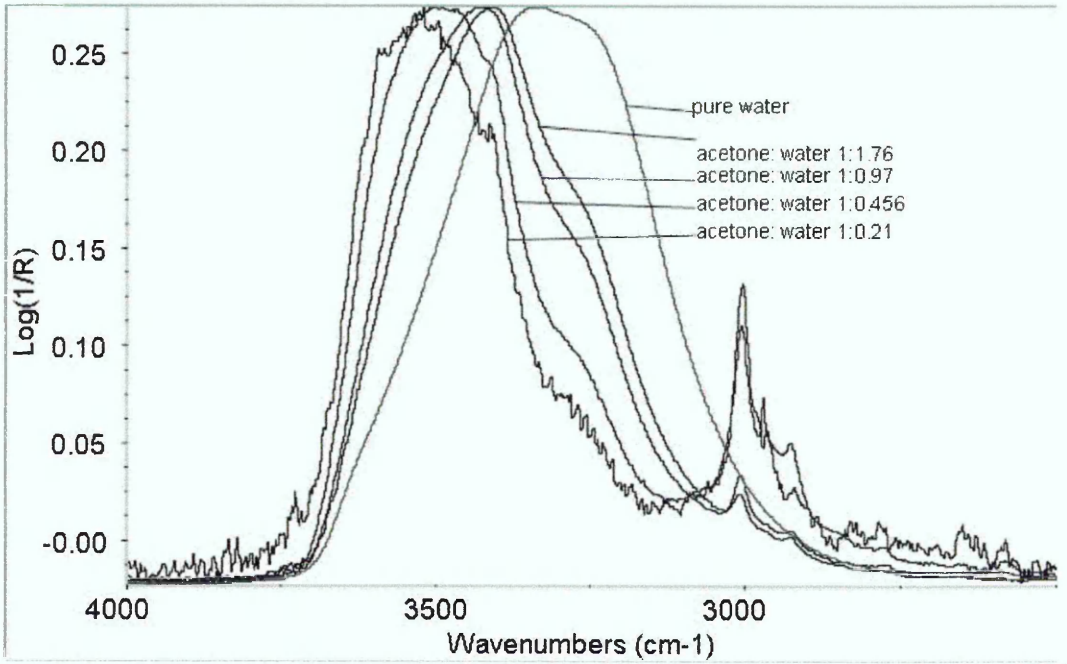

Figure 6-4 ATR spectra of pure water and acetone/ water mixtures in the 4000 - 2500 cm^{-1} region

Compared to the OH stretching mode in pure water the band in the mixture is shifted to higher wavenumbers, indicating a reduction in the overall hydrogen bonding strength of the water molecules. Furthermore, the band is narrowing with increasing acetone content in the sample. The changes to the width of this band are more subtle for mixtures with ratios of water to acetone greater than one, and more obvious once that ratio changes in favour of acetone molecules.

The shape of the ν(OH) bands for the mixtures with higher acetone content indicates the presence of several different environments for OH vibrations, since the band has a clearly visible shoulder at lower wavenumber. Max and Chapados [6.17] deduced from their analysis of acetone/ water mixture spectra by factor analysis that such mixtures are comprised of a combination of various acetone/ water complexes as well as "pure" acetone and "pure" water, and showed that the relative concentrations of these compounds were dependent on the overall ratio of acetone to water.

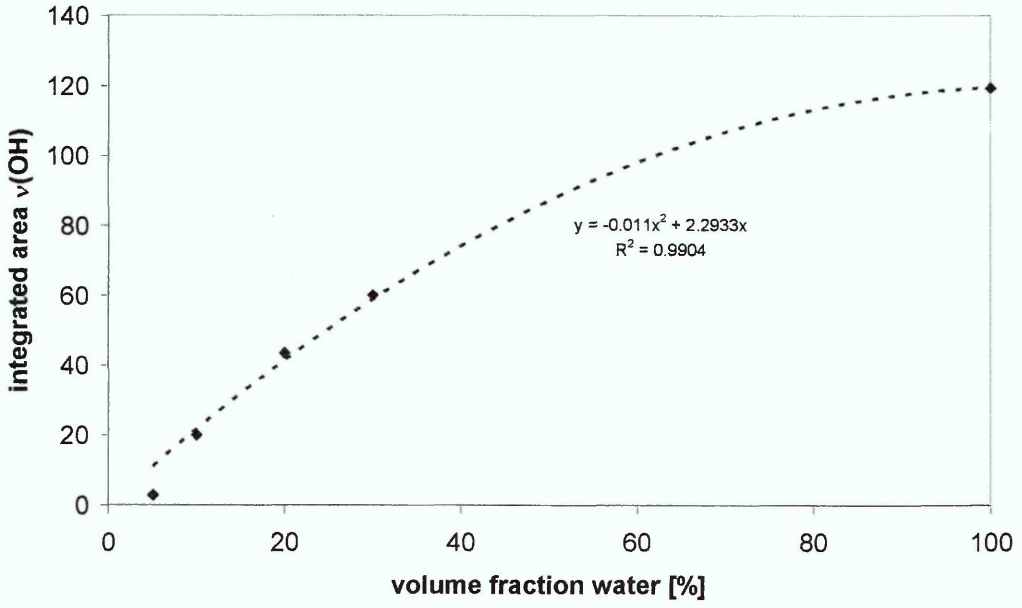

Figure 6-5 Changes in the area of the ν(OH) band at different water fractions

Plotting the area of the ν(OH) band versus the volume fraction of water (see Figure 6-5) shows that the area of the ν(OH) is higher in the mixtures than one would expect based on a linear relationship between the peak area and the concentration of water in the mixture. The refractive index of the solutions is only changing by ca. 2% over the whole range of mixtures which means that this increase is unlikely to be due to increased depth of penetration, but rather a perturbation of the water vibrations caused by the interactions with acetone.

Figure 6-6 displays the changes in the carbonyl stretching mode of acetone and the OH bending mode of water for the different acetone/ water mixtures. Analogous to the OH stretching band, positional shifts due to hydrogen bonding can be observed for both these bands. The extent of these shifts is, however, more subtle than that observed for the ν(OH) band. Peak centres of these

bands shift by a couple of wavenumbers only rather than over 100 cm^{-1} as in case of the ν(OH) band. The carbonyl band shifts to lower wavenumbers with increasing water content. The δ(OH) band on the other hand remains in a similar position for all mixtures.

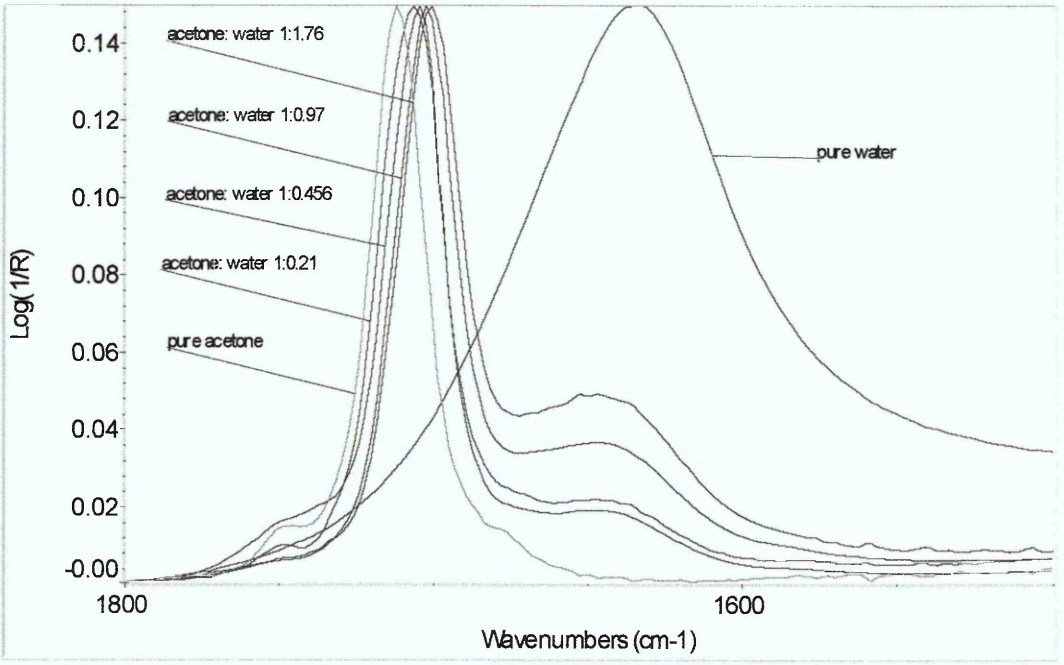

Figure 6-6 ATR spectra of pure water, pure acetone and acetone/ water mixtures in the 1800-1500cm^{-1} region

6.2 Obtaining diffusion data

6.2.1 Sample preparation and parameters for the collection of spectra

The set-up for these experiments was the same as described in chapter 5.2.1 for the measurements of liquid water diffusion into PVOH. The polymer and polymer/ clay solutions were prepared as described in chapter 3.5.2.2. The nanocomposite mixtures were continuously stirred until the film was cast to prevent the clay from settling out of solution. Sample films were prepared using the same method as described in chapter 5.2.2 and experiments performed at the 40 °C.

The solvent mixtures were prepared freshly before each experiment by mixing the desired volumes of acetone and water in a flask sealed with Parafilm using magnetic stirring for agitation for 30 minutes.

The diffusion of acetone/ water mixtures with high acetone contents into PVOH and PVOH/ Na^+ Cloisite® nanocomposites proceeds at a slower rate than the

diffusion of pure water into the samples. Therefore, spectra were collected with longer time intervals. Data was recorded for up to 5 hours. Per spectrum 10 scans with a resolution of 4 cm^{-1} were averaged and all spectra were saved as single beams. The data collection was automated using a macro to define the delays between recordings of the spectra. A background spectrum was taken after the removal of the film at the end of the experiments.

sample	Intervals for collection of spectra
Diffusion experiments with 1:1.76 and 1:1.02 acetone/ water mixtures, 1:0.456 acetone/ water mix for PVOH and PVOH + 2.5wt% Na^+ Cloisite® (all molar ratios)	- 75 spectra without delays (time to collect spectrum: 8 seconds) - 40 spectra with 5 second delays - 35 spectra with 15 second delays - 10 spectra with 30 second delays - 10 spectra with 60 second delays
Diffusion experiments with 1:0.456 acetone/ water mix for 5wt% Na^+ Cloisite® and all 1:0.21 acetone/ water mix experiments	- 60 spectra with 15 second delays - 60 spectra with 25 second delays - 100 spectra with 115 second delays - 12 spectra with 285 second delays

Table 6-1 Sampling intervals for diffusion experiments

The single beam spectra were later reprocessed in two ways. For the first set the single beam spectra were ratioed against a single beam spectrum of the clean crystal (background spectrum), while the second set of spectra was obtained from ratioing against the dry film.

To obtain the film thickness of the sample, the film was allowed to dry at the end of the measurement and was peeled off the crystal. The thickness was then measured using a micrometer.

6.2.2 Obtaining kinetic information on the diffusion of acetone/water mixtures from the ATR-FTIR spectra

Even at these lower water levels significant swelling of the samples was observed. The changes occurring in the ν(OH) region are very complex as this band is due to OH vibrations of the polymer as well as the ingressing water.

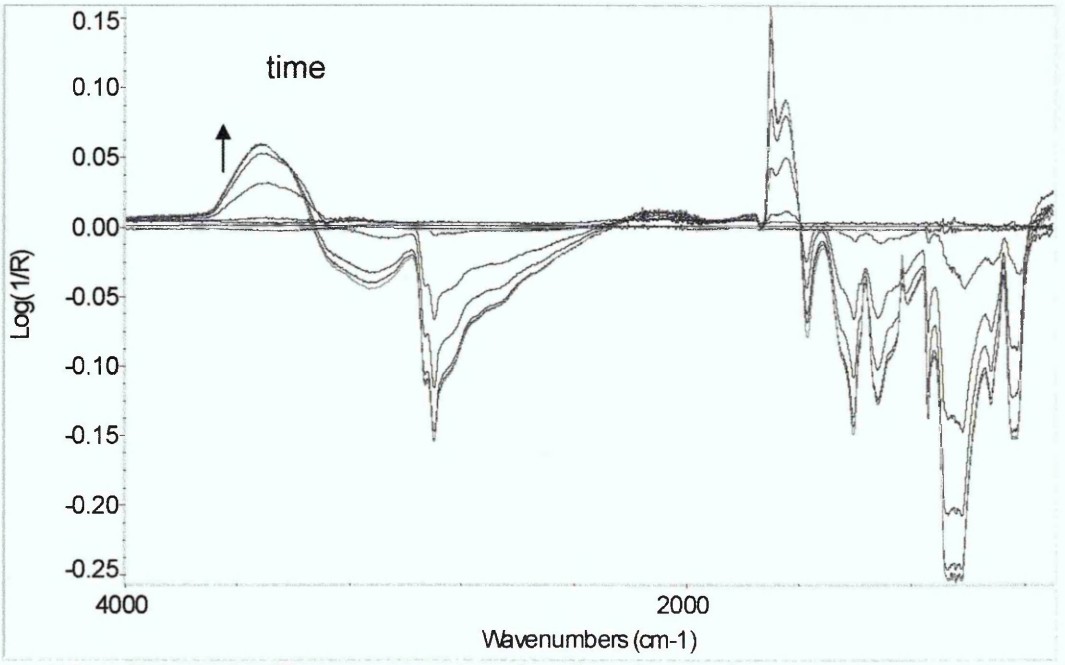

Figure 6-7 Selected difference spectra showing the evolution of bands during the diffusion of a 1:0.456 acetone/ water mixture into PVOH

The difference spectra between the dry film spectrum and spectra collected during the course of the diffusion in Figure 6-7 show that the ν(OH) region exhibits increasing intensities of the higher wavenumber region due to the rising water levels in the sample. At the same time the lower wavenumber region is reduced in intensity due to swelling of the sample and changes in the strength of the hydrogen bond of the polymer, as well as the penetrant water. Furthermore, it is possible that the refractive index of the sample changes enough, due to the swelling of the film by water, that the sampling depth is altered sufficiently to account for some of the observed changes.

This strong overlapping of bands arising from various OH vibrations makes it almost impossible to extract kinetic data for the diffusion of the water fraction from this region. Integration over the whole ν(OH) band (3700 - 3000 cm^{-1}) results in almost constant values throughout the experiments, as intensity and

width of the band changes due to swelling and water diffusion effectively cancel each other with respect to changes in the area of the band.

The changes in the δ(OH) region similarly arise from a combination of increasing water levels in the sample, changes in hydrogen bonding and swelling of the polymer. As the bending mode is less sensitive to different environments this band is less complex than the ν(OH) mode.

Overlaying of the spectra of acetone, water and PVOH (Figure 6-8) shows that the peaks for $\delta(OH)_{pure\ water}$ and $\delta(OH)_{PVOH}$ are relatively separated with peak centres at 1650 cm^{-1} and 1567 cm^{-1} respectively. The peak position of the δ(OH) band is unusually low, yet behaviour of the band appears to indicate that it is indeed arising due to OH vibrations of the polymer, since it reduces and shifts towards higher wavenumbers with increasing water content in the sample. It is also possible that this band is shifted to lower wavenumber because it might arise due to a combination of δ(OH) with C-C or CH vibrations.

Another band arising from water that is not overlaid by polymer bands is the combination band of the OH bending mode and the water libration, which appears as a broad band with a peak centre around 2100 cm^{-1}. This band is, however, very weak, which renders it unsuitable for integration in these spectra because the background noise level is relatively high compared to the band intensity. From this figure one can also see that the only acetone band that is not overlapped by strong polymer bands is the carbonyl stretching mode at 1700 cm^{-1}.

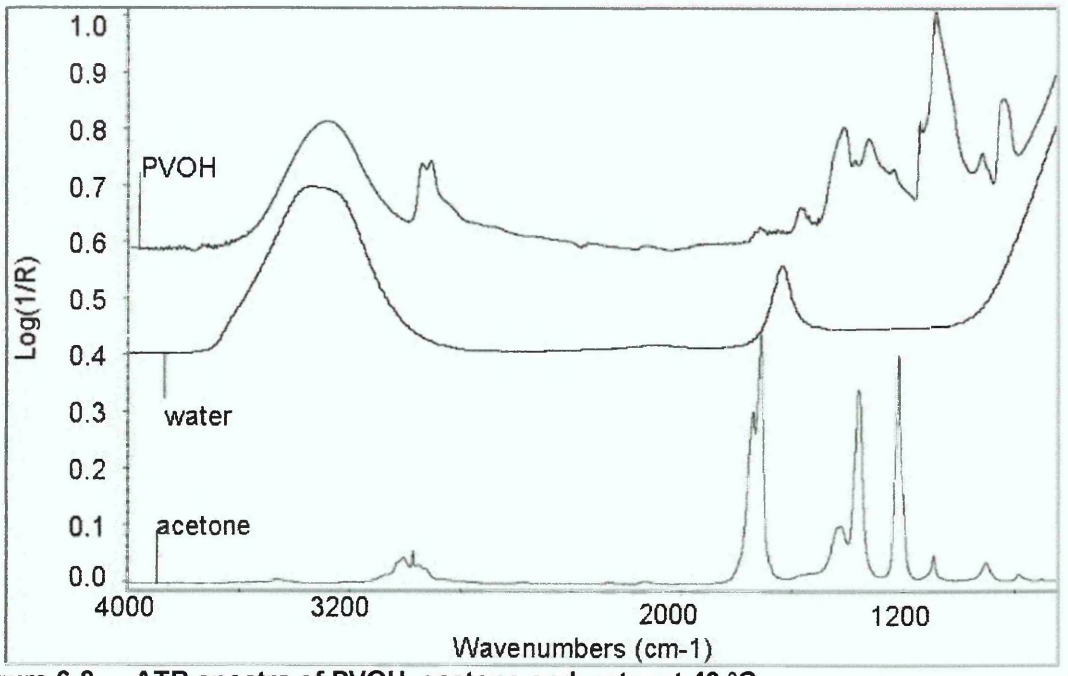

Figure 6-8 ATR spectra of PVOH, acetone and water at 40 °C

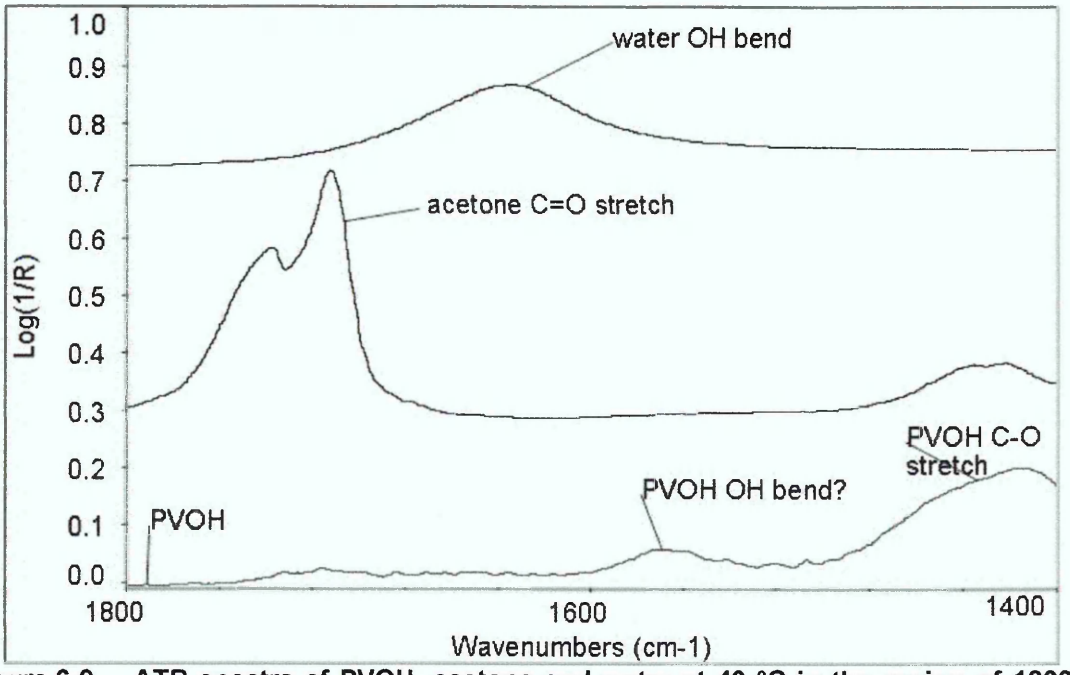

Figure 6-9 ATR spectra of PVOH, acetone and water at 40 °C in the region of 1800 – 1400 cm^{-1}

These observations led to the conclusion that the δ(OH) and the ν(C=O) are the best available options for the extraction of kinetic data from the sets of spectra. Simple integration again proved difficult, as some overlap of the OH bending modes of the polymer and the penetrant water meant that the integrated areas were changing not only due to the increase of water in the sample but also due to the swelling caused by the water ingress.

Choosing bands that are relatively close to one another to obtain the data for acetone and water diffusion meant that any differences in the times before the penetrant peaks become visible in the spectrum were due to differences in the diffusion rate, with only minor influence from the variations in sampling depth between the wavenumbers in question (d_p = 1.18 µm for ν(C=O) and 1.22 µm for δ(OH)). Any diffusion curves obtained from these bands should therefore be directly comparable.

To improve the results obtained from integration of the peaks, peak fitting of the 1800 - 1400 cm^{-1} region of the spectra was performed. A first test with fitting three bands to this region for the ν(C=O), $\delta(OH)_{water}$ and $\delta(OH)_{PVOH}$ bands resulted in a too narrow band shape for the $\delta(OH)_{water}$ band, while the $\delta(OH)_{PVOH}$ peak was too wide once it started to decrease due to the polymer interactions. Restricting the width of this peak did not improve results significantly. Therefore, a further peak was added to the fitting procedure to account for the overlap of the $\delta(OH)_{PVOH}$ with the bands around 1420 cm^{-1}, which are due to the $\delta(CH_2)$ and δ(CH+OH) modes of the PVOH.

Peak centres and peak width restrictions for all peaks were chosen with regard to the values obtained for the equilibrium spectra of diffusion of acetone/water mixtures into PVOH. Mixed Lorentzian and Gaussian peaks were used in the fitting with a maximum Gaussian content of 50%.

peak	peak centre range [cm^{-1}]	maximum peak width [cm^{-1}]
ν(C=O)	1705-1695	40
$\delta(OH)_{water}$	1655-1645	no restrictions
$\delta(OH)_{PVOH}$	1572-1562	70
Polymer band ($\delta(CH_2)$ and δ(CH+OH))	1423-1413	100

Table 6-2 Settings for peak fitting of spectra from diffusion runs

Table 6-2 summarises the settings used for the peak fitting process. Typical results for the fitting of the dry film and equilibrium spectra are shown in Figure 6-10 and Figure 6-11. These figures show the trace resulting from the fit, the residual which is obtained by subtraction of the fitted trace from the original trace, and the second derivative of the original trace in the top half of the image

and the original trace, the peaks that were fitted, and the baseline in the lower half of the image.

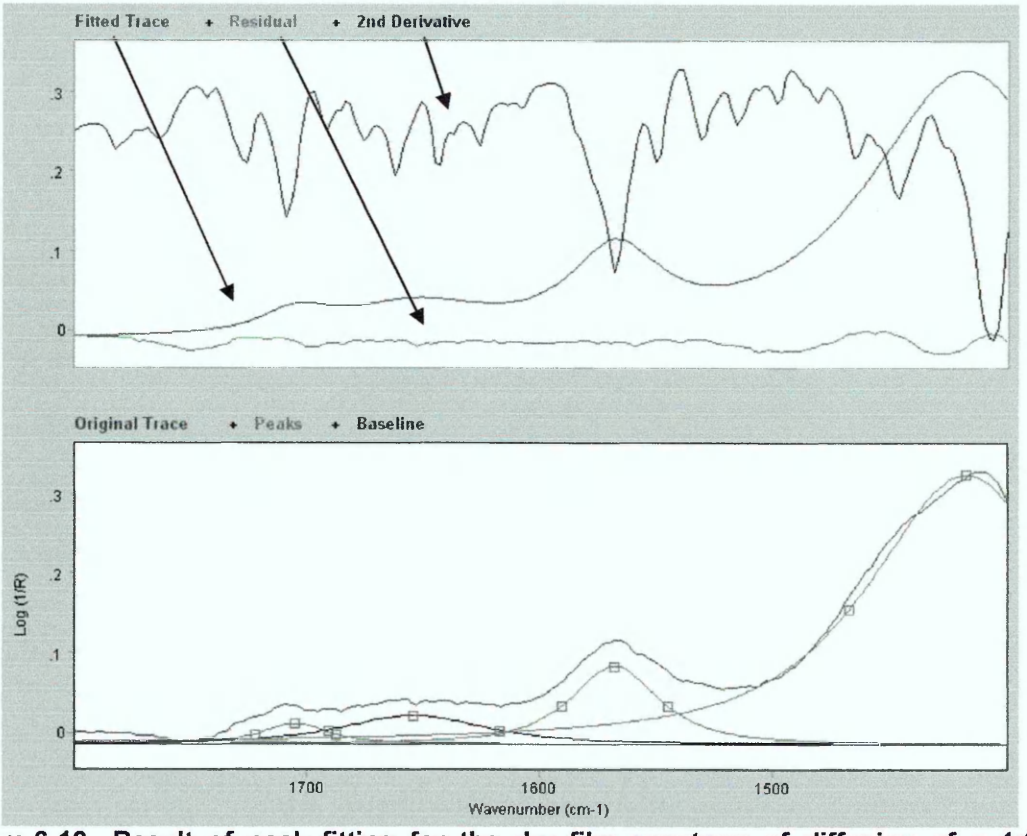

Figure 6-10 Result of peak fitting for the dry film spectrum of diffusion of a 1:0.21 acetone: water mixture into PVOH

The small ν(C-O) peak in the dry film spectra is due to remaining carboxyl groups of the polymer as the PVOH used in these experiments was only 98-99% hydrolysed. It is also obvious from these spectra that some residual water remained in the dried films.

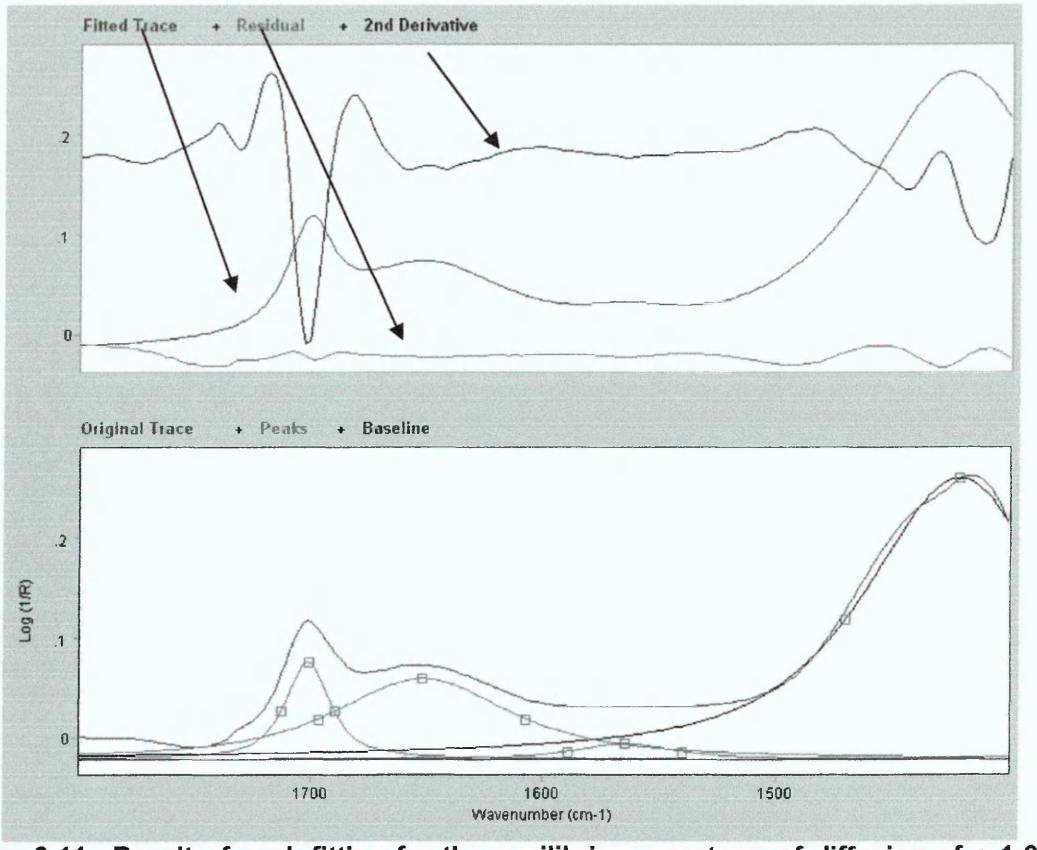

Figure 6-11 Result of peak fitting for the equilibrium spectrum of diffusion of a 1:0.21 acetone: water mixture into PVOH

6.2.3 Obtaining information on swelling, changes in crystallinity and clay levels

To assess the changes which occur within the polymer during the diffusion of acetone/ water mixtures into the sample, changes in several bands have been followed over time.

Swelling of the sample was observed from the decrease of the ν(C-O) peak over time. This peak was chosen because it is very strong in the dry polymer and is not influenced by any strong penetrant bands. Changes in the crystallinity were assessed from the ratio of the area of the shoulder at 1140 cm^{-1} to the area of the ν(C-O) peak. For the nanocomposites any changes to the amount of clay in the evanescent field were assessed by following the change in the ratio of the area of the ν(Si-O) band to the area of the ν(C-O) band. Integration limits for all these bands were set to the same values as those discussed in chapter 5.3.2 for the assessment of changes in PVOH and its nanocomposites during the diffusion of water.

6.2.4 Obtaining information on changes in the hydrogen bonding of water molecules

As discussed in chapter 5.1.1, the OH stretching region is a very good indicator for changes in the immediate environment of water molecules, especially with respect to the hydrogen bonding of these molecules. Such changes can be observed when acetone/ water mixtures are diffusing into PVOH and PVOH/ clay nanocomposites. During these experiments the OH stretching band is shifted to higher wavenumbers indicating a weakening of the hydrogen bonding network.

To further assess these changes peak fitting has been used. Again two bands have been fitted to the dry PVOH spectrum to account for strongly and weakly hydrogen bonded OH groups of the PVOH. Unlike the measurements for pure water diffusion only three bands could be fitted to account for different water structures present in the polymer film. This could be due to a significant overlap of any water OH vibrations with those of the polymer which cannot be resolved with the methods available.

These three peaks are, however, in agreement with water structures found in DSC measurements. [6.19 – 6.21] Studies performed on water swollen PVOH samples reported evidence of three states of water in such films. These three states were referred to as "free water", "freezable bound water" and "non-freezing water".

From the peak positions of the three bands it is unlikely that the peak at highest wavenumber is indeed caused by free water, as such a water structure is expected to result in a peak at around 3600 cm^{-1}. The bands will, therefore, be referred to as weakly, moderately and strongly hydrogen bonded water.

To obtain a reproducible result on the fitting of the baseline for spectra throughout the experiment three peaks were also fitted to the ν(CH) region. All peaks were fitted with a mixed Gaussian and Lorentzian band shape with a minimum Lorentzian contribution of 80%. This mixed shape can be described by the equation 6-1. An example for the resulting fit is shown in Figure 6-12.

$$Shape = (1 - x) * Gaussian + x * Lorentzian \qquad \textbf{Equation 6-1}$$

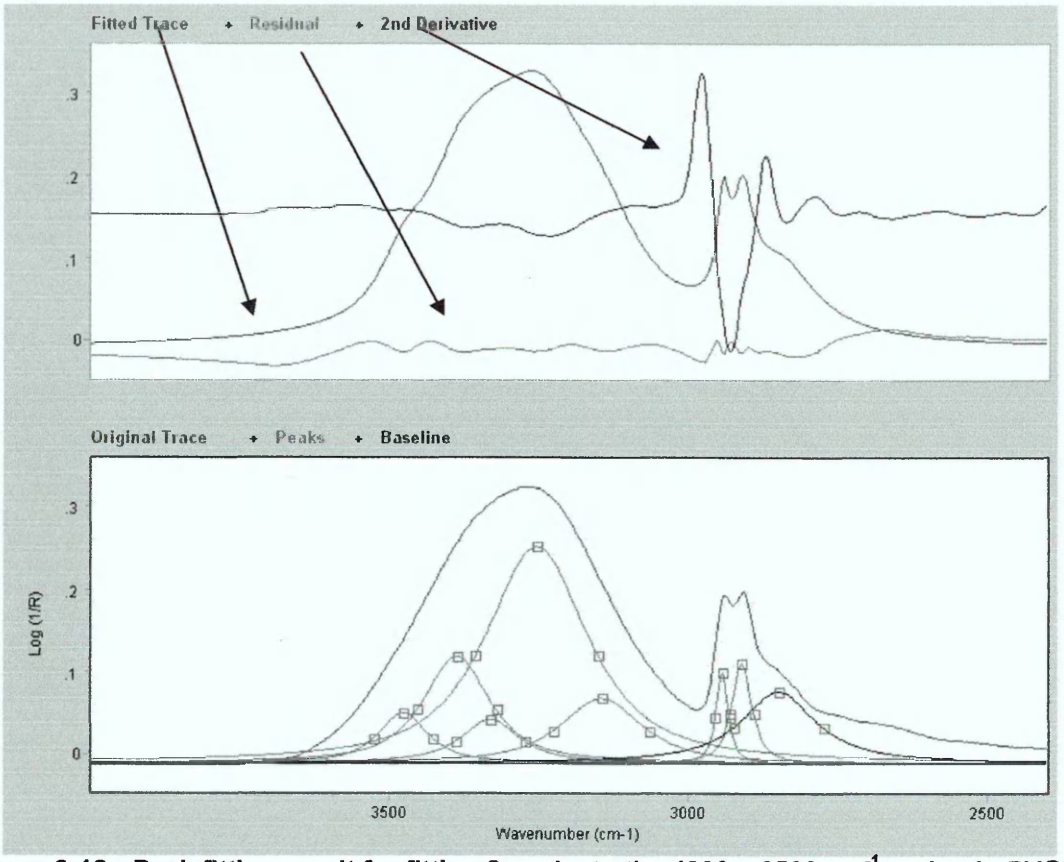

Figure 6-12 Peak fitting result for fitting 8 peaks to the 4000 – 2500 cm^{-1} region in PVOH

Parameters for the fitting process are given in Table 6-3.

Peak	restrictions
weakly hydrogen bonded water	none
weakly hydrogen bonded PVOH	position: 3386 - 3387 cm^{-1}
moderately hydrogen bonded water	none
strongly hydrogen bonded PVOH	position: 3253 - 3254 cm^{-1}
strongly hydrogen bonded water	none
$\nu_{as}(CH_2)$	position: 2940 - 2943 cm^{-1}
$\nu_{s}(CH_2)$	position: 2906 - 2909 cm^{-1}
$\nu(CH)$	position: 2848 - 2851 cm^{-1}, max. width 150 cm^{-1}

Table 6-3 Parameters for peak fitting of ν(OH) region

The restriction of the bands assigned to PVOH was chosen like this even though the spectra were recorded at a resolution of 4 cm^{-1} because this was the only way to ensure that the peak position remained fixed during the fitting process.

6.3 Results and discussion

6.3.1 Kinetic data for the diffusion of acetone/ water mixtures

Diffusion data obtained as described above was recorded for a series of measurements with molar acetone: water ratios of about 1:2, 1:1, 2:1 and 4:1 respectively. Sample films of ca. 30 µm thickness were prepared as described above. Diffusion data was collected on samples containing 0, 2.5 and 5 wt% Na^+ Cloisite®. All experiments were performed on a Thermo Nicolet Nexus FTIR spectrometer fitted with a heatable Golden Gate accessory with a diamond single reflection crystal. Spectra were collected using a macro specifying the sampling intervals as summarised in Table 6-1.

Diffusion coefficients were calculated by applying a short term approximation of the Fickian diffusion model to the data as described in chapter 4.2.

6.3.1.1 Diffusion of acetone/ water mixtures in PVOH/ Na+ Cloisite® nanocomposites

The diffusion behaviour of four different mixtures was investigated. Most of these mixtures had an excess of acetone because excess amounts of water caused the samples to swell and dissolve, making analysis of the data more complicated. (see previous chapter for discussion of problems involved in following the diffusion of water into PVOH)

The sample with the highest water content had a molar ratio of acetone to water of 1:1.76. Further experiments were performed on mixtures with equal amounts of acetone and water molecules (molar ratio of 1:1.02), and two mixtures with an excess of acetone having molar ratios of acetone: water of 1:0.456 and 1:0.21.

Diffusion coefficients were calculated by fitting the kinetic data obtained from the ν(C=O) and δ(OH) bands to the short term approximation of Fickian diffusion. Using this model, a simplified analysis of the data was possible, which however neglects the possibility of diffusion of acetone/ water complexes or changes in the diffusion model at longer times due to plasticisation of the polymer by water. Furthermore, this model does not take any effects of the clay into account. Nevertheless, use of such a basic model can give some

information on a system, since complex as the diffusion studies of solvent mixtures into PVOH nanocomposites presented here.

6.3.1.1.1 Diffusion of acetone/ water mixtures into PVOH

Diffusion experiments of various acetone/ water mixtures into PVOH were performed to establish baseline data to which the results obtained from the diffusion experiments of these mixtures into PVOH nanocomposites could be compared. The polymer used in these experiments was the low molecular weight PVOH (Mw = 31,000 – 50,000).

Typical spectra recorded during the diffusion of such mixtures are presented in Figure 6-13 and Figure 6-14. Kinetic data obtained from these spectra for the diffusion of the four different mixtures into PVOH is shown in Figure 6-15 - Figure 6-18. A summary of the diffusion parameters calculated from this data is given in Table 6-4. The negative values in the kinetic data for the acetone fraction are an artefact of the peak fitting procedure. Since the values plotted here were obtained by subtracting the area of the relevant peaks in the dry film spectra from those at each time variations in the fitting of the width of the peaks can result in smaller areas after the start of the experiment. Since the negative values in the acetone data are observed at the same time the area of the water bands increases, changes in the best fit of the δ(OH) bands are most likely influencing the result of the fitting for the ν(C=O) band.

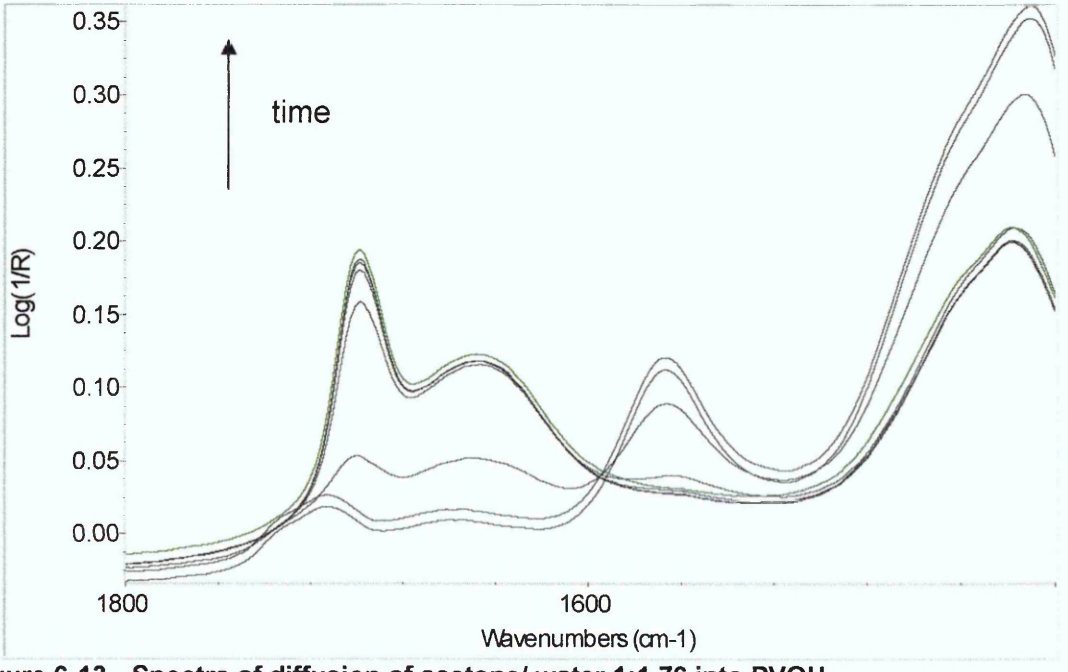

Figure 6-13 Spectra of diffusion of acetone/ water 1:1.76 into PVOH

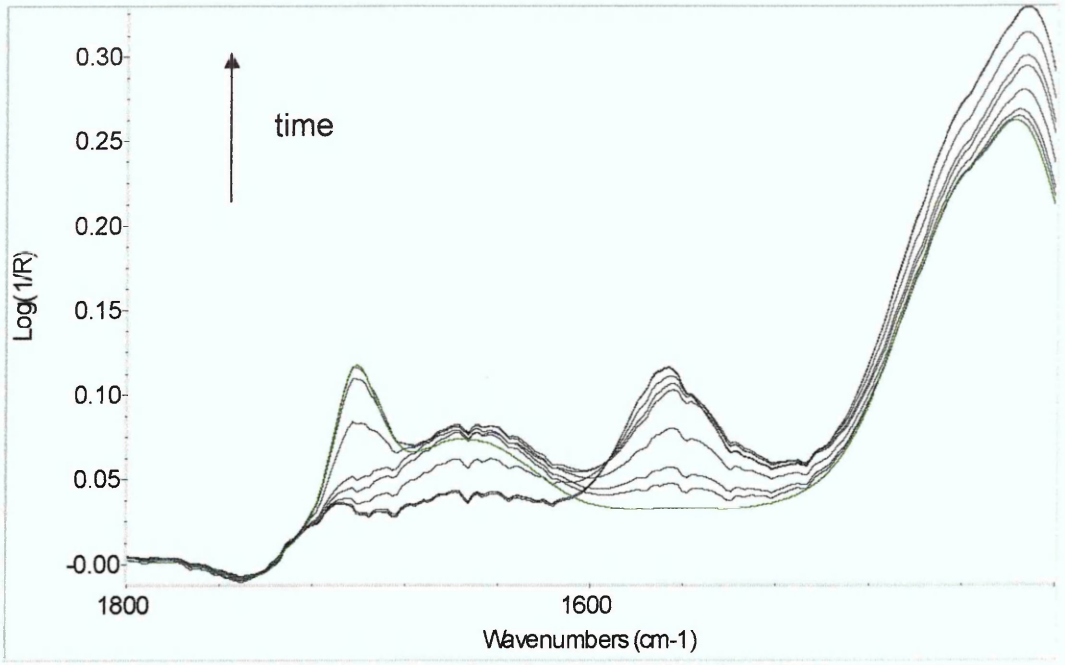

Figure 6-14 Spectra of diffusion of acetone/ water 1:0.21 into PVOH

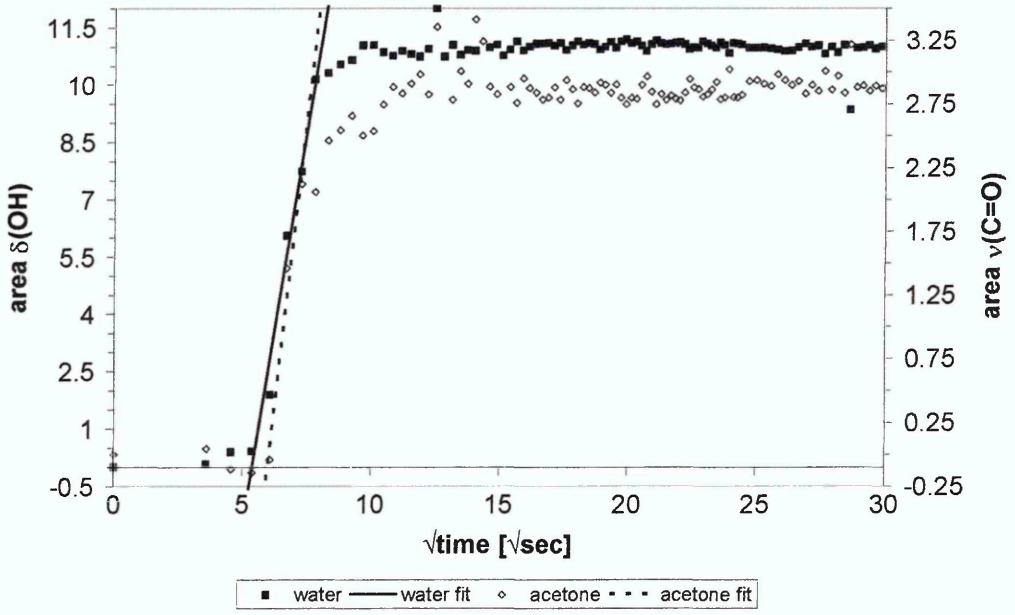

Figure 6-15 Experimental data and short term approximation of Fickian diffusion fits for diffusion of 1:1.76 acetone/ water mixture into PVOH

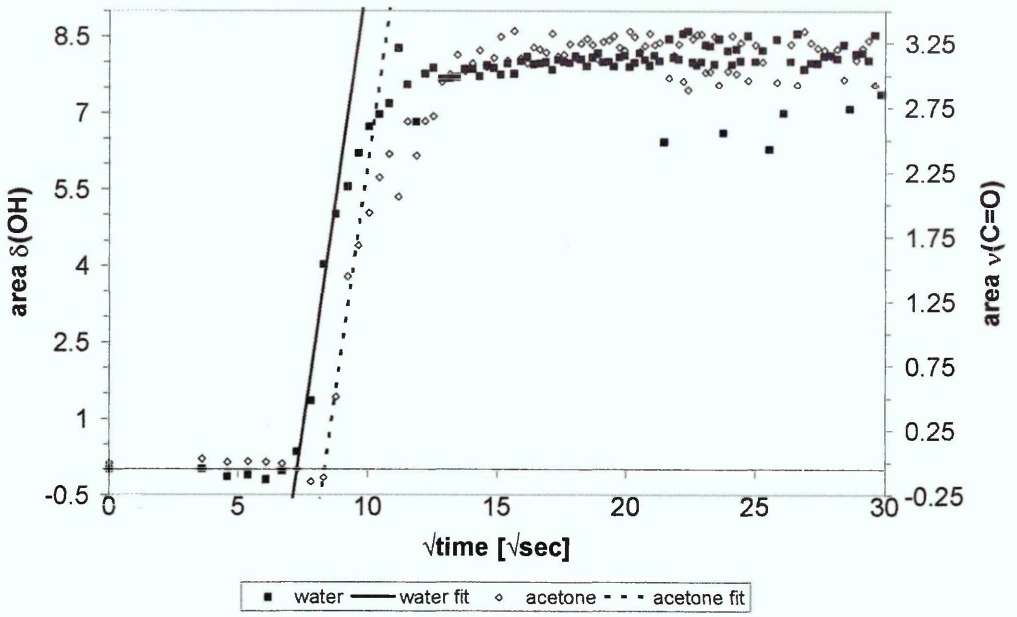

Figure 6-16 Experimental data and short term approximation of Fickian diffusion fits for diffusion of 1:1.02 acetone/ water mixture into PVOH

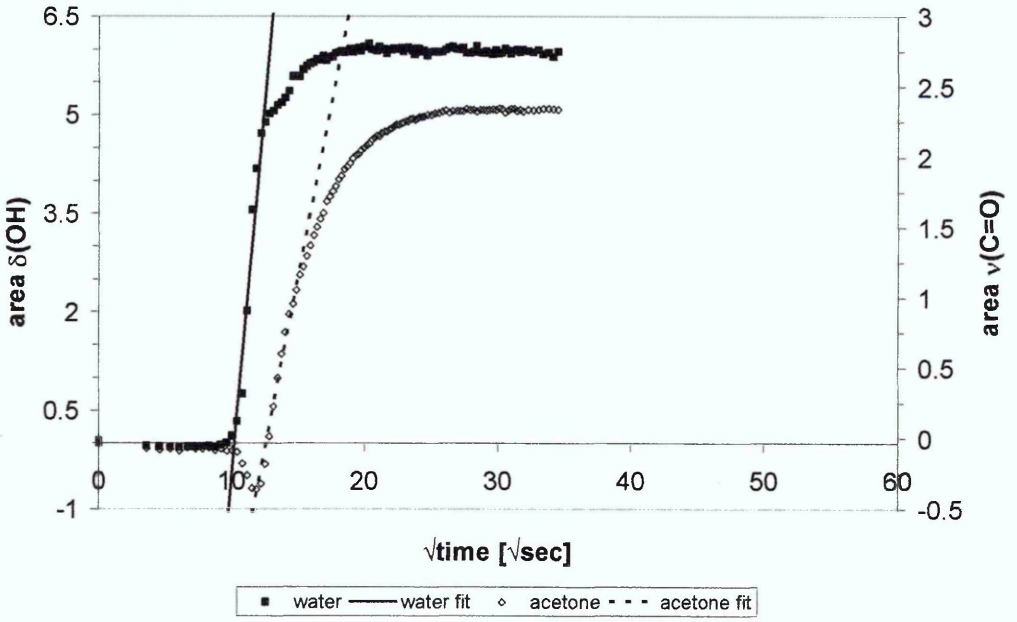

Figure 6-17 Experimental data and short term approximation of Fickian diffusion fits for diffusion of 1:0.456 acetone/ water mixture into PVOH

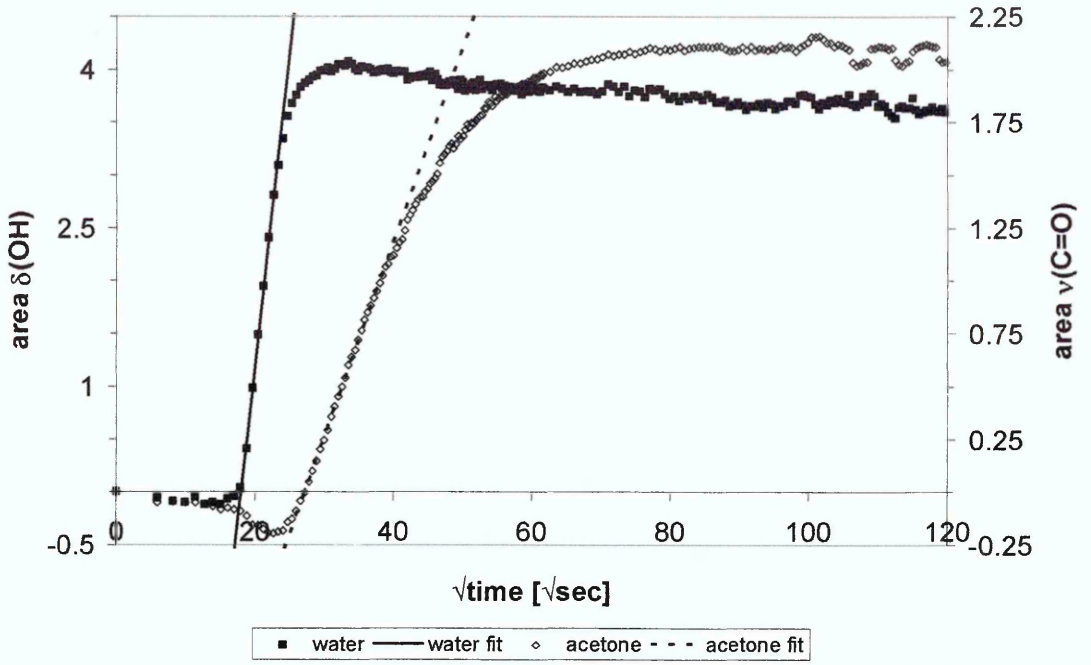

Figure 6-18 Experimental data and short term approximation of Fickian diffusion fits for diffusion of 1:0.21 acetone/ water mixture into PVOH

Acetone/ water ratio	Water		Acetone	
	Intercept/L [min/µm]	Diffusion coefficient D [cm²/sec]	Intercept/L [min/µm]	Diffusion coefficient D [cm²/sec]
1:1.76	0.017	$1.09 * 10^{-4}$	0.022	$2.03 * 10^{-5}$
1:1.02	0.034	$6.75 * 10^{-5}$	0.045	$1.07 * 10^{-5}$
1:0.456	0.072	$2.38 * 10^{-5}$	0.111	$1.10 * 10^{-6}$
1:0.21	0.225	$1.62 * 10^{-6}$	0.513	$3.85 * 10^{-8}$

Table 6-4 Summary of diffusion parameters for diffusion of acetone/ water mixtures into PVOH

Diffusion of both acetone and water is clearly dependent on the amount of water present in the mixture. Lower water contents reduce the diffusion rate of both liquids and result in longer time delays before the ingress of these solvents can be observed in the ATR spectra.

The diffusion parameters calculated for the 1:1.76 acetone/ water experiment indicate that diffusion of water proceeds at a rate comparable to that measured for pure water (values for pure water: intercept/L = 0.011 ± 0.002 min/µm; D = $6.66* 10^{-5} \pm 2.66 * 10^{-5}$ cm²/sec) as long as there is an excess of water in the mixture. The shape of the diffusion curve also remains the same as that observed during the diffusion of pure water.

The diffusion behaviour of acetone into PVOH is strongly dependent on the amount of water present. When water is in excess the diffusion of acetone and

water is found to occur parallel. It is quite likely that water is forming complexes with the acetone, which can diffuse into the sample at a faster rate than acetone on its own. Evidence for such complexes has been found in the pure liquids by Max and Chapados [6.17].

When the ratio of acetone to water is about equal, acetone is still found to diffuse into the sample at a rate similar to that of water. At this acetone/ water ratio the diffusion of acetone is, however, starting to lag behind that of water Furthermore, the shape of the diffusion curves is changing indicating a change in the diffusion mechanism.

Increasing the amount of acetone in the diffusant mixture results in further separation of the times after which diffusion of water and acetone can be observed in ATR-FTIR spectra. In the 1:0.21 acetone/ water mixture the diffusion of water has almost reached equilibrium before the diffusion of acetone can be observed. This suggests that a certain water concentration in the polymer is necessary for diffusion of acetone to occur at a rate that can be measured in ATR-FTIR experiments. No attempts have however been made to quantify this amount of water as no calibration for the water content within the polymer was available. The area of the $\delta(OH)_{water}$ band does however have to be on the order of 4 cm^{-1} before increases in the $\nu(C=O)$ band can be measured.

The shape of the diffusion curve is becoming more like a Fickian diffusion profile at longer times. With less water available for diffusion and equilibrium sorption levels of water decreasing the polymer is less likely to change into a rubbery state during the experiment. Therefore the shape of the diffusion curves is expected to become more like those observed for the diffusion of liquids into other glassy polymers.

The equilibrium values for the diffusion of water are significantly reduced with increasing acetone content in the diffusant mixtures. The equilibrium sorption of water in the 1:0.21 acetone/ water mixture is reduced to 36% of the level observed for the 1:1.76 acetone/ water mixture. The equilibrium values for the diffusion of acetone are less affected by the amount of water with equilibrium sorption being reduced to 71% for the 1:0.21 acetone/ water mixture of its value

for the 1:1.76 acetone/ water mixture. Water therefore appears to enable the diffusion of acetone into PVOH and equilibrium sorption for both solvents is influenced by the water levels available for diffusion.

6.3.1.1.2 Diffusion of acetone/ water mixtures into PVOH nanocomposites with 2.5 wt% Na+ Cloisite®

Diffusion experiments were performed on PVOH nanocomposite samples cast from solutions with 2.5 wt% clay content to investigate the influence of the clay nanoparticles on the diffusion behaviour of acetone/ water mixtures. Diffusion experiments were performed using the four different acetone/ water mixtures described above for the diffusion into neat PVOH.

Examples for diffusion curves are shown in Figure 6-19 - Figure 6-22 and a summary of the diffusion parameters obtained from the short term approximation of Fickian diffusion fits is given in Table 6-5.

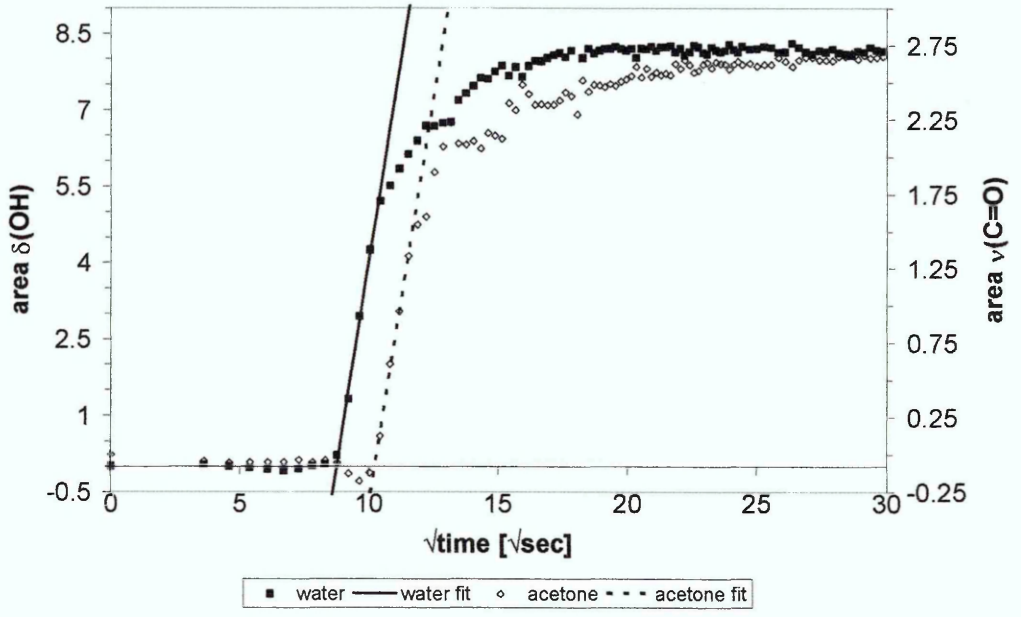

Figure 6-19 Experimental data and short term approximation of Fickian diffusion fits for diffusion of 1:1.76 acetone/ water mixture into PVOH + 2.5 wt% Na^+ Cloisite®

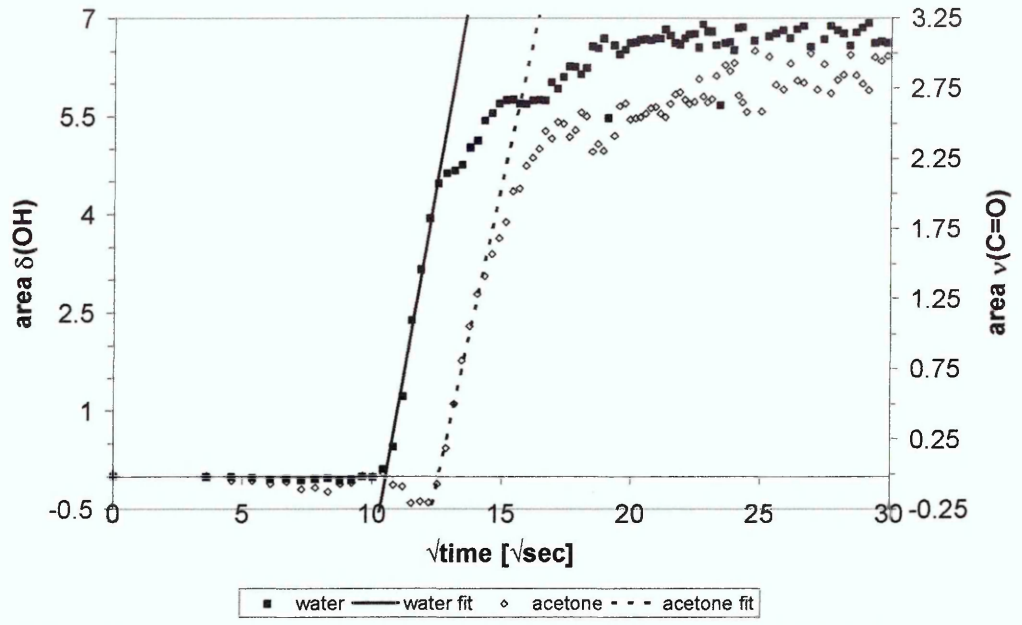

Figure 6-20 **Experimental data and short term approximation of Fickian diffusion fits for diffusion of 1:1.02 acetone/ water mixture into PVOH + 2.5 wt% Na^+ Cloisite®**

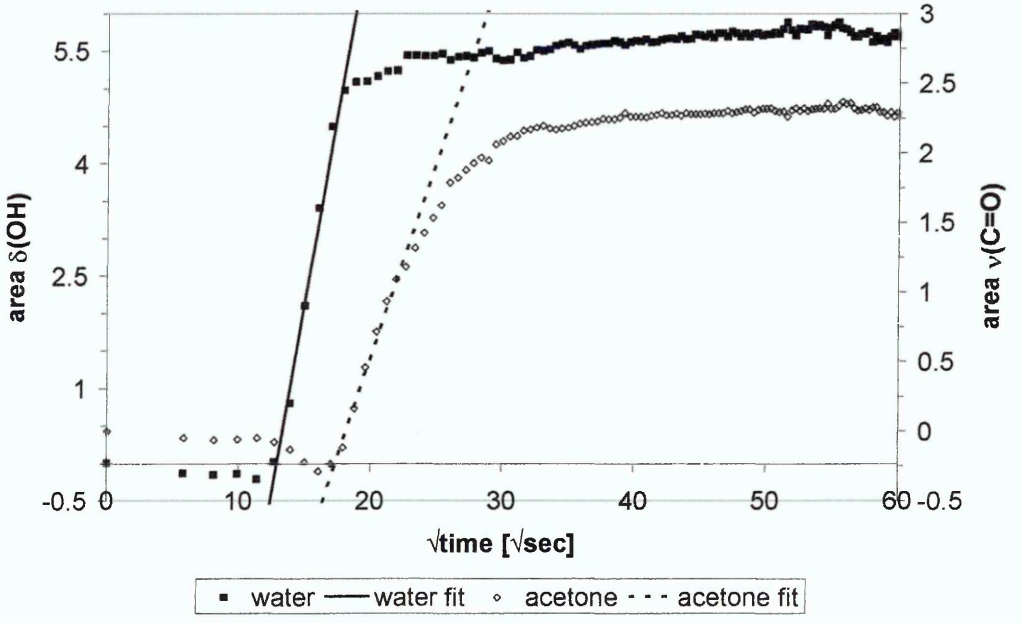

Figure 6-21 **Experimental data and short term approximation of Fickian diffusion fits for diffusion of 1:0.456 acetone/ water mixture into PVOH + 2.5 wt% Na^+ Cloisite®**

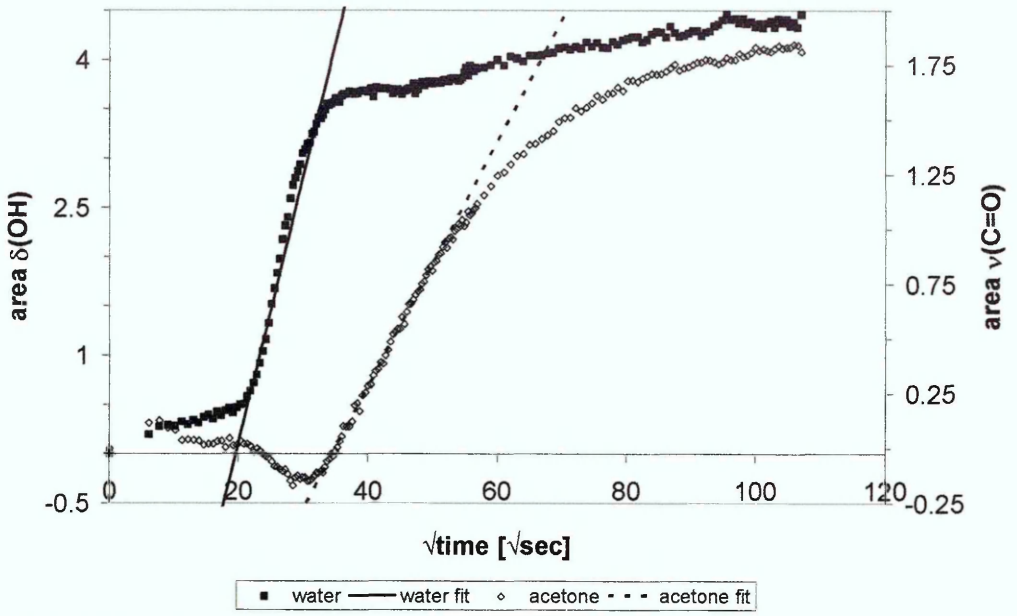

Figure 6-22 Experimental data and short term approximation of Fickian diffusion fits for diffusion of 1:0.21 acetone/ water mixture into PVOH + 2.5 wt% Na^+ Cloisite®

Acetone/ water ratio	Water		Acetone	
	Intercept/L [min/µm]	Diffusion coefficient D [cm²/sec]	Intercept/L [min/µm]	Diffusion coefficient D [cm²/sec]
1:1.76	0.038	$9.45 * 10^{-5}$	0.052	$1.09 * 10^{-5}$
1:1.02	0.054	$4.79 * 10^{-5}$	0.072	$8.71 * 10^{-6}$
1:0.456	0.099	$6.50 * 10^{-6}$	0.196	$4.97 * 10^{-7}$
1:0.21	0.265	$3.29 * 10^{-7}$	0.849	$1.41 * 10^{-8}$

Table 6-5 Summary of diffusion parameters for diffusion of acetone/ water mixtures into PVOH + 2.5 wt% Na^+ Cloisite®

For the 2.5 wt% clay nanocomposites the diffusion behaviour followed a similar pattern to that observed for the neat polymer, with diffusion rates being dependent on the amount of water present in the diffusant mixture.

The data obtained for the 1:1.76 acetone/ water mixture shows some differences compared to the diffusion of pure water into such nanocomposites. While the diffusion coefficient obtained for the water fraction in this mixture is faster than the one obtained for pure water ($D = 3.00^* 10^{-5} \pm 1.20 * 10^{-5}$ cm²/sec), the time before diffusion can be observed is significantly longer in these samples (pure water: intercept/L = 0.010 ± 0.002 min/µm). This difference is much larger than the variation observed between the diffusion of 1:1.76 acetone/ water mixture and pure water into neat PVOH. The presence of clay therefore improves the barrier properties against water at low concentrations of water. As such improvement could not be observed as clearly during the

diffusion of pure water into these nanocomposites compared to the PVOH, it is assumed that clay can only improve the barrier properties in samples that do not swell extensively.

Diffusion rates reduce significantly with a reduction of the water fraction in the diffusant mixture. For all these mixtures diffusion of acetone occurs after the diffusion of water has set in or in the case of excess acetone in the diffusant mixture, after the diffusion of water has reached equilibrium.

Equilibrium sorption values are decreasing with increasing acetone content in the diffusant mixtures. The equilibrium sorption of water in the 1:0.21 acetone/ water mixture is reduced to 44% of the level observed for the 1:1.76 acetone/ water mixture. The equilibrium values for the diffusion of acetone are less affected by the amount of water, with equilibrium sorption being reduced to 69% for the 1:0.21 acetone/ water mixture of its value for the 1:1.76 acetone/ water mixture. The value for acetone is similar to the reductions in equilibrium sorption observed in the neat polymer, while the reduction of the equilibrium sorption is lower in the nanocomposite than in the pure polymer. Whether this is due to the effect the clay has on the sorption of water or within the experimental variation remains unclear.

6.3.1.1.3 Diffusion of acetone/ water mixtures into PVOH nanocomposites with 5 wt% Na+ Cloisite®

To investigate the influence of the amount of clay present in the nanocomposite films experiments were repeated with samples that were cast from solutions with a clay loading of 5 wt%. Diffusion experiments were performed using the four different acetone/ water mixtures described above for the diffusion into neat PVOH.

Examples for diffusion curves are shown in Figure 6-23 - Figure 6-26 and a summary of the diffusion parameters obtained from the short term approximation of Fickian diffusion fits is given in Table 6-6.

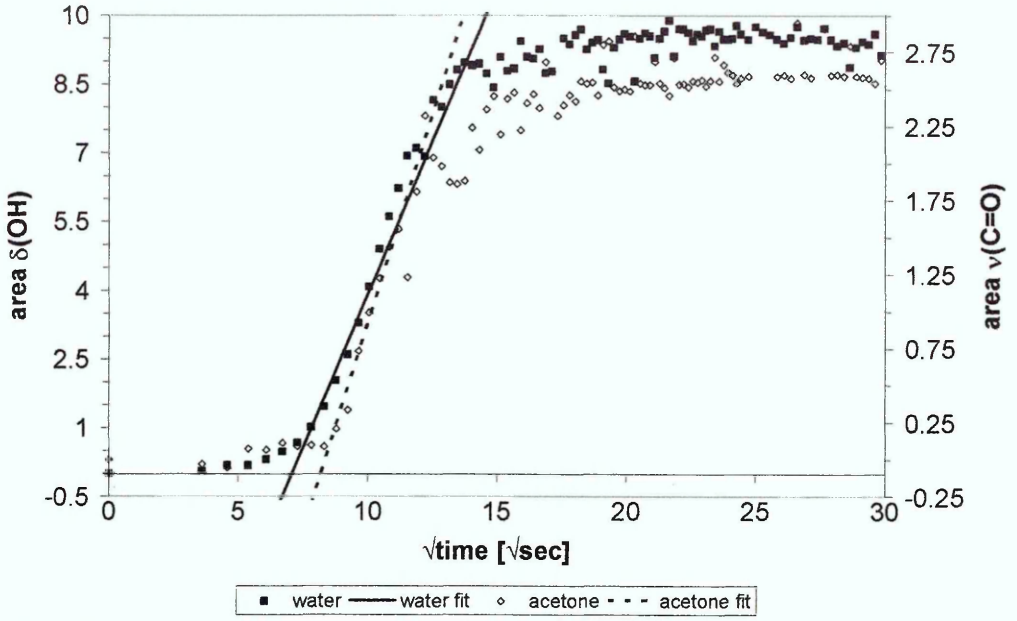

Figure 6-23 Experimental data and short term approximation of Fickian diffusion fits for diffusion of 1:1.76 acetone/ water mixture into PVOH + 5 wt% Na^+ Cloisite®

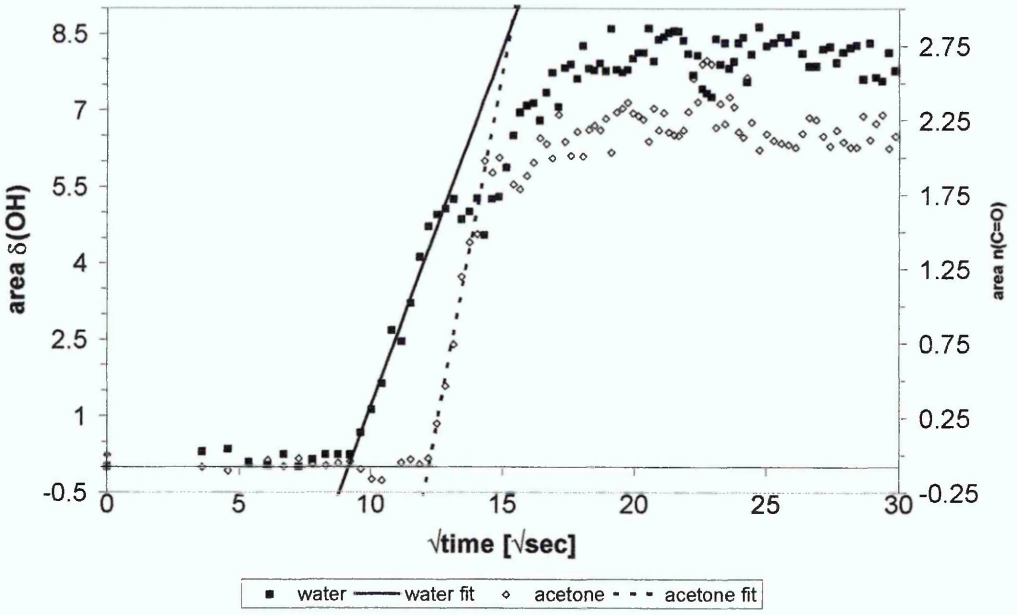

Figure 6-24 Experimental data and short term approximation of Fickian diffusion fits for diffusion of 1:1.02 acetone/ water mixture into PVOH + 5 wt% Na^+ Cloisite®

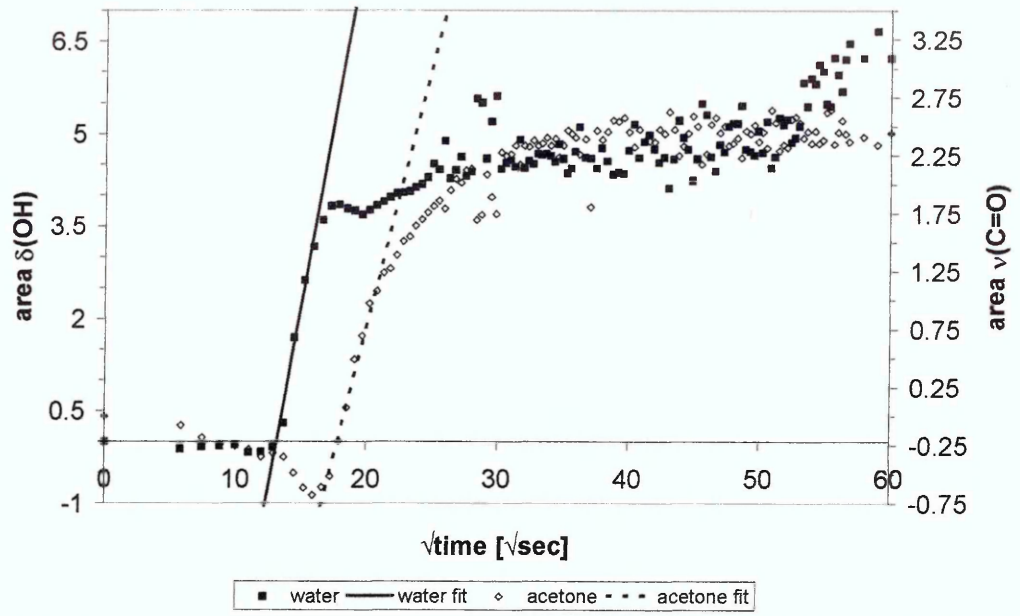

Figure 6-25 Experimental data and short term approximation of Fickian diffusion fits for diffusion of 1:0.456 acetone/ water mixture into PVOH + 5 wt% Na^+ Cloisite®

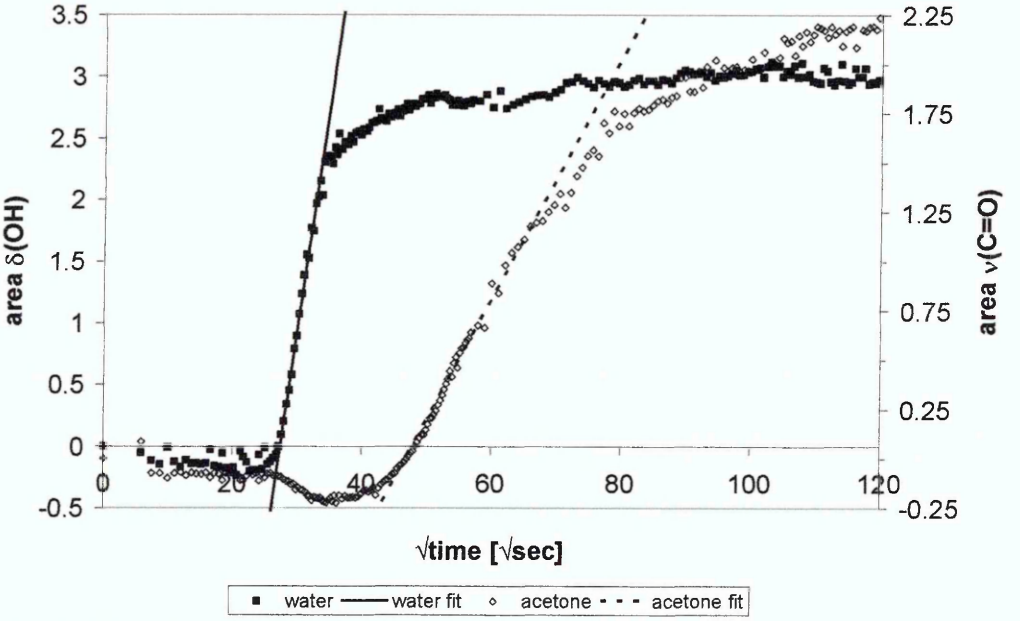

Figure 6-26 Experimental data and short term approximation of Fickian diffusion fits for diffusion of 1:0.21 acetone/ water mixture into PVOH + 5 wt% Na^+ Cloisite®

Acetone/ water ratio	Water		Acetone	
	Intercept/L [min/µm]	Diffusion coefficient D [cm²/sec]	Intercept/L [min/µm]	Diffusion coefficient D [cm²/sec]
1:1.76	0.026	$1.44 * 10^{-5}$	0.036	$2.54 * 10^{-6}$
1:1.02	0.040	$1.91 * 10^{-5}$	0.072	$8.71 * 10^{-6}$
1:0.456	0.096	$1.04 * 10^{-5}$	0.156	$1.46 * 10^{-6}$
1:0.21	0.390	$1.12 * 10^{-6}$	1.140	$3.02 * 10^{-8}$

Table 6-6 Summary of diffusion parameters for diffusion of acetone/ water mixtures into PVOH + 5 wt% Na^+ Cloisite®

The data obtained for the diffusion of acetone/ water mixtures into 5 wt% clay nanocomposites showed some irregularities, yet the general trend observed for the neat polymer and the 2.5 wt% nanocomposites remained. With increasing acetone content in the diffusant mixture a decrease of the diffusion rates for acetone and water could be observed, while delay times before diffusion became measurable in these experiments increased.

The diffusion of the water fraction of a 1:1.76 acetone/ water mixture is faster than that of pure water if one just considers the diffusion coefficient, yet the delay time before diffusion can be observed is increased for the mixture compared to the pure liquid. This surprising result is possibly due to variations in clay loading and dispersion between the samples.

Equilibrium sorption values are decreasing with increasing acetone content in the diffusant mixtures. The equilibrium sorption of water in the 1:0.21 acetone/ water mixture is reduced to 28% of the level observed for the 1:1.76 acetone/ water mixture. The equilibrium values for the diffusion of acetone are less affected by the amount of water, with equilibrium sorption being reduced to 80% for the 1:0.21 acetone/ water mixture of its value for the 1:1.76 acetone/ water mixture. While the reduction in the equilibrium level for water is stronger than that observed in either PVOH or the 2.5 wt% nanocomposite, the level of acetone is less affected by the reduction of water in the diffusant mixture in this case. These results could, however, be influenced by variations in the clay levels observed in the dry film spectra of these samples which will be discussed below.

6.3.1.1.4 Comparison of diffusion of acetone/ water mixtures into PVOH and PVOH/ Na+ Cloisite® nanocomposites

The diffusion of acetone/ water mixtures into PVOH is strongly influenced by the amount of water present in the diffusant mixture. If one plots the delay times (before diffusion sets in) and the diffusion coefficients (obtained from the data presented above) versus the concentration of water in the diffusant mixture, the variations discussed above for the various types of samples become more obvious. Such graphs are presented in Figure 6-27 and Figure 6-28. At higher water concentrations the initial delay time before diffusion can be observed is similar for acetone and water, as well as PVOH and its nanocomposites independent of clay loading. At lower water concentrations longer delay times can be observed for the diffusion of acetone. Values for the nanocomposites become longer indicating an improvement of the barrier properties of these materials against acetone/ water mixtures with low water contents.

The data for the diffusion coefficients follows a similar behaviour. While the data shows a larger spread, the diffusion coefficients of the single components are generally faster for mixtures with higher water concentrations in the diffusant. Unlike the observations made for the delay times diffusion coefficients appear to be influenced by the presence of clay in the polymer matrix for all diffusant mixtures.

This observation leads to the assumption that the delay time (before diffusion can be observed) is mainly due to voids in the polymer structure which are filled faster if higher water concentrations are present as these mixtures show a higher diffusion rate. After these "defects" in the polymer structure have been filled with liquid diffusion through the polymer can be observed which is slowed down in presence of clay due to the impenetrable nature of the clay platelets.

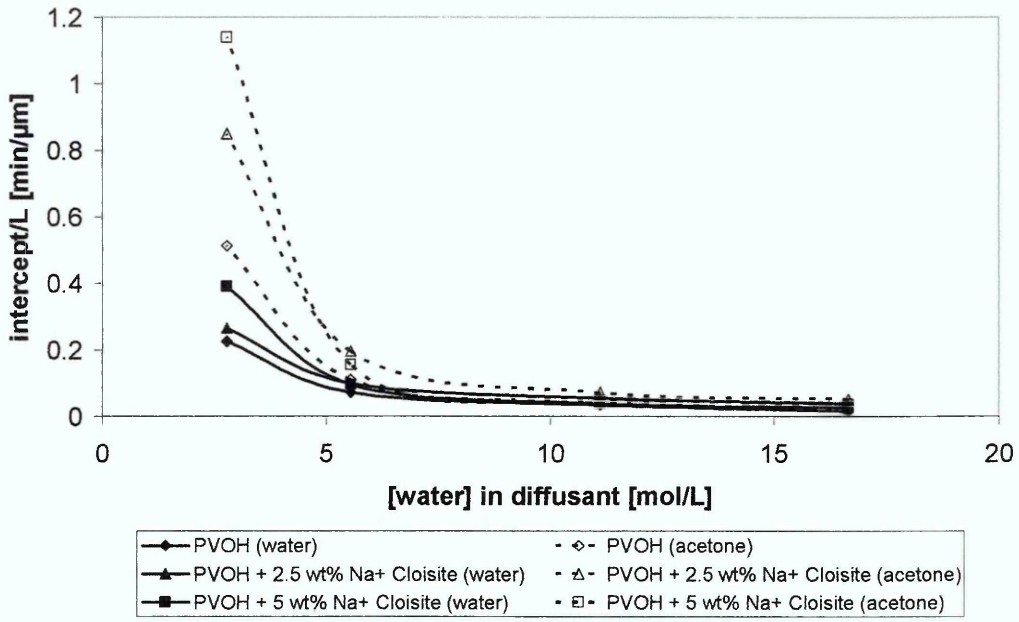

Figure 6-27 Comparison of „delay times" in dependence of water concentration in the diffusant

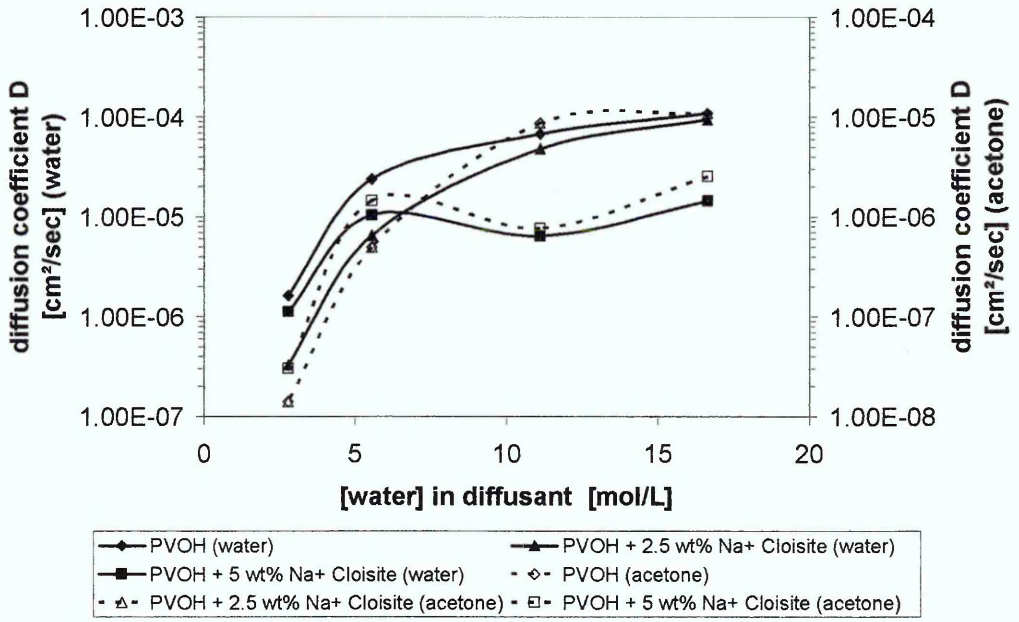

Figure 6-28 Comparison of diffusion coefficients in dependence of water concentration in the diffusant

To further investigate this dependence of acetone diffusion on the presence of water, experiments with pure acetone were performed. In fully dried films no bands for acetone could be measured over the course of a 16 hour experiment, which means that diffusion of acetone in dried PVOH is occurring only at a very reduced rate if at all. If films did, however, retain some residual moisture diffusion of acetone became measurable by ATR-FTIR experiments. Such samples were obtained by drying films cast from solution at room temperature

over night rather than heating them to 40 °C. Since no calibration was obtained for the moisture levels, it is impossible to state how much residual water in the film is necessary to observe this diffusion. Figure 6-29 presents the data obtained from such diffusion experiments. The experimental data could be fitted to a Fickian diffusion process. This suggests that the diffusion mechanism of acetone is strongly influenced by the presence of water since the diffusion behaviour is changing significantly in dependence of the water concentration.

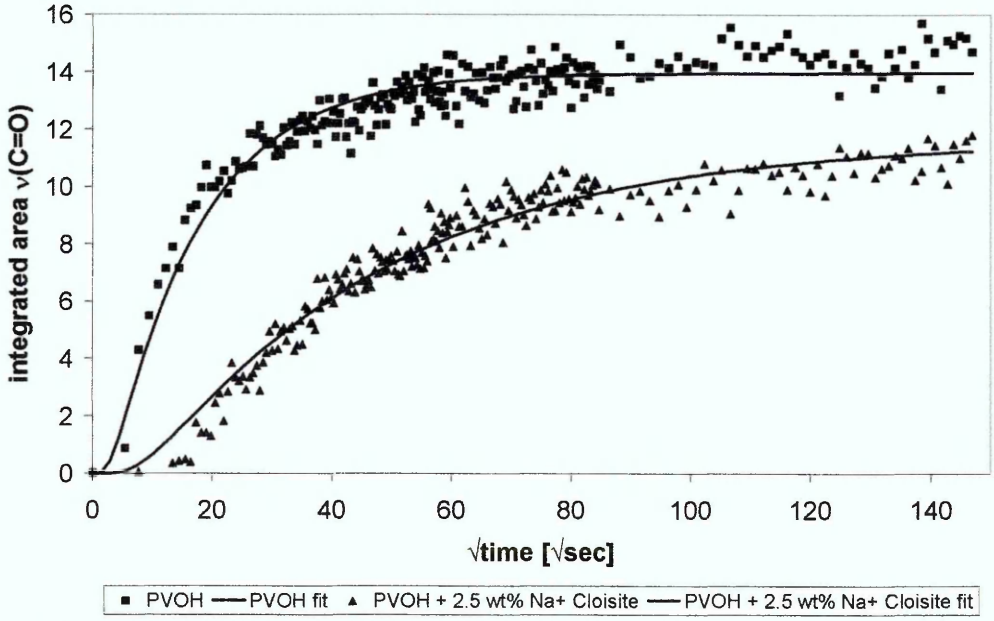

Figure 6-29 Diffusion of acetone into moist films [6.22]

Similar to the data collected for the diffusion of acetone/ water mixtures into PVOH nanocomposites, the diffusion of acetone into PVOH nanocomposite films with residual moisture was found to decrease when clay was introduced into the sample [6.22]. Diffusion coefficients obtained from the data presented in Figure 6-29 are given in Table 6-7.

Sample	Diffusion coefficient D [cm²/sec]
PVOH	1.7×10^{-7}
PVOH + 2.5wt% Na^+ Cloisite	0.6×10^{-7}

Table 6-7 Diffusion coefficients for the diffusion of acetone into moist PVOH films [6.22]

The faster diffusion coefficients obtained for these experiments compared to the diffusion coefficients of the acetone fraction in experiments with 1:0.21 acetone/ water are likely to be due to variations a of variety of parameters. Differences in the moisture levels of the dry films, crystallinity and clay loading can lead to

these faster values, as well as the different fitting procedures used to obtain the diffusion coefficients. The pure acetone diffusion data was fitted to the "full" Fickian diffusion model given by equation 4-12 and diffusion coefficients were obtained by fitting the data to the model using a non-linear regression method.

Comparisons of the diffusion parameters obtained for the nanocomposite experiments discussed above with respect to the clay loading are presented in Figure 6-30 and Figure 6-31. Delay times for diffusion of mixtures with high water concentrations are not influenced by the amount of clay present in the nanocomposite. At lower water concentrations the delay times increase with increasing clay loading. The diffusion of acetone appears to be reduced by the presence of clay to a greater extent.

The diffusion coefficients are however presenting an unexpected trend. While diffusion coefficients for the mixtures with 1:2 and 1:1 acetone/ water ratios show the expected decrease in the diffusion rate with increasing clay levels, diffusion occurs at increased rates in the nanocomposites with higher clay loadings for both components in the diffusant mixtures with excess acetone.

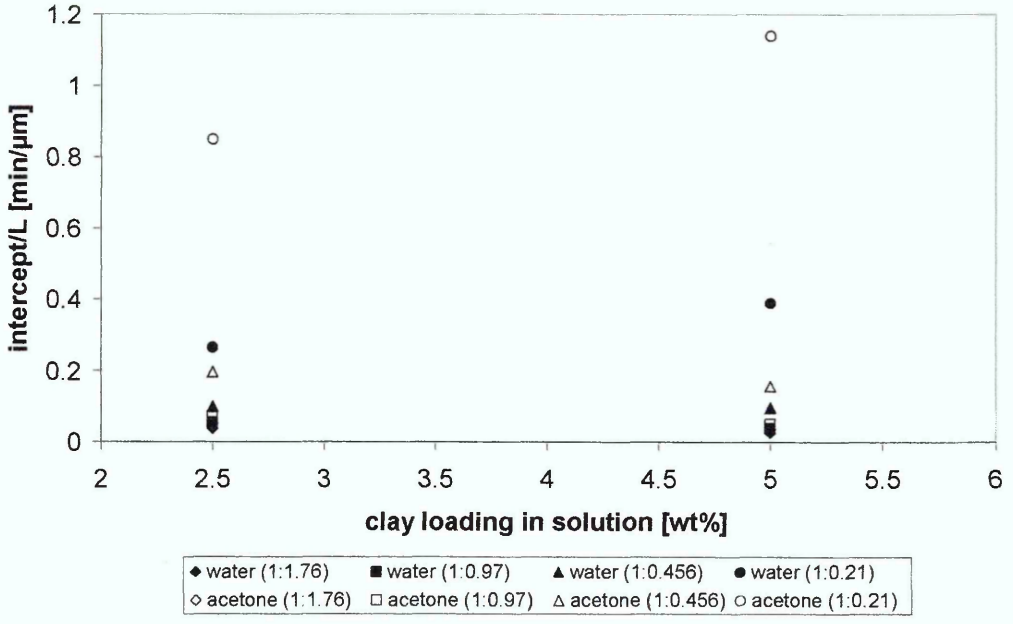

Figure 6-30 Comparison of „delay times" in dependence of clay loading in the solution from which films were cast

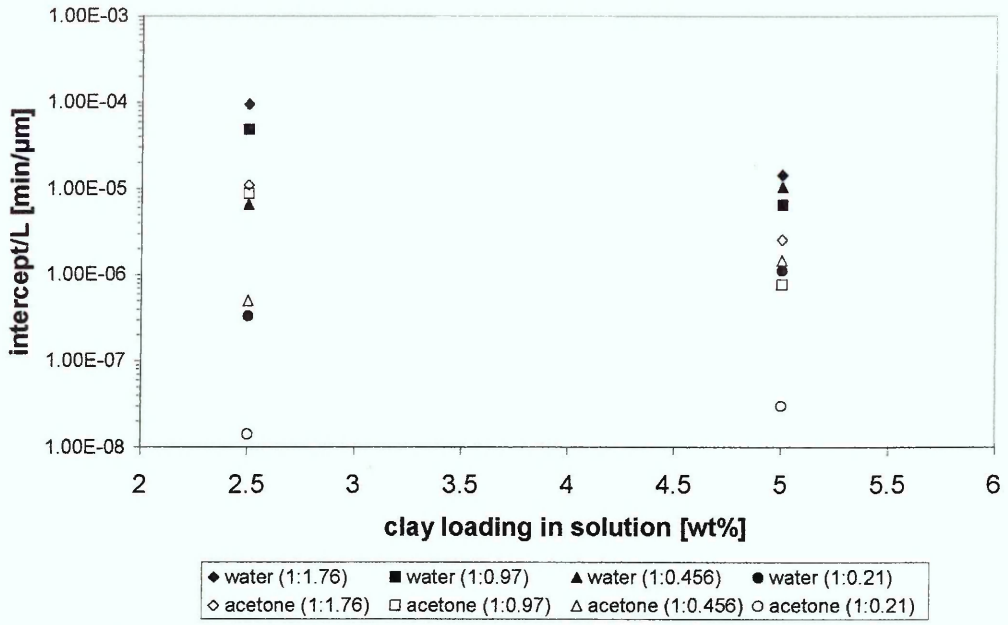

Figure 6-31 Comparison of diffusion coefficients in dependence of clay loading in the solution from which films were cast

The solutions, from which the films for all these experiments were cast, were heterogeneous mixtures. Therefore, films cast from the same solution could exhibit variations in the actual clay levels in the sample. To investigate whether the unexpected results for the diffusion rates seen in Figure 6-31 were due variations in the clay level, the data was plotted versus a "clay indicator" in the dry film ATR-FTIR spectra. This "clay indicator" was obtained by ratioing the area of the ν(Si-O) band of the clay against the area of the ν(C-O) of the PVOH. In these plots repeat runs for the various mixtures are included, so that a wider range of samples can be compared.

This wider range of samples confirmed the observations made before for the limited range of samples. At high water concentrations delay times remained uninfluenced by the amount of clay present in the sample and delays for acetone and water diffusion were similar. At 1:0.456 water/ acetone only minor changes can be observed with variations in the clay levels. While acetone diffusion has a longer delay than water diffusion before it can be observed, values vary only little with increasing clay levels. The changes observed with variations in clay levels for the diffusion of 1:0.21 acetone water mixtures had a slightly larger extent for the acetone diffusion but remained similar to those observed for the 1:0.456 mixture for the water diffusion.

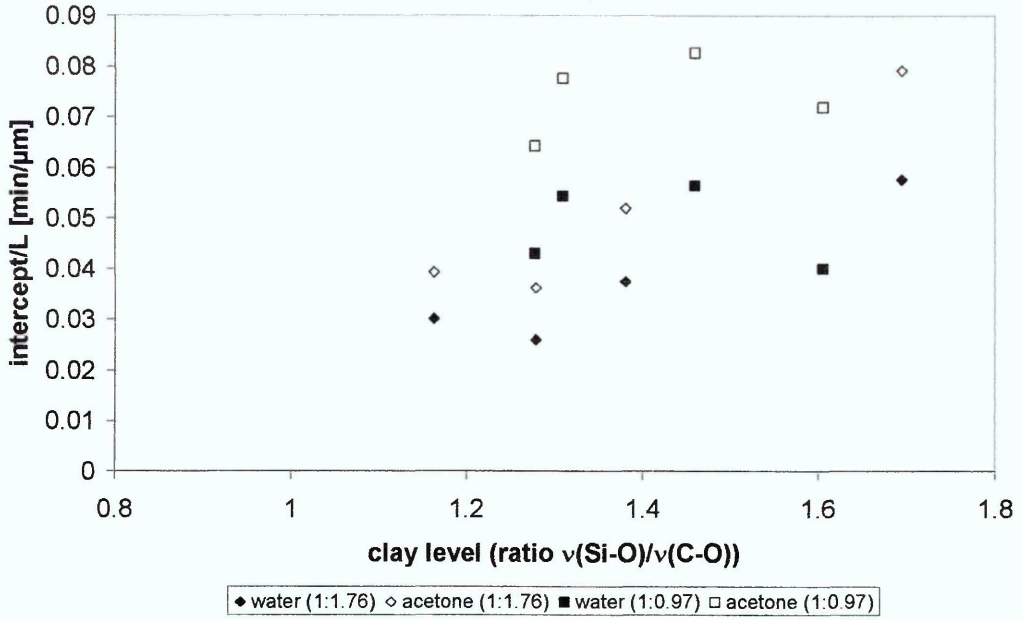

Figure 6-32 Comparison of „delay times" in dependence of clay levels obtained from ATR-FTIR spectra of the dry films for mixtures with lower acetone content

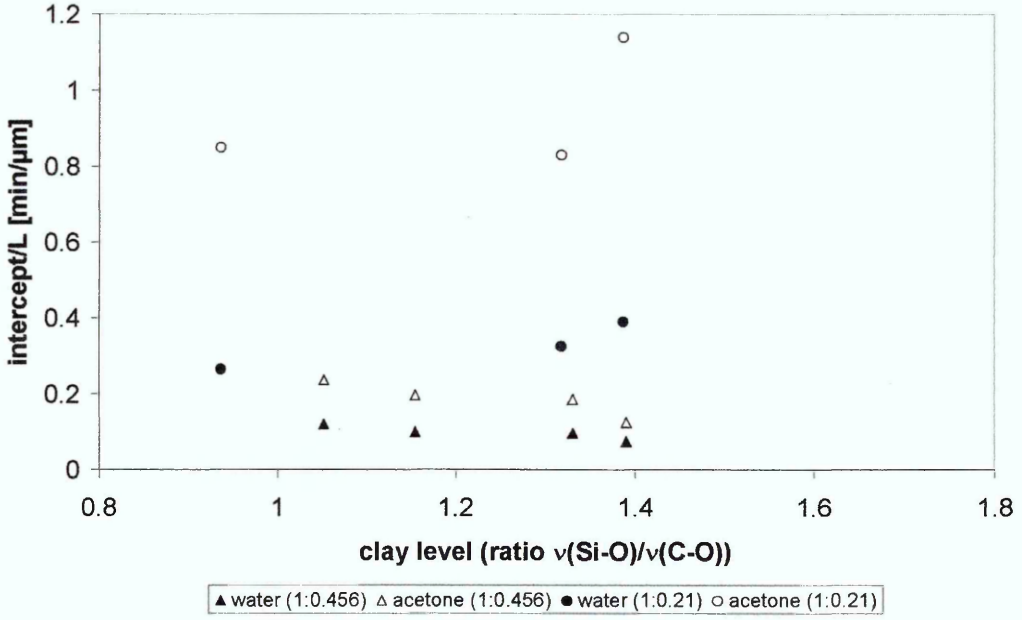

Figure 6-33 Comparison of „delay times" in dependence of clay levels obtained from ATR-FTIR spectra of the dry films for mixtures with higher acetone content

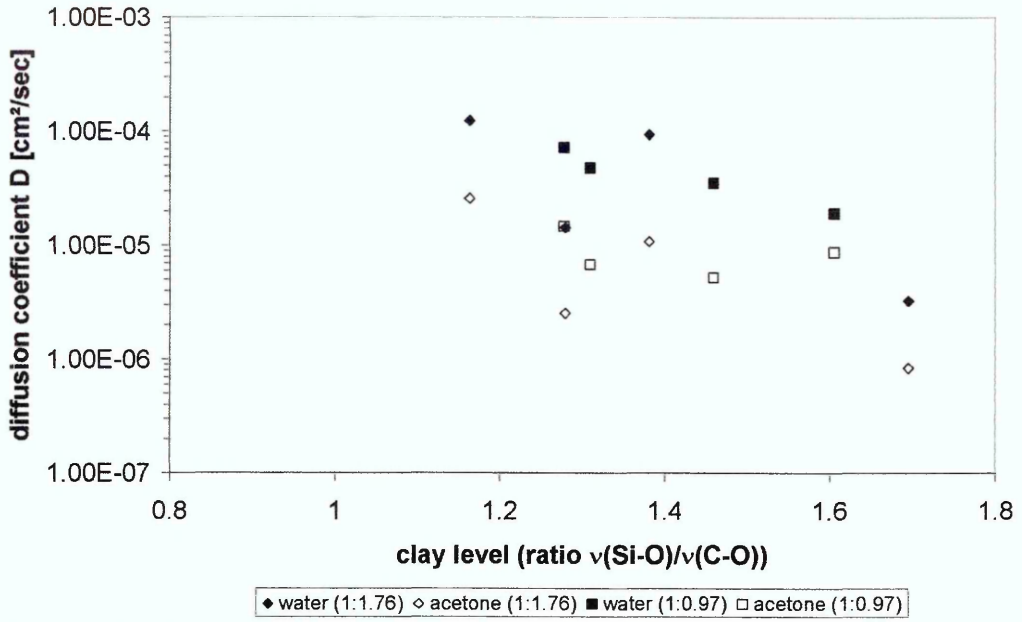

Figure 6-34 Comparison of diffusion coefficients in dependence of clay levels obtained from ATR-FTIR spectra of the dry films with lower acetone content

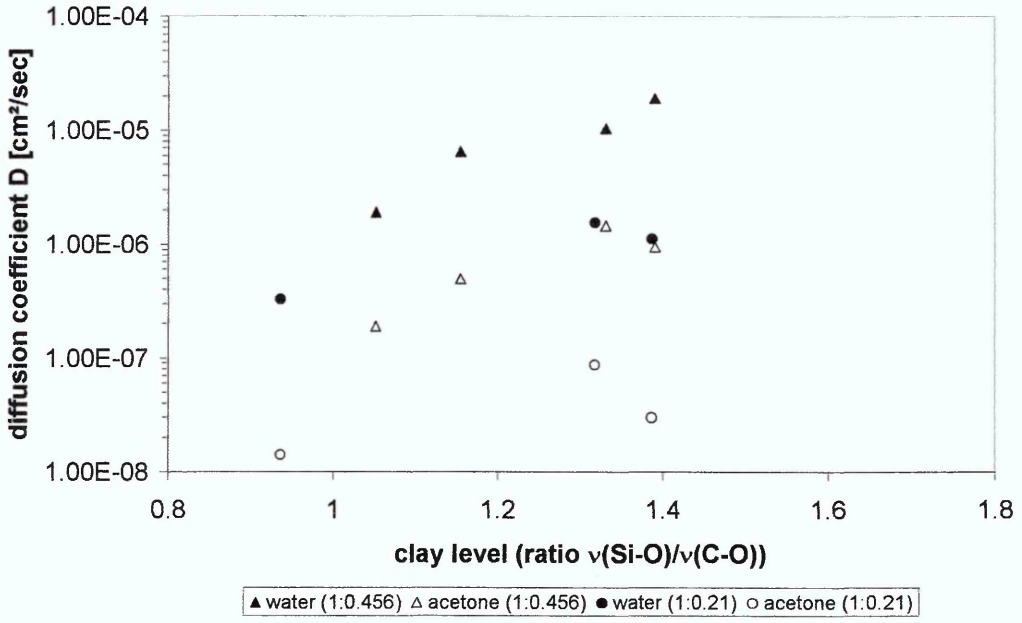

Figure 6-35 Comparison of diffusion coefficients in dependence of clay levels obtained from ATR-FTIR spectra of the dry films with higher acetone content

The data for the diffusion coefficients was also confirmed. At low acetone contents diffusion coefficients were found to decrease with increasing clay content in the sample, while mixtures with excess of acetone appear to diffuse at a faster rate once diffusion has set in.

As variations in the actual clay loading are therefore unlikely to cause these results, other parameters that could change between experiments have to be considered. Moisture content in the dry films has before been shown to have a major impact on the diffusion behaviour of liquids in PVOH. Comparison of the ν(OH) bands for the dry films used in these experiments (which are presented in Figure 6-36) did not show any obvious variations that could explain these changes. The minor variations observed in the ν(OH) band could be caused by a combination of variations in moisture in the film, number of OH groups in the polymer and hydrogen bonding within the polymer.

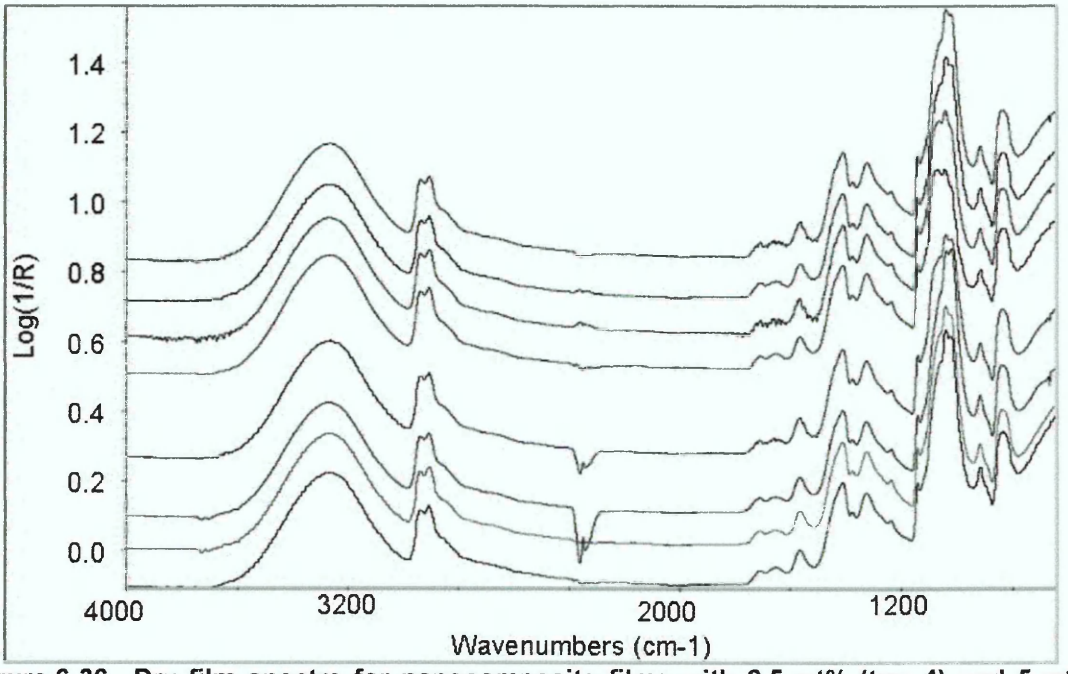

Figure 6-36 Dry film spectra for nanocomposite films with 2.5 wt% (top 4) and 5 wt% (bottom 4) Na^+ Cloisite®

Another parameter that could be responsible for these observations, are the uncertainties in preparation of the mixtures. The liquids were measured by volume using a graduated cylinder. As unexpected results only occur for samples with low water contents in the diffusants, changes in the acetone/ water ratio, due to evaporation of acetone, are a likely source for these results. This hypothesis can, however, not be proved or disproved because no spectra could be taken of the mixtures before the start of the experiment. Any background spectra, as well as the pure mixture spectra presented earlier in this chapter, were collected after the films were removed from the crystal at the end of the experiments.

6.3.1.2 Diffusion of acetone/ water mixtures into PVOH/ Li+ MCBP nanocomposites

Diffusion measurements have been carried out on PVOH/ charged reduced Li^+ MCBP nanocomposites to investigate whether the observations made for diffusion of pure water into these nanocomposites would be more obvious at lower water concentrations. Experiments were performed similar to those described above for PVOH/ Na^+ Cloisite® nanocomposites though only mixtures with molar ratios of 1:1.02 and 1:0.456 for acetone: water were investigated. Furthermore, no experiments were performed to investigate the influence of clay loading in these samples. All films that were used in the diffusion experiments described below were prepared from 5 wt% solutions. Kinetic data was obtained by peak fitting of the ν(C=O), δ(OH) and polymer peaks as described above and diffusion parameters were calculated by treating each diffusant on its own.

Diffusion experiments were performed on nanocomposites prepared with three different Li^+ MCBP clays. The clays used in these experiments were non-heated Li^+ MCBP and Li^+ MCBP heated to either 135 °C or 210 °C for 24 hours. The analysis of the nanocomposites which was discussed in chapter 3.5.3.2.2 showed that non heat treated Li^+ MCBP formed an XRD silent nanocomposite with PVOH at a clay loading of 5 wt%. Li^+ MCBP fired at 135 °C showed a raised background at this clay loading, indicating an intercalated structure with spacings higher than 60 Å. Li^+ MCBP fired at 210 °C did have a poorer dispersion than the other two samples at this clay loading and showed characteristics of a microcomposite.

6.3.1.2.1 Diffusion of 1:1.02 acetone/ water mixture into PVOH/ Li+ MCBP nanocomposites

Experimental data and short term approximation of Fickian diffusion fits for these samples are presented in Figure 6-37 - Figure 6-39 and a summary of diffusion parameters is given in Table 6-8.

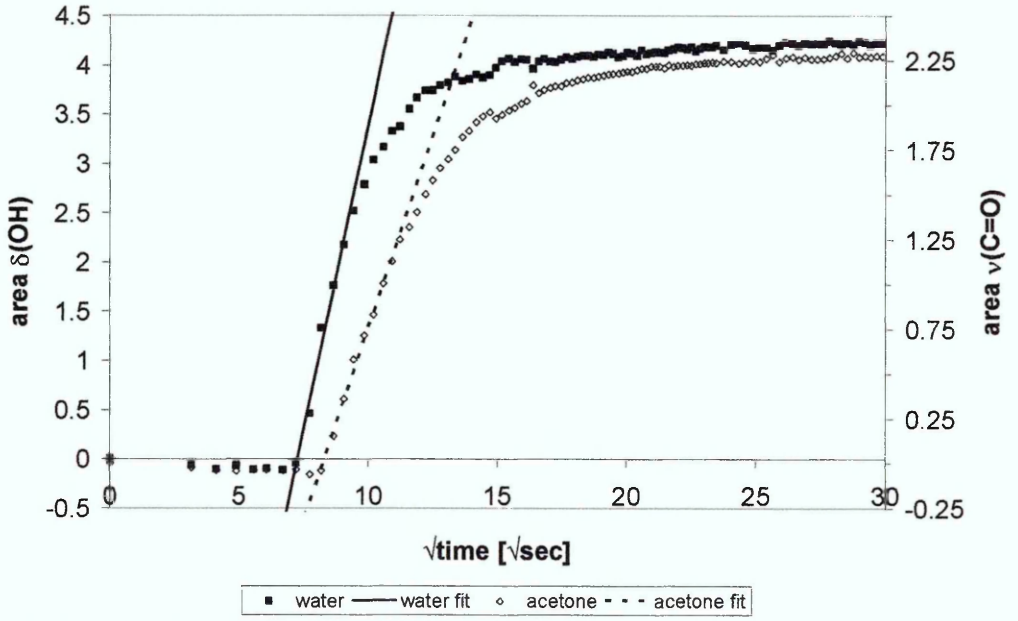

Figure 6-37 Experimental data and short term approximation of Fickian diffusion fits for diffusion of 1:1.02 acetone/ water mixture into PVOH + 5 wt% Li^+ MCBP

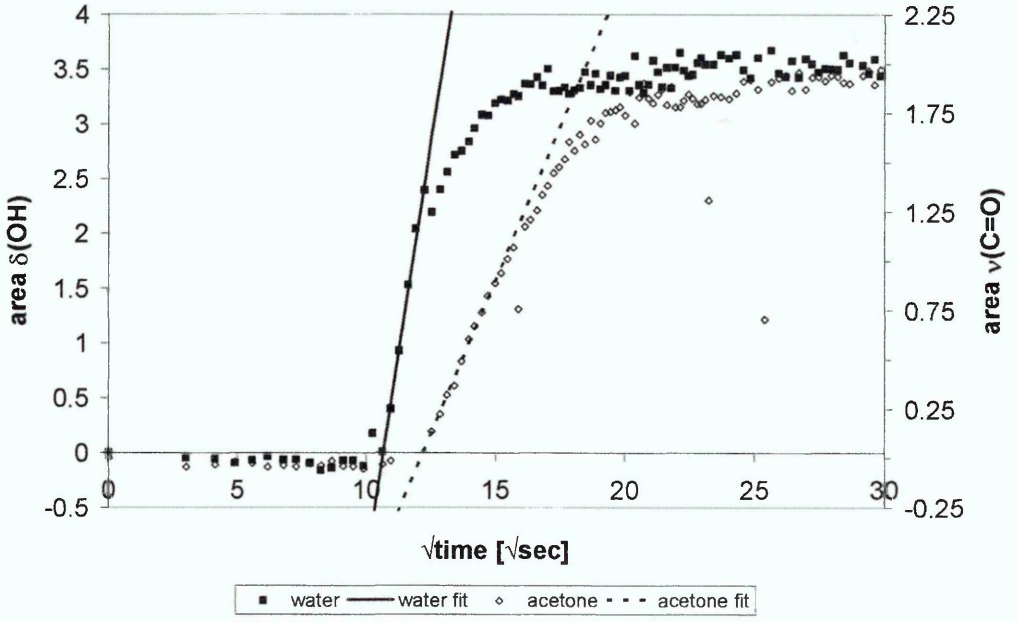

Figure 6-38 Experimental data and short term approximation of Fickian diffusion fits for diffusion of 1:1.02 acetone/ water mixture into PVOH + 5 wt% Li^+ MCBP fired at 135 °C for 24 hours

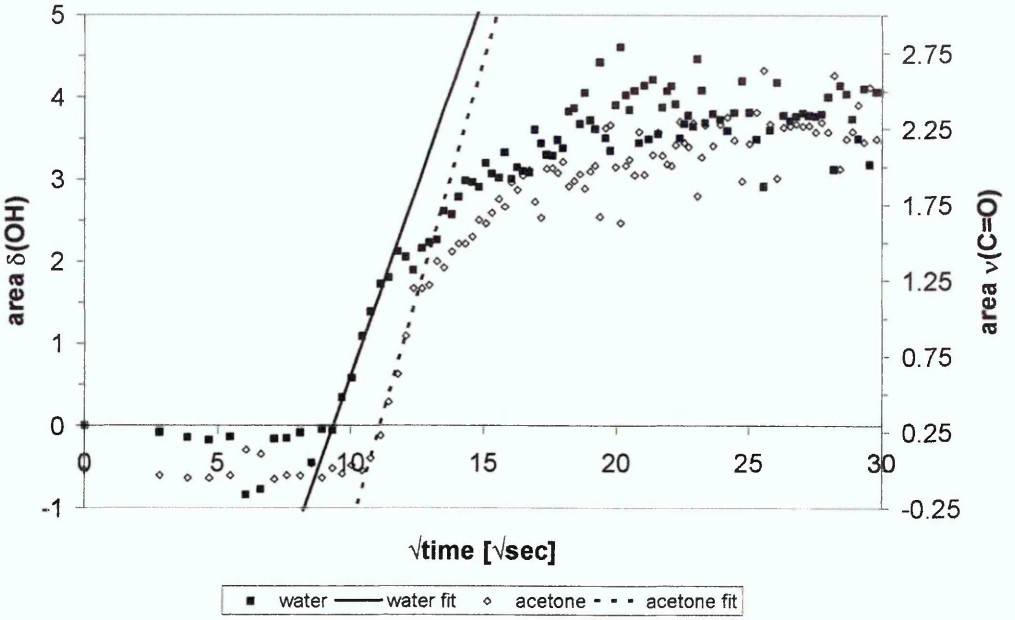

Figure 6-39 Experimental data and short term approximation of Fickian diffusion fits for diffusion of 1:1.02 acetone/ water mixture into PVOH + 5 wt% Li^+ MCBP fired at 210 °C for 24 hours

Clay	Water		Acetone	
	Intercept/L [min/µm]	Diffusion coefficient D [cm²/sec]	Intercept/L [min/µm]	Diffusion coefficient D [cm²/sec]
Li^+ MCBP	0.038	$6.44 * 10^{-6}$	0.049	$7.71 * 10^{-7}$
Li^+ MCBP fired at 135 °C	0.057	$2.06 * 10^{-5}$	0.074	$8.34 * 10^{-7}$
Li^+ MCBP fired at 210 °C	0.056	$4.52 * 10^{-6}$	0.072	$2.01 * 10^{-6}$

Table 6-8 Summary of diffusion parameters for diffusion of 1:1.02 acetone/ water mixture into PVOH + 5 wt% Li^+ MCBP

The results obtained from these samples were very mixed. Judging from the delay times before diffusion becomes measurable, the dispersion has a strong influence on the diffusion. The clay with the best dispersion had delay times comparable to those observed for the neat polymer and the Na^+ Cloisite® nanocomposites. The heated clays which formed nanocomposites with poorer dispersions when incorporated into PVOH did show increased delay times. Diffusion parameters did not show any obvious trend. For diffusion of water the nanocomposite with medium dispersion had the fastest diffusion coefficient, while the microcomposite sample had the slowest diffusion coefficient. For acetone diffusion the fastest diffusion coefficient was measured for the diffusion into the microcomposite and slowest diffusion for the sample with the best dispersion.

At this point no explanation can be given for these observations. Considering the shape of the diffusion curves presented above it is, however, possible that the diffusion parameters obtained from the fits do not give an accurate representation of the data.

6.3.1.2.2 Diffusion of 1:0.456 acetone/ water mixture into PVOH/ Li+ MCBP nanocomposites

Experimental data and short term approximation of Fickian diffusion fits for these samples are presented in Figure 6-40 - Figure 6-42 and a summary of diffusion parameters is given in Table 6-9.

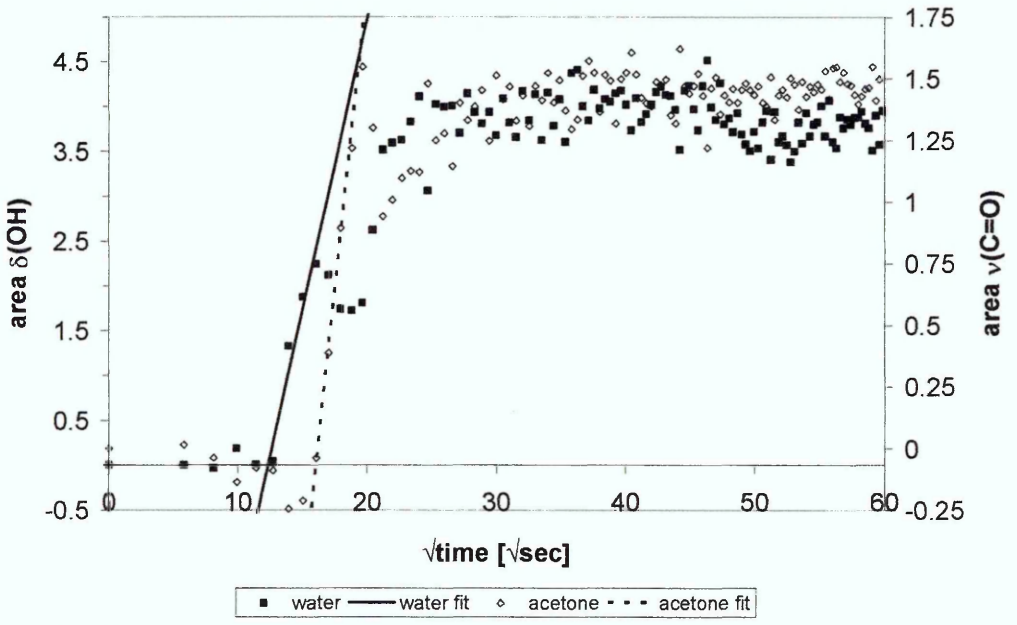

Figure 6-40 Experimental data and short term approximation of Fickian diffusion fits for diffusion of 1:0.456 acetone/ water mixture into PVOH + 5 wt% Li^+ MCBP

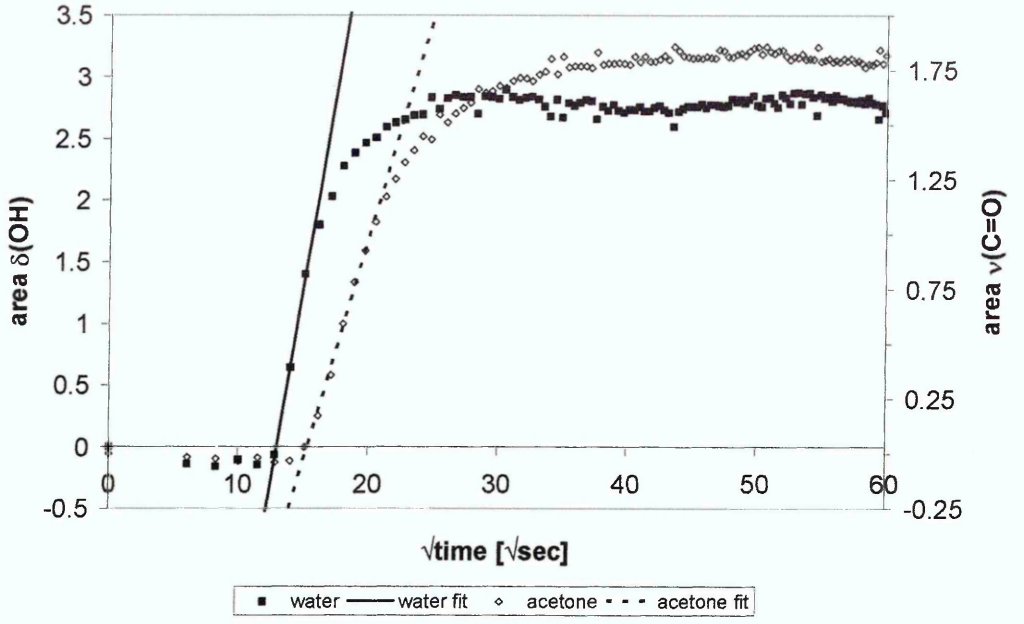

Figure 6-41 Experimental data and short term approximation of Fickian diffusion fits for diffusion of 1:0.456 acetone/ water mixture into PVOH + 5 wt% Li^+ MCBP heated at 135 °C for 24 hours

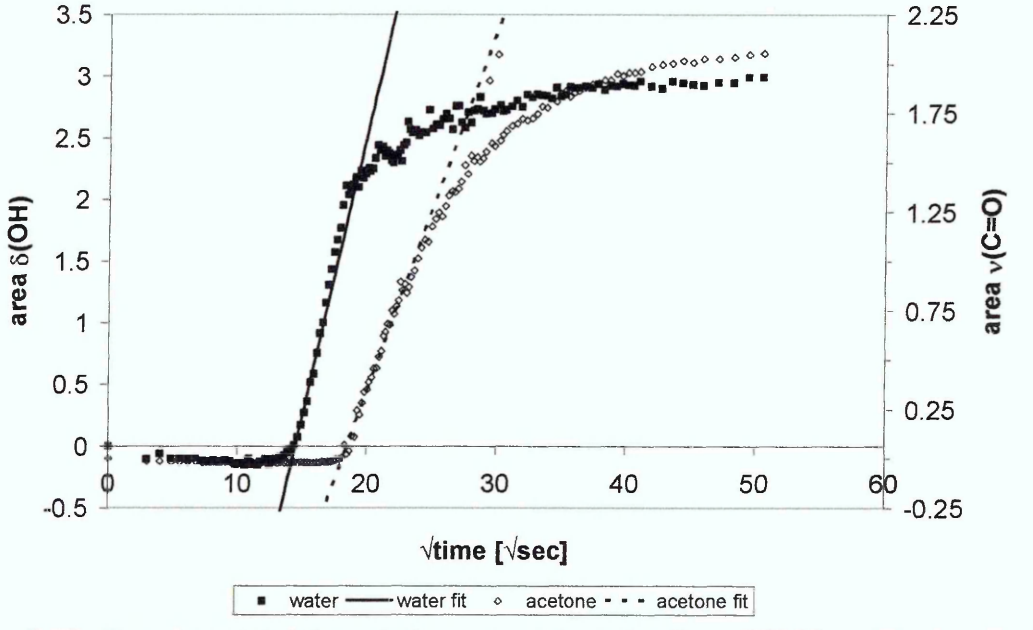

Figure 6-42 Experimental data and short term approximation of Fickian diffusion fits for diffusion of 1:0.456 acetone/ water mixture into PVOH + 5 wt% Li^+ MCBP heated at 210 °C for 24 hours

Clay	Water		Acetone	
	Intercept/L [min/µm]	Diffusion coefficient D [cm²/sec]	Intercept/L [min/µm]	Diffusion coefficient D [cm²/sec]
Li^+ MCBP	0.090	$2.69 * 10^{-6}$	0.156	$1.51 * 10^{-6}$
Li^+ MCBP fired at 135 °C	0.100	$2.52 * 10^{-6}$	0.137	$2.55 * 10^{-7}$
Li^+ MCBP fired at 210 °C	0.125	$1.33 * 10^{-6}$	0.196	$2.09 * 10^{-7}$

Table 6-9 Summary of diffusion parameters for diffusion of 1:0.456 acetone/ water mixture into PVOH + 5 wt% Li^+ MCBP

The diffusion of 1:0.456 acetone/ water mixtures followed a more obvious trend than the data for 1:1.02 acetone/ water mixtures. With poorer diffusion longer delay times are observed before diffusion can be measured by ATR-FTIR. At the same time diffusion rates decrease with poorer dispersion of the clay. These trends are surprising on first glance, as one would expect a better dispersion of the clay to result in better barrier properties.

A possible explanation for these unpredicted observations could be that the stacks of clay layers that were observed in the heat treated nanocomposites in the XRD analysis have larger aspect ratios than the better dispersed nanocomposite materials. This increase in aspect ratio of the clay could be produced if the individual clay layers only partially overlap when dispersed in the polymer, as shown in schematic representation in Figure 6-43. Lan et al. [6.23] showed that such an increase in aspect ratio leads to improved barrier properties at constant clay loadings when investigating the permeability of nanocomposites by gases.

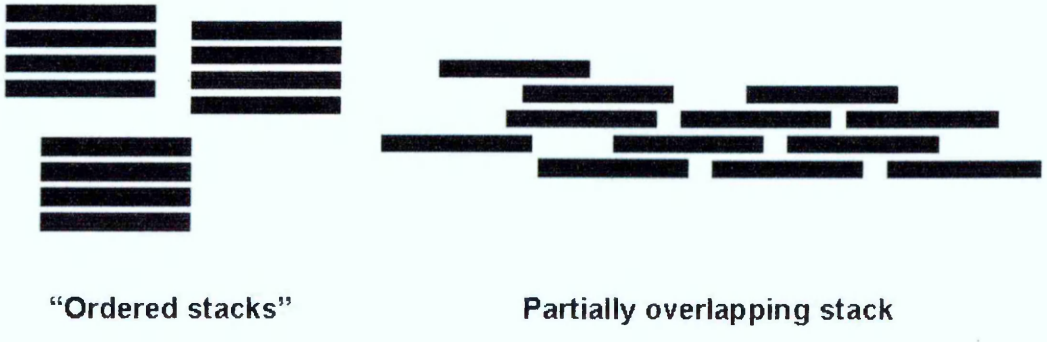

Figure 6-43 Schematic of clay ordering

Further analysis of the exact dispersion by TEM is needed to confirm this hypothesis. Furthermore, the data presented above could be influenced by variations in the clay loading in the sample films, changes in the residual moisture in the dry samples and deviations in the acetone/ water ratios of the diffusant mixtures.

6.3.1.3 Comparison of diffusion of acetone/ water mixtures into PVOH and PVOH nanocomposites with Na+ Cloisite® and Li+ MCBP

Comparing the data for the two different clays shows that the delay times (before diffusion becomes measurable) obtained from diffusion experiments into the 5 wt% Na^+ Cloisite® nanocomposites are similar to those of the PVOH/ Li^+ MCBP (non-heat treated) nanocomposites, proving that neither minor differences in the structure of the clay, nor the ion in the gallery have a strong influence on the diffusion of acetone/ water mixture into PVOH/ clay nanocomposites.

All samples with clay have slower diffusion coefficients for the diffusion of both acetone and water in these mixtures. Best barrier properties are observed for the PVOH/ clay (nano-) composites with poorer dispersion and especially those with microcomposite structures.

6.3.2 Changes in the polymer during the ingress of acetone/ water mixtures

During the diffusion of acetone/ water mixtures into PVOH and PVOH nanocomposites several changes to the structure of the polymer can be observed. As with the diffusion of pure water, diffusion of acetone/ water mixtures causes PVOH films to swell. Furthermore, changes in crystallinity and clay levels detectable in the evanescent field can be observed during these experiments.

6.3.2.1 Swelling of the polymer and polymer nanocomposite films

Swelling of PVOH films is dependent on the amount of water sorbed in the film. During diffusion of mixtures of acetone and water into PVOH and PVOH nanocomposite films swelling has been evaluated by monitoring the decrease of the ν(C-O) band of PVOH over time.

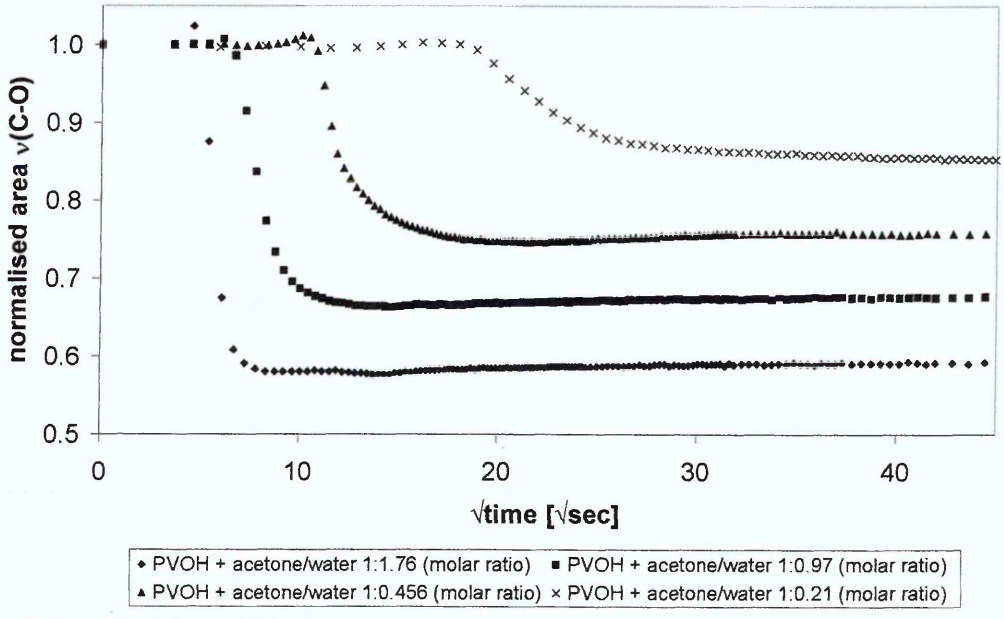

Figure 6-44 Swelling of PVOH during the diffusion of acetone/ water mixtures

Swelling can be detected in the film once water has diffused into the sample. Like the diffusion of water swelling reaches equilibrium within a few minutes for samples with lower acetone content, while higher acetone content samples swell at a slower rate.

The introduction of clay into PVOH results in a reduction of the swelling. The effect is larger for high water content penetrant mixtures but can still be observed in the low water content experiments. Higher clay levels do not

appear to have a significant effect on the swelling. (see Figure 6-45 and Figure 6-46)

Swelling in the non-heat treated Li^+ MCBP nanocomposites was found to be unusually high, almost reaching the levels observed in the unfilled polymer. The heat treated clay nanocomposites exhibited a strong decrease in the swelling which was even less than the swelling observed in Na^+ Cloisite® nanocomposites at a lower water content in the diffusant mixture. (see Figure 6-47)

The clay is likely to reduce swelling by several mechanisms. Hodge et al [6.24] noted that swelling of PVOH is governed by a two fold mechanism, the increase in the size of free volume cavities and a lubrication effect which promotes chain mobility and disrupts hydrogen bonding. Introduction of clay is likely to restrict the formation of free volume cavities as well as reducing the lubrication effect because it presents a physical barrier to the movement of polymer chains.

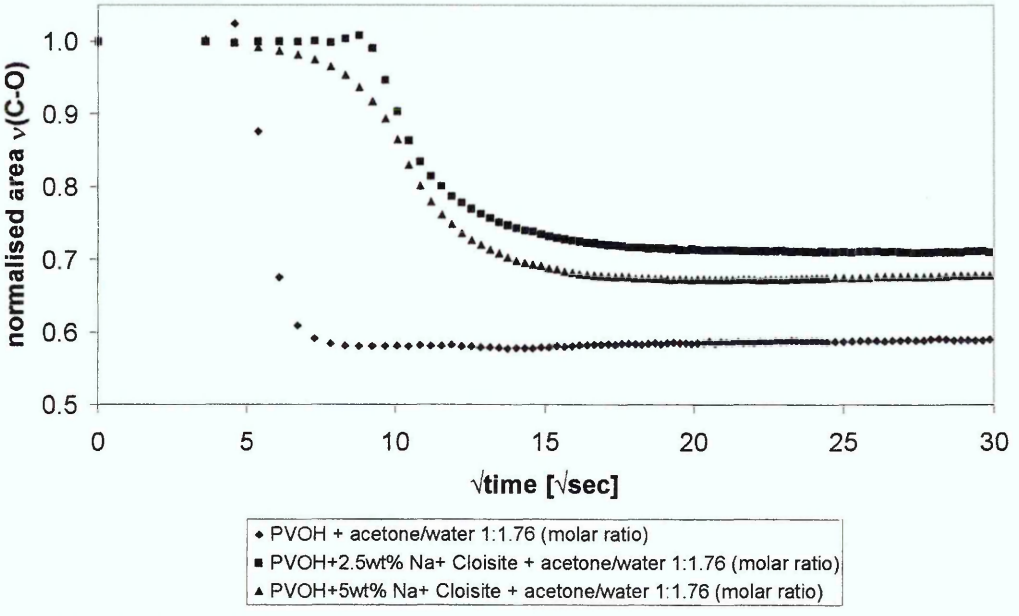

Figure 6-45 Swelling during diffusion of a 1:1.76 acetone/ water mixture into PVOH and its Na^+ Cloisite® nanocomposites

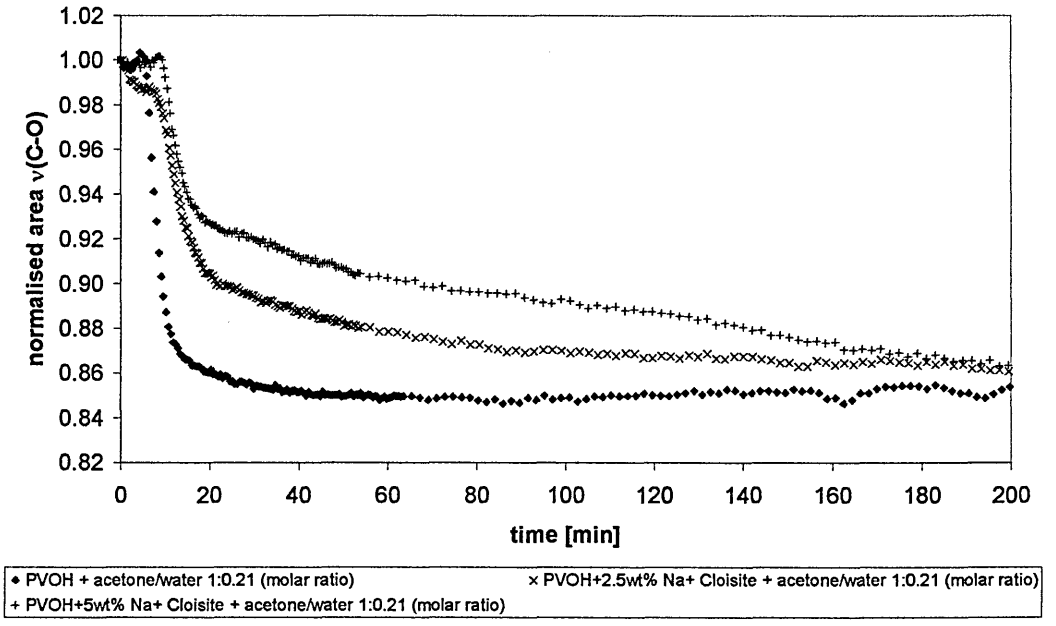

Figure 6-46 Swelling during diffusion of a 1:0.21 acetone/ water mixture into PVOH and its Na^+ Cloisite® nanocomposites

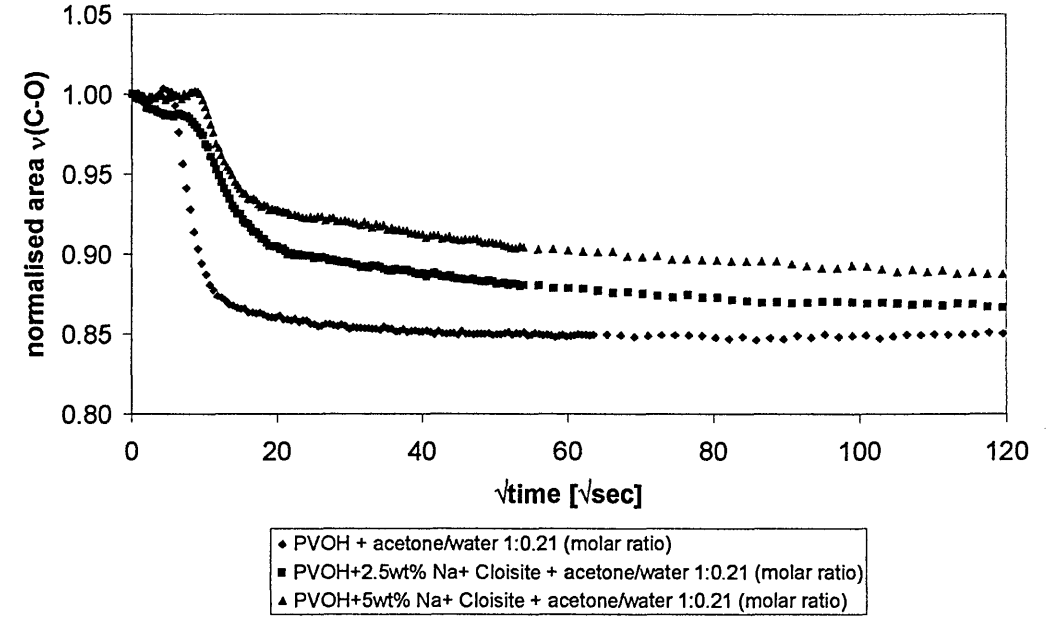

Figure 6-47 Swelling during diffusion of a 1:0.456 acetone/ water mixture into PVOH and its Li^+ MCBP nanocomposites

6.3.2.2 Crystallinity changes of the polymer and polymer nanocomposites

Diffusion through polymers generally takes place through the amorphous regions of the sample. The ingress of a solvent can, however, dissolve crystallites and lead to changes in the overall crystallinity of the film.

FTIR allows a qualitative determination of crystallinity. The band at 1141 cm^{-1} has been found to change with crystallinity [6.25 - 6.28]. Figure 6-48 presents a typical example of the changes occurring in this band over time.

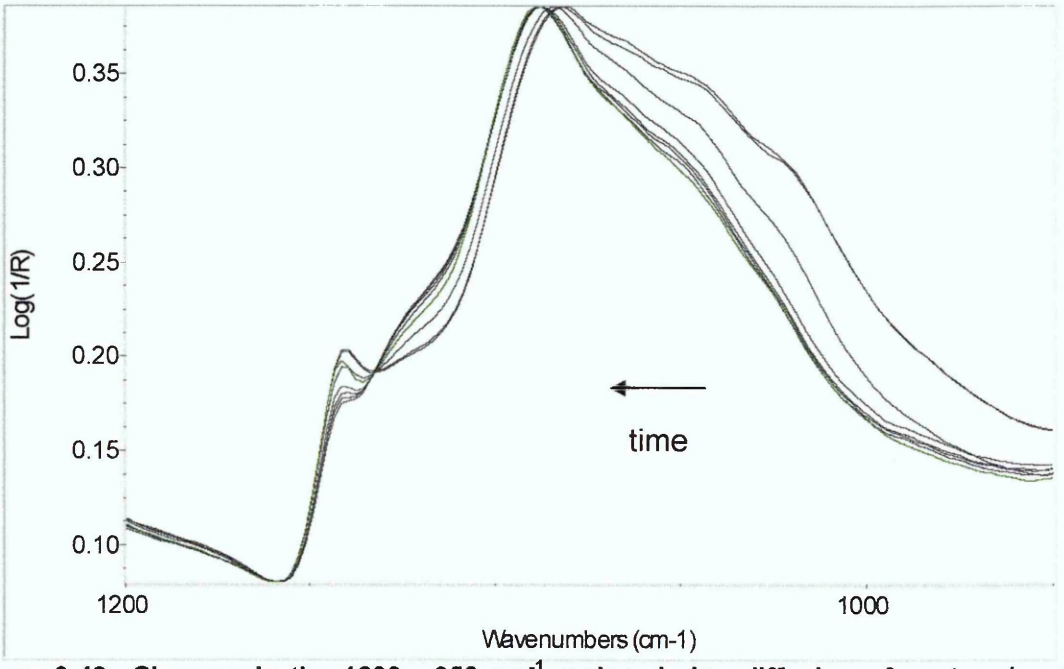

Figure 6-48 Changes in the 1200 - 950 cm^{-1} region during diffusion of acetone/ water 1:1.76 into PVOH

By ratioing this band against the ν(C-O) band changes in crystallinity can be observed independent of the swelling of the sample. Figure 6-49 - Figure 6-51 are showing the qualitative changes in crystallinity over time.

Crystallinity levels appear to be reproducible in the dry films of the pristine polymer. For the nanocomposite samples minor variations in the crystallinity levels of the dry film can be observed but the crystallinity remains of the same order in the nanocomposite as it is in the pristine polymer. Clay therefore does not appear to have a significant influence on the crystallinity of the bulk polymer when films are prepared by casting from aqueous solutions.

At high water concentrations the crystallinity of the film exhibits a sudden drop while the change is slower for lower water content samples. After reaching a minimum at about the same time as water diffusion reaches equilibrium the crystallinity slowly increases again. For the lowest water concentration (molar ratio of acetone: water 1:0.21) the decrease in crystallinity is more gradual and does not exhibit a minimum but rather remains lower than that of the dry polymer.

Peppas [6.28] observed that swelling does not affect crystallinity when PVOH hydrogels are formed. From the data presented in this thesis it is, however, obvious that changes initially occur. Relaxation and reorganisation of the polymer chains over time lead to a reformation of crystallites so that the values at equilibrium are very similar to those obtained for the dry film for the pristine polymer.

The equilibrium water content appears to have an influence on the amount of crystals forming in the swollen polymer. For samples with acetone: water ratios of 1:1 and higher water concentrations a similar level of crystallinity is reached. Samples containing less water in the penetrant mixture, and therefore in the sample at equilibrium show higher crystallinities at equilibrium. This is possibly due to fewer crystals being dissolved in the initial stages of the diffusion.

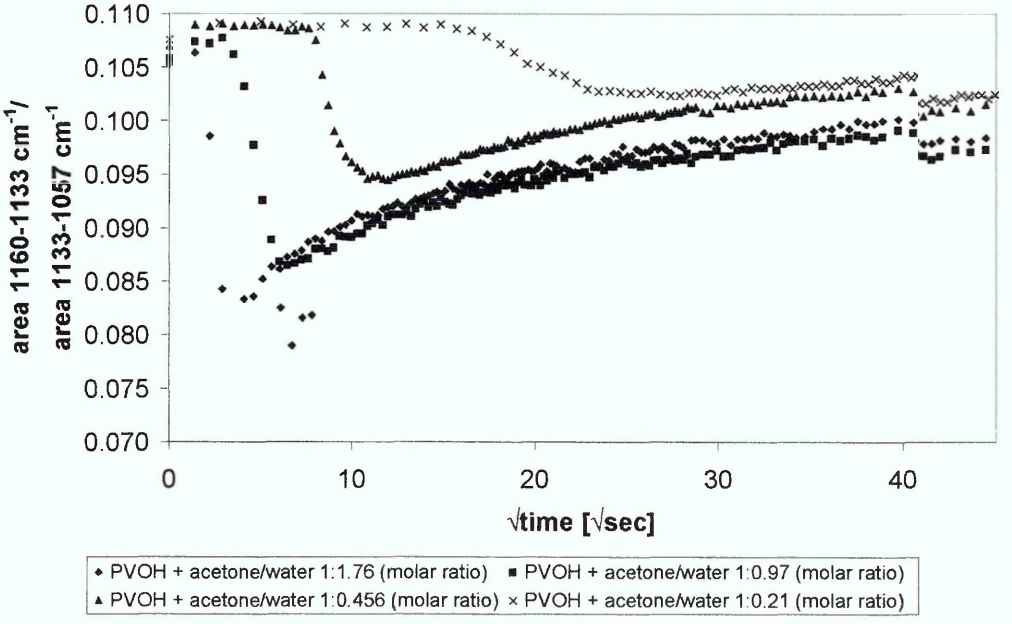

Figure 6-49 Changes in crystallinity during diffusion of acetone/ water mixtures into PVOH

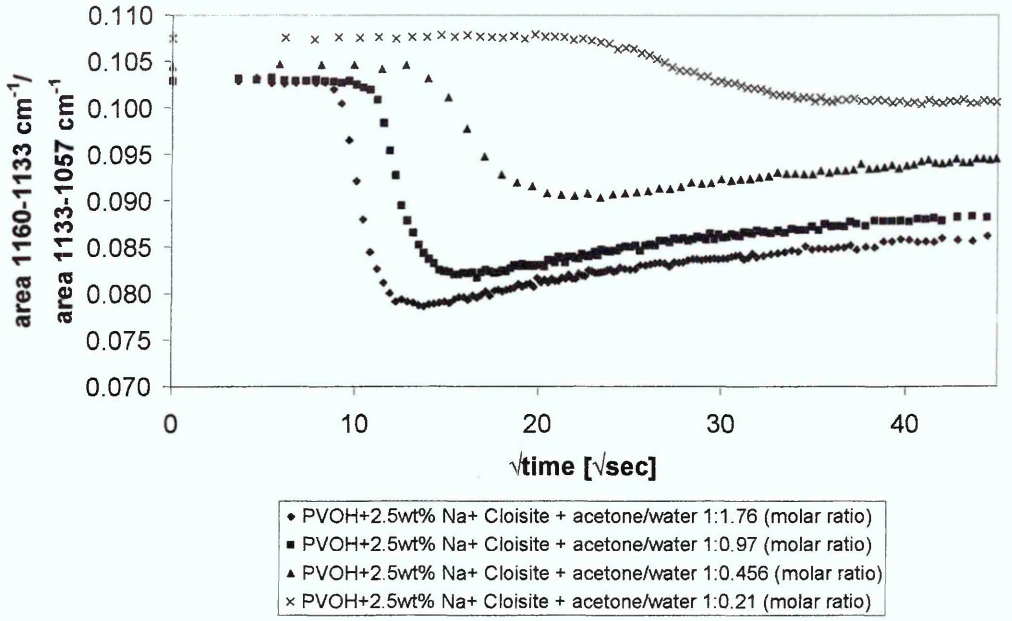

Figure 6-50 Changes in crystallinity during diffusion of acetone/ water mixtures into PVOH + 2.5 wt% Na^+ Cloisite®

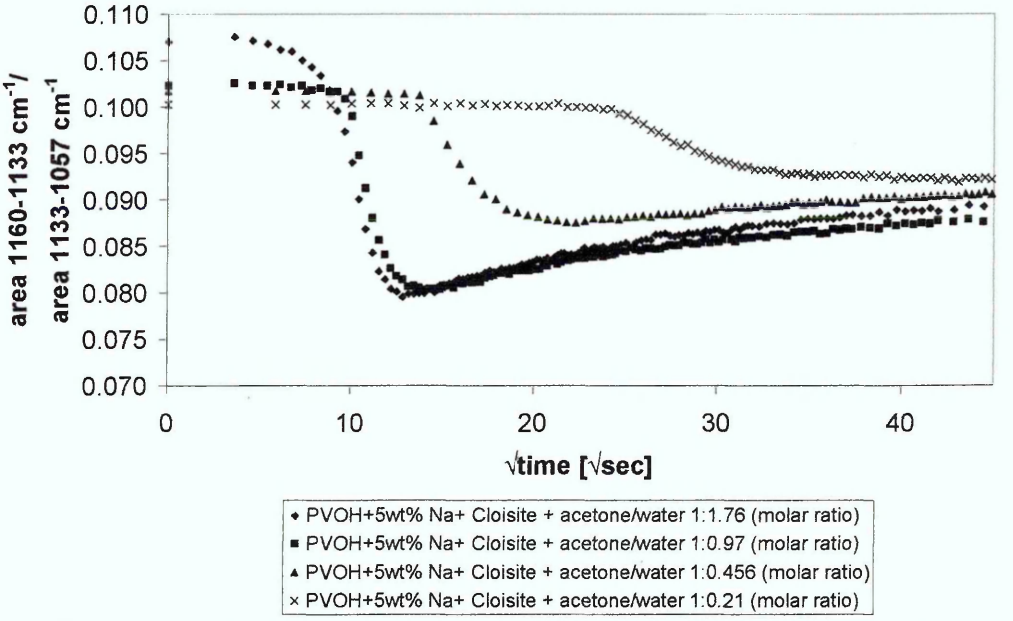

Figure 6-51 Changes in crystallinity during diffusion of acetone/ water mixtures into PVOH + 5 wt% Na^+ Cloisite®

Upon introduction of clay into the PVOH the initial drop in crystallinity remains similar to that observed in the pristine polymer. The reformation of crystals does occur at a much slower rate. This observation suggests that the rate of recovery of crystallinity, after the diffusion of water has reached equilibrium, is mainly due to the mobility of the polymer chains. As polymer chains are hindered in their movement by the presence of clay, crystals cannot be formed as readily through reorganisation of the polymer chains as in the pristine polymer. The

extent to which crystallinity is recovered is also reduced in the nanocomposites. Figure 6-52 presents a comparison of the changes occurring during diffusion of a 1:1.76 acetone/ water mixture into PVOH and PVOH nanocomposites.

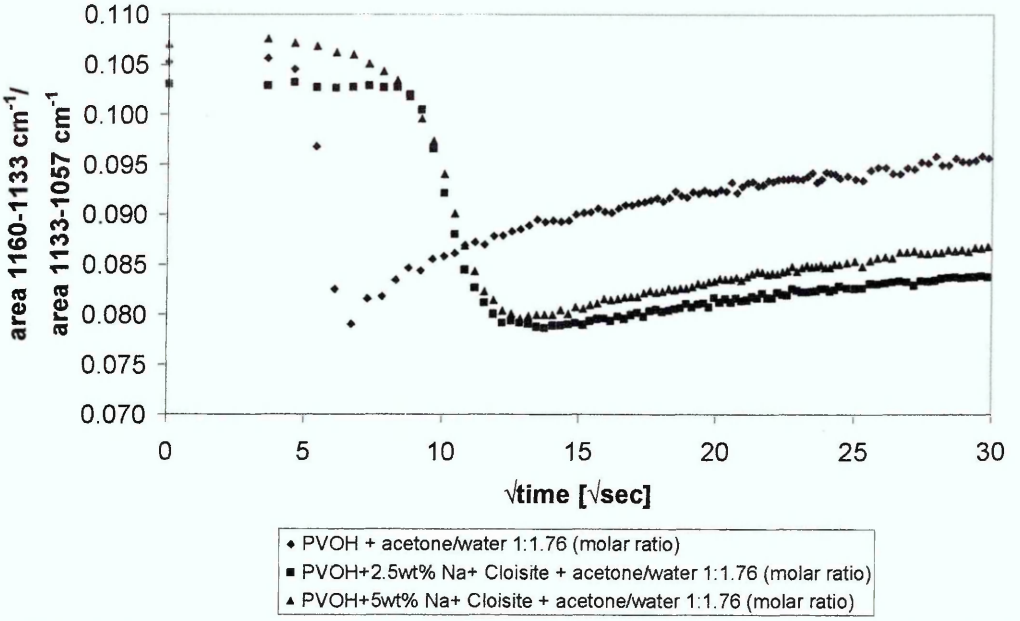

Figure 6-52 Changes in crystallinity during diffusion of a 1:1.76 acetone/ water mixture into PVOH and PVOH/ Na^+ Cloisite® nanocomposites

In the Li^+ MCBP nanocomposites slightly higher starting crystallinities can be observed for the nanocomposites prepared from charge reduced clays. Crystallinity is reducing with the ingress of water and some re-crystallisation can be observed over time.

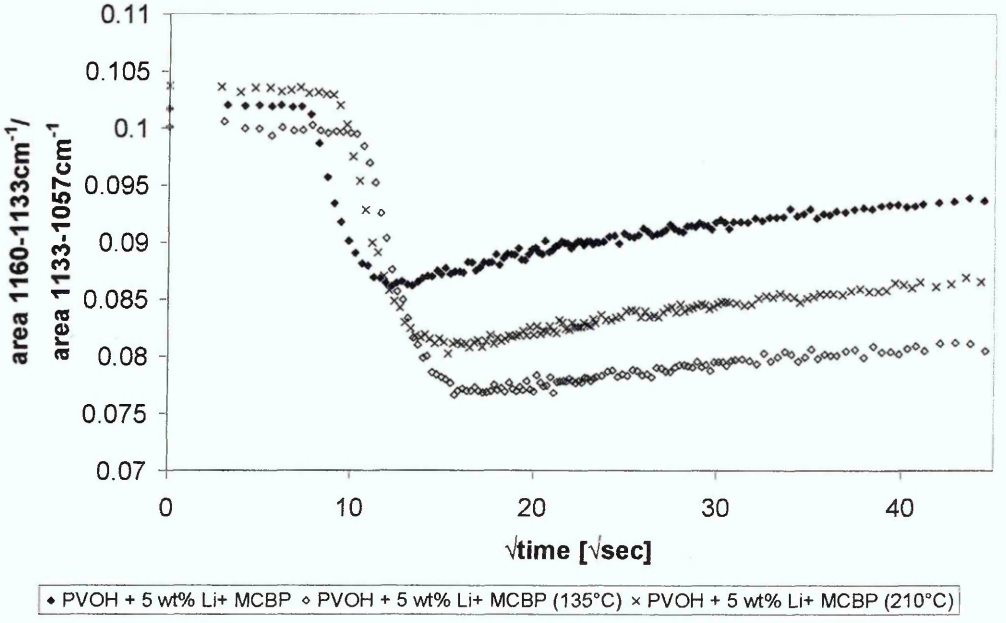

Figure 6-53 Changes in crystallinity during diffusion of a 1:1.02 acetone/ water mixture into PVOH/ Li^+ MCBP nanocomposites

6.3.2.3 Clay level changes in the nanocomposites

When the solutions that were used to cast the nanocomposites were left standing without stirring the clay would settle out over time. Monitoring the ratio of the areas of the ν(Si-O) and ν(C-O) peaks was chosen to investigate if a similar effect could be observed during the swelling of PVOH nanocomposites by water diffusing into the film.

Figure 6-54 presents a comparison of changes to the ν(Si-O)/ν(C-O) ratio over time for the diffusion of acetone/ water mixtures with varying water contents. Even though there are some variations in the initial "clay level" in the evanescent field it is obvious that the ν(Si-O)/ν(C-O) ratio of decreases. This means that the amount of clay present in the evanescent field is reduced upon diffusion of water into the film. As the decrease of this ratio is larger for higher water contents it is likely that the reduction occurs because of swelling of the PVOH matrix with the clay remaining embedded in the polymer.

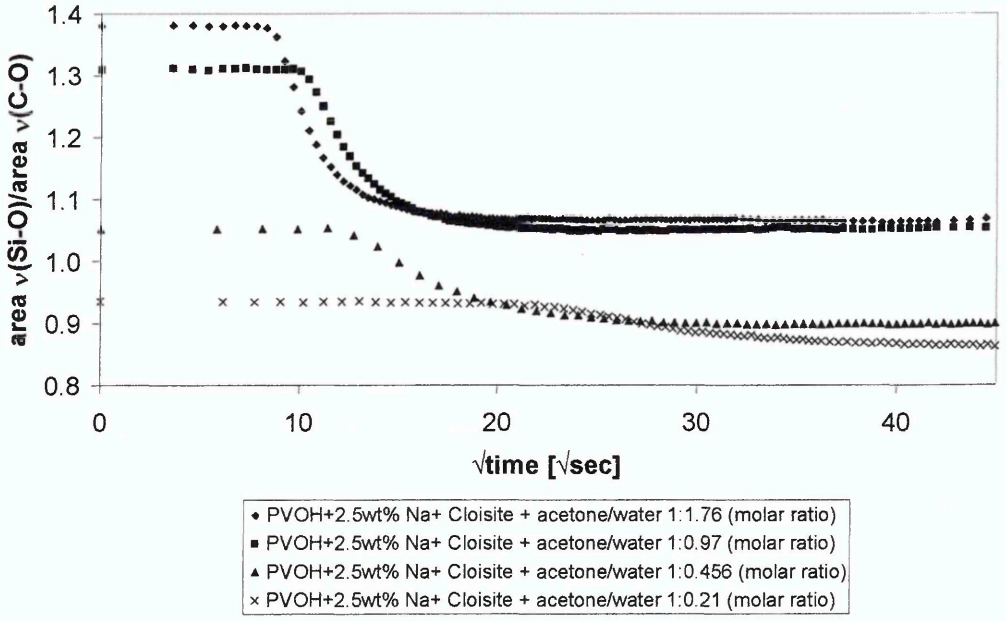

Figure 6-54 Changes in the ν(Si-O)/ν(C-O) ratio over time for PVOH + 2.5 wt% Na^+ Cloisite®

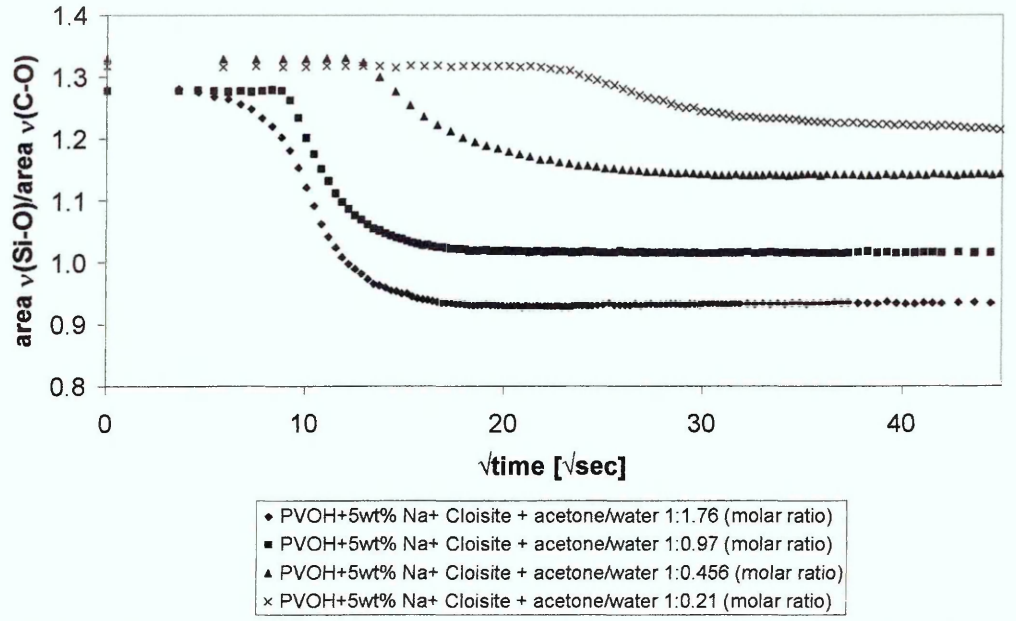

Figure 6-55 Changes in the ν(Si-O)/ν(C-O) ratio over time for PVOH + 5 wt% Na^+ Cloisite®

The results for 5 wt% nanocomposites are similar to those observed for the 2.5 wt% nanocomposite. An overview of the changes for the higher clay samples is presented in Figure 6-55. This graph also shows that for samples with the same starting levels of clay detectable in the ATR-FTIR spectrum the equilibrium level will depend on the amount of water in the penetrant mixture with higher water levels leading to a stronger reduction of the clay detectable in the spectra.

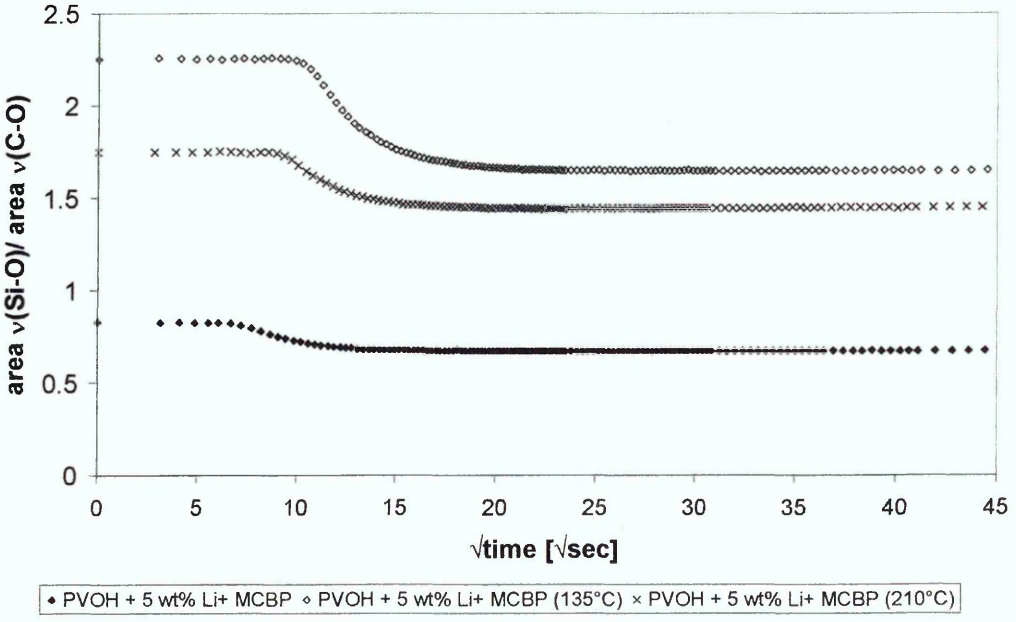

Figure 6-56 Changes in the ν(Si-O)/ν(C-O) ratio over time for PVOH / 5 wt% Li^+ MCBP nanocomposites

Clay levels in the evanescent field were found to be much higher when clay dispersion was poorer. Such higher clay levels in the evanescent field could be due to either clay settling out of the polymer dispersion upon drying when it is dispersed less well or a larger clay agglomerate over the crystal resulting in a apparent clay level in these samples. The changes over time are, however, comparable to those observed in the Na^+ Cloisite® nanocomposites.

The rate of change in the ratio of the Si-O and C-O stretching modes is also dependent on the amount of water available for diffusion. Changes occur at a faster rate the more water is present. This also supports the idea that the reduction of clay is caused by the swelling of the polymer matrix.

As the area of the ν(C-O) band is changing with water ingress the ν(Si-O) must change at a higher rate to account for the changes observed in the ratio of the two bands. Na^+ Cloisite® is a swellable clay. It is therefore possible that the clay layers swell within the polymer once water diffuses into the interlayers, thereby causing the observed apparent reduction of clay in the evanescent field over time. Another possibility is that these observed changes in the clay levels are an artefact of the integration since the bands of interest undergo changes in shape due to interaction with water. As can be seen in Figure 6-57 and Figure 6-58 the complex band around 1000 cm^{-1} shifts to higher wavenumbers.

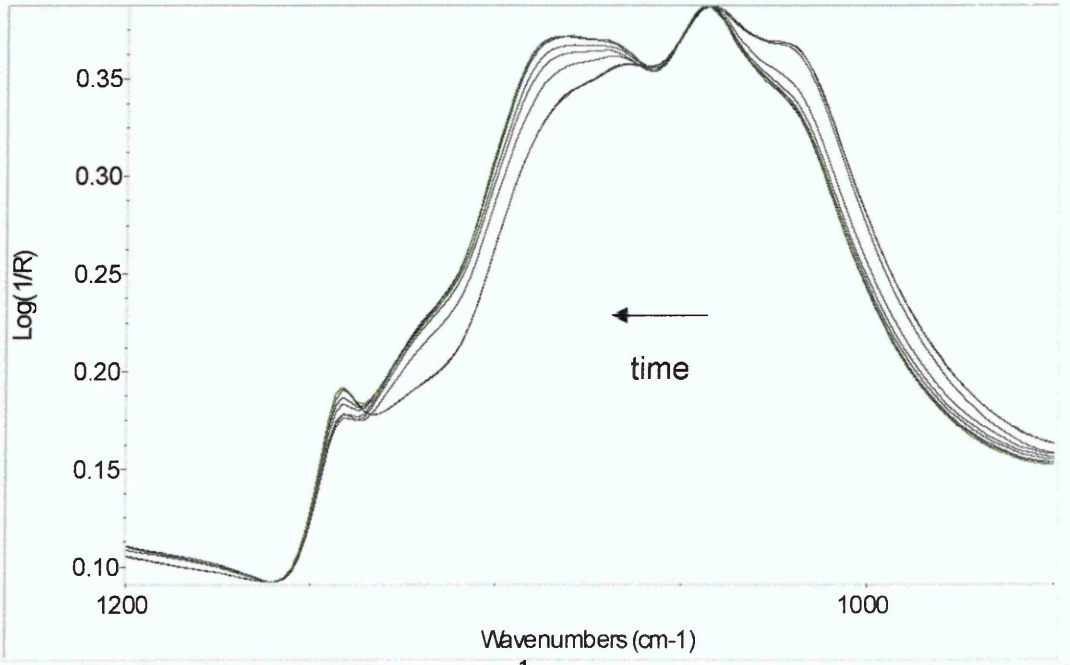

Figure 6-57 Changes in the 1200 – 950 cm^{-1} region for diffusion of acetone/ water 1:1.76 into PVOH + 2.5 wt% Na^+ Cloisite®

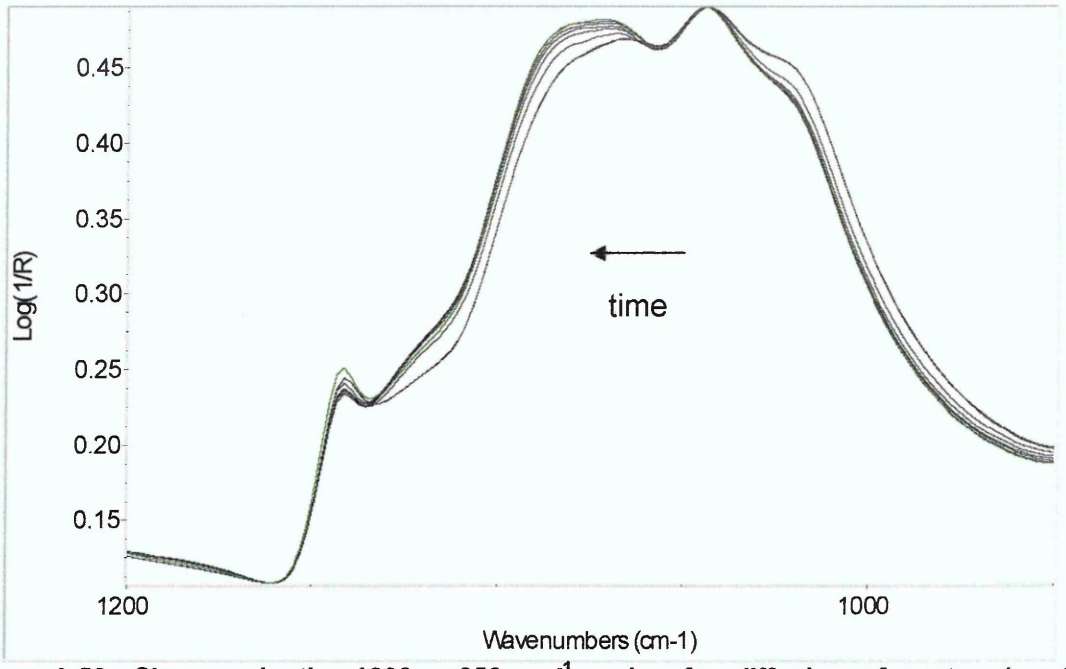

Figure 6-58 Changes in the 1200 – 950 cm^{-1} region for diffusion of acetone/ water 1:0.456 into PVOH + 2.5 wt% Na^+ Cloisite®

As the shift and change in shape is larger for the area used for the integration of the ν(C-O) peak, it is quite likely that any reductions in the ratio of the ν(Si-O) and ν(C-O) peaks are due to the increased area of the ν(C-O) band rather than a proportionally stronger decrease of the ν(Si-O) band. It is, however, certain that unlike in aqueous solutions of PVOH nanocomposites the clay in swollen PVOH nanocomposite films is not completely settling out.

6.3.3 Changes in the hydrogen bonding of water and poly (vinyl alcohol)

The OH stretching region is particularly sensitive to changes in hydrogen bonding. Fitting a single Lorentzian band to the ν(OH) peak gives some general information about the changes occurring in the equilibrium spectra in dependence of clay and water levels in the films.

6.3.3.1 Changes in the equilibrium spectra for diffusion experiments

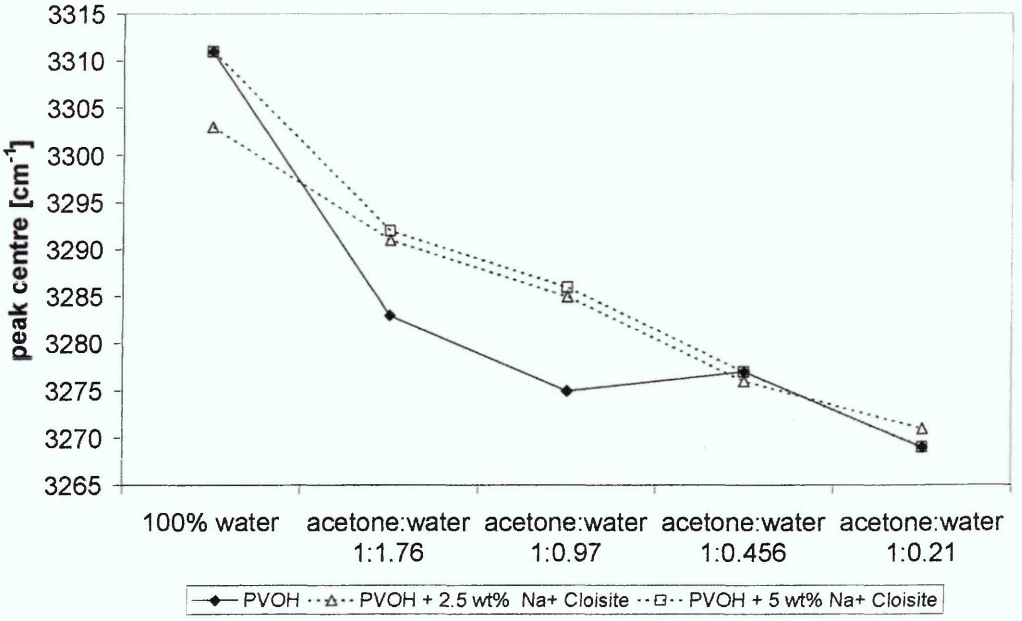

Figure 6-59 Shifts of the peak centre of the ν(OH) band in equilibrium spectra of diffusion experiments on PVOH and PVOH/ Na^+ Cloisite® nanocomposites

With a reduction of water in the penetrant mixture the peak centre of the broad ν(OH) band shifts to lower wavenumbers, indicating the presence of stronger hydrogen bonds the lower the water content in the sample. These changes can be observed in the nanocomposite and pristine polymer alike with little changes in the position in dependence of clay content as shown in Figure 6-59.

At the same time a reduction of the width of this peak can be observed when the amount of water diffusing into the film is reduced. A summary of the changes in the peak width is presented in Figure 6-60. The ν(OH) band is narrower in the nanocomposites which indicates a reduction of the number of water environments which is possibly due to the restricted movement of molecules in the presence of clay platelets.

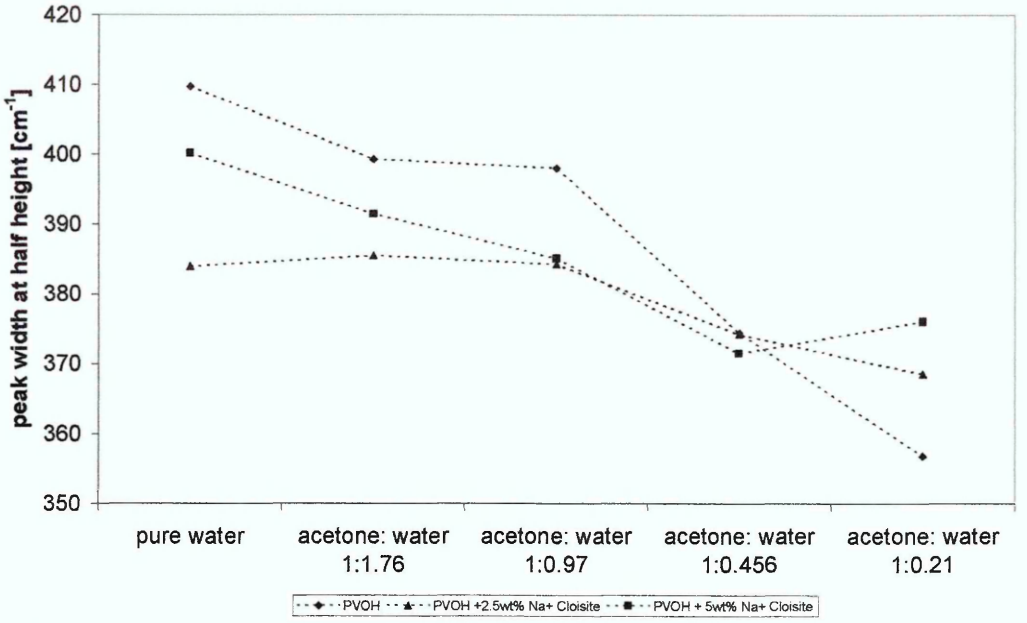

Figure 6-60 Changes of the peak width of the ν(OH) band in equilibrium spectra of diffusion experiments on PVOH and PVOH/ Na^+ Cloisite® nanocomposites

To further investigate these changes in the structure of PVOH and its interactions with water several bands were fitted to the region between 3800 cm^{-1} and 2500 cm^{-1} as described in chapter 6.2.3.

Figure 6-61 - Figure 6-63 present the changes in the relative areas of the different bands fitted to the ν(OH) region for PVOH and PVOH/ Na^+ Cloisite® nanocomposites with clay loadings of 2.5 wt% and 5 wt% respectively.

As expected the relative areas of the peaks attributed to PVOH increase with decreasing water content in the penetrant mixture. This is due to a reduction in swelling of the sample. The relative area of the water bands for strongly and weakly hydrogen bonded water reduces with decreasing water content in the penetrant mixture while there is hardly any change in the peak for moderately hydrogen bonded water. The reduced intensities of water related peaks with increasing acetone content in the penetrant are to be expected as less water is available for diffusion.

The decrease of strongly and weakly hydrogen bonding at the same time while moderate hydrogen bonding remains unchanged means that the water in the system is more alike at low water concentrations, whereas higher water concentrations give rise to various different water environments ,and therefore different strength of hydrogen bonds.

Once the molar ratio of acetone and water in the penetrant mixture reaches 1:1 the changes get less pronounced, suggesting that once hydrogen bonds between water molecules increase, the formation of a water network is the main type of hydrogen bonding of the water molecules.

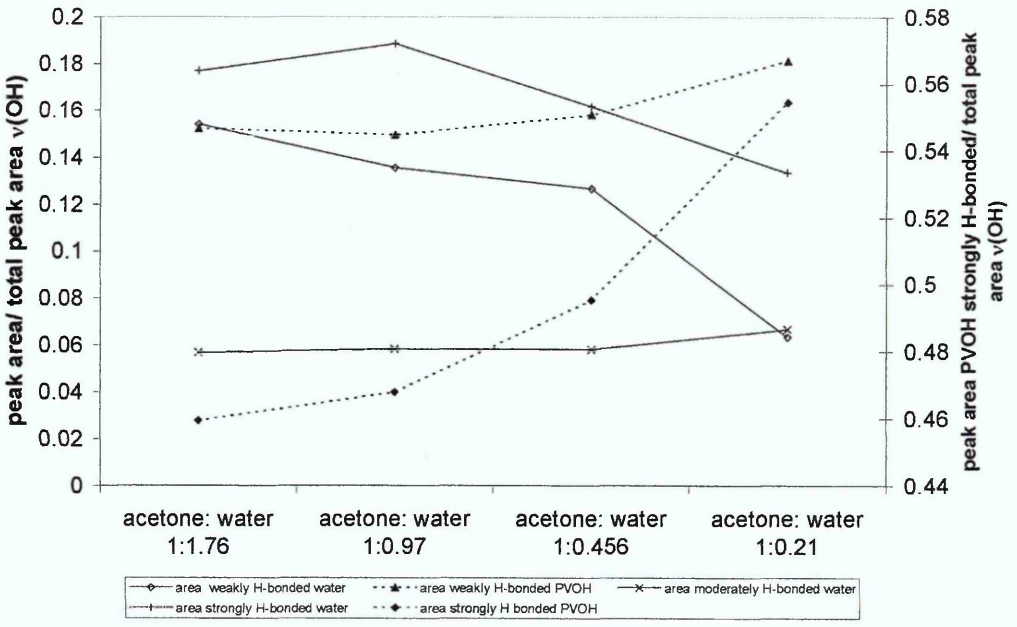

Figure 6-61: Comparison of peak areas of the peaks fitted to the ν(OH) region for the equilibrium spectra of the diffusion of acetone/ water mixtures into PVOH

The introduction of clay into PVOH changes the environment for water in the polymer and therefore influences the hydrogen bonding behaviour of water in such samples. Even though only small amounts of clay are present in the nanocomposite the influence of clay in on the hydrogen bonding can be detected by monitoring the changes occurring in the ν(OH) region.

The peaks assigned to OH vibrations of the polymer are still changing in the same manner as in the pristine polymer. The relative area of these two peaks increases with decreasing water content. The amount of weakly hydrogen bonded water is also found to decrease with decreasing water content in the mixtures while little change can be observed in the area of the moderately hydrogen bonded water.

Of the three types of hydrogen bonding observed for water the strongly hydrogen bonded water accounts for the largest fraction of water with moderately bond water representing the smallest fraction. The dominant OH

stretching vibrations are attributed to the polymer which is to be expected as the sample films are merely swollen by water.

In contrast to the changes observed for the pristine polymer the relative amount of strongly hydrogen bonded water remains constant when clay is present in the polymer films. These strong hydrogen bonds most likely occur when water molecules hydrogen bond with other water molecules to form clusters. The formation of such clusters appears to be increased when clay is present in the sample.

The overall distribution of types of hydrogen bonding present in the sample is, however, not affected by the introduction of clay into the polymer film. Strongly hydrogen bonded water still makes up the largest fraction of the water present in the film while moderately hydrogen bonded water remains the smallest fraction.

The peak areas in the equilibrium spectra of the diffusion of acetone/ water mixtures into nanocomposites of the various Li^+ MCBP clays undergo only few changes. The increase in the relative area of the strongly hydrogen bonded PVOH is likely to be due to stronger inter- and intra molecular hydrogen bonding of the polymer as clay agglomerates increase.

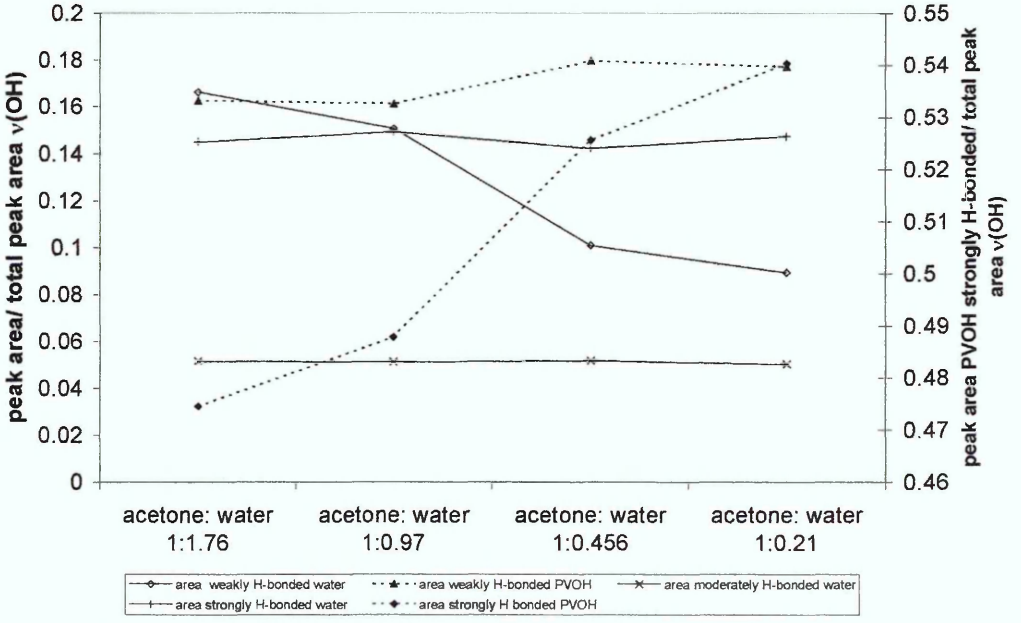

Figure 6-62 Comparison of peak areas of the peaks fitted to the ν(OH) region for the equilibrium spectra of the diffusion of acetone/ water mixtures into PVOH + 2.5 wt% Na^+ Cloisite®

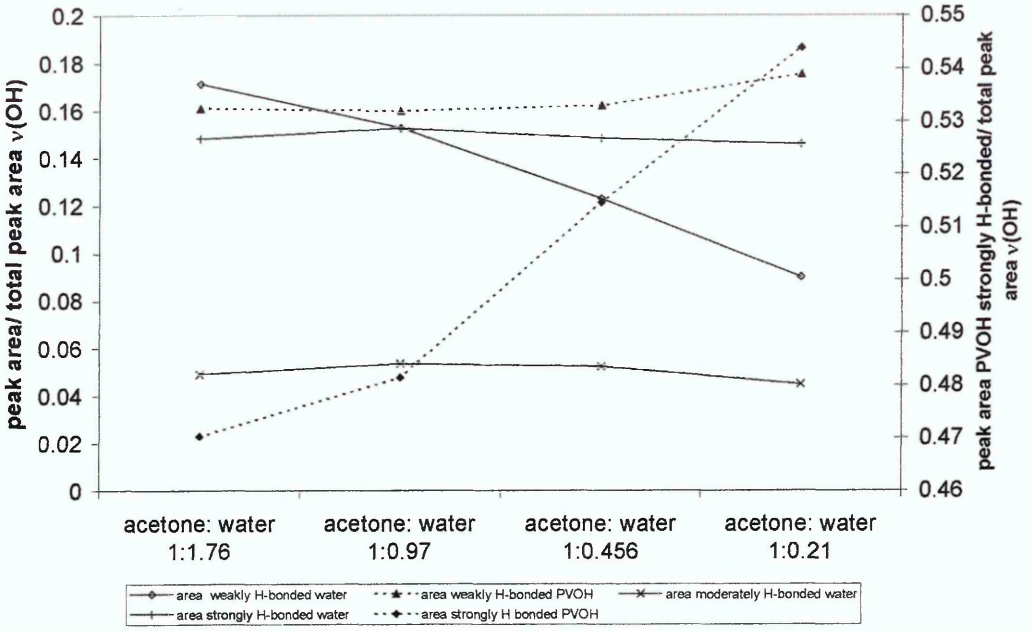

Figure 6-63 Comparison of peak areas of the peaks fitted to the ν(OH) region for the equilibrium spectra of the diffusion of acetone/ water mixtures into PVOH + 5 wt% Na^+ Cloisite®

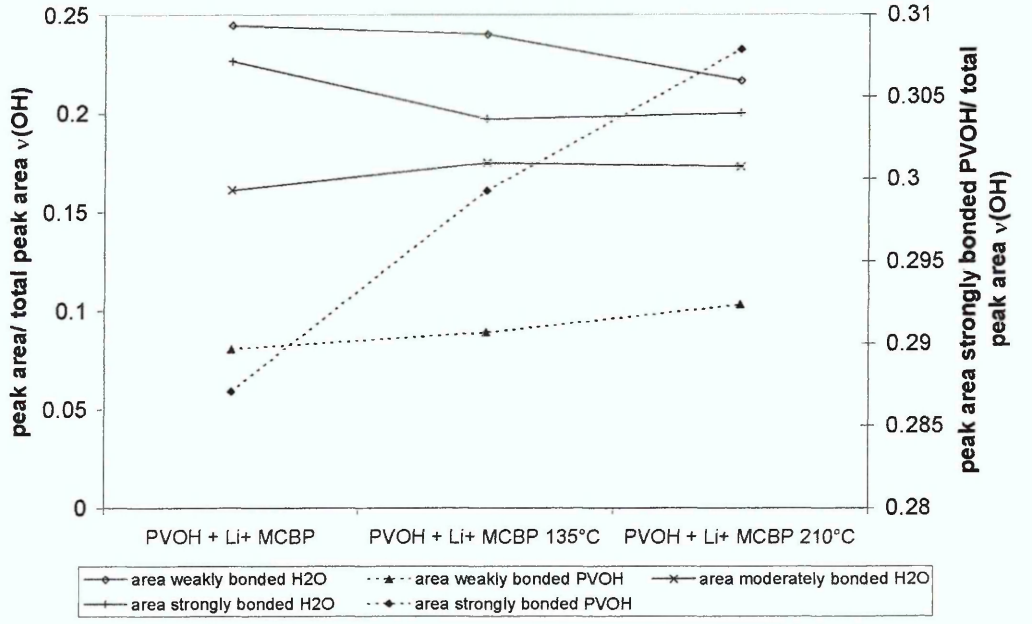

Figure 6-64 Comparison of peak areas of the peaks fitted to the ν(OH) region for the equilibrium spectra of the diffusion of acetone/ water 1:1.02 mixture into PVOH/ Li^+ MCBP nanocomposites

6.3.3.2 Changes during the diffusion of acetone/ water mixtures

Following the changes in the areas of the various peaks related to different hydrogen bonding strength during a diffusion experiment shows an initial increase of the area of strongly bonded PVOH followed by a reduction of this area to a level higher than the initial peak area once equilibrium has been reached. This increase, even though it is only small, is surprising as any bands associated with the polymer are expected to decrease due to swelling of the sample upon diffusion of water into the film. Since it is very hard to produce a completely dry PVOH film, it is possible that this peak has some contribution from water bound to the polymer which remained undetected in the dried sample used to determine the positions of the OH stretching vibrations in PVOH. The increase of this band can, therefore, be explained by an increase in the water level in the film before the swelling and relaxation of the polymer cause the peak to reduce in area again. Another possibility is that this increase is an artefact of the fitting process, caused by the fixed position for this peak.

With decreasing water content in the penetrant mixture the decrease of the peak area of the strongly hydrogen bonded PVOH is slowed down and the final peak area is higher. This is due to the reduction of swelling of the sample with higher acetone content of the penetrant mixture. Since the mobility of the polymer chains is more restricted in an unswollen sample any changes occur at a slower rate. At the same time less swelling means that more polymer is sampled by the ATR measurement resulting in a higher overall peak area of the ν(OH) band.

The weakly hydrogen bonded PVOH displays an increase in intensity which occurs at the same rate as the diffusion of water into the sample and the swelling of the sample. Therefore, this increase could be attributed either to a weakening of the polymer-polymer interactions due to the swelling or to a contribution from water diffusing into the polymer to the area of this peak. If the changes were due to a weakening of the polymer-polymer hydrogen bonds one would expect the increase of this band to occur parallel to the decrease of the band for strongly hydrogen bonded PVOH. This is, however, not the case which makes it more likely that the observed changes are due to a contribution of water hydrogen bonding vibrations to this peak.

The water band for strongly hydrogen bonded water is reducing during the diffusion of a 1:1.76 acetone/ water mixture into PVOH while an increase in weakly hydrogen bonded water can be observed as shown in Figure 6-65. The change in this band is occurring at the same rate as that observed for the δ(OH) band.

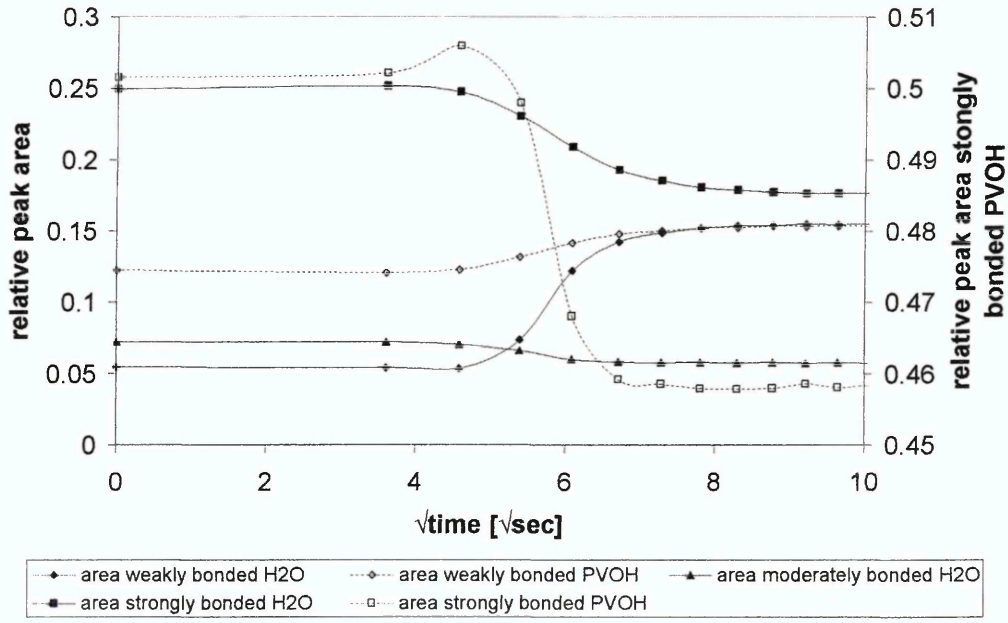

Figure 6-65 Changes in the peak areas of the ν(OH) region during diffusion a 1:1.76 of acetone/water mixture into PVOH

Reduction of the water content in the penetrant mixture results in a decrease of the initial peak area of the strongly bonded water while the weakly bonded water remains at similar intensities which means that the ratio of strongly bonded water: weakly bonded water is changing in favour of the weaker bonds as less water is available for diffusion.

This implies a change of the structure water adopts in the polymer. At higher water concentrations water molecules can hydrogen bond with other water molecules and form clusters. The hydrogen bonding in such clusters is generally stronger than that between water molecules and the polymer or water and acetone. Therefore, a reduction in the concentration and size of water clusters results in a reduction of the peak for strongly hydrogen bonded water.

A reduction of the overall water content does not lead to any significant changes in the behaviour of the bands associated with weakly and strongly hydrogen

bonded PVOH, other than the rate at which changes occur. The same is true for the changes observed for moderately and weakly hydrogen bonded water.

The shape of the curve obtained for the area of strongly hydrogen bonded water is however changing with a reduction of water in the diffusant mixture. As can be seen in the example presented in Figure 6-66 the area of this band initially increases parallel to the increase observed for the peak for strongly hydrogen bonded PVOH and then decreases over time. It is not entirely clear whether this change is an artefact of the fitting process or a real change in hydrogen bonding behaviour of water in the polymer.

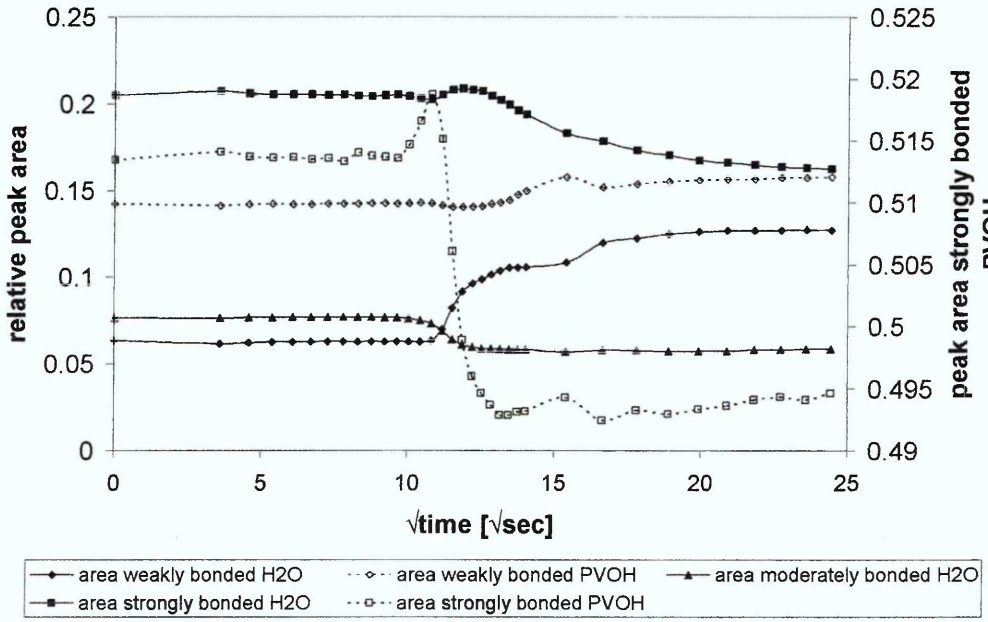

Figure 6-66 Changes in the peak areas of the ν(OH) region during diffusion a 1:0.456 of acetone/ water mixture into PVOH

These results are in contrast to those published by Sammon et al [6.29 - 6.31] for the diffusion of water into PET and PVC samples respectively. For these polymers an increase of strong hydrogen bonding of water molecules can be observed during the course of diffusion of water into the polymers. Since PET and PVC are relatively hydrophobic, it is possible that these differences of the states of water in the polymer are due to the greater interactions between water and PVOH. Furthermore, the amount of water sorbed in PVOH at equilibrium is much greater than that sorbed in either PET or PVC. Compared to these polymers PVOH exhibits increased swelling of the sample film during an experiment which increases the pore size of the polymer thereby allowing

higher water levels to be sorbed and at the same time weakening the intramolecular hydrogen bonds of the polymer.

Introduction of clay has a similar effect on the changes observed for the different bands fitted to the OH stretching region as the reduction of water in the penetrant mixture. The initial increase observed for the peak areas of the strongly hydrogen bonded water and PVOH is, however, sharper than in the pure polymer (see Figure 6-67). As the clay is also hydrophilic it can be assumed that some interactions will occur between water and clay. These interactions are however not identified on their own by the fitting process used. It is therefore possible that the unexplained increase in the peak areas of the peaks associated with strong hydrogen bonding is at least partially caused by contributions of water – clay interactions.

Results for the 5 wt% clay nanocomposites as shown in Figure 6-68 are displaying several jumps in the data that cannot be explained by the shape of the ν(OH) band in the spectra. It is possible that the neglection of any interactions of clay and water in this fitting process creates a systematic error which makes the fitting process unreliable.

If these irregularities in the data are ignored data for the 5 wt% nanocomposites is similar to that for the 2.5 wt% nanocomposites thereby confirming that any differences observed between the fits for the pristine polymer and the lower clay content nanocomposite are due to the presence of clay in the sample.

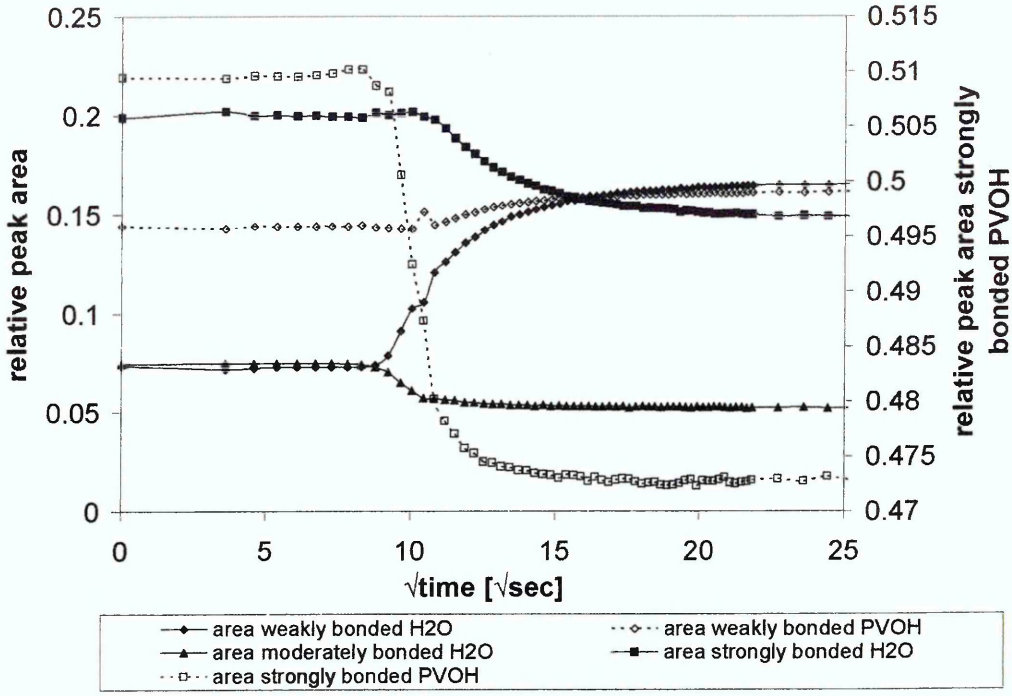

Figure 6-67 Changes in the peak areas of the ν(OH) region during diffusion a 1:1.76 of acetone/water mixture into PVOH + 2.5 wt% Na^+ Cloisite®

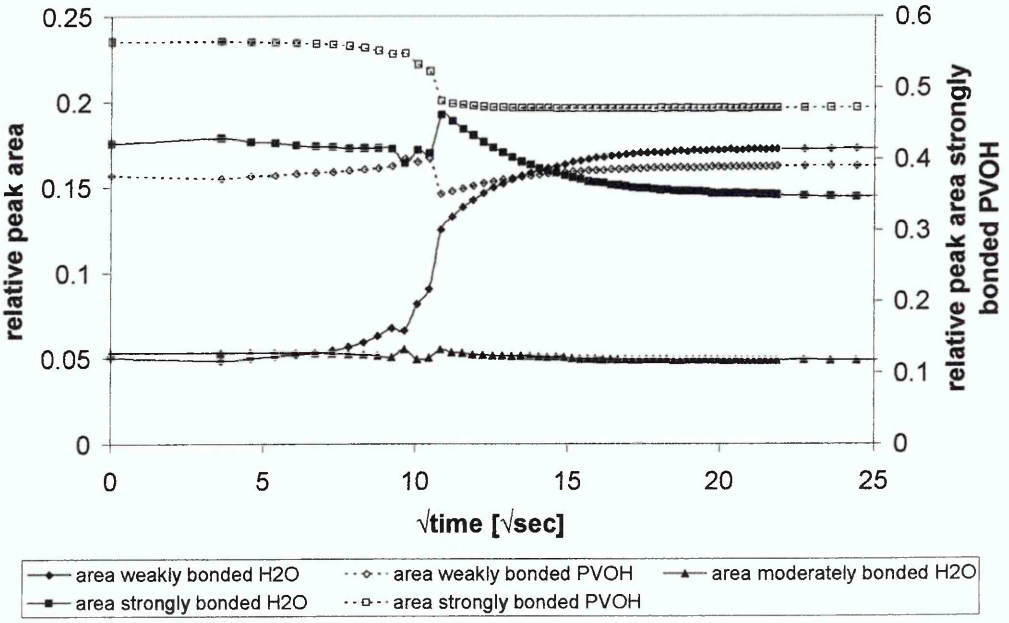

Figure 6-68 Changes in the peak areas of the ν(OH) region during diffusion a 1:1.76 of acetone/water mixture into PVOH + 5 wt% Na^+ Cloisite®

6.3.4 Summary

Diffusion of acetone/ water mixtures into PVOH and PVOH nanocomposites causes a variety of changes in the structure of the sample films. The extent of these changes strongly depends on the composition of the penetrant mixture. Presence of clay in the polymer reduces the amount of swelling and the fraction of crystallinity recovered through chain reorganisation after the initial dissolution of crystals during the swelling and gel formation process.

The shape of the diffusion curves were found to vary with water concentration in the diffusant mixture and clay loading of the samples. Nevertheless, the data was found to fit the short term approximation of Fickian diffusion.

The diffusion of acetone is generally occurring after the diffusion of water has been observed. Diffusion coefficients are slower than those observed for the diffusion of water. This observation is in agreement with studies on solvent/ non-solvent mixtures diffusing into polymers published by Ribar and Koenig [6.9].

Changes in the polymer structure were occurring at the same time that water diffusion could be measured in these systems. Even at water contents as low as 1:0.21 acetone/ water swelling of the PVOH could be observed. Parallel to the swelling of the sample a decrease in the clay levels in the evanescent field was detected. This indicates that the clay remains dispersed in the polymer when it is swollen as a phase separation of the clay and polymer would likely result in higher intensities for the clay bands due to clay settling out and sinking to towards the crystal.

Crystallinity of the samples is also influenced by the amount of water present in the film, as well as the clay loading of the nanocomposites. Initially, the ingress of water into the system results in a reduction of crystallinity. In the pure polymer an increase of crystallinity can be observed after this initial reduction indicating the formation of new crystallites through re-arrangement of polymer chains in the plasticised films. This recovery of crystallinity is impeded in the nanocomposites as clay reduces the mobility of the polymer chains.

6.4 References

6.1 Hauser J, Reinhardt GA, Stumm F, Heintz A, *J. Membrane Sci.*, **47**, 261 (1989)
6.2 Huang YM, Liu HL, Hu Y, *J. Membrane Sci.*, **222**, 123 (2003)
6.3 Dutheillet Y, Mantle M, Vesely D, Gladden I, *J. Polym. Sci.: Pt. B Polym. Phys.*, **37**, 3328 (1999)
6.4 Sackin R, Godward J, Keddle JL, McDonald PJ, *Macromol.*, **34**, 890 (2001)
6.5 Grinsted RA, Koenig JL, *Macromol.*, **25**, 1229 (1992)
6.6 Elabd YA, Barbari TA, *AIChE J.*, **48**, 1610 (2002)
6.7 Hong SU, Barbari TA, *J. Polym. Sci.: Pt. B Polym. Phys.*, **39**, 908 (2001)
6.8 Hong SU, Barbari TA, Sloan JM, *J. Polym. Sci.: Pt. B Polym. Phys.*, **36**, 337 (1998)
6.9 Ribar T, Koenig JL, *Macromol.*, **34**, 8340 (2001)
6.10 Balik CM, Simendinger WH, *Polymer*, **39**, 4723 (1998)
6.11 Onsager L, *Phys. Rev.*, **37**, 405 (1931)
6.12 Yeh JM, Yu MY, Liou SJ, *J. Appl. Polym. Sci.*, **89**, 3632 (2003)
6.13 Mizuno K, Ochi T, Shindo Y, *J. Chem. Phys.*, **109**, 9502 (1998)
6.14 Engdahl A, *Chem. Phys.*, **178**, 305 (1993)
6.15 Zhang XK, Lewars EG, March RE, Parnis JM, , *J. Chem. Phys.*, **97**, 4320 (1993)
6.16 Symons MCR, Eaton GR, *Faraday Symp. Chem. S.*, **17**, 31 (1982)
6.17 Max JJ, Chapados C, *J. Chem. Phys.*, **119**, 5632 (2003)
6.18 Venables DS, Schmuttenmaer CA, *J. Chem. Phys.*, **113**, 11222 (2000)
6.19 Gref R, Nguyen QT, Rault J, Neel J, *Eur. Polym J.*, **8**, 1007 (1992)
6.20 Gref R, Nguyen QT, Rault J, Neel J, *Eur. Polym J.*, **8**, 1015 (1992)
6.21 Ping ZH, Nquyen QT, Chen SM, Zhou JQ, Ding YD, *Polymer*, **42**, 8461 (2001)
6.22 Döppers LM, Breen C, Sammon C, *Vib. Spectrosc.*, **35**, 27 (2004)
6.23 Lan T, Kaviratna PD, Pinnavaia TJ, *Chem. Mater.*, **6**, 573 (1994)
6.24 Hodge RM, Edward GH, Simon GP, *Polymer*, **37**, 1371 (1996)
6.25 Assander HE, Windle AH, *Polymer*, **39**, 4295 (1998)
6.26 Krimm S, Liang CY, Sutherland GBBM, *J. Polym. Sci.*, **22**, 227 (1956)
6.27 Ngui MO, Mallapragada SK, *J. Polym. Sci.: Pt. B Polym. Phys.*, **36**, 2771 (1998)
6.28 Peppas NA, *Makromol. Chem.*, **178**, 595 (1977)
6.29 Sammon C, Mura C, Yarwood J, Everall N, Swart R, Hodge D, *J. Phys. Chem. B*, **102**, 3402 (1998)
6.30 Sammon C, Deng CS, Mura C, Yarwood J, *J. Mol. Liq.*, **101**, 35 (2001)
6.31 Sammon C, Deng CS, Yarwood J, *Polymer*, **44**, 2669 (2003)

7 Conclusions and further work

7.1 Poly (ethylene terephthalate)/ organo – montmorillonite nanocomposites

Nanocomposites were prepared by solution intercalation of commercially available organically modified montmorillonites. Two types of PET, a homo-polymer and a polymer containing isophthalate copolymer units, were intercalated into three clays with different organic modifications by solution intercalation using tetrachloroethane and o-chlorophenol as solvents.

All prepared nanocomposites had 001 clay peaks at lower degrees 2θ than the pristine organoclay in their x-ray diffractograms indicating a regular intercalated structure with higher clay layer spacings than the pristine organoclays. Comparison of these samples prepared from different organoclays showed that intercalation of PET into Cloisite® 20A resulted in the highest interlayer spacing while the layers of Cloisite® 30B underwent the highest percentage swelling when intercalated with PET. The high increase in layer spacing in the Cloisite® 30B is most likely due to the better compatibility of the surfactant used in this clay with PET, while the layer spacing of Cloisite® 20A nanocomposites is probably largely influenced by the size of the surfactant and its alignment within the layers.

Samples prepared from E99 (PET with 18% isophthalate units) had a more ordered structure based on the observation of the 002 reflection of the clay in the XRD traces of the nanocomposites. The higher order of the clay layers in these nanocomposites has been attributed to the bulkier structure of the co-polymer. Such a structure makes it harder to intercalate into the clay layers resulting in more ordered stacks of clay being present in the polymer matrix.

Allowing the clay to swell in the solvent for different amounts of time did not result in any changes in the structures of the final polymer. Since the mixing time after addition of polymer was, however, kept constant at two days, it is quite possible that any effects the initial dispersion of the clay in the solvent had on the intercalation of PET was compensated by this long stirring time.

The drying temperature for the PET films did not appear to have any influence on the dispersion of the clay within the polymer. Since PET is a semi-crystalline polymer that can be crystallised by annealing at elevated temperatures, higher drying temperatures did, however, result in a material with higher crystallinity. Crystallinity changes of the samples, as calculated from their ATR-FTIR spectra, did not show any major differences between the pristine polymer and the nanocomposites. The presence of clay does not appear to induce crystallinity on the scale of these measurements nor hinder the formation of crystals.

Use of different solvents or variations in the concentration of the polymer in the dispersion did not result in significant changes in the structure of the nanocomposites.

The intercalation of PET into the organoclays used in this study was not affected greatly by the parameters of preparation that were investigated. All prepared PET/ organoclay nanocomposites had an intercalated structure with layer spacings between 36 Å and 44 Å. The thermal stability of these samples in a nitrogen atmosphere was similar to that of the pristine polymer. The decomposition of the polymer in the nanocomposites did, however, start at temperatures up to 40 °C lower than the unfilled polymer. It remains unclear whether this is due to a higher solvent content in the films or a catalytic effect of the clay.

Solution intercalation of PET using OCP or TCE as solvent medium was, therefore, found to lead to similar results as those published for other solvent materials. While this method could be used to create intercalated structures, the conditions investigated did not influence the dispersion of the clay enough to result in the formation of exfoliated nanocomposites. Furthermore, reproducibility of the preparation of sample films was found to be low making measurements of diffusion by ATR-FTIR impossible.

7.2 Poly (vinyl alcohol)/ montmorillonite nanocomposites

Nanocomposites were prepared from poly (vinyl alcohol) polymers with two different mean molecular weights by intercalating them into various sodium and lithium montmorillonites using solution intercalation in aqueous solutions.

Using a wide range of polymer to clay ratios, from low clay loadings in PVOH to PVOH adsorbed on clay, different structures could be observed. From the interpretation of their XRD traces the samples could be described as exfoliated nanocomposites, intercalated nanocomposites, mixtures of microcomposites and PVOH adsorbed onto clay layers. At low clay contents, up to 10 wt%, XRD silent nanocomposites were formed, which are likely to have an exfoliated structure. Increasing the amount of clay systematically decreased the layer spacing of the clay. Clay loadings between 20 wt% and 40 wt% resulted in samples with broad 001 peaks at low angles, indicating a wide range of high layer spacings. Further increase of the clay loading up to 75 wt% gave composites with clearly intercalated structures, narrower distributions of layer spacings, and layer spacings that decreased almost linearly with increasing clay content. Samples with more than 75 wt% clay were composed of layers intercalated by polymer, and those with no polymer present. Changes in molecular weight or organic contamination of the sodium clay did not show in any significant changes of the dispersion of the clay within the polymer matrix based on the XRD results. As both polymers used had quite large distributions of molecular weights, it is possible that the effect of variations in molecular weight is not detectable by the methods used here.

Thermal stability of these samples under nitrogen could also be divided into distinct groups showing the influence of the clay on the polymer degradation. Below 40 wt% the degradation of the (nano)-composite and the neat polymer is relatively similar though the onset of degradation occurs at higher temperatures (10 - 20°C higher) in the samples with clay. At the same time the maximum decomposition temperature for the first stage of decomposition is raised by 10 – 20 °C in the nanocomposites. At clay loadings of 40 – 60 wt% this first stage of decomposition is showing two maxima, while even higher clay loadings raise the maximum decomposition temperature for this stage by 40 – 60 °C compared to the neat polymer. This latter observation is most likely to be

caused by slower breakdown of the polymer due to stronger interactions with the clay surface and slower release of the decomposition products from the sample. The second decomposition stage is also delayed in the presence of clay. Contrary to the first decomposition stage this stage exhibited a steady increase in the onset temperature with increasing clay loadings up to 65 wt% after which the onset temperature decreased again.

The charge reduction in the lithium clays strongly influenced the dispersion of the clay in the polymer. Lower layer charges resulted in poorer dispersions as these clays swell less in the presence of water and intercalation is, therefore, harder, if not impossible, to achieve. The clay with the lowest layer charge (fired at 210 °C) could not be used for the preparation of nanocomposites. Even at low clay loadings microcomposite structures could be observed in these samples as it did not swell enough to admit any polymer chains.

7.3 Diffusion of water into poly (vinyl alcohol) and its nanocomposites

Diffusion of water into PVOH and its nanocomposites was found to by a very complex procedure. The analysis of the ATR-FTIR spectra was complicated by the number of processes occurring when water interacts with PVOH. During the monitoring of the diffusion process swelling, gelling and partial dissolution of the samples could be observed. This complexity meant that only a semi-quantitative comparison of the data could be performed since no model was found that could account for all processes.

For all samples delay times could be observed before diffusion was detected. Once the diffusion process became measurable it usually reached equilibrium very fast. The delay times and diffusion coefficients were influenced by the formation of nanocomposites. Delay times were found to decrease with increasing clay content. At the same time diffusion rates were slowed down. The diffusion of water into PVOH and PVOH nanocomposites is, therefore, assumed to be a two stage process. First voids and defects in the polymer structure are filled with water. As clay particles disrupt the structure of the PVOH these defects are expected to have a higher volume in the nanocomposites, which results in shorter delay times before diffusion can be observed. Once this free volume within the sample has been filled "true" diffusion through the polymer can be observed. This diffusion process is slowed down by the presence of clay layers as these increase the tortuosity of the diffusion path.

The use of the clean clay in the preparation of nanocomposites was found to lead to higher equilibrium sorption and faster diffusion coefficients. Similar effects were noted for the nanocomposites prepared from charged reduced clays. Samples with poorer dispersion of the clay had longer time delays before diffusion could be observed and slower diffusion coefficients. Two effects have been used to explain these unexpected results. As the incorporation of clay appears to disrupt the intermolecular hydrogen bonding of the PVOH, nanocomposite samples have lower initial barrier properties towards liquid water. Poorer dispersion will, therefore, result in less disruption of the PVOH structure and better barrier properties. At the same time intercalated and

microcomposite structures can have larger aspect ratios of the clay than nanocomposites if clay layers within the stacks are only partially overlapping. Such higher aspect ratios result in better barrier properties due to higher tortuosity of the diffusion path.

Raised temperatures were generally found to result in faster diffusion. This effect was expected as diffusion is a kinetic process. Activation energies for diffusion calculated from the data were higher for the nanocomposites. While this result is unexpected, as nanocomposites are expected to have lower cohesive energy and, therefore, lower activation energies, it could not be ruled out that this observation was due to the large errors associated with the measurements of diffusion coefficients.

Diffusion was found to proceed at an increased rate in samples prepared from higher molecular weight PVOH compared with the pristine polymer. Diffusion and time delay of diffusion into the nanocomposites were found to follow a similar pattern in the high molecular weight nanocomposites compared to that of the low molecular weight samples. Comparison of diffusion coefficients for nanocomposites prepared from these two polymer types generally showed faster diffusion into the high molecular weight samples but differences were not as pronounced as they were in the pristine polymers. The effect of clean clay nanocomposites was, however, stronger in these samples with diffusion coefficients for the clean clay nanocomposites being almost an order of magnitude faster than those measured for the contaminated clay nanocomposites. The faster diffusion in the high molecular weight samples has been attributed to less dense packing of the polymer chains in this polymer.

Swelling of the polymer films was found to be similar for high and low molecular weight samples. Comparison of swelling between the neat polymer and nanocomposites showed mixed results with nanocomposites tending to swell more than the polymer on its own. Changes in crystallinity could only be followed by comparison of the spectra as integration of the relevant bands was influenced too much by the swelling and presence of water in these films. For all samples the band assigned to crystalline regions of PVOH was found to decrease with ingress of water and completely disappear from the spectra long before equilibrium was reached, which indicates that any crystallites are

dissolved during the diffusion of water into these samples. The clay levels in the nanocomposite films could similarly only be compared qualitatively from the spectra. Clay levels appeared to remain similar or decrease in all nanocomposite samples indicating that the clay remained dispersed in the PVOH gel and in cases of reduced relative intensity of the ν(Si-O) band was swollen to greater extent than the polymer by the ingressing water.

Hydrogen bonding of water within the polymer and intermolecular hydrogen bonding were found to be influenced by the presence of clay. For the equilibrium spectra of the neat polymer an increase in the weaker hydrogen bonding of water within the sample and weaker hydrogen bonding of the PVOH could be observed with increasing temperatures. These effects were enhanced by the presence of clay, yet no definite conclusions could be drawn from the data, as changes were likely to arise due to a combination of various factors such as clay loading, temperature and ambient conditions. With higher clay loading an increase in the weaker hydrogen bonded water and PVOH could be observed which means that clay is disrupting the hydrogen bonding network of both.

Following the changes in hydrogen bonding in the sorbed water throughout the diffusion experiment showed that most of the water diffusing into the polymer is weakly hydrogen bonded. Both weakly and strongly hydrogen bonded polymer is decreasing with increasing water content in the film as the polymer is swollen significantly. The incorporation of clay does not alter these general trends.

7.4 Diffusion of acetone/ water mixtures into poly (vinyl alcohol) and its nanocomposites

Diffusion measurements of acetone/ water mixtures into PVOH and PVOH nanocomposites have been performed using four mixtures with molar ratios varying from an excess of water to an excess of acetone. Diffusion was found to be strongly dependent on the water concentration within the diffusants and the resulting concentration of water within the sample films.

The diffusion curves could be divided into two groups at molar ratios of 1:2 acetone/ water and 1:1 acetone/ water diffusion of acetone was found to occur simultaneous with the diffusion of water. In mixtures with an excess of acetone the diffusion of the acetone was delayed with respect to the water diffusion and proceded at a slower rate. In these experiments the diffusion of acetone often set in at the same time water diffusion reached equilibrium. This behaviour is related to the relative concentrations of "pure acetone", acetone/ water complexes and "pure water" in the diffusant mixtures. In mixtures with high concentrations of "pure acetone" and an acetone/ water 5:1 complex (generally mixtures with excess acetone) acetone diffusion is delayed with respect to water diffusion while high concentrations in acetone/ water 2:1 complexes result in simultaneous diffusion of water and acetone.

The 1:2 acetone/ water mixture diffused into these samples at a rate comparable or faster to pure water, yet delay times before diffusion could be observed were increased.

Introduction of clay into the samples appeared to result in longer delay times before diffusion became measurable for both solvents when the mixtures had an excess of acetone. At higher water concentrations delay times before diffusion could be observed in the nanocomposites were found to be similar to those for the pristine polymer. Diffusion coefficients generally decreased with increasing acetone concentrations in the diffusants and increasing clay contents. The formation of nanocomposites, therefore, successfully improved the barrier properties of PVOH against low concentration of water and acetone in combination with water.

Diffusion of pure acetone could only be measured in films that had a high residual moisture content. In such films acetone was found to follow a Fickian diffusion profile and was slowed down significantly in a 2.5 wt% nanocomposite compared to the pristine polymer.

Comparison of delay times and diffusion coefficients with respect to the actual clay loading showed the expected decrease in the diffusion coefficients for the diffusion of the two mixtures with lower acetone content. Delay times before diffusion could be observed remained relatively unchanged. For the mixtures with excess acetone the delay times increased slightly with increasing clay contents. The diffusion coefficients for these samples were, however, found to increase with increasing clay contents. No explanation can be given for these results, yet uncertainties in the preparation of the diffusant mixtures and variations in the "dryness" of the films at the beginning of the experiment are likely to account for these observations.

Diffusion experiments of acetone/ water mixtures into (nano-) composites prepared from charged reduced clays followed the same behaviour as the diffusion of pure water into these samples. Generally barrier properties were found to be best in the samples that showed microcomposite character in their XRD traces. Further clarification of the sample structure is needed to verify whether this observation is due to partial delamination of the samples creating clay agglomerates with larger aspect ratios than the dispersion of clay on a nanoscale.

Swelling of these samples is strongly dependent on the water concentration in the diffusant. Higher amounts of water result in greater extents of swelling. Introduction of clay into the polymer further reduces the swelling possibly through restriction of polymer chain movement due to steric effects.

Crystallinity of these samples was found to reduce in the presence of water. In the neat polymer some crystallinity was recovered over the course of the experiment, since polymer chains could re-arrange into crystal structures in the plasticised polymer. While such recovery of crystallinity after initial dissolution of the crystallites could also be observed in the nanocomposite samples, the extent of the recovery was severely reduced in presence of the clay. This

reduction in ability to regain crystallinity in the nanocomposites has again been attributed to steric effects of the clay particles reducing the polymer chain movement.

Clay levels generally decreased parallel to the swelling of the sample. Any re-aggregation and phase separation of the clay has, therefore, been ruled out, as such events would result in a relative increase of the clay in the evanescent field, which in turn would result in an increase of the clay levels measurable from the ATR-FTIR spectra.

The position of the ν(OH) band in the equilibrium spectra was found to shift to lower wavenumbers with decreasing water contents in the diffusant mixtures. Position of the band remained relatively unaffected by the presence of clay in the sample. Peak width was, however, reduced in the nanocomposites and generally reduced with decreasing water concentrations in the diffusant mixtures.

Investigation of the hydrogen bonding of water and PVOH at equilibrium showed that in the pristine polymer strongly and weakly hydrogen bonded water decreased with increasing acetone concentrations in the diffusant mixtures. In the nanocomposites on the other hand only a decrease of the weakly hydrogen bonded water could be observed. Stronger hydrogen bonding is probably influenced by the presence of clay with water forming strong hydrogen bonds with the clay surfaces or hydration shells around the interlayer cations. Bands for hydrogen bonding of PVOH were found to increase in both cases with increasing acetone concentrations as swelling in the samples was reduced.

Following the changes in hydrogen bonding in the sorbed water throughout the course of the experiment showed decreases in the intermolecular hydrogen bonding of PVOH due to swelling. At the same time, an increase in weakly hydrogen bonded water and a decrease of strongly hydrogen bonded water could be observed, while the fraction of moderately hydrogen bonded water remained constant throughout the experiment. These overall trends were found for diffusion into the pristine polymer as well as the nanocomposites independent of the acetone/ water ratio of the diffusant mixture.

7.5 Further work

7.5.1 Poly (ethylene terephthalate)/ organoclay nanocomposites

Various aspects of the PET/ organoclay nanocomposites could be explored further. For the samples prepared by solution intercalation a more detailed analysis of the structure of the nanocomposites by TEM and AFM would give additional information on the dispersion of the clay platelets in the polymer matrix, as well as more localised changes in crystallinity of the polymer. The ATR-FTIR imaging data showed promising results which suggest that further investigation of larger areas probably by using transmission FTIR imaging could help in understanding the polymer structure in the nanocomposite samples. Comparison of data obtained from transmission measurements with results from ATR-FTIR imaging also enables a comparison of the surface of the material and the bulk sample. Furthermore, the influence of molecular weight of the polymer on the intercalation by solution intercalation could be explored by preparing samples from PET with different molecular weights. Using different preparation methods, such as melt intercalation or in-situ polymerisation, could also be explored as a means of obtaining a better dispersion of the clay in PET.

Similar to the data presented for PVOH nanocomposites diffusion measurements by ATR-FTIR and permeability measurements are useful to assess the barrier properties of PET nanocomposites compared to PET. Diffusion data for the diffusion of water into these films could be explored in dependence of clay loading of the nanocomposite films. Repeating these experiments at different temperatures could give information about the activation energy for the diffusion process. Further diffusion experiments could include investigation of the diffusion of alcohols into PET and PET nanocomposites in dependence of alkyl chain length and structure of the alkyl chain. Another area of interest is the diffusion of solvent/ non-solvent mixtures into such nanocomposite samples which could be explored by ATR-FTIR diffusion measurements.

7.5.2 Poly (vinyl alcohol)/ clay nanocomposites

The preparation of PVOH/ clay nanocomposites could be altered to further optimise the process. The use of different clays, with and without organic modification, should allow preparation of a wide range of materials with different degrees of dispersion. Especially for the charge reduced clays an optimisation of the time allowed to pre-swell the clay in water before addition of the polymer could lead to better dispersion of the clay particles. Another possible route to preparation of these nanocomposites could be the mixing of a dispersion of clay with a polymer solution at elevated temperatures. The investigation of the influence of molecular weight on the dispersion of clay in the polymer matrix could be expanded to include a wider range of molecular weights and probably polymers with narrower molecular weight distributions.

Structural analysis of such samples could be expanded to include TEM and AFM data. Especially for nanocomposites with low clay loadings, where no peaks are observed in the XRD traces, such analysis could shed light on the actual dispersion of the clay platelets. AFM could also be used to gain information on the morphology of samples cast onto different substrates as the optical properties of PVOH and PVOH nanocomposite films cast from aqueous solutions have been found to be transparent when cast onto smooth surfaces while rougher surfaces lead to opaque samples.

To further analyse the influence of clay on the FTIR spectrum it might be necessary to create calibration curve to quantify the clay in the evanescent field rather than using the qualitative ratio as presented in this thesis. Such quantification would enable a closer investigation whether the clay is remaining well dispersed or settling out of the dispersion when films are cast.

7.5.3 Diffusion of small molecules into poly (vinyl alcohol) and its nanocomposites

7.5.3.1 Diffusion of water

The data obtained for diffusion of liquid water into PVOH and PVOH nanocomposites could treated further to extract more details on the structural changes occurring within the polymer. Spectra that are dominated by the water absorption bands could be analysed by subtracting the spectrum of pure water to gain information on the changes in hydrogen bonding of the water once it has entered the polymer film, as well as changes in the polymer bands caused by the swelling and gelling of the films.

The kinetic data can also be analysed further in an attempt to find a more suitable model that can take the strong interactions between water and PVOH, as well as swelling and partial dissolution of the sample during the diffusion of water into such films into account. It might also be necessary to fit the data for the nanocomposite samples using a different model that takes the two phase character of the system into account.

Furthermore, a calibration to quantify the water content at the start of the experiment, as well as at equilibrium, is needed to gain better understanding of the influence of water in the dry films/ in the atmosphere on the reproducibility of these experiments. Reproducibility of the drying procedure could possibly be improved by drying samples under a nitrogen atmosphere.

Since few changes have been observed for nanocomposites with up to 5 wt% clay loading, diffusion experiments on samples with higher clay loadings might exhibit more obvious differences in the barrier properties of these samples.

The work on temperature dependence of the diffusion process could also be expanded, though it appears to be necessary to improve the reproducibility of actual clay loadings in the evanescent field, so that data for different temperatures can be evaluated independent of these changes.

To reduce the influence of swelling and dissolution experiments of water vapour diffusion could be performed. Using water vapour instead of liquid water allows monitoring the diffusion characteristics in dependence of water activity. The

data obtained from such experiments is expected to be easier to analyse, as the observed changes will mainly be due to diffusion of water molecules at low water activities. Such water vapour experiments would also have the advantage that diffusion data obtained from ATR-FTIR measurements could be compared with permeation data obtained from gravimetric analysis.

All the above mentioned experiments could also be performed on nanocomposites of various clays with PVOH. In case of charge reduced clays (heat treated Li^+ montmorillonites) diffusion parameters could be investigated as a function of layer charge, as well as dispersion of the clay and clay loading.

Furthermore, data on PVOH clay composites with higher clay loadings could be gathered to gain a better understanding on the influence of clay loading and possible any changes in the stacking of the clay layers on the diffusion characteristics of the material.

7.5.3.2 Diffusion of other small molecules

Further diffusion studies of small molecules interacting with PVOH and PVOH nanocomposites might include the study diffusion of alcohols or similar small molecules that are poor or non-solvents for PVOH. Such experiments could be performed analysing the dependence of the diffusion on the size and structure, e.g. different alkyl chain length in alcohols, on the diffusion kinetics and the overall barrier properties of PVOH in comparison to PVOH nanocomposites.

Another area of interest is the diffusion of salt solutions into PVOH and PVOH nanocomposites. These studies could be performed in dependence of the salt concentration as well as the type/ size of the cation involved. Cations could potentially show variations in their diffusion behaviour since some cations might be attracted to the clay layers and, therefore, exhibit anomalous diffusion.

In these experiments a wide range of nanocomposites could be used studying the influence of molecular weight of the polymer, clay loading, clay layer charge, cations in the clay gallery and dispersion of the clay in the polymer matrix on the diffusion of these liquids. Experiments at different temperatures could, furthermore, enable the determination of activation energies for the diffusion processes.

7.5.3.3 Diffusion of mixed liquids

Measuring the diffusion of aqueous solvent mixtures into PVOH and PVOH nanocomposites is a powerful method to study the diffusion of water into PVOH at lower concentrations. Data can be obtained on the structural changes occurring in the polymer films due to the interaction with these mixtures. The analysis presented in this thesis could be expanded by investigating the diffusion into nanocomposites with higher clay loadings as well as those with different clay dispersions due to charge reduction or different interlayer cations of the pristine clays. Further experiments could also include diffusion measurements on samples prepared from different molecular weight PVOH samples, as well as investigations of the temperature dependence of the diffusion.

Widening the range of mixtures used in diffusion measurements can give further information about the limits of water content in the film necessary for diffusion of a non solvent, such as acetone, to occur and might also provide evidence of changes in the diffusion mechanism from the kinetic data. For higher water concentrations experiments could be performed using the faster data acquisition method with just one scan per spectrum rather than the ten scans used to collect the data presented in this thesis.

The data analysis could also be improved by the use of multivariate analysis to extract information on the diffusion kinetics and changes within the polymer during the diffusion of solvent mixtures. Should the spectra show enough variation, applying this method should be able to give information on changes in the interactions between the two liquids in the mixture, as well as interactions between solvents and the polymer or polymer/ clay nanocomposite.